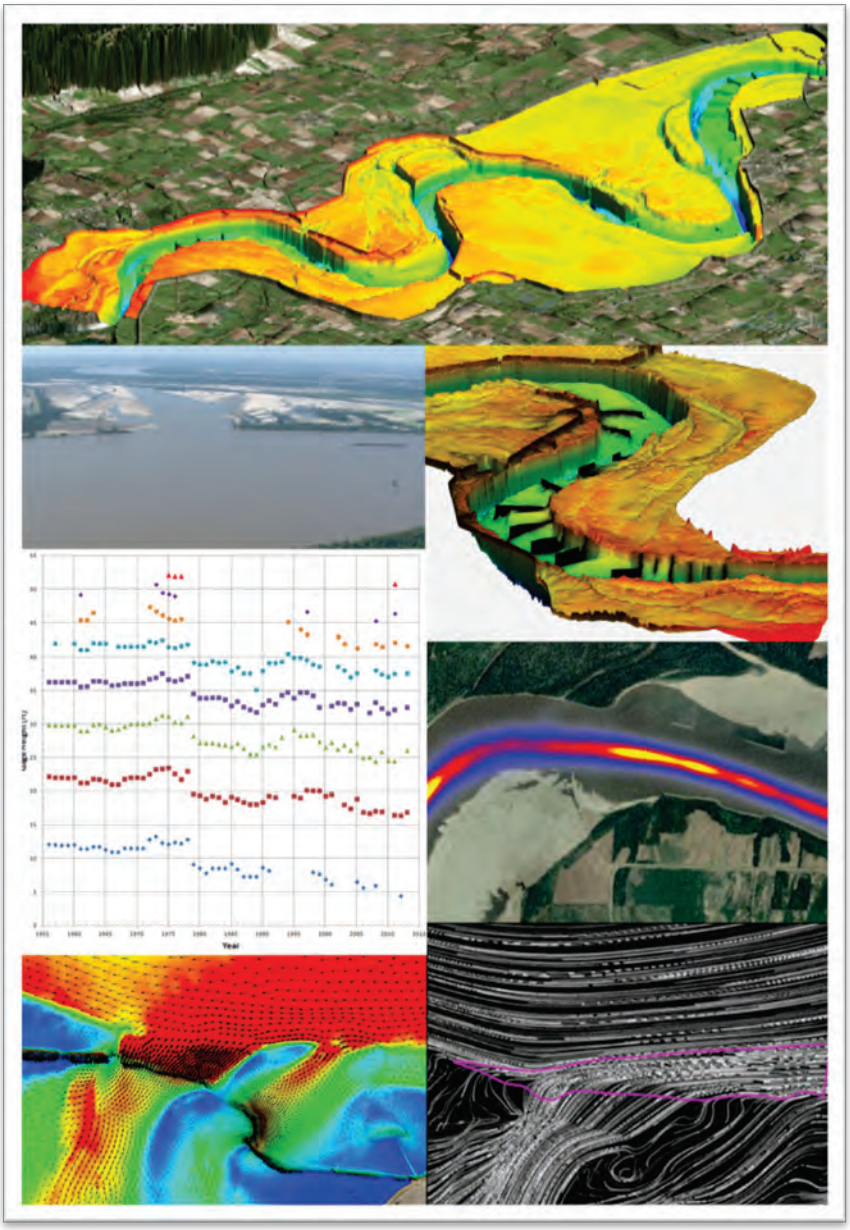
US Army Corps of Engineers®

Merriwether-Cherokee Potamology Study

MRG&P Report No. 9 • May 2017



MRG&P
Mississippi River Geomorphology & Potamology Program

Report prepared for the Mississippi River Commission

Mississippi River Geomorphology &
Potamology (MRG&P) Program

MRG&P Report No. 9
May 2017

Merriwether-Cherokee Potamology Study

Brian M. Hall, Roger A. Gaines, L. Yu Lin, and Kandi H. Waller

Memphis District Hydraulics and Hydrology Branch
U.S. Army Corps of Engineers
167 North Main Street
Memphis, TN 38103-1894

Final report

Approved for public release; distribution is unlimited.

Prepared for U.S. Army Corps of Engineers, Mississippi Valley Division
Mississippi River Geomorphology and Potamology Program
1400 Walnut Street
Vicksburg, MS 39180

Under Project 127672; "Merriwether-Cherokee Potamology Study"

Abstract

This report documents the analysis performed for the Merriwether-Cherokee Potamology Study. The investigation included the following: infrastructure analysis, Low Water Reference Plane analysis, thalweg and tertiary layer analysis, volumetric analysis, specific gage analysis, duration analysis, multidimensional modeling analysis, one-dimensional modeling analysis, and a navigation assessment. A concern was that without modification of the western spur levee and Island 13 overbank, the Mississippi River will continue to form a 9-mile cutoff. If a cutoff were to form, potential adverse impacts include changes in long-term reach dynamics, navigation outdraft conditions, increased dredging operations, hydrodynamic condition changes in close proximity to a Mississippi River Levee mainline levee (Tiptonville-Obion Levee), endangerment of existing channel improvement features ($60M), endangerment of completed crevasse repairs ($27M), and endangerment of planned crevasse repairs. The analysis conducted on the base condition indicated that there is a moderate risk for cutoff formation. Alternatives were investigated to mitigate the risk for cutoff formation. The analysis conducted on the base condition indicated that there is a severe risk for local scour at the closure structure. Local scour countermeasures were investigated to mitigate the risk of closure structure failure.

DISCLAIMER: The contents of this report are not to be used for advertising, publication, or promotional purposes. Citation of trade names does not constitute an official endorsement or approval of the use of such commercial products. All product names and trademarks cited are the property of their respective owners. The findings of this report are not to be construed as an official Department of the Army position unless so designated by other authorized documents.

DESTROY THIS REPORT WHEN NO LONGER NEEDED. DO NOT RETURN IT TO THE ORIGINATOR.

Contents

Abstract ii

Figures and Tables vi

Preface xviii

Unit Conversion Factors xx

Executive Summary xxi

1 Introduction 1

Purpose 1

Problem 1

Method 11

Infrastructure Analysis 11

Lower Water Reference Plane Analysis 11

Thalweg and Tertiary Layer Analysis 11

Volumetric Analysis 11

Specific Gage Analysis 12

Duration Analysis 12

Multidimensional Modeling Analysis 12

One-dimensional (1D) Modeling Analysis 14

Navigation Assessment 15

2 Base Condition 16

Existing infrastructure 16

Closure structure 16

River features 16

Mississippi River Levee (MRL) 21

Geomorphic assessment 21

Low water reference plane (LWRP), thalweg, and tertiary layer analysis 21

Volumetric analysis 23

Specific gage analysis 29

Duration analysis 33

Multidimensional modeling analysis 34

Model description 34

Data collection 34

Model development 35

Hydrodynamic boundary condition development 42

Sediment boundary condition and initial condition development 42

Hydrodynamic calibration and validation 51

Sediment transport function 56

Scenario simulation 57

Flow and sediment diversion analysis *71*
Water surface slope analysis *72*
Key elevations and flows *75*
One-dimensional (1D) Modeling Analysis 78
Model description *78*
Geometry development *78*
Hydrodynamic calibration and validation *79*
Boundary condition development *80*
Scenario simulation *80*
Risk assessment 85
Cutoff formation *85*
Local scour potential *85*
Closure structure failure *86*
Navigation assessment 93
Analysis *93*
Conclusion *97*

3 Alternatives 98
Descriptions of alternatives 98
Multidimensional modeling analysis 99
Geometric data *99*
Plan comparisons *110*
Flow and sediment diversion analysis *124*
Scenario simulations *127*
One-Dimensional (1D) Modeling Analysis 127
Plan parameters *127*
Scenario simulation *128*

4 Local Scour Countermeasures 130
Local scour countermeasure descriptions 130
Multidimensional modeling analysis 131
Geometric data *131*
Plan comparisons *131*
Flow and sediment diversion analysis *140*
Scenario simulations *140*

5 Risk Mitigation 142
Summary of modeled risk mitigation measures 142
Risk mitigation recommendation 144
Risk of cutoff formation *144*
Risk of closure structure failure *144*
Risk to navigation *144*
Risk at MRL *144*

6 Conclusion 145

References 147

Appendix A: Merriwether-Cherokee Potamology Study Phase I Report 149

Appendix B: Volumetric Analysis 291

Appendix C: Multidimensional Modeling Analysis 318

Appendix D: 1D Modeling Analysis 583

Report Documentation Page

Figures and Tables

Figures

Figure 1-1. Overview map. 3
Figure 1-2. Island 13 map. 4
Figure 1-3. Island 13 imagery–6 October 2010. 5
Figure 1-4. Island 13 imagery–4 May 2011. 6
Figure 1-5. Island 13 imagery–22 May 2012. 7
Figure 1-6. Island 13 imagery–29 November 2013. 8
Figure 1-7. Island 13 imagery–29 January 2015. 9
Figure 1-8. Island 13 overbank key features map. 10
Figure 2-1. Adjacent infrastructure impacted by potential cutoff. 17
Figure 2-2. Cumulative dike length by construction year. 19
Figure 2-3. River features impacted by potential cutoff. 20
Figure 2-4. LWRP, thalweg, and tertiary layer plot. 22
Figure 2-5. Hydrographic dataset segmented boundary regions. 24
Figure 2-6. Sediment volume difference by river mile segments. 25
Figure 2-7. Sediment volume difference from 1989 dataset to 1994 dataset. 26
Figure 2-8. Sediment volume difference from 1994 dataset to 2004 dataset. 27
Figure 2-9. Sediment volume difference from 2004 dataset to 2009 dataset. 28
Figure 2-10. Sediment volume difference from 2009 dataset to 2010 dataset. 30
Figure 2-11. Sediment volume difference from 2010 dataset to 2013 dataset. 31
Figure 2-12. Sediment volume difference from 1989 dataset to 2013 dataset. 32
Figure 2-13. Hickman, KY, specific gage plot. 33
Figure 2-14. Duration analysis plot for the time period 1954–2013. 34
Figure 2-15. Island 13 overbank soil sample locations. 36
Figure 2-16. Base condition element mesh for AdH model (entire model). 38
Figure 2-17. Base condition element mesh for AdH model (study overbank). 39
Figure 2-18. Base condition mesh elevation (entire model domain). 40
Figure 2-19. Base condition mesh elevation (study overbank). 41
Figure 2-20. Base condition material type (entire model domain). 43
Figure 2-21. Base condition material type (study overbank). 44
Figure 2-22. Base condition 3D surface (entire model domain). 46
Figure 2-23. Base condition 3D surface (study overbank). 47
Figure 2-24. Sediment bed initialization inflow hydrograph. 51
Figure 2-25. Calibration event 1 inflow hydrograph. 52
Figure 2-26. Calibration event 2 inflow hydrograph. 52
Figure 2-27. Calibration event 3 inflow hydrograph. 53

Figure 2-28. Validation event inflow hydrograph. 53
Figure 2-29. WSEL calibration–gage location map. 54
Figure 2-30. Hypothetical event inflow hydrograph. 58
Figure 2-31. Base condition velocity—1,900,000 cfs (entire model domain). 59
Figure 2-32. Base condition velocity—1,900,000 cfs (study overbank). 61
Figure 2-33. Base condition velocity—1,900,000 cfs (study crevasse). 62
Figure 2-34. Base condition shear stress—1,900,000 cfs (study overbank). 63
Figure 2-35. Historical event inflow hydrograph. 64
Figure 2-36. Base condition bed displacement cohesive overbank—Historical Hydrograph. 65
Figure 2-37. Base condition bed displacement noncohesive overbank—Historical Hydrograph. 66
Figure 2-38. Long-duration inflow hydrograph. 67
Figure 2-39. 1,100,000 cfs event duration histogram. 68
Figure 2-40. Base condition bed displacement cohesive overbank—1,100,000 cfs, 250 days. 69
Figure 2-41. Base condition bed displacement noncohesive overbank—1,100,000 cfs, 250 days. 70
Figure 2-42. Base condition overbank diversion data. 71
Figure 2-43. Base condition main channel sediment load upstream of crevasse. 72
Figure 2-44. Base condition overbank sediment load. 73
Figure 2-45. Average water surface slope flow paths. 74
Figure 2-46. Average water surface slope. 75
Figure 2-47. Crevasse WSEL transect location. 76
Figure 2-48. Crevasse WSEL profile. 77
Figure 2-49. HEC-6T geometry schematic. 78
Figure 2-50. HEC-6T Merriwether-Cherokee overbank reach geometry. 79
Figure 2-51. HEC-6T long-duration hydrograph. 81
Figure 2-52. HEC-6T base condition profile plot Island 13. 82
Figure 2-53. HEC-6T base condition thalweg time series Island 13. 83
Figure 2-54. HEC-6T base condition profile plot main channel. 84
Figure 2-55. Closure structure local scour potential. 86
Figure 2-56. Closure structure failure mesh elevation (study overbank). 87
Figure 2-57. Closure structure failure 3d surface (study overbank). 88
Figure 2-58. Closure structure failure overbank diversion flow. 89
Figure 2-59. Closure structure failure overbank sediment diversion load. 89
Figure 2-60. Closure structure failure shear stress—1,900,000 cfs (study overbank). 91
Figure 2-61. Closure structure failure shear stress difference—1,900,000 cfs. 92
Figure 2-62. Navigation zone of influence with flow trace at 2,400,000 cfs. 93
Figure 2-63. Navigation zone of influence with velocity field at 2,400,000 cfs. 94
Figure 2-64. LOMA live plotter. 95
Figure 2-65. Study area vessel tracks. 96
Figure 2-66. Downstream-bound vessel density map. 96

Figure 2-67. Upstream-bound vessel density map. 97
Figure 3-1. Alternative 1 mesh elevation (study overbank). 100
Figure 3-2. Alternative 1; 3D surface (study overbank). 101
Figure 3-3. Alternative 2 mesh elevation (study overbank). 102
Figure 3-4. Alternative 2; 3D surface (study overbank). 103
Figure 3-5. Alternative 3 mesh elevation (study overbank). 104
Figure 3-6. Alternative 3; 3D surface (study overbank). 105
Figure 3-7. Alternative 4 mesh elevation (study overbank). 106
Figure 3-8. Alternative 4; 3D surface (study overbank). 107
Figure 3-9. Alternative 5 material type (study overbank). 108
Figure 3-10. Alternative 6 material type (study overbank). 109
Figure 3-11. Alternative 1 shear stress—1,900,000 cfs (study overbank). 111
Figure 3-12. Alternative 1 shear stress difference—1,900,000 cfs. 112
Figure 3-13. Alternative 2 shear stress—1,900,000 cfs (study overbank). 113
Figure 3-14. Alternative 2 shear stress difference—1,900,000 cfs. 115
Figure 3-15. Alternative 3 shear stress—1,900,000 cfs (study overbank). 116
Figure 3-16. Alternative 3 shear stress difference—1,900,000 cfs. 117
Figure 3-17. Alternative 4 shear stress—1,900,000 cfs (study overbank). 118
Figure 3-18. Alternative 4 shear stress difference—1,900,000 cfs. 120
Figure 3-19. Alternative 5 shear stress—1,900,000 cfs (study overbank). 121
Figure 3-20. Alternative 5 shear stress difference—1,900,000 cfs. 122
Figure 3-21. Alternative 6 shear stress—1,900,000 cfs (study overbank). 123
Figure 3-22. Alternative 6 shear stress difference—1,900,000 cfs. 125
Figure 3-23. Alternative overbank diversion flow. 126
Figure 3-24. Alternative overbank sediment diversion load. 126
Figure 3-25. HEC-6T Alternative 5 profile plot. 128
Figure 3-26. HEC-6T Alternative 5 thalweg time series. 129
Figure 4-1. Local Scour Countermeasure 1 material type (study overbank). 132
Figure 4-2. Local Scour Countermeasure 2 mesh elevation (study overbank). 133
Figure 4-3. Local Scour Countermeasure 2; 3D surface (study overbank). 134
Figure 4-4. Local Scour Countermeasure 1 shear stress—1,900,000 cfs (study overbank). 135
Figure 4-5. Local Scour Countermeasure 1 shear stress difference—1,900,000 cfs. 137
Figure 4-6. Local Scour Countermeasure 2 shear stress—1,900,000 cfs (study overbank). 138
Figure 4-7. Local Scour Countermeasure 2 shear stress difference—1,900,000 cfs. 139
Figure 4-8. Local scour countermeasure overbank diversion flow. 141
Figure 4-9. Local scour countermeasure overbank sediment diversion load. 141
Figure B-1. Surface difference comparison from 1989 dataset to 1994 dataset (RM 840-860). 291
Figure B-2. Surface difference comparison from 1989 dataset to 1994 dataset (RM 860-878). 292

Figure B-3. Surface difference comparison from 1989 dataset to 1994 dataset (RM 878-888). 293
Figure B-4. Surface difference comparison from 1994 dataset to 2004 dataset (RM 840-860). 294
Figure B-5. Surface difference comparison from 1994 dataset to 2004 dataset (RM 860-878). 295
Figure B-6. Surface difference comparison from 1994 dataset to 2004 dataset (RM 878-888). 296
Figure B-7. Surface difference comparison from 2004 dataset to 2009 dataset (RM 840-860). 297
Figure B-8. Surface difference comparison from 2004 dataset to 2009 dataset (RM 860-878). 298
Figure B-9. Surface difference comparison from 2004 dataset to 2009 dataset (RM 878-888). 299
Figure B-10. Surface difference comparison from 2009 dataset to 2010 dataset (RM 840-860). 300
Figure B-11. Surface difference comparison from 2009 dataset to 2010 dataset (RM 860-878). 301
Figure B-12. Surface difference comparison from 2009 dataset to 2010 dataset (RM 878-888). 302
Figure B-13. Surface difference comparison from 2010 dataset to 2013 dataset (RM 840-860). 303
Figure B-14. Surface difference comparison from 2010 dataset to 2013 dataset (RM 860-878). 304
Figure B-15. Surface difference comparison from 2010 dataset to 2013 dataset (RM 878-888). 305
Figure B-16. Surface difference comparison from 1989 dataset to 2013 dataset (RM 840-860). 306
Figure B-17. Surface difference comparison from 1989 dataset to 2013 dataset (RM 860-878). 307
Figure B-18. Surface difference comparison from 1989 dataset to 2013 dataset (RM 878-888). 308
Figure C-1. WSEL calibration—MS116 Event 1. 319
Figure C-2. WSEL calibration—MS117 Event 1. 319
Figure C-3. WSEL calibration—MS116 Event 2. 320
Figure C-4. WSEL calibration—MS117 Event 2. 320
Figure C-5. Dec 2013 observed precipitation. 321
Figure C-6. 20 Dec 2013 observed precipitation. 321
Figure C-7. 21 Dec 2013 observed precipitation. 322
Figure C-8. 22 Dec 2013 observed precipitation. 322
Figure C-9. 23 Dec 2013 observed precipitation. 323
Figure C-10. 24 Dec 2013 observed precipitation. 323
Figure C-11. WSEL calibration—MS116 Event 3. 324
Figure C-12. WSEL calibration—MS117 Event 3. 324

Figure C-13. Velocity calibration—8 May 2013 velocity difference. 325
Figure C-14. Velocity calibration—8 May 2013 modeled vs. observed. 326
Figure C-15. Velocity calibration—19 Dec 2013 velocity difference. 327
Figure C-16. Velocity calibration—19 Dec 2013 modeled vs. observed. 328
Figure C-17. Velocity calibration—28 Feb 2014 Dataset 1 velocity difference. 329
Figure C-18. Velocity calibration—28 Feb 2014 Dataset 1 modeled vs. observed. 330
Figure C-19. Velocity calibration—28 Feb 2014 Dataset 2 velocity difference. 331
Figure C-20. Velocity calibration—28 Feb 2014 Dataset 2 modeled vs. observed. 332
Figure C-21. Velocity calibration—28 Feb 2014 Dataset 3 velocity difference. 333
Figure C-22. Velocity calibration—28 Feb 2014 Dataset 3 modeled vs. observed. 334
Figure C-23. Velocity calibration—9 Apr 2014 Dataset 1 velocity difference. 335
Figure C-24. Velocity calibration—9 Apr 2014 Dataset 1 modeled vs. observed. 336
Figure C-25. Velocity calibration—9 Apr 2014 Dataset 2 velocity difference. 337
Figure C-26. Velocity calibration—9 Apr 2014 Dataset 2 modeled vs. observed. 338
Figure C-27. Velocity calibration—9 Apr 2014 Dataset 3 velocity difference. 339
Figure C-28. Velocity calibration—9 Apr 2014 Dataset 3 modeled vs. observed. 340
Figure C-29. WSEL validation—MS116. 341
Figure C-30. Water Surface Elevation Validation—MS117 341
Figure C-31. Bed sediment initialization—d16 difference. 342
Figure C-32. Bed sediment initialization—d16 modeled vs. observed. 343
Figure C-33. Bed sediment initialization—d25 difference. 344
Figure C-34. Bed sediment initialization—d25 modeled vs. observed. 345
Figure C-35. Bed sediment initialization—d50 difference. 346
Figure C-36. Bed sediment initialization—d50 modeled vs. observed. 347
Figure C-37. Bed sediment initialization—d75 difference. 348
Figure C-38. Bed sediment initialization—d75 modeled vs. observed. 349
Figure C-39. Bed sediment initialization—d84 difference. 350
Figure C-40. Bed sediment initialization—d84 modeled vs. observed. 351
Figure C-41. Base condition velocity—400,000 cfs (entire model domain). 352
Figure C-42. Base condition velocity—500,000 cfs (entire model domain). 353
Figure C-43. Base condition velocity—600,000 cfs (entire model domain). 354
Figure C-44. Base condition velocity—650,000 cfs (entire model domain). 355
Figure C-45. Base condition velocity—700,000 cfs (entire model domain). 356
Figure C-46. Base condition velocity—750,000 cfs (entire model domain). 357
Figure C-47. Base condition velocity—800,000 cfs (entire model domain). 358
Figure C-48. Base condition velocity—850,000 cfs (entire model domain). 359
Figure C-49. Base condition velocity—900,000 cfs (entire model domain). 360
Figure C-50. Base condition velocity—1,100,000 cfs (entire model domain). 361
Figure C-51. Base condition velocity—1,300,000 cfs (entire model domain). 362
Figure C-52. Base condition velocity—1,500,000 cfs (entire model domain). 363

Figure C-53. Base condition velocity—1,700,000 cfs (entire model domain). 364
Figure C-54. Base condition velocity—1,900,000 cfs (entire model domain). 365
Figure C-55. Base condition velocity—2,100,000 cfs (entire model domain). 366
Figure C-56. Base condition velocity—400,000 cfs (study overbank). 367
Figure C-57. Base condition velocity—500,000 cfs (study overbank). 368
Figure C-58. Base condition velocity—600,000 cfs (study overbank). 369
Figure C-59. Base condition velocity—650,000 cfs (study overbank). 370
Figure C-60. Base condition velocity—700,000 cfs (study overbank). 371
Figure C-61. Base condition velocity—750,00 cfs (study overbank). 372
Figure C-62. Base condition velocity—800,000 cfs (study overbank). 373
Figure C-63. Base condition velocity—850,000 cfs (study overbank). 374
Figure C-64. Base condition velocity—900,000 cfs (study overbank). 375
Figure C-65. Base condition velocity—1,100,000 cfs (study overbank). 376
Figure C-66. Base condition velocity—1,300,000 cfs (study overbank). 377
Figure C-67. Base condition velocity—1,500,000 cfs (study overbank). 378
Figure C-68. Base condition velocity—1,700,000 cfs (study overbank). 379
Figure C-69. Base condition velocity—1,900,000 cfs (study overbank). 380
Figure C-70. Base condition velocity—2,100,000 cfs (study overbank). 381
Figure C-71. Base condition velocity—400,000 cfs (study crevasse). 382
Figure C-72. Base condition velocity—500,000 cfs (study crevasse). 383
Figure C-73. Base condition velocity—600,000 cfs (study crevasse). 384
Figure C-74. Base condition velocity—650,000 cfs (study crevasse). 385
Figure C-75. Base condition velocity—700,000 cfs (study crevasse). 386
Figure C-76. Base condition velocity—750,000 cfs (study crevasse). 387
Figure C-77. Base condition velocity—800,000 cfs (study crevasse). 388
Figure C-78. Base condition velocity—850,000 cfs (study crevasse). 389
Figure C-79. Base condition velocity—900,000 cfs (study crevasse). 390
Figure C-80. Base condition velocity—1,100,000 cfs (study crevasse). 391
Figure C-81. Base condition velocity—1,300,000 cfs (study crevasse). 392
Figure C-82. Base condition velocity—1,500,000 cfs (study crevasse). 393
Figure C-83. Base condition velocity—1,700,000 cfs (study crevasse). 394
Figure C-84. Base condition velocity—1,900,000 cfs (study crevasse). 395
Figure C-85. Base condition velocity—2,100,000 cfs (study crevasse). 396
Figure C-86. Base condition shear stress—900,000 cfs (study overbank). 397
Figure C-87. Base condition shear stress—1,100,000 cfs (study overbank). 398
Figure C-88. Base condition shear stress—1,300,000 cfs (study overbank). 399
Figure C-89. Base condition shear stress—1,500,000 cfs (study overbank). 400
Figure C-90. Base condition shear stress—1,700,000 cfs (study overbank). 401
Figure C-91. Base condition shear stress—1,900,000 cfs (study overbank). 402
Figure C-92. Base condition shear stress—2,100,000 cfs (study overbank). 403

Figure C-93. Base condition WSEL profile. 405
Figure C-94. Base condition WSEL—2,100,000 cfs (study overbank). 406
Figure C-95. Closure structure failure shear stress—900,000 cfs (study overbank). 408
Figure C-96. Closure structure failure shear stress—1,100,000 cfs (study overbank). 409
Figure C-97. Closure structure failure shear stress—1,300,000 cfs (study overbank). 410
Figure C-98. Closure structure failure shear stress—1,500,000 cfs (study overbank). 411
Figure C-99. Closure structure failure shear stress—1,700,000 cfs (study overbank). 412
Figure C-100. Closure structure failure shear stress—1,900,000 cfs (study overbank). 413
Figure C-101. Closure structure failure shear stress—2,100,000 cfs (study overbank). 414
Figure C-102. Closure structure failure shear stress difference—900,000 cfs. 416
Figure C-103. Closure structure failure shear stress difference—1,100,000 cfs. 417
Figure C-104. Closure structure failure shear stress difference—1,300,000 cfs. 418
Figure C-105. Closure structure failure shear stress difference—1,500,000 cfs. 419
Figure C-106. Closure structure failure shear stress difference—1,700,000 cfs. 420
Figure C-107. Closure structure failure shear stress difference—1,900,000 cfs. 421
Figure C-108. Closure structure failure shear stress difference—2,100,000 cfs. 422
Figure C-109. Closure structure failure WSEL profile. 424
Figure C-110. Closure structure failure vs. base condition WSEL profile 1,100,000 cfs. 425
Figure C-111. Closure structure failure vs. base condition WSEL profile 1,500,000 cfs. 426
Figure C-112. Closure structure failure vs. base condition WSEL profile 1,900,000 cfs. 427
Figure C-113. Closure structure failure vs. base condition WSEL profile 2,100,000 cfs. 428
Figure C-114. Alternative 1 shear stress—900,000 cfs (study overbank). 430
Figure C-115. Alternative 1 shear stress—1,100,000 cfs (study overbank). 431
Figure C-116. Alternative 1 shear stress—1,300,000 cfs (study overbank). 432
Figure C-117. Alternative 1 shear stress—1,500,000 cfs (study overbank). 433
Figure C-118. Alternative 1 shear stress—1,700,000 cfs (study overbank). 434
Figure C-119. Alternative 1 shear stress—1,900,000 cfs (study overbank). 435
Figure C-120. Alternative 1 shear stress—2,100,000 cfs (study overbank). 436
Figure C-121. Alternative 1 shear stress difference—900,000 cfs. 438
Figure C-122. Alternative 1 shear stress difference—1,100,000 cfs. 439
Figure C-123. Alternative 1 shear stress difference—1,300,000 cfs. 440
Figure C-124. Alternative 1 shear stress difference—1,500,000 cfs. 441
Figure C-125. Alternative 1 shear stress difference—1,700,000 cfs. 442
Figure C-126. Alternative 1 shear stress difference—1,900,000 cfs. 443
Figure C-127. Alternative 1 shear stress difference—2,100,000 cfs. 444
Figure C-128. Alternative 1 WSEL. 446
Figure C-129. Alternative 2 shear stress—900,000 cfs (study overbank). 448
Figure C-130. Alternative 2 shear stress—1,100,000 cfs (study overbank). 449
Figure C-131. Alternative 2 shear stress—1,300,000 cfs (study overbank). 450
Figure C-132. Alternative 2 shear stress—1,500,000 cfs (study overbank). 451

Figure C-133. Alternative 2 shear stress—1,700,000 cfs (study overbank). 452
Figure C-134. Alternative 2 shear stress—1,900,000 cfs (study overbank). 453
Figure C-135. Alternative 2 shear stress—2,100,000 cfs (study overbank). 454
Figure C-136. Alternative 2 shear stress difference—900,000 cfs. 456
Figure C-137. Alternative 2 shear stress difference—1,100,000 cfs. 457
Figure C-138. Alternative 2 shear stress difference—1,300,000 cfs. 458
Figure C-139. Alternative 2 shear stress difference—1,500,000 cfs. 459
Figure C-140. Alternative 2 shear stress difference—1,700,000 cfs. 460
Figure C-141. Alternative 2 shear stress difference—1,900,000 cfs. 461
Figure C-142. Alternative 2 shear stress difference—2,100,000 cfs. 462
Figure C-143. Alternative 2 WSEL profile. 464
Figure C-144. Alternative 3 shear stress—900,000 cfs (study overbank). 466
Figure C-145. Alternative 3 shear stress—1,100,000 cfs (study overbank). 467
Figure C-146. Alternative 3 shear stress—1,300,000 cfs (study overbank). 468
Figure C-147. Alternative 3 shear stress—1,500,000 cfs (study overbank). 469
Figure C-148. Alternative 3 shear stress—1,700,000 cfs (study overbank). 470
Figure C-149. Alternative 3 shear stress—1,900,000 cfs (study overbank). 471
Figure C-150. Alternative 3 shear stress—2,100,000 cfs (study overbank). 472
Figure C-151. Alternative 3 shear stress difference—900,000 cfs. 474
Figure C-152. Alternative 3 shear stress difference—1,100,000 cfs. 475
Figure C-153. Alternative 3 shear stress difference—1,300,000 cfs. 476
Figure C-154. Alternative 3 shear stress difference—1,500,000 cfs. 477
Figure C-155. Alternative 3 shear stress difference—1,700,000 cfs. 478
Figure C-156. Alternative 3 shear stress difference—1,900,000 cfs. 479
Figure C-157. Alternative 3 shear stress difference—2,100,000 cfs. 480
Figure C-158. Alternative 3 WSEL. 482
Figure C-159. Alternative 4 shear stress—900,000 cfs (study overbank). 484
Figure C-160. Alternative 4 shear stress—1,100,000 cfs (study overbank). 485
Figure C-161. Alternative 4 shear stress—1,300,000 cfs (study overbank). 486
Figure C-162. Alternative 4 shear stress—1,500,000 cfs (study overbank). 487
Figure C-163. Alternative 4 shear stress—1,700,000 cfs (study overbank). 488
Figure C-164. Alternative 4 shear stress—1,900,000 cfs (study overbank). 489
Figure C-165. Alternative 4 shear stress—2,100,000 cfs (study overbank). 490
Figure C-166. Alternative 4 shear stress difference—900,000 cfs. 492
Figure C-167. Alternative 4 shear stress difference—1,100,000 cfs. 493
Figure C-168. Alternative 4 shear stress difference—1,300,000 cfs. 494
Figure C-169. Alternative 4 shear stress difference—1,500,000 cfs. 495
Figure C-170. Alternative 4 shear stress difference—1,700,000 cfs. 496
Figure C-171. Alternative 4 shear stress difference—1,900,000 cfs. 497
Figure C-172. Alternative 4 shear stress difference—2,100,000 cfs. 498

Figure C-173. Alternative 4 WSEL profile. 500
Figure C-174. Alternative 5 shear stress—900,000 cfs (study overbank). 502
Figure C-175. Alternative 5 shear stress—1,100,000 cfs (study overbank). 503
Figure C-176. Alternative 5 shear stress—1,300,000 cfs (study overbank). 504
Figure C-177. Alternative 5 shear stress—1,500,000 cfs (study overbank). 505
Figure C-178. Alternative 5 shear stress—1,700,000 cfs (study overbank). 506
Figure C-179. Alternative 5 shear stress—1,900,000 cfs (study overbank). 507
Figure C-180. Alternative 5 shear stress—2,100,000 cfs (study overbank). 508
Figure C-181. Alternative 5 shear stress difference—900,000 cfs. 510
Figure C-182. Alternative 5 shear stress difference—1,100,000 cfs. 511
Figure C-183. Alternative 5 shear stress difference—1,300,000 cfs. 512
Figure C-184. Alternative 5 shear stress difference—1,500,000 cfs. 513
Figure C-185. Alternative 5 shear stress difference—1,700,000 cfs. 514
Figure C-186. Alternative 5 shear stress difference—1,900,000 cfs. 515
Figure C-187. Alternative 5 shear stress difference—2,100,000 cfs. 516
Figure C-188. Alternative 5 WSEL profile. 518
Figure C-189. Alternative 6 shear stress—900,000 cfs (study overbank). 520
Figure C-190. Alternative 6 shear stress—1,100,000 cfs (study overbank). 521
Figure C-191. Alternative 6 shear stress—1,300,000 cfs (study overbank). 522
Figure C-192. Alternative 6 shear stress—1,500,000 cfs (study overbank). 523
Figure C-193. Alternative 6 shear stress—1,700,000 cfs (study overbank). 524
Figure C-194. Alternative 6 shear stress—1,900,000 cfs (study overbank). 525
Figure C-195. Alternative 6 shear stress—2,100,000 cfs (study overbank). 526
Figure C-196. Alternative 6 shear stress difference—900,000 cfs. 528
Figure C-197. Alternative 6 shear stress difference—1,100,000 cfs. 529
Figure C-198. Alternative 6 shear stress difference—1,300,000 cfs. 530
Figure C-199. Alternative 6 shear stress difference—1,500,000 cfs. 531
Figure C-200. Alternative 6 shear stress difference—1,700,000 cfs. 532
Figure C-201. Alternative 6 shear stress difference—1,900,000 cfs. 533
Figure C-202. Alternative 6 shear stress difference—2,100,000 cfs. 534
Figure C-203. Alternative 6 WSEL profile. 536
Figure C-204. Alternatives vs. base condition WSEL profile 1,100,000 cfs. 538
Figure C-205. Alternatives vs. base condition WSEL profile 1,500,000 cfs. 539
Figure C-206. Alternatives vs. base condition WSEL profile 1,900,000 cfs. 540
Figure C-207. Alternatives vs. base condition WSEL profile 2,100,000 cfs. 541
Figure C-208. Local Scour Countermeasure 1 shear stress—900,000 cfs (study overbank). 543
Figure C-209. Local Scour Countermeasure 1 shear stress—1,100,000 cfs (study overbank). 544
Figure C-210. Local Scour Countermeasure 1 shear stress—1,300,000 cfs (study overbank). 545
Figure C-211. Local Scour Countermeasure 1 shear stress—1,500,000 cfs (study overbank). 546
Figure C-212. Local Scour Countermeasure 1 shear stress—1,700,000 cfs (study overbank). 547

Figure C-213. Local Scour Countermeasure 1 shear stress—1,900,000 cfs (study overbank). 548
Figure C-214. Local Scour Countermeasure 1 shear stress—2,100,000 cfs (study overbank). 549
Figure C-215. Local Scour Countermeasure 1 shear stress difference—900,000 cfs. 551
Figure C-216. Local Scour Countermeasure 1 shear stress difference—1,100,000 cfs. 552
Figure C-217. Local Scour Countermeasure 1 shear stress difference—1,300,000 cfs. 553
Figure C-218. Local Scour Countermeasure 1 shear stress difference—1,500,000 cfs. 554
Figure C-219. Local Scour Countermeasure 1 shear stress difference—1,700,000 cfs. 555
Figure C-220. Local Scour Countermeasure 1 shear stress difference—1,900,000 cfs. 556
Figure C-221. Local Scour Countermeasure 1 shear stress difference—2,100,000 cfs. 557
Figure C-222. Local Scour Countermeasure 1 WSEL profile. 559
Figure C-223. Local Scour Countermeasure 2 shear stress—900,000 cfs (study overbank). 561
Figure C-224. Local Scour Countermeasure 2 shear stress—1,100,000 cfs (study overbank). 562
Figure C-225. Local Scour Countermeasure 2 shear stress—1,300,000 cfs (study overbank). 563
Figure C-226. Local Scour Countermeasure 2 shear stress—1,500,000 cfs (study overbank). 564
Figure C-227. Local Scour Countermeasure 2 shear stress—1,700,000 cfs (study overbank). 565
Figure C-228. Local Scour Countermeasure 2 shear stress—1,900,000 cfs (study overbank). 566
Figure C-229. Local Scour Countermeasure 2 shear stress—2,100,000 cfs (study overbank). 567
Figure C-230. Local Scour Countermeasure 2 shear stress difference—900,000 cfs. 569
Figure C-231. Local Scour Countermeasure 2 shear stress difference—1,100,000 cfs. 570
Figure C-232. Local Scour Countermeasure 2 shear stress difference—1,300,000 cfs. 571
Figure C-233. Local Scour Countermeasure 2 shear stress difference—1,500,000 cfs. 572
Figure C-234. Local Scour Countermeasure 2 shear stress difference—1,700,000 cfs. 573
Figure C-235. Local Scour Countermeasure 2 shear stress difference—1,900,000 cfs. 574
Figure C-236. Local Scour Countermeasure 2 shear stress difference—2,100,000 cfs. 575
Figure C-237. Local Scour Countermeasure 2 WSEL profile. 577
Figure C-238. Local scour countermeasures vs. base condition WSEL profile 1,100,000 cfs. 579
Figure C-239. Local scour countermeasures vs. base condition WSEL profile 1,500,000 cfs. 580
Figure C-240. Local scour countermeasures vs. base condition WSEL profile 1,900,000 cfs. 581
Figure C-241. Local scour countermeasures vs. base condition WSEL profile 2,100,000 cfs. 582
Figure D-1. HEC-6T index flow and Hickman, KY, specific gage plot. 583
Figure D-2. HEC-6T 1993 sediment calibration at RM 846.40. 584
Figure D-3. HEC-6T 2004 sediment calibration at RM 846.40. 584
Figure D-4. HEC-6T 2010 sediment validation at RM 846.40. 584
Figure D-5. HEC-6T 1993 sediment calibration at RM 856.99. 584
Figure D-6. HEC-6T 2004 sediment calibration at RM 856.99. 584
Figure D-7. HEC-6T 2010 sediment validation at RM 856.99. 584
Figure D-8. HEC-6T 1993 sediment calibration at RM 864.76. 584
Figure D-9. HEC-6T 2004 sediment calibration at RM 864.76. 584
Figure D-10. HEC-6T 2010 sediment validation at RM 864.76. 584
Figure D-11. HEC-6T 1993 sediment calibration at RM 870.20. 584

Figure D-12. HEC-6T 2004 sediment calibration at RM 870.20. 584
Figure D-13. HEC-6T 2010 sediment validation at RM 870.20. 584
Figure D-14. HEC-6T base condition vs. Alternative 5 index flows at RM 846.20. 584
Figure D-15. HEC-6T base condition vs. Alternative 5 index flows at RM 869.08. 584
Figure D-16. HEC-6T base condition vs. Alternative 5 index flows at RM 873.04. 584
Figure D-17. HEC-6T base condition vs. Alternative 5 index flows at RM 922.00. 584

Tables

Table 2-1. Potential cutoff adjacent revetment impact. 18
Table 2-2. Island 13 overbank soil samples. 37
Table 2-3. Manning's roughness coefficients. 45
Table 2-4. Cohesive sediment model parameters. 48
Table 2-5. Noncohesive sediment model parameters. 49
Table 2-6. Initial overbank material bed distribution and layer thickness. 50
Table 2-7. Initial channel material bed distribution and layer thickness. 50
Table 2-8. Tiptonville gage WSEL calibration and validation summary. 55
Table 2-9. Caruthersville gage WSEL calibration and validation summary. 55
Table 2-10. Water surface elevation root-mean-square error. 56
Table 2-11. Velocity calibration summary. 56
Table 2-12. Bed sediment initialization summary. 57
Table 2-13. Discharge frequency for the Mississippi River at Hickman, KY. 58
Table 2-14. Base condition key flows and elevations 77
Table 3-1. Descriptions of alternatives. 98
Table 4-1. Local scour countermeasure descriptions. 130
Table 5-1. Summary of alternatives. 142
Table 5-2. Local scour countermeasure summary. 143
Table B-1. Surface difference comparison from 1989 dataset to 1994 dataset. 309
Table B-2. Surface difference comparison from 1989 dataset to 2013 dataset. 310
Table B-3. Surface difference comparison from 1994 dataset to 2004 dataset. 311
Table B-4. Surface difference comparison from 1994 dataset to 2013 dataset. 312
Table B-5. Surface difference comparison from 2004 dataset to 2009 dataset. 313
Table B-6. Surface difference comparison from 2004 dataset to 2013 dataset. 314
Table B-7. Surface difference comparison from 2009 dataset to 2010 dataset. 315
Table B-8. Surface difference comparison from 2009 dataset to 2013 dataset. 316
Table B-9. Surface difference comparison from 2010 dataset to 2013 dataset 317
Table C-1. Base condition diversion grain size distribution. 407
Table C-2. Closure structure failure diversion grain size distribution. 429
Table C-3. Alternative 1 diversion grain size distribution. 447
Table C-4. Alternative 2 diversion grain size distribution. 465
Table C-5. Alternative 3 diversion grain size distribution. 483

Table C-6. Alternative 4 diversion grain size distribution. 501
Table C-7. Alternative 5 diversion grain size distribution..... 519
Table C-8. Alternative 6 diversion grain size distribution. 537
Table C-9. Local Scour Countermeasure 1 diversion grain size distribution..... 560
Table C-10. Local Scour Countermeasure 2 diversion grain size distribution. 578

Preface

The research documented in this report was conducted as part of the Mississippi River Geomorphology and Potamology (MRG&P) Program, under Project 127672; "Merriwether-Cherokee Potamology Study." The MRG&P is part of the Mississippi River and Tributaries Program (MR&T) and is managed by the U.S. Army Corps of Engineers (USACE), Mississippi Valley Division (MVD), and Districts. The MRG&P Senior Program Manager was Mr. Freddie Pinkard, and the Technical Director was Dr. Barbara Kleiss. The MVD Commander was MG Michael C. Wehr. The MVD Director of Programs was Mr. James A. Bodron.

Mississippi River engineering direction and policy advice were provided by the Mississippi River Commission. The Commission members were MG Wehr, USACE; the Honorable Sam E. Angel; the Honorable R. D. James; the Honorable Norma Jean Mattei, Ph.D.; RDML Gerd F. Glang, National Oceanic and Atmospheric Administration; BG Richard G. Kaiser, USACE; and BG David C. Hill, USACE.

The report was prepared under the general supervision of Mr. David P. Berretta, Chief, Hydraulics and Hydrology Branch, and Mr. Donny D. Davidson, Chief, Engineering Division. COL Jeffery A. Anderson was Commander of the Memphis District (MVM). Organizational support was provided by Dr. Barbara Kleiss (MVD) and Mr. Freddie Pinkard (Vicksburg District).

The investigation was conducted by a collaboration among the following offices and agencies: MVD, MVM, and the Engineer Research and Development Center (ERDC), Coastal and Hydraulics Laboratory (CHL). Funding for the study was provided by MVD.

Direct supervision of the CHL aspects of this effort was provided by Dr. Ty V. Wamsley, Chief of the Flood and Storm Division (CERD-HF), and Dr. Loren Wehmeyer, Chief of the River Engineering Branch (CERD-HFR). The Director of CHL was Mr. José E. Sánchez.

Significant contributions to this document were made by Mr. William A. Simmerman and Mr. Darian S. Chasteen (MVD Hydraulics and Hydrology

Branch); Mr. Ronald E. Heath, Mr. Ian E. Floyd, Mr. Michael F. Winkler, and Mr. Howard E. Park (CHL); and Mr. David S. Biedenharn (Biedenharn Group, LLC). Additional acknowledgment is extended to Mr. Charles Little and Mr. Gary Bell (CHL) and Mr. Tony L. Tullos (Information Technology Laboratory), whose critical reviews, suggestions, and edits significantly improved the report.

COL Bryan S. Green was Commander of ERDC, and the Director was Dr. David W. Pittman.

Unit Conversion Factors

Multiply	By	To Obtain
cubic feet	0.02831685	cubic meters
cubic inches	1.6387064 E-05	cubic meters
cubic yards	0.7645549	cubic meters
degrees Fahrenheit	(F-32)/1.8	degrees Celsius
feet	0.3048	meters
gallons (U.S. liquid)	3.785412 E-03	cubic meters
inches	0.0254	meters
inch-pounds (force)	0.1129848	newton meters
knots	0.5144444	meters per second
miles (U.S. statute)	1,609.347	meters
miles per hour	0.44704	meters per second
pounds (force) per square foot	47.88026	pascals
pounds (force) per square inch	6.894757	kilopascals
pounds (mass)	0.45359237	kilograms
pounds (mass) per cubic foot	16.01846	kilograms per cubic meter
pounds (mass) per cubic inch	2.757990 E+04	kilograms per cubic meter
pounds (mass) per square foot	4.882428	kilograms per square meter
pounds (mass) per square yard	0.542492	kilograms per square meter
square inches	6.4516 E-04	square meters
square miles	2.589998 E+06	square meters
square yards	0.8361274	square meters
tons (2,000 pounds, mass)	907.1847	kilograms
yards	0.9144	meters

Executive Summary

This report documents the analysis performed for the Merriwether-Cherokee Potamology Study. The investigation included the following: infrastructure analysis, Low Water Reference Plane analysis, thalweg and tertiary layer analysis, volumetric analysis, specific gage analysis, duration analysis, multidimensional modeling analysis, one-dimensional modeling analysis, and a navigation assessment.

During the historic flood of 2011, the Mississippi River reached record-breaking water levels between Cairo, IL, and Memphis, TN. Downstream from Tiptonville, TN, Sheep Ridge Road Spur Levee (private) was overtopped and crevassed when the Mississippi River reached a stage of 48.35 ft on the Tiptonville gage. The length of spur levee crevassed was 3,000 ft, and the length of bankline eroded was 2,700 ft. The Mississippi River began to form a new cutoff from river mile 869 to 860. Erosion extended approximately 4,000 ft along Island 13, degrading the landscape to elevations 80 ft below natural ground. The crevasse divided the Sheep Ridge Road Spur Levee, leaving an approximately 3,000 ft section to the east of the crevasse (eastern spur levee) and an approximately 2.2-mile section to the west of the crevasse of Sheep Ridge Road Spur Levee (the western spur levee). The eastern spur levee is connected to the Tiptonville-Obion River Levee.

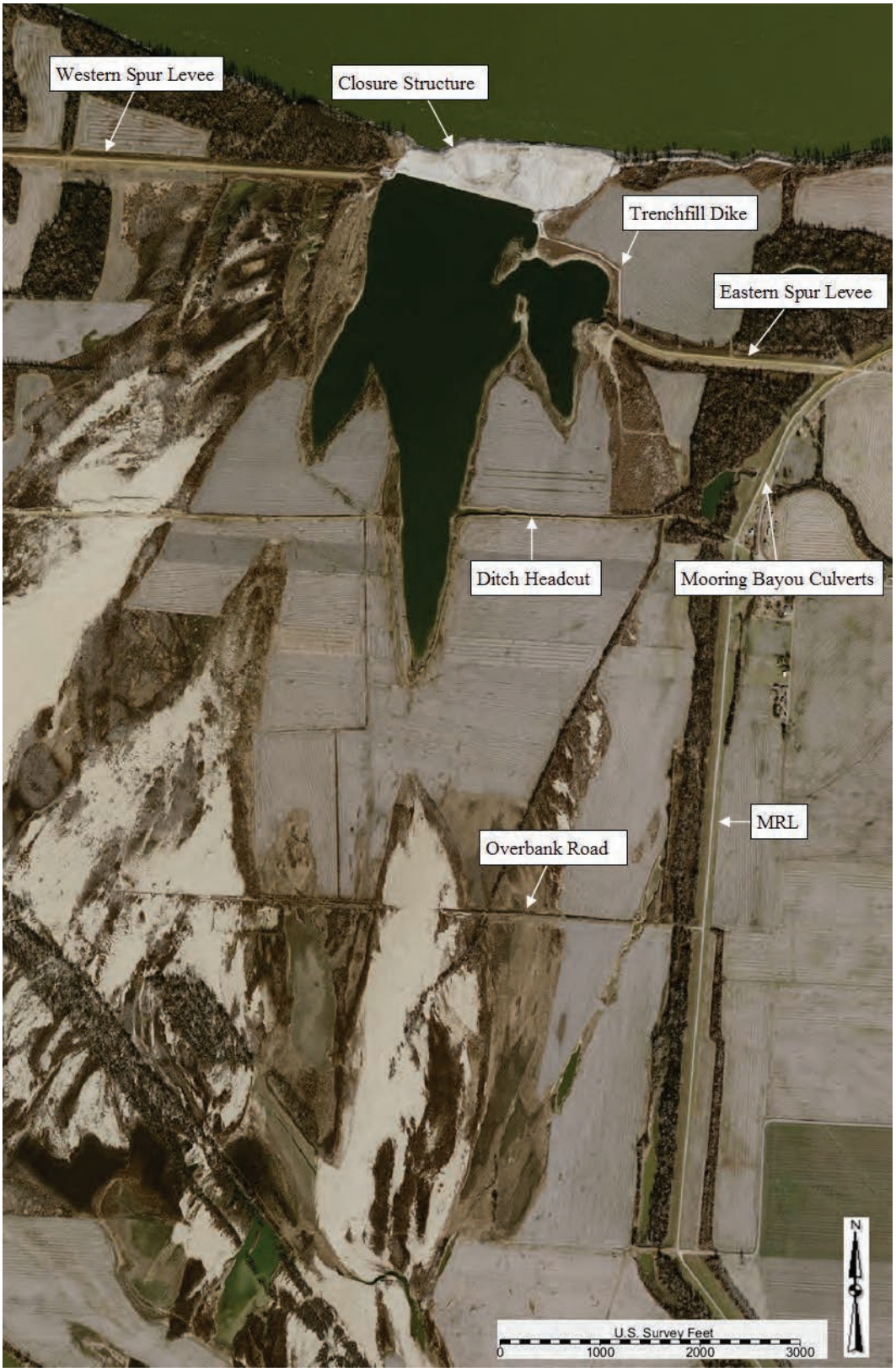
A concern was that without modification of the western spur levee and Island 13 overbank, the Mississippi River would continue to form a 9-mile cutoff. If a cutoff were to form, potential adverse impacts include changes in long-term reach dynamics, navigation outdraft conditions, increased dredging operations, hydrodynamic condition changes in close proximity to a Mississippi River Levee (MRL) mainline levee (Tiptonville-Obion River Levee), endangerment of existing channel improvement features ($60M), endangerment of completed crevasse repairs ($27M), and endangerment of planned crevasse repairs.

The following two figures identify key features of the Island 13 overbank.

Island 13 figure. Federal levee segment is depicted by a blue line. Private levee is depicted by an orange line. Dike is depicted by a red line. Articulated Concrete Mattress (ACM) is depicted by a red hatched polygon. River mile markers are above HOP.



Island 13 overbank key features figure.



Currently, completed repairs to Island 13 include the initial repairs of 2,700 ft of bankline along the Merriwether-Cherokee Revetment, construction of a 1,600 ft riprap baffle landward of the initial bankline repairs, placement of dredged fill between the initial bankline repairs and riprap baffle, placement of a riprap cap over the dredged fill, and a trenchfill dike running from the closure structure to the eastern spur levee.

Numerical model main channel flows listed in the table below were computed from the base condition hypothetical hydrograph simulation. Listed in the following table are reference elevations, gage heights, and main channel flow for four flow conditions at the crevasse location. Gage heights are listed at Tiptonville, TN, and Caruthersville, MO. Water surface elevations are listed at the closure structure. The closure structure is overtopped when the main channel flow reaches approximately 662,000 cfs. The Island 13 overbank diversion flow commences when the main channel flow upstream of the crevasse reaches 858,000 cfs.

Base condition key flows, elevations, and gage heights.

Flow Condition	Main Channel Flow, (cfs)	Closure Structure Water Surface Elevation (ft NAVD88)	Tiptonville Gage Stage (ft)	Caruthersville Gage Stage (ft)
Overtops closure structure	662,000	269.7	25.6	24.8
Overtops scour hole	746,000	272.5	28.1	27.0
Overtops overbank road	853,000	275.4	31.0	29.5
Overbank diversion flow commences	858,000	275.5	31.1	29.6

Note: Flows are rounded to the nearest 1,000 cfs. Elevations are rounded to nearest tenth.

The analysis conducted on the base condition indicated that there is a moderate risk for cutoff formation. Alternatives were investigated to mitigate the risk for cutoff formation. Alternatives that were modeled are listed in the following table.

Description of alternatives.

ID	Description	Report Figure
Alternative 1	Levee built to elevation 291.0 ft NAVD88	Figure 3-1 and Figure 3-2
Alternative 2	Levee built to elevation 282.0 ft NAVD88	Figure 3-3 and Figure 3-4
Alternative 3	Western levee degraded to elevation 281.0 ft NAVD88	Figure 3-5 and Figure 3-6
Alternative 4	Overbank road raised to elevation 276.0 ft NAVD88	Figure 3-7 and Figure 3-8
Alternative 5	Dense vegetation on the entire overbank	Figure 3-9
Alternative 6	Dense vegetation on obtained WRP easements	Figure 3-10

Alternative 5 (dense vegetation on the entire Island 13 overbank) was recommended to mitigate the long-term risk of cutoff formation. Alternative 5 has an initial development period (estimated 20–30 years) that has a moderate risk for cutoff formation during this period. Short-term risk mitigation measures are required until full implementation (mature vegetation across entire overbank is established) of Alternative 5 is achieved. Note that the Island 13 overbank reach will further develop when the closure structure is overtopped and overbank diversion flow occurs.

The analysis conducted on the base condition indicated that there is a severe risk for local scour at the closure structure. Local scour countermeasures were investigated to mitigate the risk of closure structure failure. Local scour countermeasures that were modeled are listed in the following table. The following table presents the local scour countermeasures that were investigated (but not modeled with AdH): expansion of the existing eastern trenchfill dike, protection of the eastern spur levee, and protection of the western spur levee. The expansion and reinforcing of the existing eastern trenchfill dike would create a stone trench approximately 35 ft wide and 8 ft deep. The protection of both the eastern and western spur levees would reinforce and place stone paving at the failed ends of the eastern and western spur levees.

Local scour countermeasure descriptions.

ID	Description	Report Figure
Local Scour Countermeasure 1	Rock protection around western edge of the scour hole (2,300 ft)	Figure 4-1
Local Scour Countermeasure 2	Tapered Trenchfill dike (+6 ft at toe of eastern levee, +4 ft at midpoint, +2 ft at closure structure)	Figure 4-2 and Figure 4-3

To mitigate the risk of closure structure failure, it is recommended that the following measures be implemented: Local Scour Countermeasure 1, expansion of the existing eastern trenchfill dike, protection of the eastern spur levee, and protection of the western spur levee. These local scour countermeasures are critical components that tie-in to each other (and the closure structure) to reduce the risk of closure structure failure.

The navigation analysis indicated that there is the potential for an outdraft condition at the study crevasse. The outdraft condition occurs during events that overtop the closure structure and diversion flow commences (base condition analysis indicated approximately 858,000 cfs).

The analysis indicated scour potential at the toe of the Tiptonville-Obion River Levee. It is recommended that further investigation be conducted on the scour potential and determine if MRL protection measures are required. Island 13 also contains a ditch that drains the outlet of the MRL Mooring Bayou Culverts to the scour hole. A headcut is progressing from the scour hole to the Mooring Bayou Culverts that will put the culvert stability at the MRL at risk. Grade control measures are recommended to prevent the headcut from reaching the Mooring Bayou Culvert. Further analysis should be conducted to develop grade control designs.

Points of Contact

Brian M. Hall, P.E.
Author, USACE MVM
Brian.M.Hall@usace.army.mil

Ty V. Wamsley, Ph.D.
MRG&P Technical Director, USACE MVD
Ty.V. Wamsley@usace.army.mil

Freddie Pinkard
MRG&P Senior Program Manager, USACE MVK
Freddie.Pinkard@usace.army.mil

1 Introduction

MRG&P studies are designed to provide a comprehensive analysis of physical forces that influence the flood-carrying capacity and navigability of the Mississippi River. Their purpose is to define cause-and-effect relationships that result in short- and long-term changes in the stage-discharge relationships of the Mississippi River and to develop improved design concepts and criteria for construction of channel stabilization works that will improve flood control, navigation, and environmental conditions along the river. The Lower Mississippi River Division Potamology Programs (T-1) and (P-1) were initiated to address these concerns. A summary of the programs and detailed bibliography of works related to the Lower Mississippi River Potamology Program can be found in Biedenharn et al. (2014). Historical potamology reports and studies can be accessed on the internet via http://www.mvd.usace.army.mil/Missions/MississippiRiverScienceTechnology/MSRiverGeomorphologyPotamology.aspx.

This report documents a continuation of analysis that was conducted at the Island 13 overbank and the Merriwether-Cherokee reach on the Mississippi River. Refer to Appendix A for the *Merriwether-Cherokee Potamology Study Phase I Report - HEC-RAS 1D/2D Modeling* that documents prior analysis conducted by the Memphis District.

Purpose

The objectives of the Merriwether-Cherokee Potamology Study are to assess

1. the potential for additional overbank scour and associated risk for formation of a major river cutoff
2. the effects of spur levee failure (Sheep Ridge Road) on navigation
3. the effects of spur levee failure on long-term reach behavior
4. the effects of completed repairs on cutoff formation
5. the long-term effects of further alteration to the Spur Levee.

Problem

During the historic flood of 2011, the Mississippi River reached record-breaking water levels between Cairo, IL, and Memphis, TN. Downstream

from Tiptonville, TN, Sheep Ridge Road Spur Levee (private) was overtopped and crevassed when the Mississippi River reached a stage of 48.35 ft on the Tiptonville gage. The length of spur levee crevassed was 3,000 ft, and the length of bankline eroded was 2,700 ft. The Mississippi River began to form a new cutoff from river mile (RM) 869 to 860. Erosion extended approximately 4,000 ft along Island 13, degrading the landscape to elevations 80 ft below natural ground. Figure 1-1 is a location map of the study area, and Figure 1-2 is a map of the Island 13 overbank. As seen in Figure 1-2, the crevasse divided the Sheep Ridge Road Spur Levee, leaving an approximately 3,000 ft section to the east of the crevasse (eastern spur levee) and an approximately 2.2-mile section to the west of the crevasse of Sheep Ridge Road Spur Levee (the western spur levee). The eastern spur levee is connected to the Tiptonville-Obion River Levee.

Island 13, on the left descending (east) bank of the Mississippi River, is located along RM 869 to 860. The island includes the Merriwether-Cherokee Revetment located at RM 869 and the Sheep Ridge Road Spur Levee. The spur levee is located 5 miles southwest of Tiptonville, in Lake County, TN. The Sheep Ridge Road Spur Levee ties into the Tiptonville-Obion Levee and extends parallel to the Merriwether-Cherokee Revetment riverward for approximately 5 miles.

During high water events prior to the 2011 crevasse formation, the Mississippi River would overtop the banks of Island 13 at approximately RM 869 and rise against the riverside of the spur levee. At RM 860, the Mississippi River begins to back into Island 13, overtopping fields and building a tailwater on the landside of the Sheep Ridge Road Spur levee.

Currently, completed repairs to Island 13 include the initial repairs of 2,700 ft of bankline along the Merriwether-Cherokee Revetment, construction of a 1,600 ft riprap baffle landward of the initial bankline repairs, placement of dredged fill between the initial bankline repairs and riprap baffle, placement of a riprap cap over the dredged fill, and a trench-fill dike running from the closure structure to the eastern spur levee.

Figure 1-1. Overview map. Federal levee segment is depicted by a blue line. Private levee is depicted by an orange line. Dike is depicted by a red line. Articulated Concrete Mattress (ACM) is depicted by a red hatched polygon. River mile markers are above HOP.

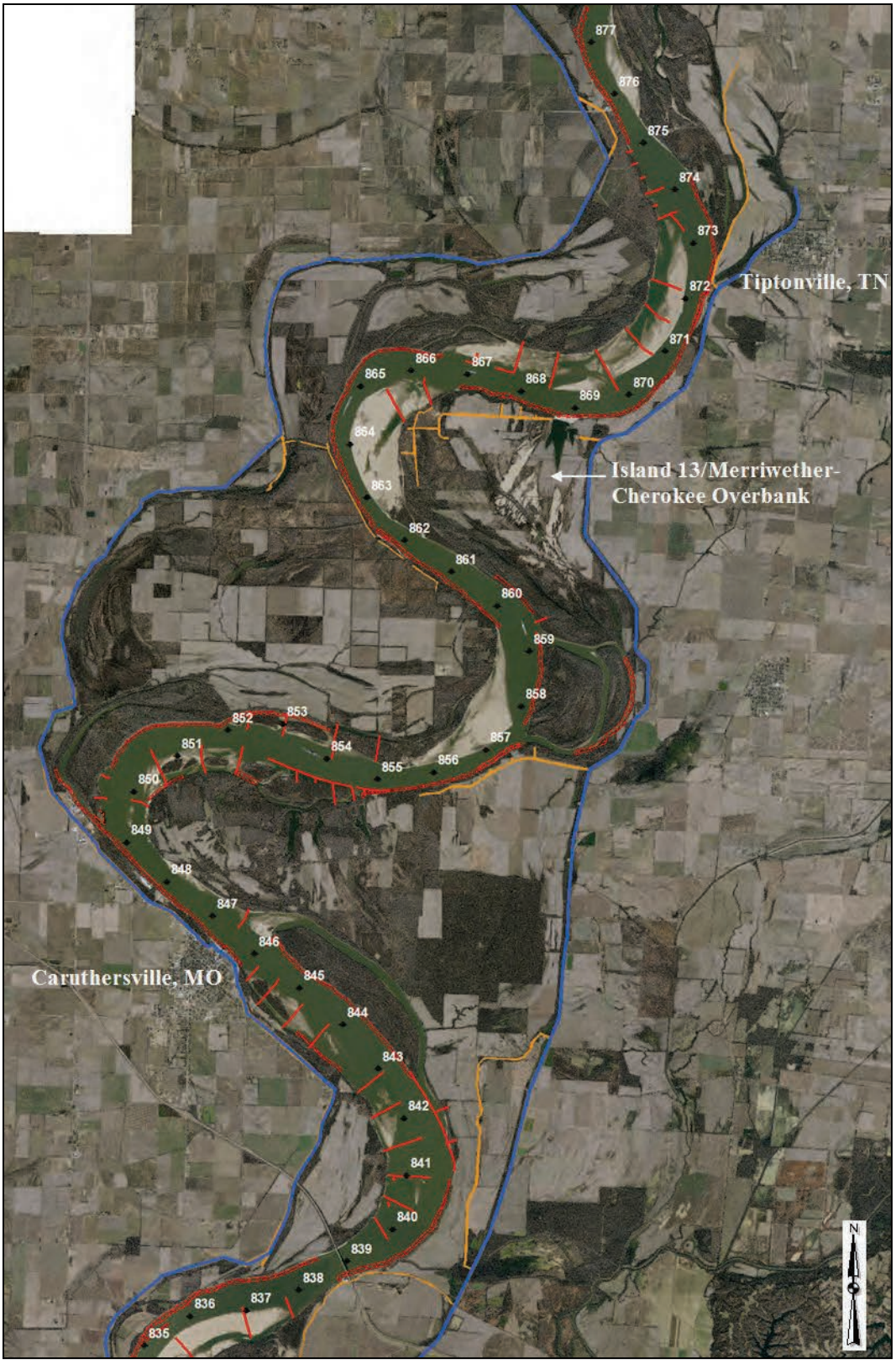


Figure 1-2. Island 13 map. Federal levee segment is depicted by a blue line. Private levee is depicted by an orange line. Dike is depicted by a red line. ACM is depicted by a red hatched polygon. River mile markers are above HOP.



Figures 1-3 through 1-7 are aerial photos of Sheep Ridge Road Spur Levee: Figure 1-3 was taken in 2010 prior to the 2011 crevasse; Figure 1-4 was taken during the 2011 flood event; Figure 1-5 was taken in 2012 after the 2011 flood event with the initial bankline repairs completed; Figure 1-6 was taken in 2013 with the baffle and dredged fill placed; and Figure 1-7 was taken in 2015 with rock cap placed. Figure 1-8 depicts key features of the Island 13 overbank.

A concern is that without modification of the western spur levee and Island 13 overbank, the Mississippi River will continue to form a 9-mile cutoff. If a cutoff were to form, potential adverse impacts include changes in long-term reach dynamics, navigation outdraft conditions, increased dredging operations, hydrodynamic condition changes in close proximity to an MRL mainline levee (Tiptonville-Obion Levee), endangerment of existing channel improvement features ($60M), endangerment of completed crevasse repairs ($27M), and endangerment of planned crevasse repairs.

Figure 1-3 was taken in 2010 prior to the 2011 crevasse.

Figure 1-3. Island 13 imagery–6 October 2010.



Figure 1-4 was taken during the 2011 flood event.

Figure 1-4. Island 13 imagery–4 May 2011.



Figure 1-5 was taken in 2012 after the 2011 flood event with the initial bankline repairs completed.

Figure 1-5. Island 13 imagery–22 May 2012.



Figure 1-6 was taken in 2013 with the baffle constructed and dredged fill placed.

Figure 1-6. Island 13 imagery–29 November 2013.

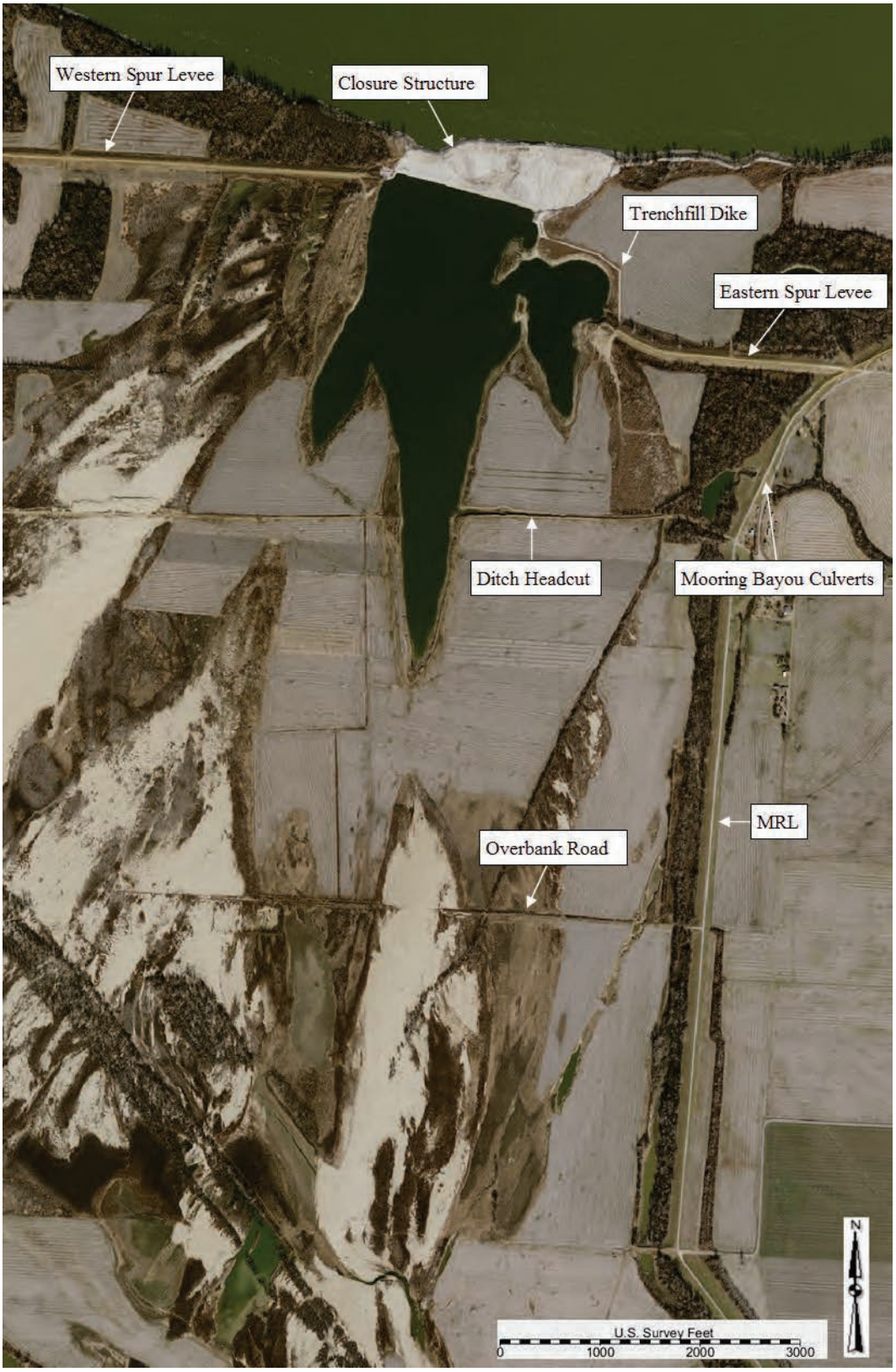


Figure 1-7 was taken in 2015 with the rock cap placed on the closure structure.

Figure 1-7. Island 13 imagery–29 January 2015.



Figure 1-8. Island 13 overbank key features map.



Method

Listed below is a description of the different analyses that were completed for this study.

Infrastructure Analysis

An analysis of navigation and flood risk management structures was performed to determine adverse impacts from a potential cutoff formation. Channel improvement features (revetments and dikes) and levees were included in the analysis.

Lower Water Reference Plane Analysis

A comparison was made among the 1974, 1993, and 2007 Low Water Reference Planes (LWRPs) to determine the vertical profile variation of the historical reach dynamics.

Thalweg and Tertiary Layer Analysis

Thalweg and tertiary elevations were obtained from *The Influence of Geology on the Lower Mississippi River*[1]. The minimum thalweg elevations from the 1962, 1975, and 1989 hydrographic surveys were compared to the tertiary elevations. The tertiary elevation data was obtained from the geological investigations by Fisk and Saucier (Fisk 1944; Saucier 1974, 1994).

Volumetric Analysis

The volumetric analysis determined the changes in sediment volume that occurred for every 2-mile segment in the reach of the Lower Mississippi River from New Madrid, MO (RM 888.0), to just upstream of I-155 Bridge (RM 840.0). Six comprehensive hydrographic datasets (1989, 1994, 2004, 2009, 2010, and 2013) were evaluated for the entire study reach.

The hydrographic survey datasets were loaded into InRoads and MicroStation (Bentley software) and segmented every 2 miles with a common border for all survey datasets. The common border was governed by the hydrographic survey dataset with the least coverage for each

[1] Biedenharn, D. S. In preparation. The influence of geology on the Lower Mississippi River. Mississippi Valley Division MRG&P Report. Vicksburg, MS: U.S. Army Corps of Engineers, Mississippi Valley Division.

respective 2-mile segment. The segmented hydrographic survey data sets were clipped by the common border and triangulated to create digital terrain models (DTM). DTM surface differences between the hydrographic datasets were computed using Fledermaus (Quality Positioning Services B.V. software). The calculated surface differences provided volumetric quantities for comparison between hydrographic datasets for each respective 2-mile segment.

Specific Gage Analysis

A specific gage analysis was conducted for the primary gage station located at Hickman, KY. A primary station reports both stage and discharge. The Hickman, KY, gage (MS-113 at RM 922) is the closest primary station to the Merriwether-Cherokee crevasse location (RM 869). An annual rating curve was developed for the discharge and stage data. Stage values were obtained from the annual rating curves for the following flows: 200,000 cfs, 400,000 cfs, 600,000 cfs, 800,000 cfs, 1,000,000 cfs, 1,200,000 cfs, 1,400,000 cfs, and 1,600,000 cfs.

Duration Analysis

A stage duration analysis was conducted for the following three locations of the Lower Mississippi River: Tiptonville, TN, gage (MS-116 at RM 872.4), Merriwether-Cherokee Crevasse (RM 869), and Caruthersville, MO, gage (MS-117 at RM 844.4). The duration curve was developed using the Standard Method (rank all data).

Multidimensional Modeling Analysis

A multidimensional hydrodynamic and sedimentation investigation was utilized to estimate hydraulic and sediment parameters through the existing spur levee crevasse, across the floodplain, and back into the Mississippi River. The two-dimensional (2D) investigation was performed with the depth-averaged, shallow-water equation version of the Adaptive Hydraulics (AdH) modeling system (version 4.4) incorporating quasi-three-dimensional (3D) sediment transport for multiple grain sizes. The computed hydraulics helped identify regions of flow concentration that have greater potential for erosion and headcut formation. The model accounted for super-elevation of the water surface in Merriwether Bend. AdH was utilized to investigate alternatives to reduce the risk of cutoff formation and local scour potential. The AdH model simulated the Lower

Mississippi River from RM 877-839. Upstream and downstream model extents were selected to ensure that the model boundary conditions did not influence results at the study location (RM 869). Calibration and validation of the modeled water surface elevation were performed utilizing two river gage stations that were located within the model domain (Tiptonville RM 872.4 and Caruthersville RM 844.4). The calibration process utilized collected acoustic Doppler current profiler (ADCP) velocity data at the crevasse location.

AdH is a finite element model that is capable of simulating 3D Navier Stokes equations, 2D and 3D shallow water equations, and groundwater equations (Berger et al. 2014). It can be used in a serial or multiprocessor mode on personal computers or parallel, high-performance computing systems. The uniqueness of AdH is its ability to dynamically refine the domain mesh in areas where more resolution is needed at certain times due to changes in flow conditions. AdH can simulate the transport of conservative constituents such as salt or dye clouds, as well as sediment transport that is coupled to bed and hydrodynamic changes. The ability of AdH to allow the domain to wet and dry as the river stage changes is important for simulating floodplain dynamics within the river system. This tool was developed at the U.S. Army Engineer Research and Development Center (ERDC).

SEDLIB is a sediment transport library developed at ERDC (Brown et al. 2012). The fundamental architecture of the sediment transport algorithms in SEDLIB is taken from the Ch3D model (Spasojevic and Holly 1994). This architecture is extended in SEDLIB to a more generalized sediment computational engine. It is capable of solving problems consisting of multiple grain sizes, cohesive and cohesionless sediment types, and multiple layers. It calculates erosion and deposition processes simultaneously and simulates such bed processes as armoring, consolidation, and discrete depositional strata evolution.

The SEDLIB library system is designed to link to any appropriate hydrodynamic code. The hydrodynamic code must be capable of performing advection diffusion calculations for a constituent. SEDLIB interacts with the parent code by providing sources and sinks to the advection diffusion solver in the parent code. The solver is then used to calculate both bed load and suspended load transport for each grain size

class. The sources and sinks are passed to the parent code via a fraction step modification of the time-derivative term.

The AdH/SEDLIB sediment model contributes several capabilities to the analysis.

- Quasi-3D flow and transport formulations that use analytical and semiempirical methods to approximate the 3D character of the flow and sediment transport phenomena. These include the ability to model the effects of helical flow through a river bendway on the suspended and bed load sediment transport, by utilizing the bendway vorticity transport algorithm given by Bernard (1992).
- Simulation of multigrain class suspended load and bed load sediment transport phenomena. It is also equipped to handle generalized multigrain class bed processes, including armoring, sorting, erosion to a solid boundary, and the storage of discrete depositional strata.
- An unstructured model mesh that permits very high resolution in areas of interest and high fidelity resolution of shoreline geometry only where needed.
- The ability to extend the boundaries sufficiently far from the project area so as not to prescribe the answer, ensuring that the results are not biased by judgments concerning boundary conditions.

For this study, the AdH model, linked to the SEDLIB sediment model, was applied in depth-averaged mode to analyze the risk of cutoff formation and local scour potential. The AdH/SEDLIB model is equipped with quasi-3D capabilities that represent the effects of the vertical variation of velocity and sediment in a river. Note that AdH sediment transport simulation requires all calculations (and model input) to be in SI units. Selected model output was converted to English units for report publication.

The U.S. Army Corps of Engineers, Memphis District (USACE MVM), Hydraulics and Hydrology Branch, partnered with the ERDC Coastal and Hydraulics Laboratory (CHL), River Engineering Branch, to collaborate and receive AdH training.

One-dimensional (1D) Modeling Analysis

A one-dimensional (1D) hydrodynamic and sedimentation investigation was utilized to evaluate long-term (years to decades) reach conditions. The 1D investigation was performed with HEC-6T (version 11 Aug 2009). The

HEC-6T program produces a 1D model that simulates the response of the riverbed profile to sediment inflow, bed-material gradation, and hydraulic parameters. The model simulates a series of steady-state discharge events, their effects on the sediment transport capacity at cross section, and the resulting degradation or aggradation. The program calculates hydraulic parameters using a standard-step backwater method.

The HEC-6T numerical model computations account for all the basic processes of sedimentation: erosion, entrainment, transportation, deposition, and compaction of the bed for the range of particle sizes found in the Mississippi River. The model calculates aggradation and degradation of the streambed profile over the course of a hydrologic event. It does not simulate bank erosion or natural adjustments in channel widths.

Navigation Assessment

The USACE MVM Hydraulics and Hydrology Branch partnered with the ERDC CHL Navigation Branch to collect and process Automatic Identification System (AIS) vessel track data and analyze numerical model results to assess potential navigation impacts on the Mississippi River.

AIS is required for all self-propelled vessels of 1600 or more gross tons when operating in the navigable waters of the United States. AIS provides vessel information (e.g., position, course, speed), receives AIS data from other vessels, and exchanges data with shore-based facilities. AIS aids to navigation (ATON) stations can receive and transmit to the AIS units on vessels. Lock Operations Management Application (LOMA) is a USACE ERDC-developed interface that receives and processes AIS data from all United States Coast Guard (USCG) and USACE ATON stations.

For this assessment, a temporary LOMA unit (on loan from ERDC) was installed at Caruthersville, MO. AIS data for RM 812–908 was collected and analyzed from 17 April 2015 to 2 May 2015.

2 Base Condition

The base condition represented the fall 2014 condition at Island 13 and the study reach. The base condition included the completion of initial repairs of 2,700 ft of bankline along the Merriwether-Cherokee revetment, construction of a 1,600 ft riprap baffle landward of the bankline, placement of dredged fill between the bankline and riprap baffle, placement of a riprap cap over the dredged fill, and a trenchfill dike running from the closure structure to the eastern spur levee.

Existing infrastructure

Existing adjacent infrastructure that would be directly impacted by a cutoff formation includes revetments (articulated concrete mattress [ACM] and upper bank paving), dikes, levees, and the Merriwether-Cherokee closure structure. Figure 2-1 depicts the adjacent infrastructure that would be directly impacted by a potential cutoff.

Closure structure

The investment in the closure structure is approximately $27 million as of fall 2014. This investment includes the completion of initial repairs of 2,700 ft of bankline along the Merriwether-Cherokee Revetment, construction of a 1,600 ft riprap baffle landward of the bankline, placement of dredged fill between the bankline and riprap baffle, placement of a riprap cap over the dredged fill, and a trenchfill dike running from the closure structure to the eastern spur levee. The closure structure has a minimum crest elevation of 269.7 ft NAVD88. Note that the closure structure has a crest elevation approximately 8 ft lower than the average top bank elevation upstream and downstream of the closure structure.

River features

If a cutoff were to form, approximately $60 million worth of existing adjacent channel improvement infrastructure would no longer function as designed. The total length of adjacent revetment impacted is approximately 70,000 ft. Table 2-1 lists specific adjacent revetments and lengths that would be impacted. Figure 2-2 depicts the cumulative dike length constructed per river mile by construction year (colors represent year of construction). There is a significant amount of dike structures that would be directly impacted from RM 869–864 if a cutoff were to form.

Figure 2-1. Adjacent infrastructure impacted by potential cutoff.



Table 2-1. Potential cutoff adjacent revetment impact.

Revetment Name	River Mile (1962 AHP)	Descending Bank	Revetment Length (ft)
Merriwether-Cherokee	867–869	Left	15,000
Little Cypress	860–866	Right	40,280
Above Lee Towhead	860	Left	4,943
Lee Towhead	858–859	Left	9,860
Total			70,083

In addition to the adjacent structures that would no longer function as designed, there would be additional channel improvement and river features impacted if a cutoff were to form. (Refer to the Chapter 2 report section titled “One-Dimensional (1D) Modeling Analysis” for the results from the synthetic long duration hydrograph simulation of the Mississippi River main channel bed profile.) The HEC-6T analysis estimated that the main channel in locations both upstream and downstream of the crevasse would experience bed lowering in excess of 10 ft. Figure 2-2 depicts the cumulative dike length constructed per river mile by construction year (colors represent year of construction) upstream and downstream of the crevasse. Figure 2-3 depicts features that would be impacted upstream of the study location. The large bed lowering would cause damages that far exceed the damages estimated for the adjacent structures (local structures in study reach). The potential damages to navigation and channel improvement features as a result of the bed lowering include the following: the undermining of existing dikes and revetments, increased dredging operations in the cutoff reach, and increased dredging operations in harbors impacted by the bed lowering. The bed lowering would also cause environmental issues and adversely impact the habitat of endangered species by degrading notched dike fields and gravel bars. Modification to the existing channel improvement structures upstream and downstream of the cutoff channel and the construction of new channel improvement structures in the cutoff channel would be required to maintain navigation if a cutoff were to form.

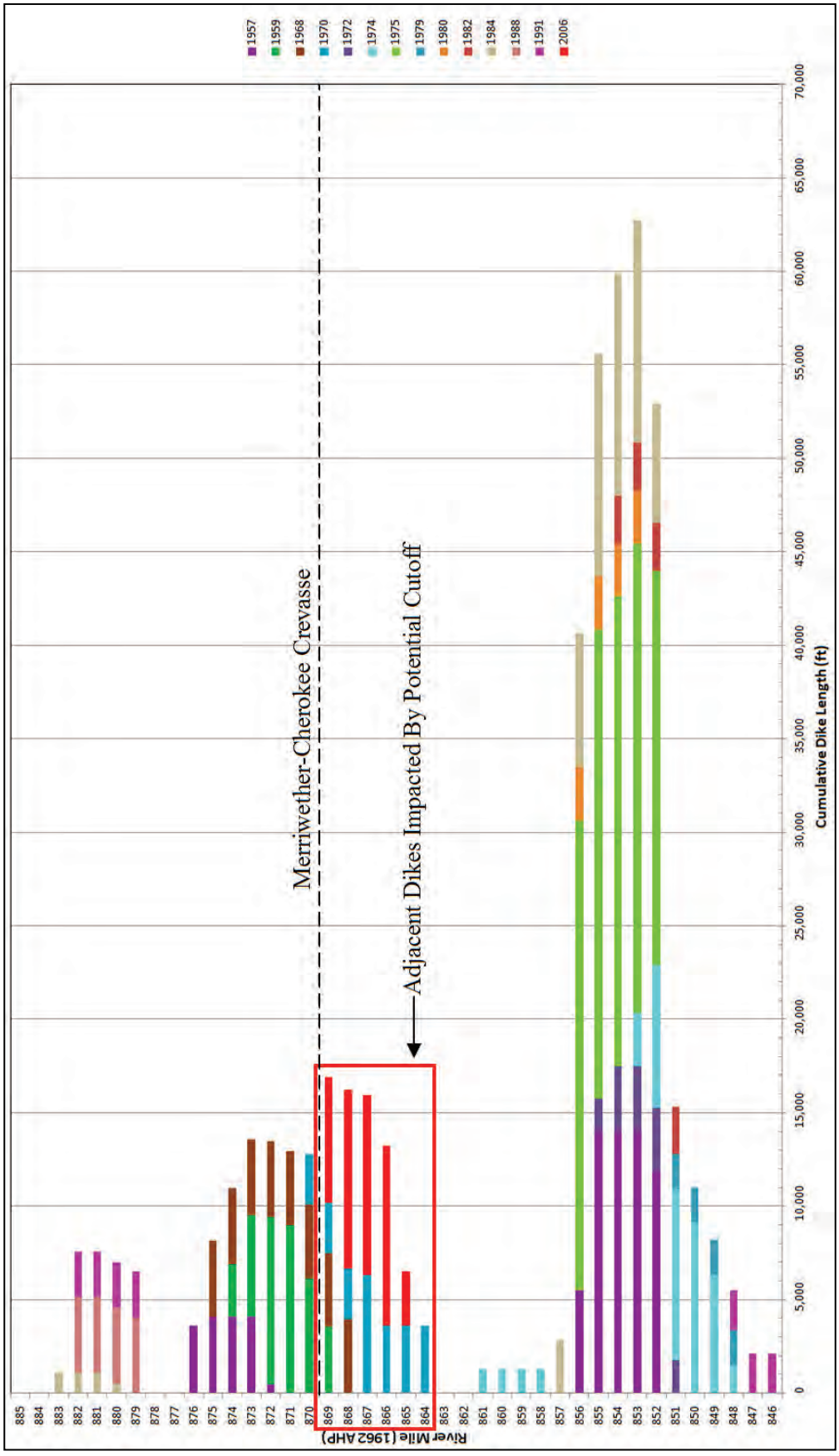
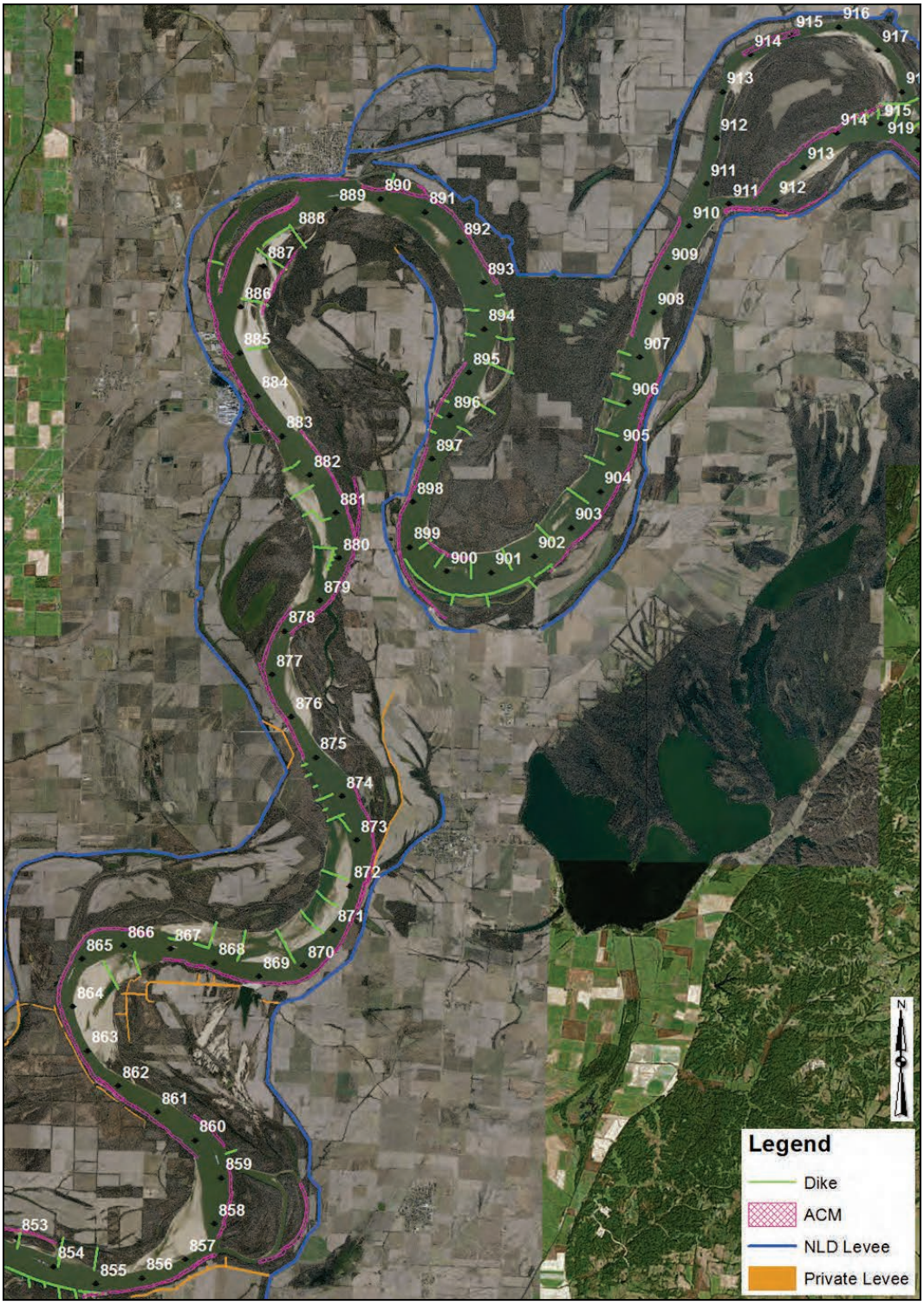


Figure 2-2. Cumulative dike length by construction year.

Figure 2-3. River features impacted by potential cutoff.



Mississippi River Levee (MRL)

The potential cutoff formation would directly impact approximately 7 miles of MRL. These impacts would include significant increases in hydrodynamic forces and levee toe scour potential. The levee impacted would be National Levee Database (NLDB), Hickman, KY, to Obion River Levee System (NLDB System #4005000003) Tiptonville-Obion River Levee Segment (NLDB Segment #4004000013). Mooring Bayou Culverts (three 60 in. circular culverts) are located in this segment of the MRL. The Mooring Bayou Culverts drain to the Island 13 scour hole. A headcut is progressing from the scour hole to the Mooring Bayou Culverts.

Geomorphic assessment

This section contains details of the analysis conducted for the geomorphic assessment.

Low water reference plane (LWRP), thalweg, and tertiary layer analysis

Figure 2-4 depicts the 1974 LWRP, 1993 LWRP, 2007 LWRP, minimum thalweg elevation profile (from 1962, 1975, and 1989), and the tertiary elevation profile. The LWRP analysis indicated that general bed lowering occurred from 1974 to 2007 within the Memphis District. From the LWRP analysis it was observed that the study reach (RM 869) experienced 2–4 ft of lowering from 1993 to 2007. Analysis indicates that further bed lowering is expected for the study reach. As this bed lowering works through the study reach, the following is expected to occur: the main channel will convey more flow before overbank flow occurs, the potential cutoff channel may experience a reduction (slight) in frequency and duration of diversion flow, there will be an increased head differential across the overbank reach making erosion more severe, and the increased erosion potential will increase the rate of overbank channel development. If a cutoff were to form, changes in the reach dynamics (bed lowering and bed response) would be expected throughout the river system and not solely at the Merriwether-Cherokee crevasse location.

It is evident from the thalweg and tertiary analysis that a tertiary layer exists at Caruthersville, MO, and Hickman, KY. The tertiary layer at Hickman, KY, consists of highly resistant clay layers. These layers are acting as a temporary grade control. Greater bed lowering will occur as the tertiary layers continue to degrade.

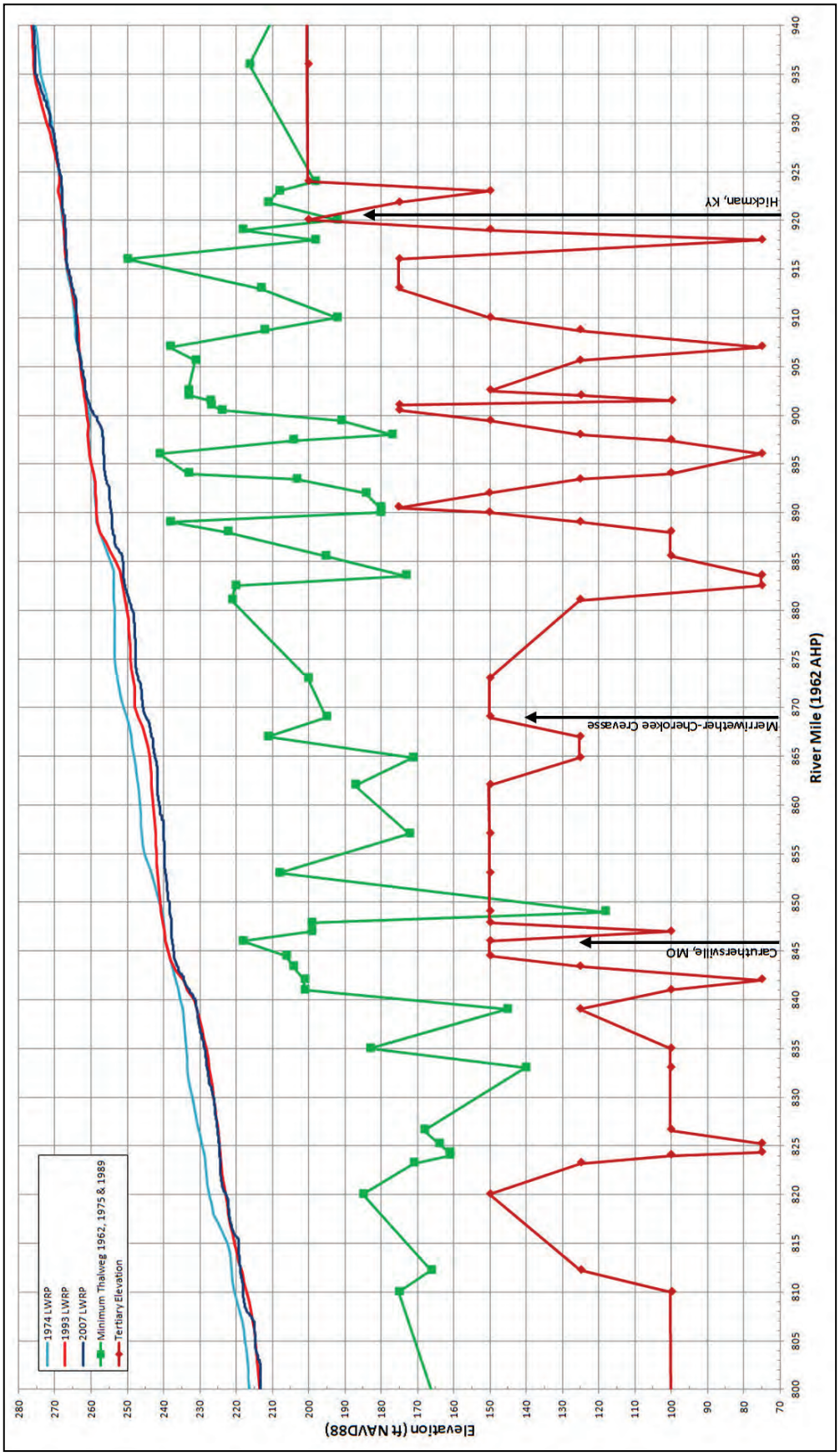


Figure 2-4. LWRP, thalweg, and tertiary layer plot.

Volumetric analysis

Figure 2-5 depicts the 24 segments of the Mississippi River where a surface difference comparison was performed on the hydrographic datasets. The horizontal datum for the hydrographic datasets was NAD83 Zone 16. The vertical datum was U.S. Survey Feet NAVD88.

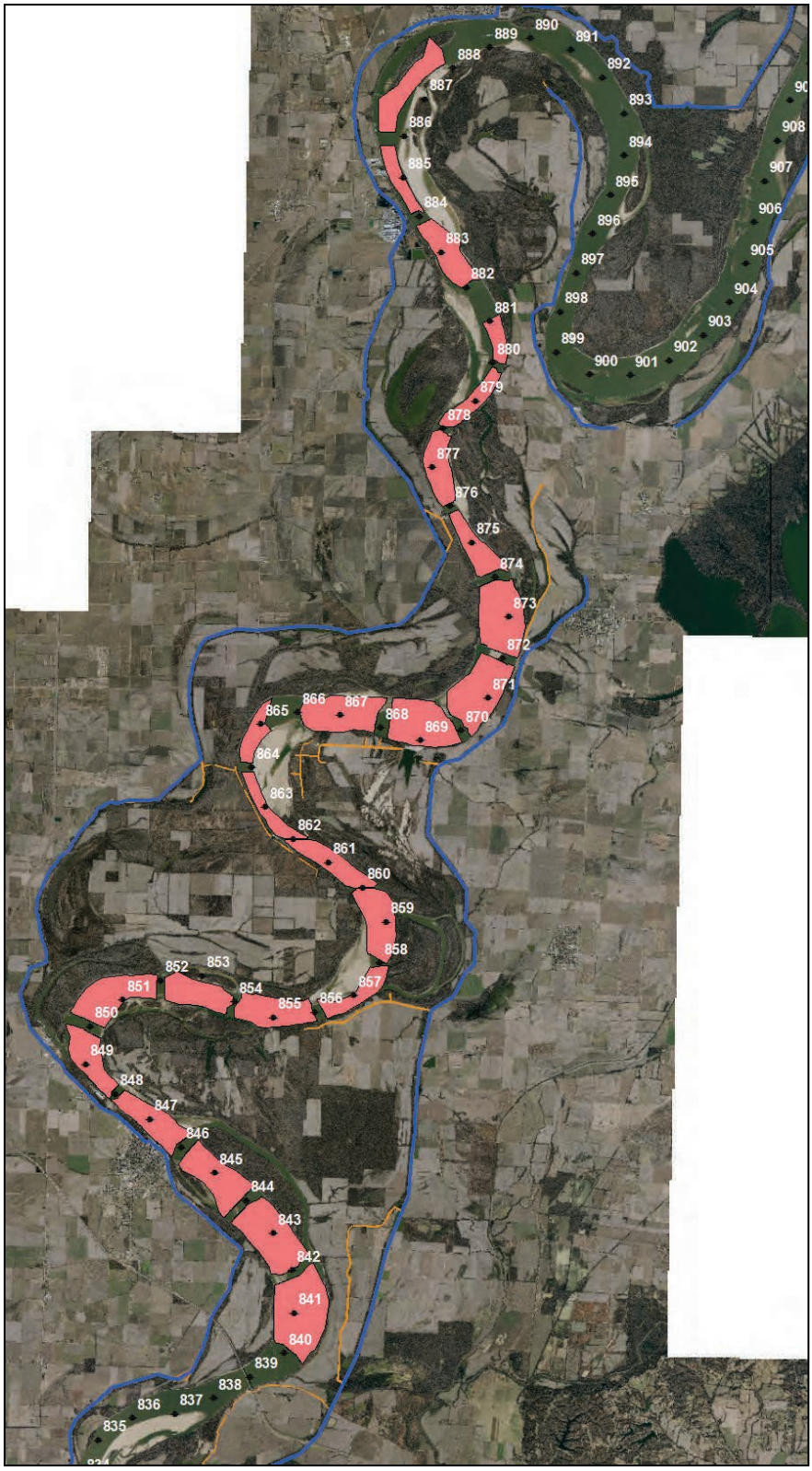
Figure 2-6 depicts the sediment volume differences for the following dataset comparisons: 1989 to 1994, 1994 to 2004, 2004 to 2009, 2009 to 2010, 2010 to 2013, and 1989 to 2013. Note that some dataset comparisons contained no data or erroneous survey data.

Figure 2-7 depicts the difference in sediment volume between the 1989 dataset to 1994 dataset. Two segments (RM 888–886 and 846–844) experienced a net increase in sediment volume. Twenty-two segments experienced a net decrease in sediment volume. Segment RM 858–856 experienced the greatest net sediment loss of 26,808,849 cy. Two major factors that contributed to the loss in sediment volume for this dataset comparison were the additions to dike fields (new dikes, extensions, raises, and notches) and that there were 299 dredging days in the studied reach during this period.

Figure 2-8 depicts the difference in sediment volume between the 1994 dataset to 2004 dataset. One segment (RM 888–886) experienced a minimal decrease in sediment volume. Twenty-three segments experienced a net increase in sediment volume. Several factors contributed to the gain in sediment volume for this dataset comparison. Two dikes were raised and extended at Stewart Towhead from RM 870 to 867 on the right descending bank that resulted in a growing sandbar. One new dike was constructed, and two dikes were raised and extended at the Caruthersville Linwood Dike Field (RM 846–840) that resulted in a growing sandbar.

Figure 2-9 depicts the difference in sediment volume between the 2004 dataset to 2009 dataset. Twenty segments experienced a net increase in sediment volume. Two segments (RM 866–864 and 856–854) experienced a minimal decrease in sediment volume.

Figure 2-5. Hydrographic dataset segmented boundary regions. Pink polygons depict the segmented regions.



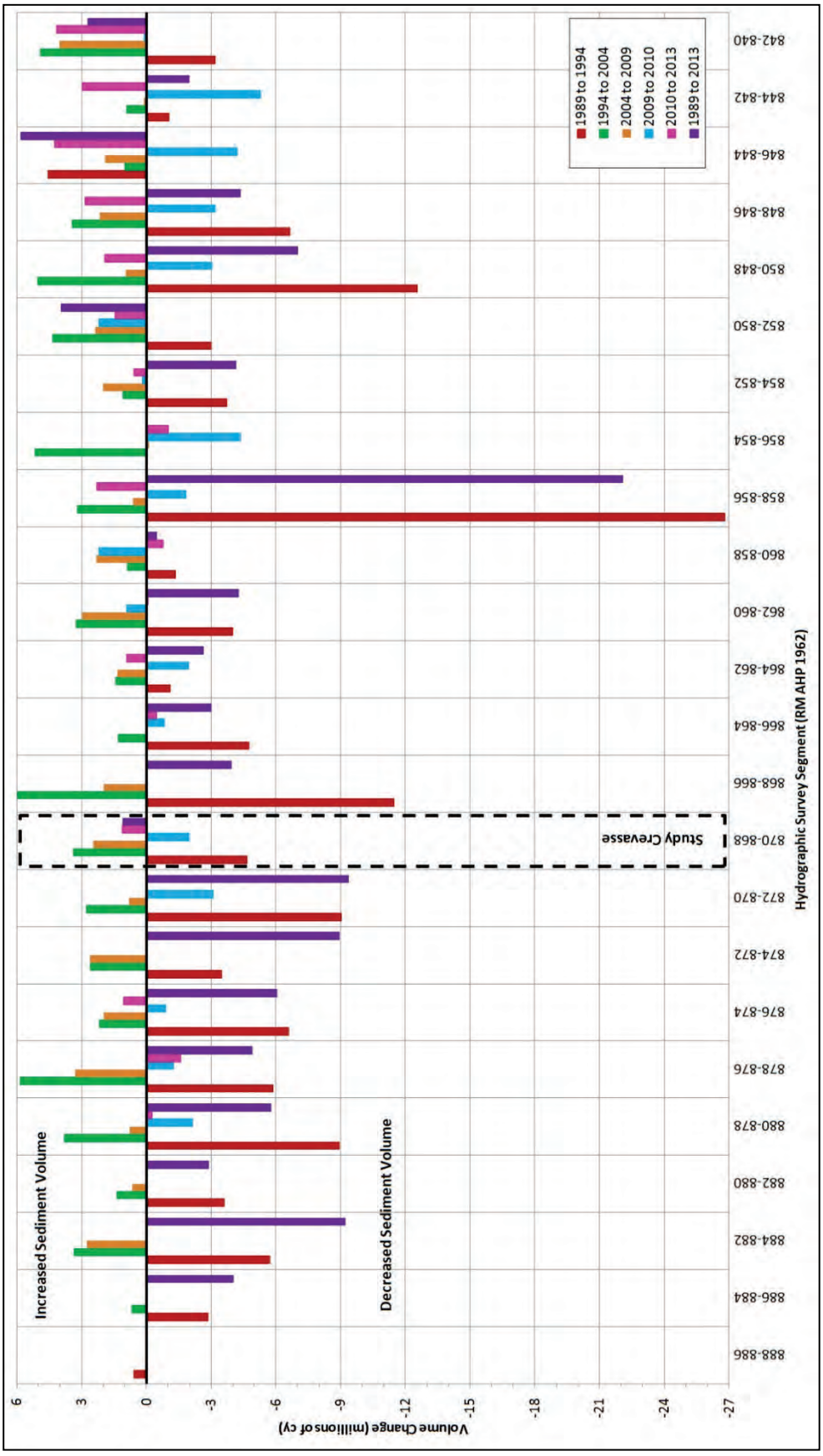


Figure 2-6. Sediment volume difference by river mile segments.

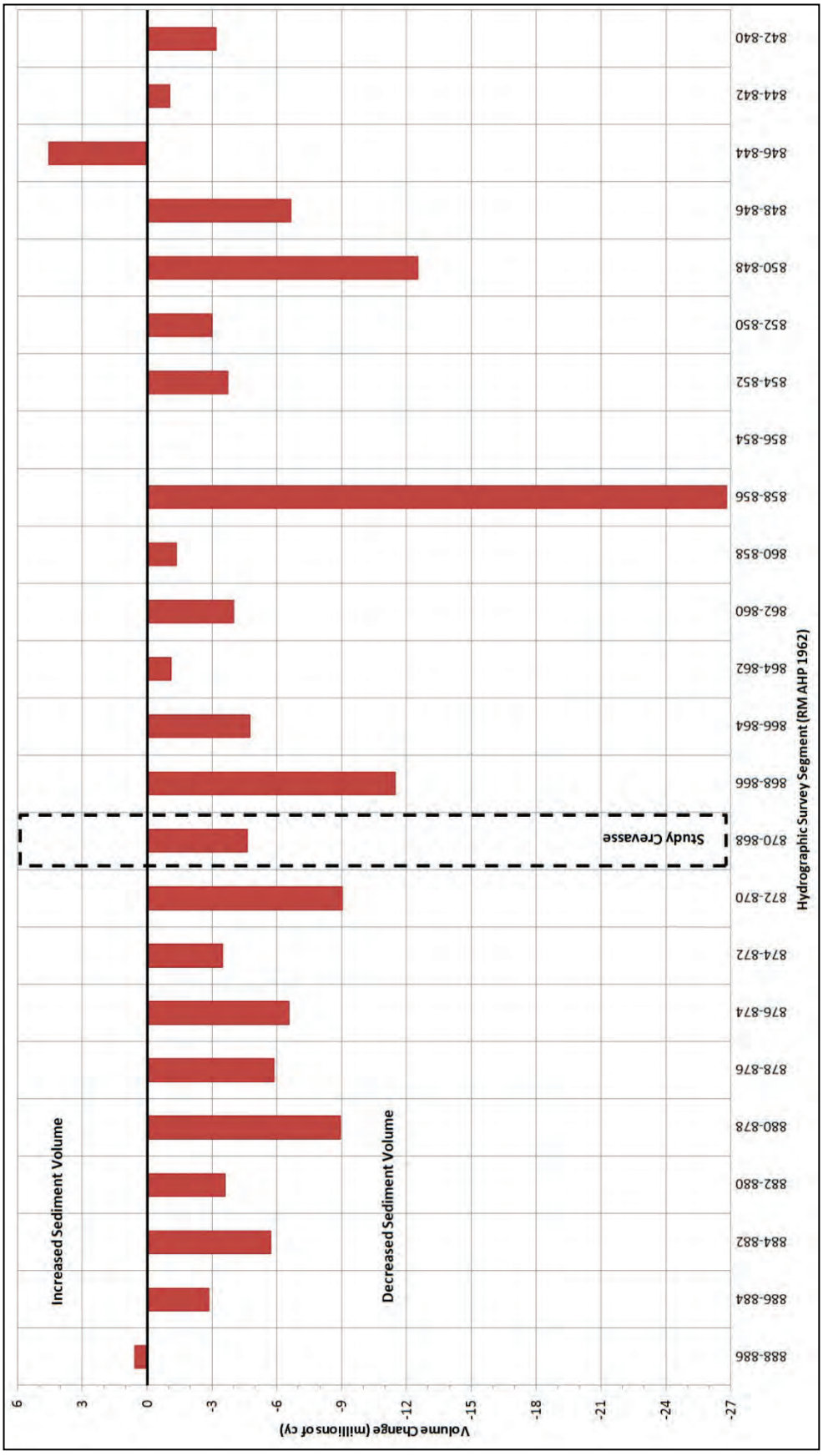


Figure 2-7. Sediment volume difference from 1989 dataset to 1994 dataset.

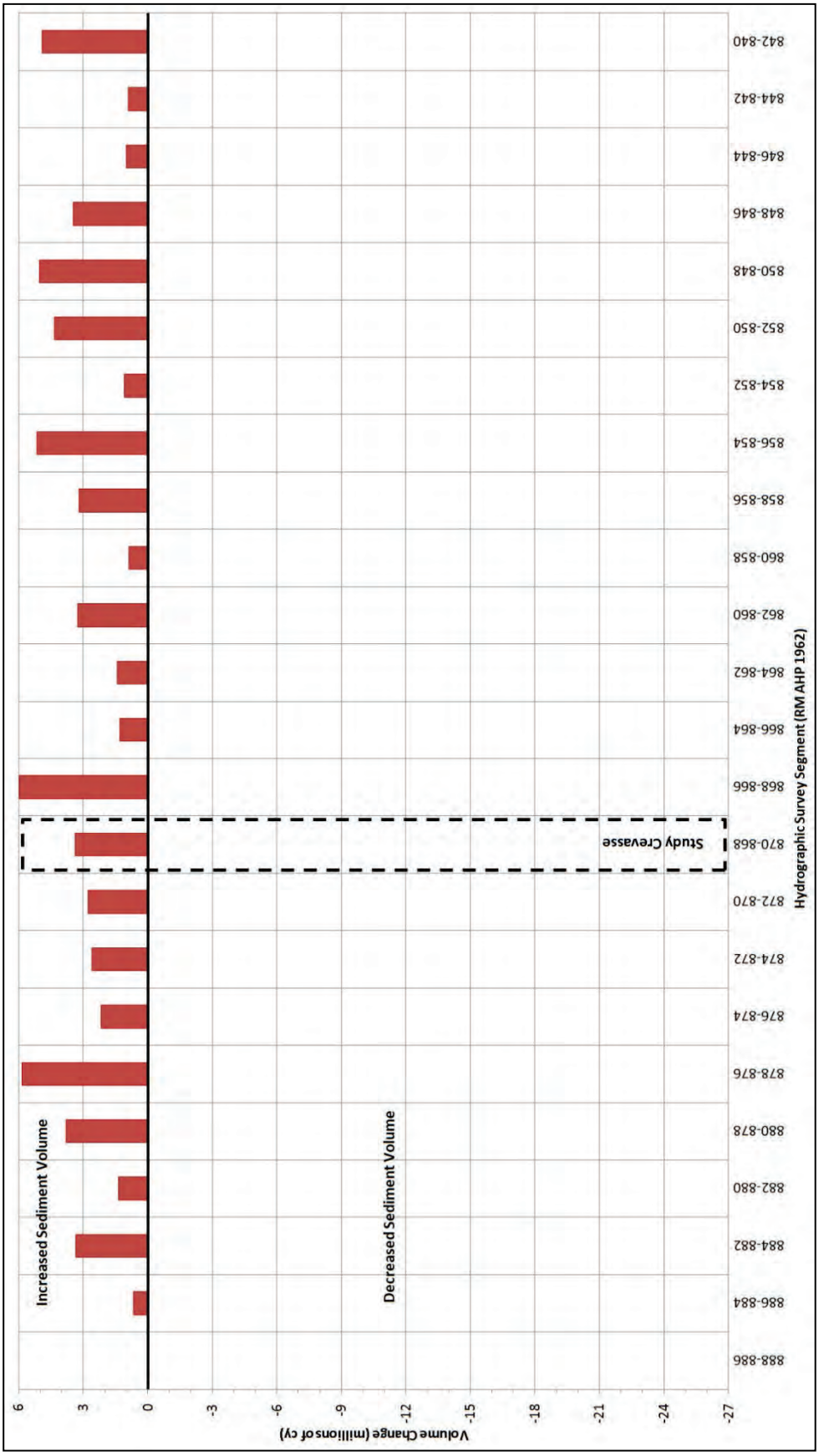


Figure 2-8. Sediment volume difference from 1994 dataset to 2004 dataset.

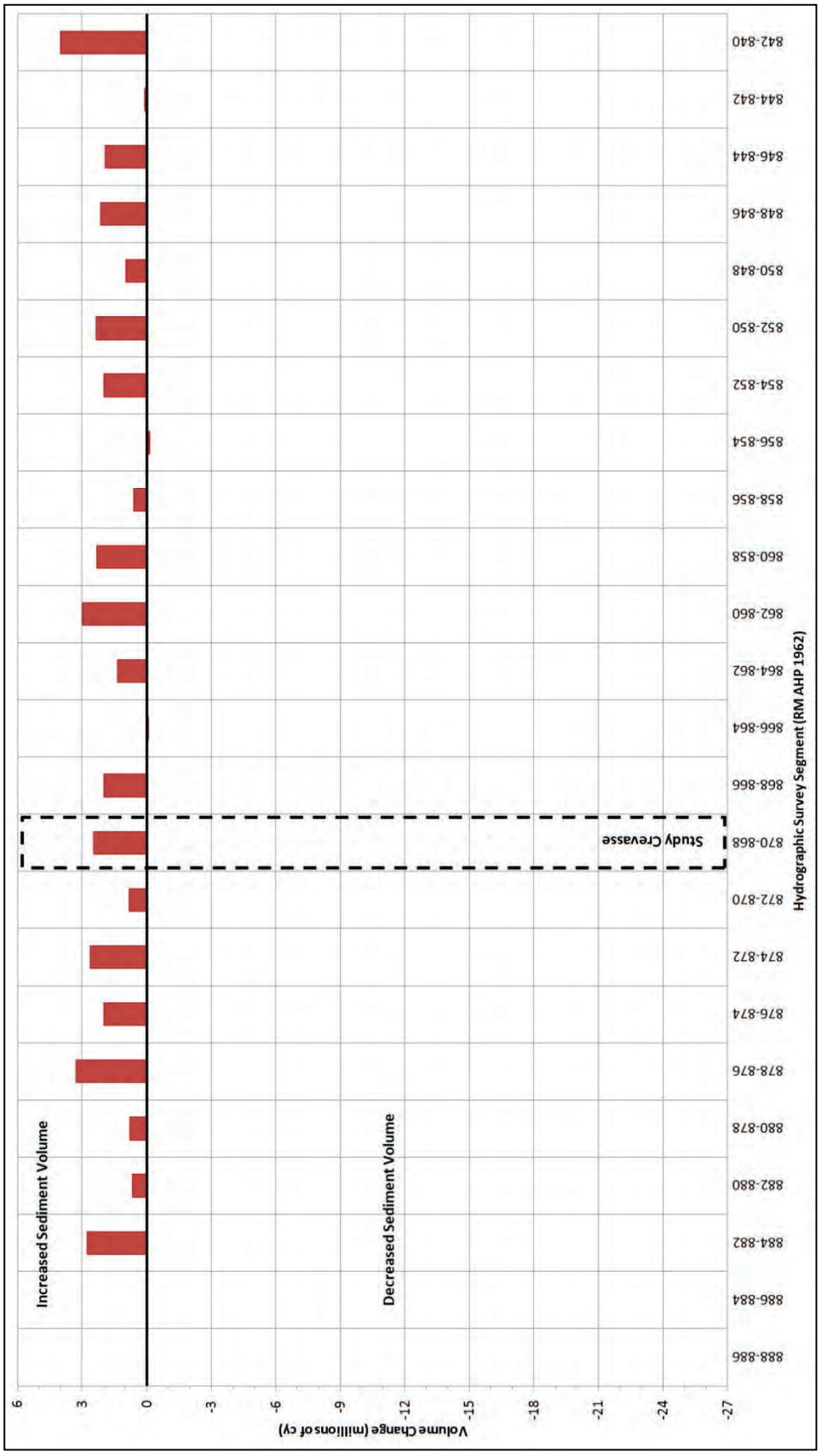


Figure 2-9. Sediment volume difference from 2004 dataset to 2009 dataset.

Figure 2-10 depicts the difference in sediment volume between the 2009 dataset to 2010 dataset. Five segments experienced a net increase in sediment volume. Thirteen segments experienced a decrease in sediment volume. One segment (RM 874–872) experienced approximately no change in sediment volume. There were 5 days of dredging in the lower reach of this study area. There were no new additions to dike fields in the study area during this time period.

Figure 2-11 depicts the difference in sediment volume between the 2010 dataset to 2013 dataset. Eleven segments experienced a net increase in sediment volume. Six segments experienced a decrease in sediment volume.

Figure 2-12 depicts the difference in sediment volume between the 1989 dataset to 2013 dataset. Four segments experienced a net increase in sediment volume. Eighteen segments experienced a decrease in sediment volume.

Appendix B contains additional data from the volumetric analysis:

- spatial plots of the dataset surface comparisons (Figures B-1 through B-18)
- tabular output of the dataset surface comparisons (Tables B-1 through B-9).

Specific gage analysis

Figure 2-13 depicts the specific gage record at Hickman, KY (RM 922). The specific gage analysis evaluated discharge and stage data from the period of record 1956–2013. The analysis indicated that stages for out-of-bank discharges remained relatively stable for the entire period of record. Base Condition bankfull flow ranges from approximately 800,000 to 1,000,000 cfs. The stages for in-channel flows remained relatively stable from 1956–1978; however, a decreasing trend is observed for in-channel flows from 1978 to 2013.

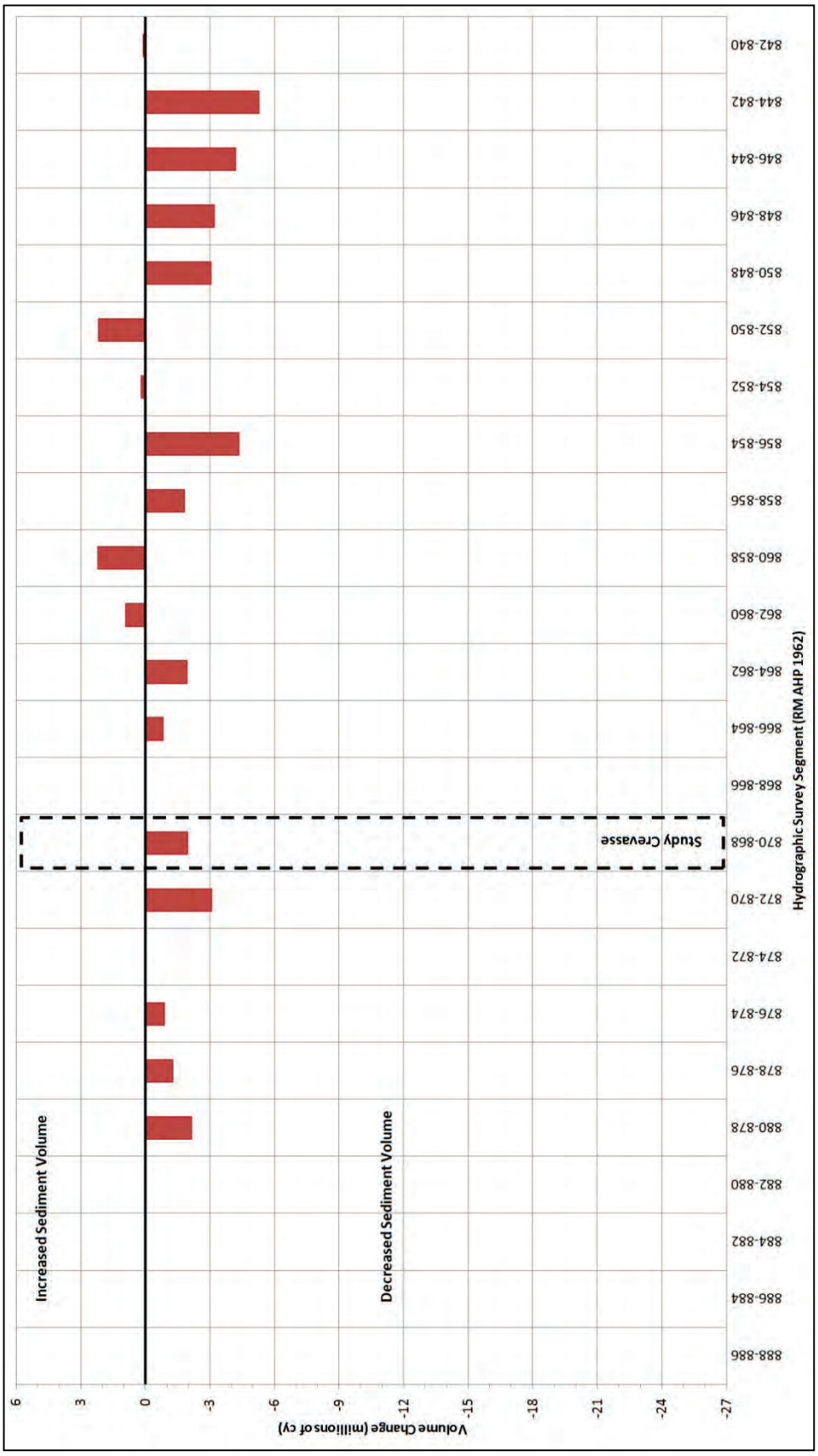


Figure 2-10. Sediment volume difference from 2009 dataset to 2010 dataset.

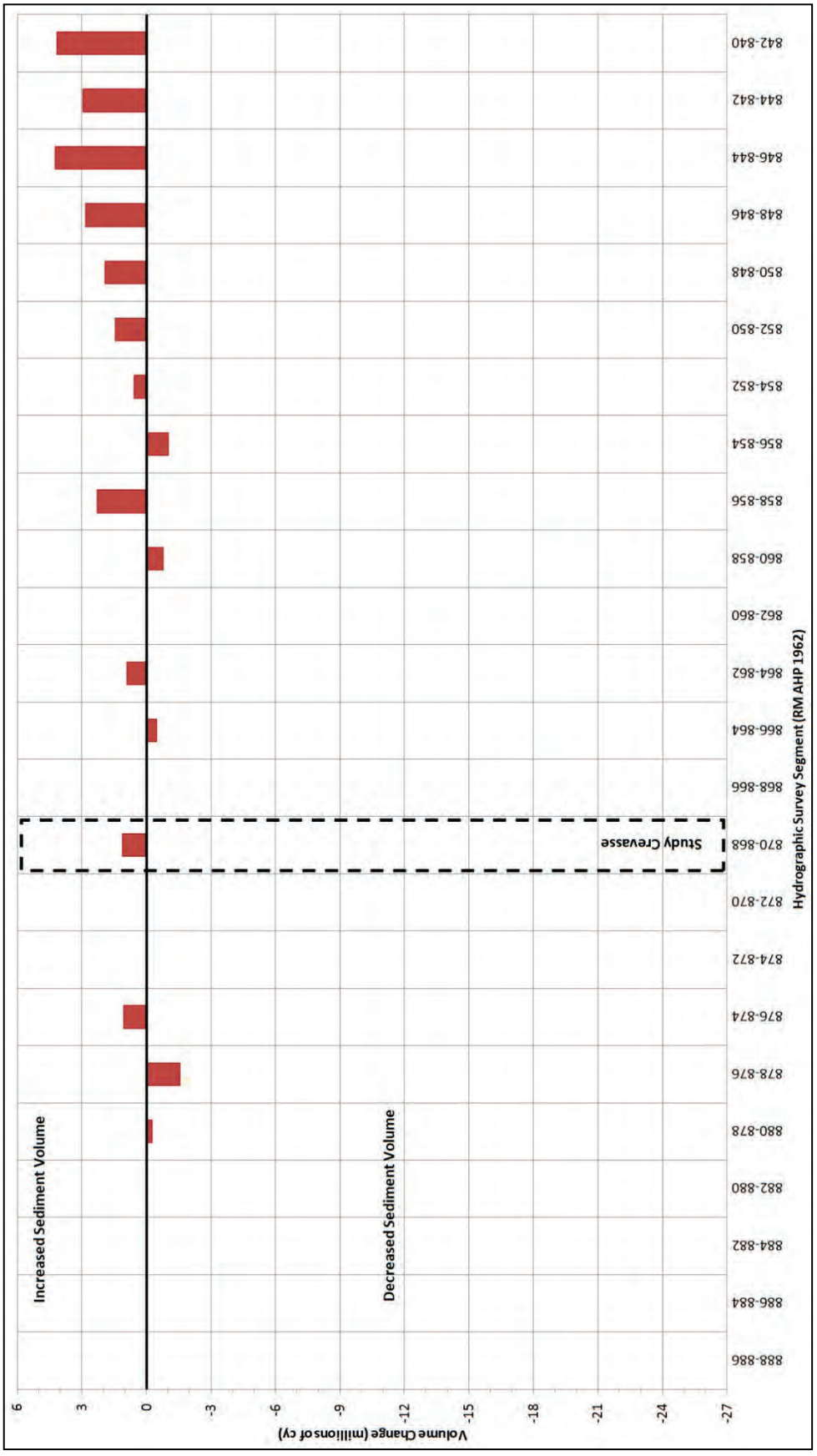


Figure 2-11. Sediment volume difference from 2010 dataset to 2013 dataset.

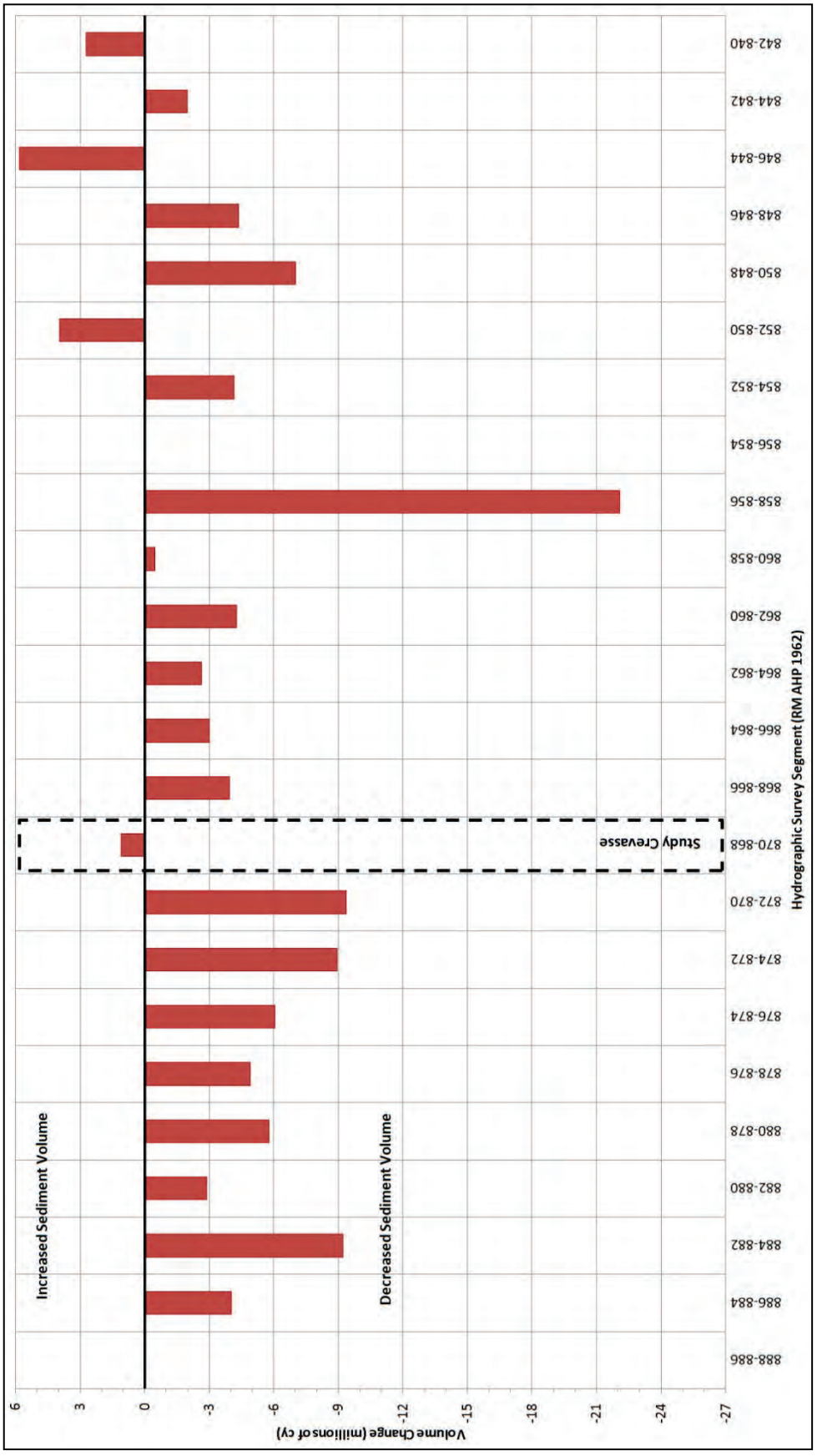
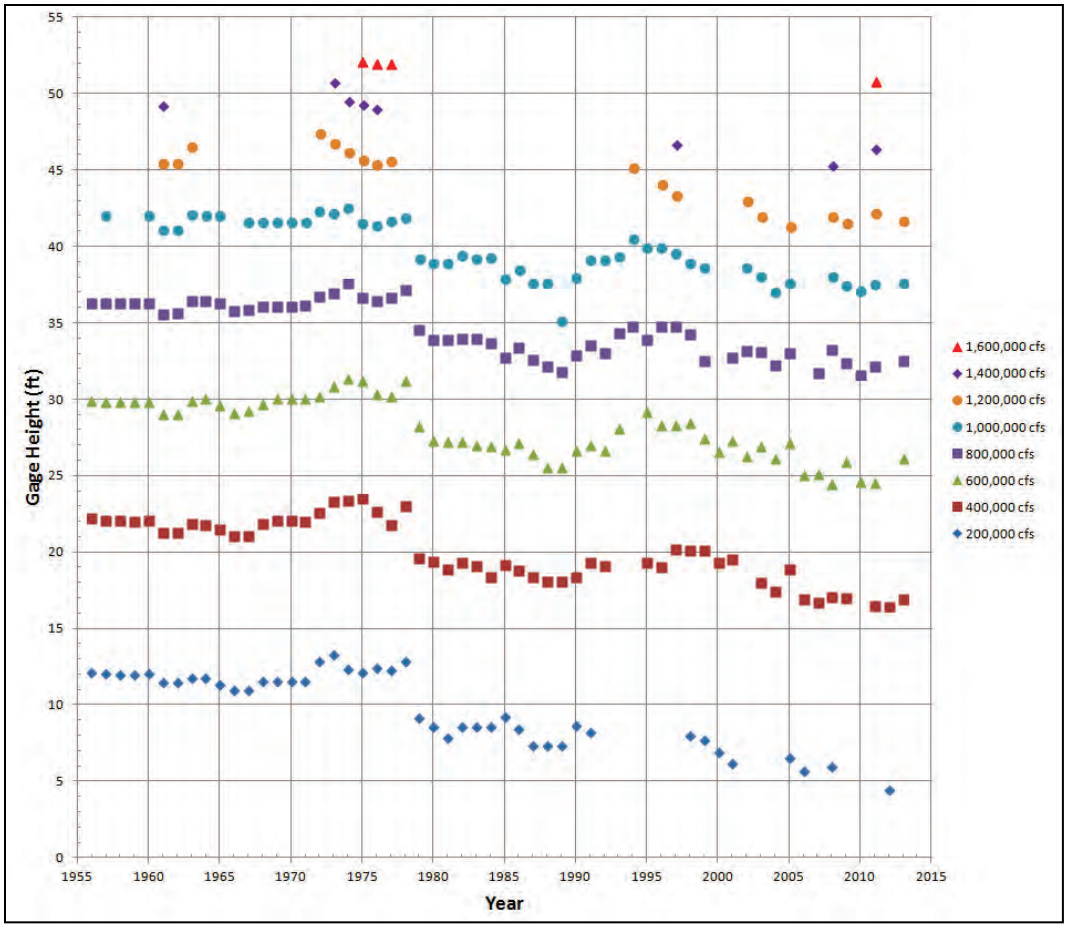


Figure 2-12. Sediment volume difference from 1989 dataset to 2013 dataset.

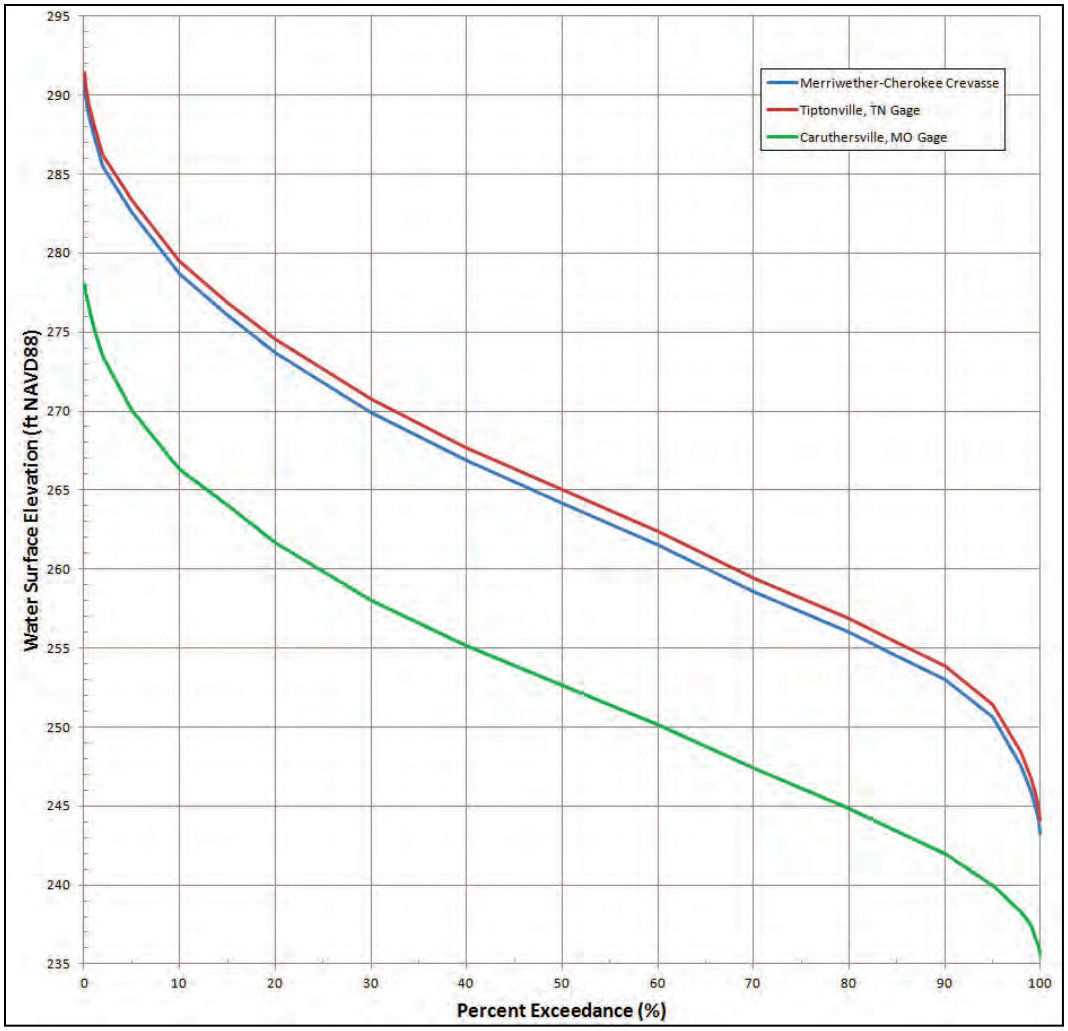
Figure 2-13. Hickman, KY, specific gage plot.



Duration analysis

The duration analysis evaluated the period of record from 1954–2013. Figure 2-14 depicts the duration analysis plot for Tiptonville, TN (RM 872.4), Merriwether-Cherokee Crevasse (RM 869), and Caruthersville, MO (RM 844.4). The closure structure is overtopped at an elevation of 269.7 ft NAVD88 and has been exceeded approximately 30% of the time. Flow commences across the Island 13 overbank at an elevation of 275.5 ft NAVD88 (at the closure structure) and has been exceeded approximately 16% of the time. Note that this analysis represented the base condition (fall 2014), and as the overbank reach bed elevations lower, the frequency and discharge rate of the diversion flow will increase.

Figure 2-14. Duration analysis plot for the time period 1954–2013.



Multidimensional modeling analysis

The following sections detail the base condition AdH model.

Model description

AdH was utilized to investigate the risk of cutoff formation and local scour potential. The AdH model simulated the Lower Mississippi River from RM 877–839.

Data collection

Model mesh elevation data was a composite created from several survey sources. The majority of the channel data in the model was obtained from the 2013 single-beam hydrographic survey. Detailed channel data from the

2013 and 2014 multibeam hydrographic surveys of revetments were utilized for revetment locations. The bathymetry of the scour hole was obtained from a 2011 multibeam hydrographic survey. Overbank elevation data was obtained from a 2005 lidar data set. Spur levee profile data was obtained from a 2013 field survey. The closure structure elevations were obtained from a 2014 field survey (post stone-cap construction). Dike elevation data were obtained from as-built river engineering data.

Channel sediment particle size distributions were obtained from the 2013 Mississippi River Bed Sampling effort (Gaines and Priestas 2015). Island 13 overbank top soil layer (depth range 0 to 6 in.) particle size distributions were obtained from a 2014 field survey. Figure 2-15 depicts the locations of the 15 soil samples that were collected and analyzed. Table 2-2 lists the Island 13 overbank soil sample's percent composition. The Island 13 overbank top soil layer is a cohesive soil type. Historic Island 13 overbank borings were investigated to determine soil type variations with respect to increasing depth. It was determined that a thin (approximately 10 ft) cohesive top sediment layer rests on top of a noncohesive sediment layer. Note that samples 22 and 22B were 2011 crevasse splay sediment samples.

Model development

The mesh was developed using the Surface-water Modeling System (SMS), a graphical user interface developed by ERDC for increasing the modeling productivity for a variety of USACE numerical models, including AdH. The entire model mesh is depicted in Figure 2-16. The Island 13 overbank model mesh is depicted in Figure 2-17. The base mesh consists of 279,920 nodes and 557,682 elements. The model extends from just below New Madrid Bend (RM 877) to the I-155 Bridge (RM 839). The model extends the width of the floodplain (levee to levee). The mesh includes all of the known river training structures and bank protection measures in the river. The horizontal datum for the mesh is NAD83 Zone 16. The vertical datum is NAVD88. The mesh elevation for the entire model domain is depicted in Figure 2-18. The mesh elevation for the Island 13 overbank is depicted in Figure 2-19.

Figure 2-15. Island 13 overbank soil sample locations.



Table 2-2. Island 13 overbank soil samples.

Sample ID	Grain Size Distribution Percent Composition										
	Fine Clay	Clay	Very Fine Silt	Fine Silt	Medium Silt	Coarse Silt	Very Fine Sand	Fine Sand	Medium Sand	Coarse Sand	Very Coarse Sand
Upper diameter (mm)	0.002	0.004	0.008	0.016	0.031	0.062	0.125	0.250	0.500	1.000	2.000
Lower diameter (mm)	0.001	0.002	0.004	0.008	0.016	0.031	0.062	0.125	0.250	0.500	1.000
1	10.8	12.2	13.3	18.2	19.9	15.7	8.0	1.2	0.3	0.1	0.2
2	3.3	4.6	11.1	10.1	17.6	27.8	17.4	5.5	2.0	0.3	0.2
3	0.9	1.1	2.9	6.5	11.2	31.2	26.5	14.1	5.4	0.2	0.0
4	2.1	0.8	2.6	6.0	14.0	41.3	28.0	4.1	1.0	0.1	0.0
5	5.2	9.4	6.2	15.3	14.4	31.4	13.1	3.3	1.8	0.0	0.0
14	0.9	6.3	4.6	11.0	13.3	26.3	25.4	10.3	1.9	0.0	0.0
17	0.0	18.1	26.9	15.9	11.1	16.0	8.3	2.7	1.1	0.1	0.0
18	0.7	0.0	3.8	5.7	11.8	32.4	35.6	9.0	1.0	0.0	0.0
19	0.0	2.5	3.5	6.2	14.5	42.3	25.9	4.1	1.0	0.1	0.0
20	1.5	1.5	4.9	7.7	11.7	30.3	34.0	7.4	1.0	0.0	0.0
21	0.0	12.1	9.2	9.4	9.3	23.3	24.1	9.9	2.7	0.1	0.0
23	5.6	9.5	12.3	14.4	11.8	24.3	13.2	4.2	3.5	1.0	0.2
24	4.7	9.9	11.2	13.7	14.0	27.4	16.7	1.6	0.8	0.1	0.0
22 (2011 crevasse splay)	0.2	0.0	0.7	1.0	2.1	3.7	8.3	24.8	52.6	6.3	0.4
22B (2011 crevasse splay)	3.7	11.8	11.2	14.1	12.4	22.9	12.4	6.1	5.1	0.3	0.1

Figure 2-16. Base condition element mesh for AdH model (entire model).



Figure 2-17. Base condition element mesh for AdH model (study overbank).



Figure 2-18. Base condition mesh elevation (entire model domain).

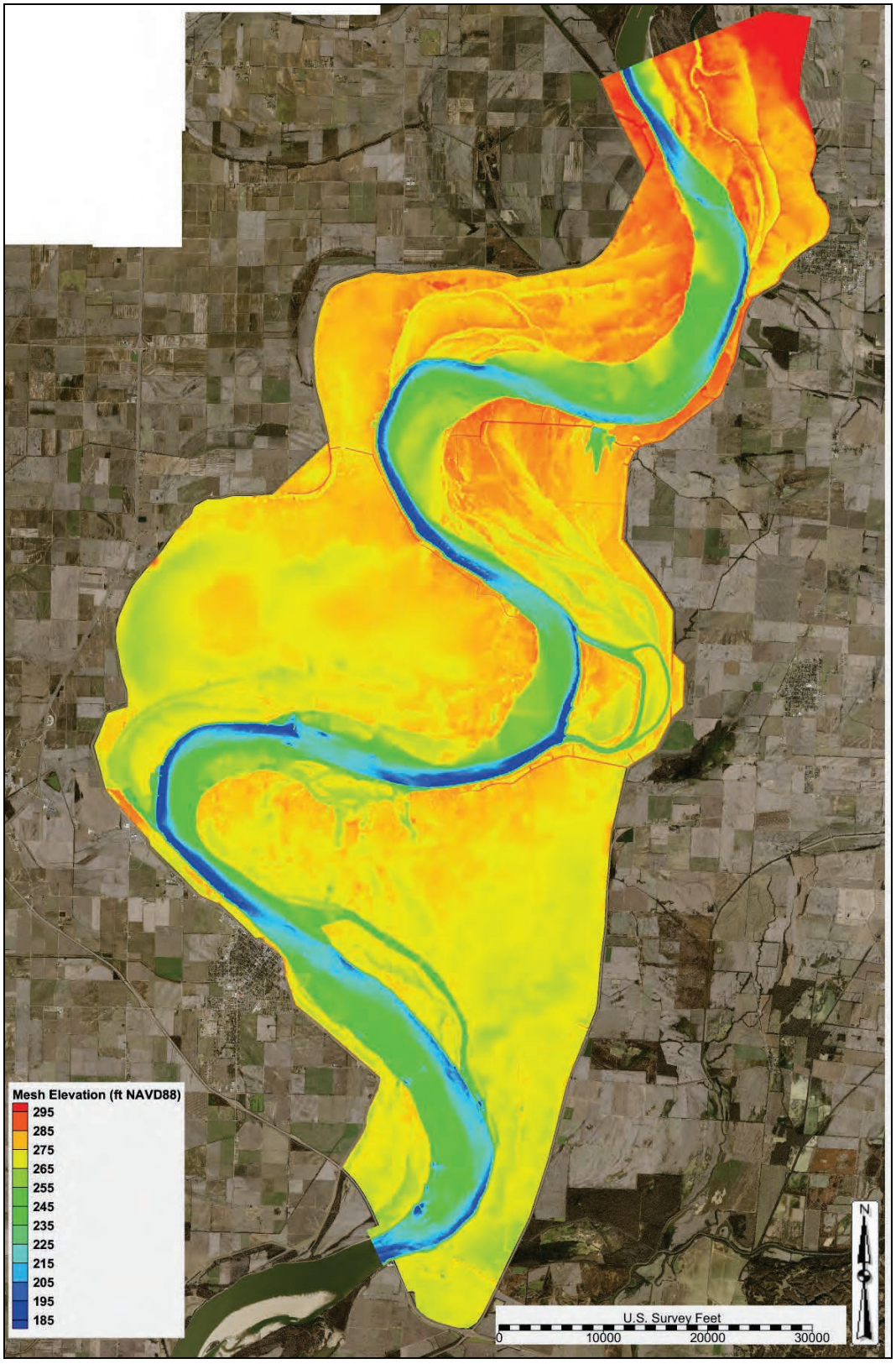
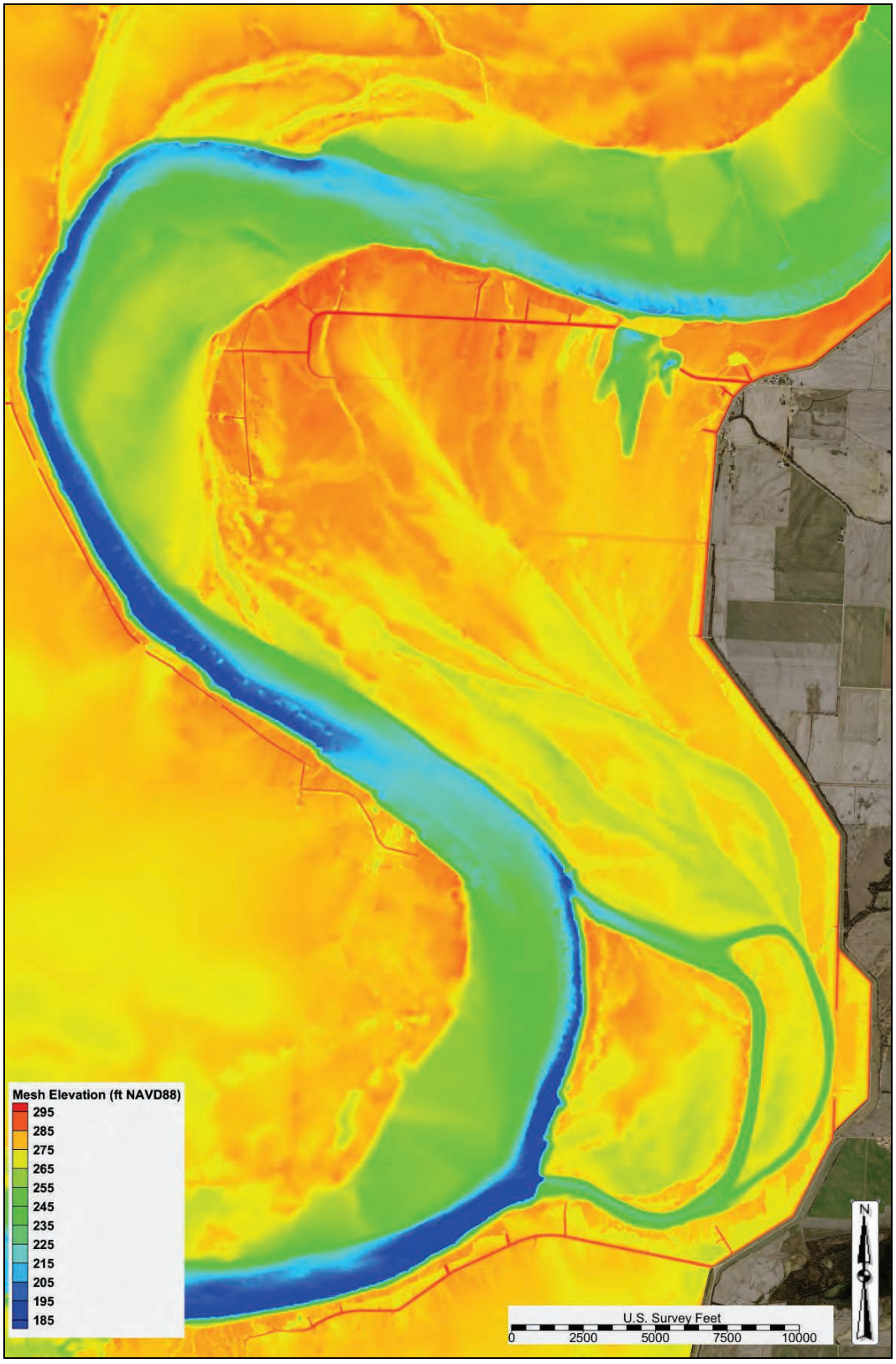


Figure 2-19. Base condition mesh elevation (study overbank).



The mesh contains 28 unique material types that define model parameters (e.g., Manning's roughness coefficients, bed grain size distribution, and bed layer thickness). The material types for the entire model domain are depicted in Figure 2-20. The material types for the Island 13 overbank are depicted in Figure 2-21. Note that most of the Island 13 overbank is cleared land. Table 2-3 contains the Manning's roughness coefficients for each material type.

Figure 2-22 depicts the 3D surface of the entire model domain. Note that several private levees, dikes, old meander scars, and river chutes are visible in the mesh. Figure 2-23 depicts the 3D surface of the Island 13 overbank. The closure structure, eastern spur levee, and western spur levee are detailed. Note the flow direction arrow in the figures.

Hydrodynamic boundary condition development

Mississippi River gage stations did not exist at the required boundary condition locations needed for the AdH model extent. Upstream (discharge) and downstream (water surface elevation) AdH boundary conditions were obtained from model output from the MVM portion of the Mississippi River HEC-RAS Unsteady Flow Model that was developed for the Mississippi River and Tributaries Program (MR&T) Flowline Study. The Mississippi River HEC-RAS Unsteady Flow Model was calibrated to the 2011 event and validated to the 2002 and 2008 events. Detailed calibration and validation data for the HEC-RAS model can be obtained from the Mississippi Valley Division (MVD) report titled *Reach-by-Reach HEC-RAS Models for the 2015 MR&T Mississippi River Flowline Study*.

Sediment boundary condition and initial condition development

For an alluvial river system, the transport of sediment is tied very closely to the reservoir of sediment available in the sediment bed. Therefore, the characterization of the sediment bed is of primary importance. Grain size classes were defined according to the American Geophysical Union (AGU) scale (Lane 1947).

Figure 2-20. Base condition material type (entire model domain).

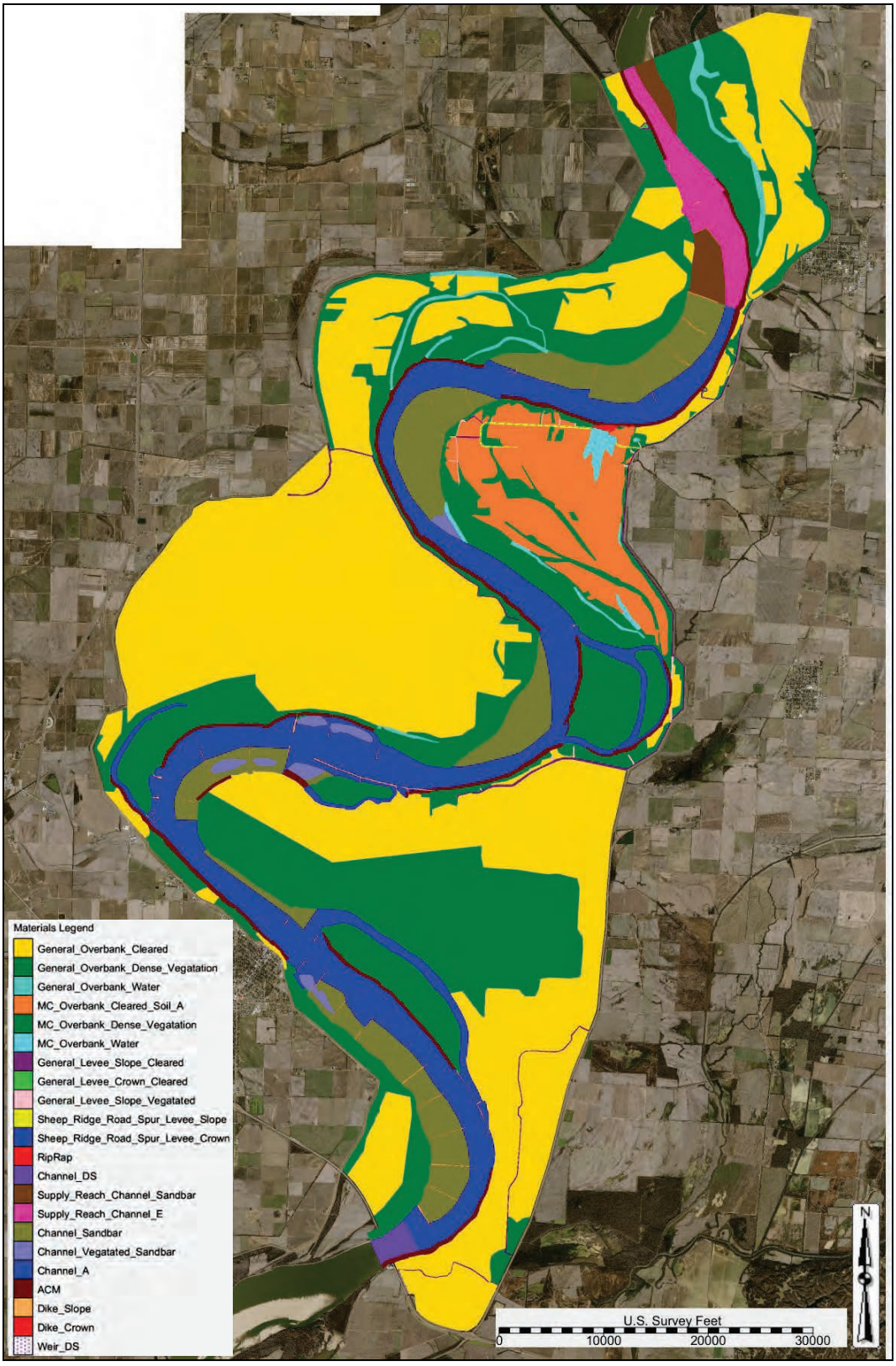


Figure 2-21. Base condition material type (study overbank).

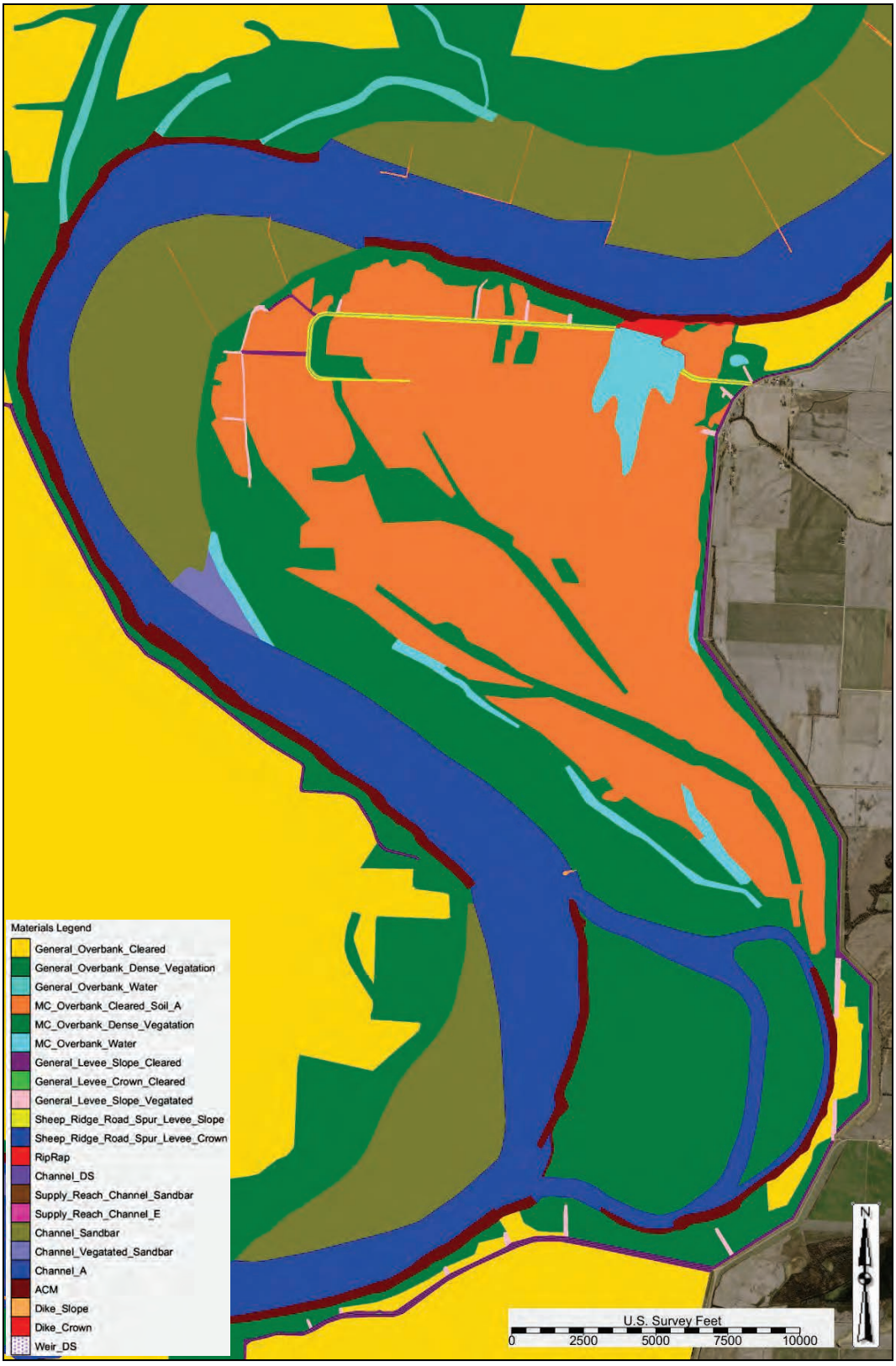


Table 2-3. Manning's roughness coefficients.

Material Type	Manning's Roughness Coefficient (n)
General Overbank Cleared	0.040
General Overbank Dense Vegetation	0.080
General Overbank Water	0.030
MC Overbank Cleared Soil A	0.040
MC Overbank Cleared Soil B	0.040
MC Overbank Dense Vegetation	0.080
MC Overbank Water	0.030
General Levee Slope Cleared	0.030
General Levee Crown Cleared	0.030
General Levee Slope Vegetated	0.080
General Levee Crown Vegetated	0.080
Sheep Ridge Road Spur Levee Slope	0.030
Sheep Ridge Road Spur Levee Crown	0.030
Riprap	0.035
Channel DS	0.031
Supply Reach Channel Sandbar	0.031
Supply Reach Channel E	0.031
Supply Reach Channel F	0.031
Channel Sandbar	0.031
Channel Vegetated Sandbar	0.031
Channel A	0.031
Channel B	0.031
Channel C	0.031
Channel D	0.031
ACM	0.031
Dike Slope	0.035
Dike Crown	0.035
Weir DS	0.040
Weir Reference String	0.040
Weir String	0.040
Tailwater Elevation Edgestring	0.031
Discharge Edgestring	0.031

Figure 2-22. Base condition 3D surface (entire model domain).

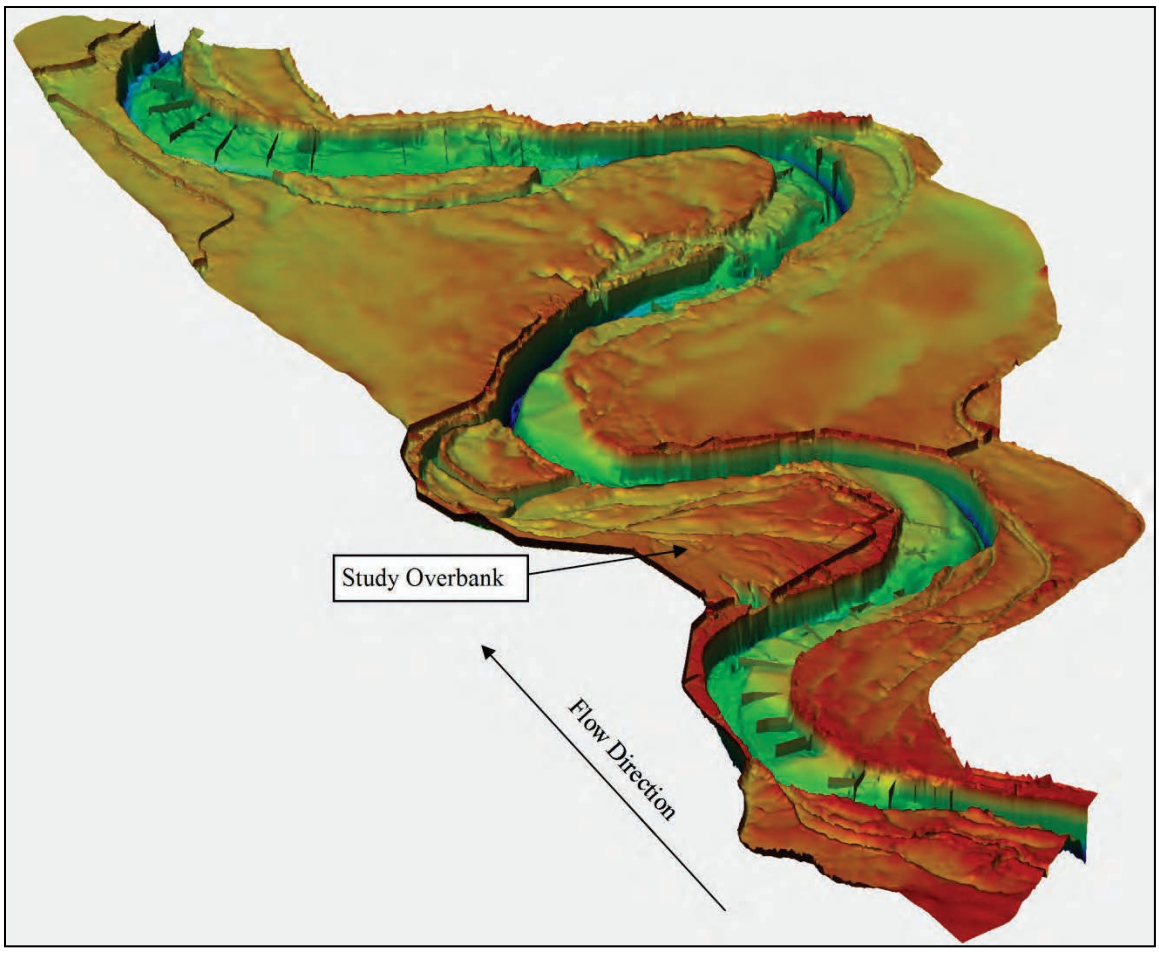


Figure 2-23. Base condition 3D surface (study overbank).

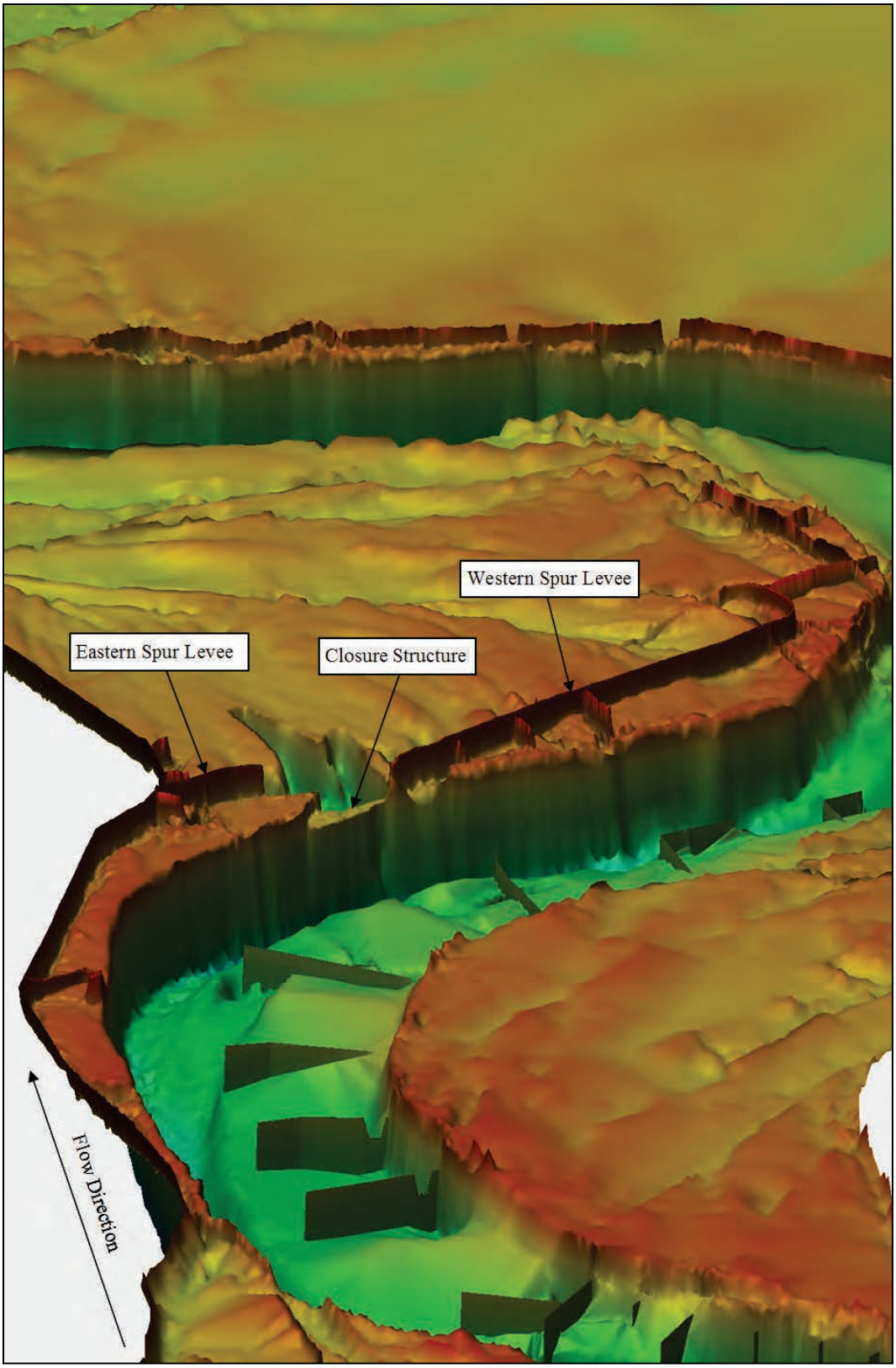


Table 2-4 lists the cohesive sediment model parameters utilized for the AdH simulation. The primary goal of the investigation was to determine overbank scour (cutoff formation). The following assumptions were made with regards to cohesive transport in the model: (1) only the erosion of cohesive sediments were modeled (cohesive sediment deposition was not modeled), and (2) all cohesive sediment was assumed to be a coarse silt grain size class. The critical shear stress for cohesive sediment was determined from equation 2-1 (Mitchener et al. 1996; Whitehouse et al. 2000). A bed density of 1,600 kg/m^3 was utilized (Mehta 2014). In AdH, the cohesive erosion rate was governed by Equation 2-2. An erosion rate constant of 0.0002 kg m^{-2} s^{-1} was utilized (Whitehouse et al. 2000; Winterwerp and van Kesteren 2004). An erosion rate exponent of 1 was utilized (Whitehouse et al. 2000; Winterwerp and van Kesteren 2004).

Table 2-4. Cohesive sediment model parameters.

Grain Size Class	Minimum Diameter (mm)	Maximum Diameter (mm)	Geometric Mean Diameter (mm)	Specific Gravity	Bulk Density (kg/m^3)	Critical Shear for Erosion (Pa)	Erosion Rate Constant (kg m^{-2} s^{-1})	Critical Shear for Deposition (Pa)	Free Settling Velocity (m/s)
Coarse Silt	0.031	0.062	0.0438	2.65	1600	1.06	0.0002	0.01	0.0001

$$\tau_c = X1\left(\rho_B - 1000\right)^{X2} \tag{2-1}$$

where:

τ_c = critical shear stress for erosion (Pa)
$X1$ = 0.015 (SI units)
$X2$ = 0.73 (SI units)
ρ_B = bed density (kg/m^3)

$$F_E = M\left(\frac{\tau}{\tau_c} - 1\right)^n \tag{2-2}$$

where:

F_E = erosion flux
M = erosion rate constant (kg m^{-2} s^{-1})
τ = shear stress (Pa)
τ_c = critical shear stress for erosion (Pa)
n = erosion rate exponent.

Table 2-5 lists the noncohesive sediment model parameters utilized for the AdH simulation. The specific gravity of all noncohesive sediment classes was set to 2.65, and the in situ porosity of the sediment bed was set to 0.35.

Table 2-5. Noncohesive sediment model parameters.

Grain Size Class	Minimum Diameter (mm)	Maximum Diameter (mm)	Geometric Mean Diameter (mm)	Specific Gravity	Grain Porosity
Very Fine Sand	0.062	0.125	0.088	2.65	0.35
Fine Sand	0.125	0.250	0.177	2.65	0.35
Medium Sand	0.250	0.500	0.354	2.65	0.35
Coarse Sand	0.500	1.000	0.707	2.65	0.35
Very Coarse Sand	1.000	2.000	1.414	2.65	0.35
Very Fine Pebble	2.000	4.000	2.828	2.65	0.35
Fine Pebble	4.000	8.000	5.657	2.65	0.35
Medium Pebble	8.000	16.000	11.314	2.65	0.35
Coarse Pebble	16.000	32.000	22.627	2.65	0.35

Initial overbank bed characteristics were developed from the 2014 Island 13 overbank soil sampling. The initial bed distribution for the overbank material types is listed in Table 2-6. Initial river channel bed characteristics were determined based on a reach averaging of the 2013 Mississippi River Bed sampling data. The initial bed distribution for the river channel material types is listed in Table 2-7.

The inflowing sediment boundary condition was set to the local equilibrium value. For the equilibrium value, the model computes an equilibrium concentration for each noncohesive grain class at the model boundary, and that value is used as the boundary condition for that time-step. In addition to the equilibrium condition, a supply reach was also utilized from RM 877–872. For the supply reach in the model, the bed elevation was held constant, and sediment transport was performed; this allowed for the development of suspended sediment load.

Table 2-6. Initial overbank material bed distribution and layer thickness.

Layer ID	Layer Thickness (m)	Grain Size Distribution Fraction Composition									
		Coarse Silt	Very Fine Sand	Fine Sand	Medium Sand	Coarse Sand	Very Coarse Sand	Very Fine Pebble	Fine Pebble	Medium Pebble	Coarse Pebble
1	19	0.000	0.019	0.093	0.387	0.364	0.094	0.023	0.010	0.008	0.002
2	3	0.711	0.211	0.058	0.017	0.002	0.001	0.000	0.000	0.000	0.000
3	0	0.711	0.211	0.058	0.017	0.002	0.001	0.000	0.000	0.000	0.000
4	0	0.711	0.211	0.058	0.017	0.002	0.001	0.000	0.000	0.000	0.000
5	0	0.711	0.211	0.058	0.017	0.002	0.001	0.000	0.000	0.000	0.000

Note: Layer 1 is the bottom layer, and Layer 5 is the top layer.

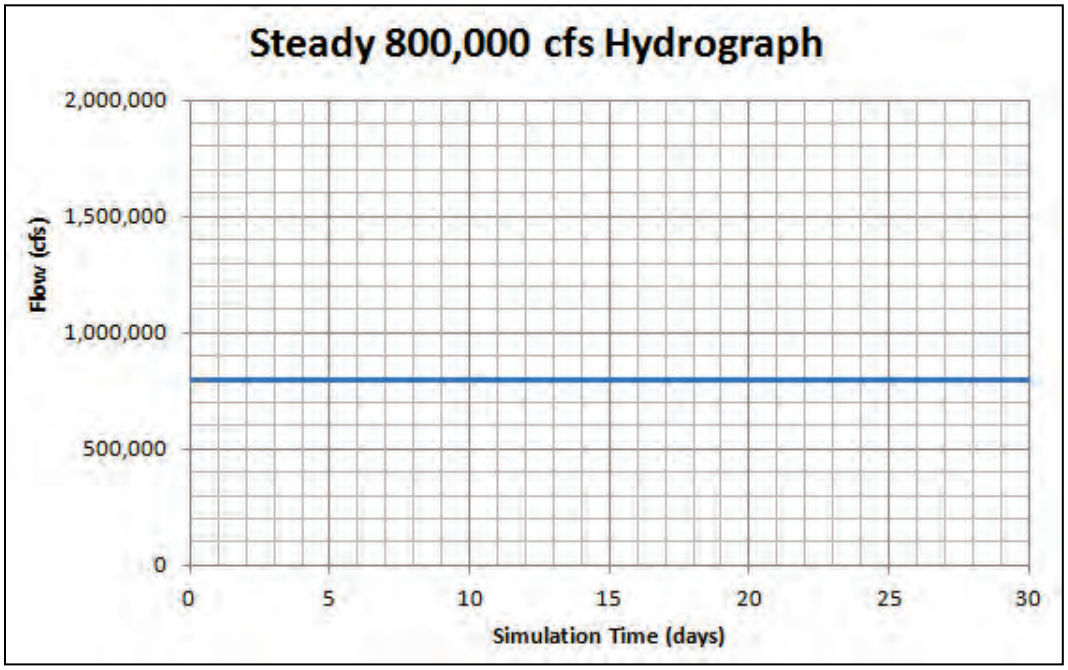
Table 2-7. Initial channel material bed distribution and layer thickness.

Layer ID	Layer Thickness (m)	Grain Size Distribution Fraction Composition									
		Coarse Silt	Very Fine Sand	Fine Sand	Medium Sand	Coarse Sand	Very Coarse Sand	Very Fine Pebble	Fine Pebble	Medium Pebble	Coarse Pebble
1	21	0.000	0.019	0.093	0.387	0.364	0.094	0.023	0.010	0.008	0.002
2	1	0.000	0.019	0.093	0.387	0.364	0.094	0.023	0.010	0.008	0.002
3	0	0.000	0.019	0.093	0.387	0.364	0.094	0.023	0.010	0.008	0.002
4	0	0.000	0.019	0.093	0.387	0.364	0.094	0.023	0.010	0.008	0.002
5	0	0.000	0.019	0.093	0.387	0.364	0.094	0.023	0.010	0.008	0.002

Note: Layer 1 is the bottom layer, and Layer 5 is the top layer.

The channel sediment bed was initialized by modeling a constant 800,000 cfs for 30 days. Figure 2-24 depicts the hydrograph utilized for the initialization of the channel sediment bed. During the bed initialization simulation, the mesh bed elevations were held constant, but the grain size distribution was allowed to vary spatially in a manner consistent with the local bed shear stress regime. This adjusted bed grain size class distribution was then used as the initial condition for all subsequent simulations; during these simulations, the bed elevation was permitted to change in the study area so that the changing morphology would interact with the flow field.

Figure 2-24. Sediment bed initialization inflow hydrograph.



Hydrodynamic calibration and validation

Hydrodynamic calibration was performed using historic water surface elevation data and ADCP velocity data.

Water surface elevation (WSEL) was calibrated to three historic events (Figures 2-25, 2-26, and 2-27) and validated to one historic event (Figure 2-28). Figure 2-29 depicts the two gage locations, Tiptonville, TN, and Caruthersville, MO, where historic water surface elevation data was available within the modeled domain.

Figure 2-25. Calibration event 1 inflow hydrograph.

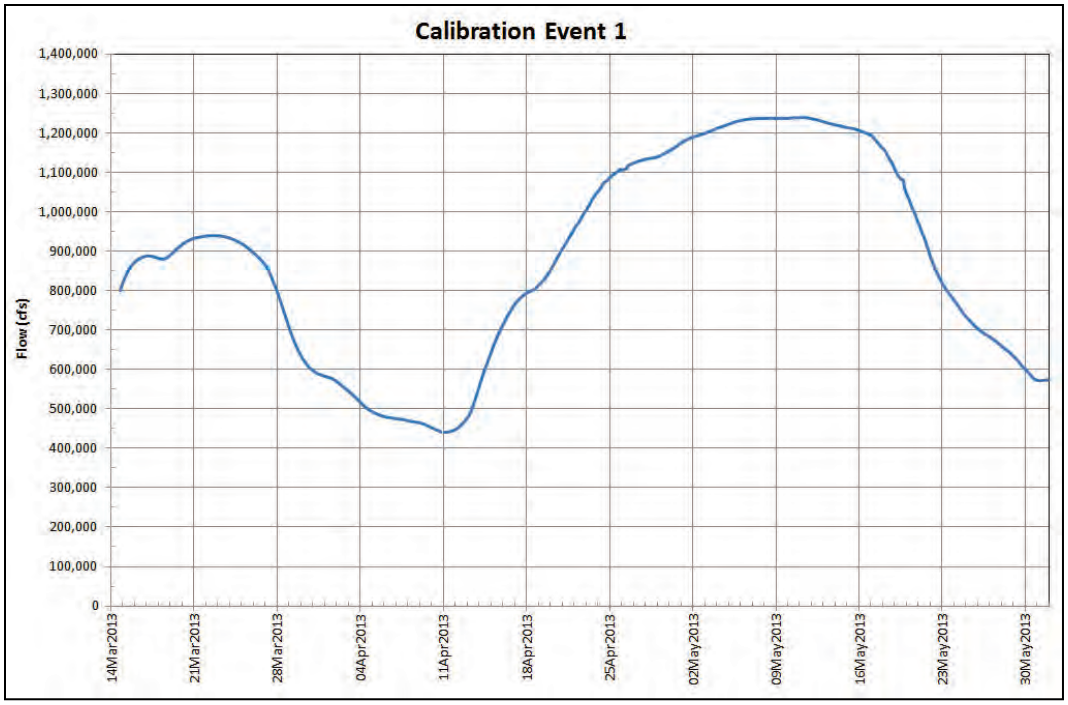


Figure 2-26. Calibration event 2 inflow hydrograph.

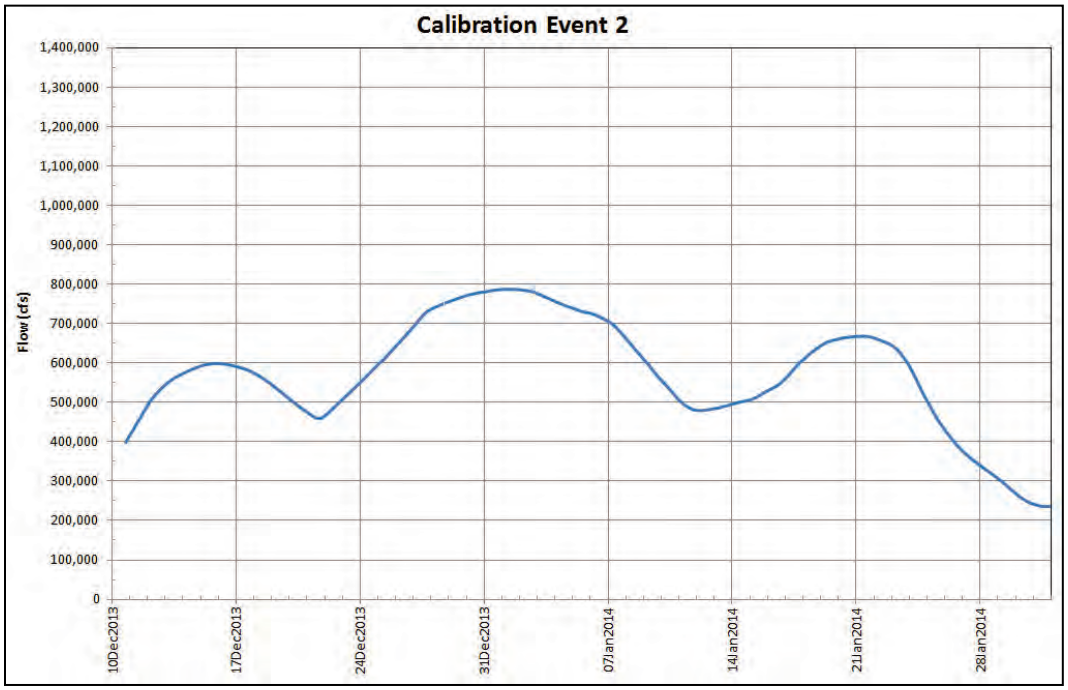


Figure 2-27. Calibration event 3 inflow hydrograph.

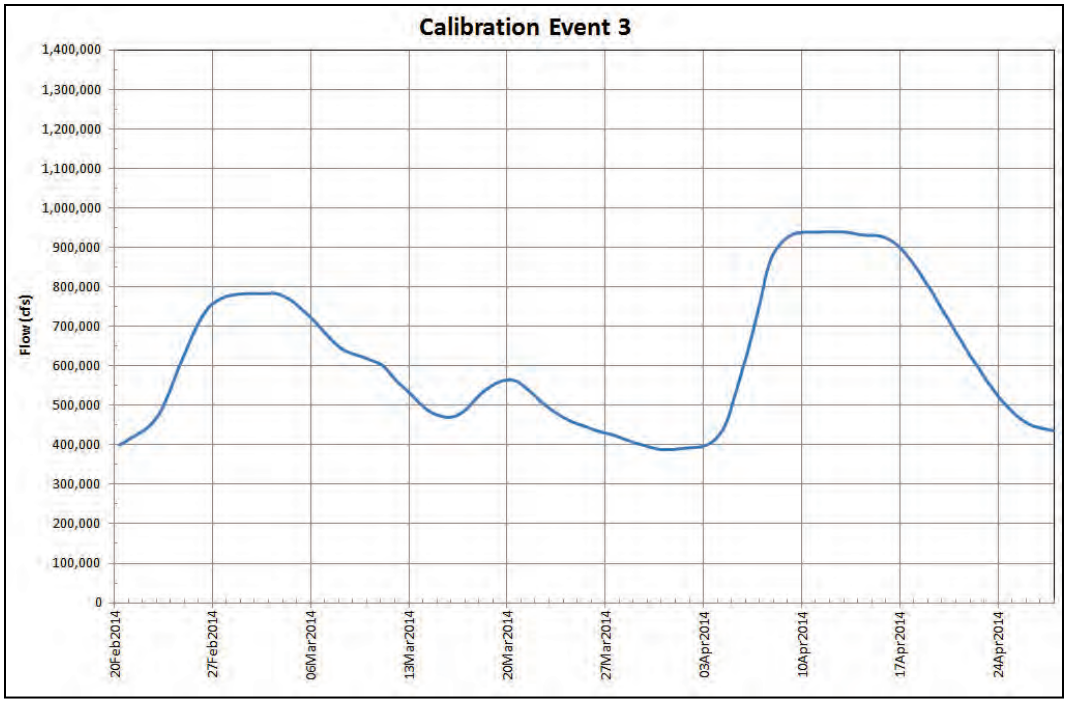


Figure 2-28. Validation event inflow hydrograph.

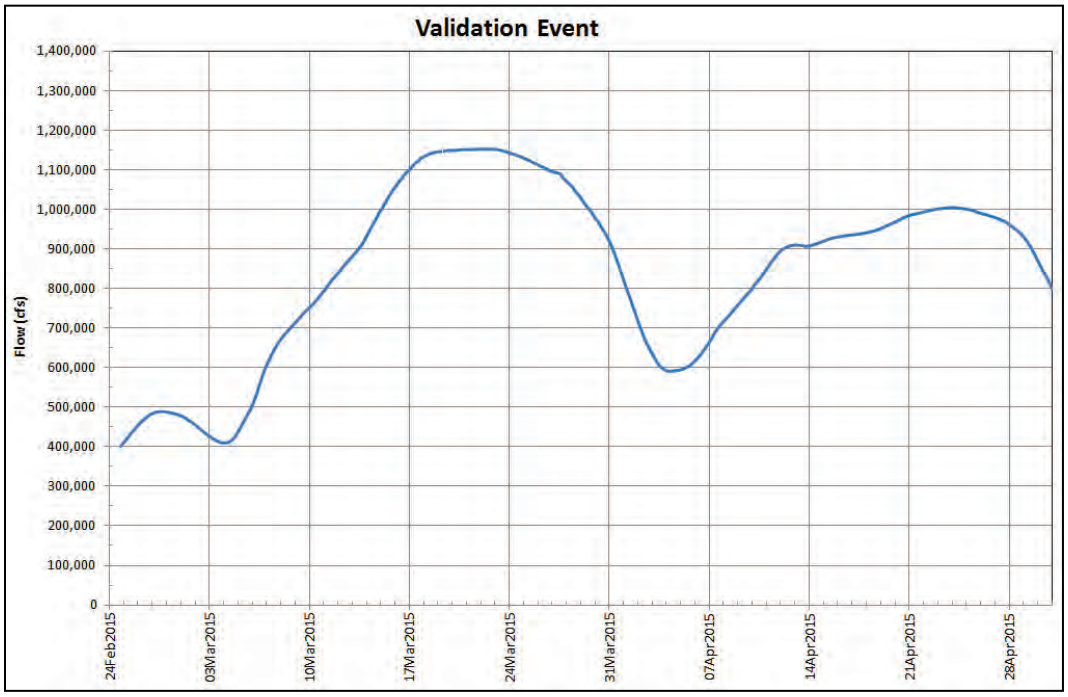


Figure 2-29. WSEL calibration–gage location map.



The results from the Tiptonville gage WSEL calibration and validation for selected peaks from each simulation are listed in Table 2-8. The WSELs for the selected peaks at Tiptonville were calibrated to ± 0.7 ft. The validation event peaks for the Tiptonville gage were within ± 0.9 ft.

Table 2-8. Tiptonville gage WSEL calibration and validation summary.

Simulation	Date	Observed WSEL (ft NAVD88)	Modeled WSEL (ft NAVD88)	WSEL Difference Modeled–Observed (ft NAVD88)
Calibration Event 1	3/22/2013	278.41	278.52	0.11
Calibration Event 1	5/11/2013	283.90	284.55	0.65
Calibration Event 2	12/15/2013	268.83	268.88	0.05
Calibration Event 2	1/1/2014	274.47	274.41	-0.06
Calibration Event 2	1/21/2014	270.84	270.47	-0.37
Calibration Event 3	3/1/2014	274.16	274.49	0.33
Calibration Event 3	3/20/2014	267.35	267.17	-0.18
Calibration Event 3	4/12/2014	278.31	278.20	-0.11
Validation Event	2/27/2015	265.44	265.02	-0.42
Validation Event	3/22/2015	283.23	282.61	-0.62
Validation Event	4/24/2015	280.18	279.33	-0.85

The results from the Caruthersville gage WSEL calibration and validation for selected peaks from each simulation are listed in Table 2-9. The WSELs for the selected peaks at Caruthersville were calibrated to ± 0.6 ft. The validation event peaks for the Caruthersville gage were within ± 0.4 ft.

Table 2-9. Caruthersville gage WSEL calibration and validation summary.

Simulation	Date	Observed WSEL (ft NAVD88)	Modeled WSEL (ft NAVD88)	WSEL Difference Modeled–Observed (ft NAVD88)
Calibration Event 1	3/22/2013	266.65	267.14	0.49
Calibration Event 1	5/11/2013	273.26	273.03	-0.23
Calibration Event 2	12/16/2015	257.94	258.41	0.47
Calibration Event 2	1/1/2014	263.10	263.42	0.32
Calibration Event 2	1/21/2014	259.62	259.93	0.31
Calibration Event 3	3/2/2014	262.94	263.48	0.54
Calibration Event 3	3/20/2014	256.53	257.09	0.56
Calibration Event 3	4/13/2014	266.56	266.92	0.36
Validation Event	2/28/2015	254.78	255.18	0.40
Validation Event	3/23/2015	271.48	271.43	-0.05
Validation Event	4/24/2015	268.33	268.32	-0.01

The WSEL root-mean-square error from the calibration and validation simulations at Tiptonville and Caruthersville is detailed in Table 2-10.

Table 2-10. Water surface elevation root-mean-square error.

Simulation	Tiptonville Gage Root-Mean-Square Error (ft NAVD88)	Caruthersville Gage Root-Mean-Square Error (ft NAVD88)
Calibration Event 1	0.50	0.68
Calibration Event 2	1.05	1.05
Calibration Event 3	0.66	0.97
Validation Event	0.70	0.27

A summary of the ADCP velocity calibration is listed in Table 2-11. Note that the velocity difference (modeled–observed) for all datasets analyzed had a standard deviation less than 2 ft/s.

Table 2-11. Velocity calibration summary.

Date	ADCP Dataset Number	Standard Deviation Velocity Difference Modeled–Observed (ft/s)	Mean Velocity Difference Modeled–Observed (ft/s)
5/8/2013	1	1.92	1.00
12/19/2013	1	1.32	-0.10
2/28/2014	1	1.15	0.59
2/28/2014	2	1.45	0.53
2/28/2014	3	1.56	-0.06
4/9/2014	1	0.71	-0.16
4/9/2014	2	1.18	-0.02
4/9/2014	3	0.78	-0.30

Appendix C contains the following detailed hydrodynamic calibration and validation data:

- Tiptonville and Caruthersville observed vs. modeled WSEL Hydrographs for calibration and validation events (Figures C-1 through C4 and C-11 through C-12)
- December 2013 event observed precipitation (Figures C-5 through C-10)
- Velocity observed vs. modeled maps (spatially view data) and graphs (Figures C-13 through C-28).

Sediment transport function

The Wright-Parker transport function was utilized for the noncohesive suspended entrainment and the Meyer Peter Mueller with the Wong Park

Correction transport function was utilized for the noncohesive bedload entrainment. Table 2-12 summarizes the results from the bed initialization simulation (800,000 cfs for 30 days) and how the modeled bed particle size distribution compared to the 2013 observed data for the selected transport functions.

Table 2-12. Bed sediment initialization summary.

Particle Size Distribution	Standard Deviation Size Difference Modeled–Observed (mm)	Mean Size Difference Modeled–Observed (mm)
d16	0.15	-0.10
d25	0.20	-0.12
d50	0.52	-0.16
d75	1.67	0.26

Appendix C contains the following detailed bed sediment initialization data:

- Bed particle size distribution (d16, d25, d50, and d75) modeled vs. observed maps (spatially view data) and graphs (Figures C-31 through C-40).

Scenario simulation

A hypothetical inflow hydrograph (Figure 2-30) was created to perform plan comparisons and obtain model output at specified flow increments. This hydrograph had flows ranging from 800,000 cfs to 2,500,000 cfs.

The discharge frequency data for the Mississippi River at Hickman, KY, is listed in Table 2-13. Note that these frequency flows are provided for reference only and do not directly correlate to flow hydrographs created and utilized for this study.

Figure 2-30. Hypothetical event inflow hydrograph.

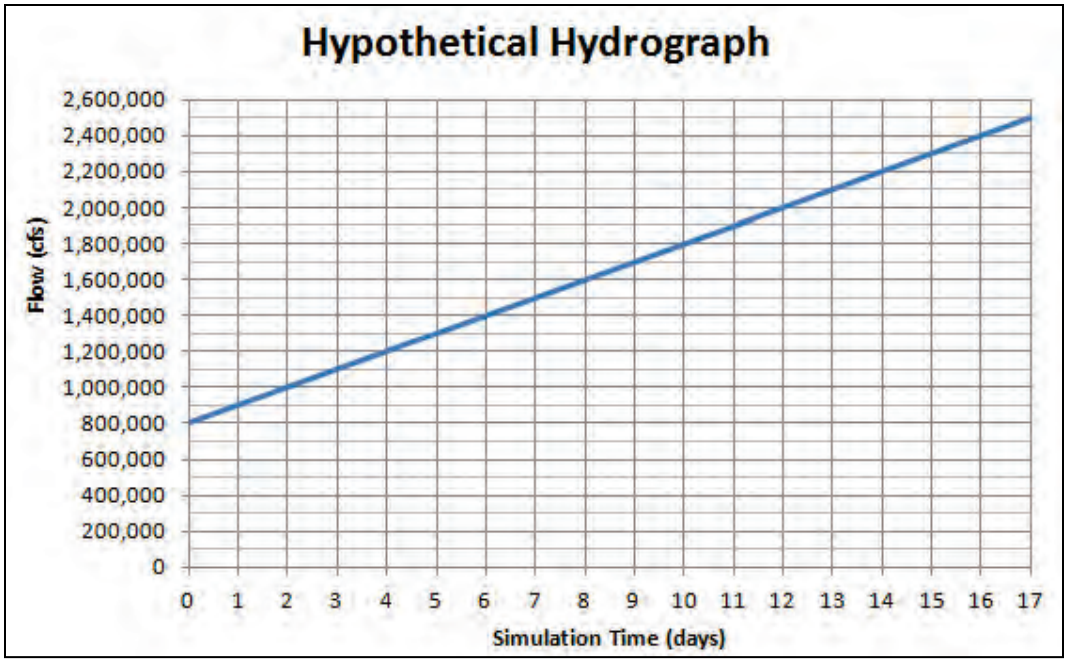
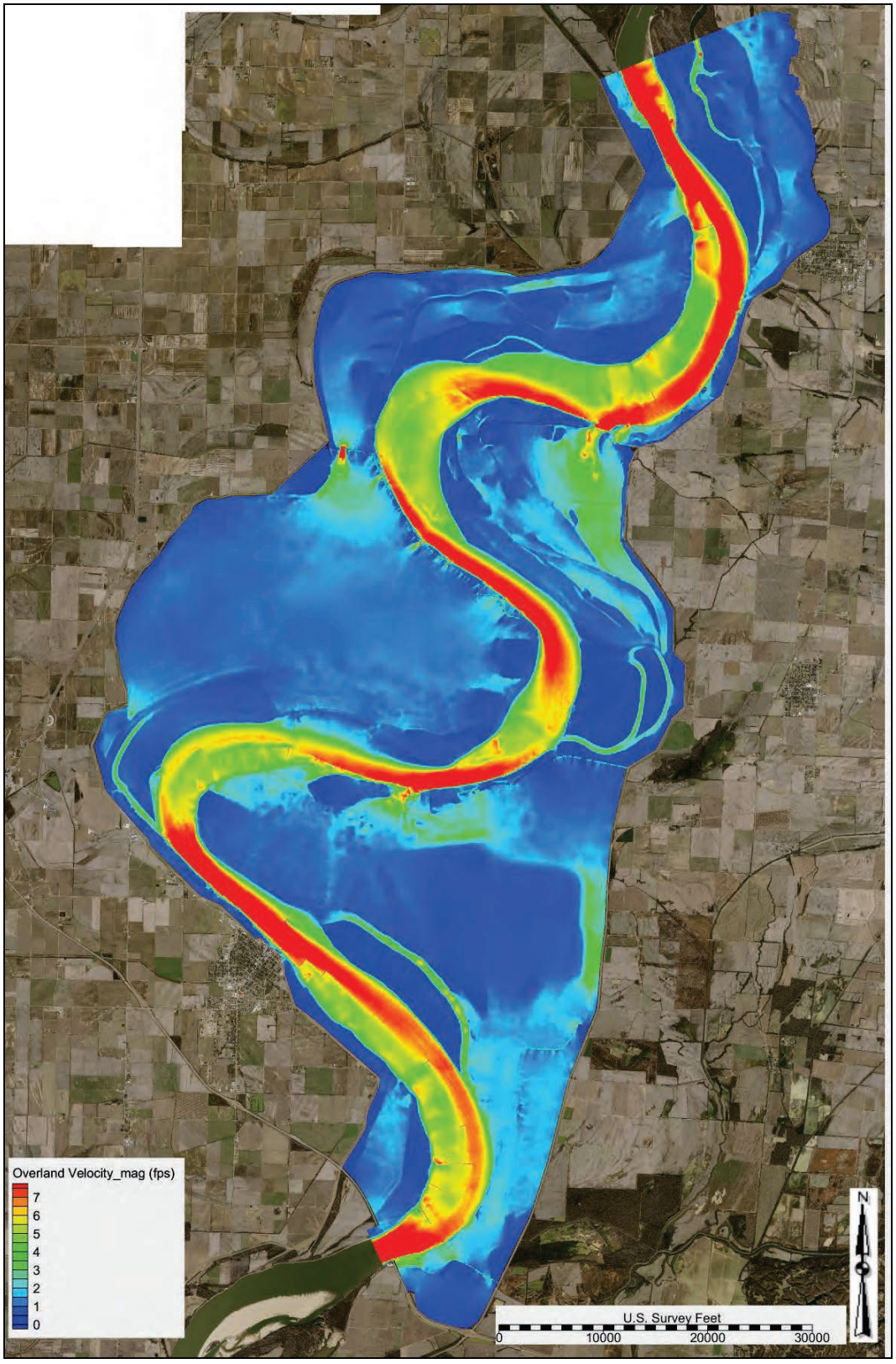


Table 2-13. Discharge frequency for the Mississippi River at Hickman, KY.

Annual Probability of Exceedance (%)	Chance Exceedance Peak Discharge (cfs)
50	1,000,000
20	1,265,000
10	1,435,000
4	1,640,000
2	1,810,000
1	1,895,000

The velocity output at 1,900,000 cfs from the Hypothetical Hydrograph simulation for the entire model domain is depicted in Figure 2-31. Note that the higher overbank velocity regions are found in overbank regions that contain cleared land (no dense vegetation or tree screens).

Figure 2-31. Base condition velocity—1,900,000 cfs (entire model domain).



The velocity output at 1,900,000 cfs from the Hypothetical Hydrograph simulation for the study overbank is depicted in Figure 2-32. Note the regions of high velocity on the closure structure, western edge of scour hole, overbank region immediately east of the closure structure, and at the toe of the Tiptonville-Obion River Levee.

The velocity output at 1,900,000 cfs from the Hypothetical Hydrograph simulation for the study crevasse is depicted in Figure 2-33. Note the regions of high velocity on the closure structure, western edge of scour hole, overbank region immediately east of the closure structure (cleared land). The velocity vectors display the flow diverted into the overbank and the eddy formations off the eastern and western spur levees.

The bed shear stress output at 1,900,000 cfs from the Hypothetical Hydrograph simulation for the study overbank is depicted in Figure 2-34. The critical shear stress, that is the incipient threshold for flow to entrain particles in a movable bed, for sand is approximately 0.02089 lb/ft^2 (1 Pa) (Nalluri 2009). Colored regions in the figure indicate that the critical shear stress for sand has been exceeded. Note the regions of high shear stress on the closure structure, western edge of scour hole, overbank region south of the scour hole, overbank region immediately east of the closure structure, and at the toe of the Tiptonville-Obion River Levee.

Scenario simulations were performed utilizing the second peak of the 2011 Flood. The historical flow hydrograph at the upstream boundary condition for the AdH model is depicted in Figure 2-35. This Historical Hydrograph had a peak of approximately 2,100,000 cfs and a duration of 70 days.

The bed displacement output from the Historical Hydrograph simulation for the study overbank modeled as a cohesive soil type is depicted in Figure 2-36. This simulation assumed that the study overbank had a cohesive top soil layer 10 ft thick across the entire Island 13 overbank. A positive (+ value and blue color) bed displacement represented aggradation (deposition) and a negative (- value and red color) bed displacement represented degradation (scour). Deposition is simulated in the main channel immediately downstream of the closure structure. Scour is simulated at the toe of the closure structure baffle, western and southern edges of the scour hole, eastern spur levee, and the toe of the Tiptonville-Obion River Levee.

Figure 2-32. Base condition velocity—1,900,000 cfs (study overbank).

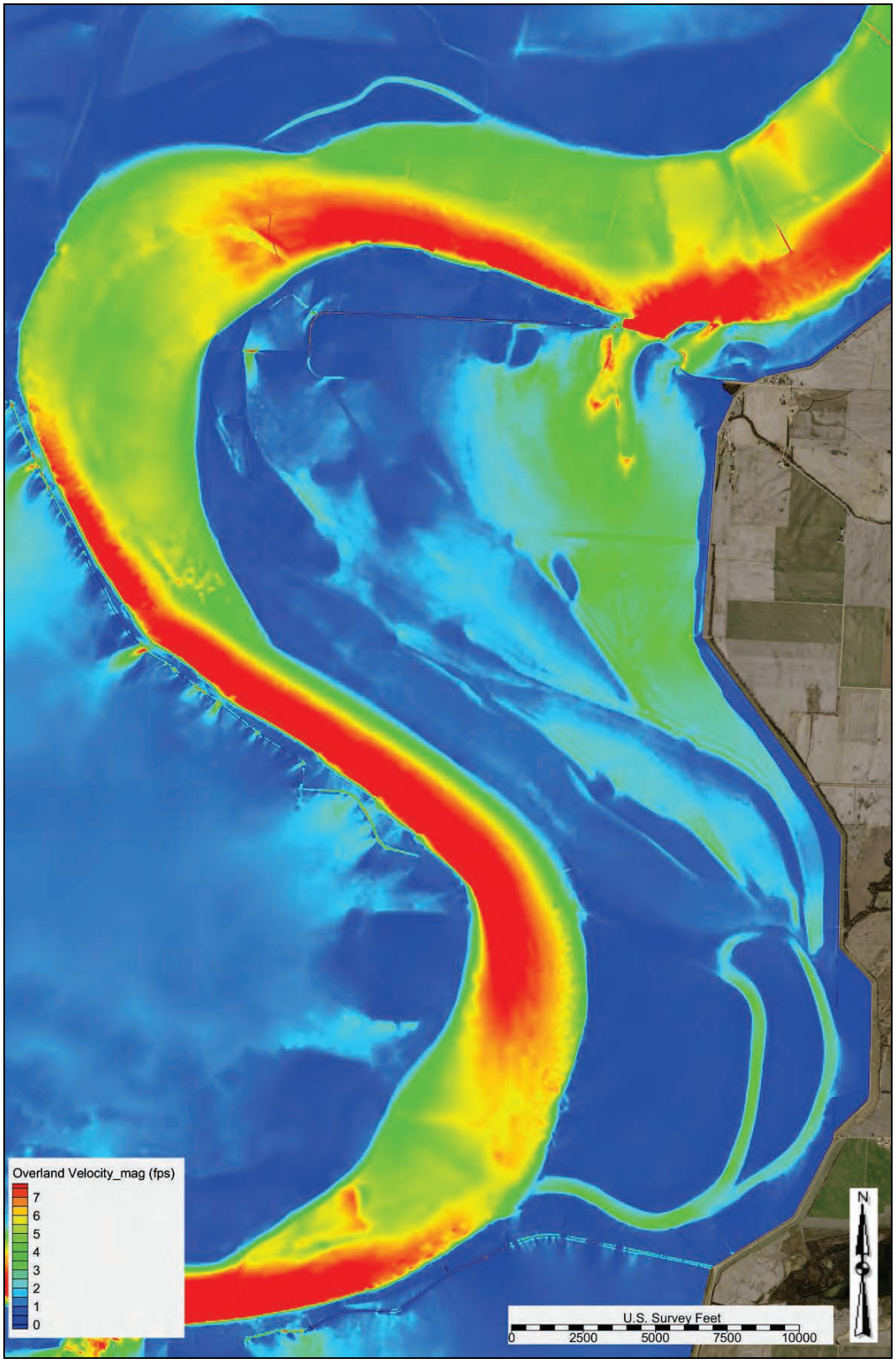


Figure 2-33. Base condition velocity—1,900,000 cfs (study crevasse).

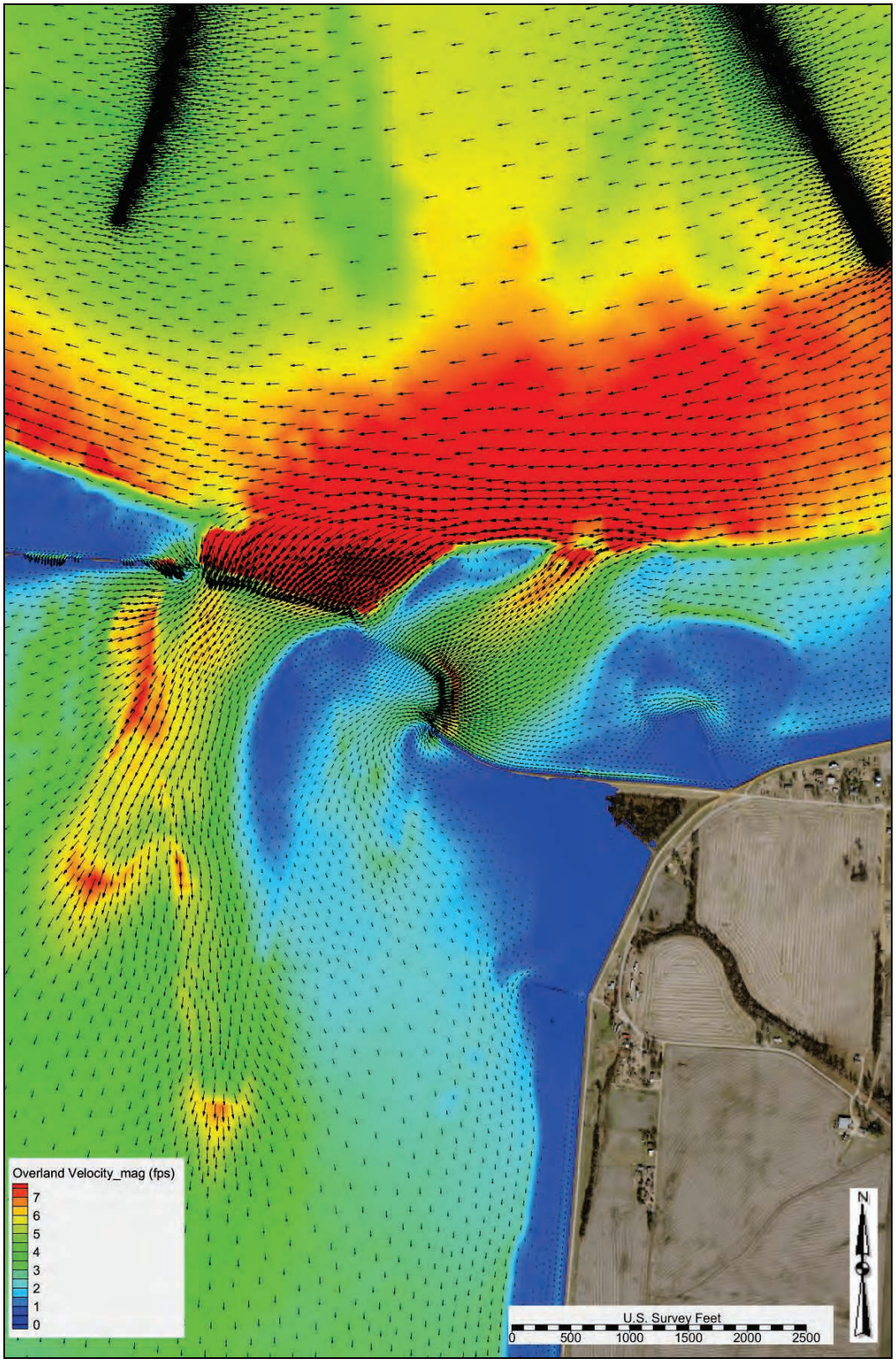


Figure 2-34. Base condition shear stress—1,900,000 cfs (study overbank).

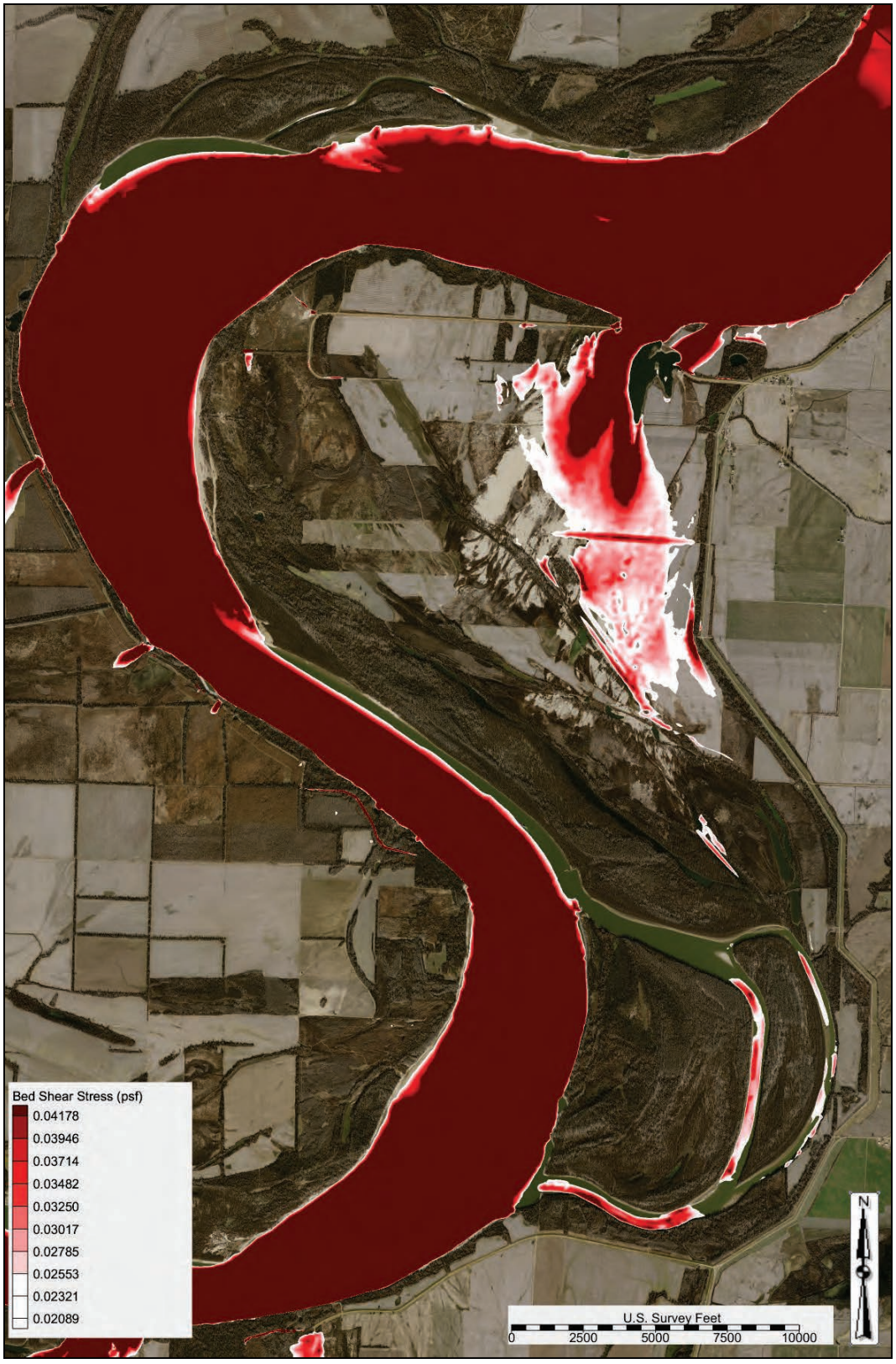
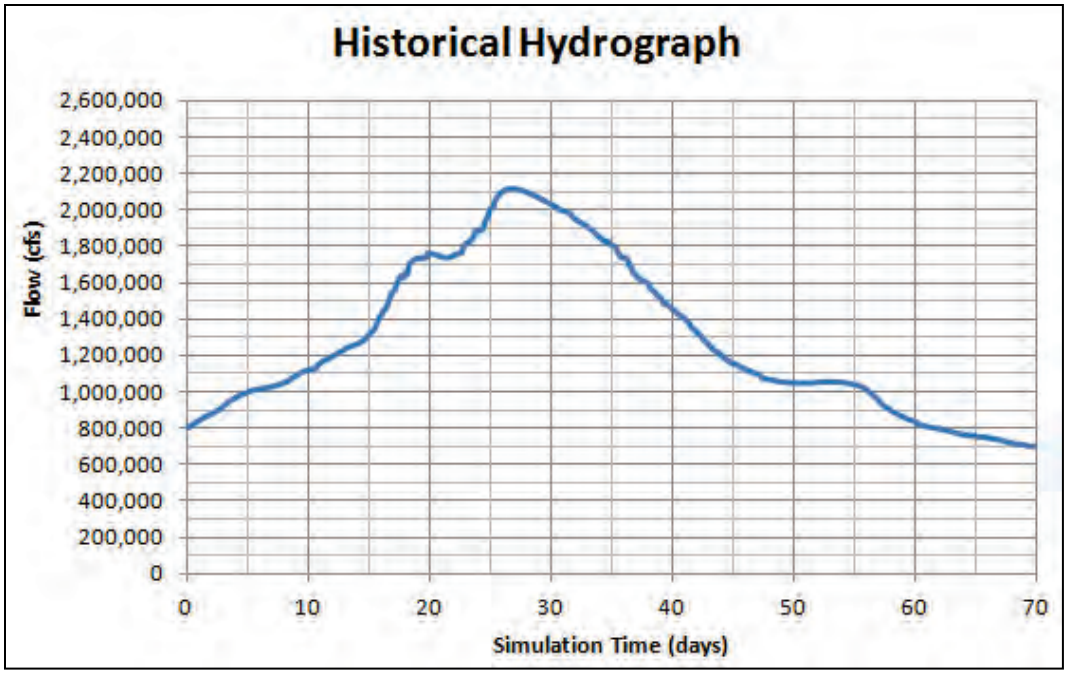


Figure 2-35. Historical event inflow hydrograph.



The bed displacement output from the Historical Hydrograph simulation for the study overbank modeled as a noncohesive soil type is depicted in Figure 2-37. This simulation assumed that the study overbank had a noncohesive top soil layer across the entire Island 13 overbank. A noncohesive overbank simulation was performed to estimate overbank scour progression if the cohesive top soil layer did not exist completely and uniformly across the Island 13 overbank. A positive (+ value and blue color) bed displacement represented aggradation (deposition) and a negative (- value and red color) bed displacement represented degradation (scour). Deposition is simulated in the main channel immediately downstream of the closure structure. Scour is simulated at the toe of the closure structure baffle, western and southern edge of the scour hole, eastern spur levee, and the toe of the Tiptonville-Obion River Levee. Significant additional scour (as compared to the cohesive simulation) was simulated in the overbank region immediately to the east of the closure structure, which would have the potential to flank and fail the closure structure.

Figure 2-36. Base condition bed displacement cohesive overbank—Historical Hydrograph.

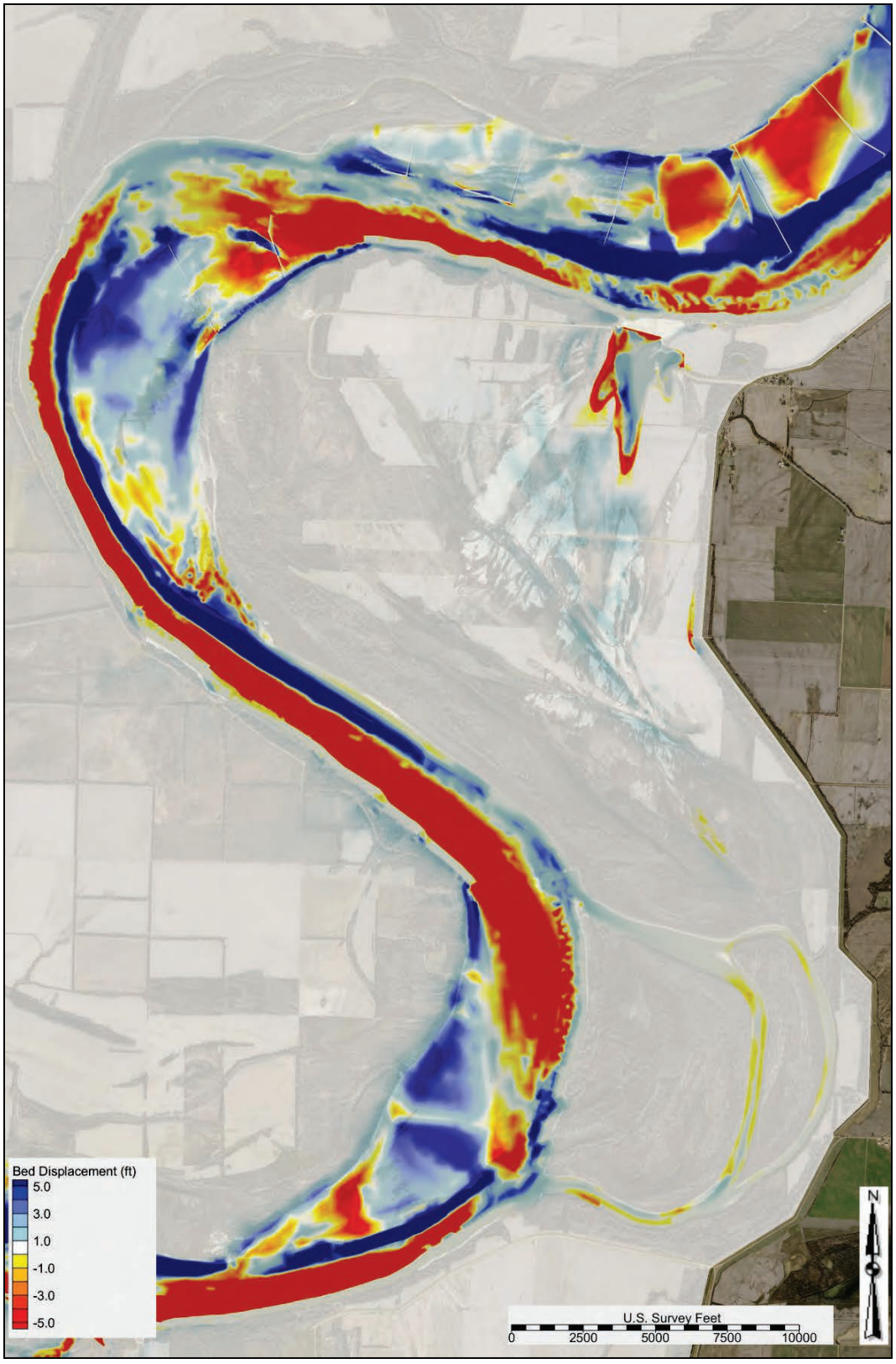
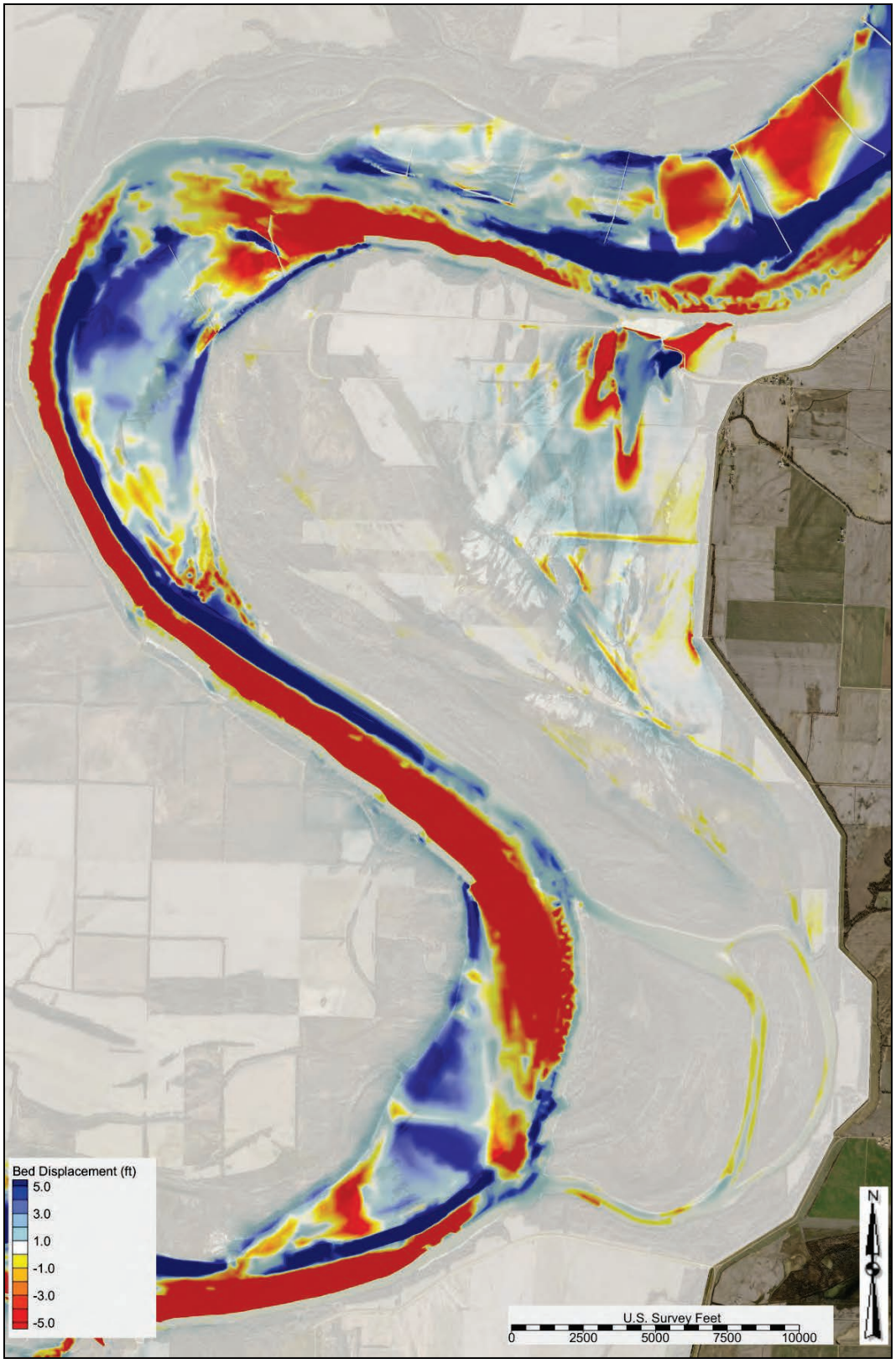
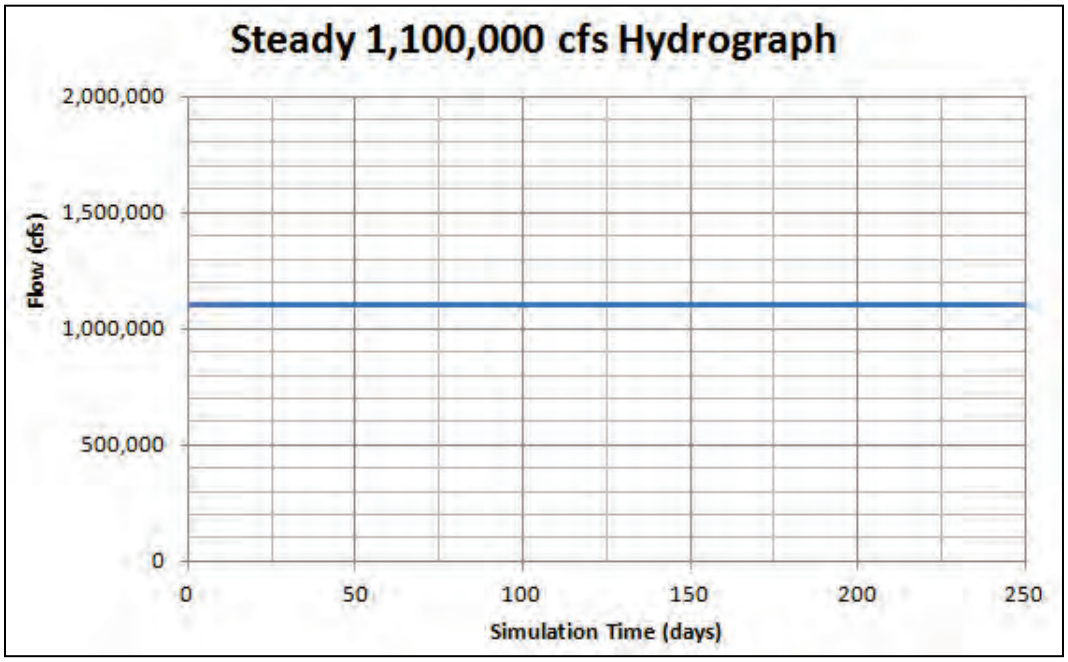


Figure 2-37. Base condition bed displacement noncohesive overbank—Historical Hydrograph.



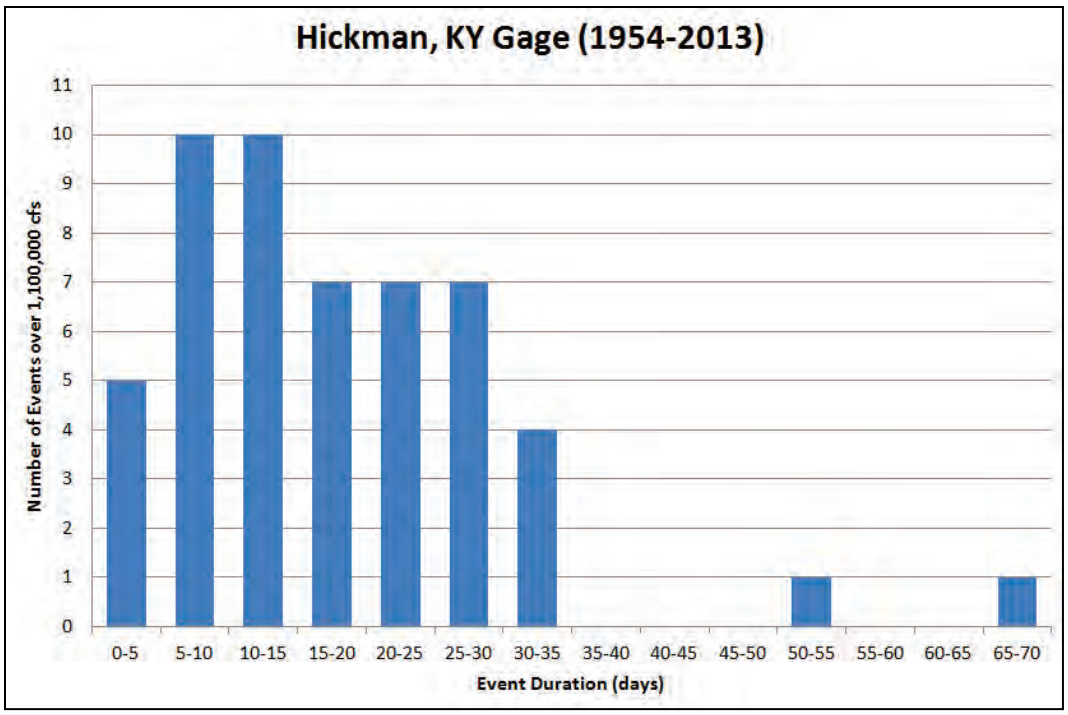
Scenario simulations were performed utilizing a long-duration hydrograph with a steady 1,100,000 cfs. The 1,100,000 cfs flow had a magnitude much less than the 2011 peak flow (2,100,000 cfs) but still diverted flow through the Island 13 overbank. The long-duration hydrograph at the upstream boundary condition for the AdH model is depicted in Figure 2-38. The Steady 1,100,000 cfs Hydrograph was simulated for a duration of 250 days.

Figure 2-38. Long-duration inflow hydrograph.



A duration analysis was performed at the Hickman, KY, gage to determine how often the flow of 1,100,000 cfs had been exceeded. Figure 2-39 depicts the results of the independent events that exceeded 1,100,000 cfs for 1 or more consecutive days from 1954 to 2013. From 1954 to 2013 there were 52 independent events that exceeded 1,100,000 cfs. From 1954 to 2013 there were 910 days that exceeded 1,100,000 cfs. The longest duration of flow that exceeded 1,100,000 cfs was 66 days in 1973.

Figure 2-39. 1,100,000 cfs event duration histogram.



The bed displacement output from the long-duration hydrograph simulation for the study overbank modeled as a cohesive soil type is depicted in Figure 2-40. This simulation assumed that the study overbank had a cohesive top soil layer 10 ft thick across the entire Island 13 overbank. A positive (+ value and blue color) bed displacement represented aggradation (deposition) and a negative (- value and red color) bed displacement represented degradation (scour). Scour is simulated at the western and southern edge of the scour hole and at the toe of the Tiptonville-Obion River Levee.

The bed displacement output from the long-duration hydrograph simulation for the study overbank modeled as a noncohesive soil type is depicted in Figure 2-41. This simulation assumed that the study overbank had a noncohesive top soil layer across the entire Island 13 overbank. A noncohesive overbank simulation was performed to estimate overbank scour progression if the cohesive top soil layer did not exist completely and uniformly across the Island 13 overbank. A positive (+ value and blue color) bed displacement represented aggradation (deposition), and a negative (- value and red color) bed displacement represented degradation (scour). Significant additional scour (as compared to the cohesive simulation) was simulated at the western and southern edge of the scour hole, the overbank region to the south of the scour hole, and the toe of the Tiptonville-Obion River Levee.

Figure 2-40. Base condition bed displacement cohesive overbank—1,100,000 cfs, 250 days.

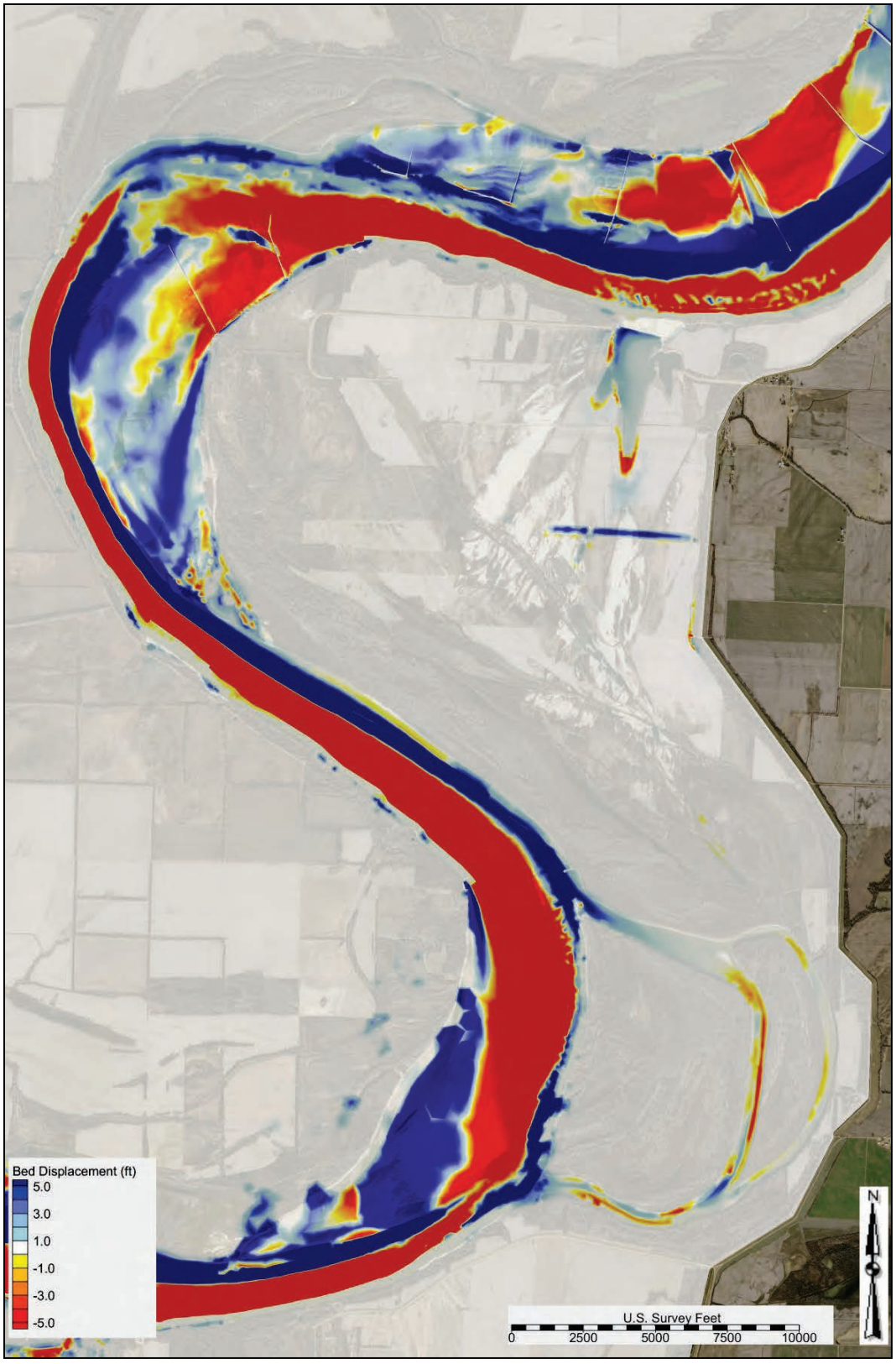
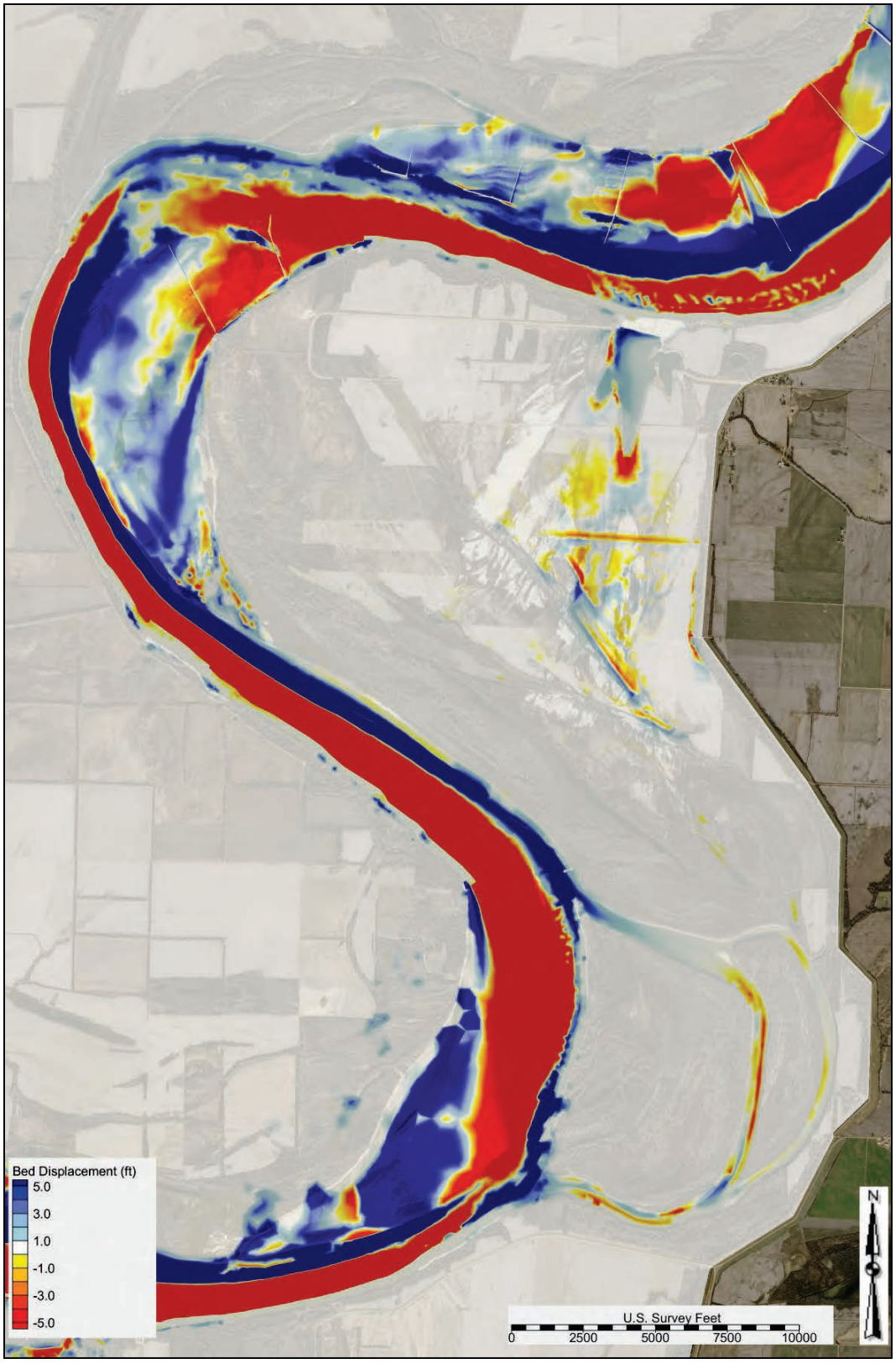


Figure 2-41. Base condition bed displacement noncohesive overbank—1,100,000 cfs, 250 days.



Appendix C contains the following detailed base condition scenario data from the Hypothetical Hydrograph simulation:

- velocity output at flows ranging from 400,000 to 2,100,000 cfs for the entire model domain, study overbank, and study crevasse (Figures C-41 through C-85)
- shear stress output at flows ranging from 900,000 to 2,100,000 cfs for the study overbank (Figures C-86 through C-92)
- WSEL profiles in the study reach for the following flows: 1,100,000 cfs, 1,500,000 cfs, 1,900,000 cfs, and 2,100,000 cfs (Figure C-93)
- WSEL map at 2,100,000 cfs that depicts super elevation and head differentials that exist in the study reach (Figure C-94).

Flow and sediment diversion analysis

An analysis was performed to determine the amount of flow and sediment diverted across the Island 13 overbank. Figure 2-42 depicts the flow percentage and sediment load percentage diverted across the Island 13 overbank from the main channel. The sediment load diverted is a smaller percentage than the flow diverted.

Figure 2-42. Base condition overbank diversion data.

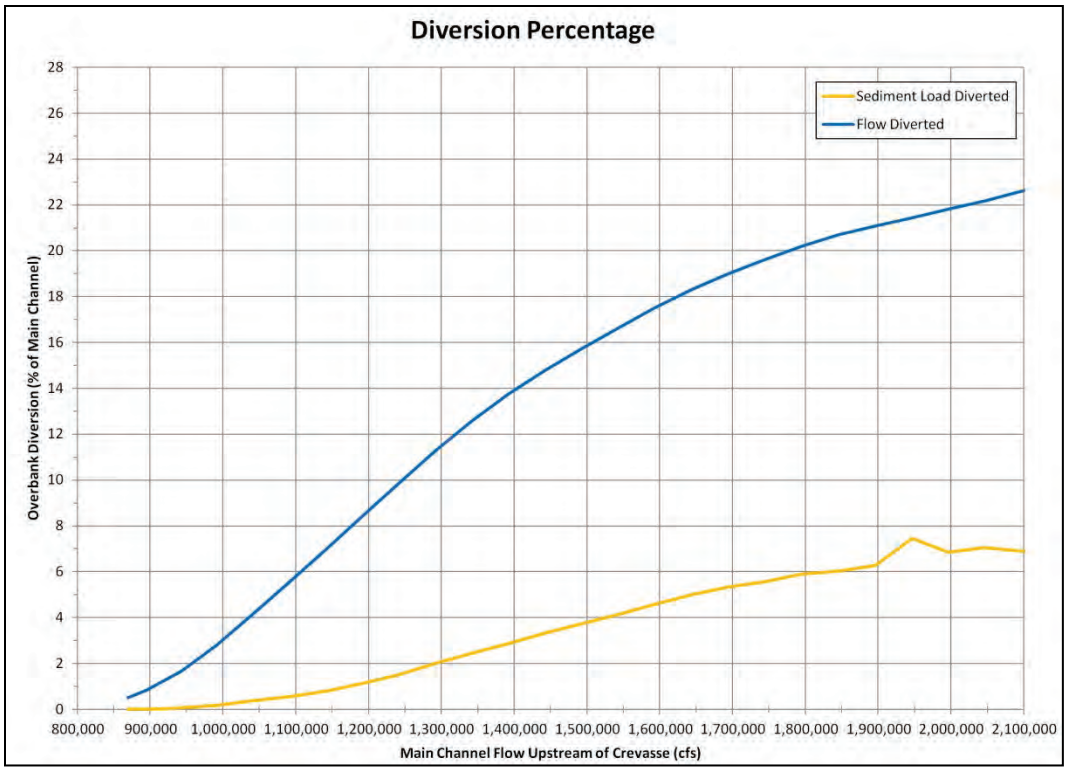
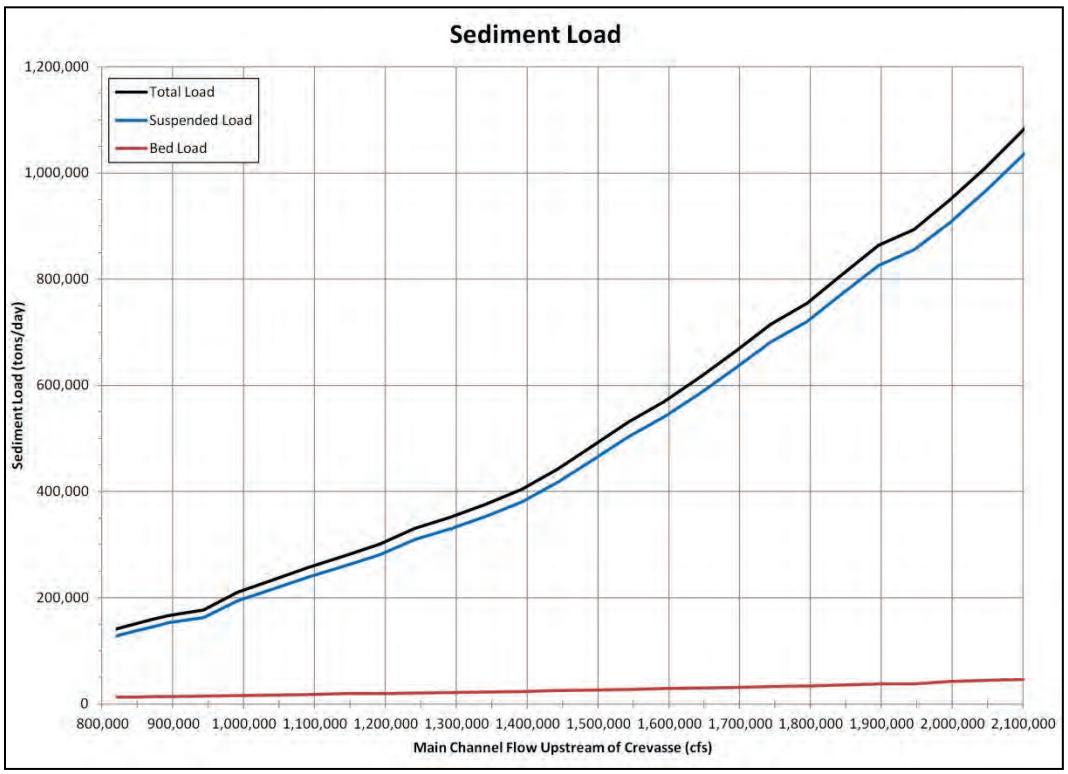


Figure 2-43 depicts the modeled total sediment load, suspended sediment load, and bed load in the Mississippi River upstream of the crevasse. The suspended sediment load is a large percentage of the total sediment load being transported.

Figure 2-43. Base condition main channel sediment load upstream of crevasse.



Depicted in Figure 2-44 is the diversion sediment load (tons/day) across the Island 13 overbank.

Appendix C contains the following detailed base condition scenario data from the Hypothetical Hydrograph simulation:

- sediment diversion grain size distribution for flows ranging from 870,000 to 2,000,000 cfs (Table C-1).

Water surface slope analysis

A water surface slope analysis was performed for the Island 13 diversion flow path. Depicted in Figure 2-45 is a comparison between the main channel flow path and Island 13 overbank flow path.

Figure 2-44. Base condition overbank sediment load.

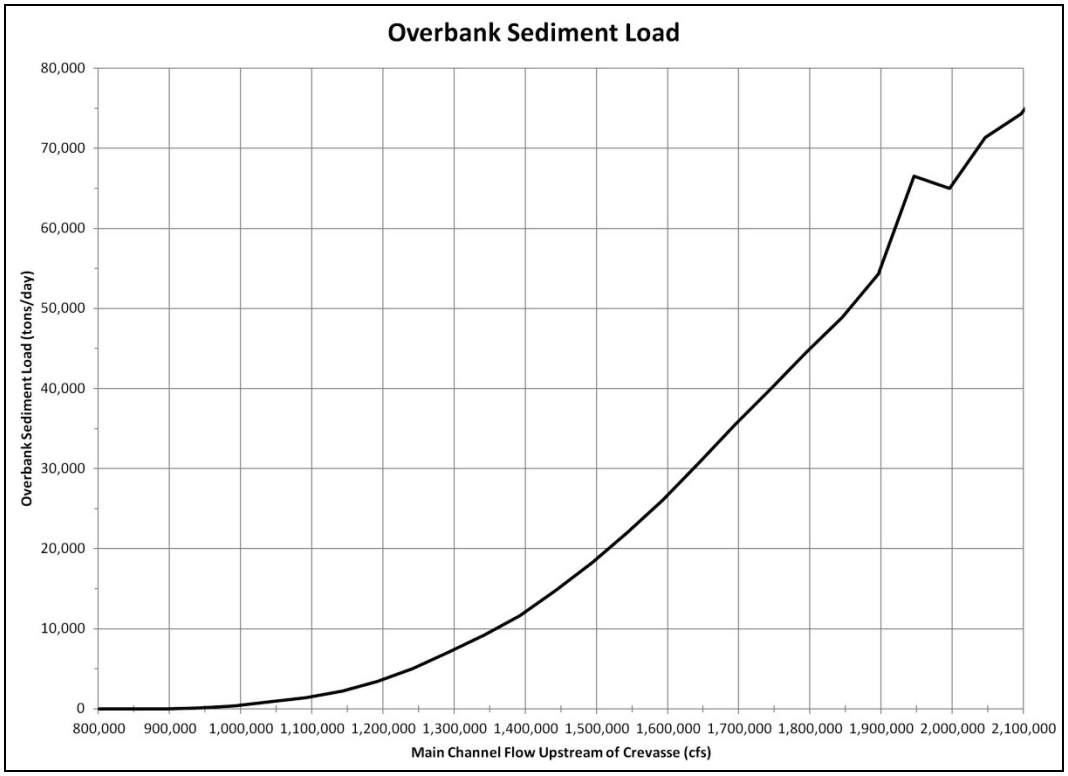


Figure 2-46 depicts the water surface slope of the main channel compared to the Island 13 overbank reach from 875,000 cfs to 2,100,000 cfs. The diversion overbank reach had a significantly greater water surface elevation slope than the main channel by approximately 0.2 ft/mile. This WSEL analysis was a reach-averaged method, meaning that the slope was computed from two common starting and ending locations for each respective flow path, and the local changes in slope that occurred between the starting and ending locations were not included.

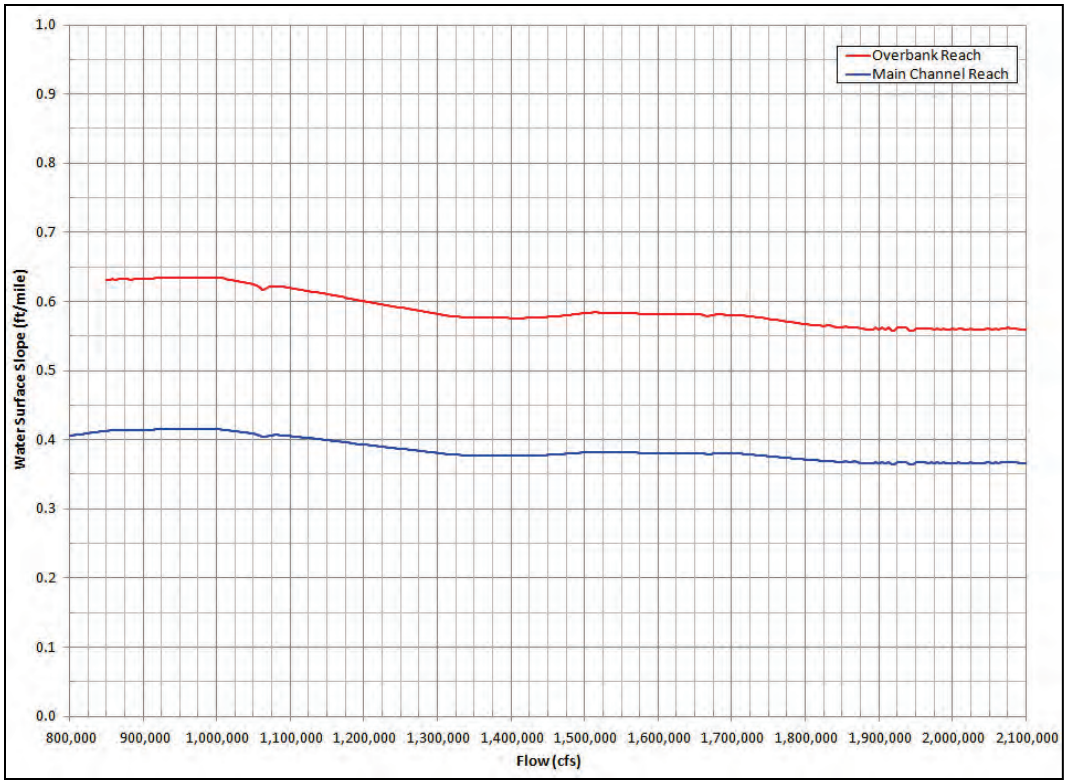
A detailed analysis of the water surface profile through the crevasse was performed. Figure 2-47 depicts the location of the transect through the crevasse for which the detailed water surface profile was investigated.

Depicted in Figure 2-48 are the detailed water surface profiles through the crevasse at flows ranging from 850,000 cfs to 2,100,000 cfs. Water surface slope and the head differential increase greatly across the closure structure above 1,000,000 cfs and continue to increase as flows increase.

Figure 2-45. Average water surface slope flow paths.



Figure 2-46. Average water surface slope.



Key elevations and flows

Listed in Table 2-14 are reference elevations, gage heights, and main channel flow for four flow conditions at the crevasse location. Gage heights are listed at Tiptonville, TN, and Caruthersville, MO. WSELs are listed at the closure structure, Tiptonville gage, and Caruthersville gage. The closure structure is overtopped when the main channel flow reaches approximately 662,000 cfs. The Island 13 overbank diversion flow commenced when the main channel flow upstream of the crevasse reached 858,000 cfs. These values were computed from the Hypothetical Hydrograph simulation. Future events that occur will have different hydrologic loading conditions (different combinations of upstream flow, downstream tailwater, and local inflow) that will produce WSELs and gage heights other than those produced from the Hypothetical Hydrograph simulation.

Figure 2-47. Crevasse WSEL transect location.

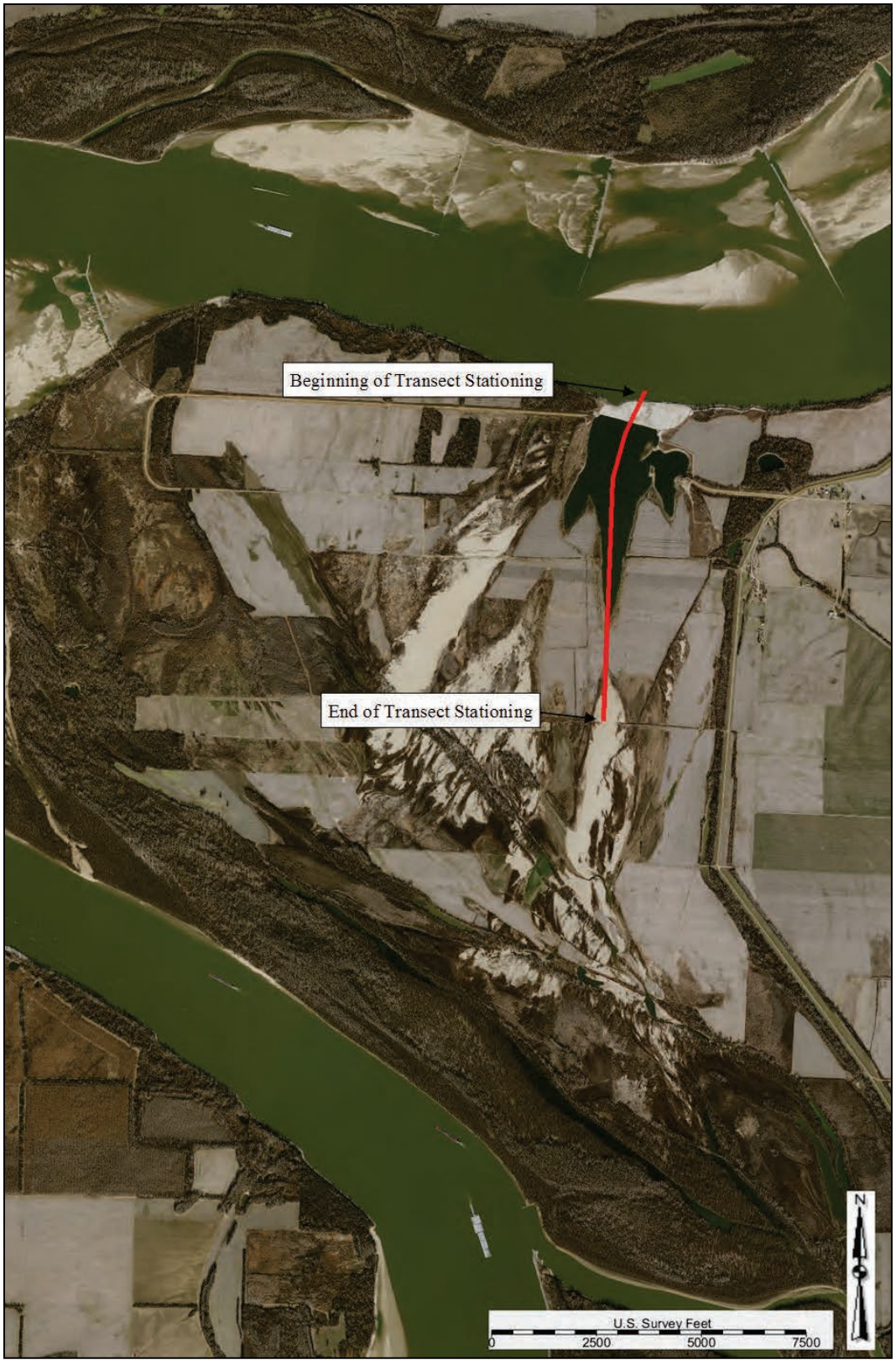


Figure 2-48. Crevasse WSEL profile.

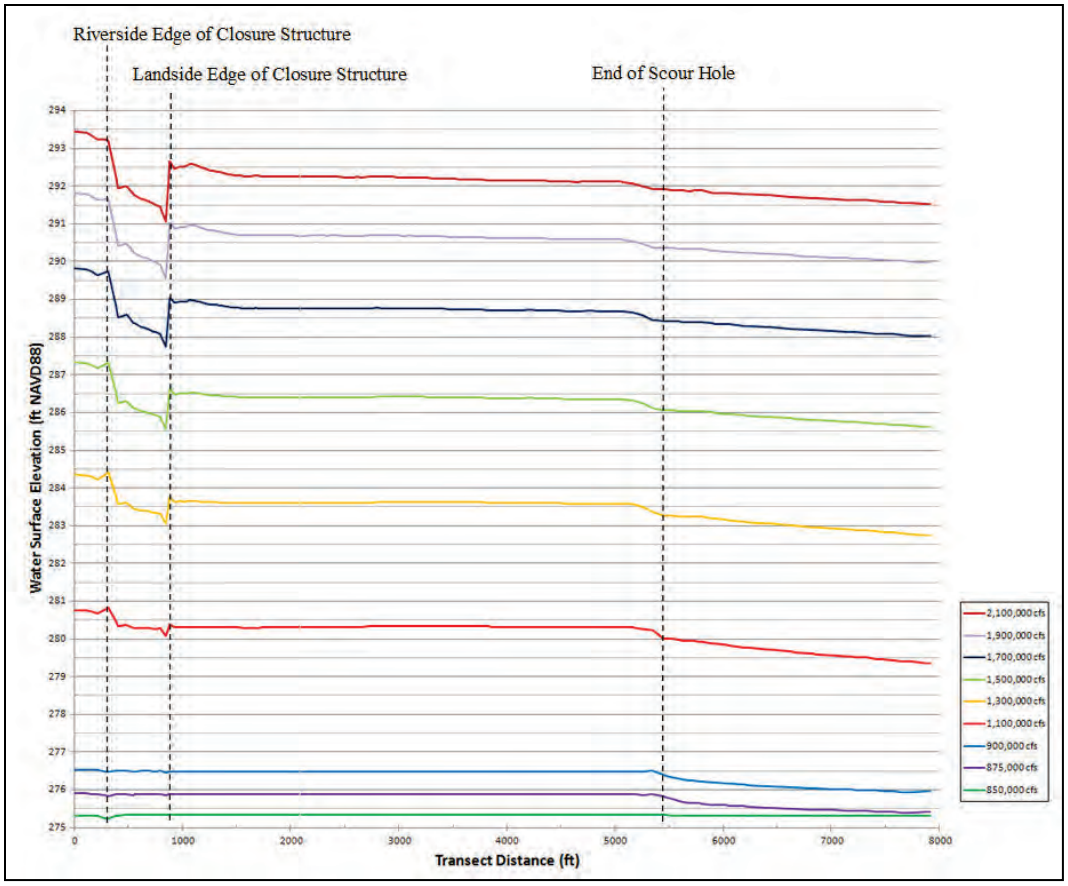


Table 2-14. Base condition key flows and elevations.

Flow Condition	Main Channel Flow (cfs)	Closure Structure WSEL (ft NAVD88)	Tiptonville Gage WSEL (ft NAVD88)	Tiptonville Gage Stage (ft)	Caruthersville Gage WSEL (ft NAVD88)	Caruthersville Gage Stage (ft)
Overtops closure structure	662,000	269.7	270.9	25.6	260.4	24.8
Overtops scour hole	746,000	272.5	273.4	28.1	262.6	27.0
Overtops overbank road	853,000	275.4	276.3	31.0	265.1	29.5
Overbank diversion flow commences	858,000	275.5	276.4	31.1	265.2	29.6

Note: Flows are rounded to the nearest 1,000 cfs. Elevations are rounded to nearest tenth.

One-dimensional (1D) Modeling Analysis

The following sections detail the base condition HEC-6T model.

Model description

HEC-6T was utilized to investigate long-term (years to decades) hydrodynamic and sediment conditions in study reach conditions.

Geometry development

Additional cross sections from Tiptonville, TN (RM 872.4), to Caruthersville, MO (RM 846.4), were added to the study reach of the Mississippi River, and a new tributary was added representing the diversion flow that occurred through the Merriwether-Cherokee Island 13 overbank reach. Figure 2-49 depicts a schematic diagram of the HEC-6T geometry layout that contains the study modifications. Figure 2-50 depicts the geometry layout for the Merriwether-Cherokee Island 13 overbank reach.

Figure 2-49. HEC-6T geometry schematic.

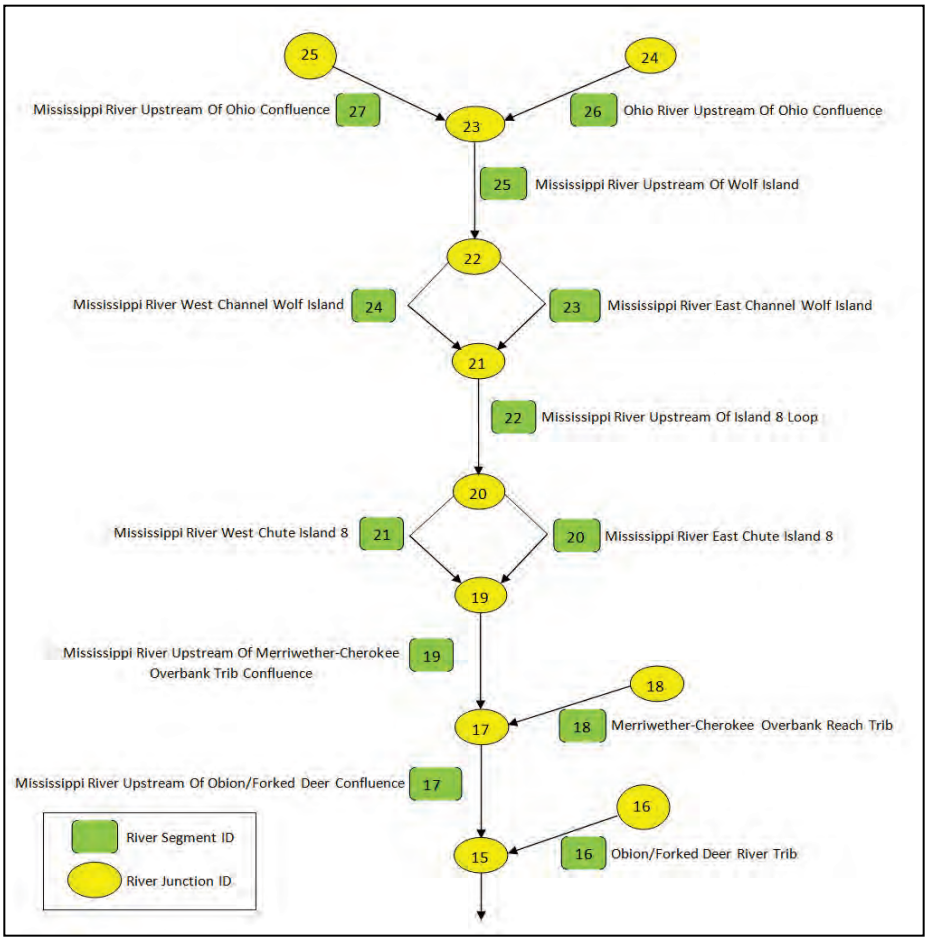
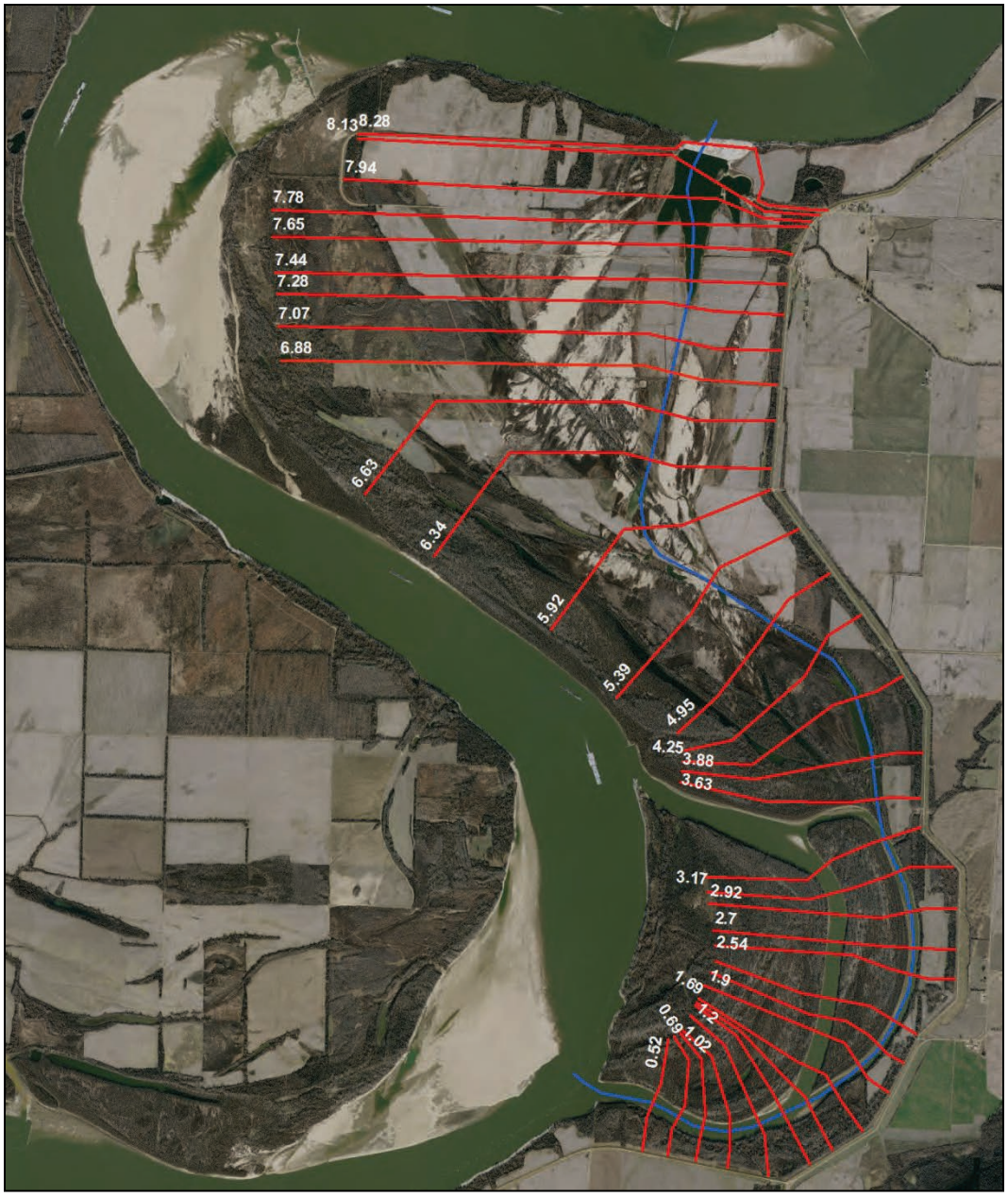


Figure 2-50. HEC-6T Merriwether-Cherokee overbank reach geometry.



Hydrodynamic calibration and validation

A continuous HEC-6T simulation was performed utilizing historical flow data from 1988 to 2010. The model was recalibrated due to the additional cross sections added to the study reach and the new tributary representing the study overbank. The model was calibrated to 1993 and 2004 historic stage data and hydrographic surveys of the bed profile. The model was validated to 2010 stage data and hydrographic surveys of the bed profile. A HEC-6T index flow analysis was conducted at the Hickman, KY, gage (RM

922.0) to further confirm model calibration. The HEC-6T index flows were selected to match the flow utilized in the specific gage analysis. Appendix C contains detailed calibration and validation data.

Boundary condition development

The flow and sediment diversion rating curves utilized for the Merriwether-Cherokee /Island 13 overbank reach in the HEC-6T model were developed from the AdH model simulations. A minimum flow of 50 cfs was required for numerical stability, which was maintained for the model simulation of the Merriwether-Cherokee/Island 13 overbank tributary. Erosion limits for the overbank reach were developed from historical 2011 flood imagery that depicted the active flow conveyance regions.

Historic daily flow data from 1 Oct 1990 to 31 Dec 2011 were repeated (looped back to back) to create a long-duration hydrograph of 20,000 days (approximately 55 years). Figure 2-51 depicts the hydrograph utilized in HEC-6T for the long-duration simulation. The synthetic long-duration dataset contained two 2011 events within the approximately 55-year hydrograph.

Scenario simulation

Figure 2-52 depicts the initial and final (day 20,000 or approximately 55 years) Merriwether-Cherokee/Island 13 overbank reach bed profiles. The HEC-6T analysis estimated that the general Island 13 overbank reach would experience a bed lowering of approximately 15 ft. Note that this is based off of the synthetic long-duration hydrograph and assumed that the Island 13 overbank consisted of noncohesive bed sediment.

Figure 2-53 depicts Island 13 overbank cross sections thalweg elevations through the 55-year simulation. Figure 2-50 depicts the cross section IDs and their respective overbank locations. Section 7.94 is located in the scour hole, and the thalweg elevation remained relatively constant throughout the simulation. Sections located in the middle portion of the Island 13 overbank reach (ID 6.88 through 3.88) experienced extensive bed lowering.

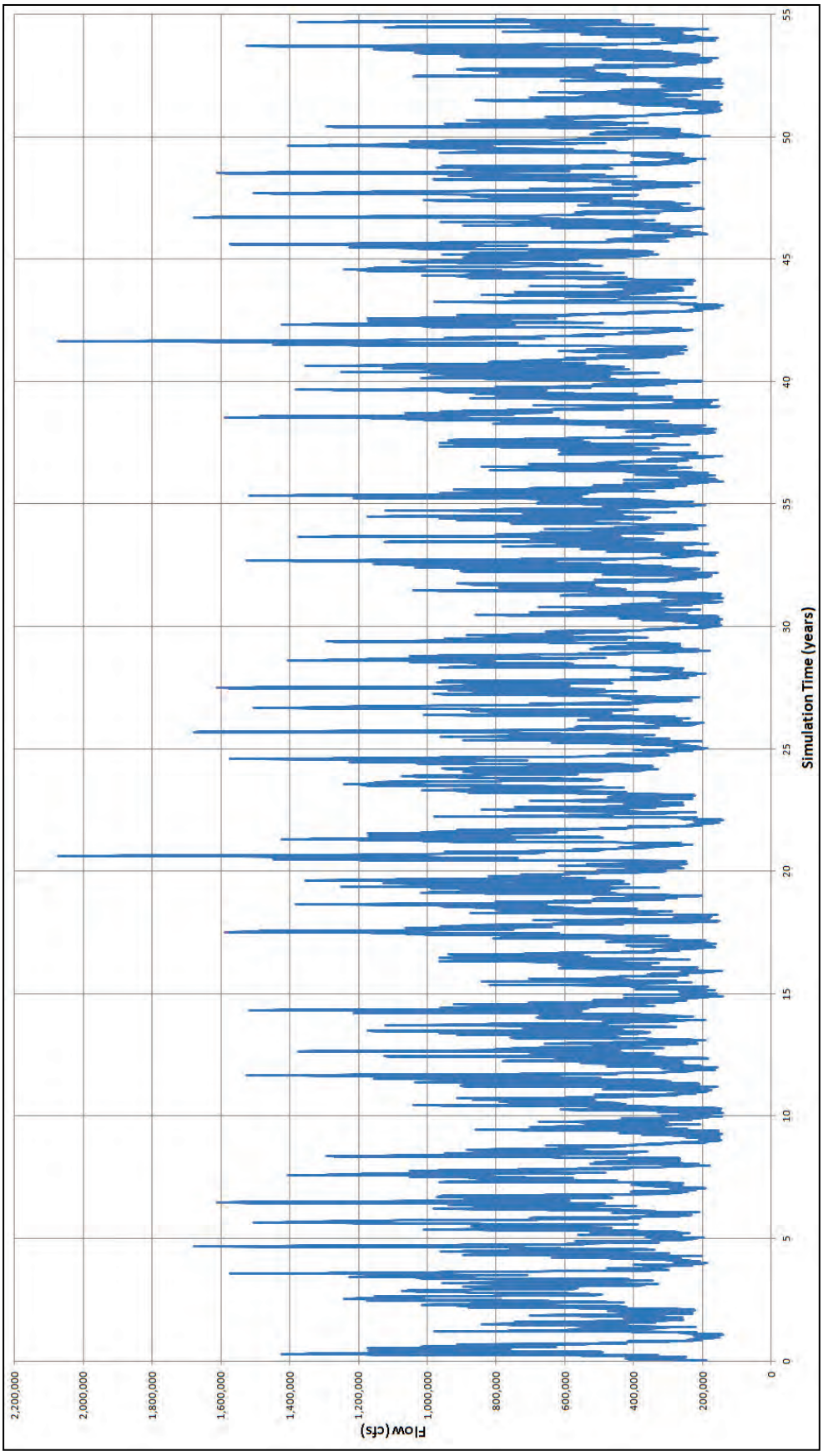


Figure 2-51. HEC-6T long-duration hydrograph.

Figure 2-52. HEC-6T base condition profile plot Island 13.

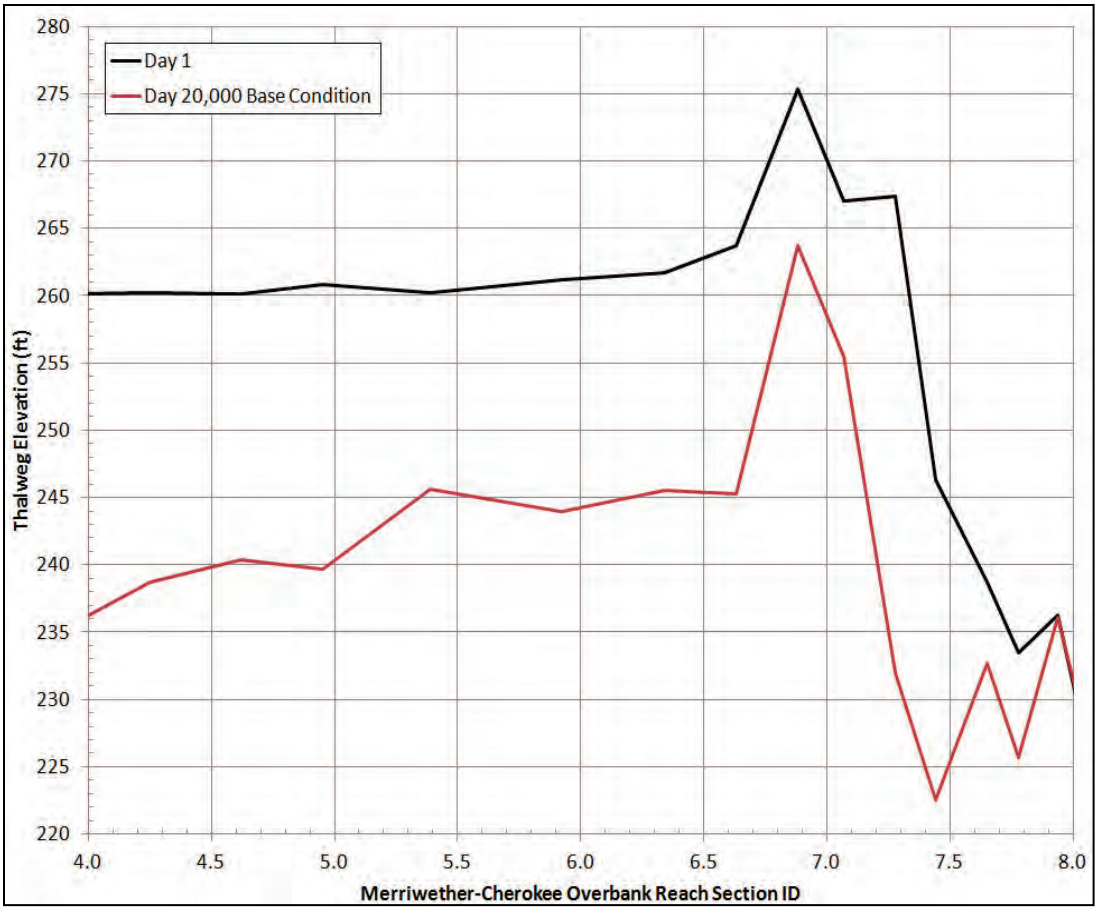
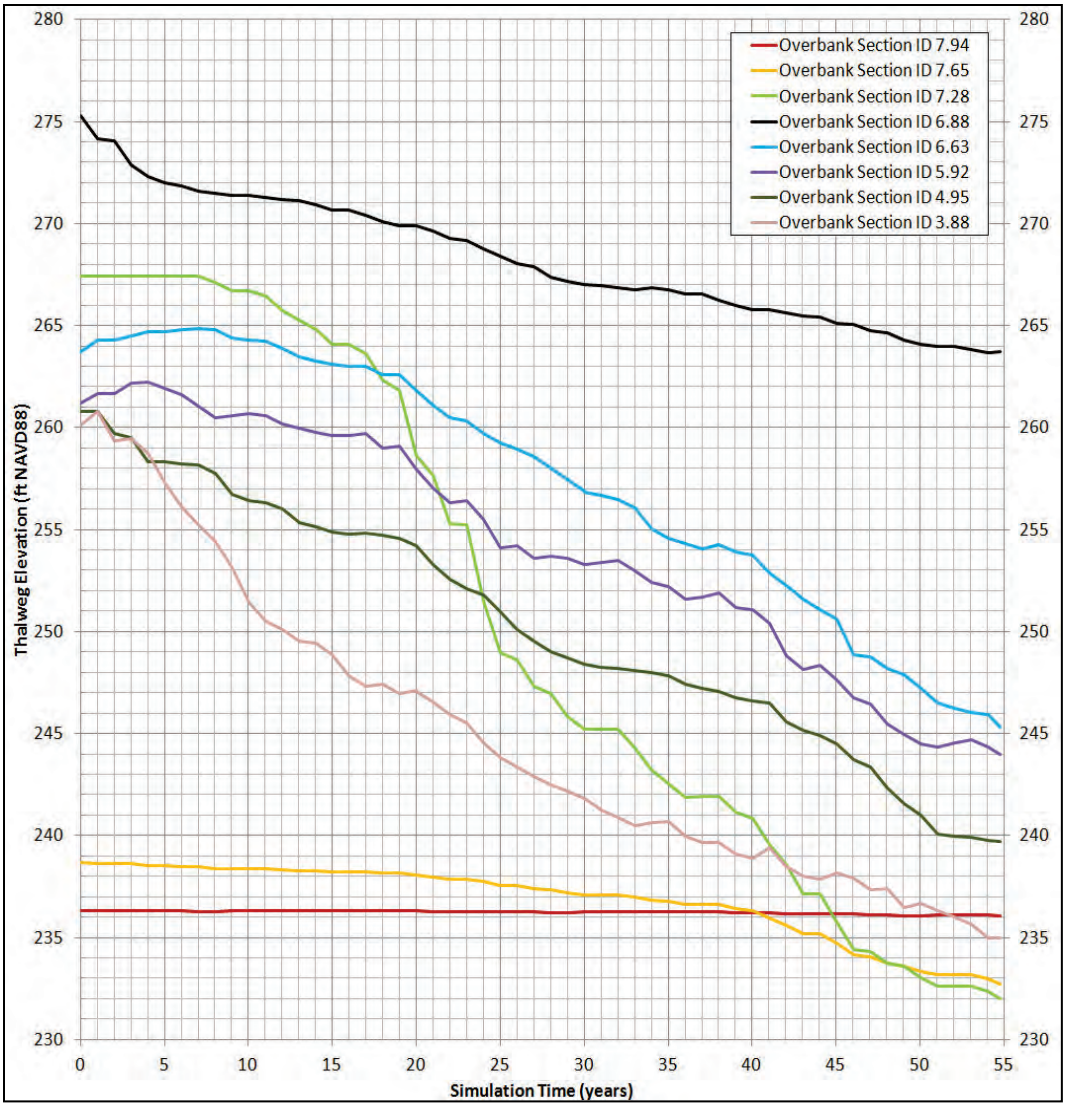


Figure 2-54 depicts the initial and final (day 20,000 or approximately 55 years) Mississippi River reach (RM 820–905) bed profiles. The HEC-6T analysis estimated that the main channel in locations both upstream and downstream of the crevasse would experience bed lowering in excess of 10 ft. Note that this is based off of the synthetic long-duration hydrograph. The bed lowering estimated at RM 857.5 is at the location where the cutoff flow rejoins the main channel flow.

Appendix C contains the following detailed base condition scenario data:

- HEC-6T index flow vs. specific gage plot at Hickman, KY (Figure D-1)
- calibration and validation cross-section analysis at four model locations (RM 846.40, RM 856.99, RM 864.76, and RM 870.2) for 1993, 2004, and 2010 (Figures D-2 through D-13).

Figure 2-53. HEC-6T base condition thalweg time series Island 13.



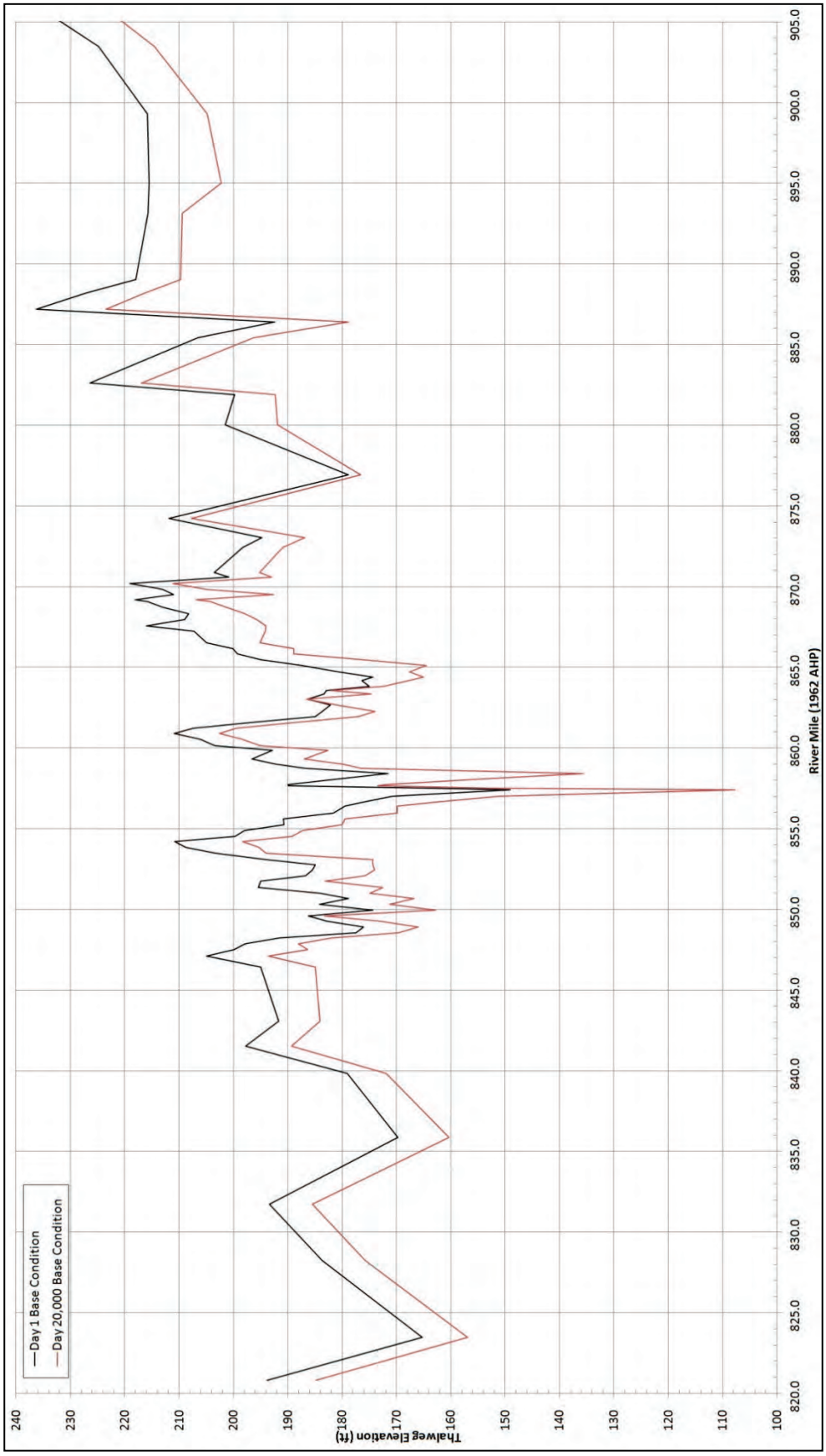


Figure 2-54. HEC-6T base condition profile plot main channel.

Risk assessment

An assessment was performed to determine the risk of cutoff formation and the risk of closure structure failure. A qualitative risk assessment was used based on the following three categories: minimal, moderate, and severe.

Cutoff formation

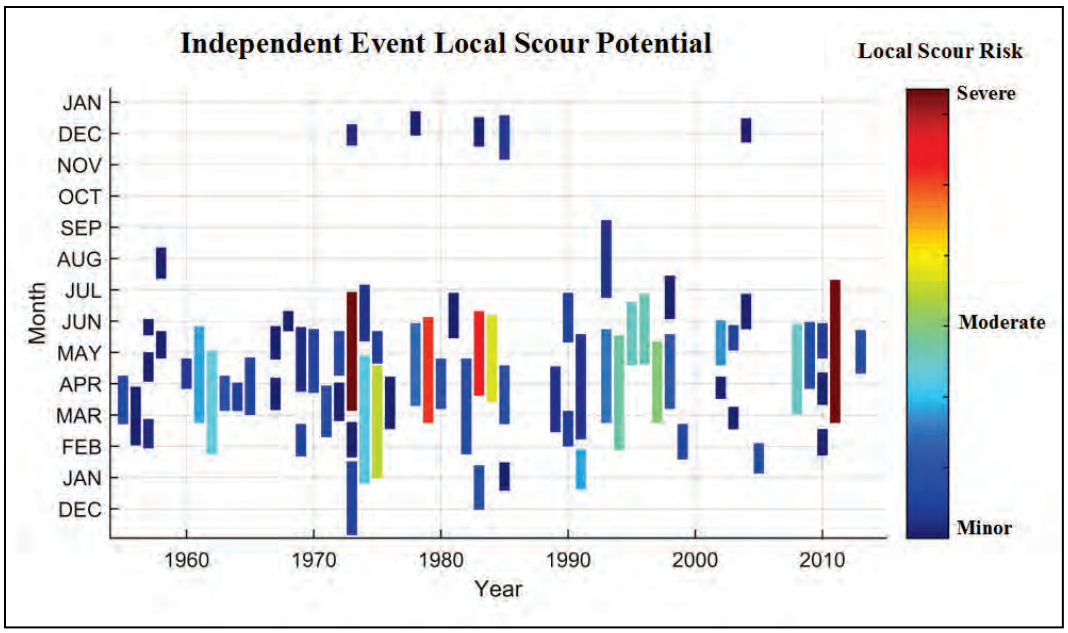
The analysis conducted on the base condition indicated that there is a moderate risk for cutoff formation. The short-term simulations (AdH) and the long-term simulations (HEC-6T) indicated a potential for overbank scour, bed lowering, and cutoff formation. Alternatives were investigated to mitigate the risk for cutoff formation. Section 3 of the report contains detailed descriptions and analysis of the alternatives.

Local scour potential

From the Historical Hydrograph AdH simulation, a relationship was developed between the main channel flow upstream of the crevasse and scour rate at the toe of the closure structure. A MATLAB script was created to estimate the cumulative scour potential for each independent high water event (flows that would overtop the closure structure) from a period record dataset. The potential scour estimate was generated by combining period-of-record flow data and the scour-to-flow relationship developed from the AdH analysis. This scour rate relationship was then applied to the period of record flow data from 1954 to 2013. Potential scour less than 5 ft was categorized as having minor scour risk. Potential scour that ranged from 5 to 15 ft was categorized as having moderate scour risk. Potential scour estimated in excess of 15 ft was categorized as having severe scour risk.

Figure 2-55 depicts the local scour potential at the closure structure for independent events from 1954 to 2013. The height of the bar (y-axis) represents event duration. Note that the 2011 flood (approximately 2,100,000 cfs peak) and the third peak of the 1973 flood (approximately 1,500,000 cfs peak) both resulted in a severe local scour potential at the closure structure. Note that several (greater than 15) events from the period of record analyzed estimate moderate or severe risk to the closure structure. The analysis conducted on the base condition indicated that there is a severe risk for local scour at the closure structure. Local scour countermeasures were investigated to mitigate the risk of closure structure failure. Section 4 of this report contains detailed descriptions and analysis of the local scour countermeasures.

Figure 2-55. Closure structure local scour potential.



Closure structure failure

AdH analysis was performed to investigate potential impacts if failure of the closure structure were to occur. Figure 2-56 depicts the mesh elevation (plan view) of the closure structure failure scenario. Figure 2-57 depicts the 3D mesh surface of the closure structure scenario.

Figure 2-58 depicts a comparison of the Island 13 overbank diversion flow between the base condition and a failure of the closure structure. Failure of the closure structure will increase the amount of flow diverted across the Island 13 overbank. It was estimated that diversion flow would increase by approximately 4% for a failure of the closure structure when the main channel flow is 2,100,000 cfs upstream of the crevasse.

Figure 2-59 depicts a comparison of the Island 13 overbank diversion sediment load between the base condition and a failure of the closure structure. Failure of the closure structure will increase the amount of sediment diverted across the Island 13 overbank. It was estimated that the diversion sediment load would increase by approximately 7% for a failure of the closure structure when the main channel flow is 2,100,000 cfs upstream of the crevasse.

Figure 2-56. Closure structure failure mesh elevation (study overbank).

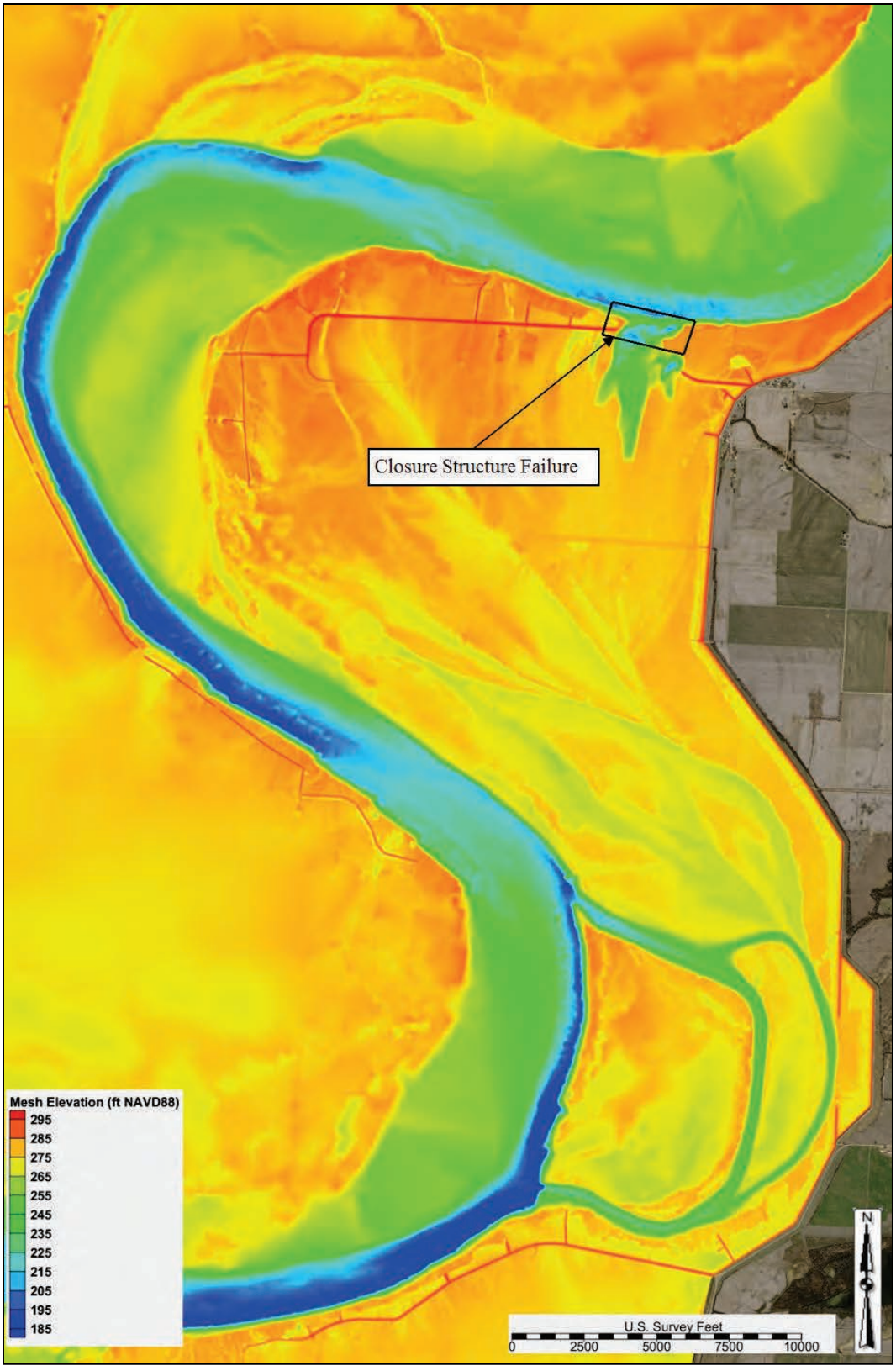


Figure 2-57. Closure structure failure 3d surface (study overbank).

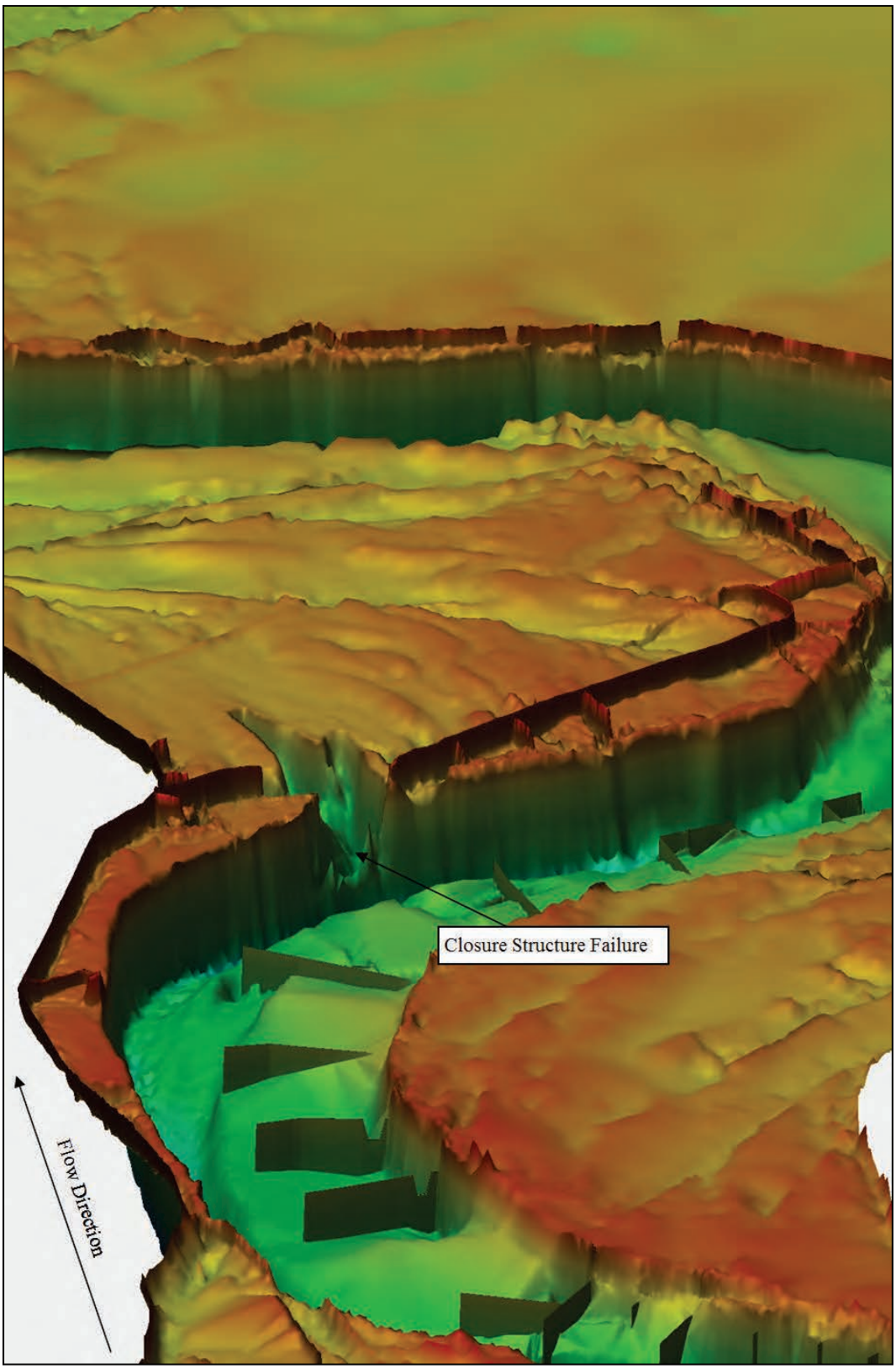


Figure 2-58. Closure structure failure overbank diversion flow.

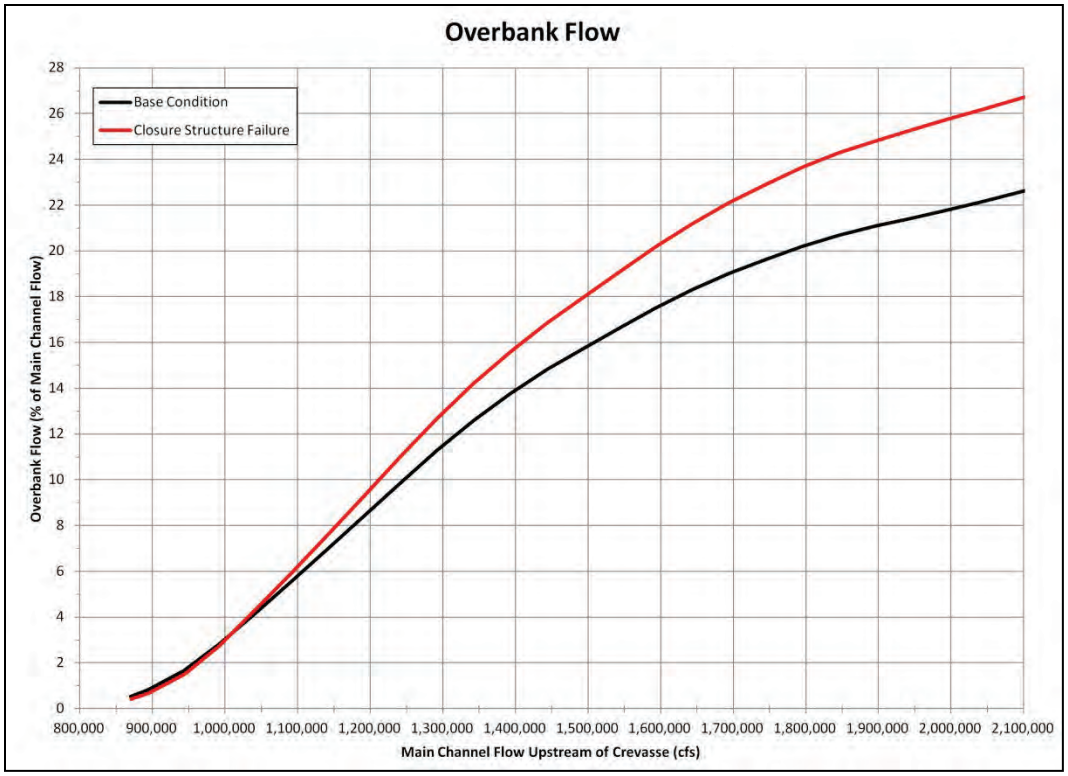
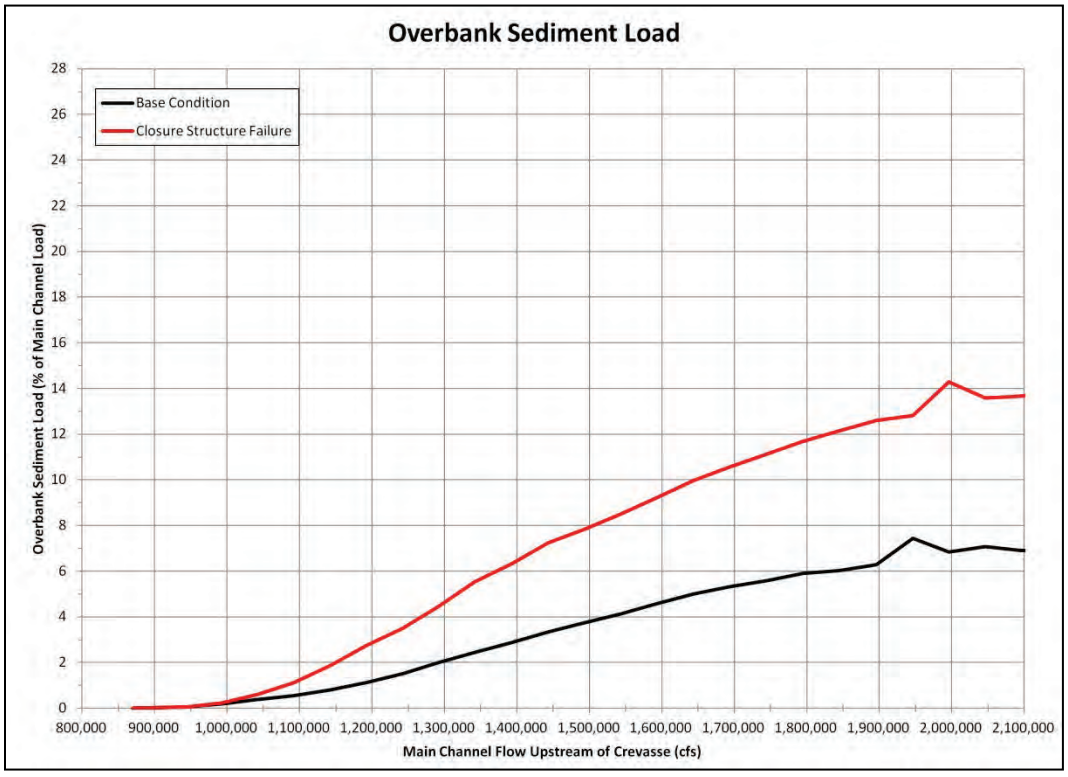


Figure 2-59. Closure structure failure overbank sediment diversion load.



The bed shear stress output at 1,900,000 cfs from the Hypothetical Hydrograph simulation for the closure structure failure scenario is depicted in Figure 2-60. Note the regions of high shear stress on the closure structure, western edge of the scour hole, overbank region south of the scour hole, overbank region immediately east of the closure structure, and at the toe of the Tiptonville-Obion River Levee.

The bed shear stress difference comparison between the closure structure failure and the base condition at 1,900,000 cfs from the Hypothetical Hydrograph simulation is depicted in Figure 2-61. A positive shear stress difference (+ value and red and orange) indicated that the failure of the closure structure increased shear stress. A negative shear stress difference (-value and blue) indicated that the failure of the closure structure decreased shear stress. A zero shear stress difference (zero value and white) indicated that the failure of the closure structure had no change on shear stress. Note that shear stress increased in the scour hole, at the perimeter of the scour hole, and at the toe of the Tiptonville-Obion River Levee.

Appendix C contains the following detailed closure structure failure scenario data from the Hypothetical Hydrograph simulation:

- shear stress output at flows ranging from 900,000 to 2,100,000 cfs for the study overbank (Figures C-95 through C-101)
- shear stress difference plots compared to the base condition output at flows ranging from 900,000 to 2,100,000 cfs for the study overbank (Figures C-102 through C-108)
- WSEL profiles in the study reach for the following flows: 1,100,000 cfs, 1,500,000 cfs, 1,900,000 cfs, and 2,100,000 cfs (Figure C-109)
- closure structure failure vs. base condition WSEL profiles for the following flows: 1,100,000 cfs, 1,500,000 cfs, 1,900,000 cfs, and 2,100,000 cfs (Figures C-110 through C-113)
- sediment diversion grain size distribution for flows ranging from 870,000 -2,000,000 cfs (Table C-2).

Figure 2-60. Closure structure failure shear stress—1,900,000 cfs (study overbank).

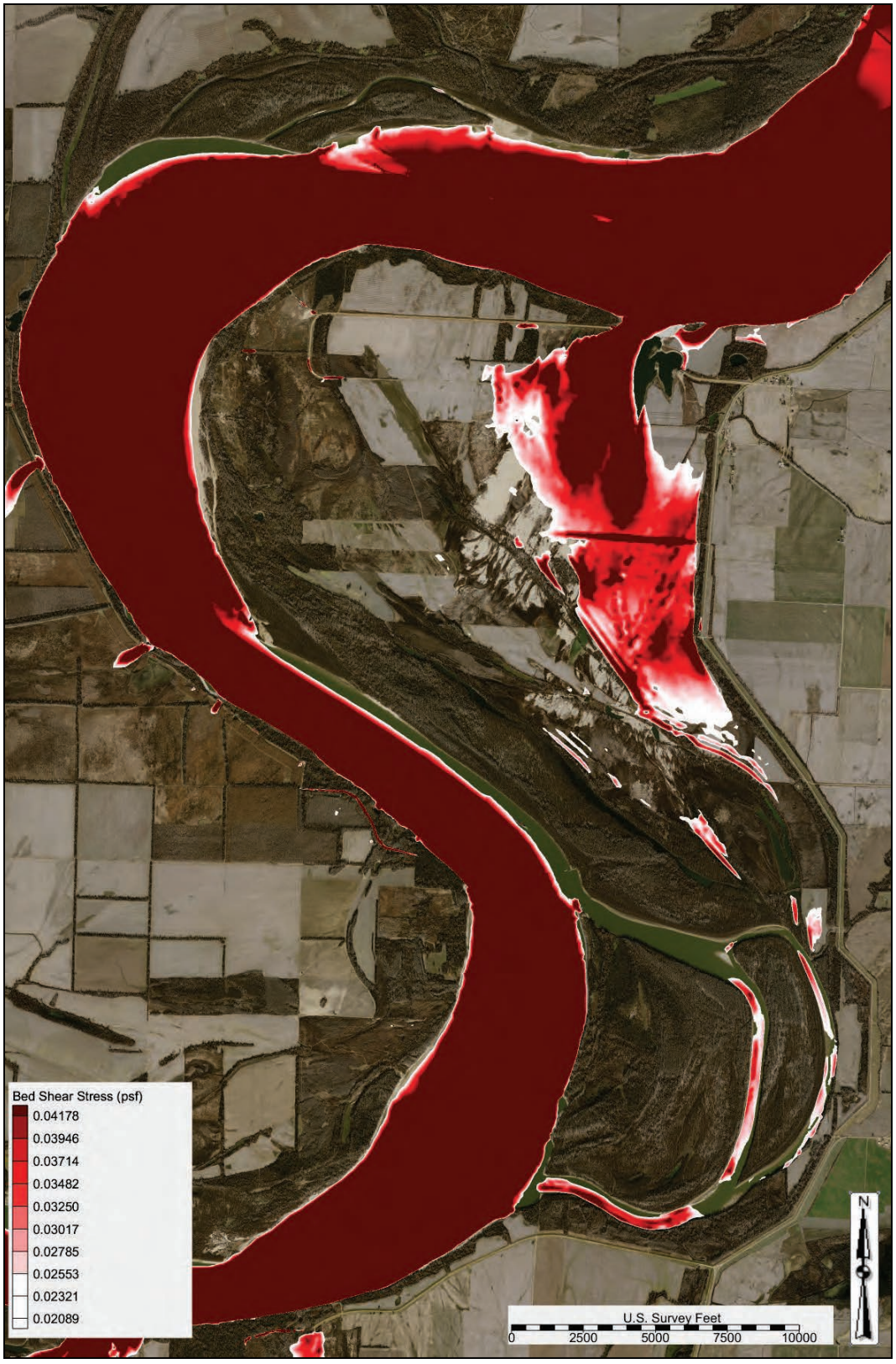
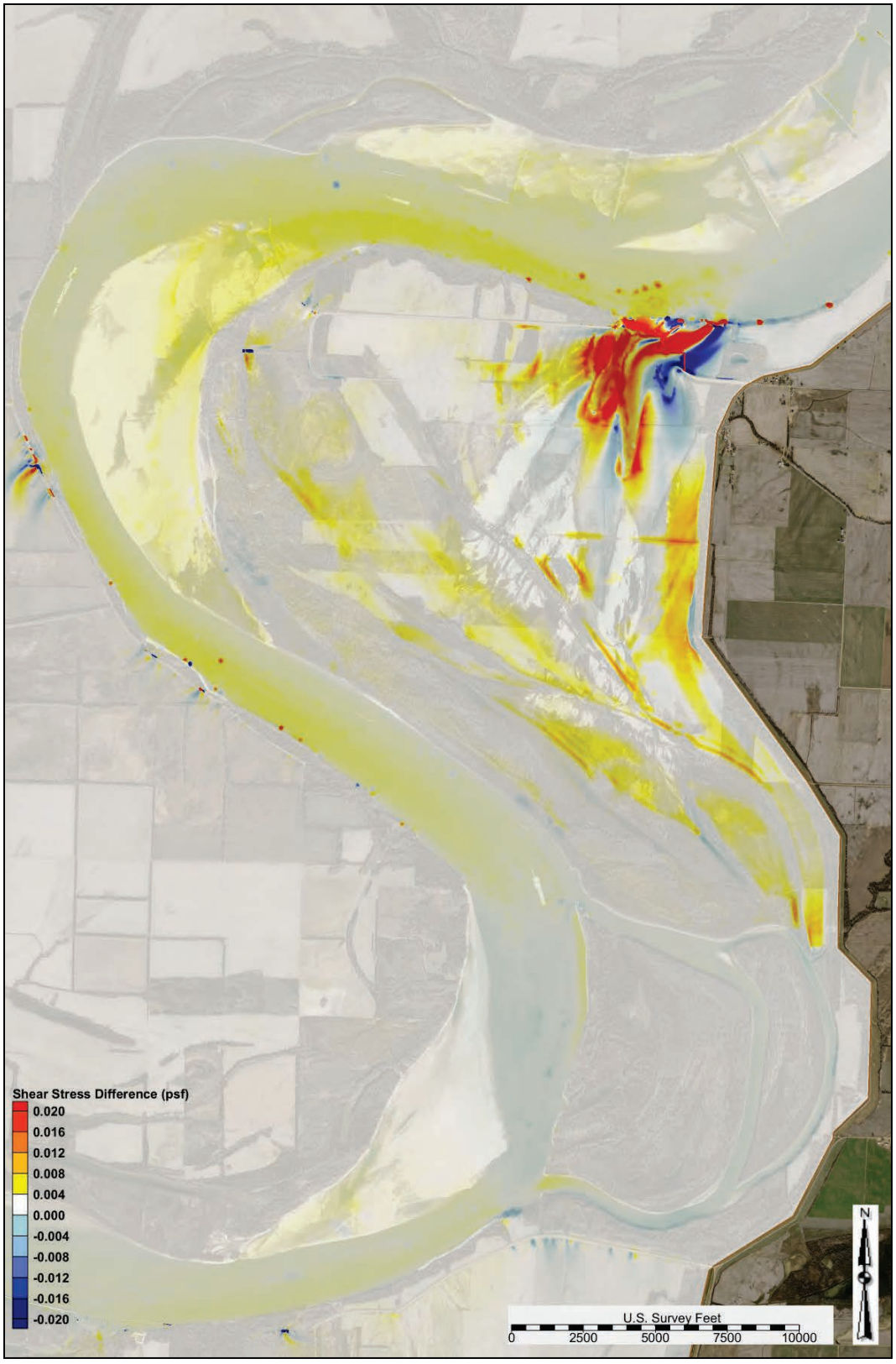


Figure 2-61. Closure structure failure shear stress difference—1,900,000 cfs.



Navigation assessment

The navigation assessment evaluated AdH and LOMA data.

Analysis

An AdH velocity vector analysis and a flow trace analysis were performed for flows ranging from 600,000 to 2,500,000 cfs. These analyses determined that a *zone of influence* existed at the crevasse location that potentially could produce outdraft currents at certain flows. Outdraft is defined as a condition whereby natural or man-induced crosscurrents develop in a river. Figure 2-62 depicts the zone of influence (shown as the magenta line) and the flow trace field at 2,400,000 cfs. Figure 2-63 depicts the zone of influence (shown as the magenta line) and the velocity vector field at 2,400,000 cfs.

AIS data was collected and analyzed from 17 Apr 2015 to 2 May 2015. During this collection period, flow overtopped the closure structure. Approximately 250 vessels transited the study reach during this collection period containing both upstream-bound and downstream-bound vessels. Figure 2-64 depicts the live plotter interface within LOMA that allowed for the real-time tracking of vessels.

Figure 2-62. Navigation zone of influence with flow trace at 2,400,000 cfs.

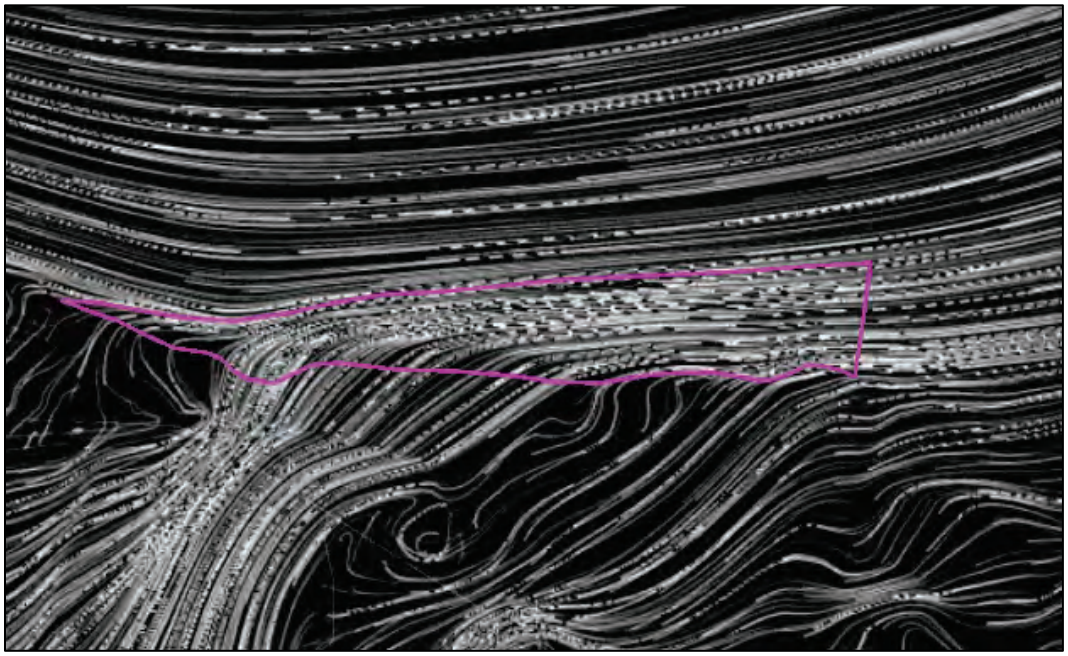


Figure 2-63. Navigation zone of influence with velocity field at 2,400,000 cfs.

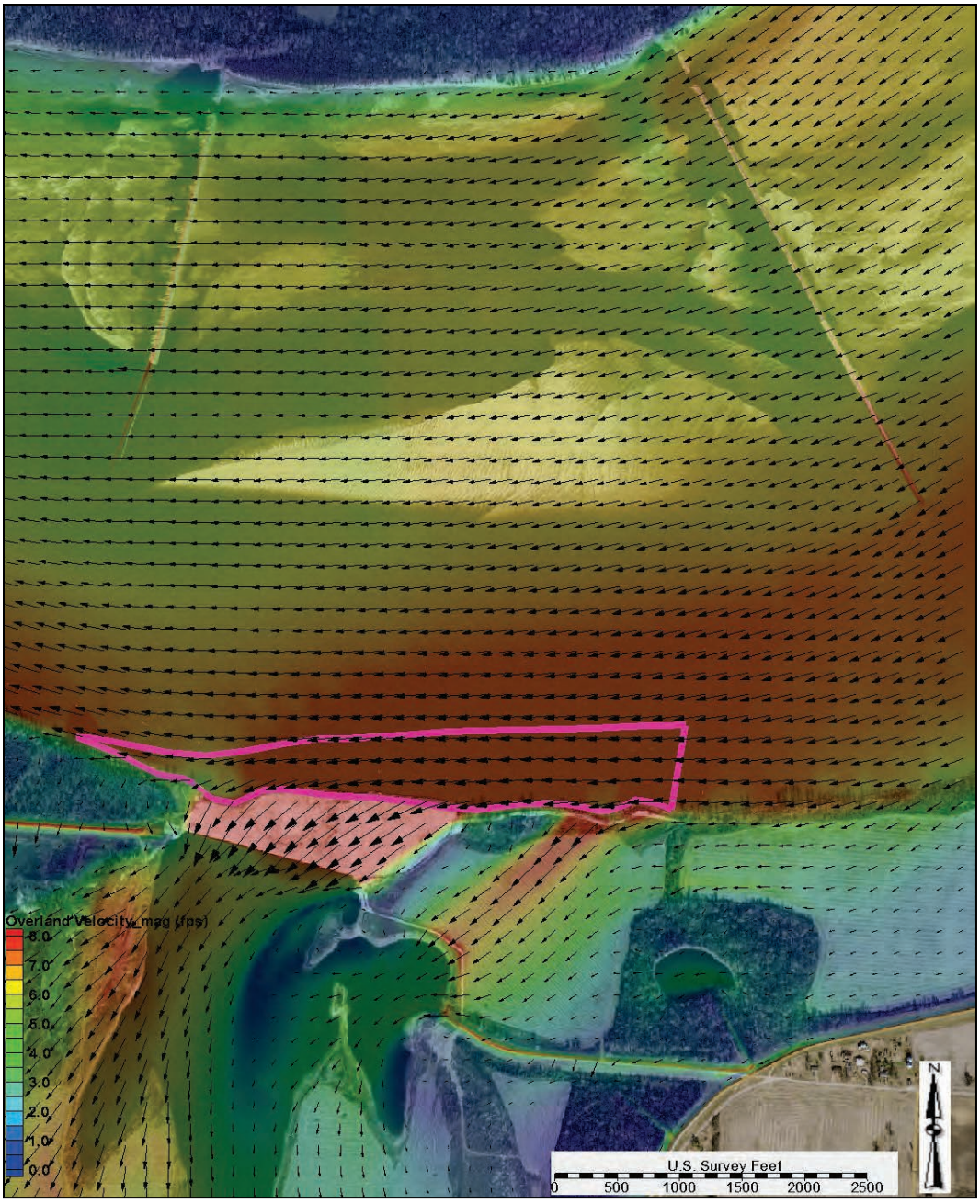


Figure 2-64. LOMA live plotter.

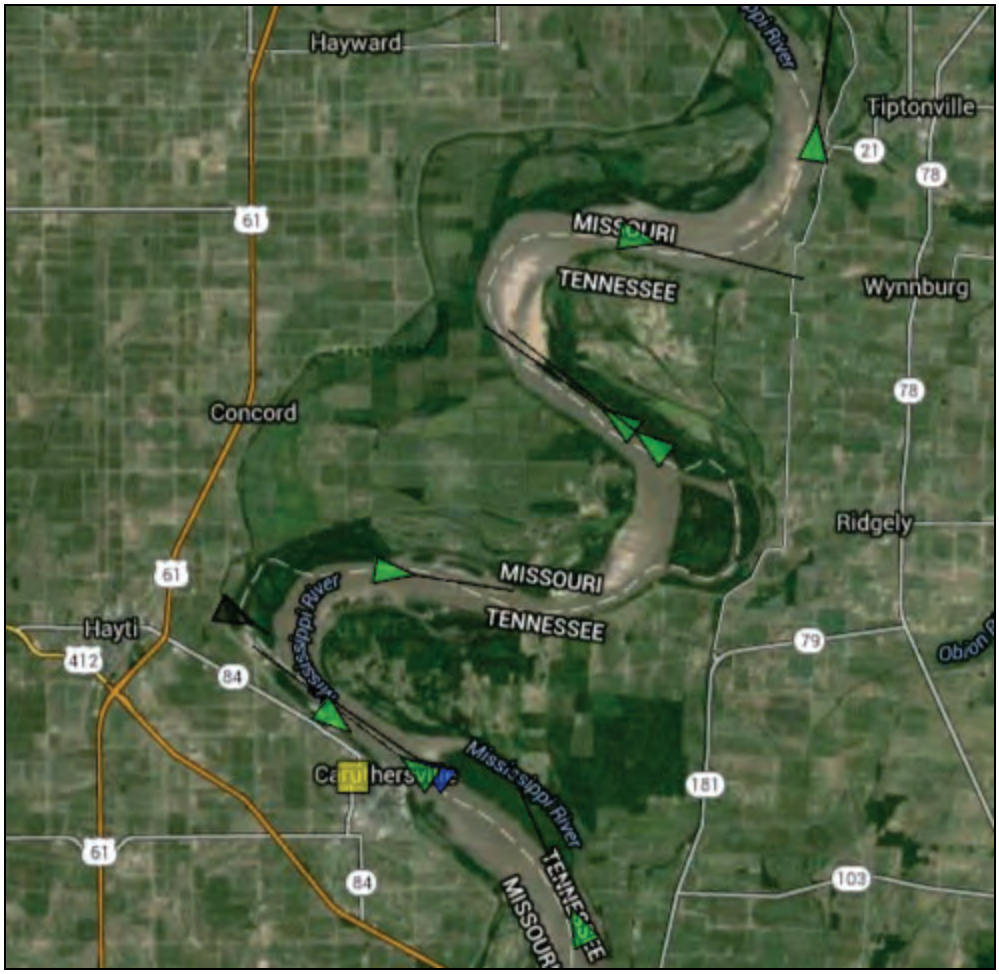


Figure 2-65 depicts the vessel tracks that were collected from 17 Apr 2015 to 2 May 2015 in the study reach. Note that the zone of influence is also depicted. During the collection period, an upstream-bound tow navigated too close to the descending left bank (into the zone of influence) and landed (grounded) on the closure structure due to a strong outdraft.

Figure 2-66 depicts the intensity map of the average downstream-bound (downbound) sailing line that was observed from 17 Apr 2015 to 2 May 2015. Note that the imagery is dated prior to the 2011 crevasse formation.

Figure 2-67 depicts the intensity map of the average upstream-bound (upbound) sailing line that was observed from 17 Apr 2015 to 2 May 2015. Note that the imagery is dated prior to the 2011 crevasse formation.

Figure 2-65. Study area vessel tracks.

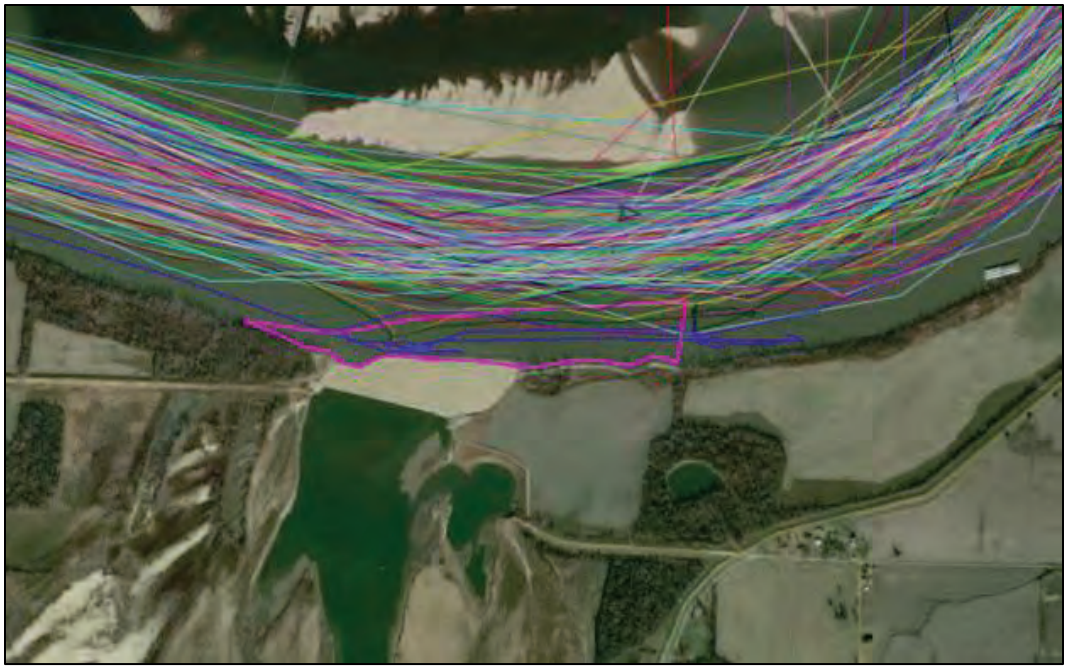
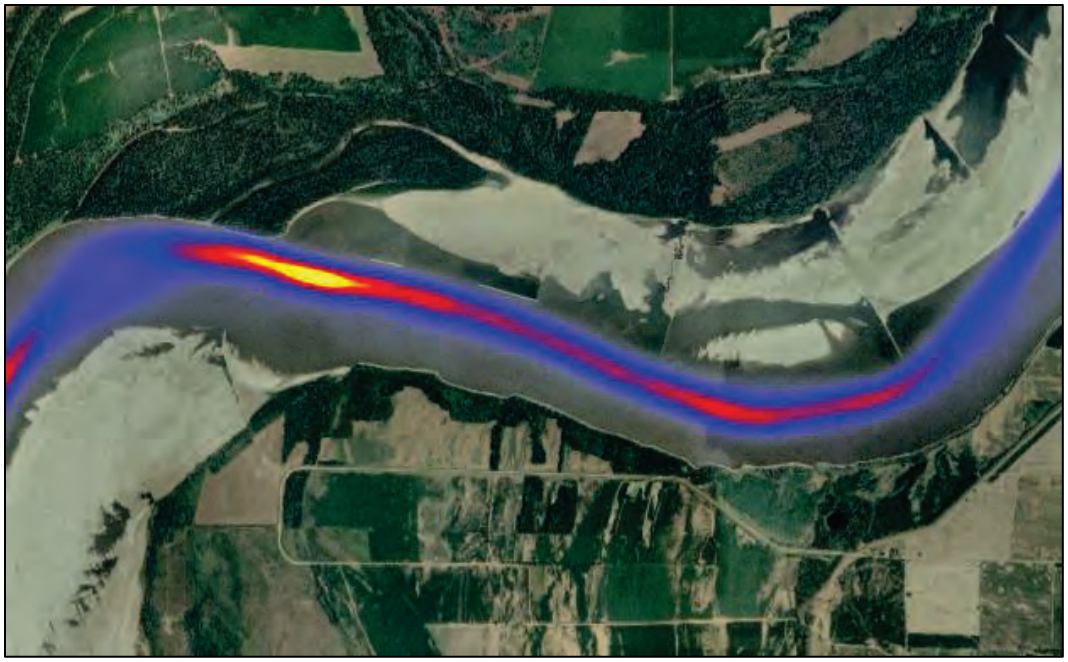


Figure 2-66. Downstream-bound vessel density map.



Figure 2-67. Upstream-bound vessel density map.



Conclusion

During flow events that overtop the closure structure and diversion flow commences (base condition analysis indicated approximately 858,000 cfs), there is the potential for an outdraft condition at the study crevasse.

The zone of influence is defined as the region where outdraft conditions may impact vessels. The zone of influence extended approximately 1,100 ft downstream from the western corner of the closure structure and extended approximately 1,800 ft upstream from the eastern corner of the closure structure. The zone of influence extends approximately 700 ft into the main channel from the top bank at the widest portion.

In the study bend (Merriwether-Cherokee bend RM 866–870) a distinct difference was observed in the vessel paths for upstream-bound and downstream-bound traffic. Downstream-bound vessel traffic favored the left descending bank, and upstream-bound vessel traffic favored the right descending bank for the Merriwether-Cherokee bend.

3 Alternatives

Alternatives were investigated to mitigate the risk for cutoff formation. To develop alternatives, meetings were held by an experienced team of engineers from ERDC CHL River Engineering Branch and MVM Hydraulics and Hydrology Branch. From the meetings, a considerable list of preliminary alternatives was compiled. Based on discussions within the team, the preliminary list was reduced to a final list of the alternatives that were determined to be feasible. The study results from each of these feasible alternatives are presented herein.

Descriptions of alternatives

Alternative 1 simulated the construction of a spur levee to the original elevation (291.0 ft NAVD88) with a new alignment around the scour hole. Alternative 2 simulated the construction of a spur levee to the top bank elevation (282.0 ft NAVD88) with a new alignment around the scour hole. Alternative 3 simulated the degradation of the western spur levee to natural grade (removal of western spur levee). Alternative 4 simulated the construction of the overbank road to a constant elevation (276.0 ft NAVD88) as a low grade control and hard point in the overbank bed profile. Alternative 5 simulated dense tree plantings over the entire Island 13 overbank region (convert cleared land into forest). Alternative 6 simulated dense tree plantings on Natural Resources Conservation Service (NRCS) Wetlands Reserve Program (WRP) easements that were obtained by the spring of 2015. Table 3-1 lists a description of the alternatives that were investigated to mitigate the risk for cutoff formation.

Table 3-1. Descriptions of alternatives.

ID	Description
Alternative 1	Levee built to elevation 291.0 ft NAVD88
Alternative 2	Levee built to elevation 282.0 ft NAVD88
Alternative 3	Western levee degraded to elevation 281.0 ft NAVD88
Alternative 4	Overbank road raised to elevation 276.0 ft NAVD88
Alternative 5	Dense vegetation on the entire overbank
Alternative 6	Dense vegetation on obtained WRP easements

Multidimensional modeling analysis

The six alternatives were modeled utilizing AdH to assess the risk for cutoff formation.

Geometric data

An AdH mesh was created to represent each respective alternative. Listed below is a description of the mesh for all alternatives.

Alternative 1 simulated the construction of a spur levee to the original elevation (291.0 ft NAVD88) with a new alignment around the scour hole. Figure 3-1 depicts the study overbank mesh elevation for Alternative 1. Figure 3-2 depicts the 3D mesh surface for Alternative 1.

Alternative 2 simulated the construction of a spur levee to the top bank elevation (282.0 ft NAVD88) with a new alignment around the scour hole. Figure 3-3 depicts the study overbank mesh elevation for Alternative 2. Figure 3-4 depicts the 3D mesh surface for Alternative 2.

Alternative 3 simulated the degradation of the western spur levee to elevation 281.0 ft NAVD88 (removal of western spur levee). Figure 3-5 depicts the study overbank mesh elevation for Alternative 3. Figure 3-6 depicts the 3D mesh surface for Alternative 3.

Alternative 4 simulated the construction of the overbank road to a constant elevation (276.0 ft NAVD88) as a low grade control and hard point in the overbank bed profile. Figure 3-7 depicts the study overbank mesh elevation for Alternative 4. Figure 3-8 depicts the 3D mesh surface for Alternative 4.

Alternative 5 simulated dense tree plantings over the entire Island 13 overbank region (convert cleared land into forest). Figure 3-9 depicts the study overbank mesh material type for Alternative 5.

Alternative 6 simulated dense tree plantings on NRCS WRP easements that were obtained by the spring of 2015. Figure 3-10 depicts the study overbank mesh material type for Alternative 6.

Figure 3-1. Alternative 1 mesh elevation (study overbank).

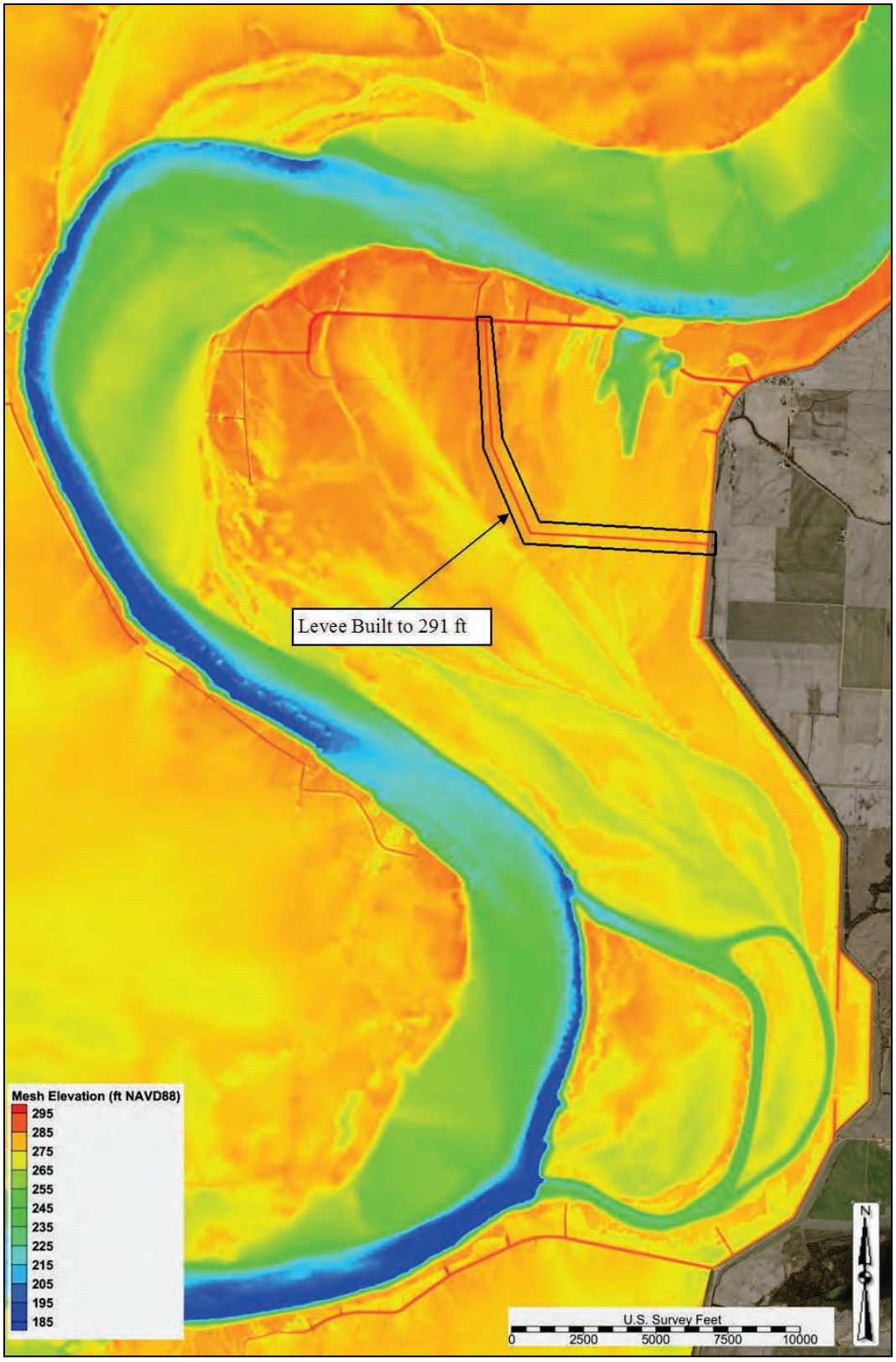


Figure 3-2. Alternative 1; 3D surface (study overbank).

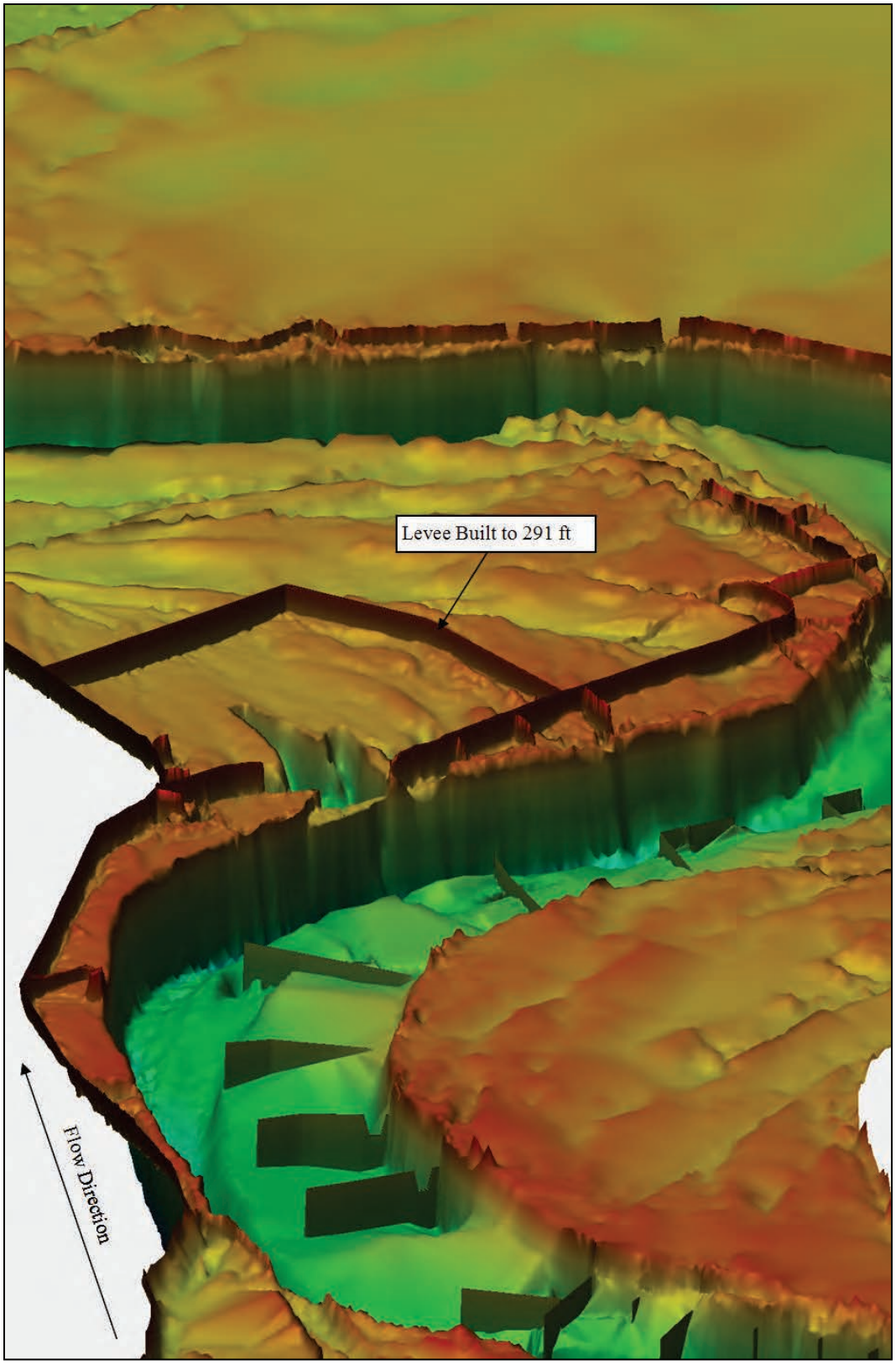


Figure 3-3. Alternative 2 mesh elevation (study overbank).

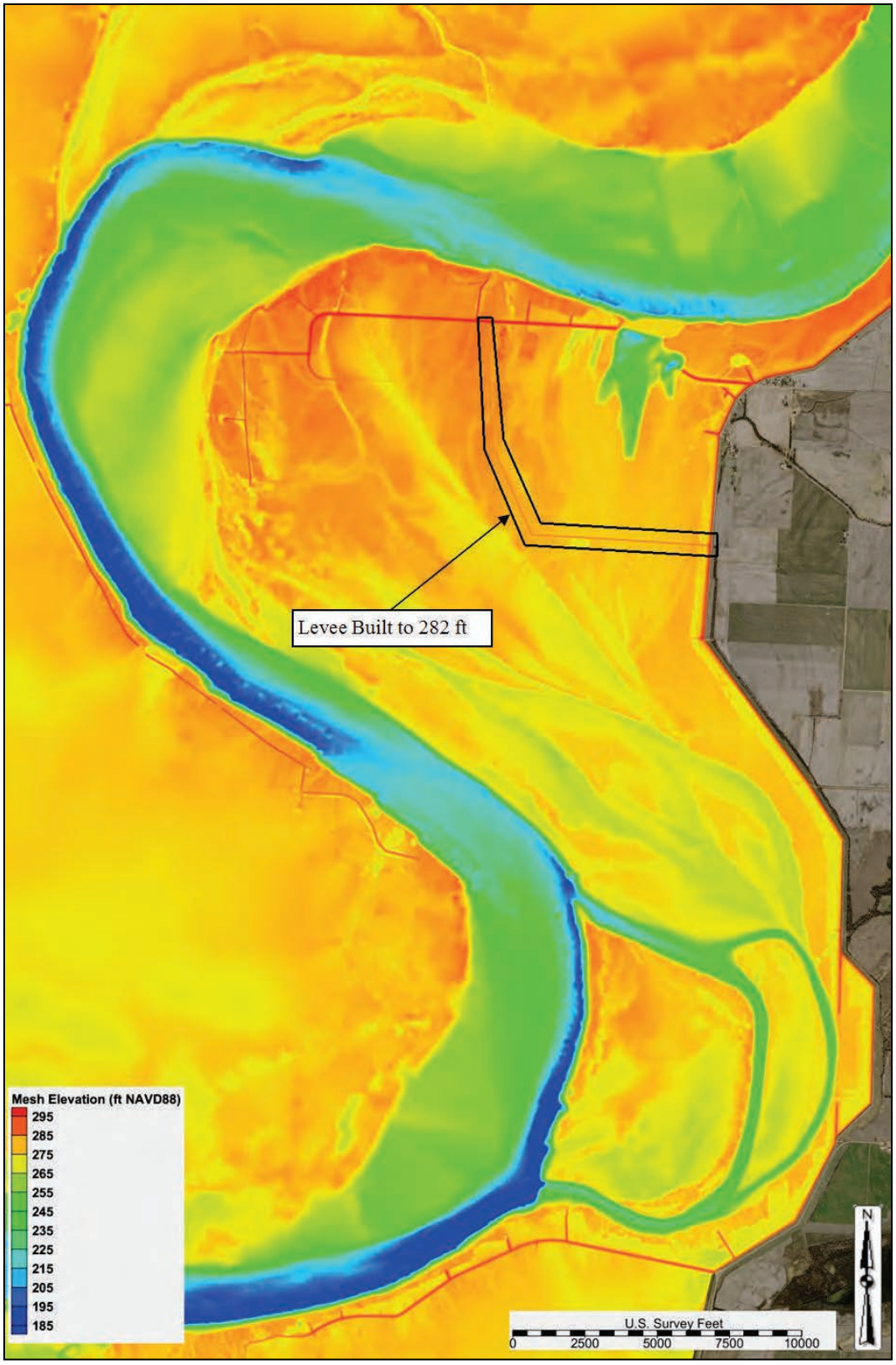


Figure 3-4. Alternative 2; 3D surface (study overbank).

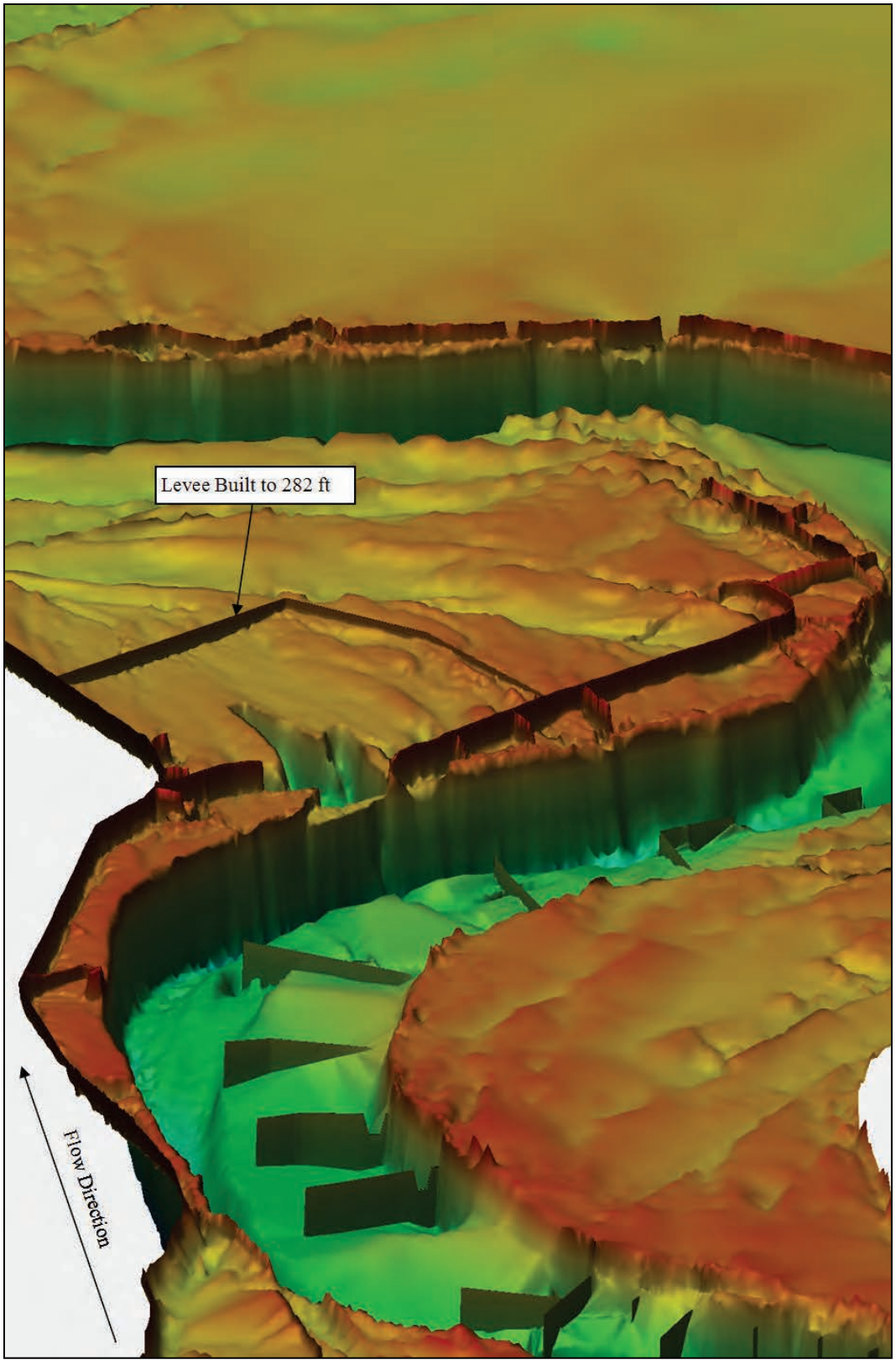


Figure 3-5. Alternative 3 mesh elevation (study overbank).

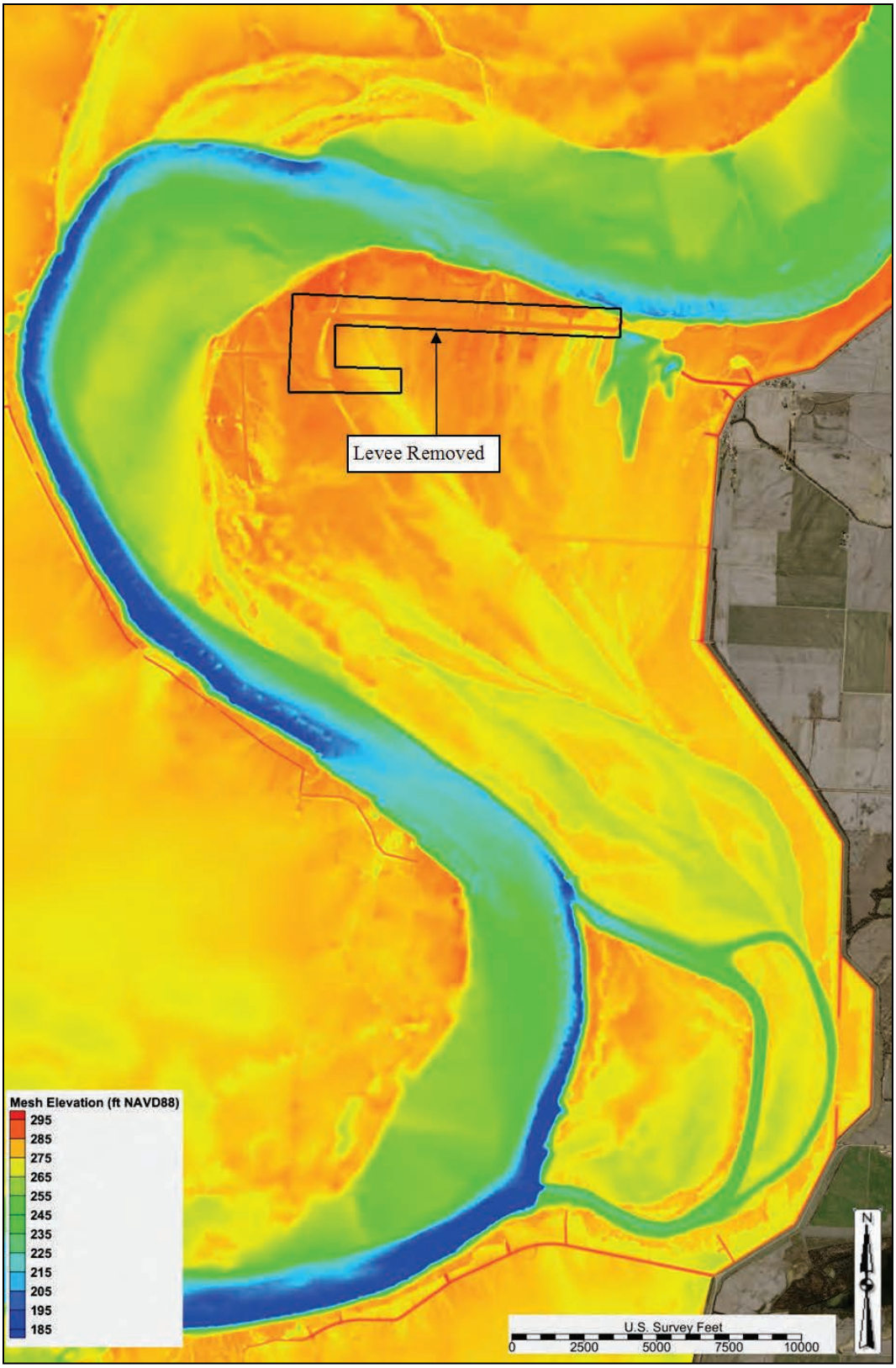


Figure 3-6. Alternative 3; 3D surface (study overbank).

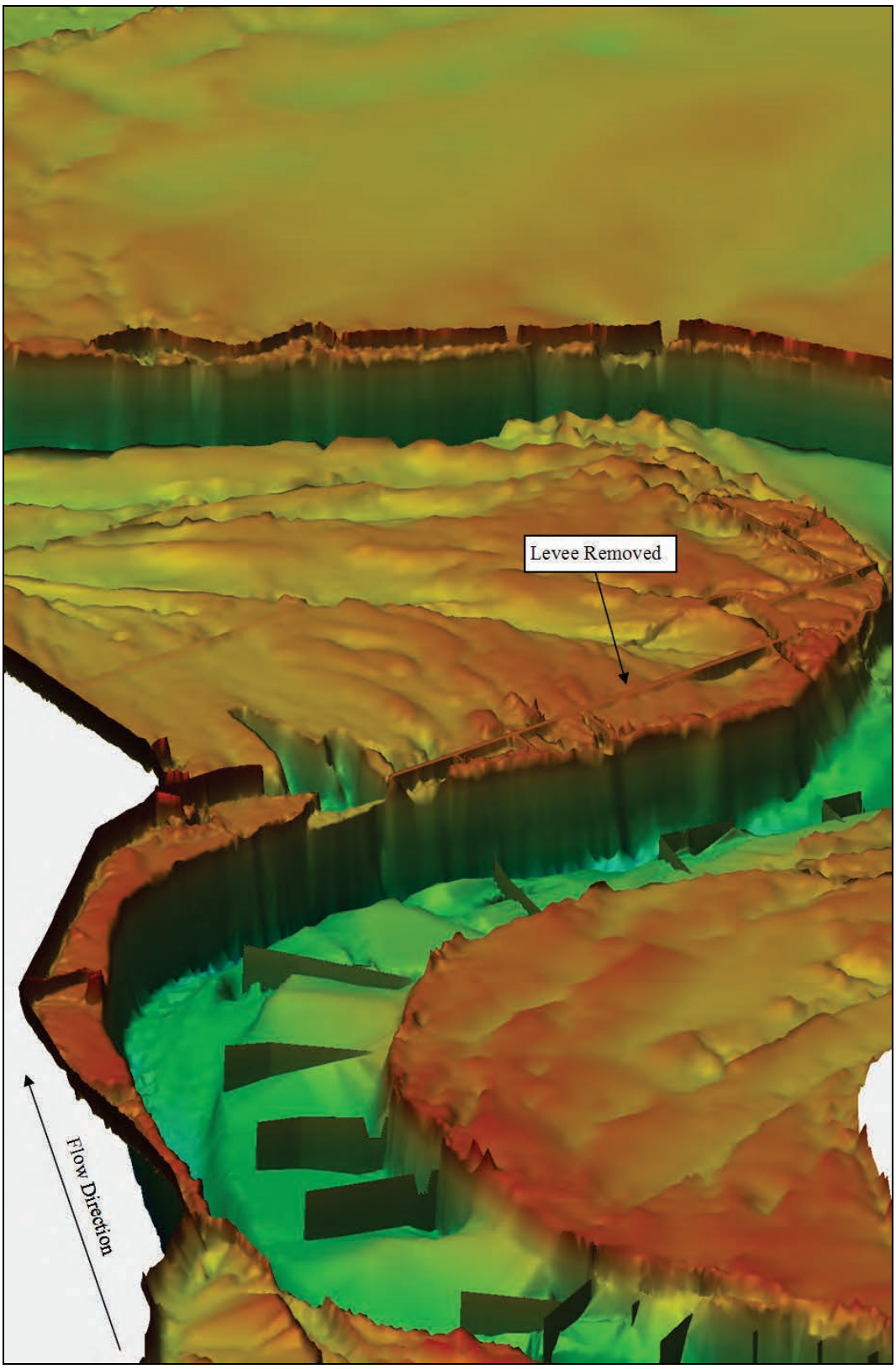


Figure 3-7. Alternative 4 mesh elevation (study overbank).

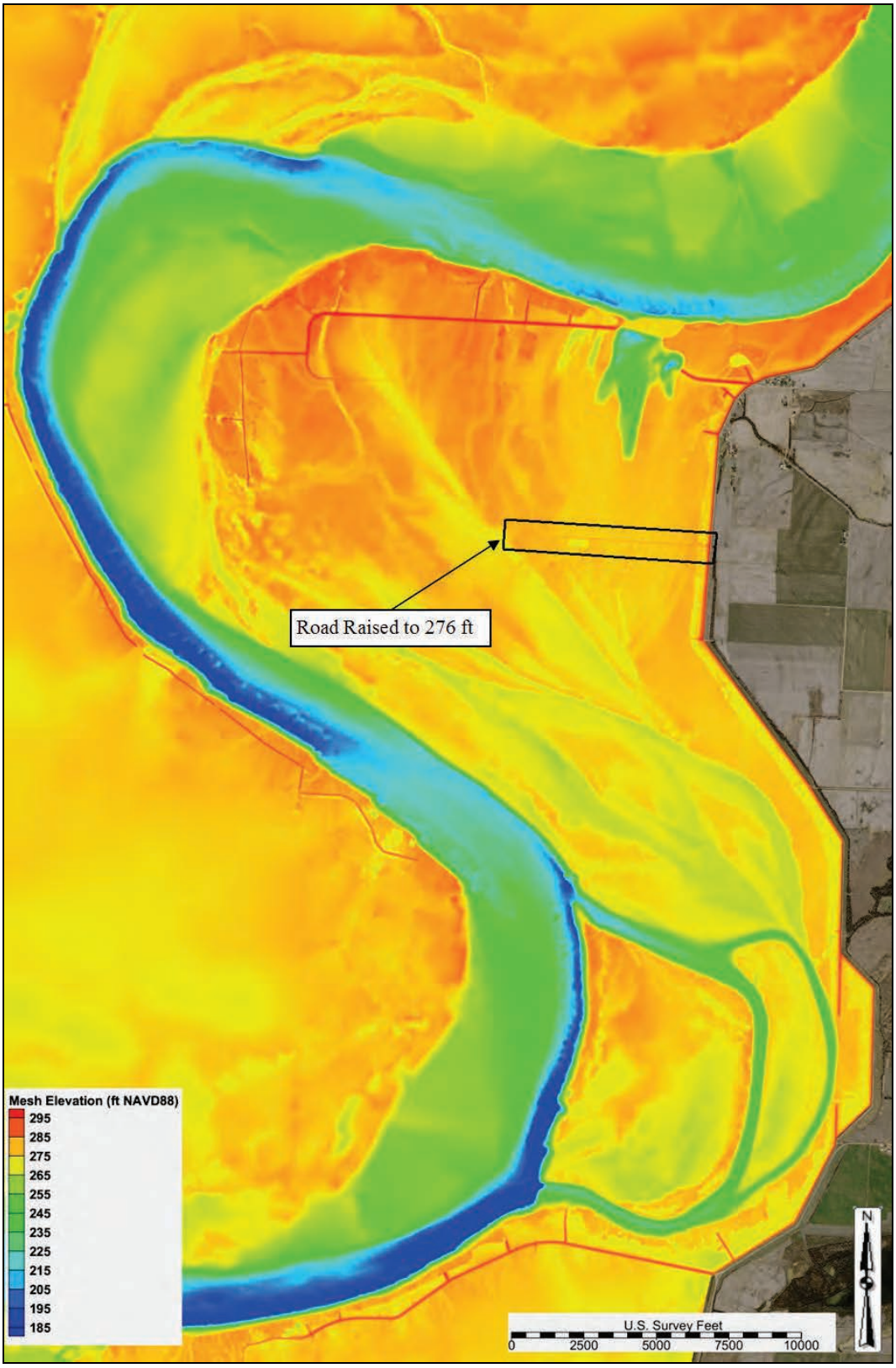


Figure 3-8. Alternative 4; 3D surface (study overbank).

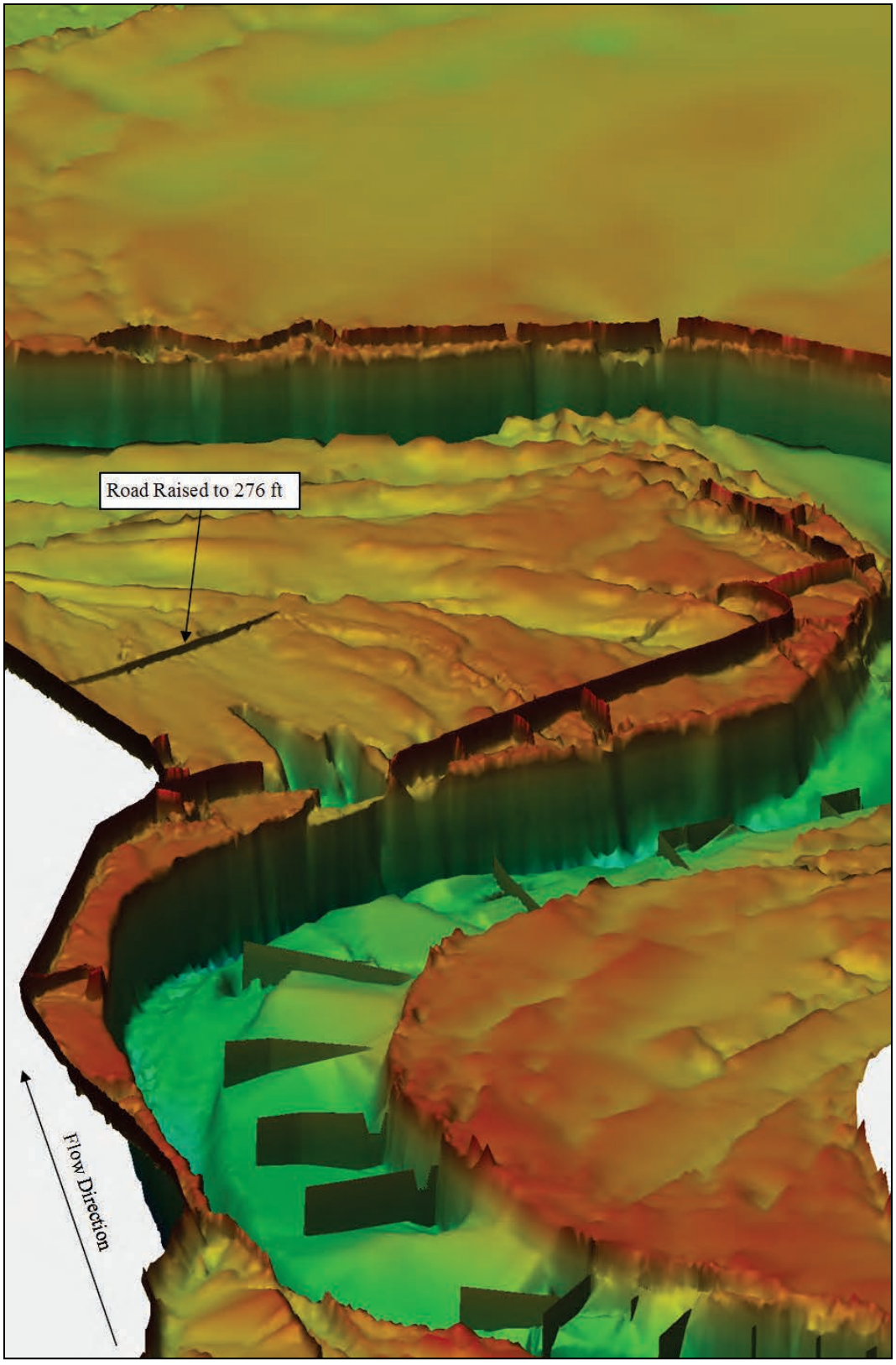


Figure 3-9. Alternative 5 material type (study overbank).

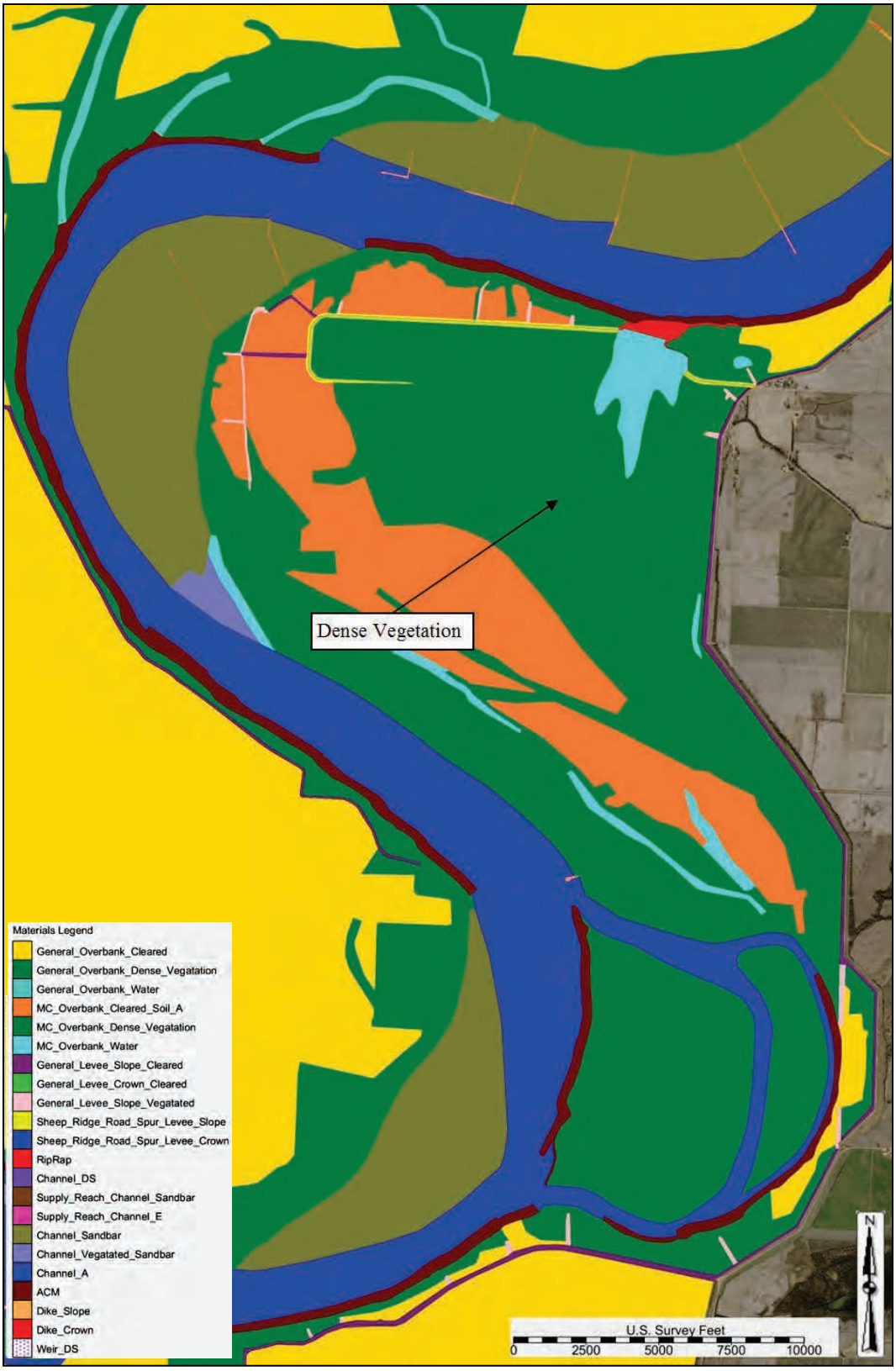
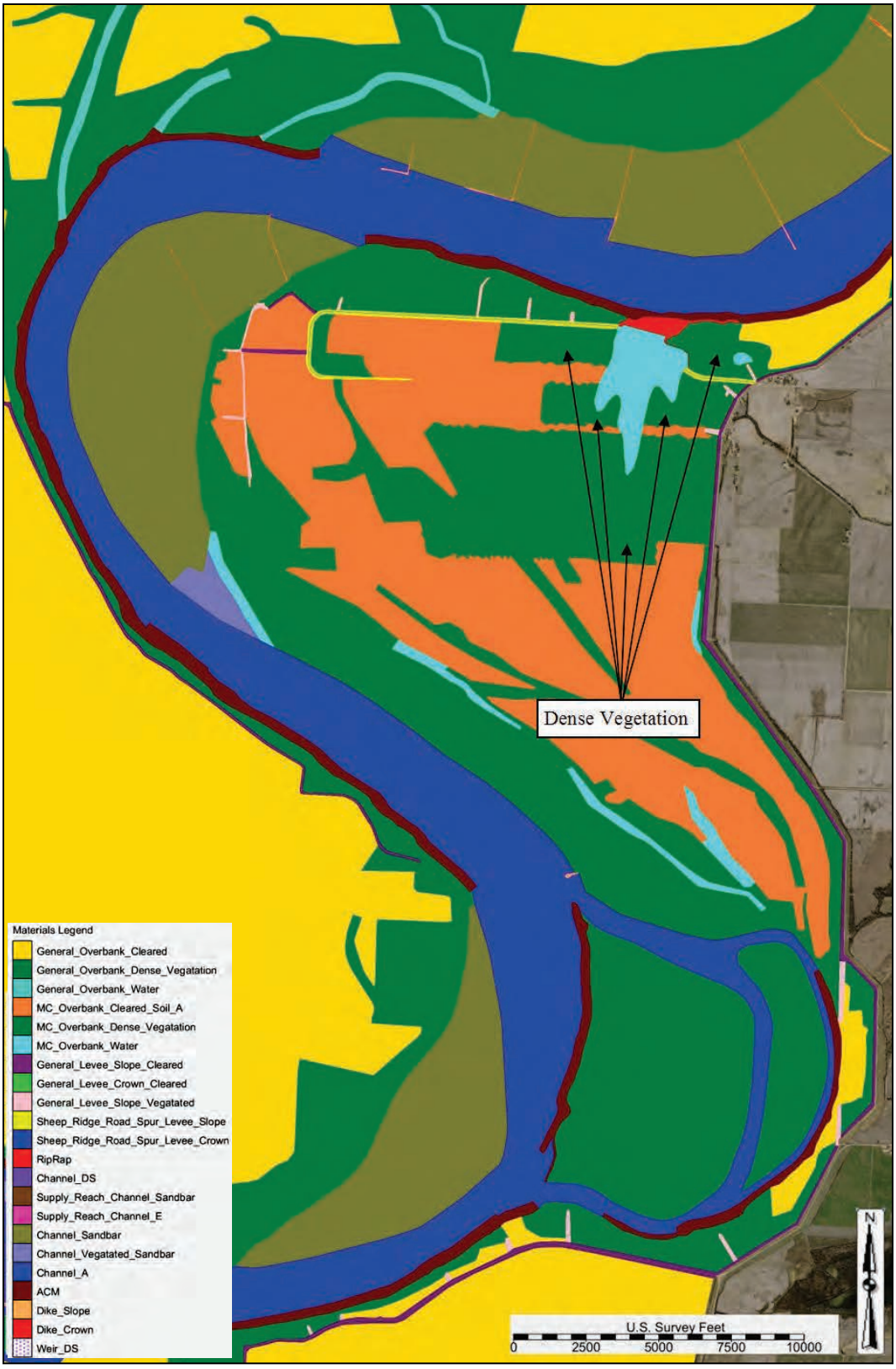


Figure 3-10. Alternative 6 material type (study overbank).



Plan comparisons

The Hypothetical Hydrograph was simulated for all six alternatives.

The bed shear stress output at 1,900,000 cfs from the Hypothetical Hydrograph simulation for Alternative 1 is depicted in Figure 3-11. Note the regions of high shear stress on the closure structure, western edge of the scour hole, the overbank region immediately east of the closure structure, and the crown of the new spur levee. Refer to Figure 2-34 for the base condition shear stress output at 1,900,000 cfs.

ID	Description
Alternative 1	Levee built to elevation 291.0 ft NAVD88

The bed shear stress difference comparison between Alternative 1 and the base condition at 1,900,000 cfs from the Hypothetical Hydrograph simulation is depicted in Figure 3-12. A positive shear stress difference (+ value and red and orange) indicated that the alternative increased shear stress. A negative shear stress difference (- value and blue) indicated that the alternative decreased shear stress. A zero shear stress difference (zero value and white) indicated that the alternative had no change on shear stress. Note that shear stress was greatly reduced across the entire Island 13 overbank with exception of the western tie-in of the closure structure and the crown of the new spur levee (weir flow).

ID	Description
Alternative 1	Levee built to elevation 291.0 ft NAVD88

The bed shear stress output at 1,900,000 cfs from the Hypothetical Hydrograph simulation for Alternative 2 is depicted in Figure 3-13. Note the regions of high shear stress on the closure structure, western edge of the scour hole, overbank region south of the scour hole, overbank region immediately east of the closure structure, at the toe of the Tiptonville-Obion River Levee, and the crown of the new spur levee.

ID	Description
Alternative 2	Levee built to elevation 282.0 ft NAVD88

Figure 3-11. Alternative 1 shear stress—1,900,000 cfs (study overbank).



Figure 3-12. Alternative 1 shear stress difference—1,900,000 cfs.

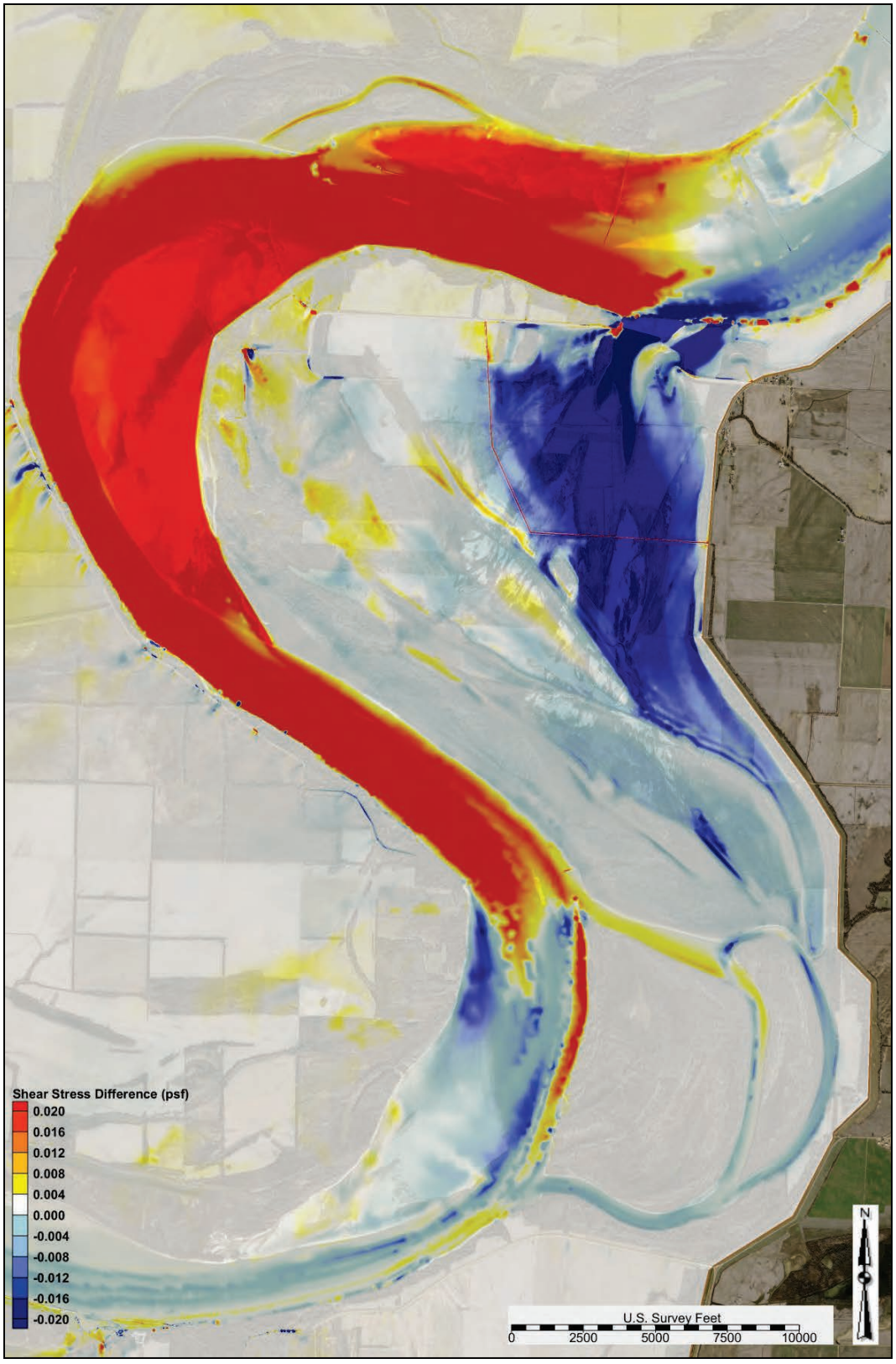


Figure 3-13. Alternative 2 shear stress—1,900,000 cfs (study overbank).



The bed shear stress difference comparison between Alternative 2 and the base condition at 1,900,000 cfs from the Hypothetical Hydrograph simulation is depicted in Figure 3-14. Note that for the majority of the study overbank no change was observed in the shear stress with the exception of the increased shear stress on the crown of the new spur levee.

ID	Description
Alternative 2	Levee built to elevation 282.0 ft NAVD88

The bed shear stress output at 1,900,000 cfs from the Hypothetical Hydrograph simulation for Alternative 3 is depicted in Figure 3-15. Note the regions of high shear stress on the closure structure, western edge of the scour hole, the overbank region immediately east of the closure structure, and at the toe of the Tiptonville-Obion River Levee.

ID	Description
Alternative 3	Western levee degraded to elevation 281.0 ft NAVD88

The bed shear stress difference comparison between Alternative 3 and the base condition at 1,900,000 cfs from the Hypothetical Hydrograph simulation is depicted in Figure 3-16. Note that for the majority of the study overbank a slight increase was observed in the shear stress with the exception of the decreased shear stress on the closure structure and the western edge of the scour hole.

ID	Description
Alternative 3	Western levee degraded to elevation 281.0 ft NAVD88

The bed shear stress output at 1,900,000 cfs from the Hypothetical Hydrograph simulation for Alternative 4 is depicted in Figure 3-17. Note the regions of high shear stress on the closure structure, western edge of the scour hole, overbank region south of the scour hole, overbank region immediately east of the closure structure, and at the toe of the Tiptonville-Obion River Levee.

ID	Description
Alternative 4	Overbank road raised to elevation 276.0 ft NAVD88

Figure 3-14. Alternative 2 shear stress difference—1,900,000 cfs.

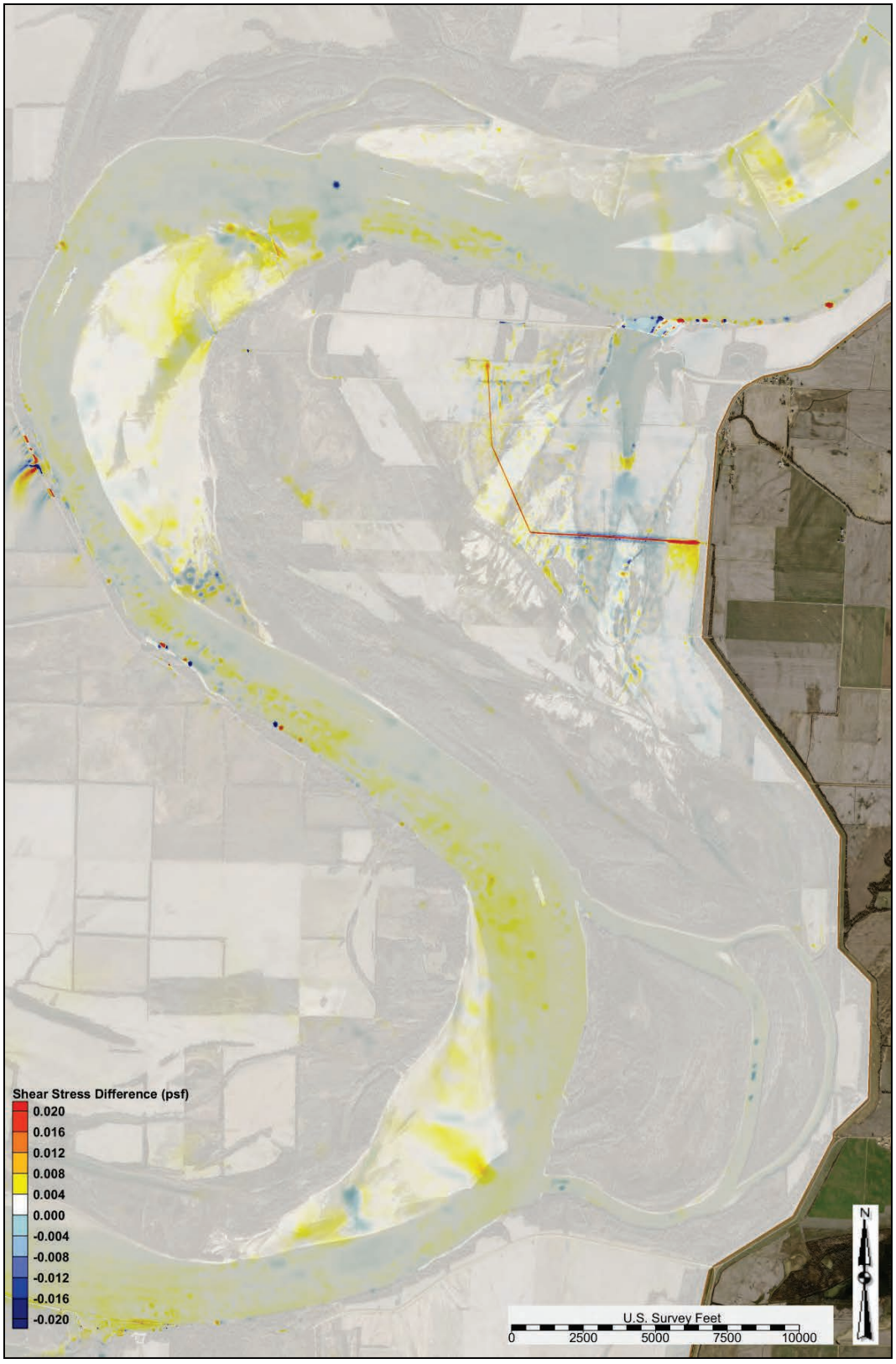


Figure 3-15. Alternative 3 shear stress—1,900,000 cfs (study overbank).

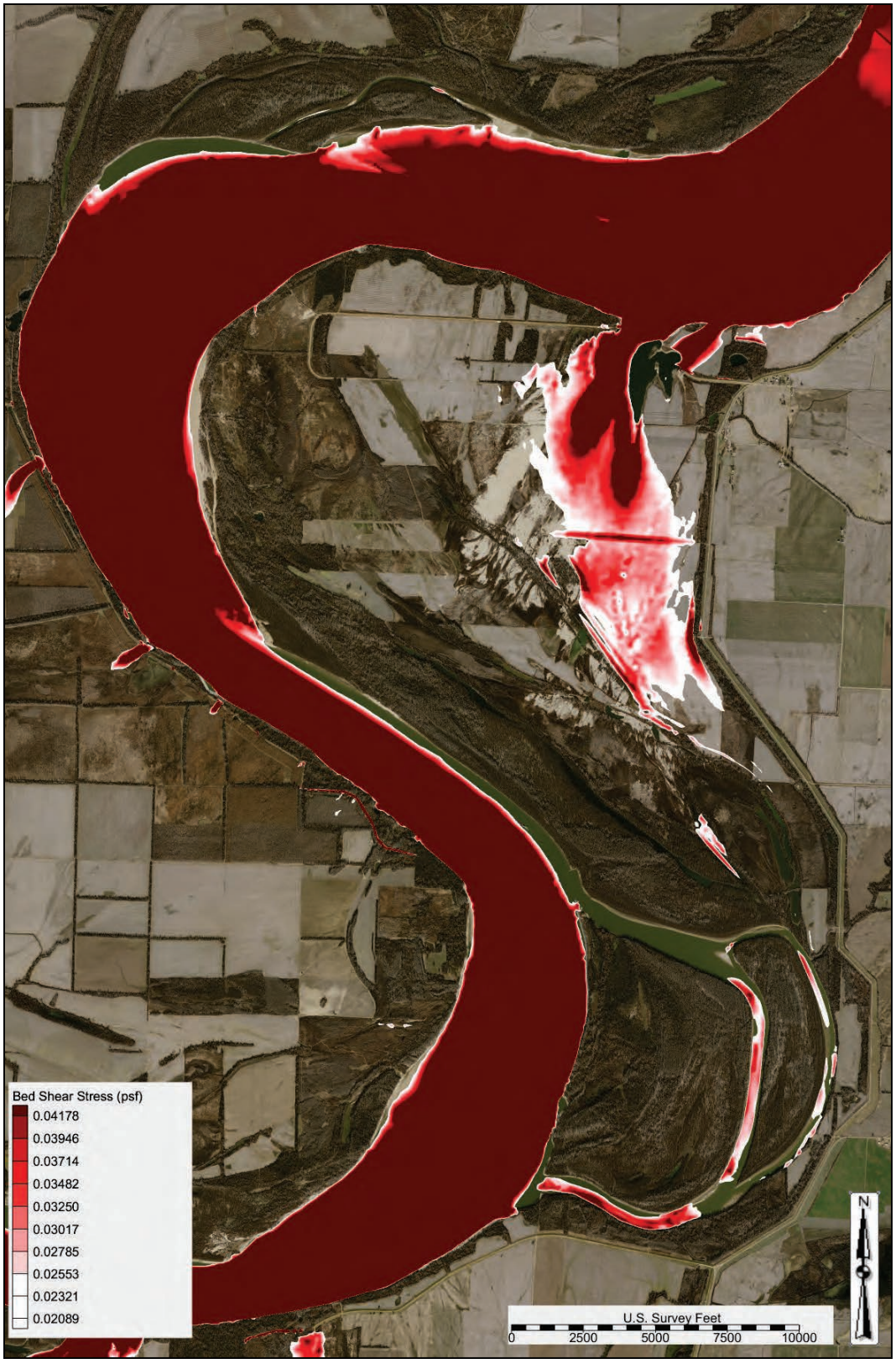


Figure 3-16. Alternative 3 shear stress difference—1,900,000 cfs.

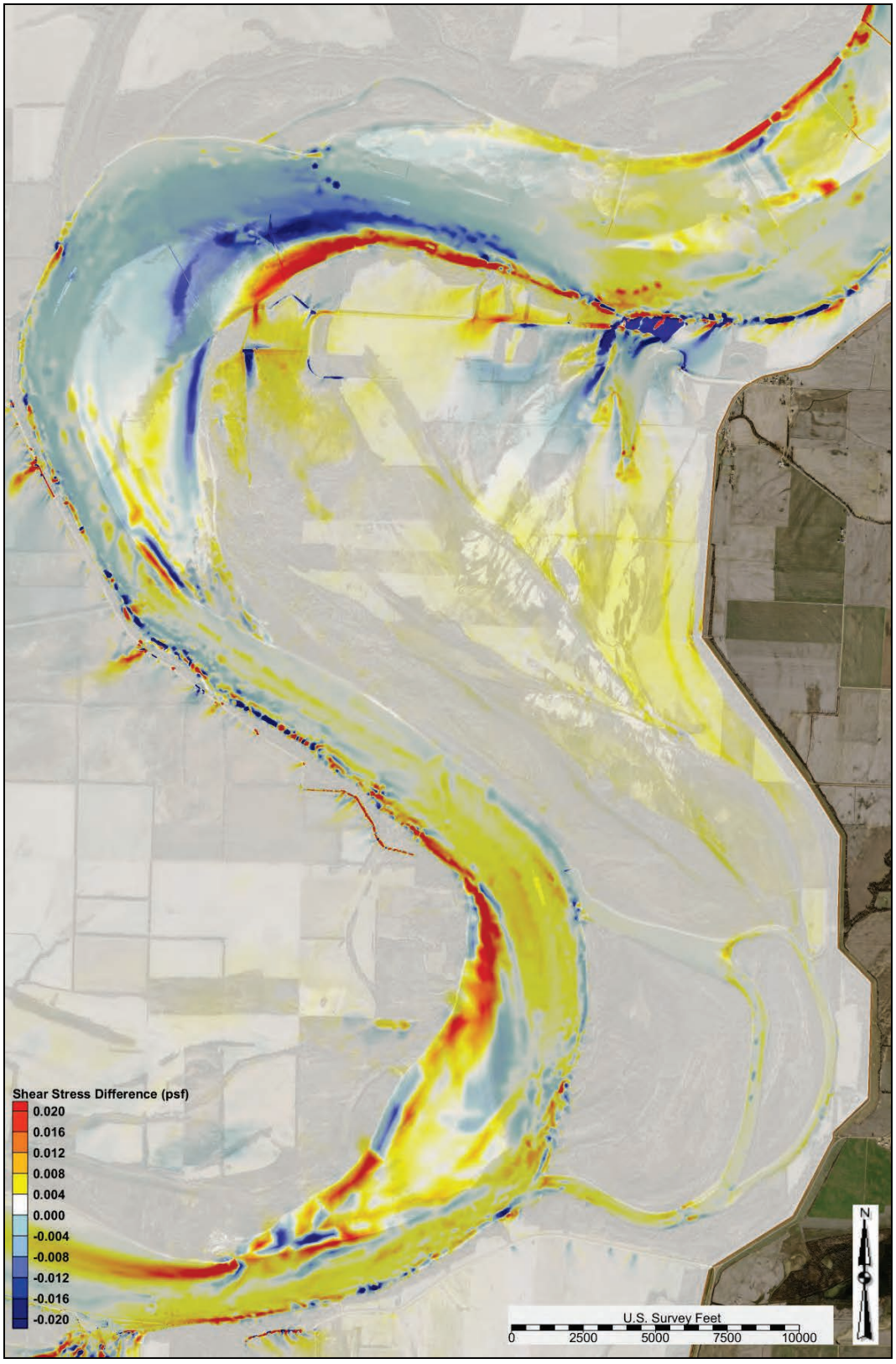
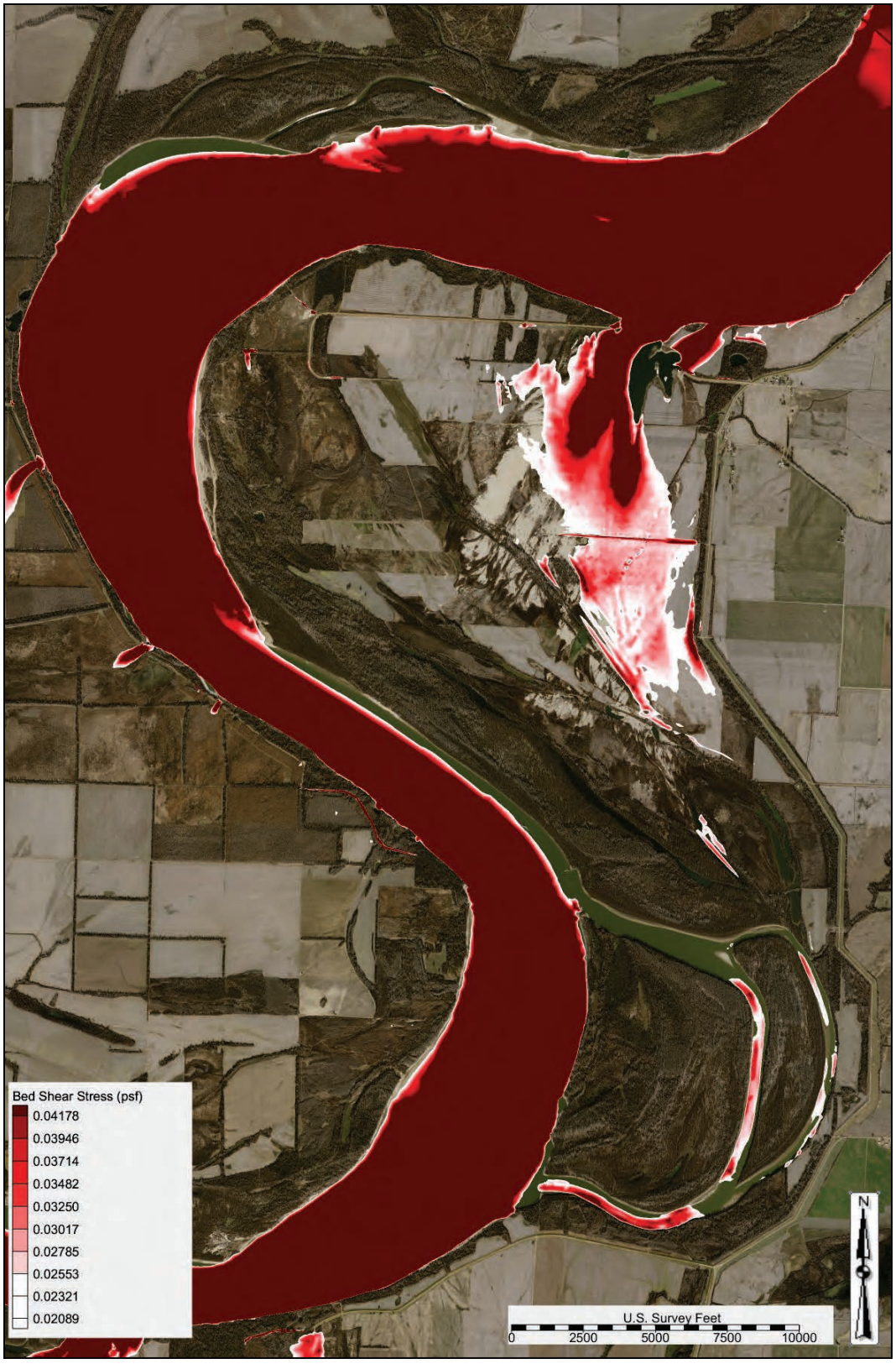


Figure 3-17. Alternative 4 shear stress—1,900,000 cfs (study overbank).



The bed shear stress difference comparison between Alternative 4 and the base condition at 1,900,000 cfs from the Hypothetical Hydrograph simulation is depicted in Figure 3-18. Note that for the majority of the study overbank no change was observed in the shear stress.

ID	Description
Alternative 4	Overbank road raised to elevation 276.0 ft NAVD88

The bed shear stress output at 1,900,000 cfs from the Hypothetical Hydrograph simulation for Alternative 5 is depicted in Figure 3-19. Note the regions of high shear stress on the closure structure, western edge of the scour hole, southern edge of the scour hole, and at the toe of the Tiptonville-Obion River Levee.

ID	Description
Alternative 5	Dense vegetation on the entire overbank

The bed shear stress difference comparison between Alternative 5 and the base condition at 1,900,000 cfs from the Hypothetical Hydrograph simulation is depicted in Figure 3-20. Note that shear stress was greatly reduced across the entire Island 13 overbank with exception of the western and eastern tie-ins of the closure structure and the ditch at the toe of the Tiptonville-Obion River Levee.

ID	Description
Alternative 5	Dense vegetation on the entire overbank

The bed shear stress output at 1,900,000 cfs from the Hypothetical Hydrograph simulation for Alternative 6 is depicted in Figure 3-21. Note the regions of high shear stress on the closure structure, western edge of the scour hole, southern edge of the scour hole, the region west of the scour hole that remained cleared land, and at the toe of the Tiptonville-Obion River Levee.

ID	Description
Alternative 6	Dense vegetation on obtained WRP easements

Figure 3-18. Alternative 4 shear stress difference—1,900,000 cfs.

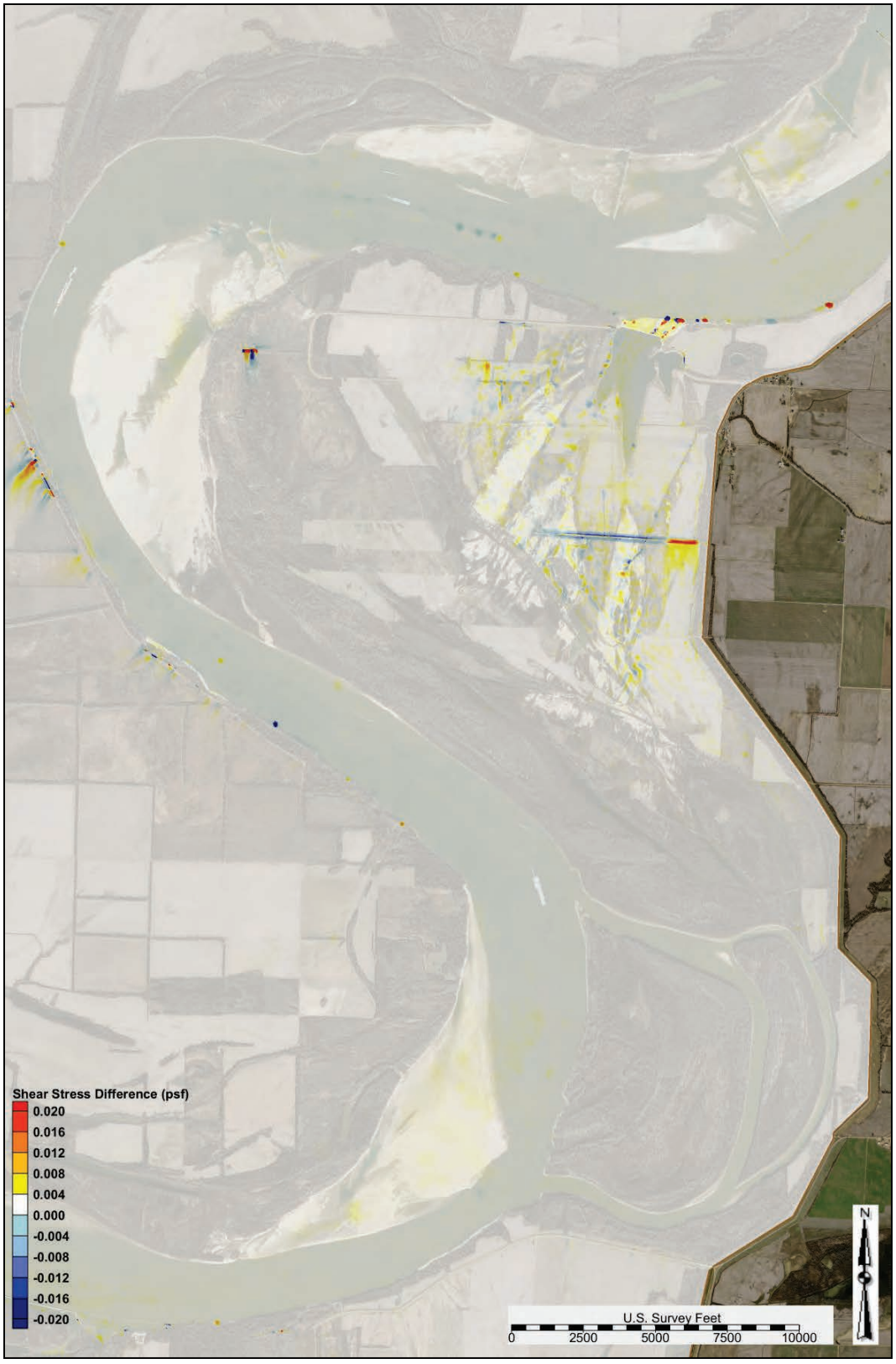


Figure 3-19. Alternative 5 shear stress—1,900,000 cfs (study overbank).



Figure 3-20. Alternative 5 shear stress difference—1,900,000 cfs.

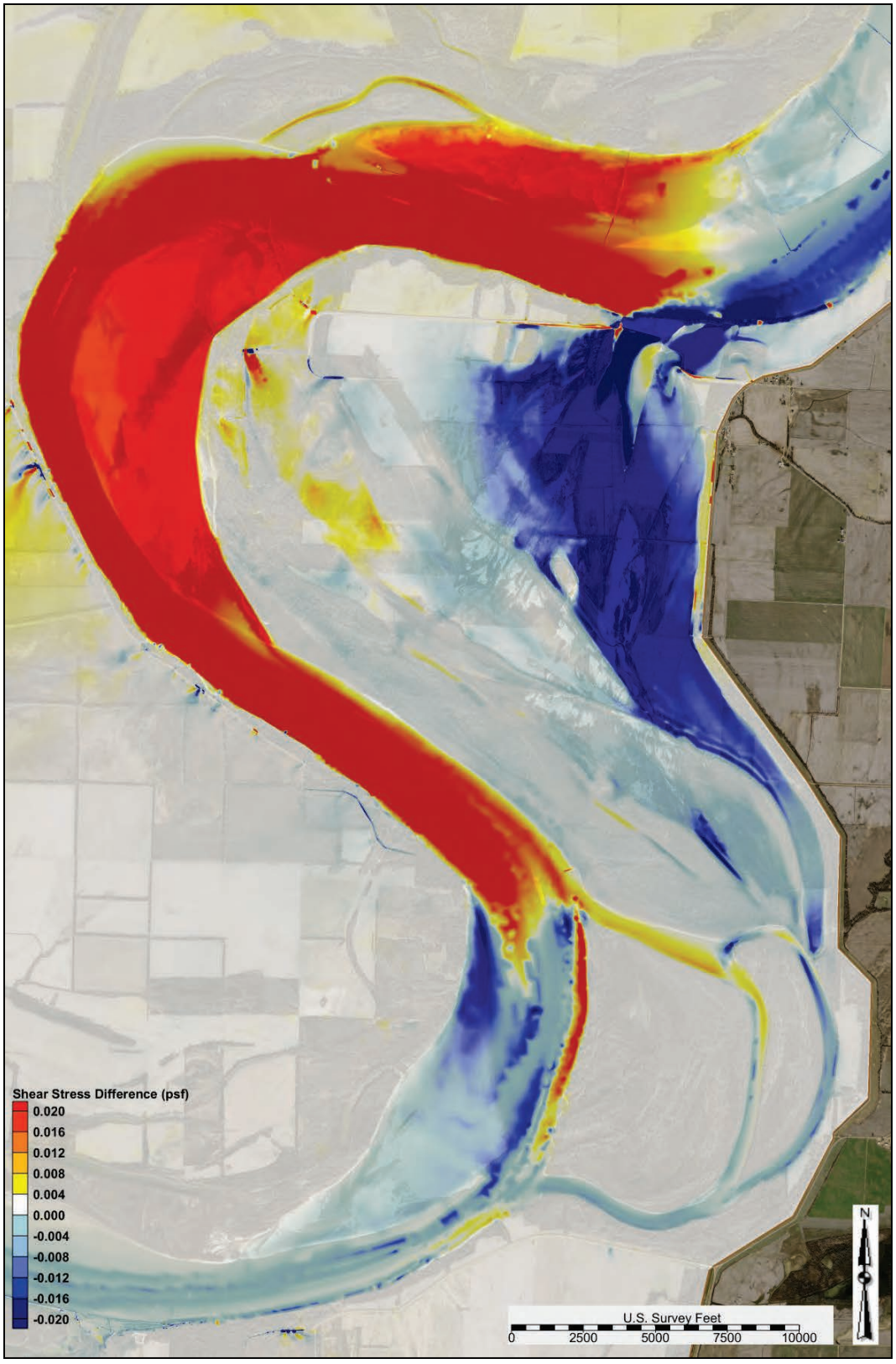


Figure 3-21. Alternative 6 shear stress—1,900,000 cfs (study overbank).



The bed shear stress difference comparison between Alternative 6 and the base condition at 1,900,000 cfs from the Hypothetical Hydrograph simulation is depicted in Figure 3-22. Note that shear stress was greatly reduced across the majority of the Island 13 overbank with exception of the western and eastern tie-ins of the closure structure, the region west of the scour hole that remained cleared land, and the ditch at the toe of the Tiptonville-Obion River Levee.

ID	Description
Alternative 6	Dense vegetation on obtained WRP easements

Flow and sediment diversion analysis

Figure 3-23 depicts a comparison of the Island 13 overbank diversion flow between the base condition and the alternatives. Alternative 1 eliminated diversion flow until the main channel flow exceeded 1,650,000 cfs upstream of the crevasse. Alternative 2 eliminated diversion flow until the main channel flow exceeded 1,100,000 cfs upstream of the crevasse. Alternative 3 increased diversion flow. Alternative 4 had minimal impact on diversion flow. Alternatives 5 and 6 greatly reduced diversion flow. At 1,900,000 cfs, Alternative 5 reduced the diversion flow by approximately 13%. At 1,900,000 cfs, Alternative 6 reduced the diversion flow by approximately 10%.

Figure 3-24 depicts a comparison of the Island 13 overbank diversion sediment load between the base condition and the alternatives. Alternative 1 eliminated diversion sediment load until the main channel flow exceeded 1,650,000 cfs upstream of the crevasse. Alternative 2 eliminated diversion sediment load until the main channel flow exceeded 1,100,000 cfs upstream of the crevasse. Alternatives 3 and 4 had minimal impact on diversion sediment load. Alternatives 5 and 6 greatly reduced diversion sediment load. At 1,900,000 cfs, Alternative 5 reduced the diversion sediment load by approximately 5%. At 1,900,000 cfs, Alternative 6 reduced the diversion sediment load by approximately 4%.

Figure 3-22. Alternative 6 shear stress difference—1,900,000 cfs.

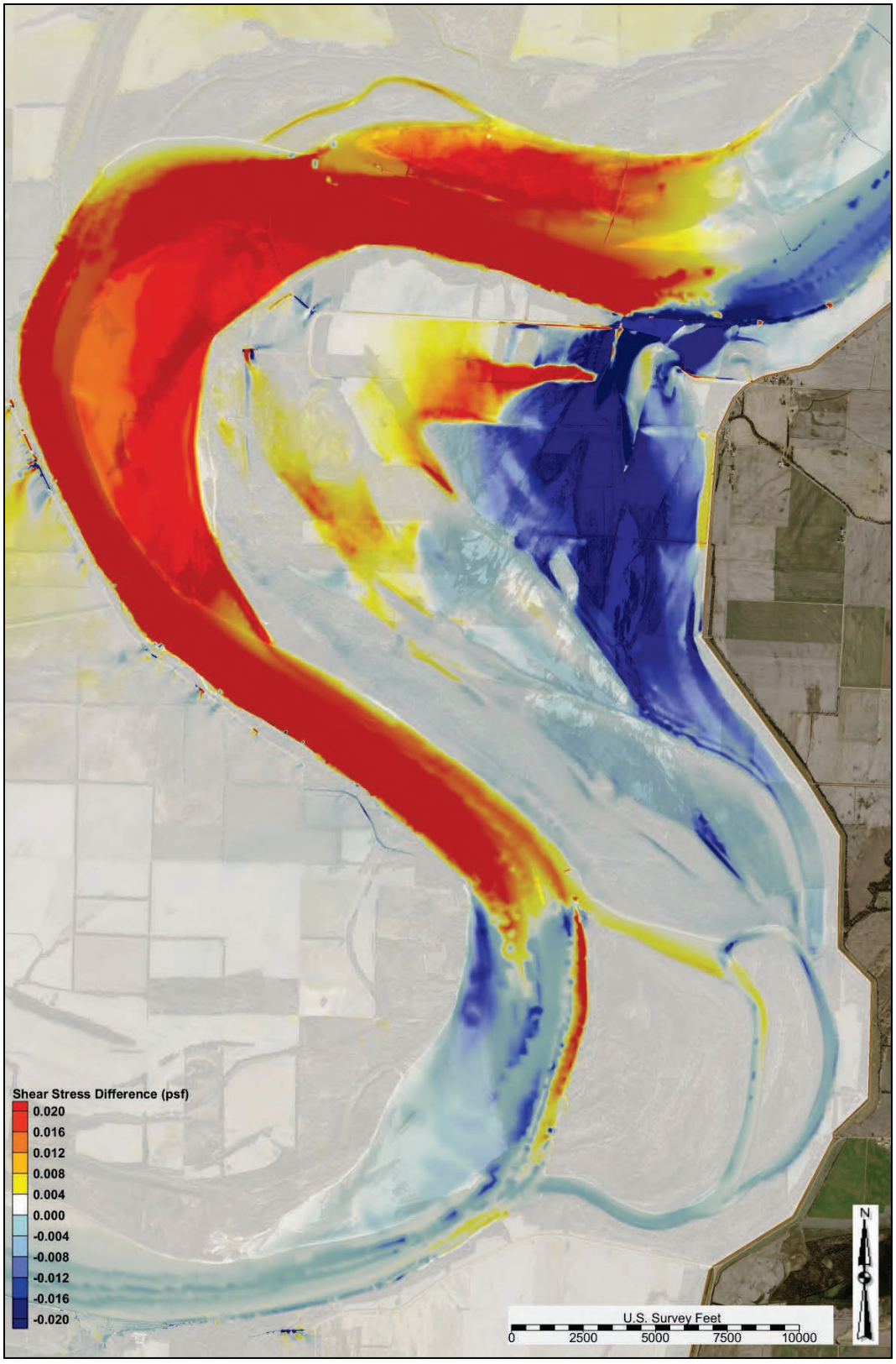


Figure 3-23. Alternative overbank diversion flow.

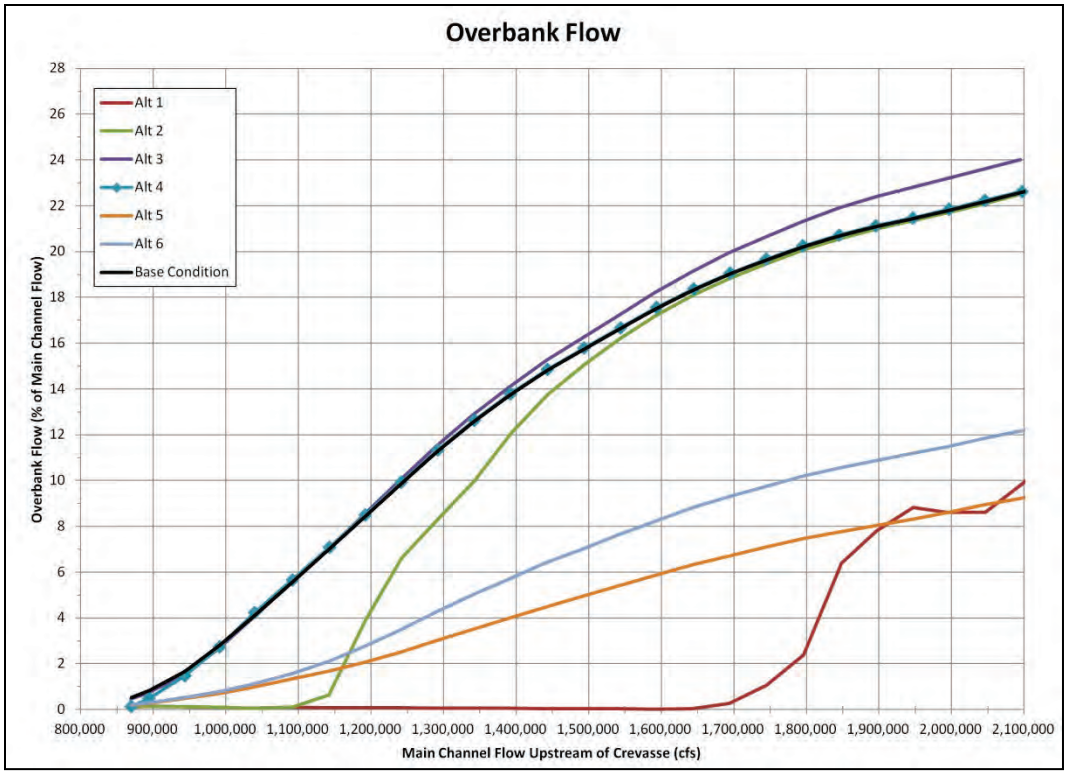
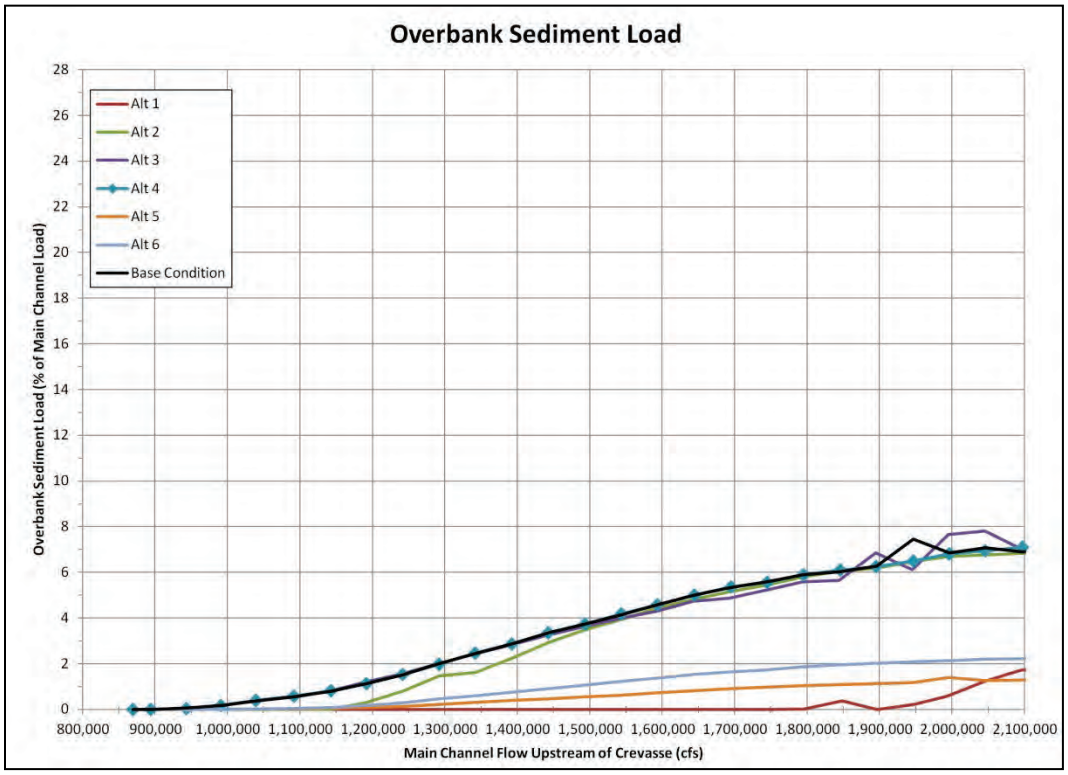


Figure 3-24. Alternative overbank sediment diversion load.



Scenario simulations

The modeled alternatives were evaluated for a range of flows (800,000–2,500,000 cfs). Appendix C contains the following detailed data for the modeled alternatives from the Hypothetical Hydrograph simulations:

- shear stress output at flows ranging from 900,000 to 2,100,000 cfs for the study overbank (Alternative 1: Figures C-114 through C-120; Alternative 2: Figures C-129 through C-135; Alternative 3: Figures C-144 through C-150; Alternative 4: Figures C-159 through C-165; Alternative 5: Figures C-174 through C-180; and Alternative 6: Figures C-189 through C-195)
- shear stress difference plots compared to the base condition output at flows ranging from 900,000 to 2,100,000 cfs for the study overbank (Alternative 1: Figures C-121 through C-127; Alternative 2: Figures C-136 through C-142; Alternative 3: Figures C-151 through C-157; Alternative 4: Figures C-166 through C-172; Alternative 5: Figures C-181 through C-187; and Alternative 6: Figures C-196 through C-202)
- water surface elevation profiles in the study reach for the following flows: 1,100,000 cfs, 1,500,000 cfs, 1,900,000 cfs, and 2,100,000 cfs (Alternative 1: Figure C-128; Alternative 2: Figure C-143; Alternative 3: Figure C-158; Alternative 4: Figure C-173; Alternative 5: Figure C-188; and Alternative 6: Figure C-203)
- alternatives vs. base condition water surface elevation profiles for the following flows: 1,100,000 cfs, 1,500,000 cfs, 1,900,000 cfs, and 2,100,000 cfs (Figures C-204 through C-207)
- sediment diversion grain size distribution for flows ranging from 870,000 to 2,000,000 cfs (Table C-3 through C-8).

One-dimensional (1D) modeling analysis

Alternative 5 was modeled utilizing HEC-6T to investigate long-term study reach conditions and the risk for cutoff formation. Due to 1D model limitations and study milestones, only Alternative 5 was modeled in HEC-6T.

Plan parameters

A HEC-6T geometry file was created for Alternative 5. Modifications were made to the Manning's roughness values that represented dense vegetation for Island 13 overbank, the diversion flow rating curve, and the diversion sediment load rating curve for the overbank reach.

Scenario simulation

Figure 3-25 depicts the initial and final (day 20,000 or approximately 55 years) Merriwether-Cherokee/Island 13 overbank reach bed profile for both the base condition and Alternative 5. From the analysis, Alternative 5 reduced the overbank bed lowering by approximately 3 to 8 ft over the 55-year simulation. Note that this analysis is based off of the synthetic long-duration hydrograph and assumed that the Island 13 overbank consisted of noncohesive sediment. Figure 3-26 depicts Island 13 overbank cross sections thalweg elevations for Alternative 5 through the 55-year simulation. Figure 2-50 depicts the cross section IDs and their respective overbank locations.

Appendix C contains the following detailed base condition scenario data:

- HEC-6T base condition vs. Alternative 5 index flow comparison at four model locations (RM 846.40, RM 856.99, RM 864.76, and RM 870.2) (Figures D-14 through D-17).

Figure 3-25. HEC-6T Alternative 5 profile plot.

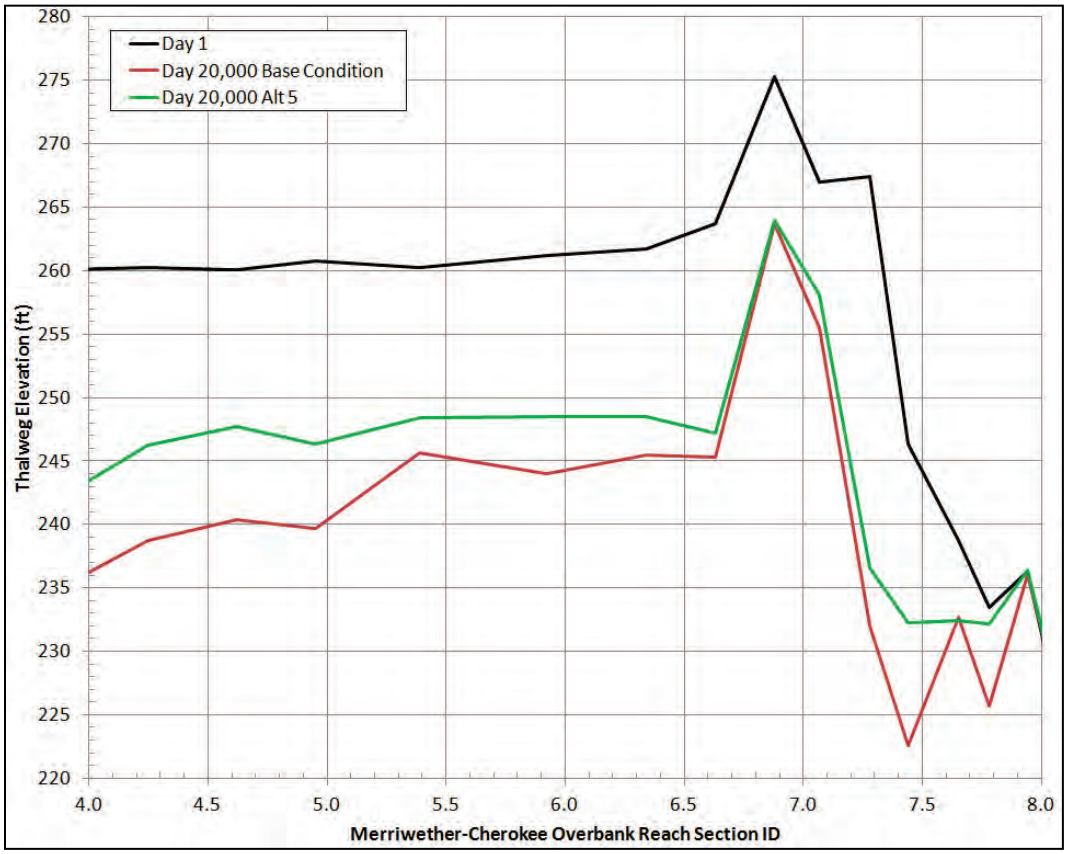
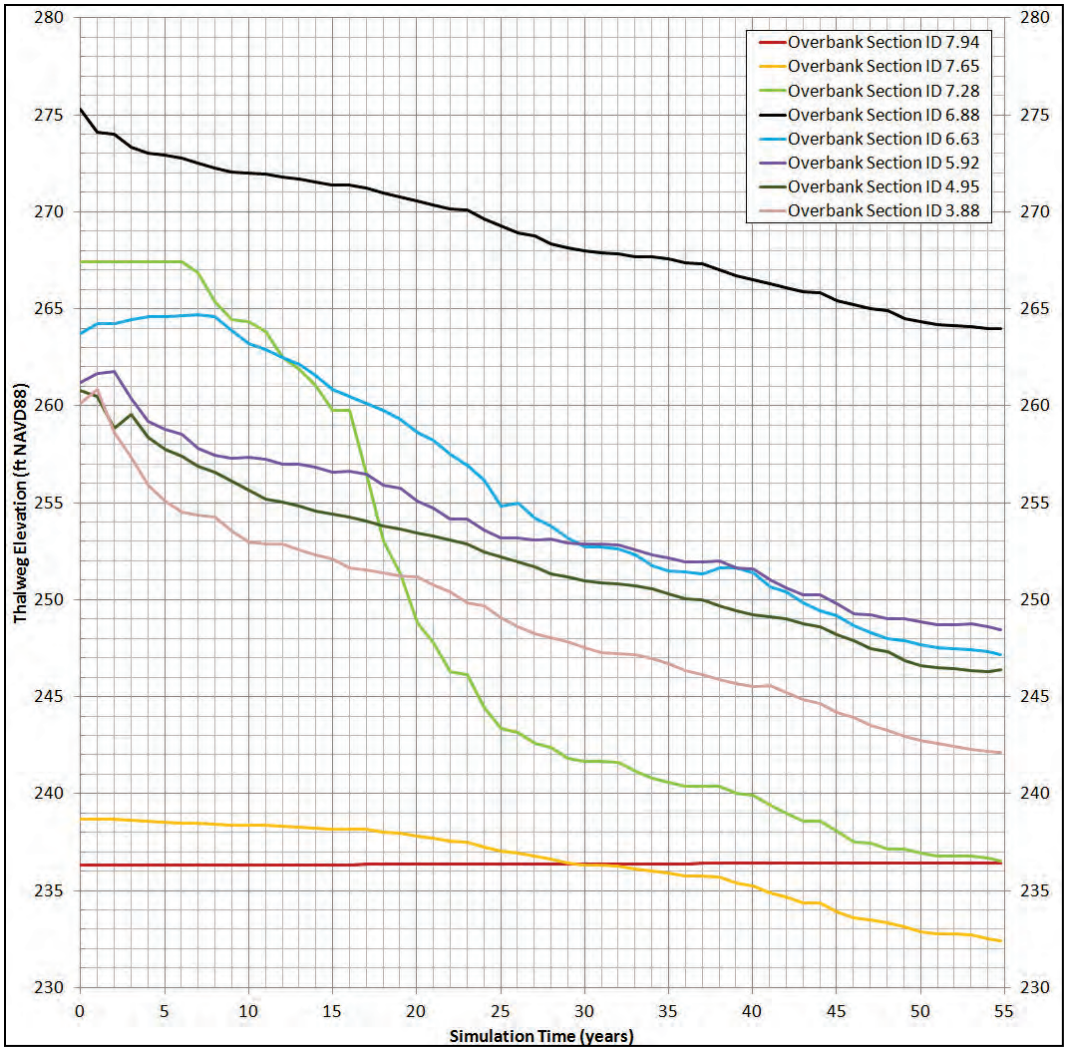


Figure 3-26. HEC-6T Alternative 5 thalweg time series.



4 Local Scour Countermeasures

Local scour countermeasures were investigated to mitigate the risk of closure structure failure. Collaboration sessions were held by the MVM Hydraulics and Hydrology Branch to devise a list of preliminary local scour countermeasures. The final list of local scour countermeasures to be studied was determined from a combination of the collaboration session's discussion and historical river design experience from all session participants (past successes and failures were considered). The study results from each of the local scour countermeasures from the final list are presented herein.

Local scour countermeasure descriptions

Local Scour Countermeasure 1 analyzed the addition of rock protection around the western edge of the scour hole (approximately 2,300 ft). Local Scour Countermeasure 2 simulated a tapered trenchfill dike at the eastern tie-in of the closure structure (excavated rockfill trench with rock +6 ft above grade at the toe of eastern levee and tapered to a +4 ft above grade at the midpoint and tapered to a +2 ft above grade at the closure structure). Table 4-1 lists a description of the modeled local scour countermeasures that were investigated to mitigate the risk of closure structure failure. Local Scour Countermeasures 1 and 2 were evaluated using AdH and a shear stress analysis.

Table 4-1. Local scour countermeasure descriptions.

ID	Description
Local Scour Countermeasure 1	Rock protection around western edge of the scour hole (2,300 ft)
Local Scour Countermeasure 2	Tapered Trenchfill dike (+6 ft at toe of eastern levee, +4 ft at midpoint, +2 ft at closure structure)

The following local scour countermeasures were investigated utilizing traditional river engineering non-modeling screening methods: expansion of the existing eastern trenchfill dike, protection of the eastern spur levee, and protection of the western spur levee. The expansion and reinforcing of the existing eastern trenchfill dike would create a stone trench approximately 35 ft wide and 8 ft deep. The protection of both the eastern and western spur levees would reinforce and place stone paving at the failed

ends of the eastern and western spur levees. Further detailed evaluation and analysis of these measures will be completed in a follow-on design study.

Multidimensional modeling analysis

Two local scour countermeasures were modeled utilizing AdH.

Geometric data

An AdH mesh was created to represent each respective local scour countermeasure. Listed below is a description of the mesh for all local scour countermeasures.

Local Scour Countermeasure 1 simulated the addition of rock protection around the western edge of the scour hole (approximately 2,300 ft). This was represented by a modified material type in the mesh. Figure 4-1 depicts the study overbank mesh material for Local Scour Countermeasure 1.

Local Scour Countermeasure 2 simulated a tapered trenchfill dike at the eastern tie-in of the closure structure (+6 ft at toe of eastern levee, +4 ft at midpoint, +2 ft at closure structure). Figure 4-2 depicts the study overbank mesh elevation for Local Scour Countermeasure 2. Figure 4-3 depicts the 3D mesh surface for Local Scour Countermeasure 2.

Plan comparisons

The Hypothetical Hydrograph was simulated for both local scour countermeasures.

The bed shear stress output at 1,900,000 cfs from the Hypothetical Hydrograph simulation for Local Scour Countermeasure 1 is depicted in Figure 4-4. Note the regions of high shear stress on the closure structure, the overbank region immediately east of the closure structure, and the eastern and western tie-ins of the closure structure.

Figure 4-1. Local Scour Countermeasure 1 material type (study overbank).

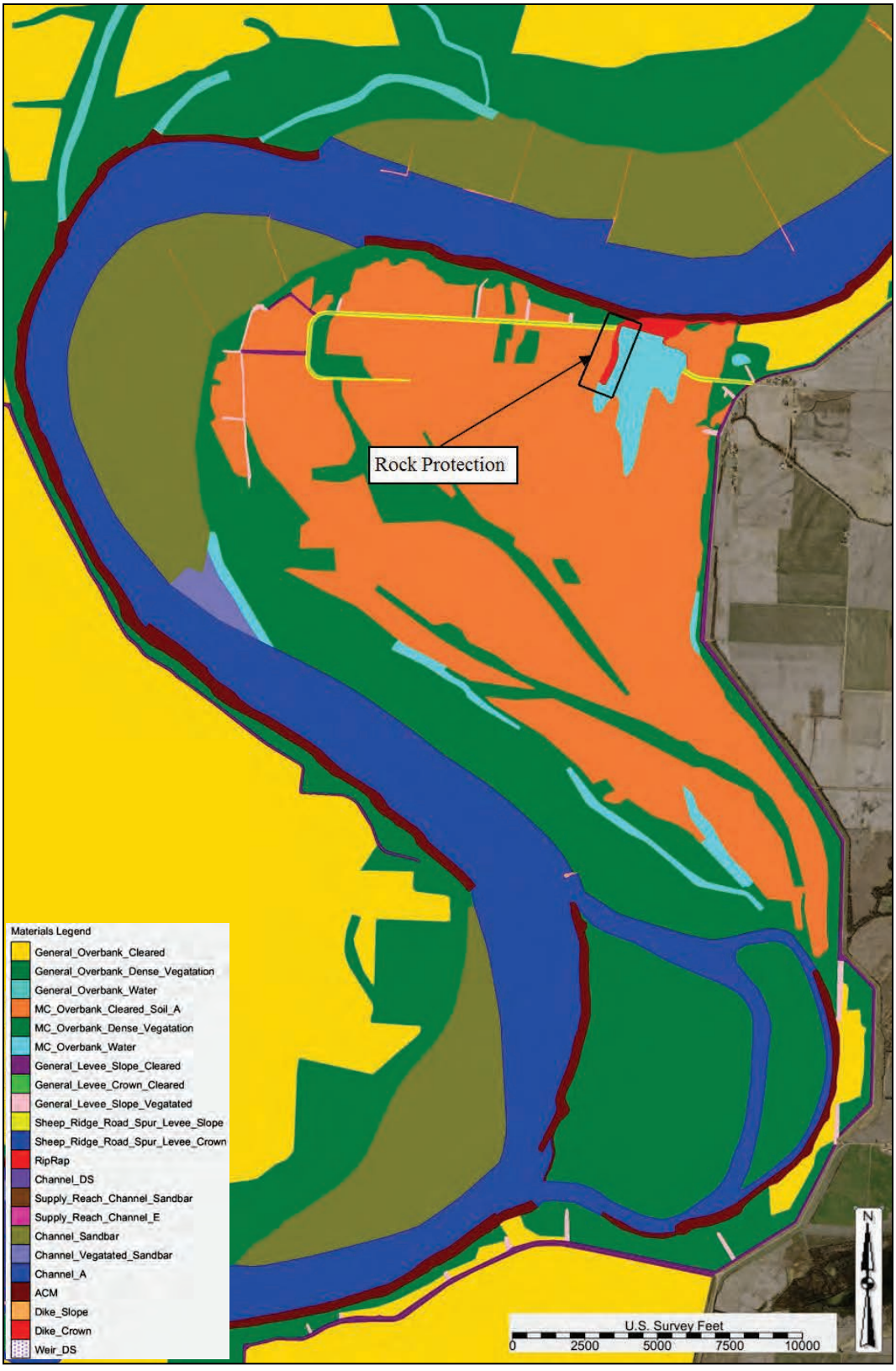


Figure 4-2. Local Scour Countermeasure 2 mesh elevation (study overbank).

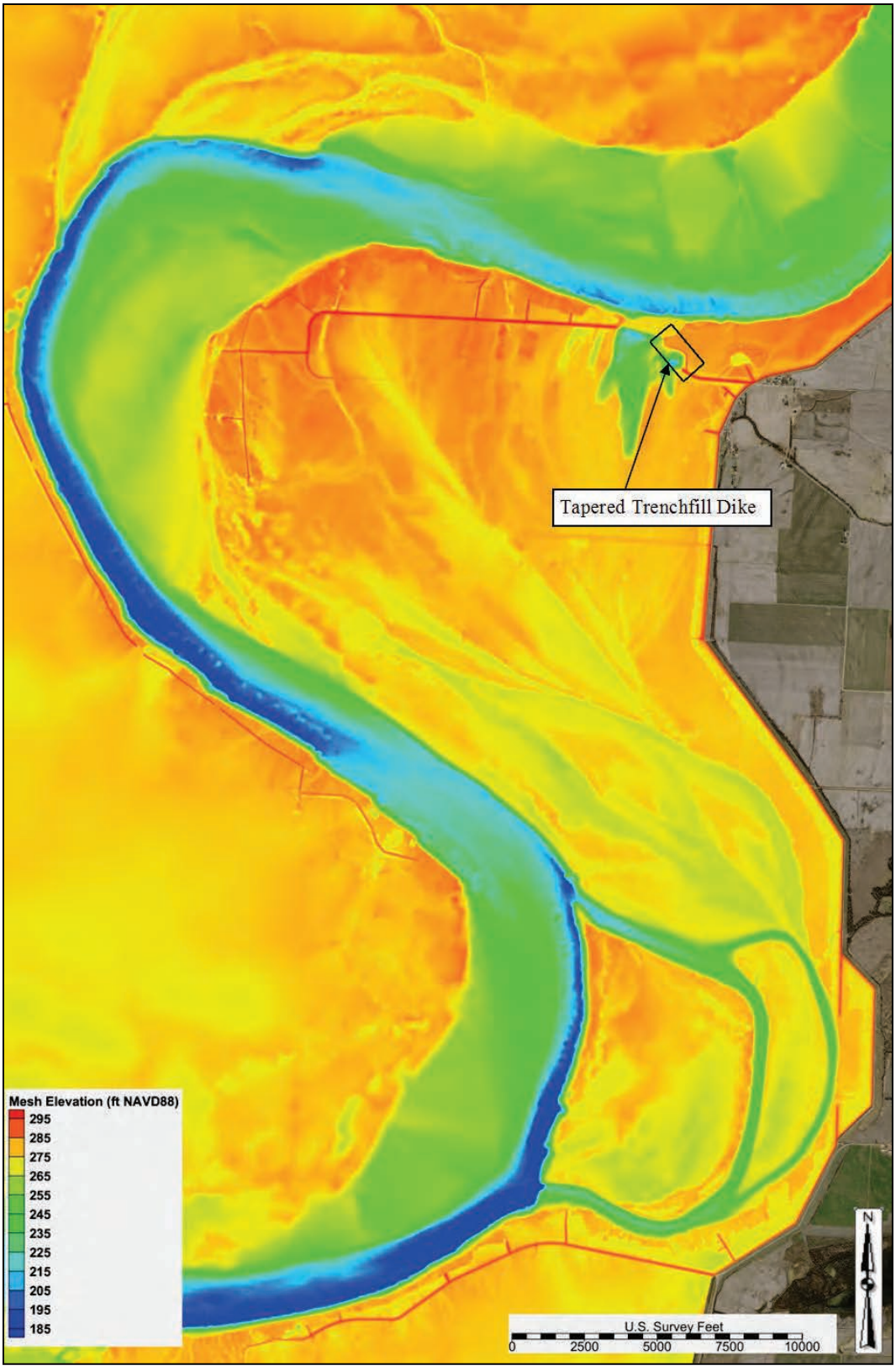


Figure 4-3. Local Scour Countermeasure 2; 3D surface (study overbank).

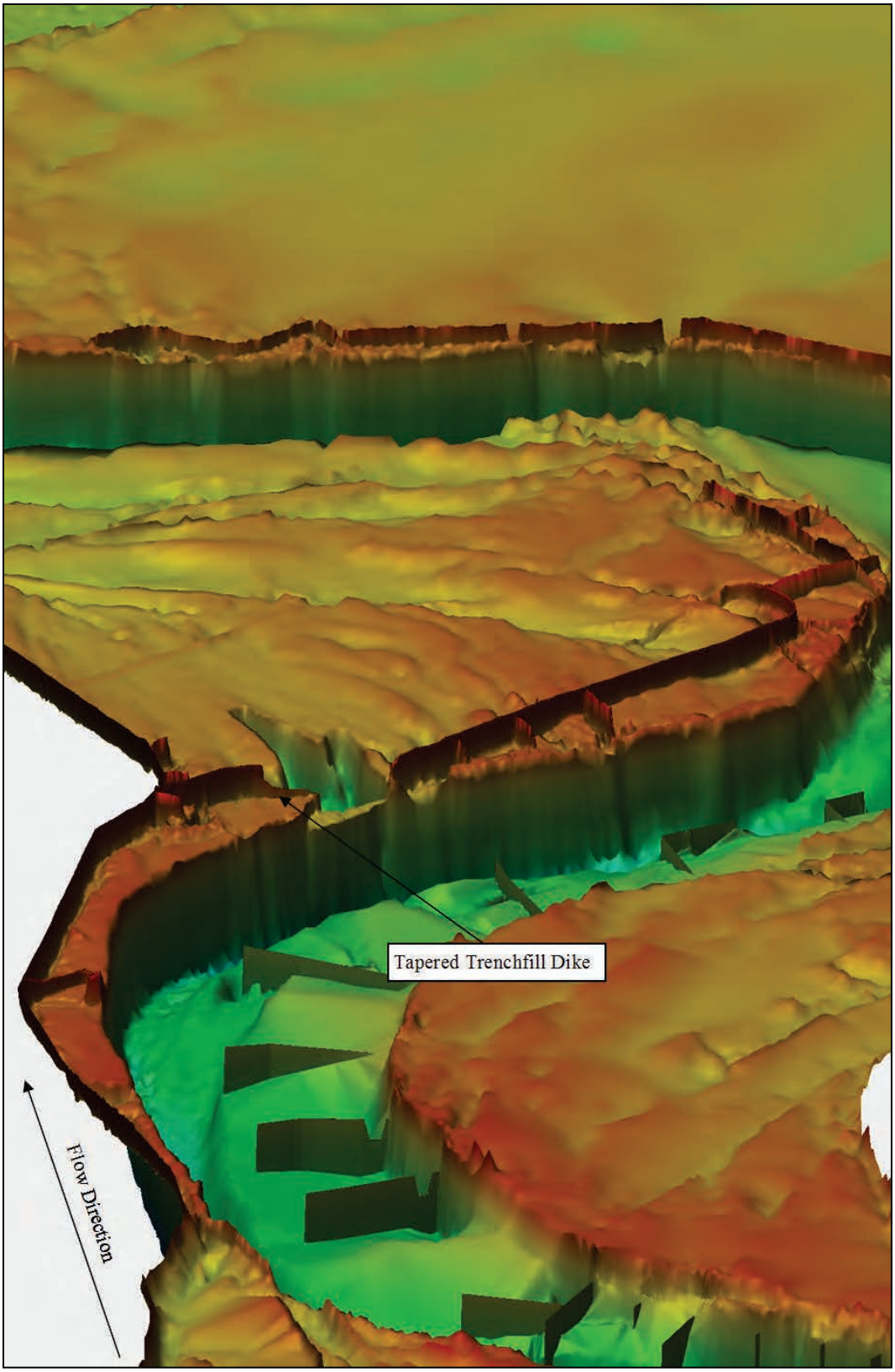
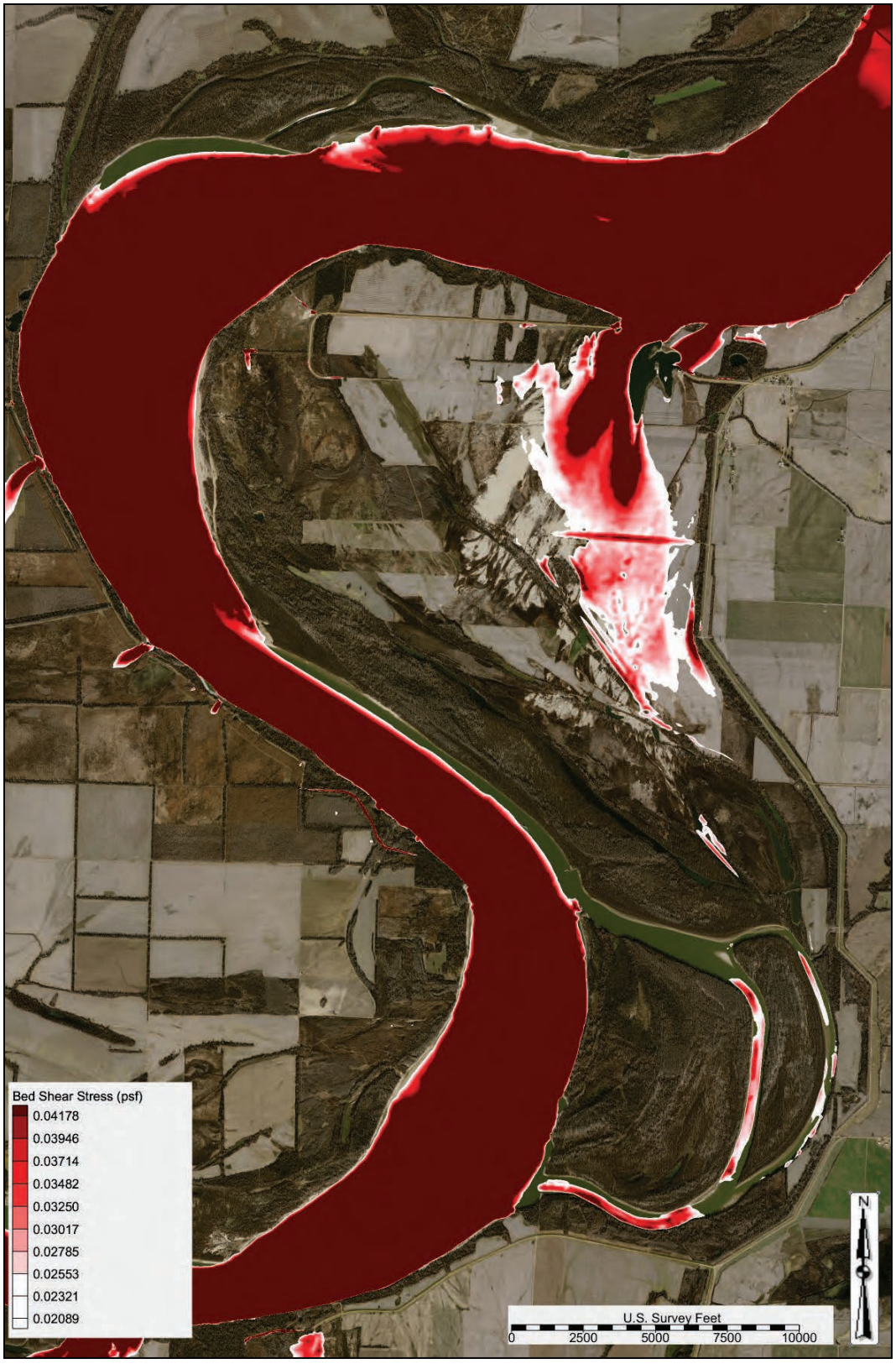


Figure 4-4. Local Scour Countermeasure 1 shear stress—1,900,000 cfs (study overbank).



The bed shear stress difference comparison between local scour countermeasure 1 and the base condition at 1,900,000 cfs from the Hypothetical Hydrograph simulation is depicted in Figure 4-5. Note that shear stress was greatly reduced at the location of the rock protection on the western edge of the scour hole.

The bed shear stress output at 1,900,000 cfs from the Hypothetical Hydrograph simulation for Local Scour Countermeasure 2 is depicted in Figure 4-6. Note the regions of high shear stress on the closure structure, the overbank region immediately east of the closure structure, and the eastern and western tie-ins of the closure structure.

The bed shear stress difference comparison between Local Scour Countermeasure 2 and the base condition at 1,900,000 cfs from the Hypothetical Hydrograph simulation is depicted in Figure 4-7 Note that shear stress was greatly increased on closure structure, the eastern and western tie-ins of the closure structure, and the overbank region immediately east of the closure structure.

Figure 4-5. Local Scour Countermeasure 1 shear stress difference—1,900,000 cfs.

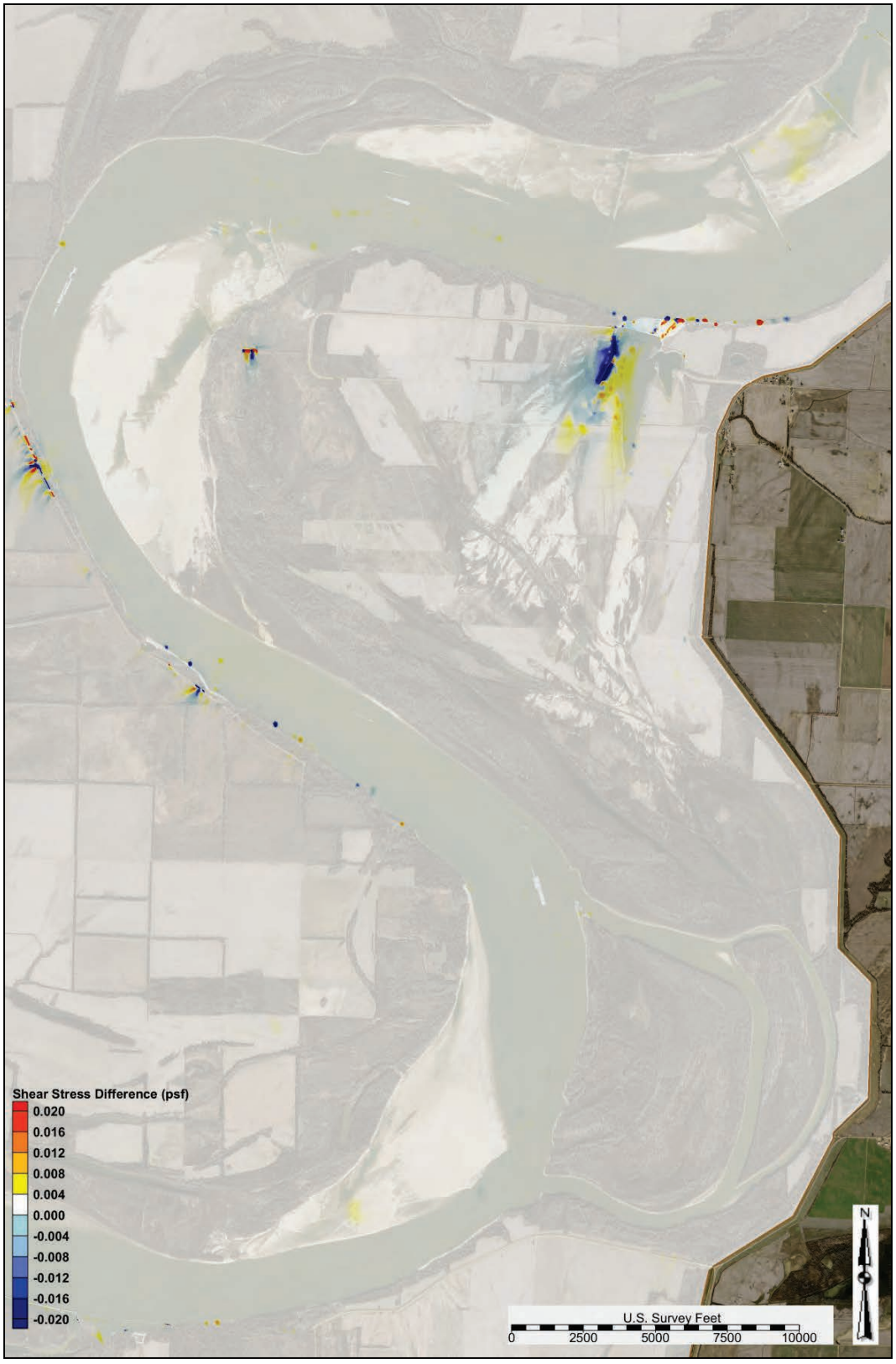


Figure 4-6. Local Scour Countermeasure 2 shear stress—1,900,000 cfs (study overbank).

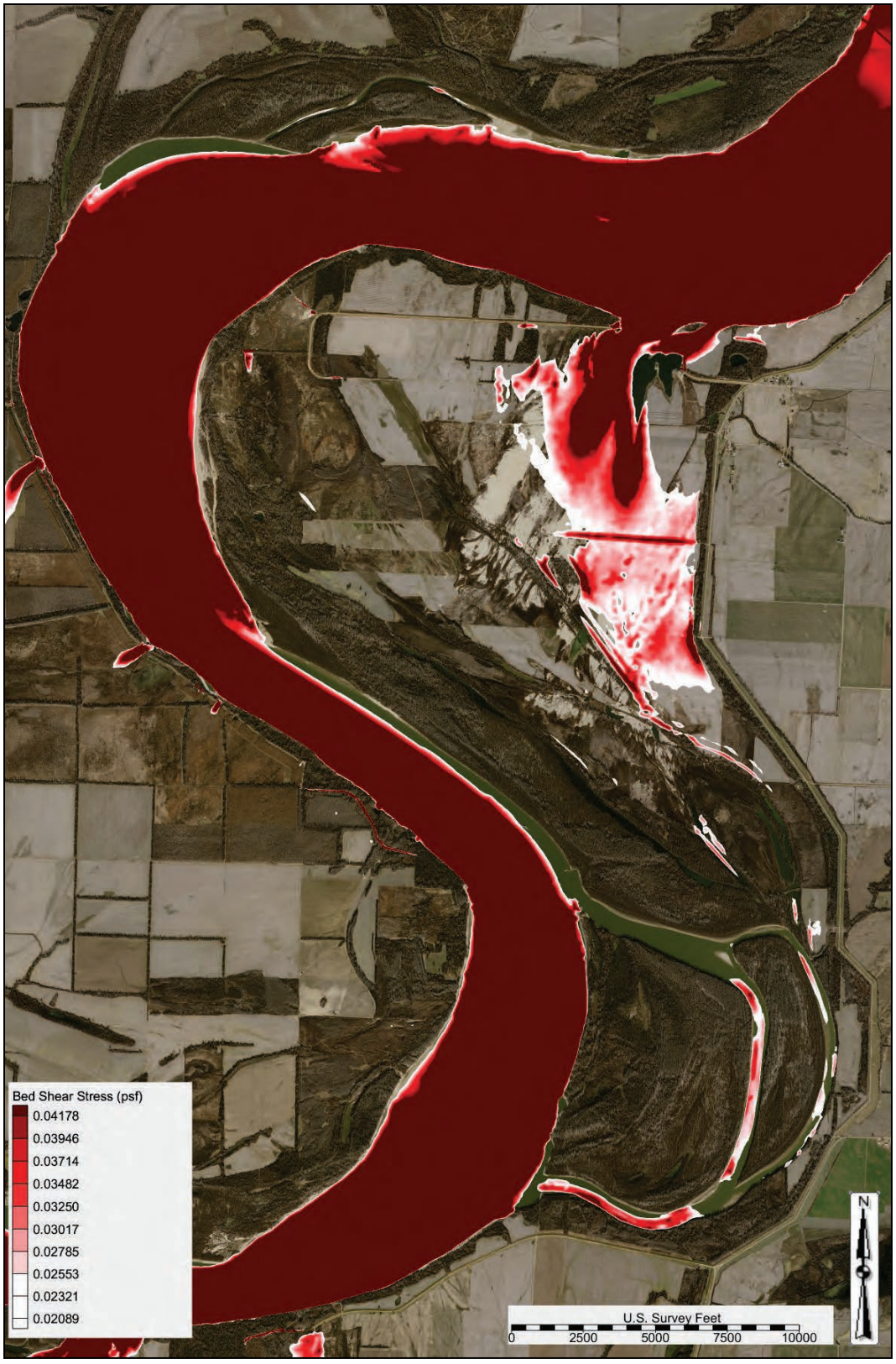
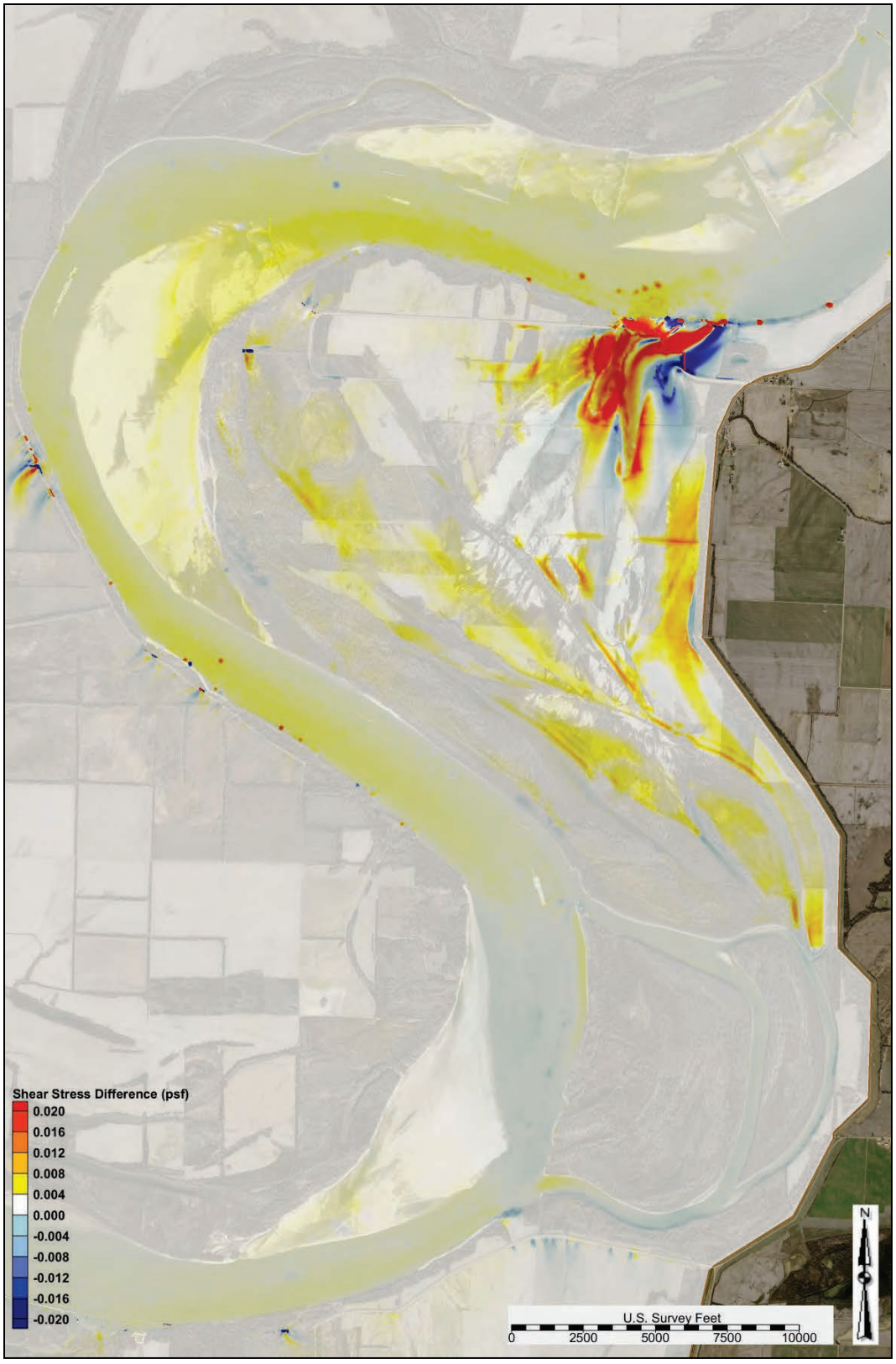


Figure 4-7. Local Scour Countermeasure 2 shear stress difference—1,900,000 cfs.



Flow and sediment diversion analysis

Figure 4-8 depicts a comparison of the Island 13 overbank diversion flow between the base condition and the local scour countermeasures. Local Scour Countermeasure 1 had minimal impact on the diversion flow. Local Scour Countermeasure 2 slightly decreased the diversion flow.

Figure 4-9 depicts a comparison of the Island 13 overbank diversion sediment load between the base condition and the local scour countermeasures. Local Scour Countermeasure 1 slightly decreased the diversion sediment load. Local Scour Countermeasure 2 had slightly increased the diversion sediment load.

Scenario simulations

The modeled local scour countermeasures were evaluated for a range of flows (800,000–2,500,000 cfs). Appendix C contains the following detailed data for the modeled local scour countermeasures from the Hypothetical Hydrograph simulations:

- shear stress output at flows ranging from 900,000 to 2,100,000 cfs for the study overbank (Local Scour Countermeasure 1: Figures C-208 through C-214 and Local Scour Countermeasure 2: Figures C-223 through C-229)
- shear stress difference plots compared to the base condition output at flows ranging from 900,000 to 2,100,000 cfs for the study overbank (Local Scour Countermeasure 1: Figures C-215 through C-221 and Local Scour Countermeasure 2: Figures C-230 through C-236)
- WSEL profiles in the study reach for the following flows: 1,100,000 cfs, 1,500,000 cfs, 1,900,000 cfs, and 2,100,000 cfs (Local Scour Countermeasure 1: Figure C-222 and Local Scour Countermeasure 2: Figure C-237)
- local scour countermeasures vs. base condition WSEL profiles for the following flows: 1,100,000 cfs, 1,500,000 cfs, 1,900,000 cfs, and 2,100,000 cfs (Figures C-238 through C-241)
- sediment diversion grain size distribution for flows ranging from 870,000 to 2,000,000 cfs (Table C-9 through C-10).

Figure 4-8. Local scour countermeasure overbank diversion flow.

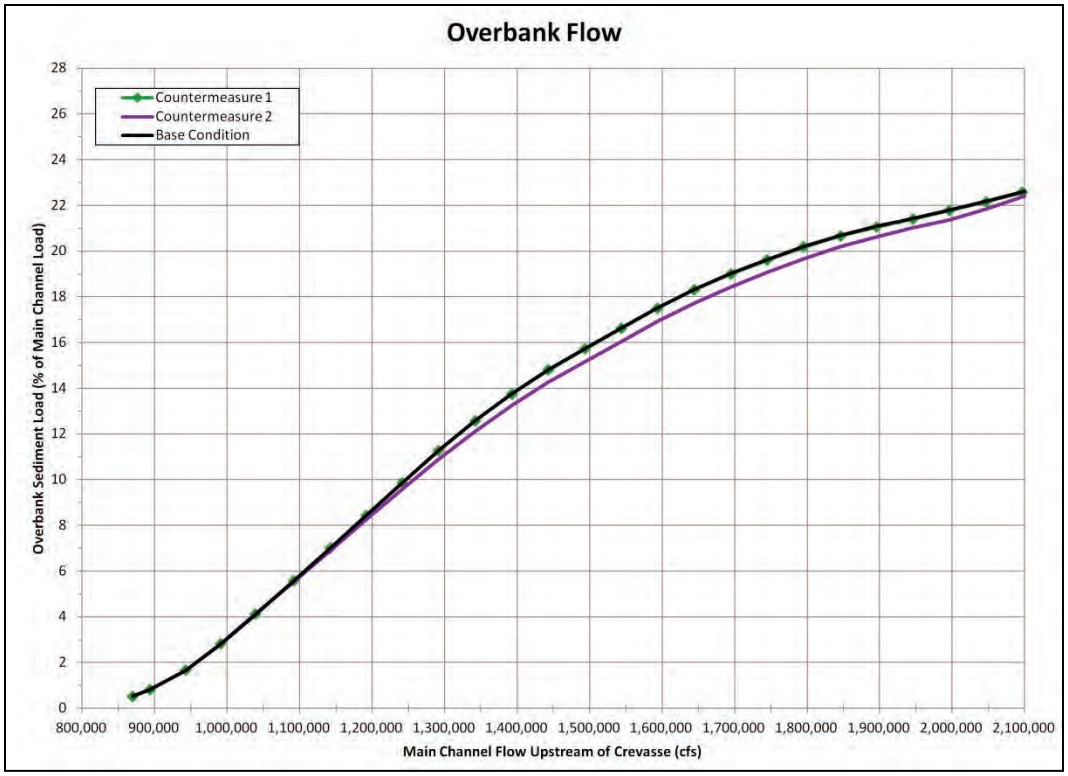
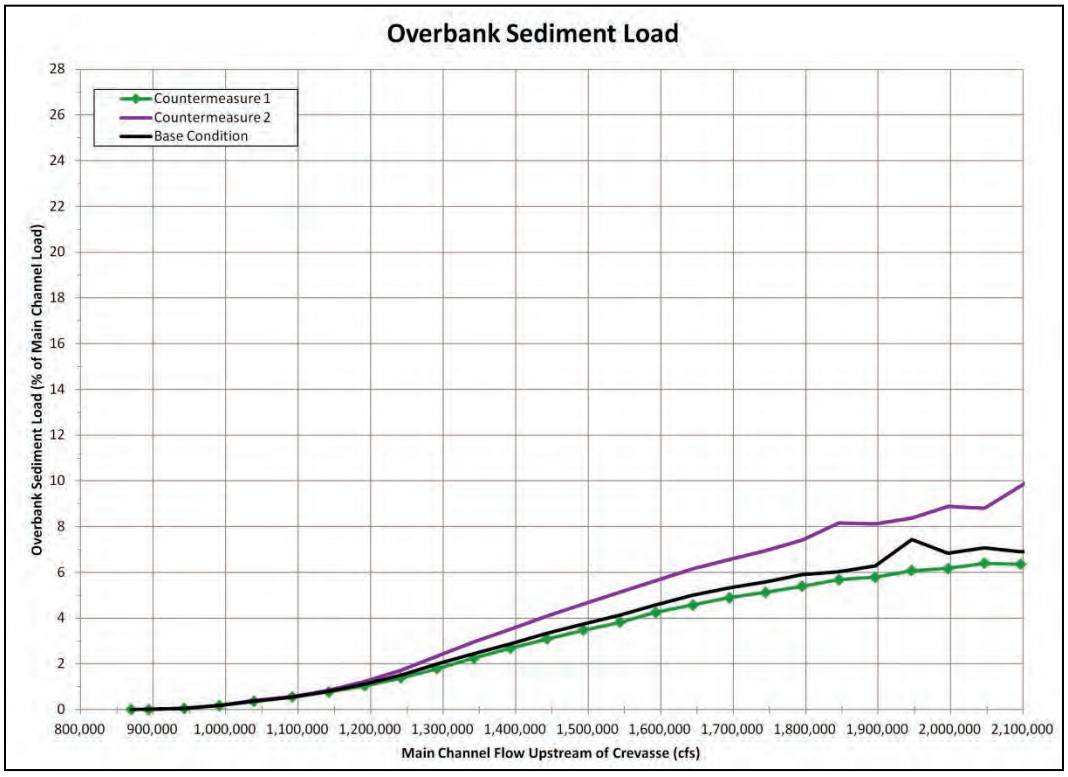


Figure 4-9. Local scour countermeasure overbank sediment diversion load.



5 Risk Mitigation

Summary of modeled risk mitigation measures

Listed in Table 5-1 is a summary of the six alternatives. The analysis indicated that Alternatives 1, 5, and 6 reduced but did not eliminate the risk for cutoff formation for higher magnitude flood events. Alternatives 2, 3, and 4 were ineffective at reducing the risk for cutoff formation for high-magnitude flood events.

Listed in Table 5-2 is a summary of the modeled local scour counter-measures. The analysis indicated that Local Scour Countermeasure 1 reduced the risk for closure structure failure. Local Scour Countermeasure 2 was ineffective at reducing the risk for closure structure failure.

Table 5-1. Summary of alternatives.

ID	Description	Pro	Con
Alternative 1	Levee built to elevation 291.0 ft NAVD88	-Virtually eliminates cutoff risk up to 1.65Mcfs	-Conflicts with current and future NRCS WRP easements -ROM estimate in excess of $23 Million -Prevents diversion flow until 1.65Mcfs, then protection measures would be needed to prevent levee failure -Authorization concerns
Alternative 2	Levee built to elevation 282.0 ft NAVD88	-Virtually eliminates cutoff risk up to 1.1Mcfs	-Does not reduce cutoff risk for flows over 1.1Mcfs -Conflicts with current and future NRCS WRP easements -Authorization concerns
Alternative 3	Western levee degraded to elevation 281.0 ft NAVD88		-Does not reduce cutoff risk -Conflicts with current and future NRCS WRP easements -Authorization concerns
Alternative 4	Overbank road raised to elevation 276.0 ft NAVD88		-Does not reduce cutoff risk -Conflicts with current and future NRCS WRP easements -Authorization concerns

ID	Description	Pro	Con
Alternative 5	Dense vegetation on the entire overbank	-Reduces cutoff risk -WRP easements obtained by NRCS for significant portion of overbank -NRCS plans to obtain nearly all remaining overbank tracks and place in WRP -Environmental benefits	-Estimated 20–30 year period to obtain full implementation, moderate risk for cutoff formation during this period -Replanting cycle expected as a result of tree mortality due to periodic high water/floods -Additional short-term risk mitigation measures required during initial 20–30 year period
Alternative 6	Dense vegetation on obtained WRP easements	-Reduces cutoff risk -Environmental benefits	-Estimated 20–30 year period to obtain full implementation, moderate risk for cutoff formation during this period Cleared land remains in western portion of crevasse location resulting in higher risk for erosion -Replanting cycle expected as a result of tree mortality due to periodic high water/floods -Additional short-term risk mitigation measures required during initial 20–30 year period

Table 5-2. Local scour countermeasure summary.

ID	Description	Pro	Con
Local Scour Countermeasure 1	Rock protection around western edge of the scour hole (2,300 ft)	-Reduces local scour risk adjacent to rock	-Cost -NRCS WRP easement infringement
Local Scour Countermeasure 2	Tapered trenchfill dike (+6 ft at toe of eastern levee, +4 ft at midpoint, +2 ft at closure structure		-Does not reduce local scour risk -Cost -NRCS WRP easement infringement
Eastern Trenchfill Dike	Trenchfill dike 35 ft wide and 8 ft deep	-Provides launch stone to protect against overbank scour to the east of the closure structure	-Cost
Eastern Spur Levee Protection	Stone paving on end of spur levee	-Reinforces and protects end of levee adjacent to the scour hole	-Cost
Western Spur Levee Protection	Stone paving on end of spur levee	-Reinforces and protects end of levee adjacent to the scour hole	-Cost

Risk mitigation recommendation

Risk of cutoff formation

The analysis conducted on the base condition indicated that there is a moderate risk for cutoff formation. Alternative 5 was recommended to mitigate the long-term risk of cutoff formation. Alternative 5 has an initial development period (estimated 20–30 years) that has a moderate risk for cutoff formation during this period. Short-term risk mitigation measures are required until full implementation (mature vegetation across entire overbank is established) of Alternative 5 is achieved. Note that the Island 13 overbank reach will further develop when the closure structure is overtopped and overbank diversion flow occurs.

Risk of closure structure failure

The analysis conducted on the base condition indicated that there is a severe risk for local scour at the closure structure. To mitigate the risk of closure structure failure, it is recommended that the following measures be implemented: Local Scour Counter Measure 1, expansion of the existing eastern trenchfill dike, protection of the eastern spur levee, and protection of the western spur levee. These local scour countermeasures are critical components that tie-in to each other (and the closure structure) to reduce the risk of closure structure failure.

Risk to navigation

The navigation analysis indicated that there is the potential for an outdraft condition at the study crevasse. The outdraft condition occurs during events that overtop the closure structure and diversion flow commences (base condition analysis indicated approximately 858,000 cfs).

Risk at MRL

The analysis indicated scour potential at the toe of the Tiptonville-Obion River Levee. It is recommended that further investigation be conducted on the scour potential and determine if MRL protection measures are required. Island 13 also contains a ditch that drains the outlet of the MRL Mooring Bayou Culverts to the scour hole. A headcut is progressing from the scour hole to the Mooring Bayou Culverts that will put at risk culvert stability at the MRL. Grade control measures are recommended to prevent the headcut from reaching the Mooring Bayou Culvert. Further analysis should be conducted to develop grade control designs.

6 Conclusion

The study indicated that there is a risk of cutoff formation, risk of closure structure failure, risk to navigation, and risk at the Tiptonville-Obion River Levee.

Alternative 5 was recommended to mitigate the long-term risk of cutoff formation. Coordination with the NRCS commenced in the spring of 2015 to achieve full vegetation across the entire Island 13 overbank. Additional analysis is required to investigate mitigation measures for the short-term risk of cutoff formation. It is recommended that a monitoring program be established to monitor the risk of cutoff formation. The monitoring program would survey the scour hole extent once each year that overbank flow occurs until full vegetation is established. General overbank scour should be monitored by collecting and analyzing aerial imagery each year that overbank flow occurs until full vegetation is established. Tree plantings and tree losses should be monitored after events that overtop the closure structure. Trees should be replanted as required to provided 90% coverage in each WRP easement. Trees lost in the critical overbank flow path should be replanted in order to avoid formation of a nonvegetated preferred flow path.

To mitigate the risk of closure structure failure, it is recommended that the following measures be implemented: Local Scour Countermeasure 1, expansion of the existing eastern trenchfill dike, protection of the eastern spur levee, and protection of the western spur levee. A task order was issued in summer of 2015 to further protect and complete construction of the closure structure. It is recommended that upon completion of the 2015 closure structure task order, that the multidimensional model be updated to include the new closure structure features. The key elevations and flows table (Table 2-14) should be updated to incorporate the most current features that exist in the field.

The navigation analysis indicated that there is the potential for an outdraft condition at the study crevasse. The outdraft condition occurs during events that overtop the closure structure and diversion flow commences (base condition analysis indicated approximately 858,000 cfs). It is recommended to collect ADCP data in the vicinity of the crevasse during

events that overtop the closure structure and diversion flow commences to obtain additional data regarding the outdraft condition.

The analysis indicated scour potential at the toe of the Tiptonville-Obion River Levee. It is recommended that further investigation be conducted on the scour potential and determine if MRL protection measures are required. Island 13 also contains a ditch that drains the outlet of the MRL Mooring Bayou Culverts to the scour hole. A headcut is progressing from the scour hole to the Mooring Bayou Culverts that will put the culvert stability at the MRL at risk. Grade control measures are recommended to prevent the headcut from reaching the Mooring Bayou Culvert. Further analysis should be conducted to develop grade control designs.

References

Berger, R.C., J. N. Tate, G. L. Brown, and G. Savant. 2014. *Adaptive hydraulics user manual*. Vicksburg, MS: U.S. Army Engineer Research and Development Center.

Bernard, R. 1992. *Depth-average numerical modeling for curved channels*. Technical Report HL-92-9. Vicksburg, MS: U.S. Army Corps of Engineers, Waterways Experiment Station.

Biedenharn, D. S., W. A. Stroupe, and J. H. Brooks. 2014. *A review of the lower Mississippi River potamology program*. MRG&P Report No. 1. Vicksburg, MS: U.S. Army Engineer Research and Development Center.

Brown, G. L., J. N. Tate, and G. Savant. 2012. *SEDLIB multiple grain sized mixed sediment library: Technical manual*. http://www.google.com/url?sa=t&rct=j&q=&esrc=s&source=web&cd=1&ved=0ahUKEwj914HynuvLAhUU5WMKHS7WCn0QFggcMAA&url=http%3A%2F%2Fadh.usace.army.mil%2Fnew_webpage%2Fdocumentation%2FSEDLIB_Manual-Version1.2.pdf&usg=AFQjCNHW8qxZ_y3Ux20TBKLwj2pKDOI0Uw&bvm=bv.118353311,d.cGc.

Fisk, H. N. 1944. *Geological investigation of the alluvial valley of the Lower Mississippi River*. Vicksburg, MS: War Department, Corps of Engineers, U.S. Army, Mississippi River Commission.

Gaines, R. A., and A. M. Priestas. 2015. *Particle size distributions of bed sediments along the Mississippi River, Grafton, Illinois, to Head of Passes, Louisiana, November 2013*. Mississippi Valley Division MRG&P Report No. 7. Vicksburg, MS: U.S. Army Corps of Engineers, Mississippi Valley Division.

Heath, R. E., G. L. Brown, C. D. Little, T. C. Pratt, J. J. Ratcliff, D. D. Abraham, D. Perkey, N. B. Ganesh, K. Martin, and D. P. May. 2015. *Old River Control Complex sedimentation investigation*. ERDC/CHL TR-15-8. Vicksburg, MS: U.S. Army Engineer Research and Development Center.

Lane, E. W. 1947. Report on the subcommittee on sediment terminology. *Transactions, American Geophysical Union* 28(6):936–938.

Mehta, A. J. 2014. *An introduction to hydraulics of fine sediment transport*. Advanced Series on Ocean Engineering, vol. 38. Hackensack: World Scientific.

Mitchener, H. J., R. J. S. Whitehouse, R. L. Soulsby, and V. A. Lawford. 1996. *Estuarine morphodynamics. Development of SedErode – instrument for in-situ mud erosion measurements*. HR Wallingford Report TR 17. United Kingdom: HR Wallingford Ltd.

Nalluri, C., R. E. Featherstone, and M. J. Marriott. 2009. *Civil engineering hydraulics, 5th Edition*. United Kingdom: Wiley-Blackwell.

Saucier, R. T. 1974. *Quaternary geology of the Lower Mississippi Valley*. Arkansas Archeological Survey Research Series No. 6. http://www.google.com/url?sa=t&rct=j&q=&esrc=s&source=web&cd=3&ved=0ahUKEwjFzKupo-vLAhUM2mMKHU9iCAwQFggoMAI&url=http%3A%2F%2Fbiotech.law.lsu.edu%2Fclimate%2Fmississippi%2Fsausier%2FQuaternary_Geo_LMV.pdf&usg=AFQjCNHDJYmaU2MRL-4Agj6mQa4p-gzqoQ&bvm=bv.118353311,d.cGc.

Saucier, R. T. 1994. *Geomorphology and quaternary geologic history of the Lower Mississippi Valley*. Vicksburg, MS: U.S. Army Corps of Engineers, Waterways Experiment Station.

Spasojevic, M., and F. Holly, Jr. 1994. *Three-dimensional numerical simulation of mobile-bed hydrodynamics*. Technical Report HL-94-2. Vicksburg, MS: U.S. Army Corps of Engineers, Waterways Experiment Station.

Whitehouse, R. J. S., R. L. Soulsby, W. Roberts, and H. J. Mitchener. 2000. *Dynamics of estuarine muds: A manual for practical applications*. London: HR Wallingford, DETR, Thomas Telford.

Winterwerp, J. C., and W. G. M. Van Kesteren. 2004. *Introduction to the physics of cohesive sediment in the marine environment*. Developments in Sedimentology series, vol. 56. Boston, Amsterdam: Elsevier.

Appendix A: Merriwether-Cherokee Potamology Study Phase I Report

Appendix A contains the *Merriwether-Cherokee Potamology Study Phase I Report - HEC-RAS 1D/2D Modeling* that documented prior analysis conducted by the Memphis District.



US Army Corps
of Engineers ®
Memphis District

Merriwether-Cherokee Potamology Study
Phase I Report

HEC-RAS 1D/2D Modeling

31 January 2014

(this page intentionally blank)

Merriwether-Cherokee Potamology Study Phase I Report

HEC-RAS 1D/2D Modeling

Hydraulics Branch
Memphis District
Corps of Engineers
Prepared By: Brian M. Hall

31 January 2014

(this page intentionally blank)

Abstract: This report was prepared by Brian M. Hall (CEMVM-EC-H) and documents the Phase I analysis of the Merriwether-Cherokee Potamology Study. Computer application of Hydrologic Engineering Centers River Analysis System (HEC-RAS) supported the evaluation of the Lower Mississippi River from river miles 871 to 864. The following conditions were modeled and analyzed: current 2013 conditions, pre-2011 crevasse conditions, four alternatives to Sheep Ridge Road Spur Levee, and two scenarios that model increased channel bed elevations for a portion of the reach.

(this page intentionally blank)

Executive Summary

This report documents the Phase I analysis of the Merriwether-Cherokee Potamology Study. Computer application of Hydrologic Engineering Centers River Analysis System (HEC-RAS) supported the evaluation of the Lower Mississippi River from river miles 871 to 864. The following conditions were modeled and analyzed: current 2013 conditions, pre-2011 crevasse conditions, four alternatives to Sheep Ridge Road Spur Levee, and two scenarios that model increased channel bed elevations for a portion of the reach.

During the historic flood of 2011, the Mississippi River reached record breaking water levels between Cairo, Illinois and Memphis, Tennessee. Downstream from Tiptonville, Tennessee, Sheep Ridge Road Spur Levee (private) was overtopped and crevassed when the Mississippi River reached a stage of 48.35 feet on the Tiptonville gage. The length of levee crevassed was 3,000 feet, and the length of bankline erode was 2,700 feet. The Mississippi River began to form a new cutoff from river mile (RM) 869 to 860. Erosion extended approximately 4,000 feet along Island 13, degrading the landscape to elevations 80 feet below natural ground. The crevasse divided the Sheep Ridge Road Spur Levee, leaving an approximate 3,000-foot section to the east of the crevasse (eastern spur levee) and an approximate 2.2-mile section to the west of the crevasse of Sheep Ridge Road Spur Levee (the western spur levee).

A concern is that without modification or degradation of the western spur levee, the Mississippi River will continue to form a 9-mile cutoff. If a cutoff were to form, potential adverse impacts include: changes in long term reach dynamics, navigation outdraft conditions, increased dredging operations, hydrodynamic condition changes in close proximity to a MRL mainline levee (Tiptonville-Obion Levee), endangerment of existing channel improvement features ($60M), endangerment of completed crevasse repairs ($18.5M), and endangerment of planned crevasse repairs ($9.5M).

The HEC-RAS analysis demonstrated that the base condition plan is hydrodynamically different compared to the pre-2011 crevasse, both in the main channel and in the Island 13 overbank region. Furthermore, the analysis indicated that all western spur levee modification alternatives would reduce velocities and shear stresses in certain regions of the Island 13 overbank; however, these alternatives also increase velocities and shear stresses in other portions of the overbank (specifically, downstream of the overbank scour hole and the western overbank region of Island 13). The analysis also indicated that both the changes in diversion flow through the crevasse and the adjustment to channel bed elevations affect the sediment transport potential in the river.

The HEC-RAS analysis does not address channel adjustment that will result from decreased sediment transport potential, nor is HEC-RAS capable of simulating the interaction between decreased channel capacity due to deposition and the flow distribution between main channel and the overbank crevasse. This effect is coupled and requires a multiple dimensional model that has the ability to simulate sediment transport and a mobile boundary.

The Phase I results underscore the need for further analysis to complete the objectives specified for the Merriwether-Cherokee Potamology Study. A recommendation is that this study should proceed to the next modeling phase, which will include the use of the 2D depth-averaged Adaptive Hydraulics (AdH) program, with sediment transport and a 1D sedimentation model.

(this page intentionally blank)

Contents

Executive Summary vii
1 Purpose 1
2 Problem 1
3 Method 2
3.1 Hydrodynamics 6
3.2 Sediment Transport Capacity 8
4 Results 9
5 Conclusion 11
References 13
Plates 15
Appendix A. HEC-RAS Analysis 23
A.1 Cross Section Maximum Water Surface Profiles 25
A.2 2D Flow Area Velocity - Simulation Hour 648 28
A.3 2D Flow Area Shear Stress - Simulation Hour 648 37
A.4 2D Flow Area Velocity - Simulation Hour at Maximum 46
A.5 2D Flow Area Shear Stress - Simulation Hour at Maximum 55
A.6 2D Flow Area Velocity - Node Maximum 64
A.7 2D Flow Area Shear Stress - Node Maximum 73
A.8 2D Flow Area Velocity - Difference from Base Condition Plan 82
A.9 2D Flow Area Shear Stress - Difference from Base Condition Plan 90
A.10 2D Flow Area Time Series Data 98
A.11 Sediment Transport Capacity 116
A.12 Calibration of 2D Overbank Region 119
Appendix B. CEERD-HF-RS MFR 125
End of Report 129

Tables

Table 3-1. Conversion from RAS River Station to Navigation River Mile 3
Table 3-2. HEC-RAS Plan Description 5
Table 3-3. HEC-RAS Steady Flow Sediment Transport Boundary Conditions 8
Table 3-4. 1989 Channel Gradation at RM 867.3 Above Head of Passes (from Nordin and Queen, 1992) 9
Table 3-5. Diversion Flow Plan Comparison 10
Table 3-6. Plan Results Comparison 10
Table 3-7. Reach Average Sediment Transport Potential 11

Table A-1. Plan Description 23
Table A-2. Simulation Time Window Relationship 24

Figures

Figure 3-1. Levee Modification Classification 5
Figure 3-2. Sheep Ridge Road Western Spur Levee Alternatives Plan Files 6
Figure 3-3. Upstream Boundary Condition Hypothetical Flow Hydrograph 7

Figure A-1. Maximum Water Surface Profiles Plans 11-16 at RM 872-844 26
Figure A-2. Maximum Water Surface Profiles Plans 11-16 at RM 871-864 26
Figure A-3. Maximum Water Surface Profiles Plans 11,12,17,18 at RM 872-844 27
Figure A-4. Maximum Water Surface Profiles Plans 11,12,17,18 at RM 871-864 27
Figure A-5. Plan 11 2D Velocity at Simulation Hour 648 29
Figure A-6. Plan 12 2D Velocity at Simulation Hour 648 30
Figure A-7. Plan 13 2D Velocity at Simulation Hour 648 31
Figure A-8. Plan 14 2D Velocity at Simulation Hour 648 32
Figure A-9. Plan 15 2D Velocity at Simulation Hour 648 33
Figure A-10. Plan 16 2D Velocity at Simulation Hour 648 34
Figure A-11. Plan 17 2D Velocity at Simulation Hour 648 35
Figure A-12. Plan 18 2D Velocity at Simulation Hour 648 36
Figure A-13. Plan 11 Shear Stress at Simulation Hour 648 38
Figure A-14. Plan 12 Shear Stress at Simulation Hour 648 39
Figure A-15. Plan 13 Shear Stress at Simulation Hour 648 40
Figure A-16. Plan 14 Shear Stress at Simulation Hour 648 41
Figure A-17. Plan 15 Shear Stress at Simulation Hour 648 42
Figure A-18. Plan 16 Shear Stress at Simulation Hour 648 43
Figure A-19. Plan 17 Shear Stress at Simulation Hour 648 44
Figure A-20. Plan 18 Shear Stress at Simulation Hour 648 45
Figure A-21. Plan 11 Velocity at Simulation Hour 532 47
Figure A-22. Plan 12 Velocity at Simulation Hour 314 48
Figure A-23. Plan 13 Velocity at Simulation Hour 314 49
Figure A-24. Plan 14 Velocity at Simulation Hour 314 50
Figure A-25. Plan 15 Velocity at Simulation Hour 314 51
Figure A-26. Plan 16 Velocity at Simulation Hour 314 52
Figure A-27. Plan 17 Velocity at Simulation Hour 312 53
Figure A-28. Plan 18 Velocity at Simulation Hour 310 54
Figure A-29. Plan 11 Shear Stress at Simulation Hour 528 56
Figure A-30. Plan 12 Shear Stress at Simulation Hour 310 57
Figure A-31. Plan 13 Shear Stress at Simulation Hour 310 58
Figure A-32. Plan 14 Shear Stress at Simulation Hour 310 59
Figure A-33. Plan 15 Shear Stress at Simulation Hour 310 60
Figure A-34. Plan 16 Shear Stress at Simulation Hour 310 61
Figure A-35. Plan 17 Shear Stress at Simulation Hour 312 62
Figure A-36. Plan 12 Shear Stress at Simulation Hour 310 63
Figure A-37. Plan 11 Velocity Node Maximum 65
Figure A-38. Plan 12 Velocity Node Maximum 66
Figure A-39. Plan 13 Velocity Node Maximum 67

Figure A-40. Plan 14 Velocity Node Maximum 68
Figure A-41. Plan 15 Velocity Node Maximum 69
Figure A-42. Plan 16 Velocity Node Maximum 70
Figure A-43. Plan 17 Velocity Node Maximum 71
Figure A-44. Plan 18 Velocity Node Maximum 72
Figure A-45. Plan 11 Shear Stress Node Maximum 74
Figure A-46. Plan 12 Shear Stress Node Maximum 75
Figure A-47. Plan 13 Shear Stress Node Maximum 76
Figure A-48. Plan 14 Shear Stress Node Maximum 77
Figure A-49. Plan 15 Shear Stress Node Maximum 78
Figure A-50. Plan 16 Shear Stress Node Maximum 79
Figure A-51. Plan 17 Shear Stress Node Maximum 80
Figure A-52. Plan 18 Shear Stress Node Maximum 81
Figure A-53. Plan 11 Velocity Difference from Base Condition 83
Figure A-54. Plan 13 Velocity Difference from Base Condition 84
Figure A-55. Plan 14 Velocity Difference from Base Condition 85
Figure A-56. Plan 15 Velocity Difference from Base Condition 86
Figure A-57. Plan 16 Velocity Difference from Base Condition 87
Figure A-58. Plan 17 Velocity Difference from Base Condition 88
Figure A-59. Plan 18 Velocity Difference from Base Condition 89
Figure A-60. Plan 11 Shear Stress Difference from Base Condition 91
Figure A-61. Plan 13 Shear Stress Difference from Base Condition 92
Figure A-62. Plan 14 Shear Stress Difference from Base Condition 93
Figure A-63. Plan 15 Shear Stress Difference from Base Condition 94
Figure A-64. Plan 16 Shear Stress Difference from Base Condition 95
Figure A-65. Plan 17 Shear Stress Difference from Base Condition 96
Figure A-66. Plan 18 Shear Stress Difference from Base Condition 97
Figure A-67. Time Series Data Output Location Node Number 99
Figure A-68. Node 410 Velocity Time Series Data for P11-P16 100
Figure A-69. Node 410 Velocity Time Series Data for P11,P12,P17,P18 100
Figure A-70. Node 410 Shear Stress Time Series Data for P11-P16 101
Figure A-71. Node 410 Shear Stress Time Series Data for P11,P12,P17,P18 101
Figure A-72. Node 967 Velocity Time Series Data for P11-P16 102
Figure A-73. Node 967 Velocity Time Series Data for P11,P12,P17,P18 102
Figure A-74. Node 967 Shear Stress Time Series Data for P11-P16 103
Figure A-75. Node 967 Shear Stress Time Series Data for P11,P12,P17,P18 103
Figure A-76. Node 1495 Velocity Time Series Data for P11-P16 104
Figure A-77. Node 1495 Velocity Time Series Data for P11,P12,P17,P18 104
Figure A-78. Node 1495 Shear Stress Time Series Data for P11-P16 105
Figure A-79. Node 1495 Shear Stress Time Series Data for P11,P12,P17,P18 105
Figure A-80. Node 1528 Velocity Time Series Data for P11-P16 106
Figure A-81. Node 1528 Velocity Time Series Data for P11,P12,P17,P18 106
Figure A-82. Node 1528 Shear Stress Time Series Data for P11-P16 107
Figure A-83. Node 1528 Shear Stress Time Series Data for P11,P12,P17,P18 107
Figure A-84. Node 1568 Velocity Time Series Data for P11-P16 108
Figure A-85. Node 1568 Velocity Time Series Data for P11,P12,P17,P18 108

Figure A-86. Node 1568 Shear Stress Time Series Data for P11-P16 109
Figure A-87. Node 1568 Shear Stress Time Series Data for P11,P12,P17,P18 109
Figure A-88. Node 1593 Velocity Time Series Data for P11-P16 110
Figure A-89. Node 1593 Velocity Time Series Data for P11,P12,P17,P18 110
Figure A-90. Node 1593 Shear Stress Time Series Data for P11-P16 111
Figure A-91. Node 1593 Shear Stress Time Series Data for P11,P12,P17,P18 111
Figure A-92. Node 7681 Velocity Time Series Data for P11-P16 112
Figure A-93. Node 7681 Velocity Time Series Data for P11,P12,P17,P18 112
Figure A-94. Node 7681 Shear Stress Time Series Data for P11-P16 113
Figure A-95. Node 7681 Shear Stress Time Series Data for P11,P12,P17,P18 113
Figure A-96. Node 13591 Velocity Time Series Data for P11-P16 114
Figure A-97. Node 13591 Velocity Time Series Data for P11,P12,P17,P18 114
Figure A-98. Node 13591 Shear Stress Time Series Data for P11-P16 115
Figure A-99. Node 13591 Shear Stress Time Series Data for P11,P12,P17,P18 115
Figure A-100. Toffaleti Sediment Transport Capacity P11-P12 117
Figure A-101. Toffaleti Sediment Transport Capacity P11,P12,P17,P18 117
Figure A-102. Laursen-Copeland Sediment Transport Capacity P11-P12 118
Figure A-103. Laursen-Copeland Sediment Transport Capacity P11,P12,P17,P18 118
Figure A-104. 08 May 2013 ADCP Velocity Measurement 120
Figure A-105. Modeled Velocity Output - 8 May 2013 1200 121
Figure A-106. Modeled Velocity Difference from ADCP Velocity - 8 May 2013 1200 122
Figure A-107. Modeled vs. ADCP Velocity Along Transect - 8 May 2013 1200 123
Figure A-108. Calibration and Sensitivity Analysis - 8 May 2013 1200 123

Plates

Plate 1. Merriwether-Cherokee Potamology Location Map 16
Plate 2. Merriwether-Cherokee Crevasse Map 17
Plate 3. Sheep Ridge Road Spur Levee - October 6, 2010 18
Plate 4. Sheep Ridge Road Spur Levee - May 4, 2011 18
Plate 5. Sheep Ridge Road Spur Levee - May 22, 2012 19
Plate 6. Merriwether-Cherokee HEC-RAS Model Extent 20
Plate 7. Merriwether-Cherokee HEC-RAS Model 2D Flow Area Extent 21
Plate 8. Base Condition Geometry - RAS Plan 12 22
Plate 9. Pre 2011 Crevasse Geometry - RAS Plan 11 22

1 Purpose

The objectives of the Merriwether-Cherokee Potamology Study are to assess:

1. The potential for additional overbank scour and associated risk for formation of a major river cut-off,
2. The effects of Spur Levee failure (Sheep Ridge Road) on navigation,
3. The effects of Spur Levee failure on long-term reach behavior,
4. The effects of completed repairs on cut-off formation, and
5. The long-term effects of further alteration to the Spur Levee.

This report documents the Phase I analysis of the Merriwether-Cherokee Potamology Study. Computer application of Hydrologic Engineering Centers River Analysis System (HEC-RAS) supported the evaluation of the Lower Mississippi River from river miles 871 to 864. The following conditions were modeled and analyzed: current 2013 conditions, pre-2011 crevasse conditions, four alternatives to Sheep Ridge Road Spur Levee, and two scenarios that model increased channel bed elevations for a portion of the reach.

2 Problem

During the historic flood of 2011, the Mississippi River reached record breaking water levels between Cairo, Illinois and Memphis, Tennessee. Downstream from Tiptonville, Tennessee, Sheep Ridge Road Spur Levee (private) was overtopped and crevassed when the Mississippi River reached a stage of 48.35 feet on the Tiptonville gage. The length of spur levee crevassed was 3,000 feet, and the length of bankline erode was 2,700 feet. The Mississippi River began to form a new cutoff from river mile (RM) 869 to 860. Erosion extended approximately 4,000 feet along Island 13, degrading the landscape to elevations 80 feet below natural ground. Plate 1 is a location map of the study area, and Plate 2 is a map of the crevasse. As seen in Plate 2, the crevasse divided the Sheep Ridge Road Spur Levee, leaving an approximate 3,000-foot section to the east of the crevasse (eastern spur levee) and an approximate 2.2-mile section to the west of the crevasse of Sheep Ridge Road Spur Levee (the western spur levee). Plates 3 - 5 are aerial photos of Sheep Ridge Road Spur Levee: Plate 3 was taken prior to the 2011 crevasse; Plate 4 was taken during the 2011 flood event; and Plate 5 was taken after the 2011 flood event with the bankline restored.

Island 13, on the left descending (east) bank of the Mississippi River, is located along RM 869 to 860. The island includes the Merriwether-Cherokee Revetment located at RM 869 and the Sheep Ridge Road Spur Levee. The spur levee is located 5 miles southwest of Tiptonville, in Lake County, Tennessee. The Sheep Ridge Road Spur Levee ties into the Tiptonville-Obion Levee and extends parallel to the Merriwether-Cherokee Revetment riverward for approximately 5 miles.

During high water events, the Mississippi River overtops the banks of Island 13 at approximate RM 869 and rises against the riverside of the spur levee. At RM 860, the Mississippi River begins to back into Island 13, overtopping fields and building a tailwater on the landside of the spur levee.

Currently completed repairs to Island 13 include the re-establishment of 2,700 feet of bankline along the Merriwether-Cherokee Revetment, construction of a 1,600 feet riprap baffle landward of the restored bankline, and placement of dredged fill between the restored bankline and riprap baffle. Future repairs include the placement of a riprap cap and clay blanket over the dredged fill, with a tree screen planted on the clay blanket and placement of articulated concrete mattress along the repaired bankline.

A concern is that without modification or degradation of the western spur levee, the Mississippi River will continue to form a 9-mile cutoff. If a cutoff were to form, potential adverse impacts include: changes in long term reach dynamics, navigation outdraft conditions, increased dredging operations, hydrodynamic condition changes in close proximity to a MRL mainline levee (Tiptonville-Obion Levee), endangerment of existing channel improvement features ($60M), endangerment of completed crevasse repairs ($18.5M), and endangerment of planned crevasse repairs ($9.5M).

3 Method

HEC-RAS was utilized to evaluate river reach conditions for the study area. The Merriwether-Cherokee Potamology HEC-RAS model extended from the Tiptonville, Tennessee gage at RM 872.4 to the Caruthersville, Missouri gage at RM 846.4. Reference Plate 6 and Plate 7 for model extents. The HEC-RAS model river stationing was developed utilizing the 2011 Mississippi river alignment. Table 3-1 relates the HEC-RAS model river station (RS) to the Navigation river mile (1962 Above Head of Passes mileage).

The HEC-RAS model geometry was developed from existing 2011 model and updated to include additional cross sections. For all plans, the model channel geometry was developed from the 2009-2010 Mississippi River hydrographic survey bathymetry dataset. Floodplain and overbank data was obtained from the 2005 MVM Mississippi River LIDAR dataset. Sheep Ridge Road Spur Levee station-elevation data was obtained from the August 2013 MVM survey of the levee. Bathymetry data for the overbank scour hole was obtained from the June 2011 MVM hydrographic survey of the crevasse.

Four types of modifications have been proposed for the western spur levee. Figure 3-1 shows four types of levee degrading alternatives for the western spur levee: Type A would degrade the entire length of the western spur levee to a specified elevation; Type B would degrade a specified length of the levee to natural ground in a rising stairstep pattern in the downstream direction; Type C would degrade a specified length of the levee to natural ground; Type D would degrade a specified length of the levee at a specified upward slope in the downstream direction. In addition to the degrading alternatives, two simulations were performed to assess impacts of additional deposition within the main channel due to diversion of flow through the crevasse. Eight geometry plans were analyzed for the study reach: current 2013 conditions, pre-2011 crevasse conditions, four alternatives to Sheep Ridge Road Spur Levee, and two scenarios that model increased channel bed elevations for a portion of the reach. The modeled plans and associated geometry descriptions are listed in Table 3-2. The western spur levee was modeled as lateral structure RS 887.84. Figure 3-2 presents station-elevation data for the western spur levee for Plans 12 - 16 (base condition and four alternatives).

HEC-RAS was utilized to conduct a hydrodynamic analysis and to assess fixed bed sediment transport potential for each plan.

Table 3-1. Conversion from RAS River Station to Navigation River Mile

HEC-RAS River Station	Navigation River Mile 1962 Above Head of Passes
890.01	870.86
889.74	870.59
889.35	870.20
888.97	869.82
888.65	869.50
888.64	869.49
888.31	869.16
888.30	869.15
888.24	869.09
887.85	868.70
887.84	868.69
887.46	868.31
887.09	867.94
886.68	867.53
886.34	867.19
885.94	866.79
885.57	866.42
885.16	866.01
885.15	866.00
884.80	865.65
884.45	865.30
884.05	864.90
883.67	864.52
883.29	864.14
883.02	863.87
882.65	863.50
882.40	863.25
882.15	863.00
881.78	862.63
881.77	862.62
881.40	862.25
881.00	861.85
880.65	861.50
880.26	861.11
879.88	860.73
879.51	860.36
879.13	859.98
878.70	859.55
878.40	859.25
877.82	858.67

HEC-RAS River Station	Navigation River Mile 1982 Above Head of Passes
877.81	858.66
877.48	858.33
877.47	858.32
877.20	858.05
876.83	857.68
876.48	857.33
876.11	856.96
876.04	856.89
876.03	856.88
875.88	856.73
875.87	856.72
875.75	856.60
875.33	856.18
874.96	855.81
874.57	855.42
874.20	855.05
873.85	854.70
873.43	854.28
873.06	853.91
872.69	853.54
872.33	853.18
871.94	852.79
871.55	852.40
871.13	851.98
870.78	851.63
870.41	851.26
870.03	850.88
869.68	850.53
869.26	850.11
868.90	849.75
868.54	849.39
868.15	849.00
867.76	848.61
867.39	848.24
867.01	847.86
866.64	847.49
866.27	847.12
865.90	846.75
865.51	846.36
865.13	845.98
864.70	845.55
864.36	845.21
863.96	844.81

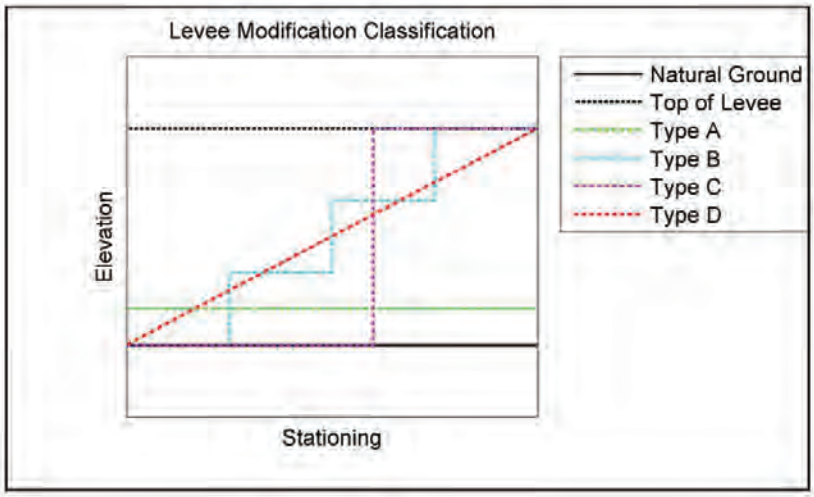


Figure 3-1. Levee Modification Classification

Table 3-2. HEC-RAS Plan Description

RAS Plan	Geometry Description
P11	Pre-2011 Crevasse
P12	Base Condition (Current 2013)
P13	Levee Alternative 1, Levee Mod Type A (Elev 283.5 ft)
P14	Levee Alternative 2, Levee Mod Type A (Elev 288.0 ft)
P15	Levee Alternative 3, Levee Mod Type C (US half to Elev 283.5 ft)
P16	Levee Alternative 4, Levee Mod Type D (sloped US (Elev 283.5 ft) to DS (Elev 291.7ft)
P17	5 ft Channel Bed Elevation increase in Cross Sections (RAS RS 887.85 - 882.15)
P18	10 ft Channel Bed Elevation increase in Cross Sections (RAS RS 887.85 - 882.15)

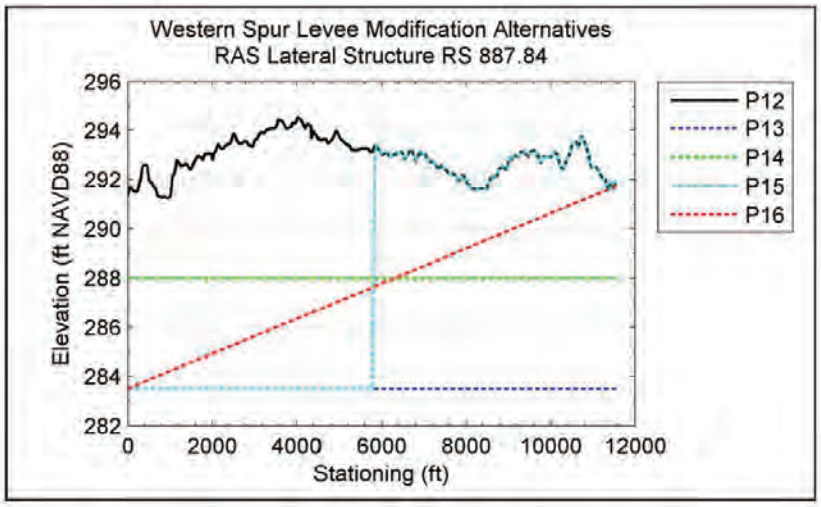


Figure 3-2. Sheep Ridge Road Western Spur Levee Alternatives Plan Files

3.1 Hydrodynamics

HEC-RAS Version 4.2.0 August Beta (Alpha 2D Flow Areas) was utilized to perform the hydrodynamic analysis; a program feature was added by HEC personnel to perform two-dimensional (2D) hydrodynamic flow routing within the unsteady flow analysis portion of HEC-RAS. HEC-RAS produced a combined one-dimensional (1D) and 2D unsteady-flow routing. The Mississippi River main channel was modeled using 1D cross sections and the Island 13 overbank region was modeled using 2D flow elements (2D flow area). Refer to Plates 6 - 9 for graphical representations of the combined 1D and 2D modeling approach. The 2D flow element size utilized for this study was 100 ft x 100 ft. Lateral structures were included to hydraulically connect the 2D flow area and the 1D cross sections. The 2D flow area was calibrated by adjusting lateral structure weir coefficients and 2D flow area Manning's n-value to the 8 May 2013 Acoustic Doppler Current Profilers (ADCP) survey that measured the flow velocity through the crevasse. Detailed calibration results are presented in Appendix A, Section A.12. For modeled plans, the downstream boundary condition assumed normal depth conditions. The upstream boundary condition was a hypothetical unsteady flow hydrograph that included a seven day model warm-up duration, as shown in Figure 3-3. The hypothetical unsteady flow hydrograph had a minimum flow of 200,000 cubic feet per second (cfs) and maximum flow of 2,200,000 cfs. The peak flow, rates of rise, and rates of fall for the hypothetical hydrograph were patterned after the 2011 flood hydrograph. The MR&T Project Design Flood peak for this reach is 2,360,000 cfs (hypo-flood event 58A-EN).

Current HEC-RAS 2D modeling limitations are listed below:

1. Only one 2D flow area is allowed,
2. The 2D flow area can only have one Manning's n-value to represent the terrain surface, and
3. 2D output viewing in HEC-RAS was limited to water depth grids.

MATLAB scripts were written to spatially analyze all 2D output and to calculate hydraulic parameters (velocity, shear stress, and time series data) for the 2D nodes. Shear stress is expressed as:

$$\tau_0 = \gamma R S_0 \quad \text{(3-1)}$$

$\tau_0 = Shear\ stress, lb/ft^2$

$\gamma = Unit\ weight\ of\ water, lb/ft^3$

$R = Hydraulic\ radius, ft$

$S_0 = Energy\ Slope, ft/ft.$

The hydraulic radius was assumed to be the water depth at the node location. The energy slope was assumed to be the friction slope. The friction slope was back-solved utilizing the Manning's equation.

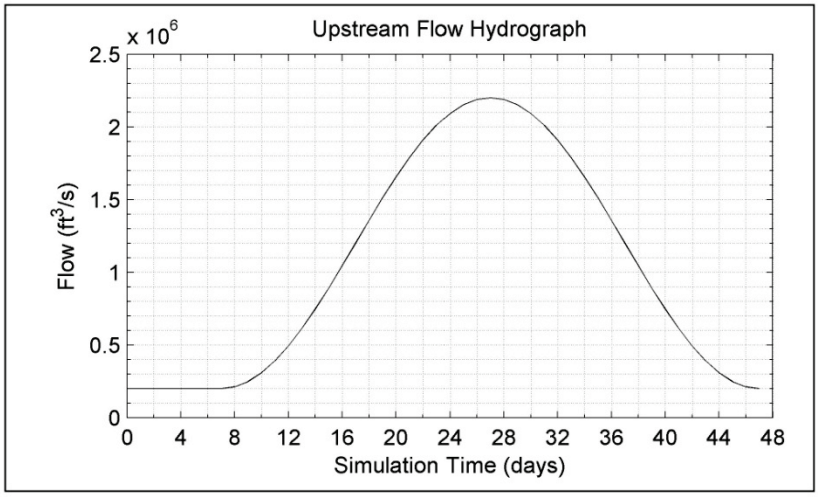


Figure 3-3. Upstream Boundary Condition Hypothetical Flow Hydrograph

3.2 Sediment Transport Capacity

HEC-RAS Version 4.1.0 was utilized to calculate the fixed bed steady flow sediment transport capacity. This version was chosen because the Hydraulic Design Function tools were not available for use in HEC-RAS Version 4.2.0 August Beta (Alpha 2D Flow Areas). The sediment transport capacity was estimated for the channel reach downstream of the crevasse (RM 867.53 - 863.00). The HEC-RAS Hydraulic Design Functions feature was used to estimate sediment transport capacity for non-cohesive sediment at the fixed bed, 1D cross sections, based on hydraulic parameters and known bed sediment properties. The sediment transport capacity computations did not account for sediment inflow, erosion, and deposition. The boundary conditions for the steady flow sediment analysis were obtained from the unsteady hydrodynamic output. Channel boundary conditions for each plan were the associated conditions that occurred in the unsteady analysis at the maximum flow rate directly upstream of the crevasse. Table 3-3 lists the sediment transport boundary conditions. Bed sediment properties for the reach were obtained from the report *Particle Size Distributions of Bed Sediments Along the Thalweg of the Mississippi River, Cairo, Illinois, to Head of Passes, September 1989 Potamology Report Program (P-1) Report 7*.[1] The channel properties utilized for the sediment transport analysis are listed in Table 3-4.

Table 3-3. HEC-RAS Steady Flow Sediment Transport Boundary Conditions

RAS Plan	Upstream BC Channel Q (cfs)	Downstream BC WSEL (ft)	Channel Q Difference from Base Condition
P11	1,841,594	289.34	69,459
P12	1,772,135	289.32	-
P13	1,629,649	289.29	-142,486
P14	1,716,636	289.31	-55,499
P15	1,693,151	289.31	-78,984
P16	1,703,247	289.31	-68,888
P17	1,766,583	289.32	-5,552
P18	1,752,683	289.32	-19,452

Table 3-4. 1989 Channel Gradation at RM 867.3 Above Head of Passes (from Nordin and Queen, 1992)

Particle Size (mm)	Percent Finer (%)
16	100.0
8	97.3
4	95.3
2	90.8
1	76.2
0.5	25.7
0.25	4.0
0.125	0.0

4 Results

Detailed results from the hydrodynamic analysis are presented in Appendix A, Sections A.1 - A.10. Diversion flow through the crevasse begins at approximately 580,000 cfs for the base condition plan. As listed in Table 3-5, Plan 12 (base condition) had a diversion flow percentage of 10.0; P11 (pre-2011 crevasse) had the minimum diversion flow percentage of 6.3; and P13 (western spur levee alternative 1) had the maximum diversion flow percentage of 17.5. Table 3-6 presents selected 2D output for each plan. The peak discharge upstream of the crevasse occurred at simulation hour 648. At simulation hour 648, the maximum velocity in the 2D overbank region for Plan 12 was 5.3 ft/s. The western spur levee alternative plan with the maximum decrease in shear stress (when compared to Plan 12) was Plan 13 at a node near the crevasse. The western spur levee alternative plan with the maximum increase in shear stress (when compared to Plan 12) was Plan 15 at a node in the western portion of the Island 13 overbank. The critical shear stress force of a particular material is the unit shear stress force which will not cause erosion of the material on a horizontal surface. The critical shear stress force for sandy loam soil (non-colloidal) is 0.0418 lb/ft^2 (Nalluri et al. 2009). Note that further field evaluation is needed to investigate overbank material type. The maximum shear stress for Plan 12 occurred at simulation hour 310. Simulation hour 310 had an upstream boundary condition flow of 602,000 cfs (Table A-2 and Figure 3-3).

Table 3-5. Diversion Flow Plan Comparison

RAS Plan	Max Flow Upstream RM 869.82 (cfs)	Max Flow Downstream RM 863.00 (cfs)	Diversion Flow (cfs)	Diversion Flow (%)
P11	2,199,908	2,062,120	137,788	6.3
P12	2,199,908	1,980,677	219,231	10.0
P13	2,199,910	1,815,001	384,909	17.5
P14	2,199,913	1,915,912	284,001	12.9
P15	2,199,909	1,888,527	311,382	14.2
P16	2,199,907	1,900,296	299,611	13.6
P17	2,199,906	1,979,148	220,758	10.0
P18	2,199,907	1,975,608	224,299	10.2

Table 3-6. Plan Results Comparison

Result Parameter	P11	P12	P13	P14	P15	P16	P17	P18
Max Velocity (ft/s) Simulation Hour 648	13.7	5.3	4.5	5.0	4.8	4.9	5.3	5.4
Max Shear Stress (lb/ft^2) Simulation Hour 648	8.492	1.030	0.748	0.915	0.837	0.868	1.039	1.058
Max Velocity (ft/s)	14.7	13.8	13.8	13.8	13.8	13.8	14.5	14.1
Simulation Hour of Max Velocity	532	314	314	314	314	314	312	310
Max Shear Stress (lb/ft^2)	10.634	9.477	9.477	9.477	9.477	9.477	11.771	12.307
Simulation Hour of Max Shear Stress	528	310	310	310	310	310	312	310
Velocity Difference from P12 (ft/s) Max Increase	12.3	-	2.7	1.1	2.1	1.0	0.0	0.1
Velocity Difference from P12 (ft/s) Max Decrease	-2.8	-	-1.3	-0.9	-1.3	-1.2	0.0	0.0
Shear Stress Difference from P12 (lb/ft^2) Max Increase	8.428	-	0.361	0.073	0.367	0.139	0.008	0.027
Shear Stress Difference from P12 (lb/ft^2) Max Decrease	-0.757	-	-0.283	-0.115	-0.193	-0.162	-0.002	-0.006

Detailed results from the sediment transport capacity analysis are presented in Appendix A, Section A.11. Table 3-7 lists the reach average (RM 867.53 - 863.00) sediment transport potential for the Toffaleti function and the Laursen-Copeland function. The analysis showed that Plans 12 - 16 (base condition and the four levee alternative plans) have less sediment transport potential than Plan 11 (pre-2011 crevasse). This indicates that deposition would occur in the main channel due to diversion of flow through the crevasse. Plan 17 and Plan 18 (increased channel bed elevation scenarios to represent different levels of deposition) also had a decrease in sediment transport potential when compared to Plan 11. These results indicate that both the changes in diversion flow through the crevasse and the adjustment to bed elevations impact the sediment transport potential in the river.

Table 3-7. Reach Average Sediment Transport Potential

RAS Plan	Toffaleti Function (tons/day)	Laursen-Copeland Function (tons/day)	Toffaleti Difference from Pre-2011 Crevasse (%)	Laursen-Copeland Difference from Pre-2011 Crevasse (%)
P11	64,859	397,394	-	-
P12	61,209	331,956	-6	-16
P13	54,424	232,781	-16	-41
P14	58,553	290,025	-10	-27
P15	57,428	273,525	-11	-31
P16	57,912	280,531	-11	-29
P17	61,332	339,931	-5	-14
P18	61,548	355,856	-5	-10

5 Conclusion

The HEC-RAS analysis demonstrated that the base condition plan is hydrodynamically different compared to the pre-2011 crevasse, both in the main channel and in the Island 13 overbank region. Furthermore, the analysis indicated that all western spur levee modification alternatives would reduce velocities and shear stresses in certain regions of the Island 13 overbank; however, these alternatives also increase velocities and shear stresses in other portions of the overbank (specifically, downstream of the overbank scour hole and the western overbank region of Island 13). The analysis also indicated that both the changes in diversion flow through the crevasse and the adjustment to channel bed elevations affect the sediment transport potential in the river.

The HEC-RAS analysis does not address channel adjustment that will result from decreased sediment transport potential, nor is HEC-RAS capable of simulating the interaction between decreased channel capacity due to deposition and the flow distribution between main channel and the overbank crevasse. This effect is coupled and requires a multiple dimensional model that has the ability to simulate sediment transport and a mobile boundary.

The Phase I HEC-RAS results underscore the need for further analysis to complete the five objectives specified for the Merriwether-Cherokee Potamology Study. A recommendation is that this study should proceed to the next modeling phase, which will include the use of the 2D depth-averaged Adaptive Hydraulics (AdH) program, with sediment transport and a 1D sedimentation model.

AdH can be used to evaluate the complex floodplain hydraulics and sedimentation impacts of existing and proposed river reach conditions. AdH can be used to model the entire study area two-dimensionally and also accounts for super-elevation of the water surface in reach bends. AdH can assess affects on sedimentation and flow, both in the floodplain and river. The sedimentation analysis in AdH is typically used for simulation periods ranging from only a single flood event to as long as a few years. AdH can provide estimates of sediment deposition rates and sediment diversion coefficients. The sediment diversion coefficients thus determined could

then be utilized by a 1D sedimentation model (i.e., MVD HEC-6T regional model) for the longer simulation period of multiple decades needed to evaluate long-term bed response.

The Merriwether-Cherokee Potamology Study was discussed in detail with engineers at the USACE Engineer Research and Development Center (ERDC) Coastal & Hydraulics Laboratory River Engineering Branch (CEERD-HF-RS) under the Water Operations Technical Support (WOTS) Program. Information received from the discussions is listed below:

1. Guidance in the selection of the modeling approach to assess additional overbank scour,
2. List of tasks needed for model development,
3. Recommended techniques to evaluate alternatives and modeling results, and
4. Detailed plan of action for future model study.

The recommendation to proceed to the next modeling phase is supported by CEERD-HF-RS in a document entitled Memorandum for Record Subject: Merriwether-Cherokee Potamology Study (Appendix B).

References

1. Nordin, C. F., & Queen, B. S., *Particle Size Distributions of Bed Sediments Along the Thalweg of the Mississippi River, Cairo, Illinois, to Head of Passes, September 1989 Potamology Report Program (P-1) Report 7*, Vicksburg, MS, September, 1992.

2. Nalluri, C., Featherstone, R.E., Marriott, M.J., *Civil Engineering Hydraulics 5th Edition*, West Sussex, United Kingdom: Wiley-Blackwell, 2009

(this page intentionally blank)

Plates

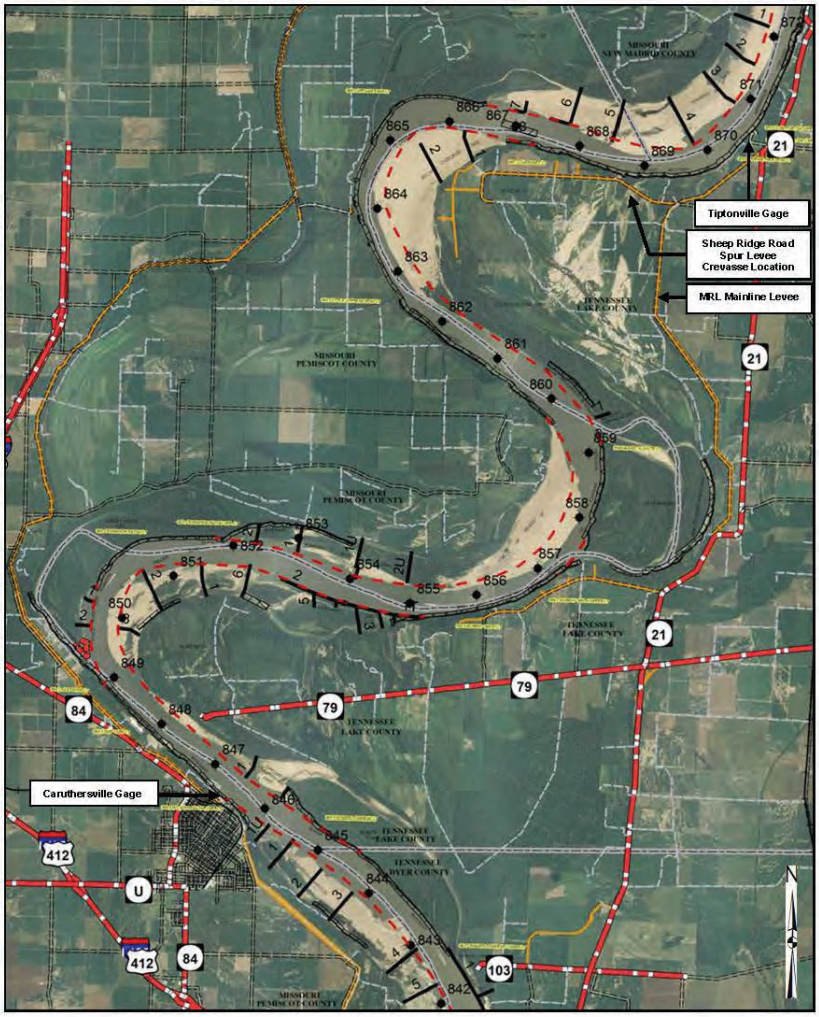


Plate 1. Merriwether-Cherokee Potamology Location Map

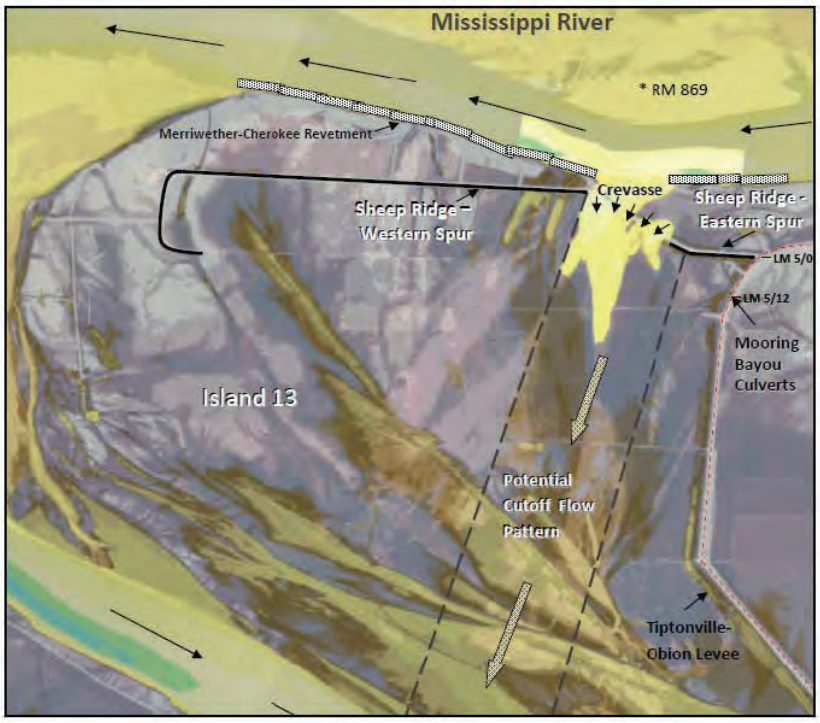


Plate 2. Merriwether-Cherokee Crevasse Map



Plate 3. Sheep Ridge Road Spur Levee - October 6, 2010



Plate 4. Sheep Ridge Road Spur Levee - May 4, 2011



Plate 5. Sheep Ridge Road Spur Levee - May 22, 2012

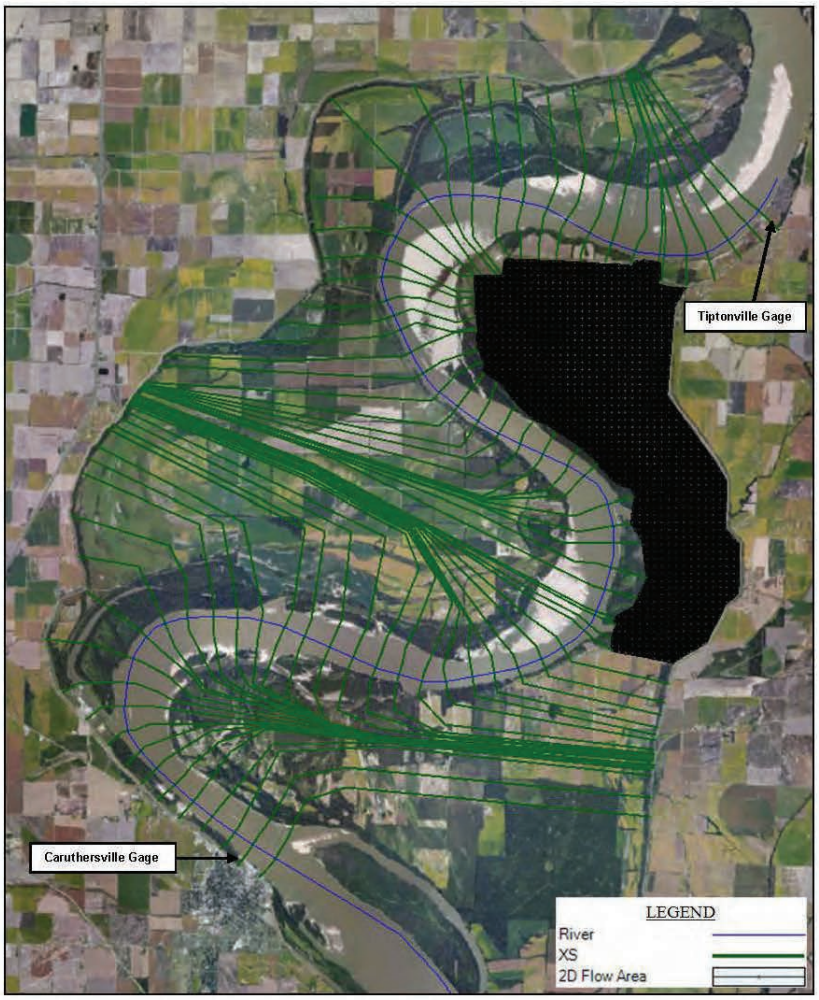


Plate 6. Merriwether-Cherokee HEC-RAS Model Extent

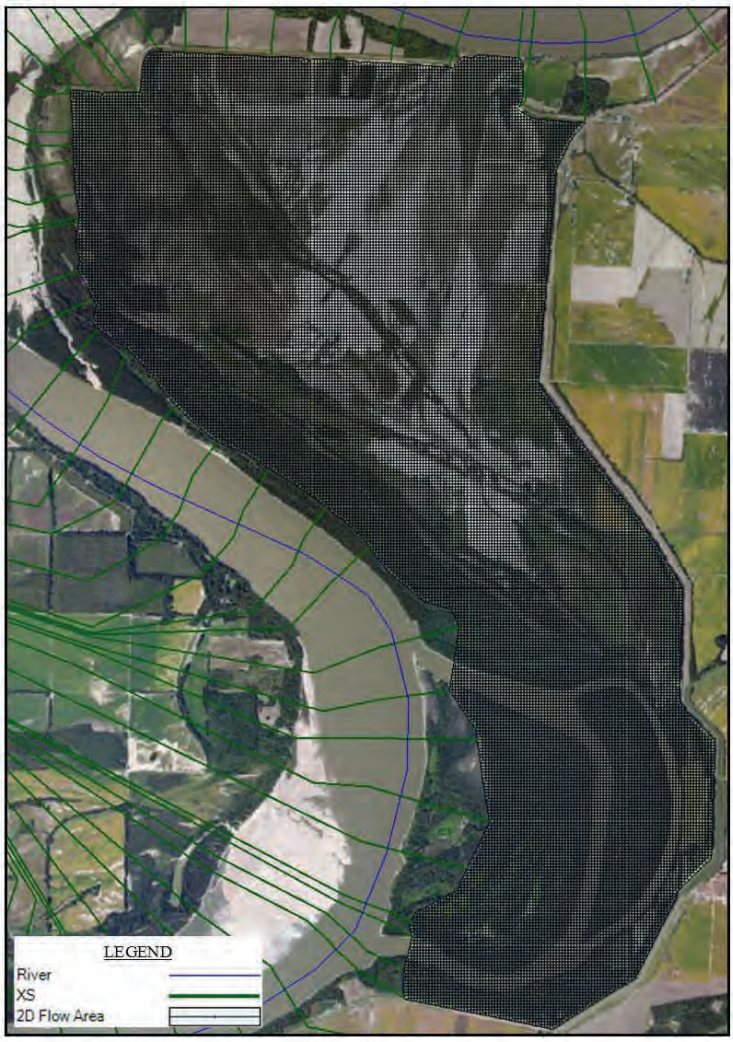


Plate 7. Merriwether-Cherokee HEC-RAS Model 2D Flow Area Extent

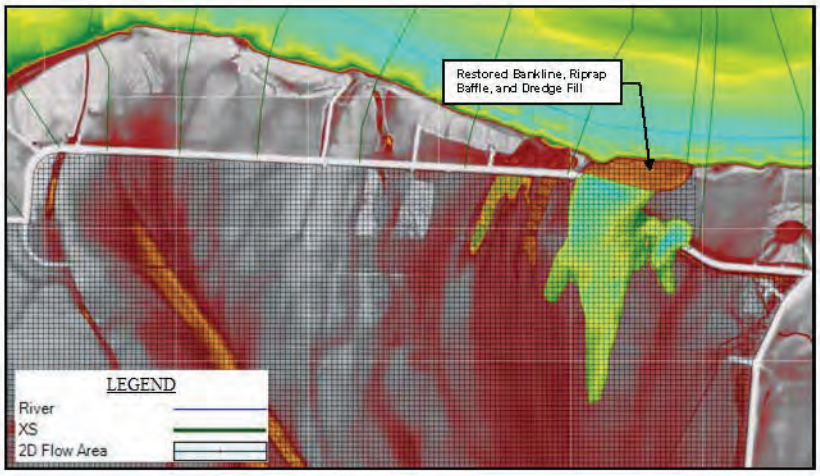


Plate 8. Base Condition Geometry - RAS Plan 12

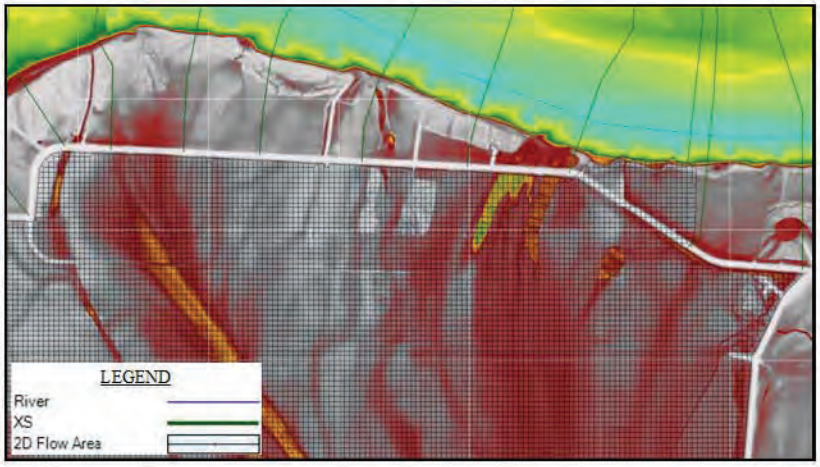


Plate 9. Pre 2011 Crevasse Geometry - RAS Plan 11

Appendix A. HEC-RAS Analysis

Appendix A contains the Phase I HEC-RAS analysis output. 2D Flow Area output was processed utilizing MATLAB. Table A-1 describes the geometry associated with each HEC-RAS plan file. Scales and color bars for like figures were held constant for plan comparison. Table A-2 lists the conversion relationship between model simulation date, simulation day, and simulation hour.

Table A-1. Plan Description

RAS Plan	Geometry Description
P11	Pre-2011 Crevasse
P12	Base Condition (Current 2013)
P13	Levee Alternative 1, Levee Mod Type A (Elev 283.5 ft)
P14	Levee Alternative 2, Levee Mod Type A (Elev 288.0 ft)
P15	Levee Alternative 3, Levee Mod Type C (US half to Elev 283.5 ft)
P16	Levee Alternative 4, Levee Mod Type D (sloped US (Elev 283.5 ft) to DS (Elev 291.7ft)
P17	5 ft Channel Bed Elevation increase in Cross Sections (RAS RS 887.85 - 882.15)
P18	10 ft Channel Bed Elevation increase in Cross Sections (RAS RS 887.85 - 882.15)

Table A-2. Simulation Time Window Relationship

Simulation Date	Simulation Day	Simulation Hour	Upstream Flow (cfs)
2/2/2099 12:00 AM	0	0	200,000
2/3/2099 12:00 AM	1	24	200,000
2/4/2099 12:00 AM	2	48	200,000
2/5/2099 12:00 AM	3	72	200,000
2/6/2099 12:00 AM	4	96	200,000
2/7/2099 12:00 AM	5	120	200,000
2/8/2099 12:00 AM	6	144	200,000
2/9/2099 12:00 AM	7	168	200,000
2/10/2099 12:00 AM	8	192	212,000
2/11/2099 12:00 AM	9	216	248,000
2/12/2099 12:00 AM	10	240	308,000
2/13/2099 12:00 AM	11	264	390,000
2/14/2099 12:00 AM	12	288	492,000
2/15/2099 12:00 AM	13	312	612,000
2/16/2099 12:00 AM	14	336	746,000
2/17/2099 12:00 AM	15	360	890,000
2/18/2099 12:00 AM	16	384	1,044,000
2/19/2099 12:00 AM	17	408	1,200,000
2/20/2099 12:00 AM	18	432	1,356,000
2/21/2099 12:00 AM	19	456	1,510,000
2/22/2099 12:00 AM	20	480	1,654,000
2/23/2099 12:00 AM	21	504	1,788,000
2/24/2099 12:00 AM	22	528	1,908,000
2/25/2099 12:00 AM	23	552	2,010,000
2/26/2099 12:00 AM	24	576	2,092,000
2/27/2099 12:00 AM	25	600	2,152,000
2/28/2099 12:00 AM	26	624	2,188,000
3/1/2099 12:00 AM	27	648	2,200,000
3/2/2099 12:00 AM	28	672	2,188,000
3/3/2099 12:00 AM	29	696	2,152,000
3/4/2099 12:00 AM	30	720	2,092,000
3/5/2099 12:00 AM	31	744	2,010,000
3/6/2099 12:00 AM	32	768	1,908,000
3/7/2099 12:00 AM	33	792	1,788,000
3/8/2099 12:00 AM	34	816	1,654,000
3/9/2099 12:00 AM	35	840	1,510,000
3/10/2099 12:00 AM	36	864	1,356,000
3/11/2099 12:00 AM	37	888	1,200,000
3/12/2099 12:00 AM	38	912	1,044,000
3/13/2099 12:00 AM	39	936	890,000
3/14/2099 12:00 AM	40	960	746,000
3/15/2099 12:00 AM	41	984	612,000
3/16/2099 12:00 AM	42	1,008	492,000
3/17/2099 12:00 AM	43	1,032	390,000
3/18/2099 12:00 AM	44	1,056	308,000
3/19/2099 12:00 AM	45	1,080	248,000
3/20/2099 12:00 AM	46	1,104	212,000
3/21/2099 12:00 AM	47	1,128	200,000

A.1 Cross Section Maximum Water Surface Profiles

Figures located in A.1 depict the maximum 1D cross section water surface profiles for Plans 11-16.

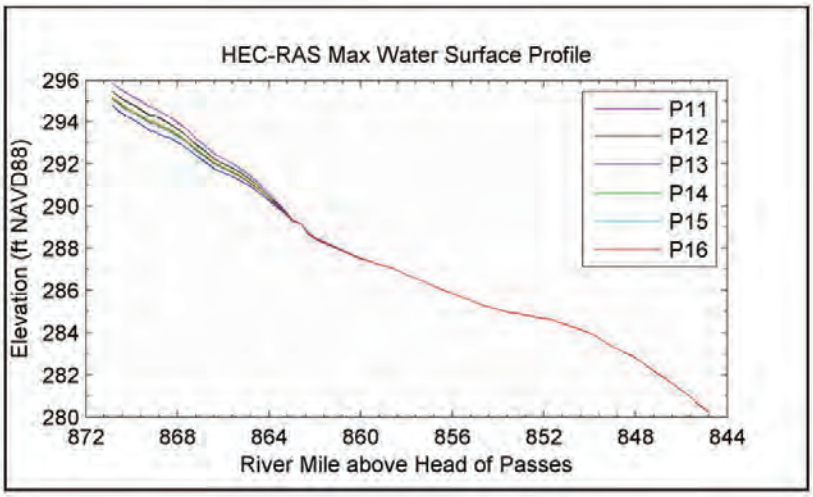


Figure A-1. Maximum Water Surface Profiles Plans 11-16 at RM 872-844

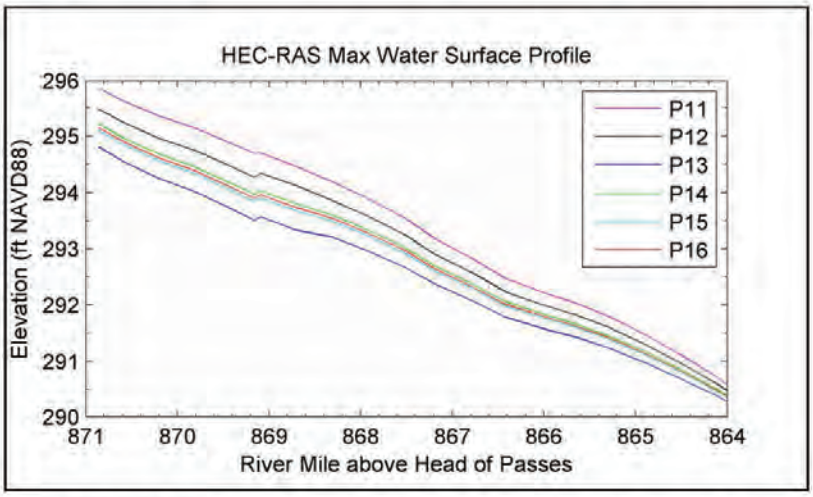


Figure A-2. Maximum Water Surface Profiles Plans 11-16 at RM 871-864

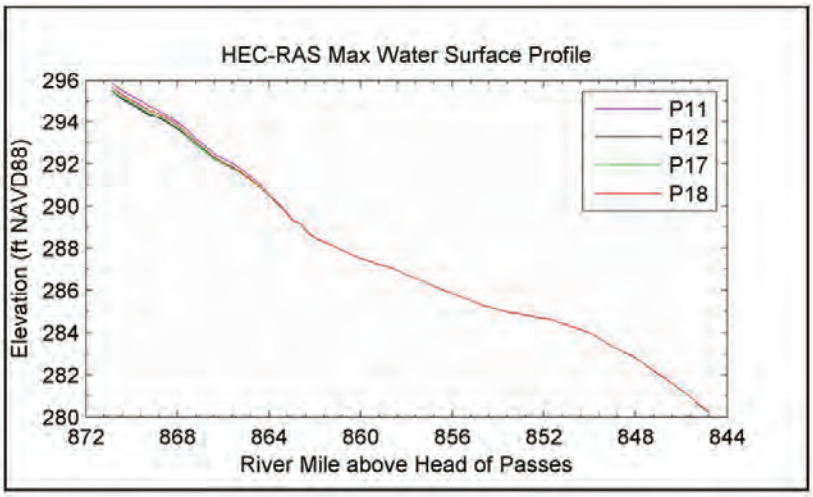


Figure A-3. Maximum Water Surface Profiles Plans 11,12,17,18 at RM 872-844

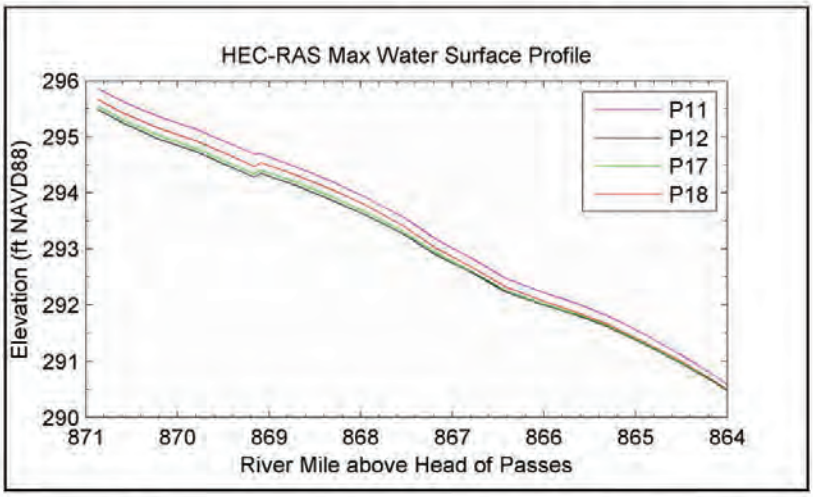


Figure A-4. Maximum Water Surface Profiles Plans 11,12,17,18 at RM 871-864

A.2 2D Flow Area Velocity - Simulation Hour 648

The peak discharge upstream of the crevasse occurred at simulation hour 648. Figures located in A.2 depict the velocity in the 2D overbank region at simulation hour 648 for Plans 11-16. The black "o" in the figure identifies the node location with the highest magnitude for each figure respectively. Note that the black arrows represent velocity vectors (a scale velocity vector of 5 ft/s is located on each figure).

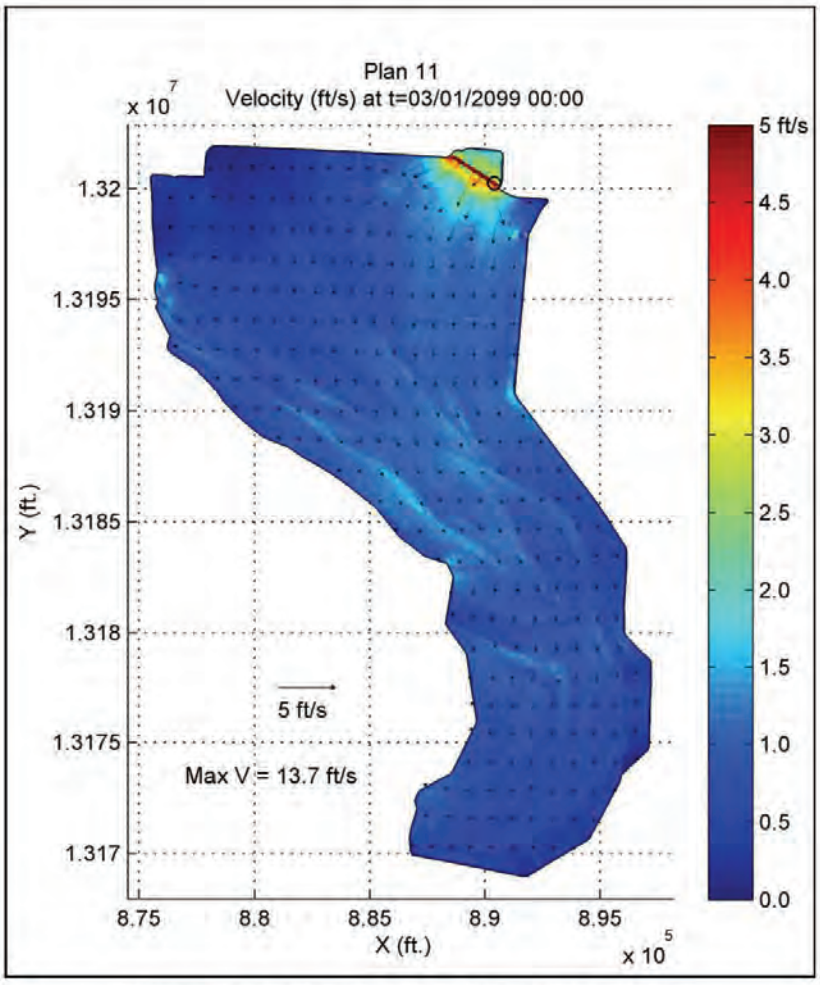


Figure A-5. Plan 11 2D Velocity at Simulation Hour 648

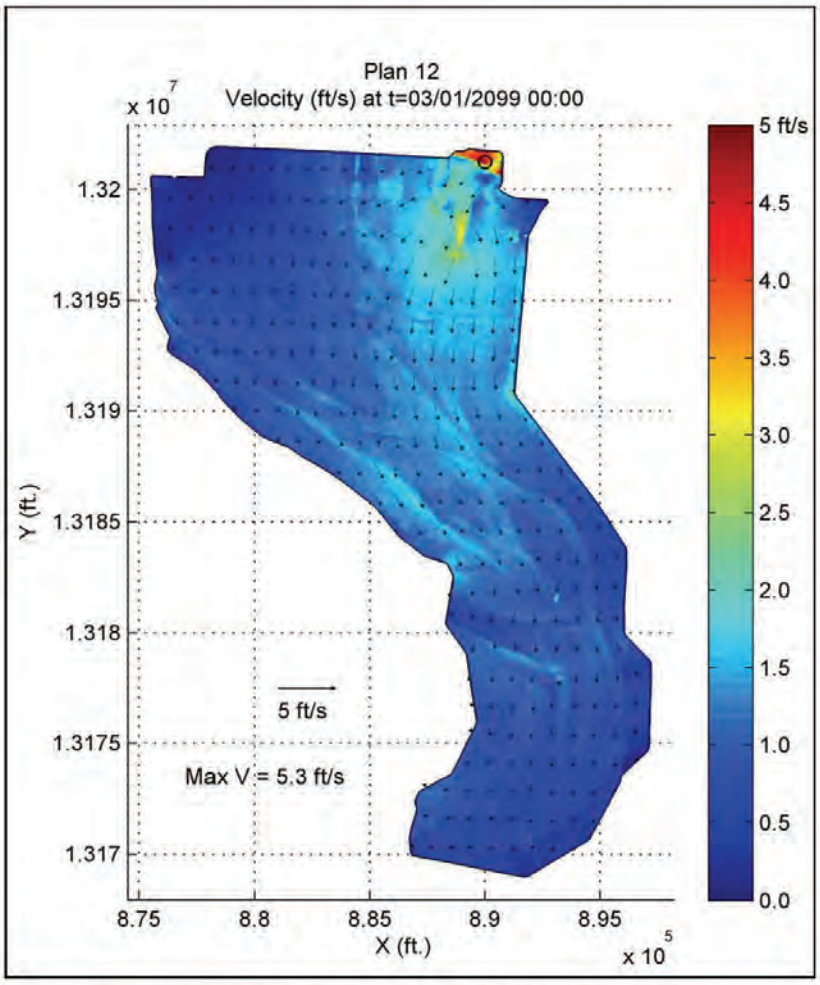


Figure A-6. Plan 12 2D Velocity at Simulation Hour 648

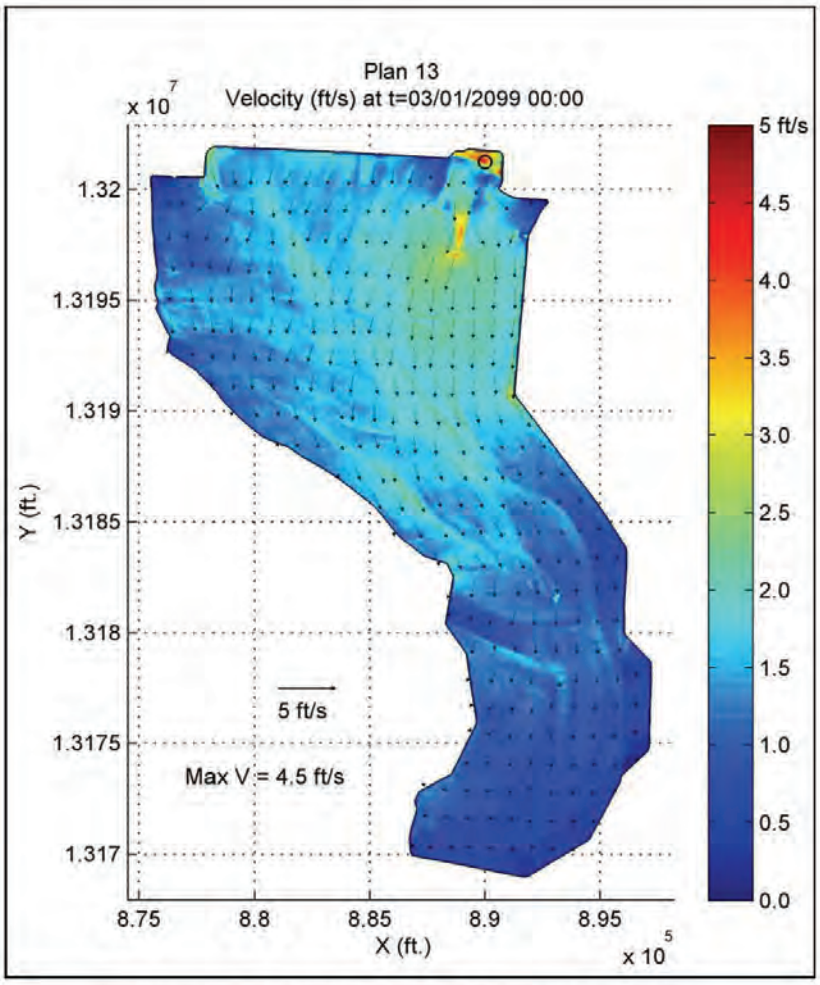


Figure A-7. Plan 13 2D Velocity at Simulation Hour 648

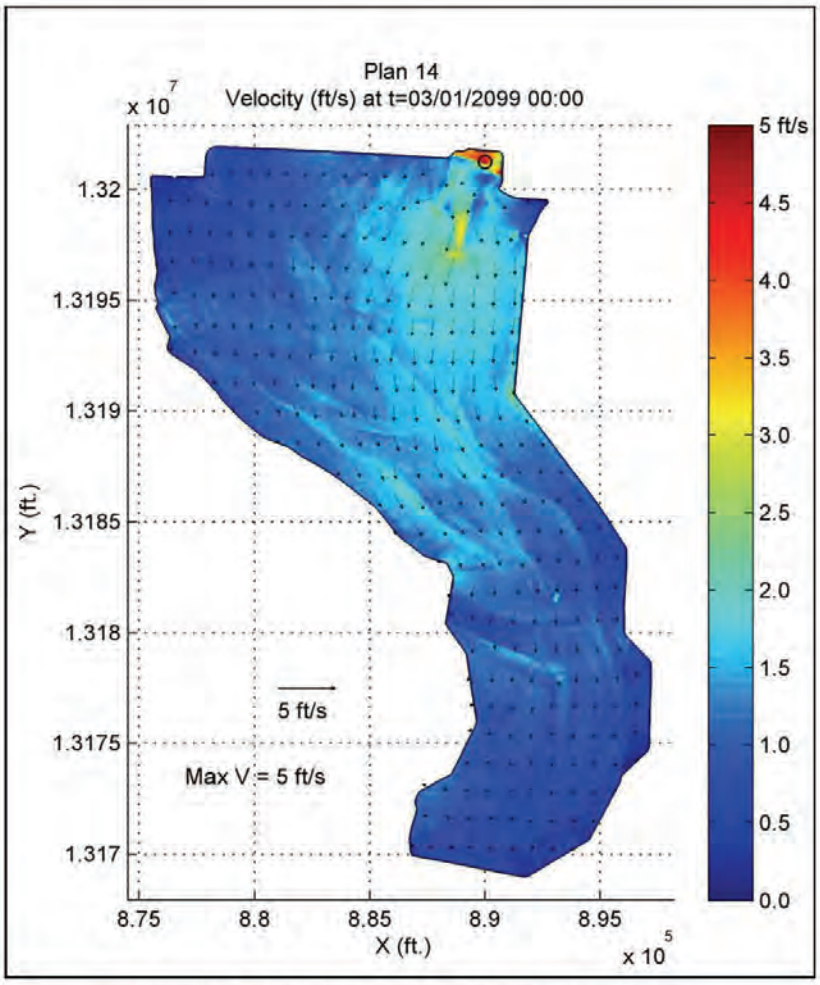


Figure A-8. Plan 14 2D Velocity at Simulation Hour 648

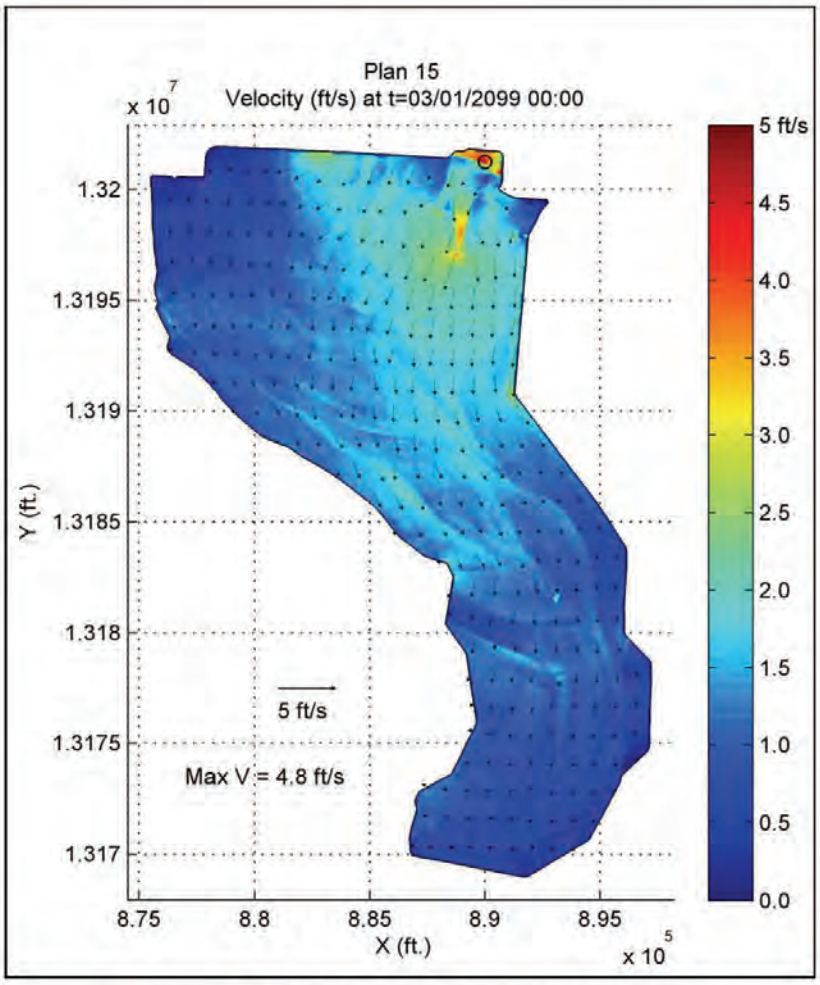


Figure A-9. Plan 15 2D Velocity at Simulation Hour 648

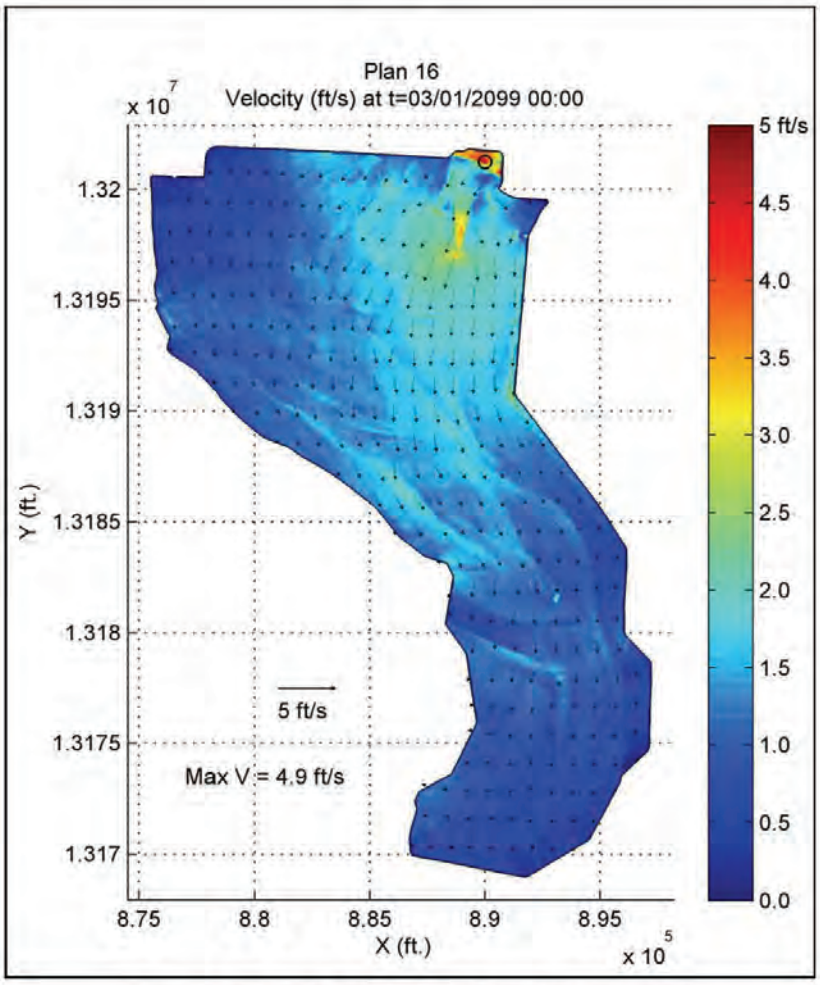


Figure A-10. Plan 16 2D Velocity at Simulation Hour 648

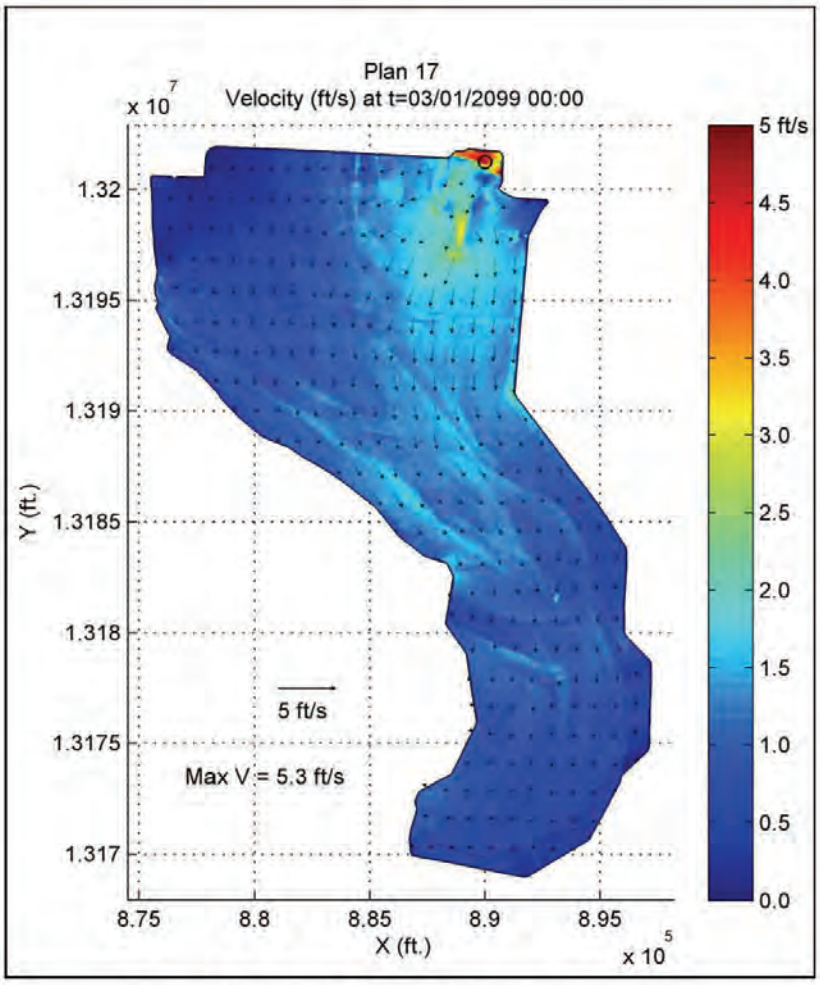


Figure A-11. Plan 17 2D Velocity at Simulation Hour 648

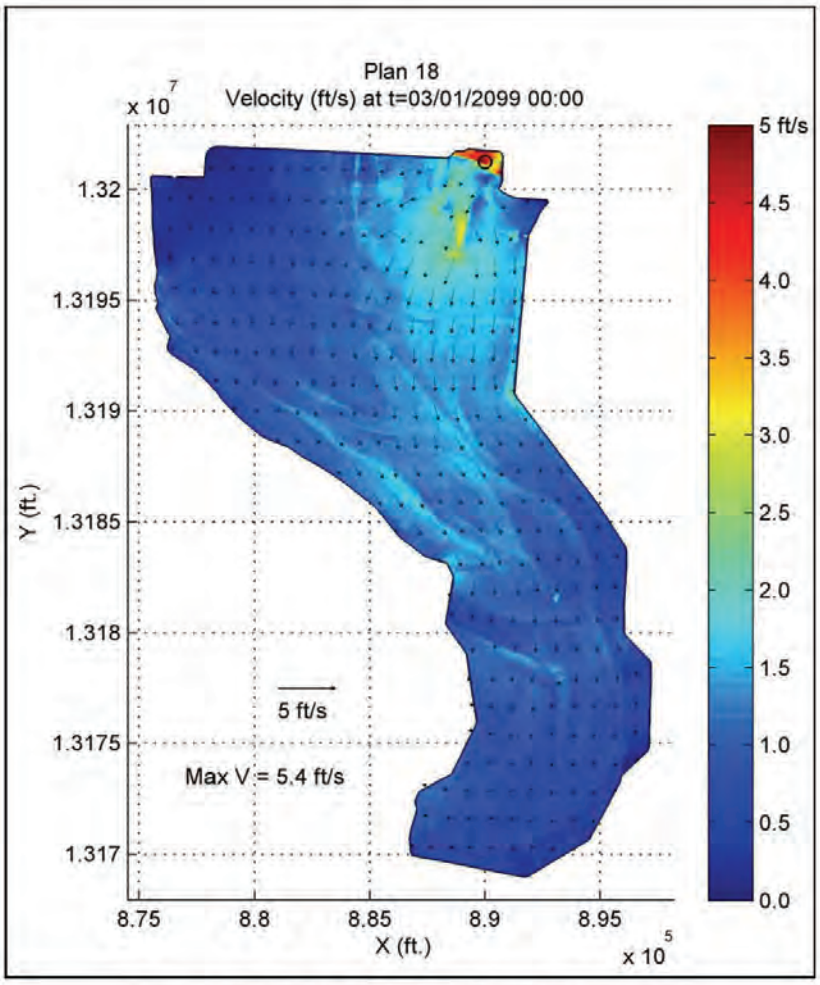


Figure A-12. Plan 18 2D Velocity at Simulation Hour 648

A.3 2D Flow Area Shear Stress - Simulation Hour 648

The peak discharge upstream of the crevasse occurred at simulation hour 648. Figures located in A.3 depict the shear stress in the 2D overbank region at simulation hour 648 for Plans 11-16. The black "o" in the figure identifies the node location with the highest magnitude for each figure respectively. Note that the black arrows represent velocity vectors (a scale velocity vector of 5 ft/s is located on each figure).

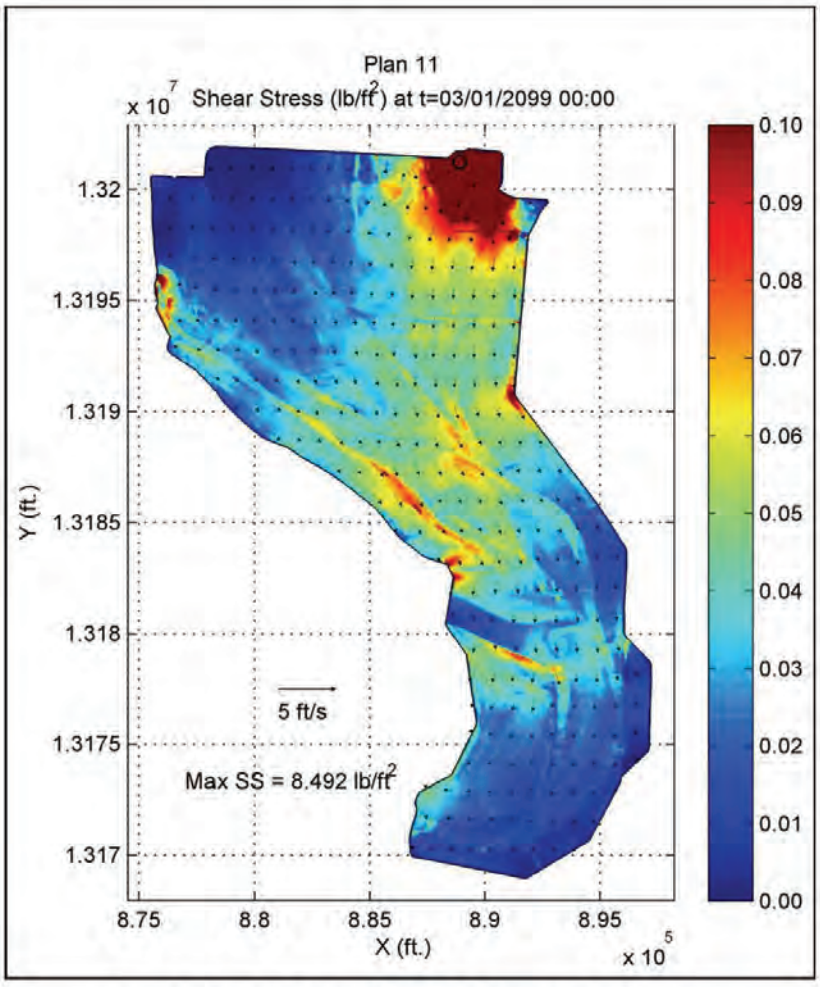


Figure A-13. Plan 11 Shear Stress at Simulation Hour 648

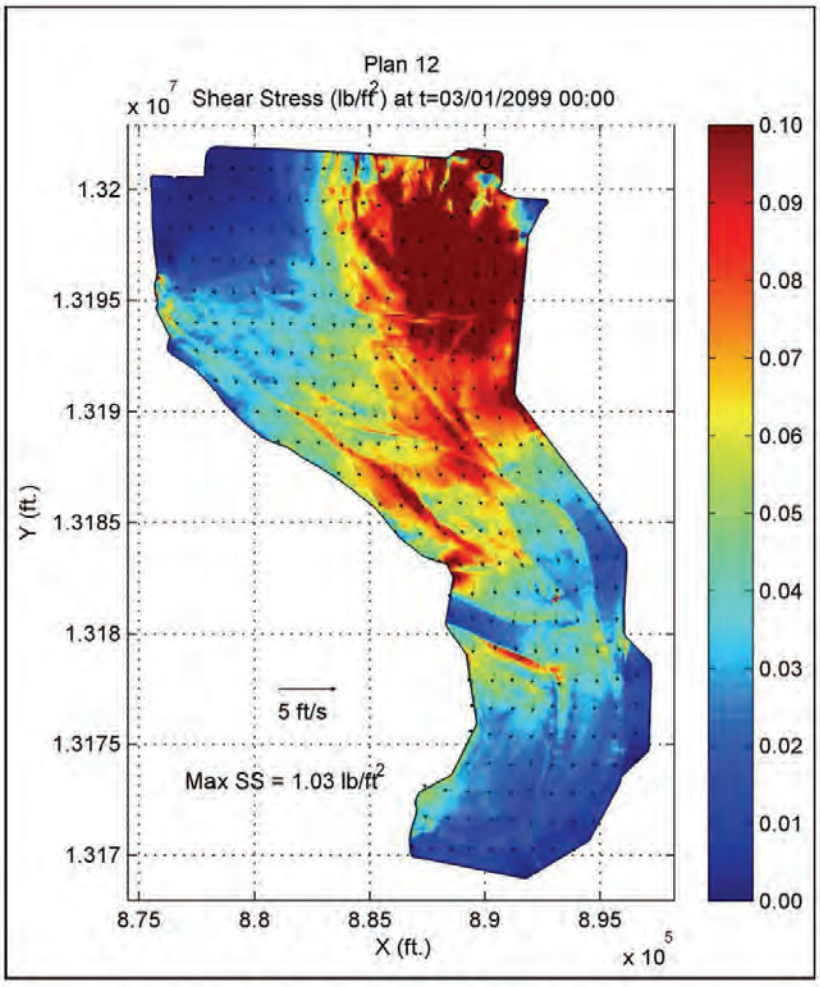


Figure A-14. Plan 12 Shear Stress at Simulation Hour 648

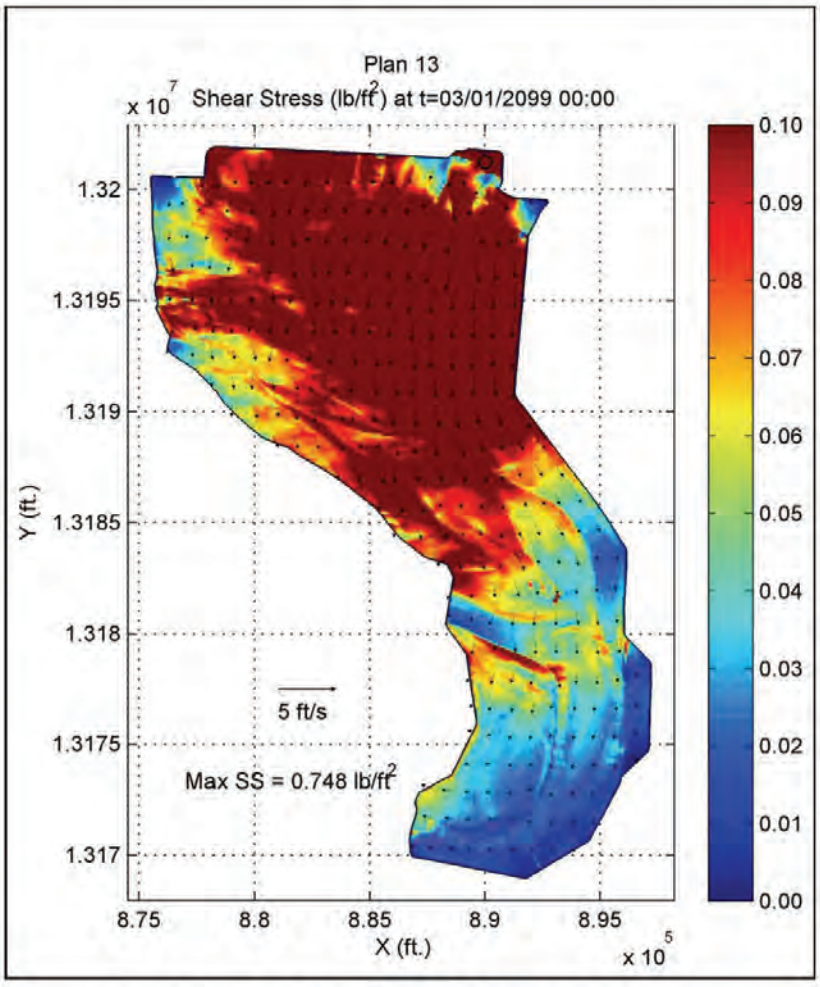


Figure A-15. Plan 13 Shear Stress at Simulation Hour 648

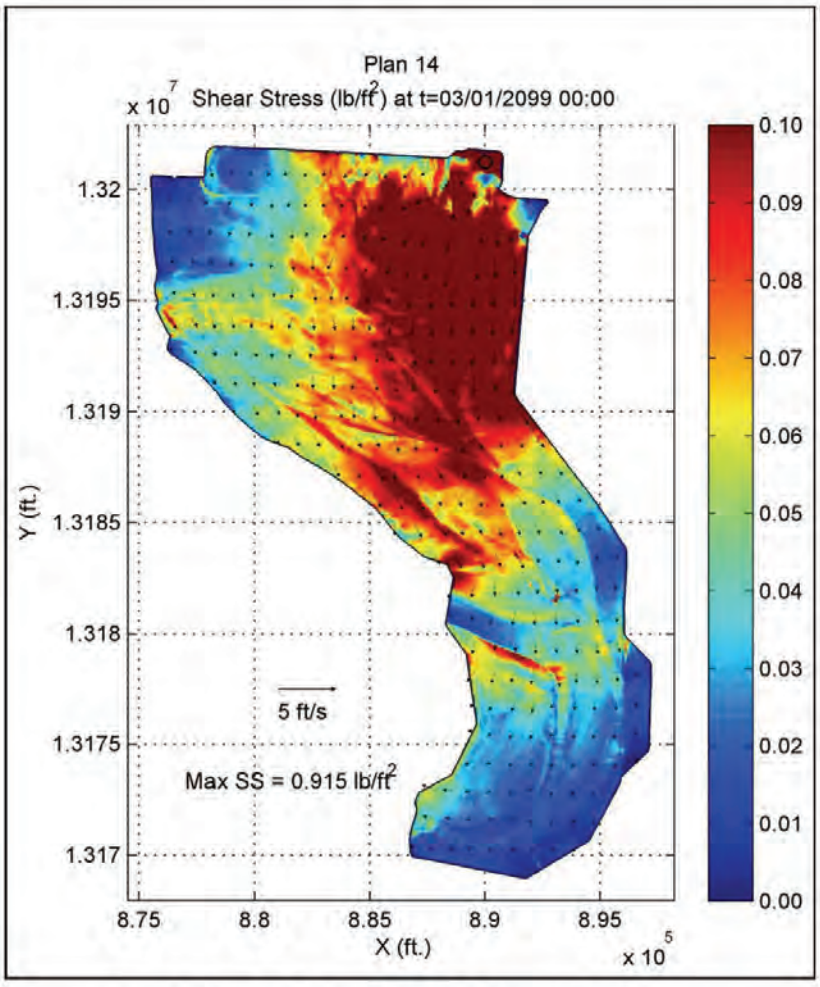


Figure A-16. Plan 14 Shear Stress at Simulation Hour 648

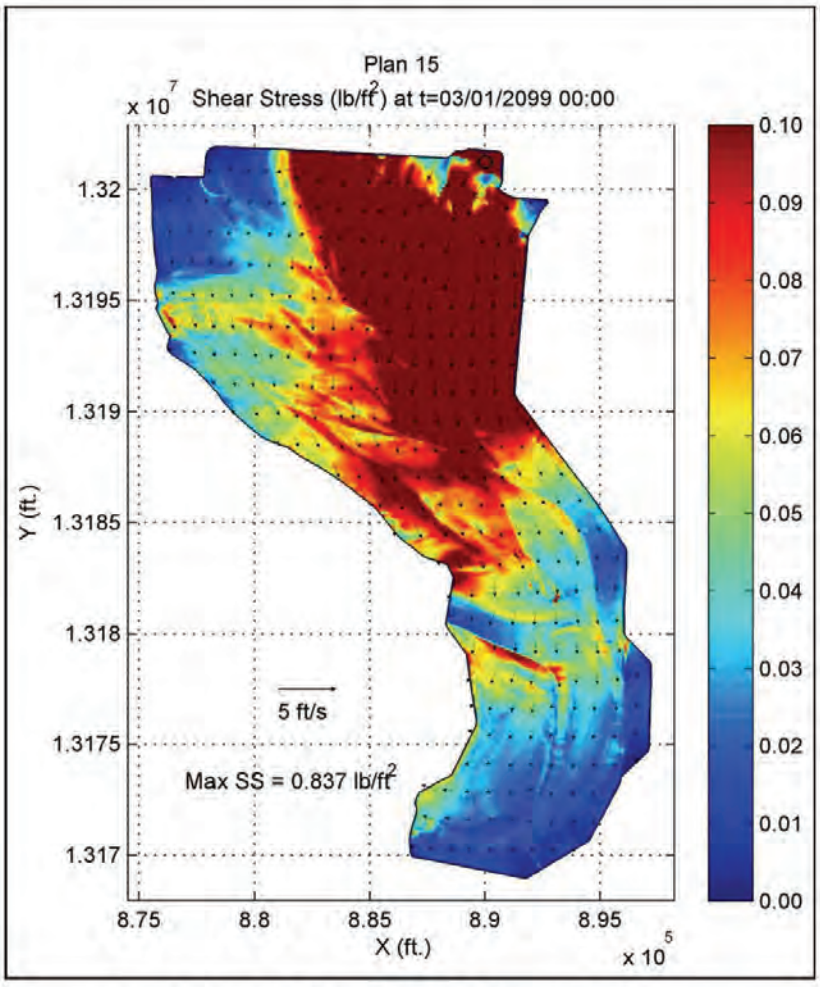


Figure A-17. Plan 15 Shear Stress at Simulation Hour 648

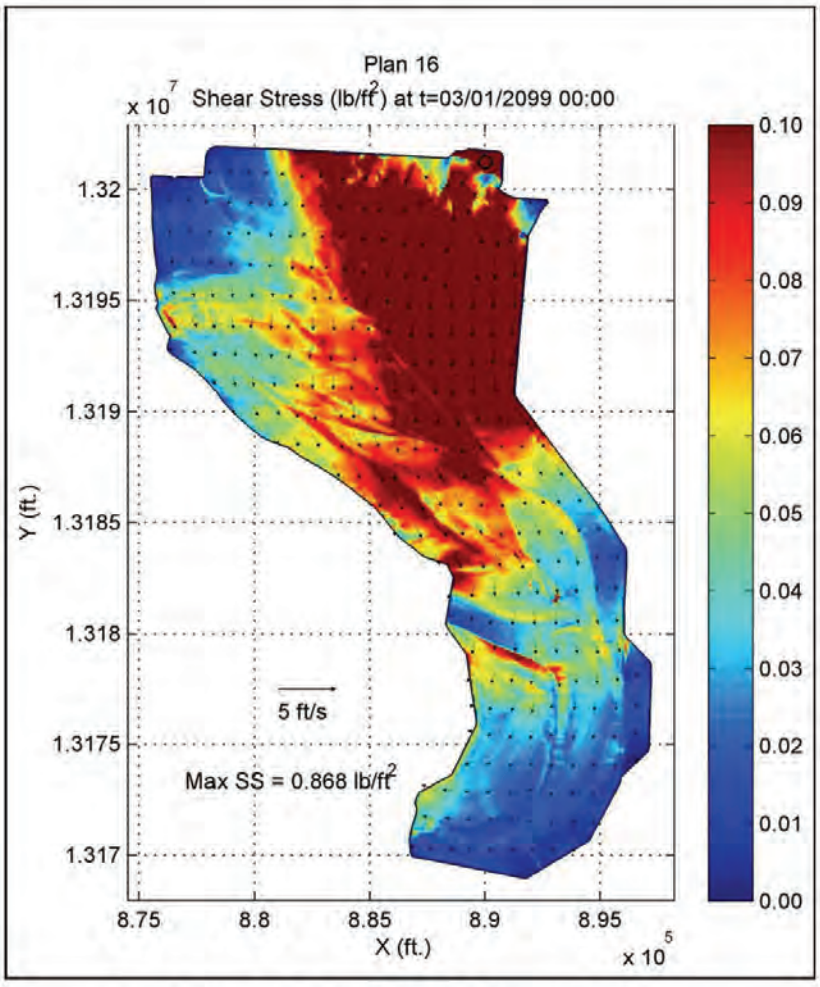


Figure A-18. Plan 16 Shear Stress at Simulation Hour 648

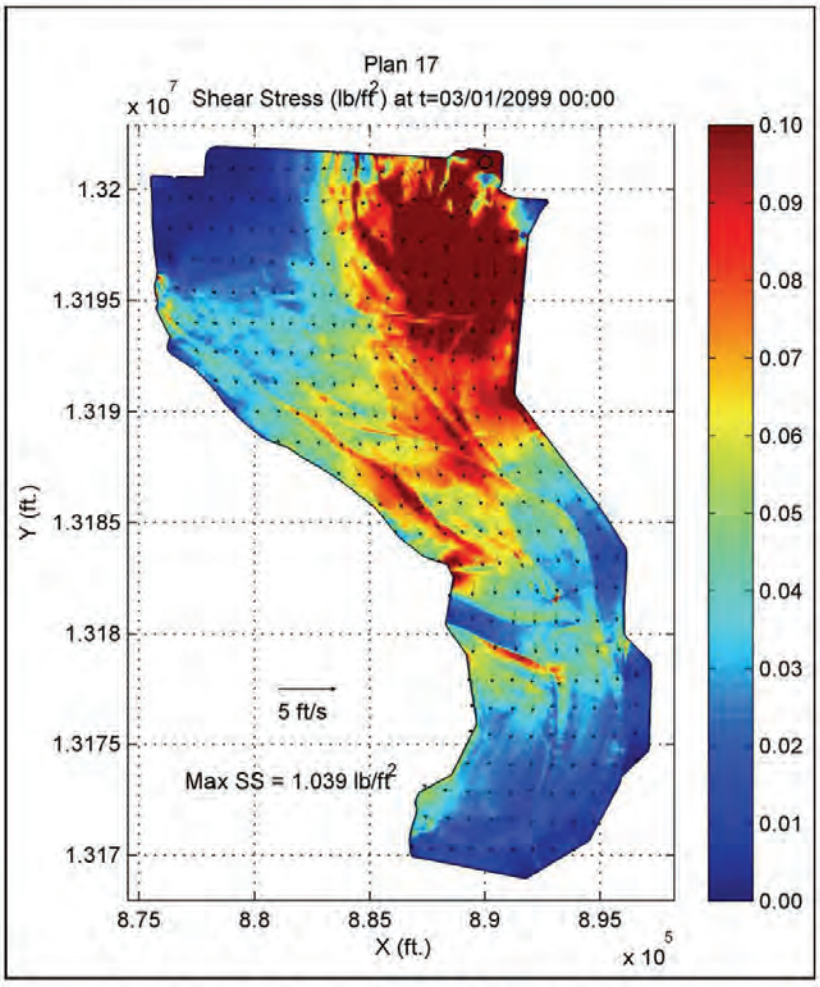


Figure A-19. Plan 17 Shear Stress at Simulation Hour 648

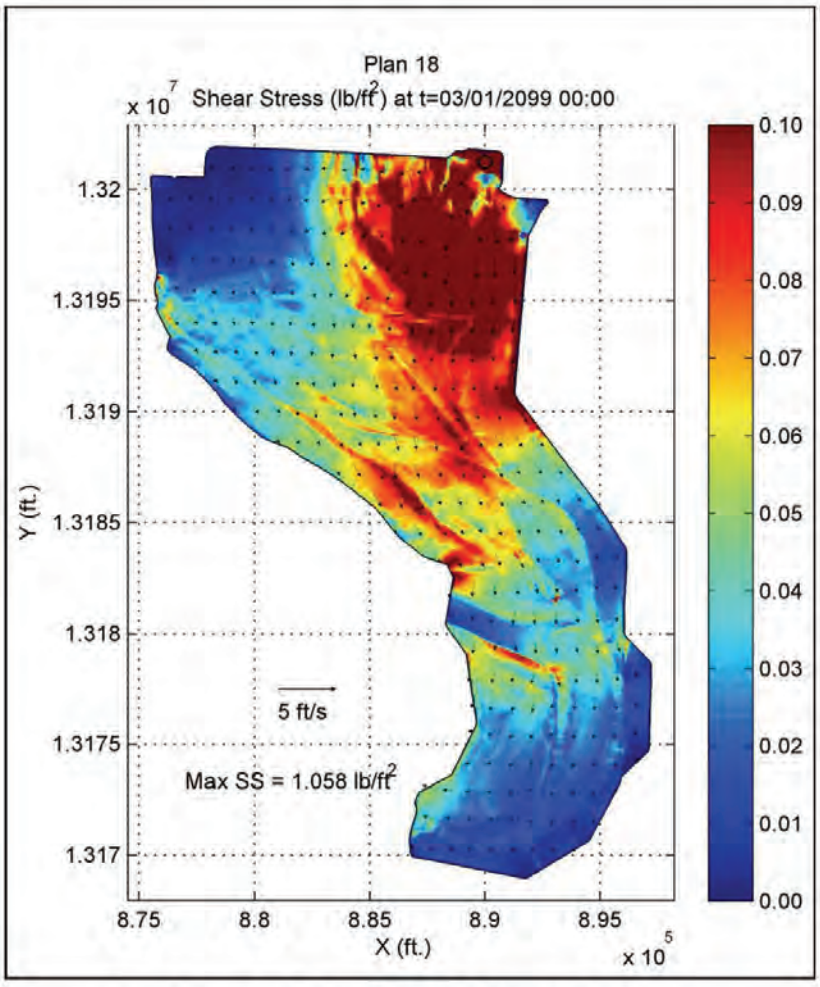


Figure A-20. Plan 18 Shear Stress at Simulation Hour 648

A.4 2D Flow Area Velocity - Simulation Hour at Maximum

Figures located in A.4 depict the velocity in the 2D overbank region at the simulation hour in which the maximum velocity occurred for each plan respectively. Note that the simulation hour/date for each figure is not the same for this series of graphics. The black "o" in the figure identifies the node location with the highest magnitude for each figure respectively. Note that the black arrows represent velocity vectors (a scale velocity vector of 5 ft/s is located on each figure). Note that the darkest color blue in the color scale bar represents zero velocity.

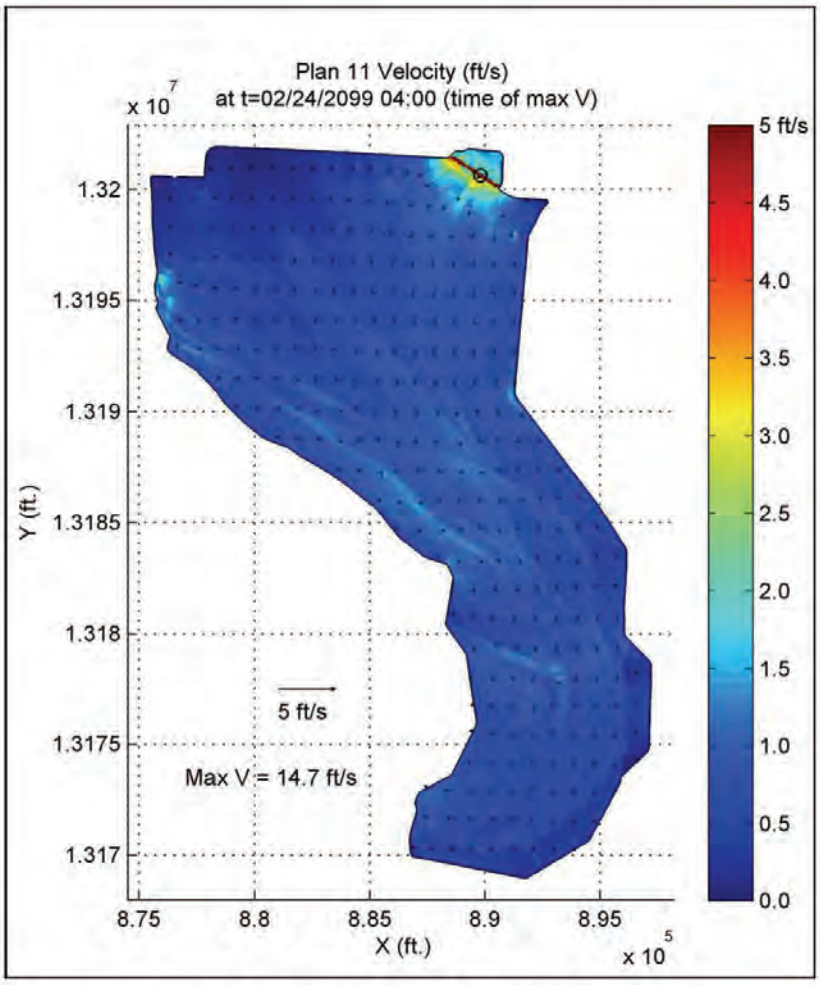


Figure A-21. Plan 11 Velocity at Simulation Hour 532

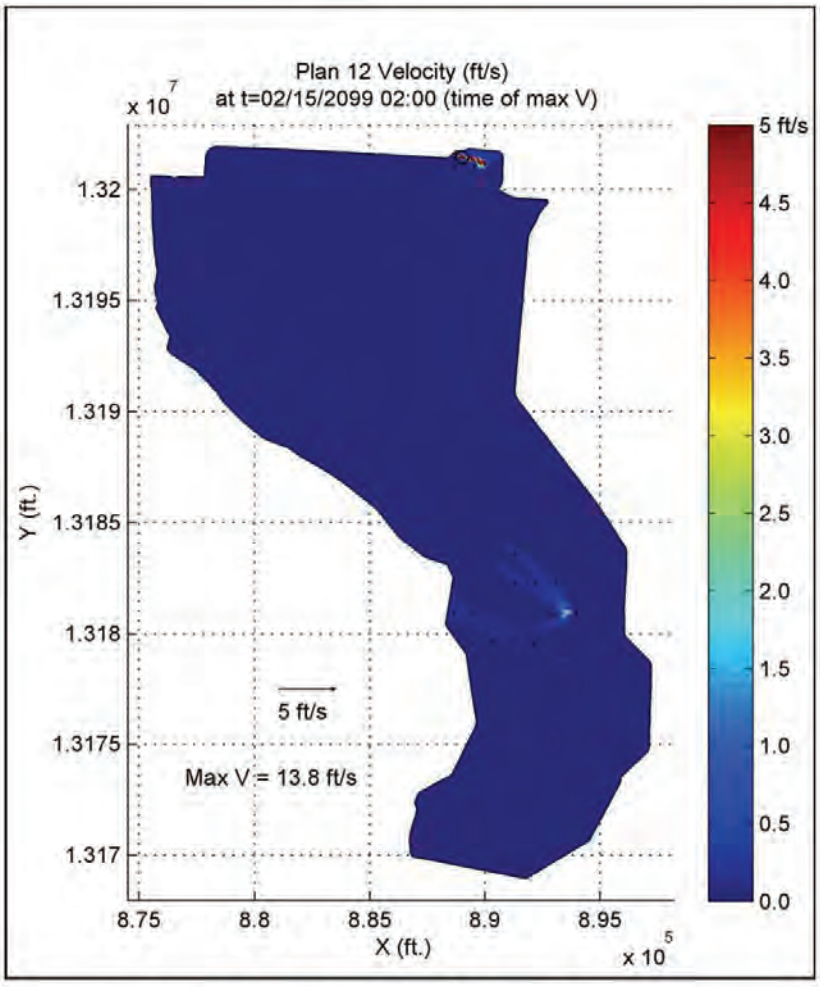


Figure A-22. Plan 12 Velocity at Simulation Hour 314

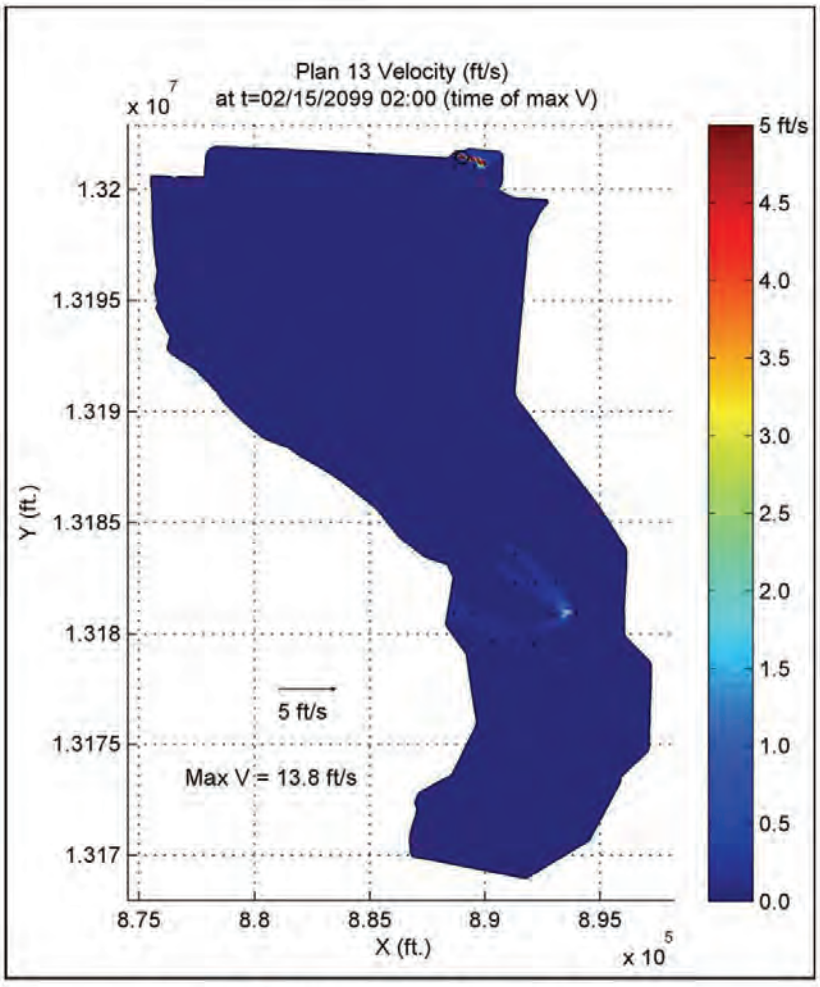


Figure A-23. Plan 13 Velocity at Simulation Hour 314

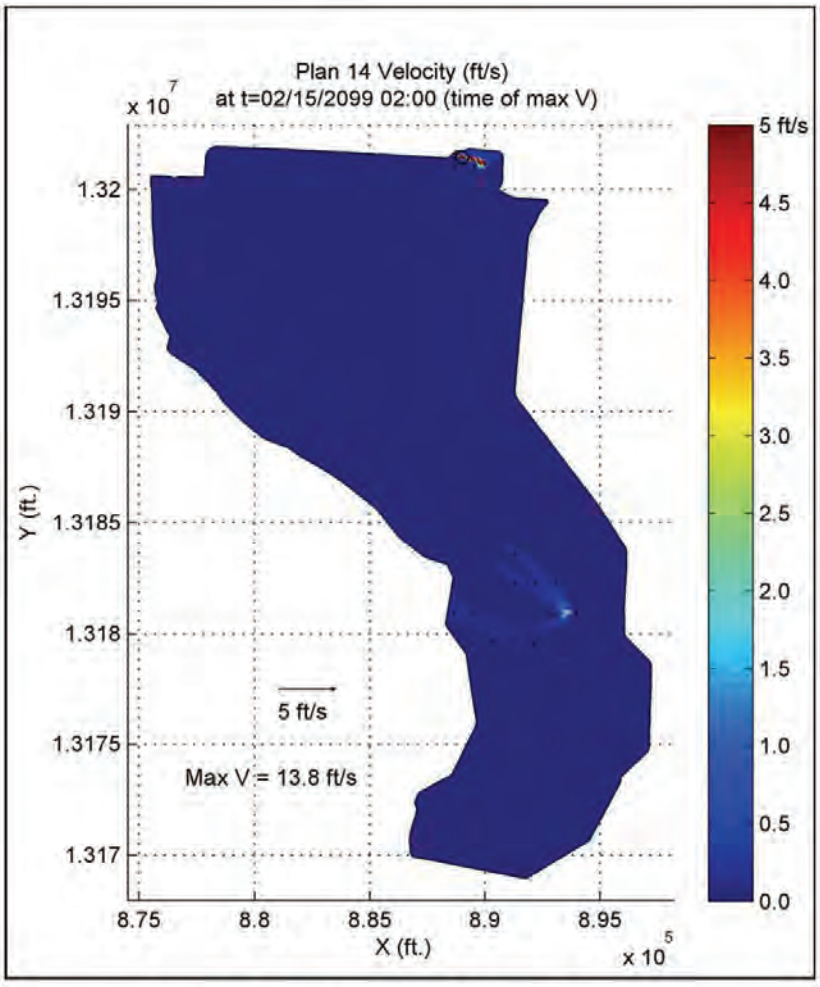


Figure A-24. Plan 14 Velocity at Simulation Hour 314

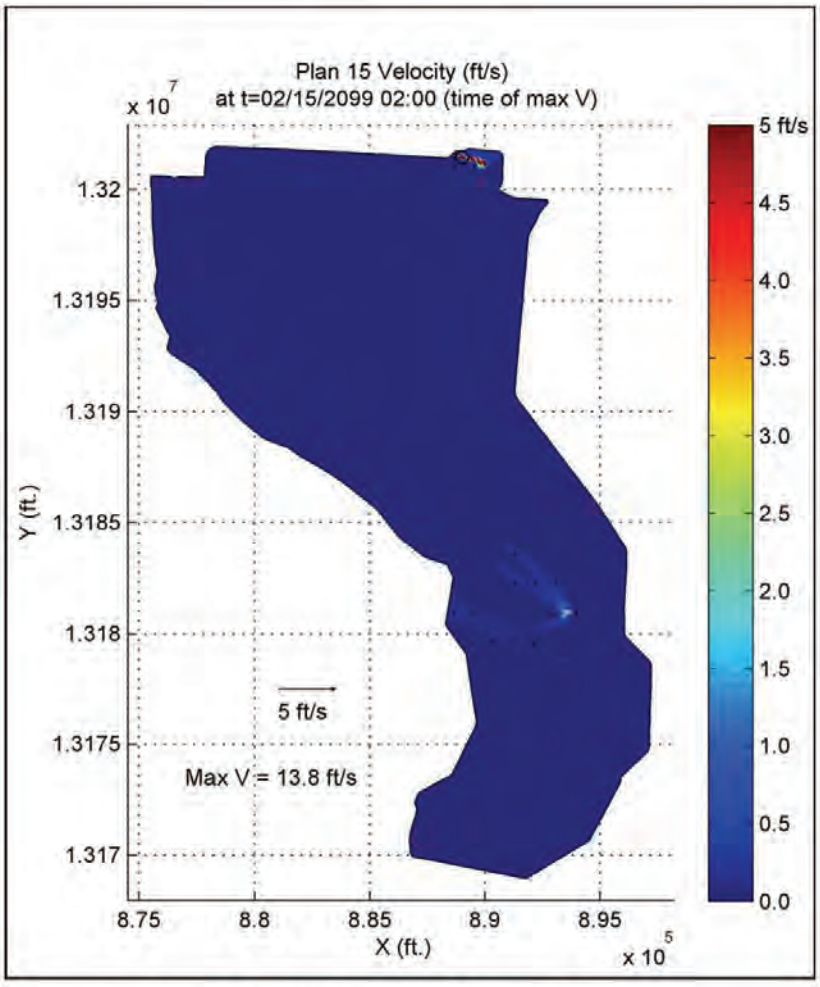


Figure A-25. Plan 15 Velocity at Simulation Hour 314

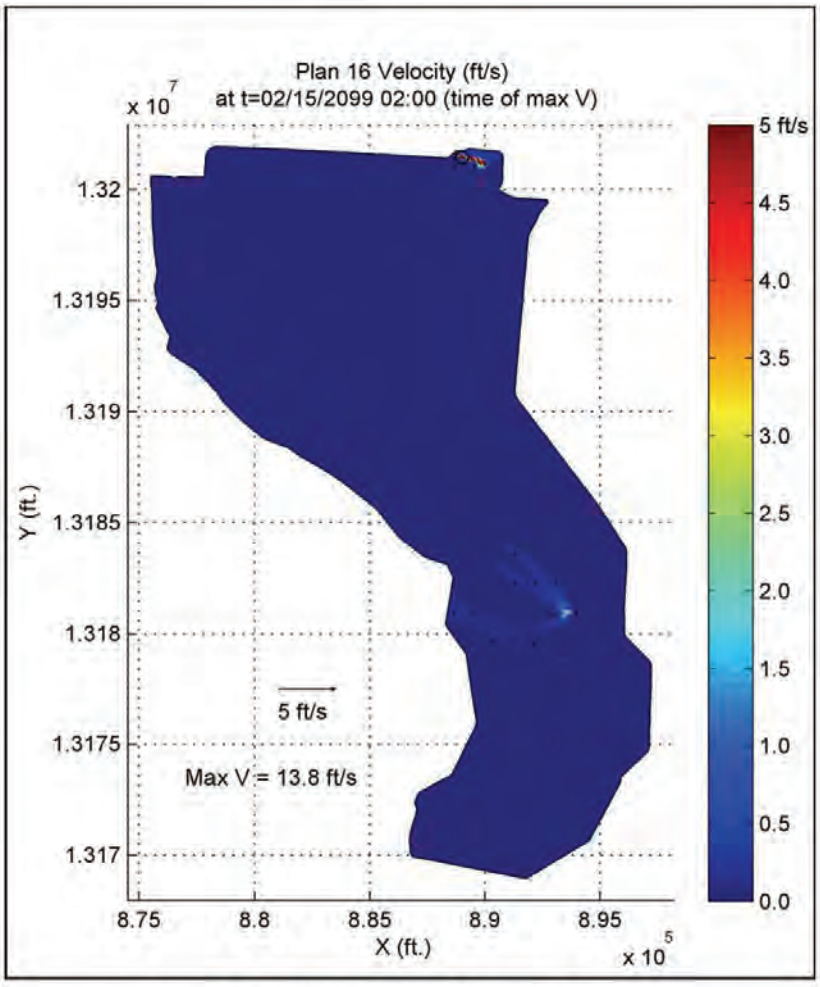


Figure A-26. Plan 16 Velocity at Simulation Hour 314

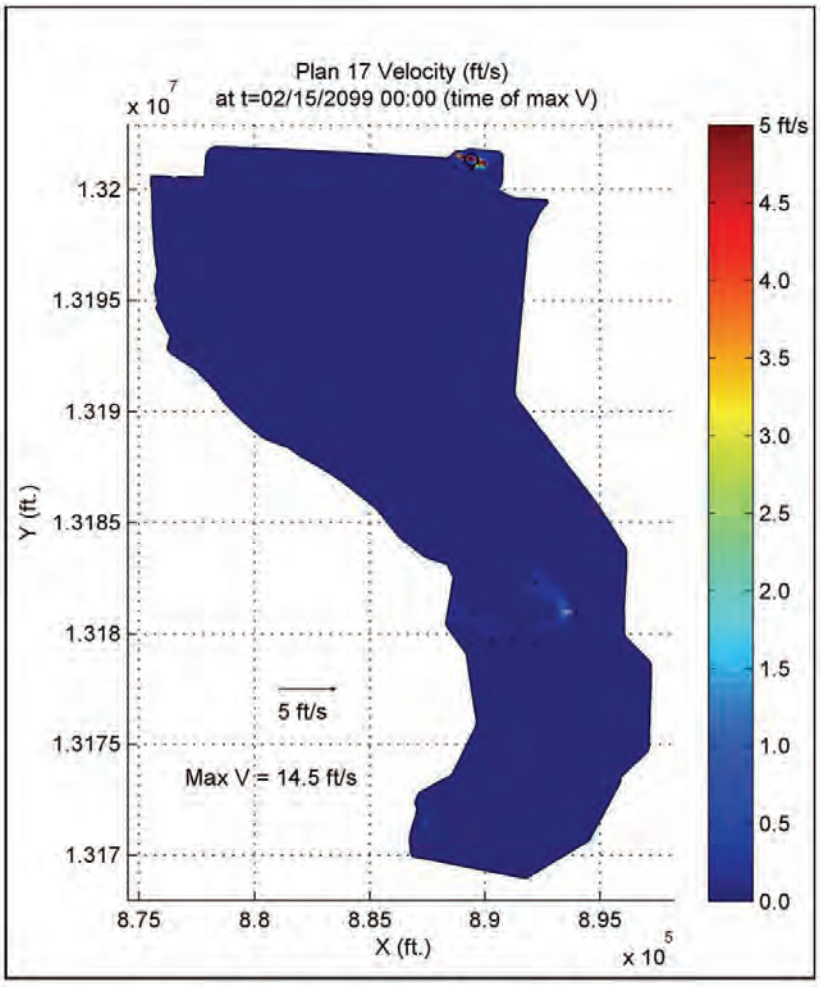


Figure A-27. Plan 17 Velocity at Simulation Hour 312

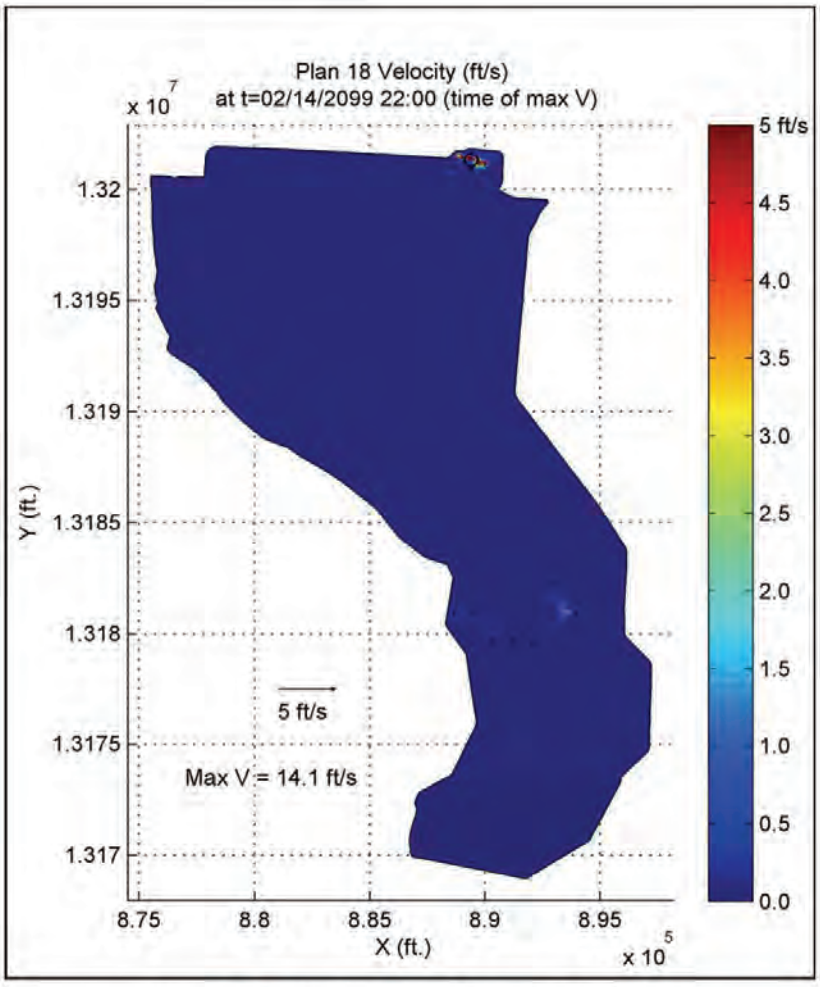


Figure A-28. Plan 18 Velocity at Simulation Hour 310

A.5 2D Flow Area Shear Stress - Simulation Hour at Maximum

Figures located in A.5 depict the shear stress in the 2D overbank region at the simulation hour in which the maximum shear stress occurred for each plan respectively. Note that the simulation hour/date for each figure is not the same for this series of graphics. Note that the color "white" symbolizes no shear stress for this series of graphics. For plots where portions of the overbank region are colored white, flow is initially beginning to divert through the crevasse (white colored regions of the overbank are dry during this simulation time). The black "o" in the figure identifies the node location with the highest magnitude for each figure respectively. Note that the black arrows represent velocity vectors (a scale velocity vector of 5 ft/s is located on each figure).

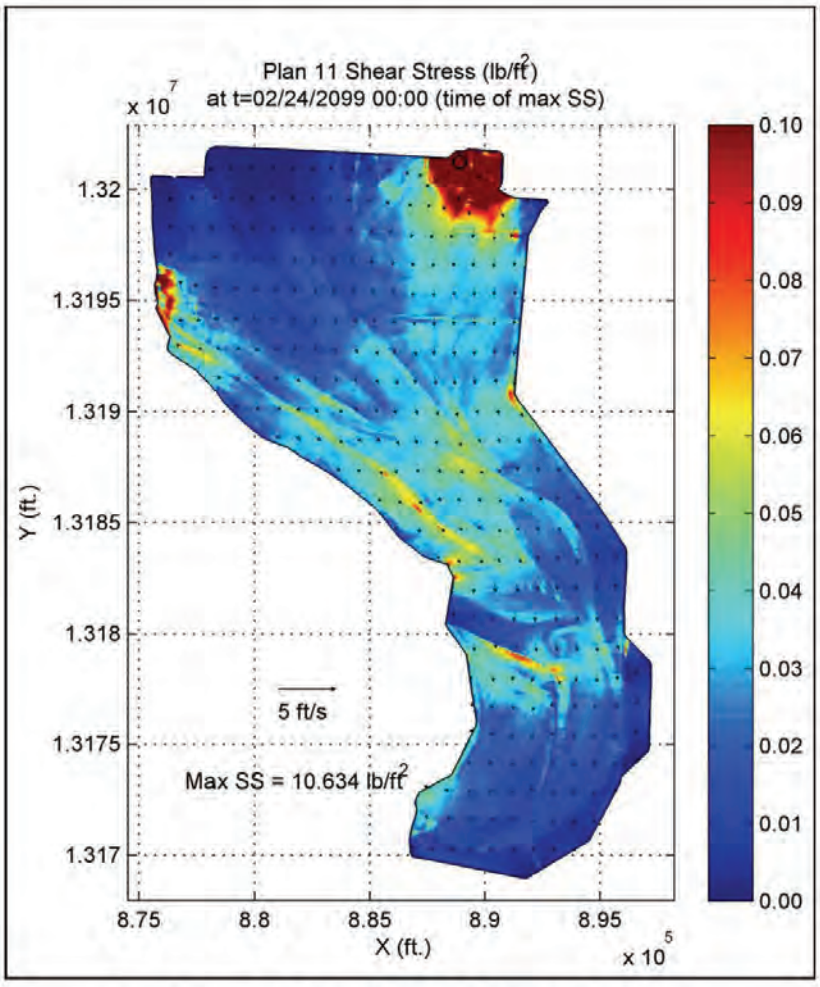


Figure A-29. Plan 11 Shear Stress at Simulation Hour 528

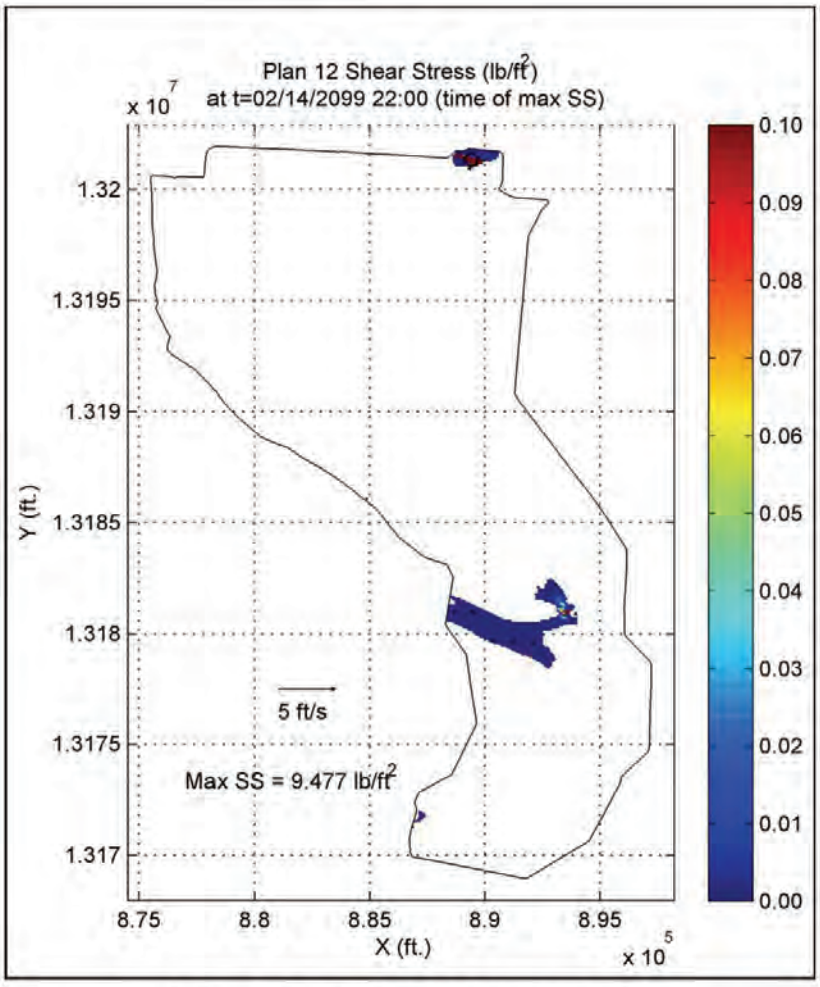


Figure A-30. Plan 12 Shear Stress at Simulation Hour 310

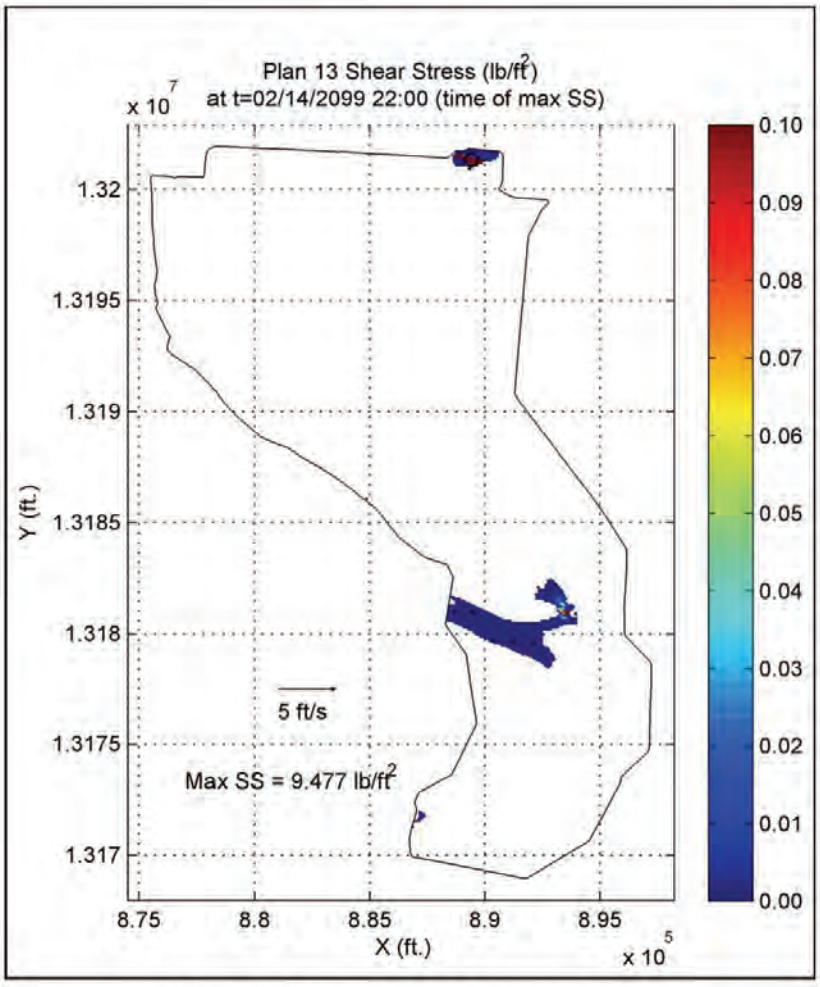


Figure A-31. Plan 13 Shear Stress at Simulation Hour 310

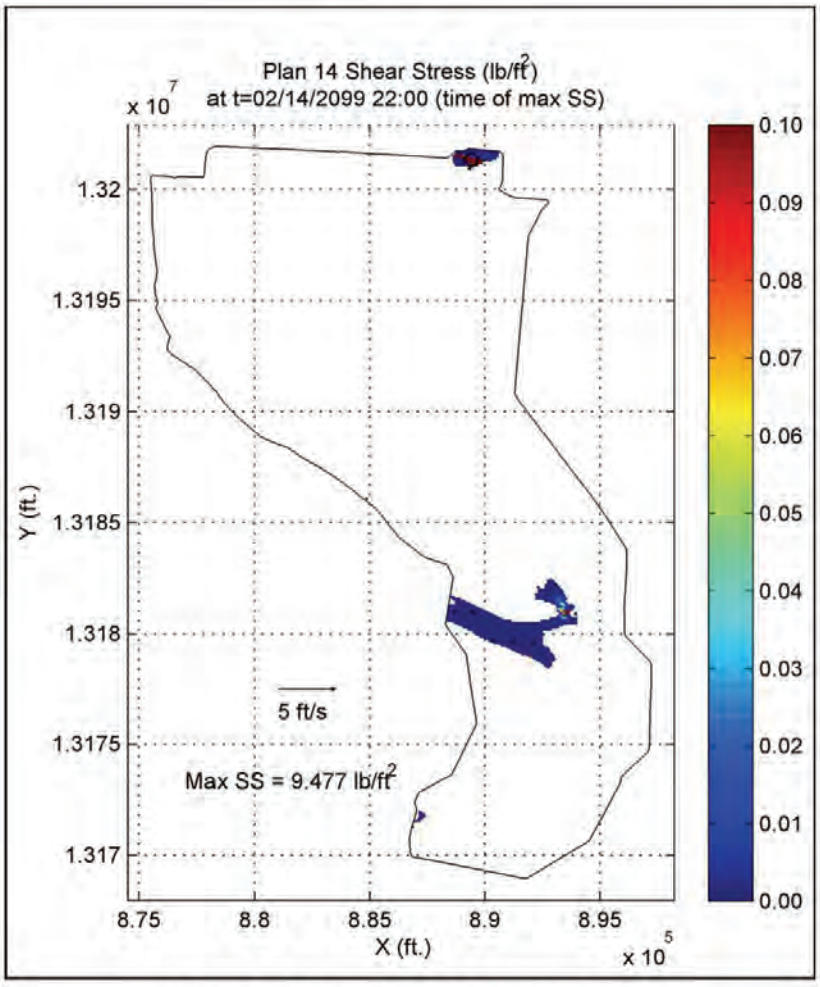


Figure A-32. Plan 14 Shear Stress at Simulation Hour 310

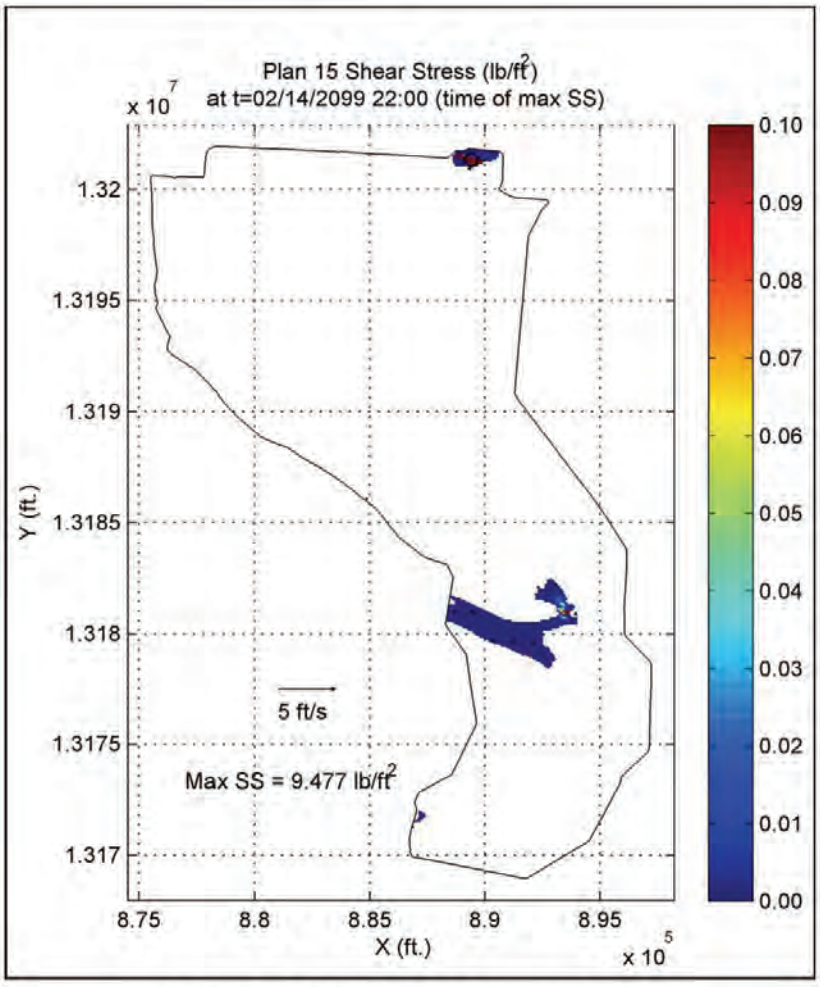


Figure A-33. Plan 15 Shear Stress at Simulation Hour 310

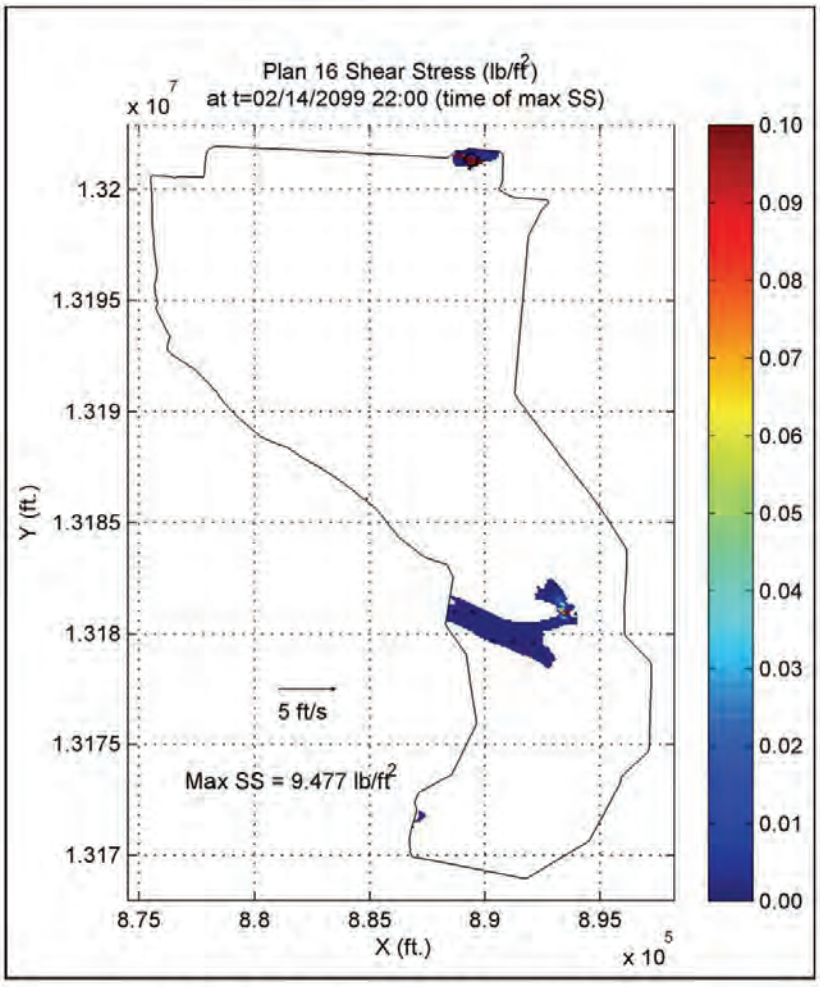


Figure A-34. Plan 16 Shear Stress at Simulation Hour 310

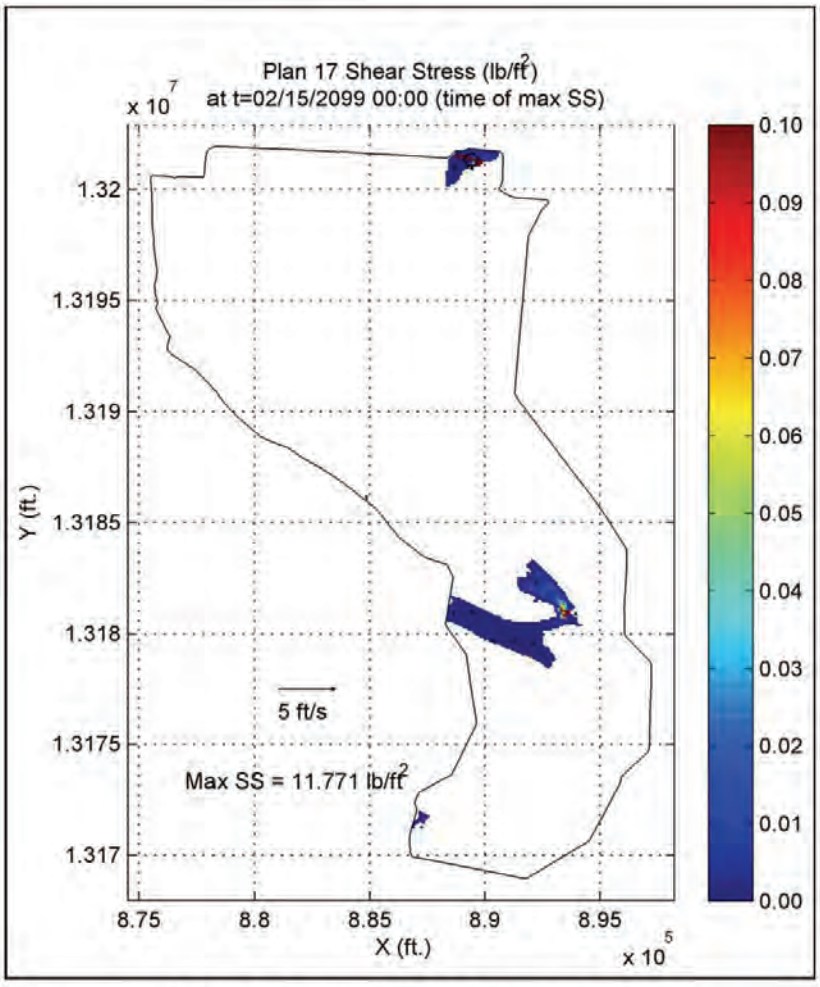


Figure A-35. Plan 17 Shear Stress at Simulation Hour 312

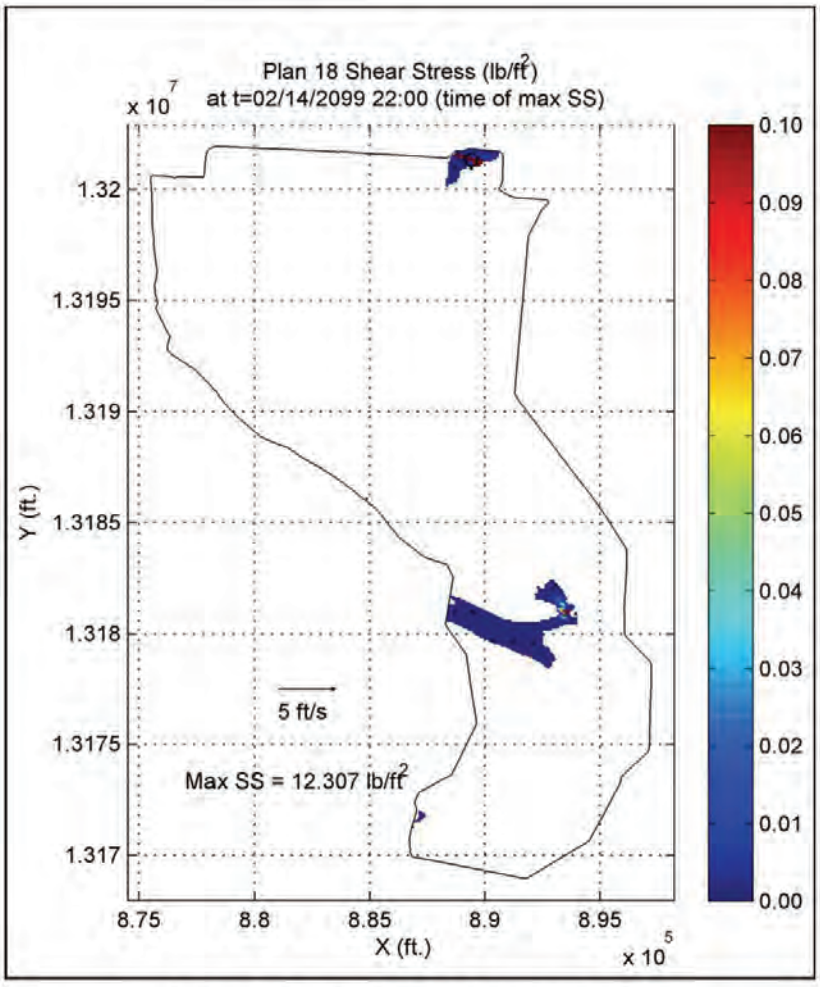


Figure A-36. Plan 12 Shear Stress at Simulation Hour 310

A.6 2D Flow Area Velocity - Node Maximum

Figures located in A.6 depict the maximum velocity that occurred at each node in the 2D overbank region throughout out the entire simulation for each plan respectively. The black "o" in the figure identifies the node location with the highest magnitude for each figure respectively.

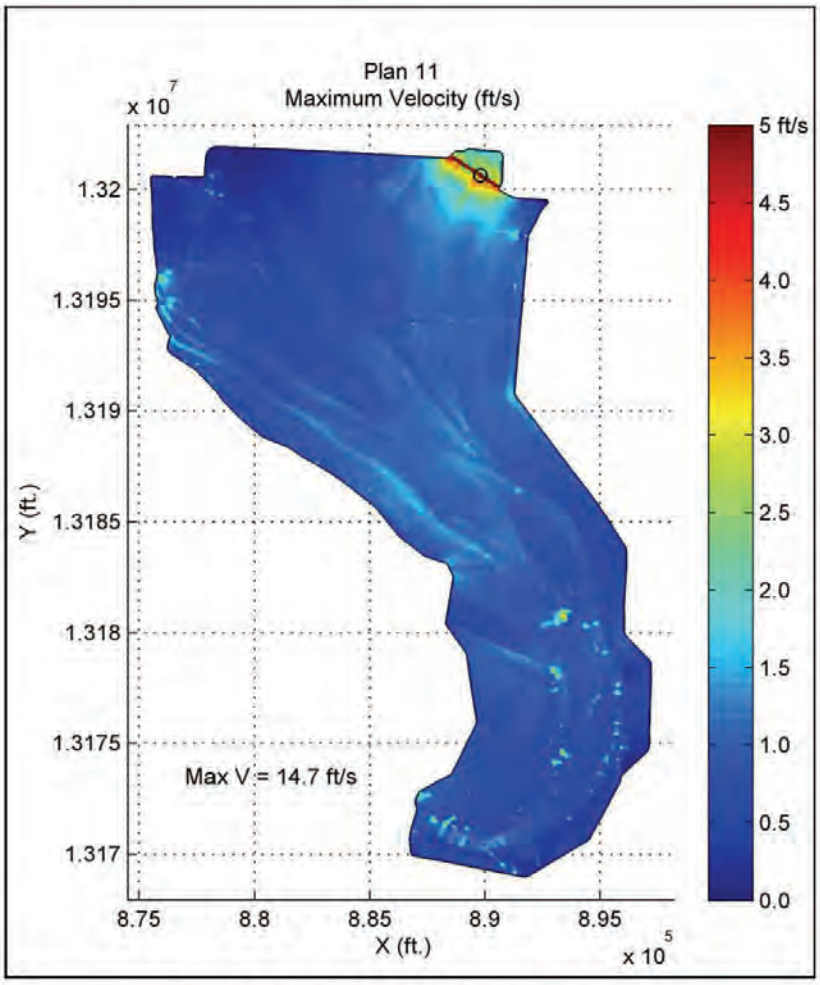


Figure A-37. Plan 11 Velocity Node Maximum

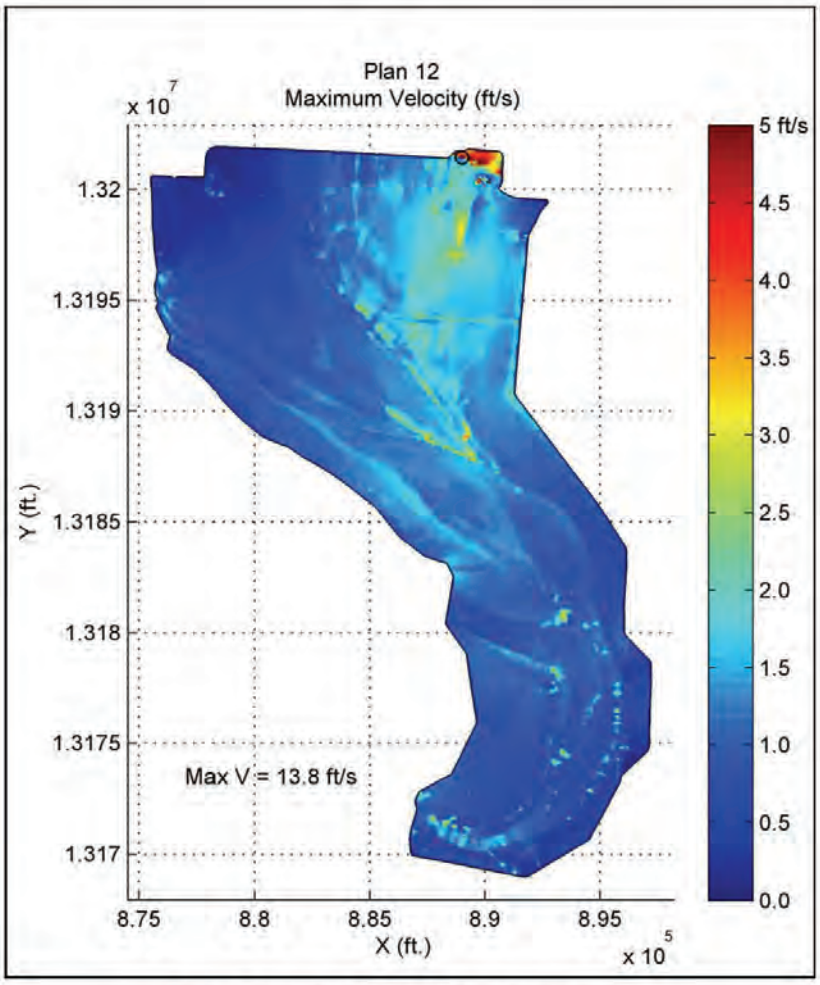


Figure A-38. Plan 12 Velocity Node Maximum

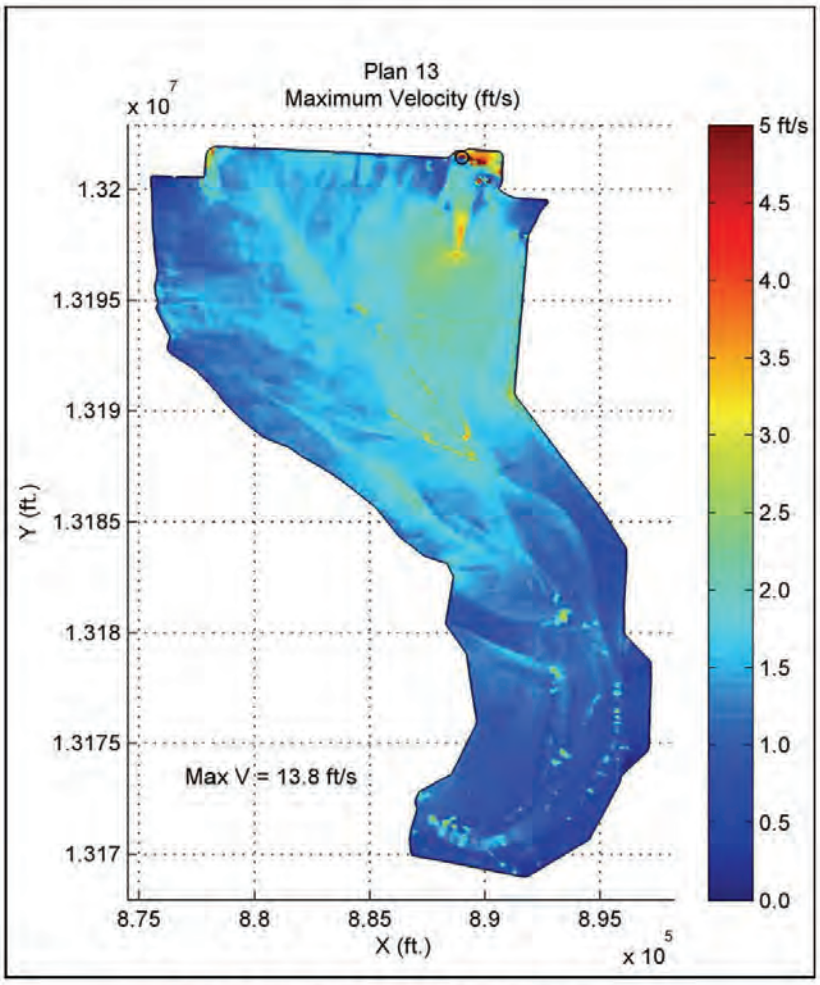


Figure A-39. Plan 13 Velocity Node Maximum

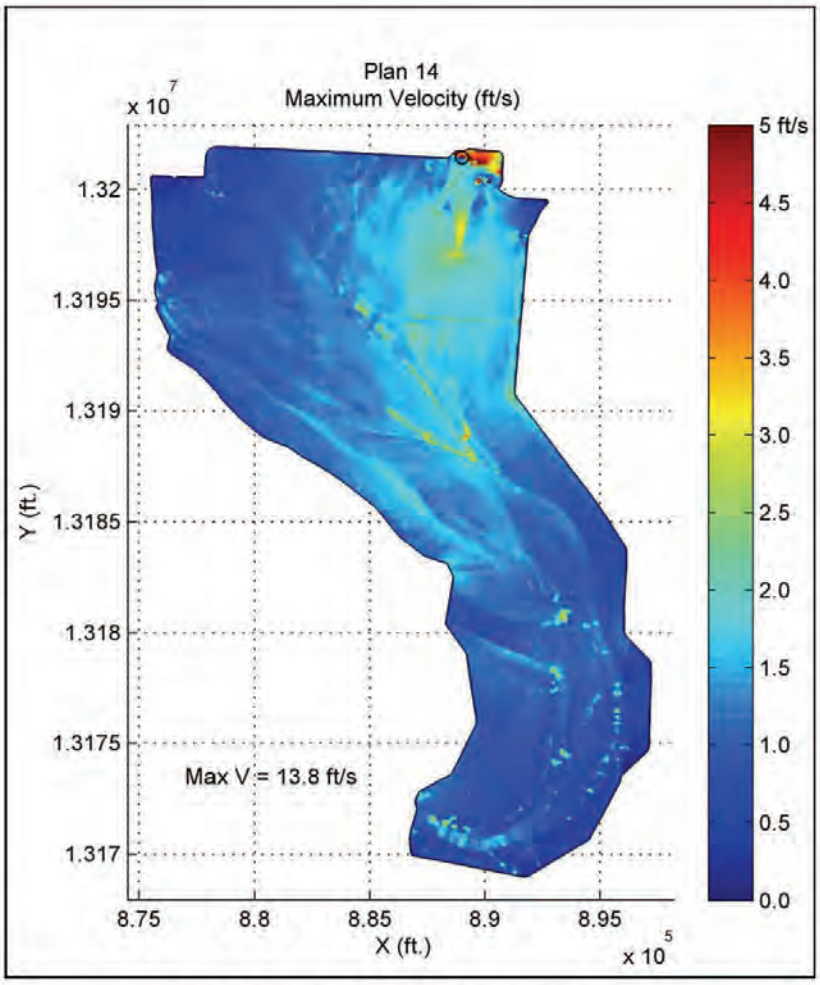


Figure A-40. Plan 14 Velocity Node Maximum

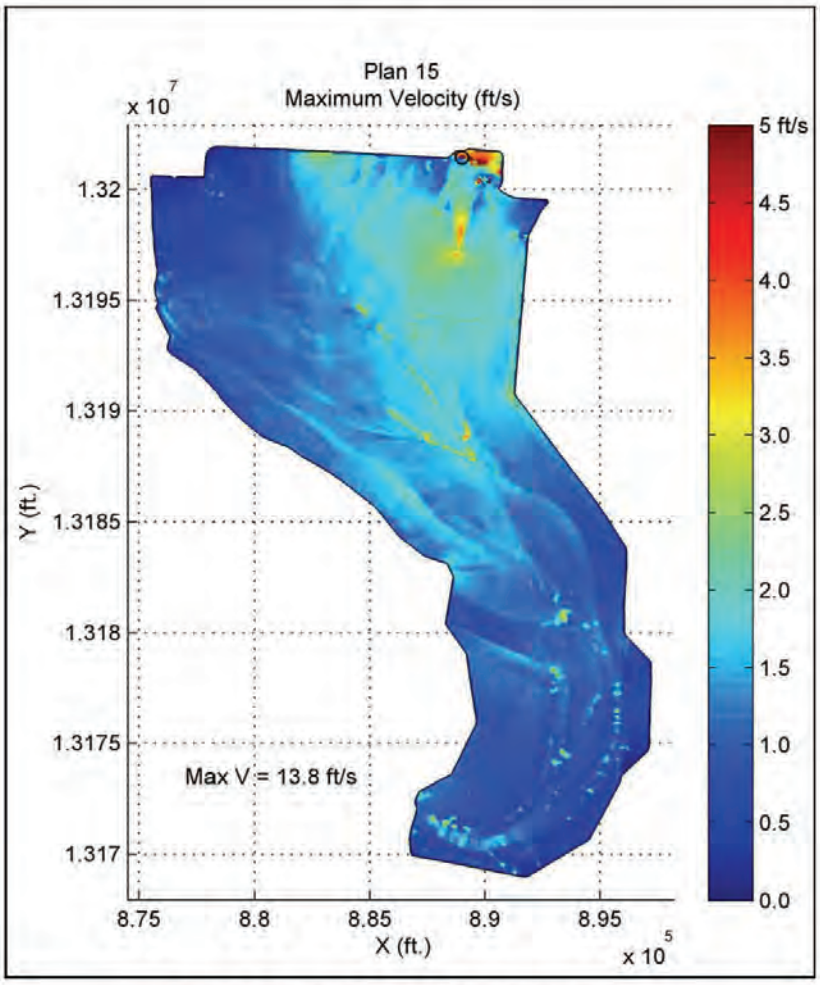


Figure A-41. Plan 15 Velocity Node Maximum

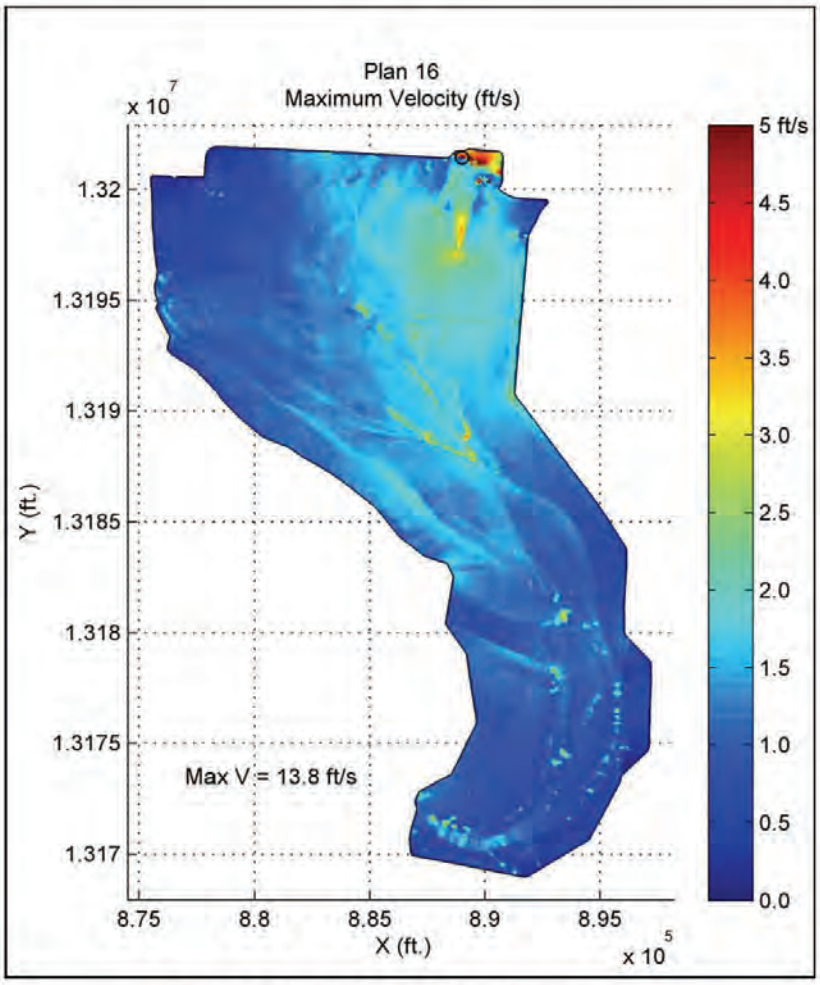


Figure A-42. Plan 16 Velocity Node Maximum

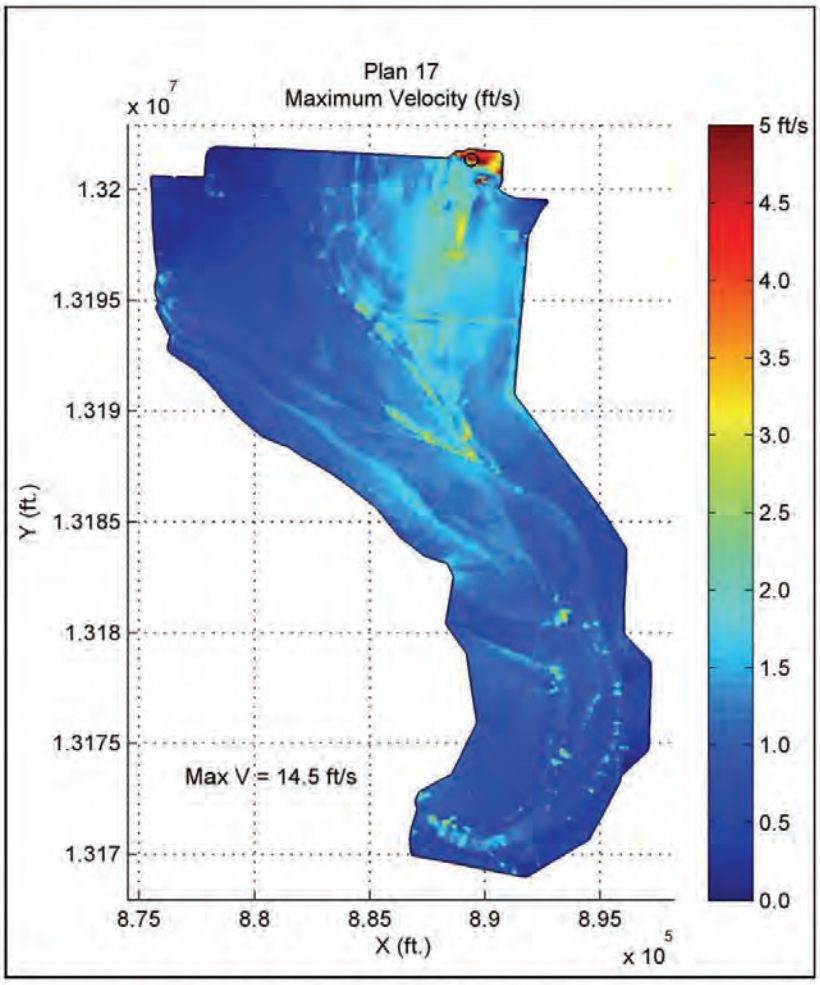


Figure A-43. Plan 17 Velocity Node Maximum

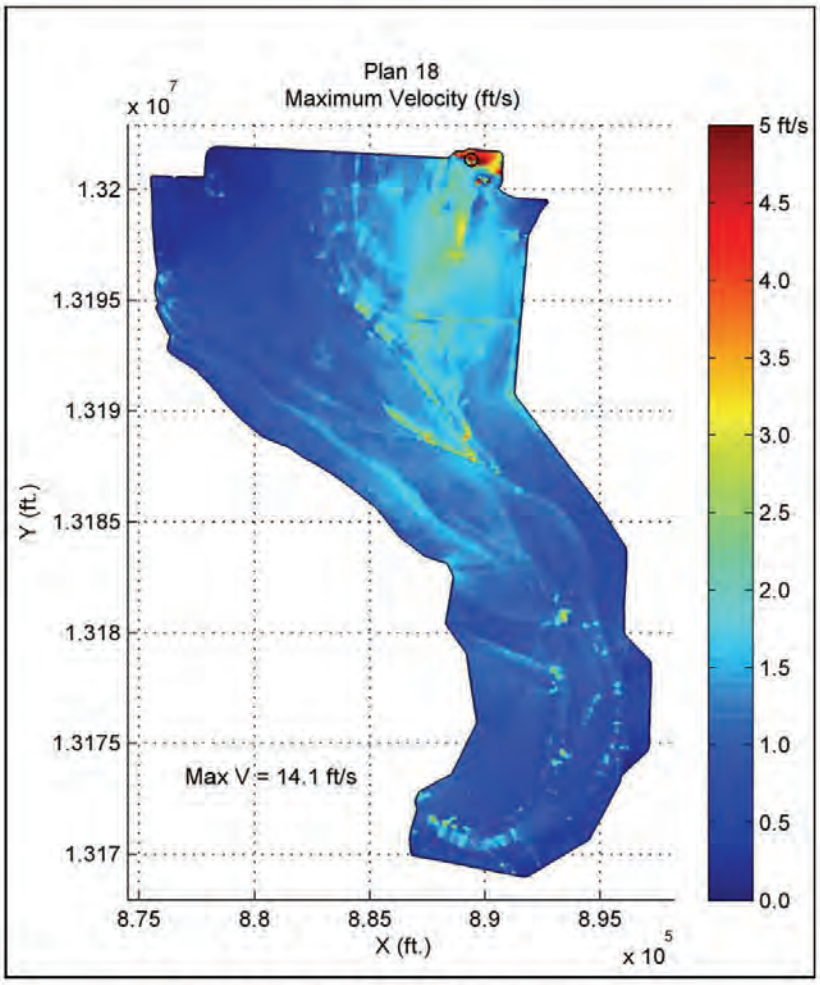


Figure A-44. Plan 18 Velocity Node Maximum

A.7 2D Flow Area Shear Stress - Node Maximum

Figures located in A.7 depict the maximum shear stress that occurred at each node in the 2D overbank region throughout out the entire simulation for each plan respectively. The black "o" in the figure identifies the node location with the highest magnitude for each figure respectively.

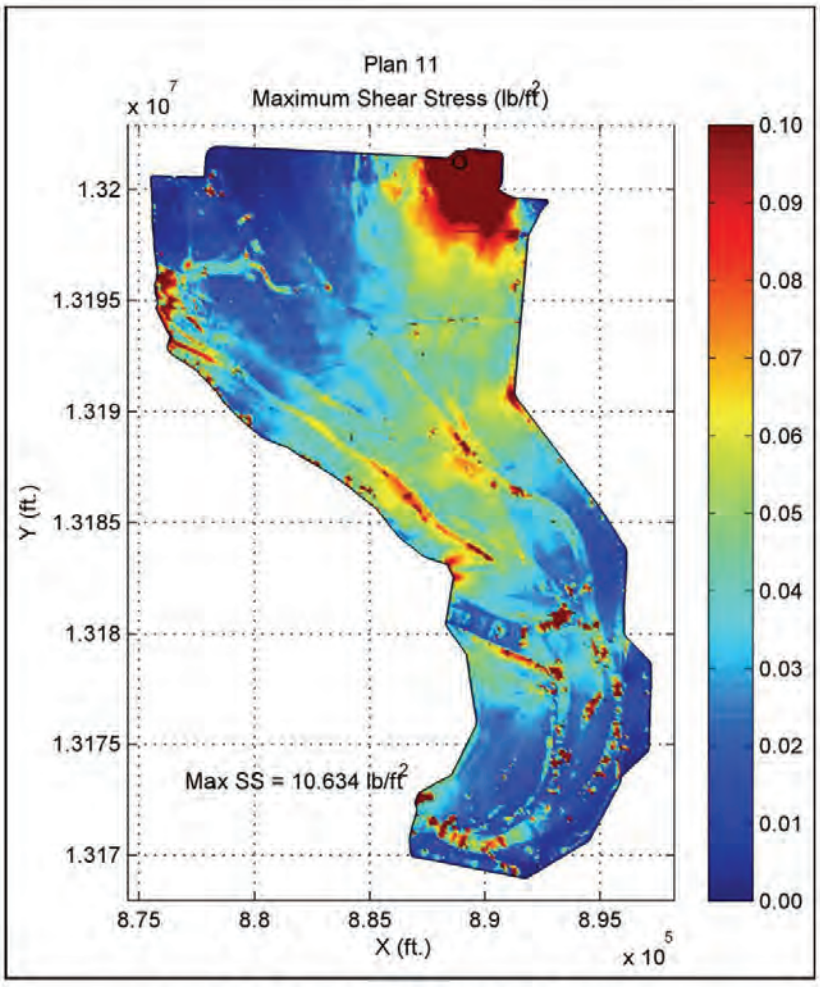


Figure A-45. Plan 11 Shear Stress Node Maximum

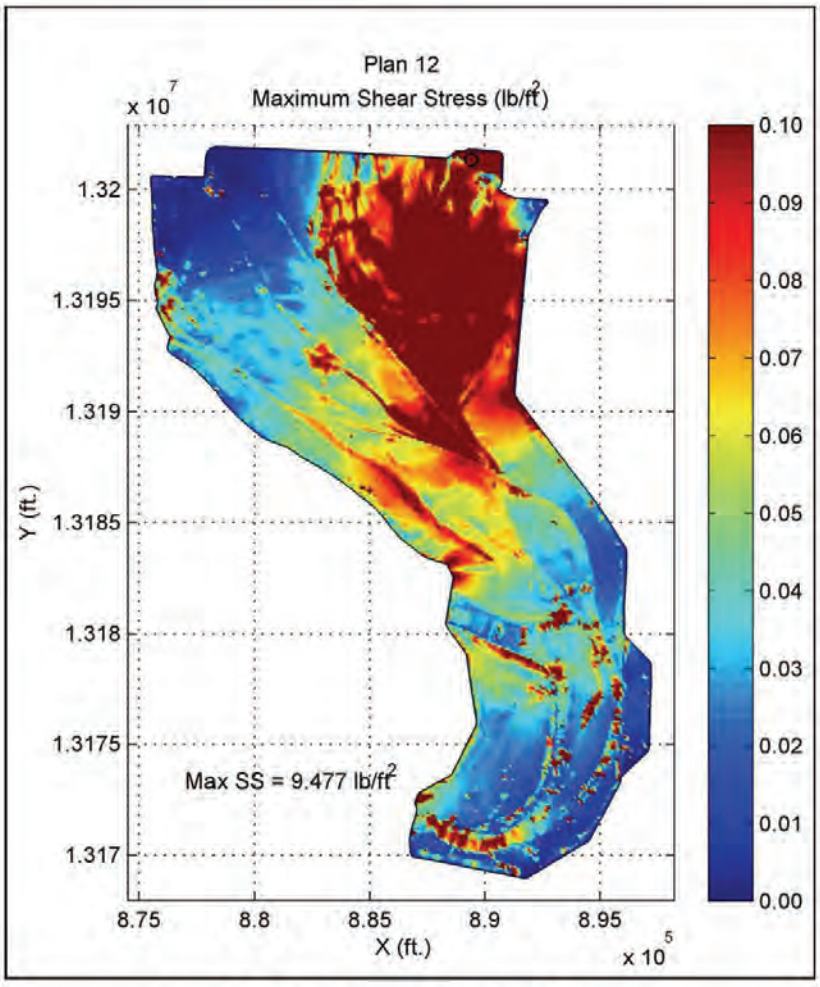


Figure A-46. Plan 12 Shear Stress Node Maximum

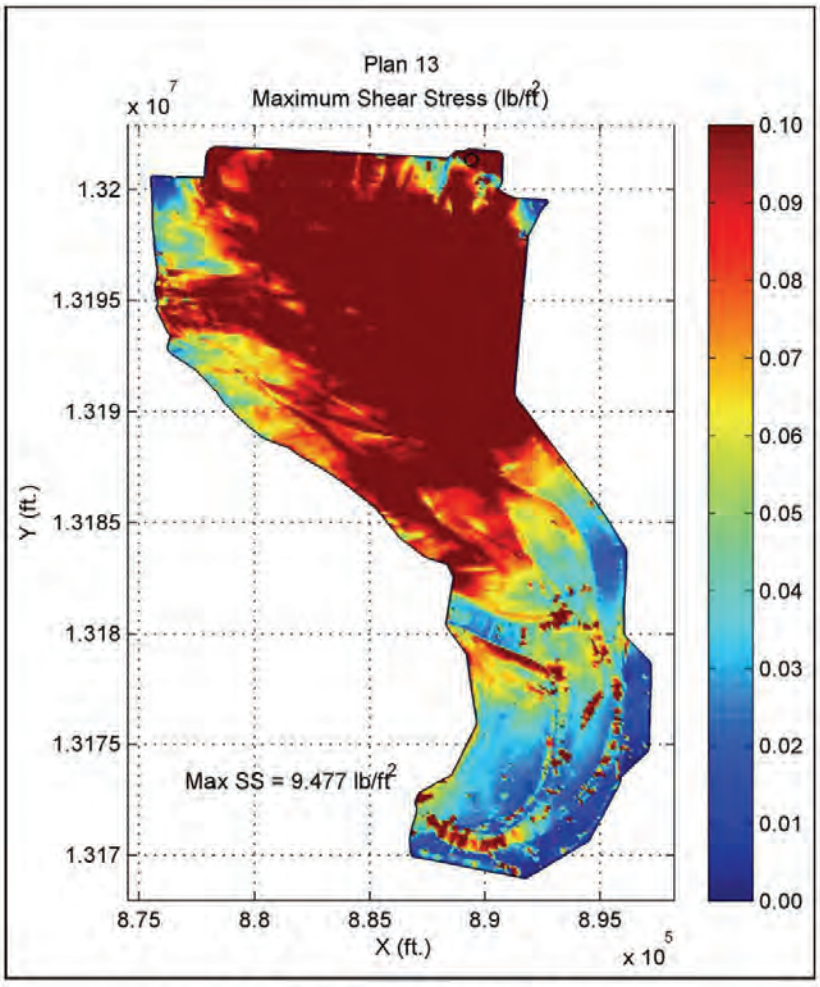


Figure A-47. Plan 13 Shear Stress Node Maximum

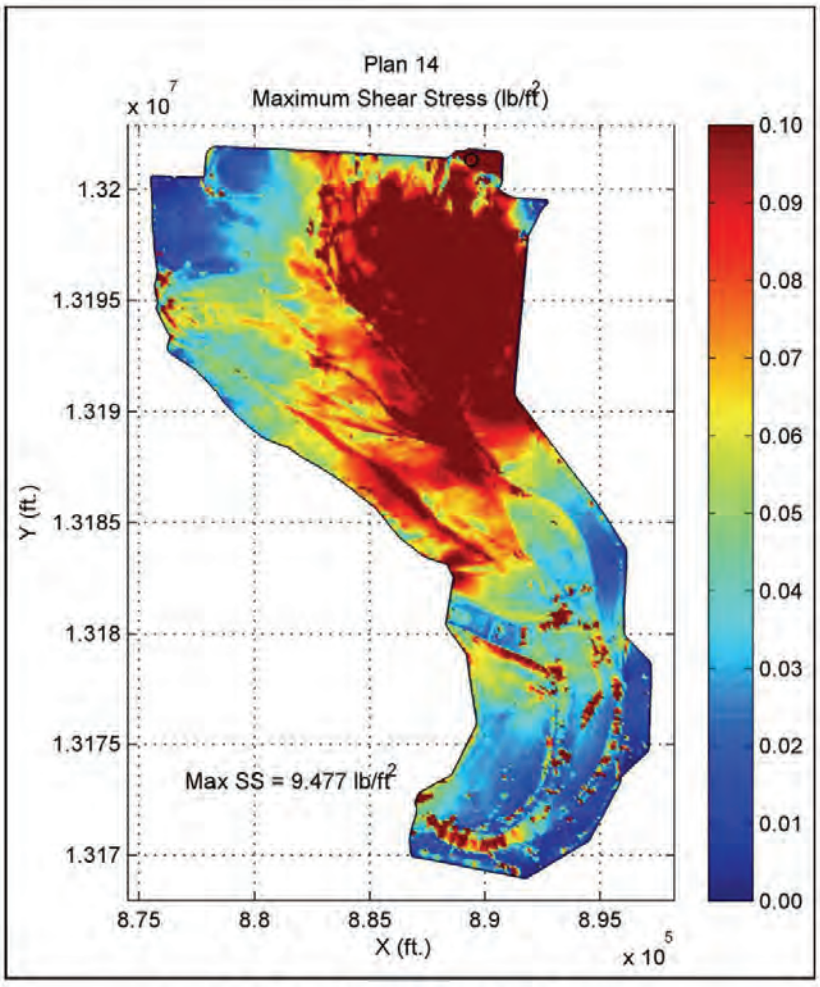


Figure A-48. Plan 14 Shear Stress Node Maximum

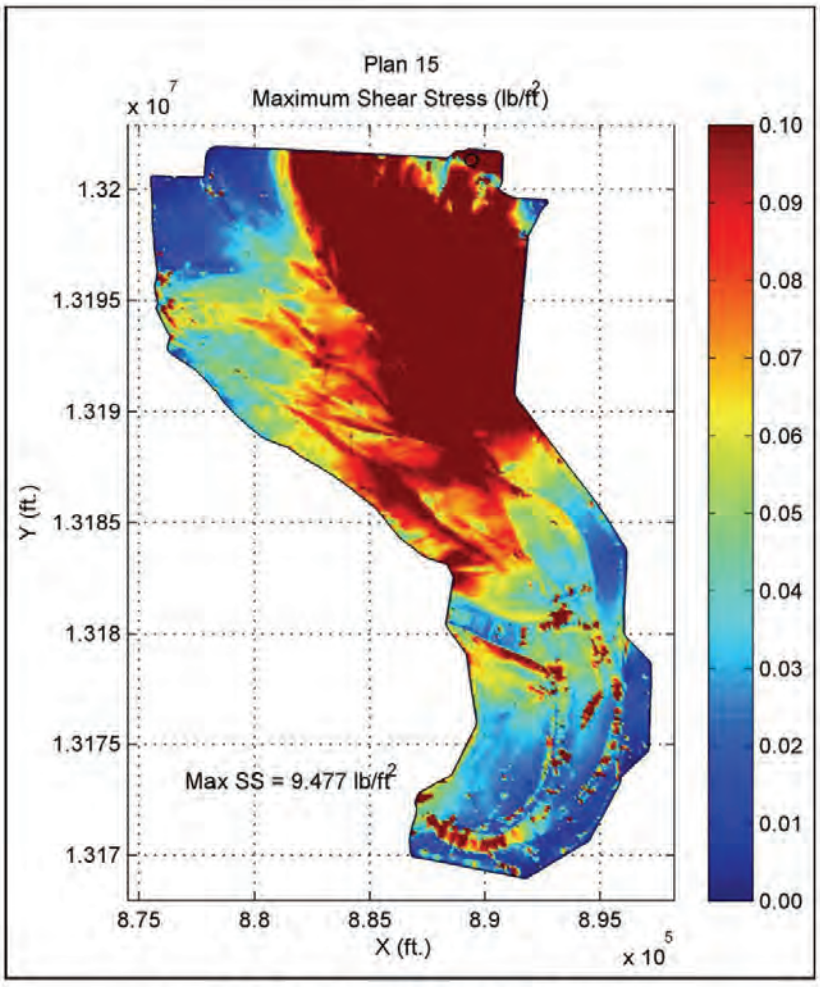


Figure A-49. Plan 15 Shear Stress Node Maximum

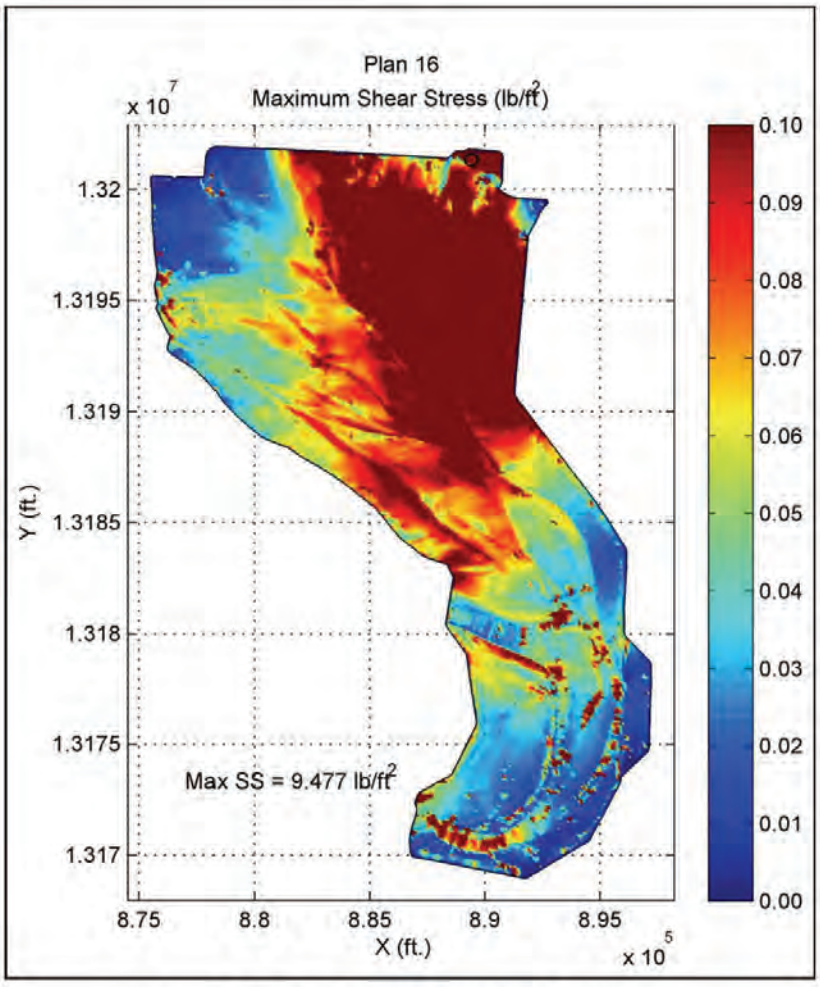


Figure A-50. Plan 16 Shear Stress Node Maximum

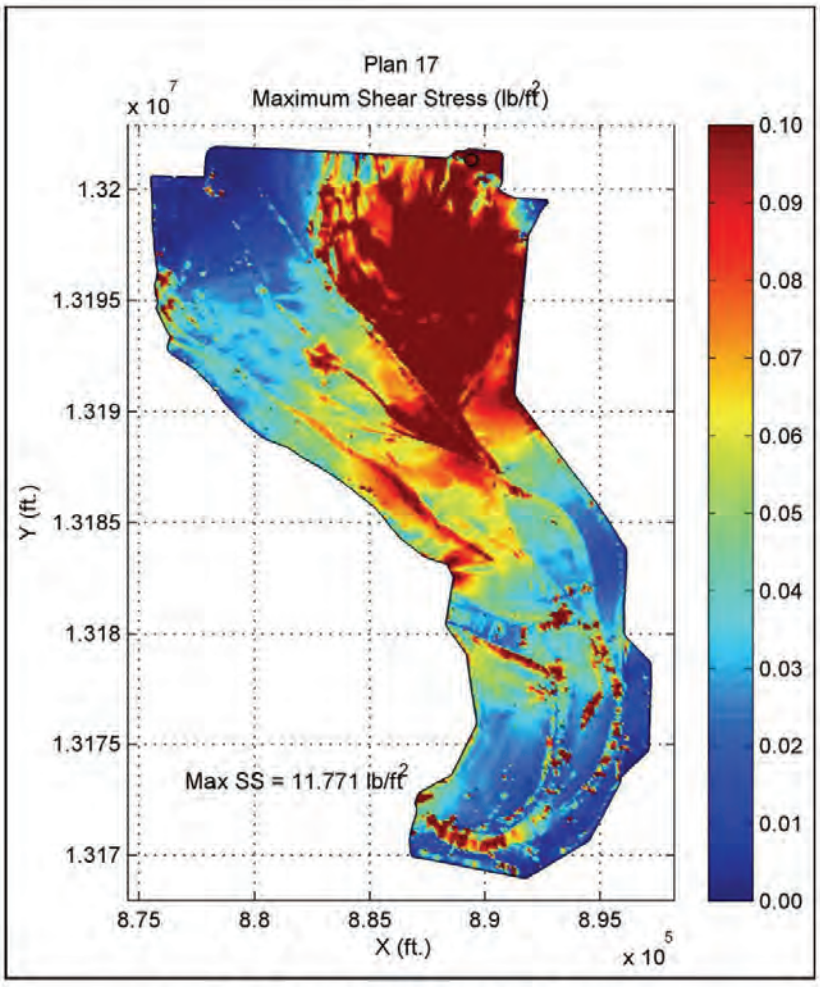


Figure A-51. Plan 17 Shear Stress Node Maximum

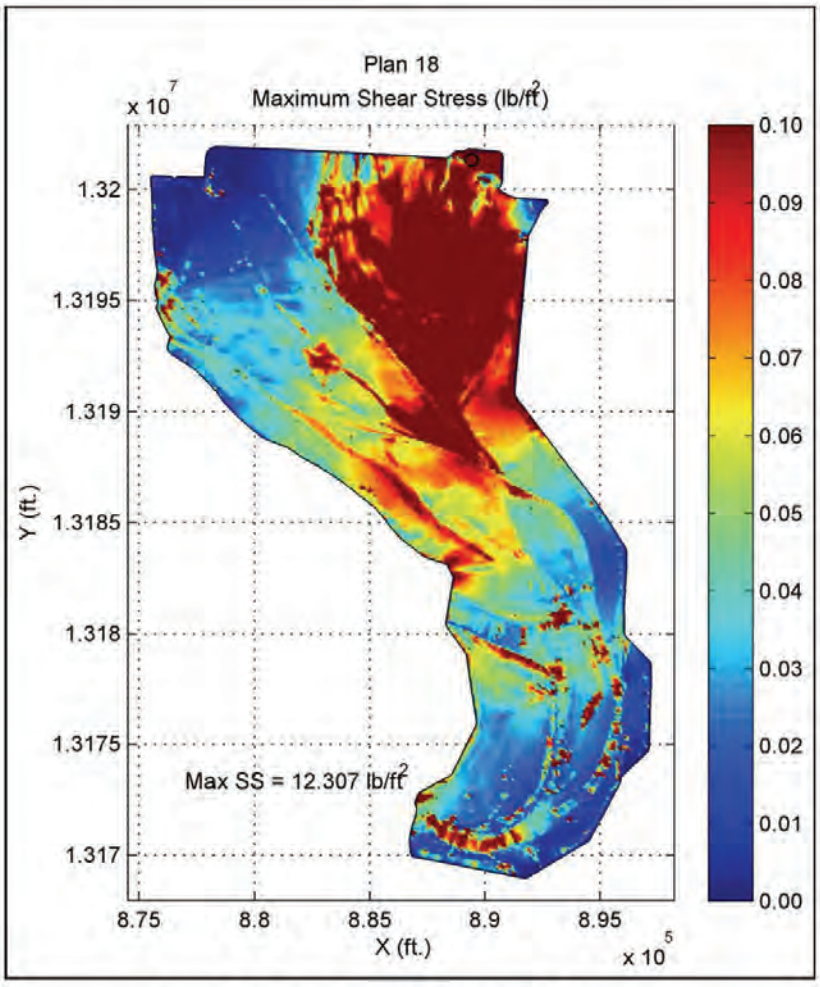


Figure A-52. Plan 18 Shear Stress Node Maximum

A.8 2D Flow Area Velocity - Difference from Base Condition Plan

Figures located in A.8 depict the respective plan's velocity difference from Plan 12 (base condition) in the 2D overbank region at simulation hour 648. The white "o" in the figure identifies the node location with the maximum increase for each figure respectively. The white "x" in the figure identifies the node location with the maximum decrease for each figure respectively.

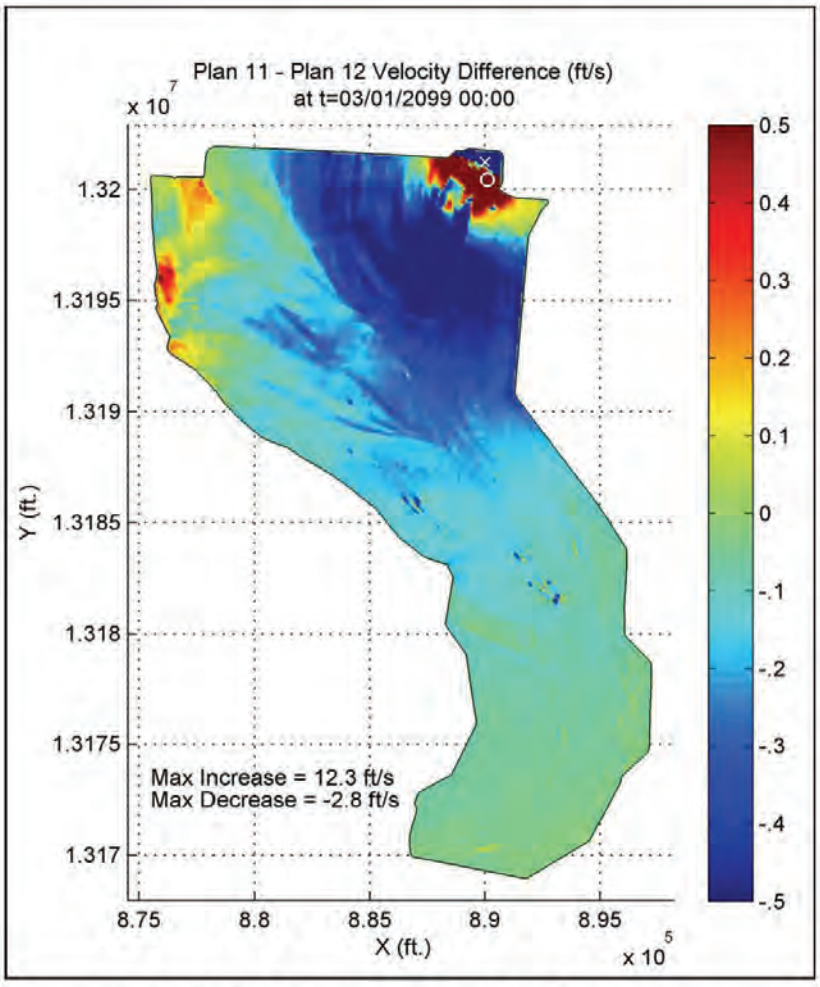


Figure A-53. Plan 11 Velocity Difference from Base Condition

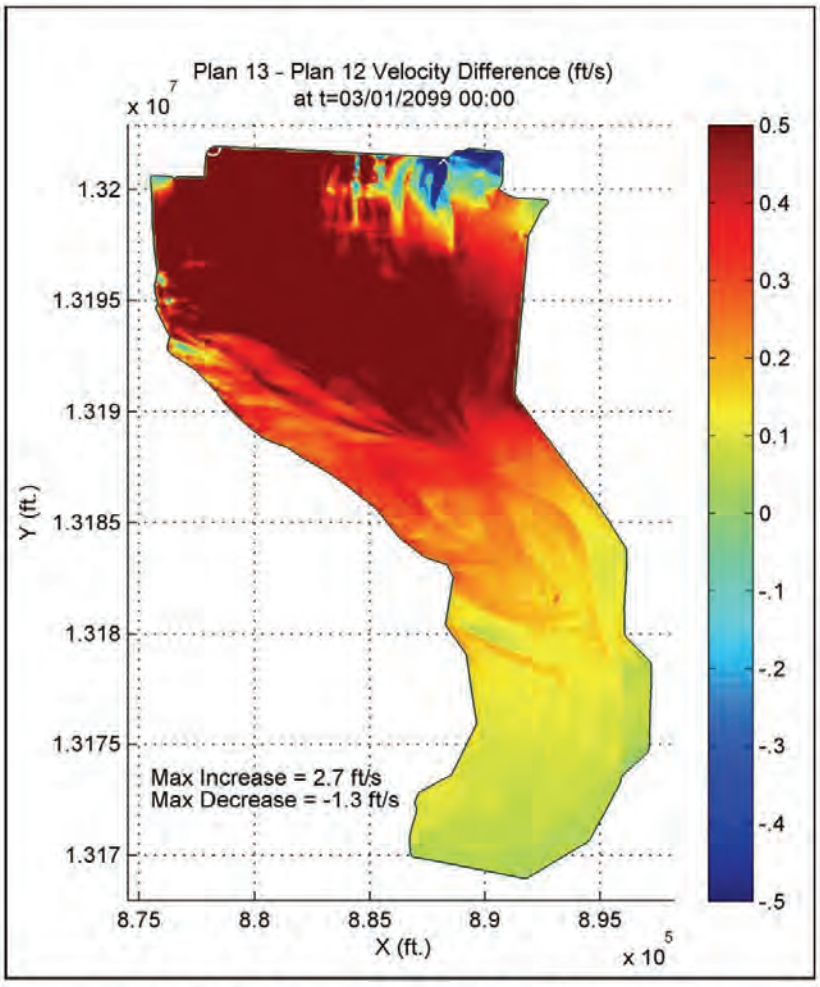


Figure A-54. Plan 13 Velocity Difference from Base Condition

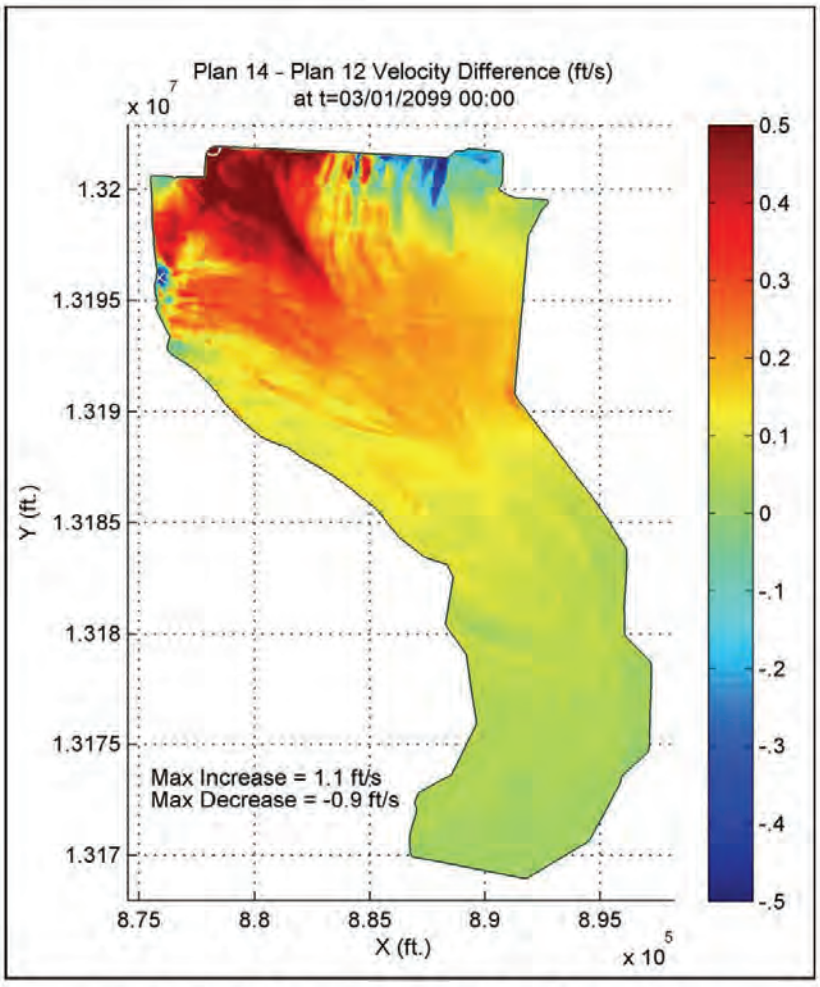


Figure A-55. Plan 14 Velocity Difference from Base Condition

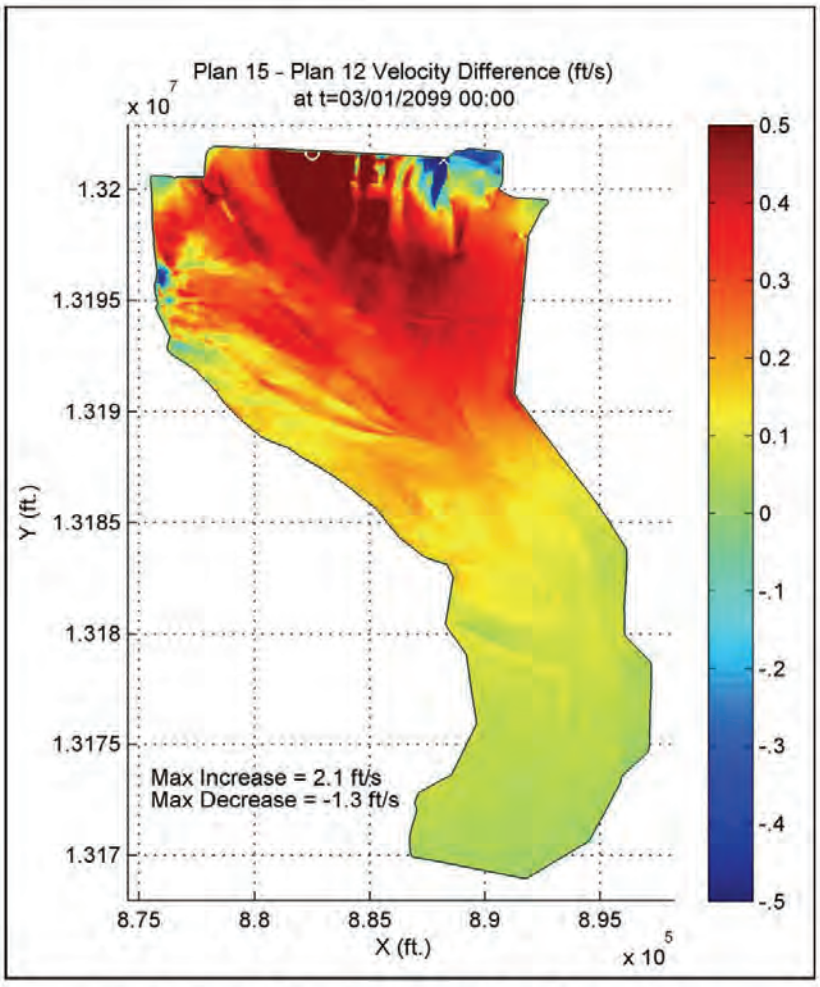


Figure A-56. Plan 15 Velocity Difference from Base Condition

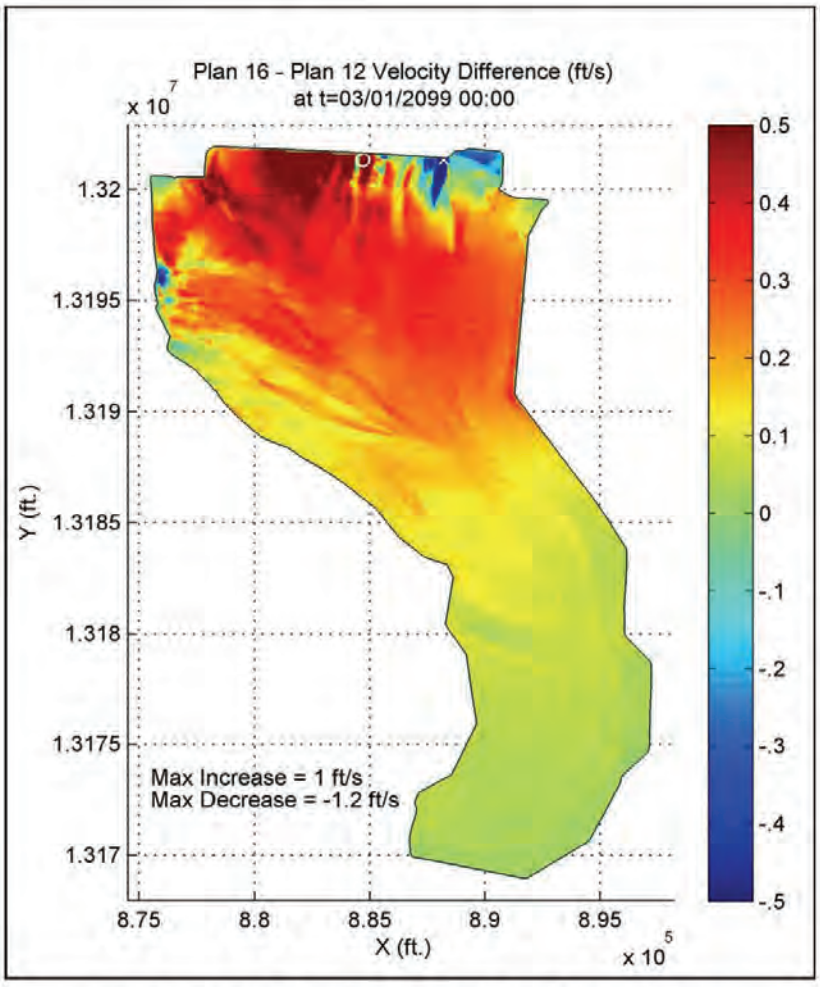


Figure A-57. Plan 16 Velocity Difference from Base Condition

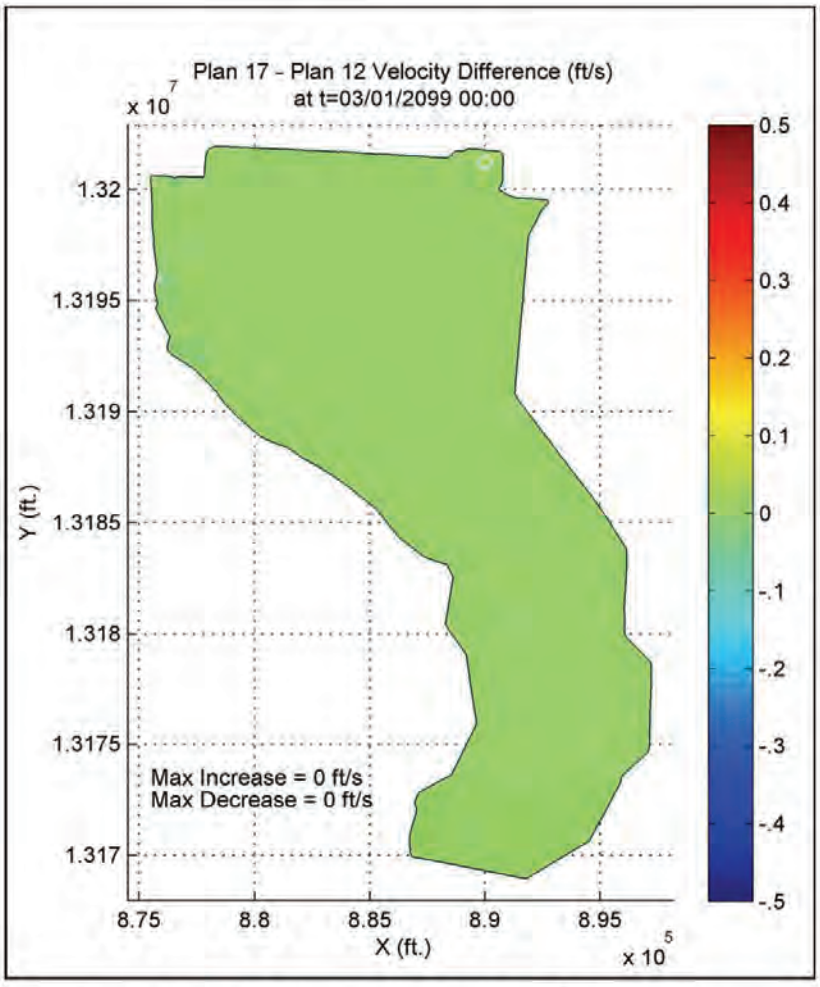


Figure A-58. Plan 17 Velocity Difference from Base Condition

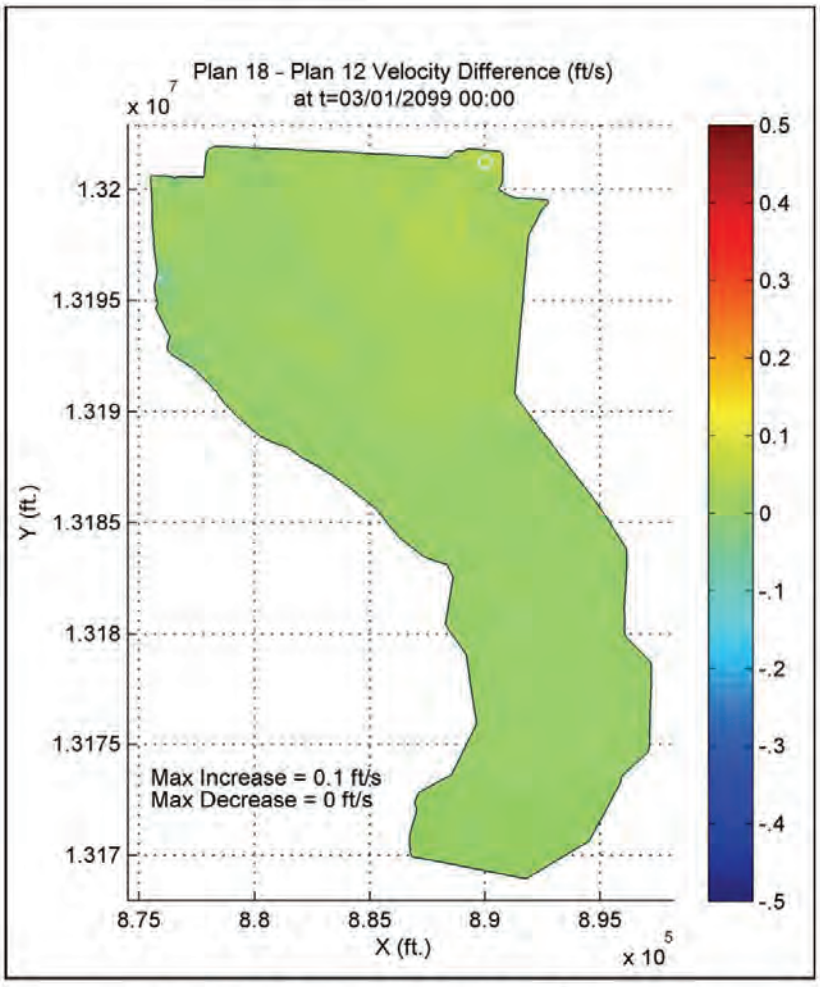


Figure A-59. Plan 18 Velocity Difference from Base Condition

A.9 2D Flow Area Shear Stress - Difference from Base Condition Plan

Figures located in A.9 depict the respective plan's shear stress difference from Plan 12 (Base Condition) in the 2D overbank region at simulation hour 648. The white "o" in the figure identifies the node location with the maximum increase for each figure respectively. The white "x" in the figure identifies the node location with the maximum decrease for each figure respectively.

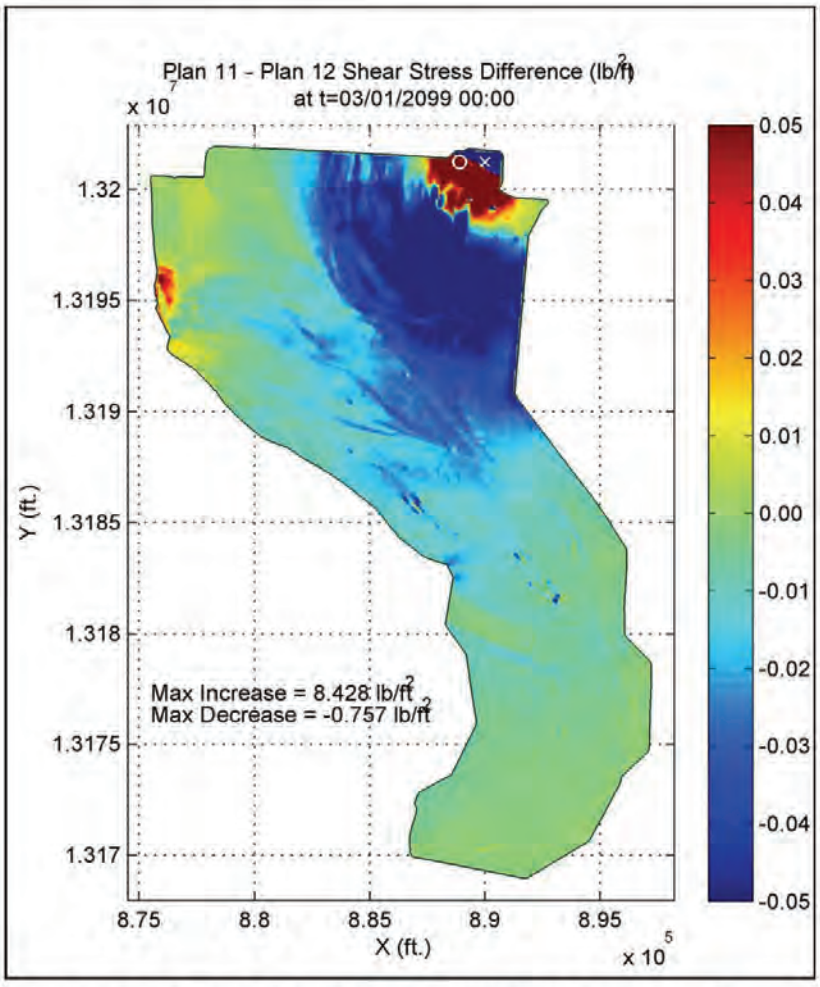


Figure A-60. Plan 11 Shear Stress Difference from Base Condition

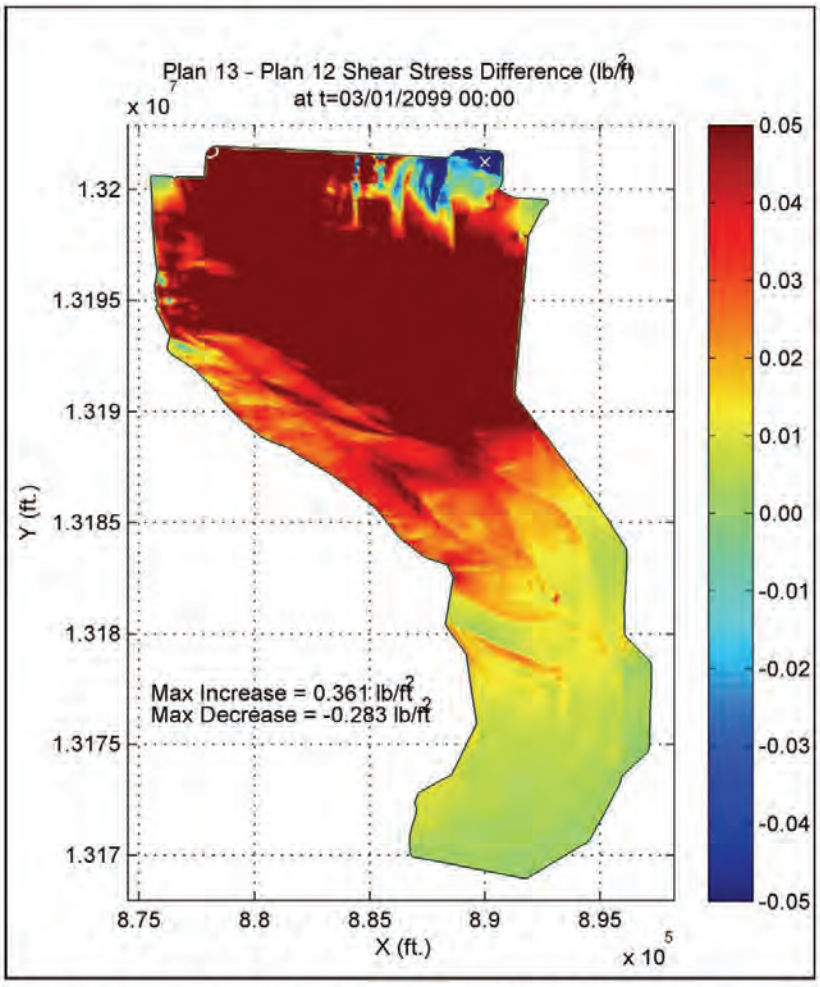


Figure A-61. Plan 13 Shear Stress Difference from Base Condition

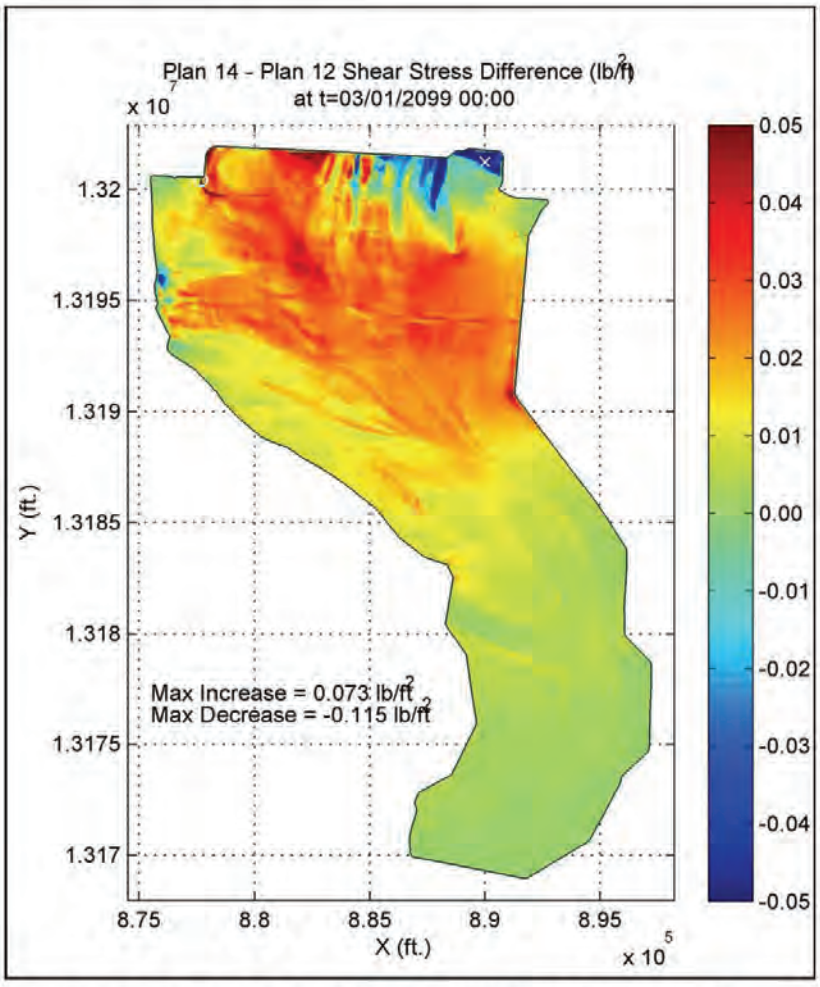


Figure A-62. Plan 14 Shear Stress Difference from Base Condition

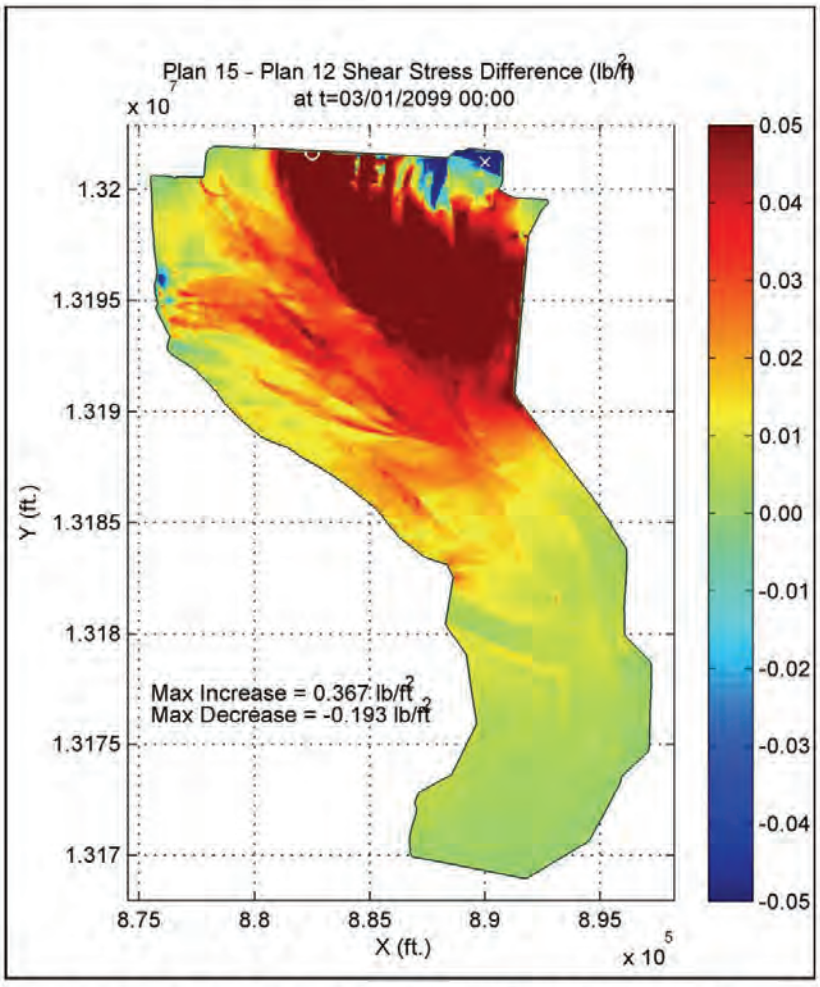


Figure A-63. Plan 15 Shear Stress Difference from Base Condition

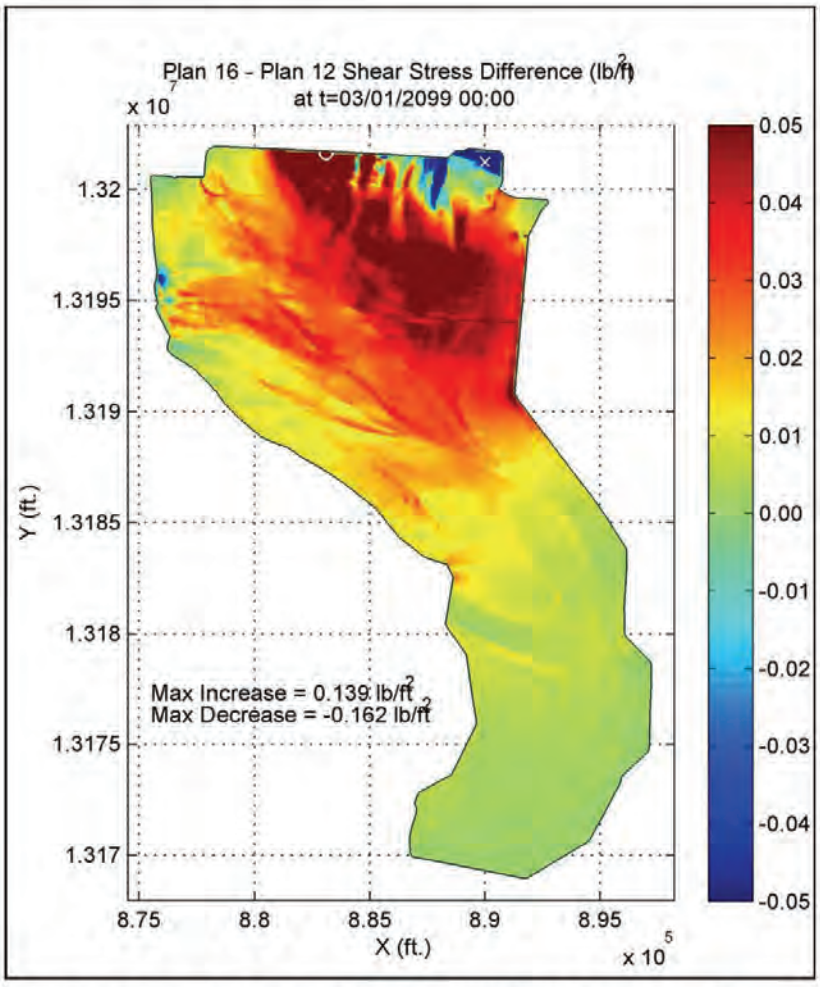


Figure A-64. Plan 16 Shear Stress Difference from Base Condition

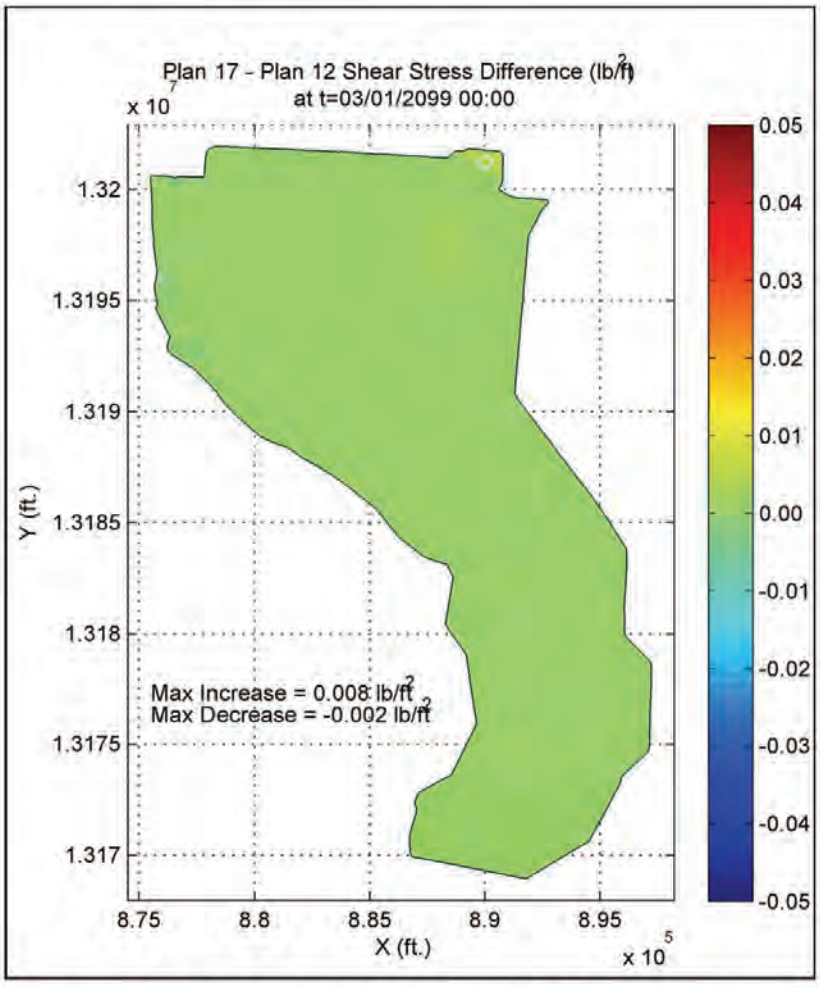


Figure A-65. Plan 17 Shear Stress Difference from Base Condition

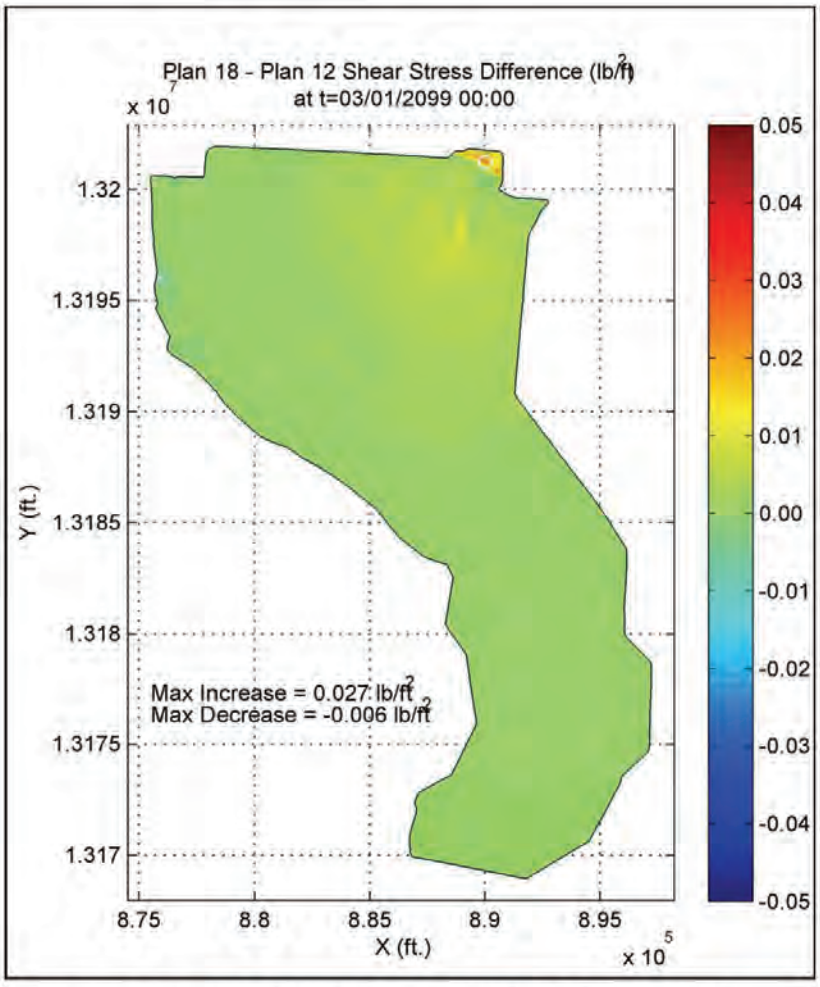


Figure A-66. Plan 18 Shear Stress Difference from Base Condition

A.10 2D Flow Area Time Series Data

The velocity and shear stress time series data at eight (8) 2D overbank node locations are presented in A.10. Figure A-67 indicates location and ID of the selected nodes. Velocity and shear stress values presented in the time series data are magnitude values. The critical shear stress force of a particular material is the unit shear stress force which will not cause erosion of the material on a horizontal surface. The critical shear stress force depicted in the shear stress time series data is for sandy loam soil (non-colloidal) and has a value of 0.0418 lb/ft^2 (Nalluri et al. 2009). Note that further field evaluation is needed to investigate overbank material type.

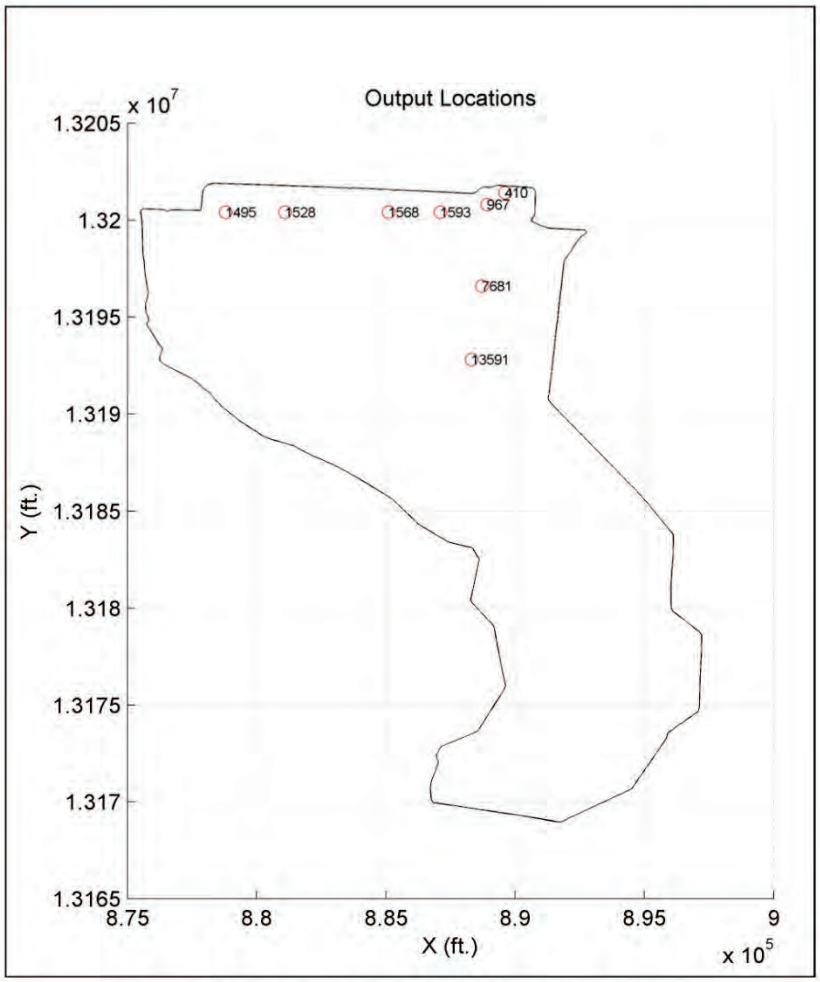


Figure A-67. Time Series Data Output Location Node Number

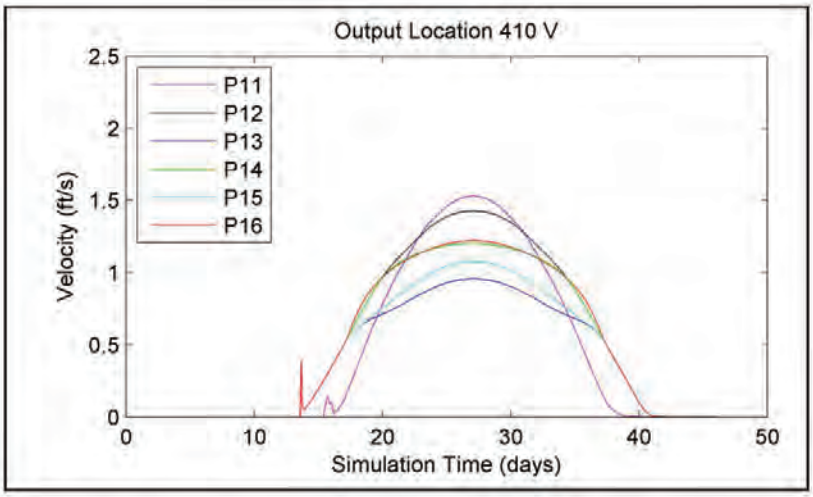


Figure A-68. Node 410 Velocity Time Series Data for P11-P16

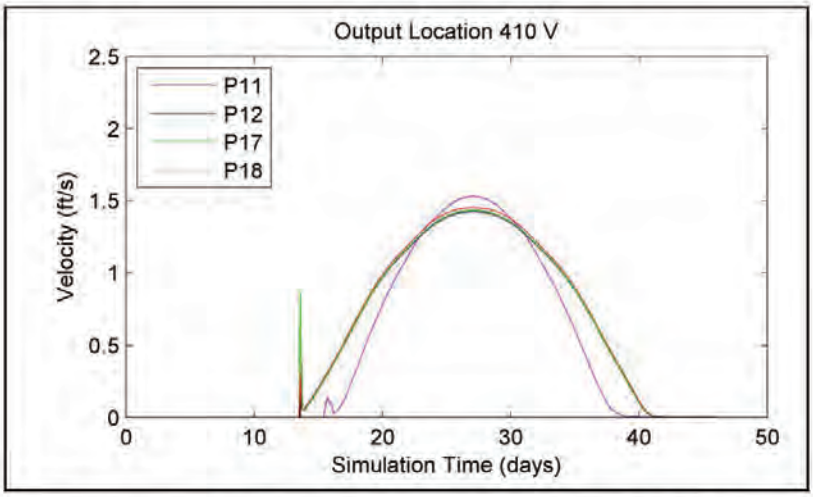


Figure A-69. Node 410 Velocity Time Series Data for P11,P12,P17,P18

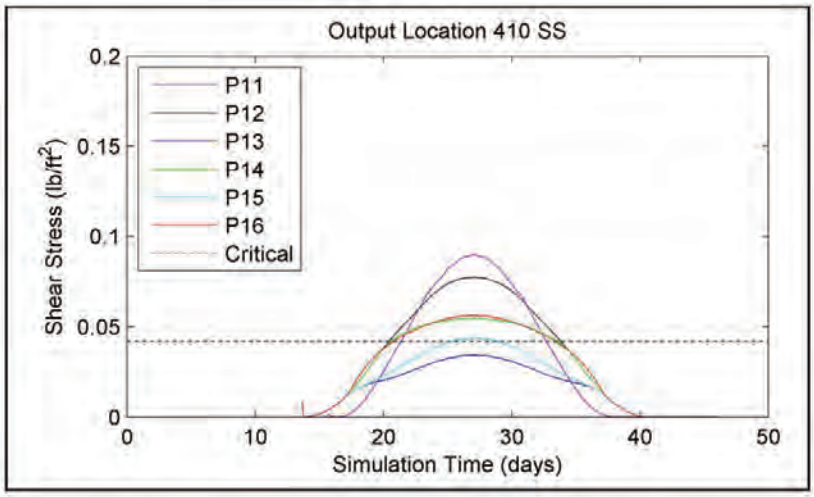


Figure A-70. Node 410 Shear Stress Time Series Data for P11-P16

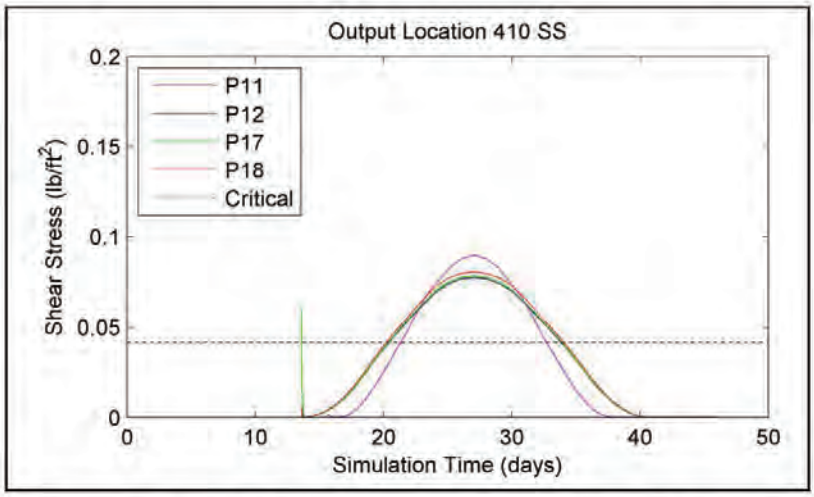


Figure A-71. Node 410 Shear Stress Time Series Data for P11,P12,P17,P18

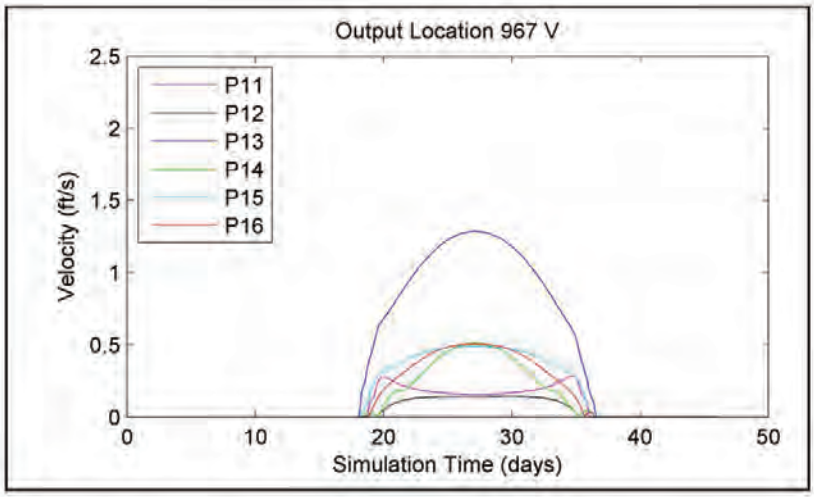


Figure A-72. Node 967 Velocity Time Series Data for P11-P16

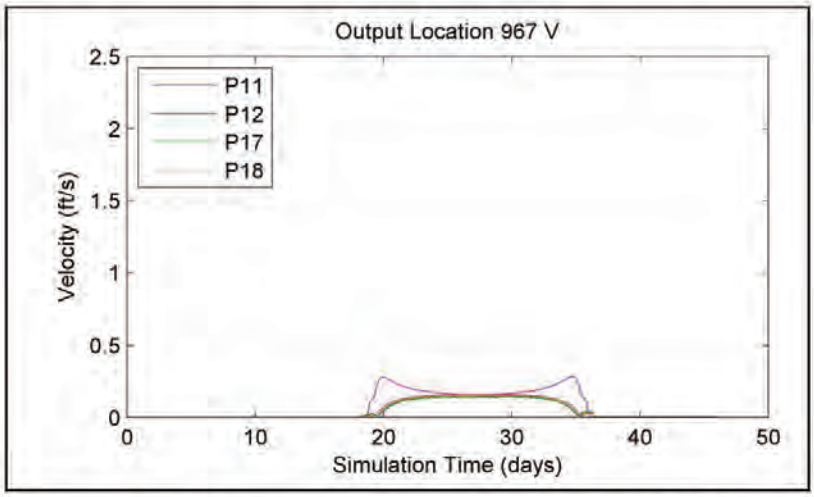


Figure A-73. Node 967 Velocity Time Series Data for P11,P12,P17,P18

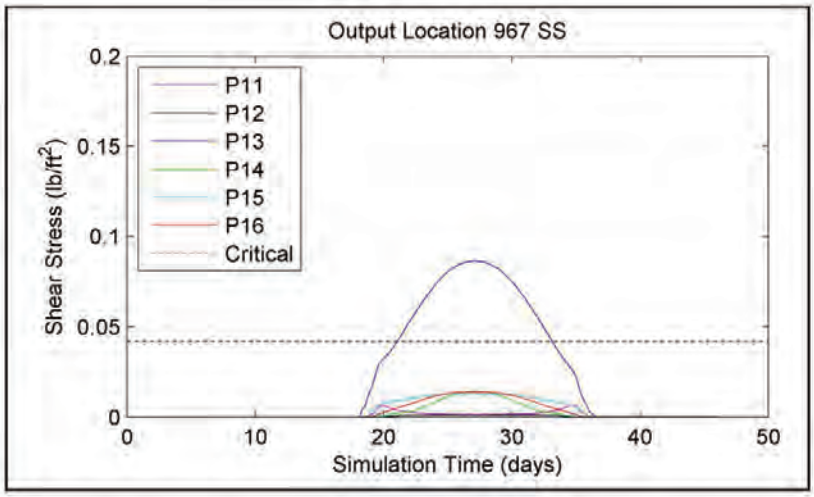


Figure A-74. Node 967 Shear Stress Time Series Data for P11-P16

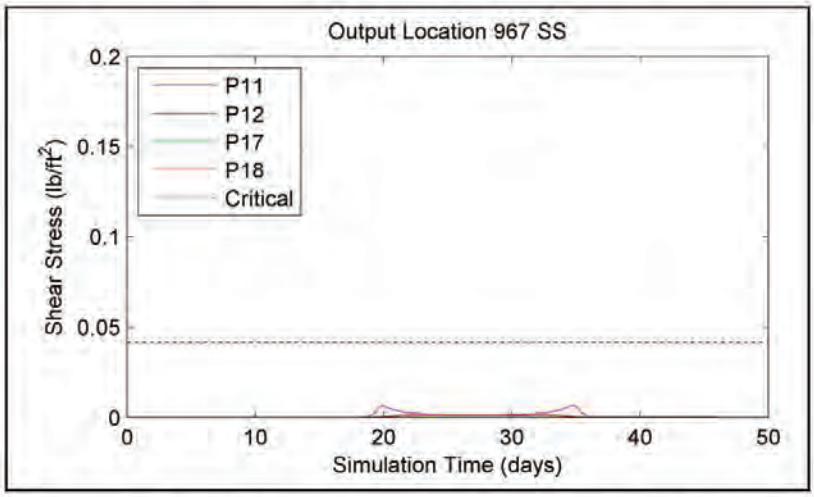


Figure A-75. Node 967 Shear Stress Time Series Data for P11,P12,P17,P18

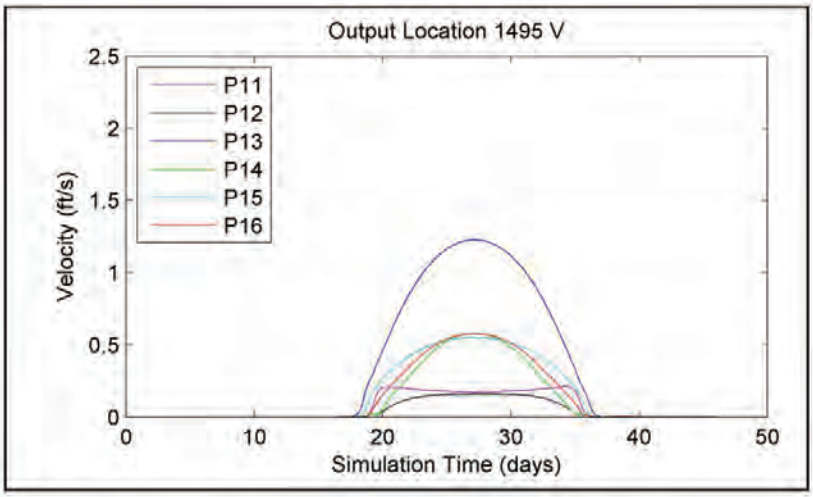


Figure A-76. Node 1495 Velocity Time Series Data for P11-P16

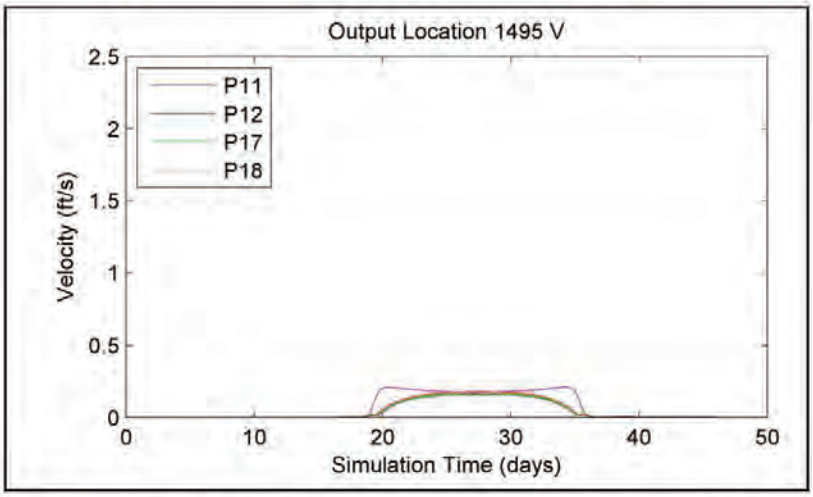


Figure A-77. Node 1495 Velocity Time Series Data for P11,P12,P17,P18

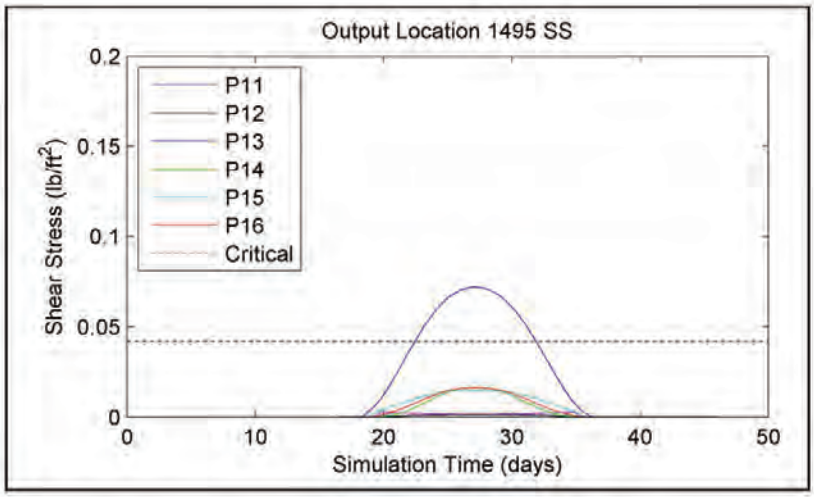


Figure A-78. Node 1495 Shear Stress Time Series Data for P11-P16

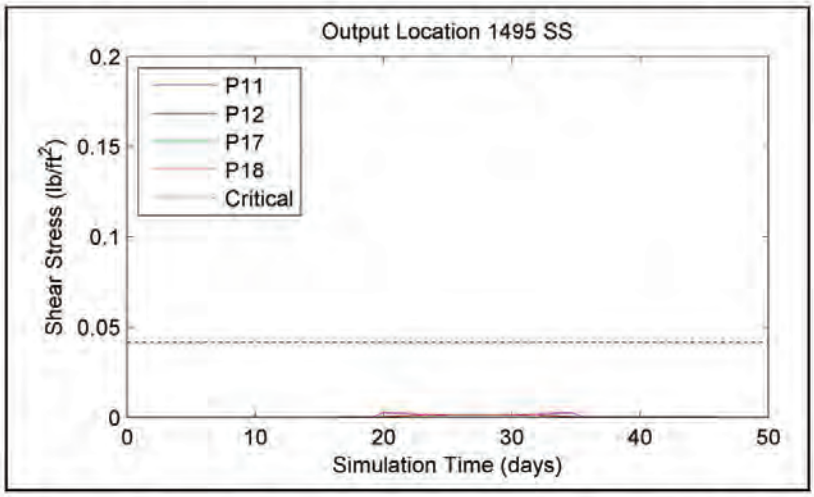


Figure A-79. Node 1495 Shear Stress Time Series Data for P11,P12,P17,P18

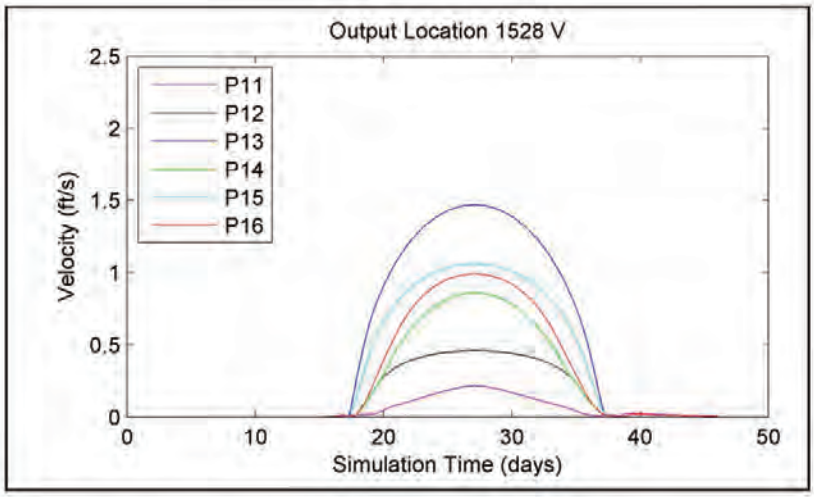


Figure A-80. Node 1528 Velocity Time Series Data for P11-P16

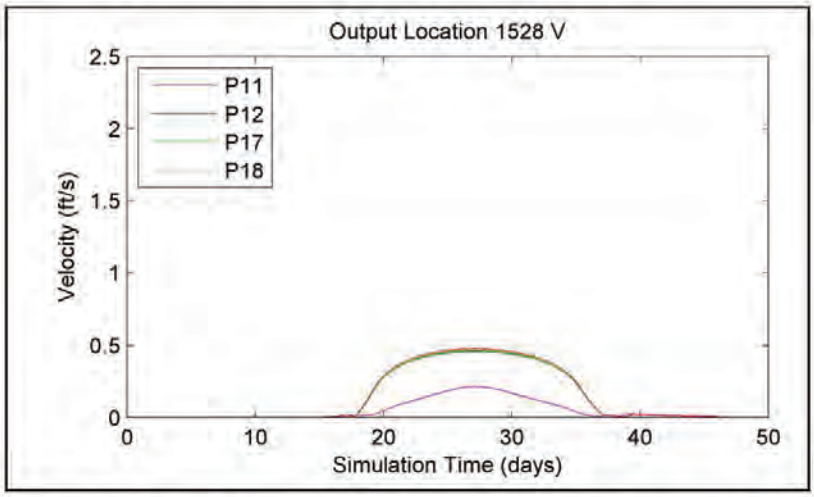


Figure A-81. Node 1528 Velocity Time Series Data for P11,P12,P17,P18

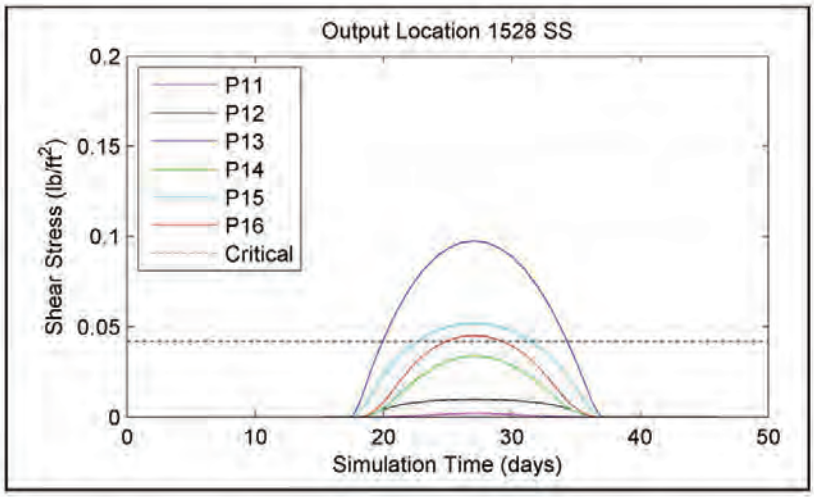


Figure A-82. Node 1528 Shear Stress Time Series Data for P11-P16

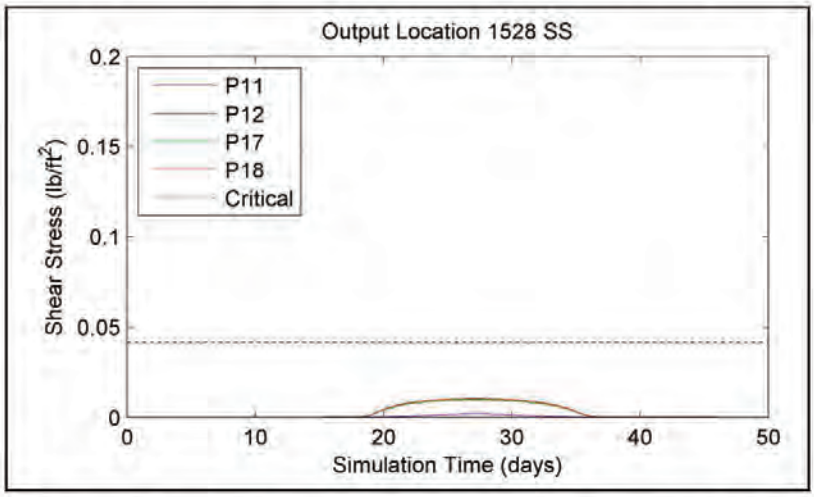


Figure A-83. Node 1528 Shear Stress Time Series Data for P11,P12,P17,P18

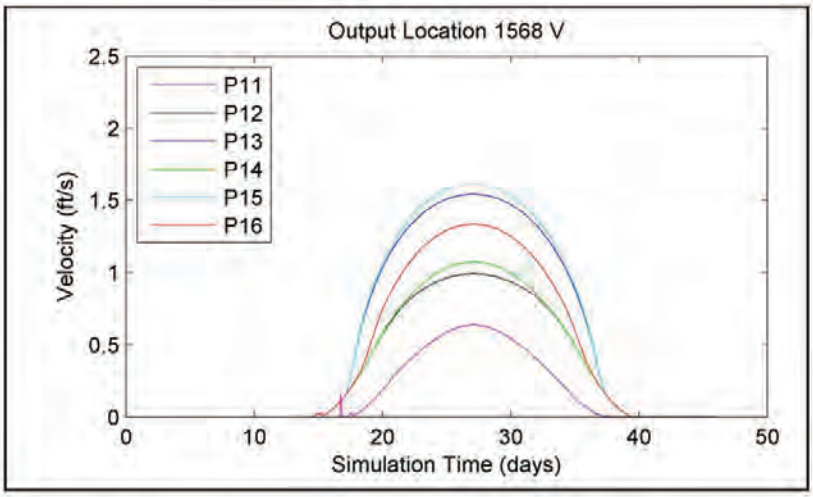


Figure A-84. Node 1568 Velocity Time Series Data for P11-P16

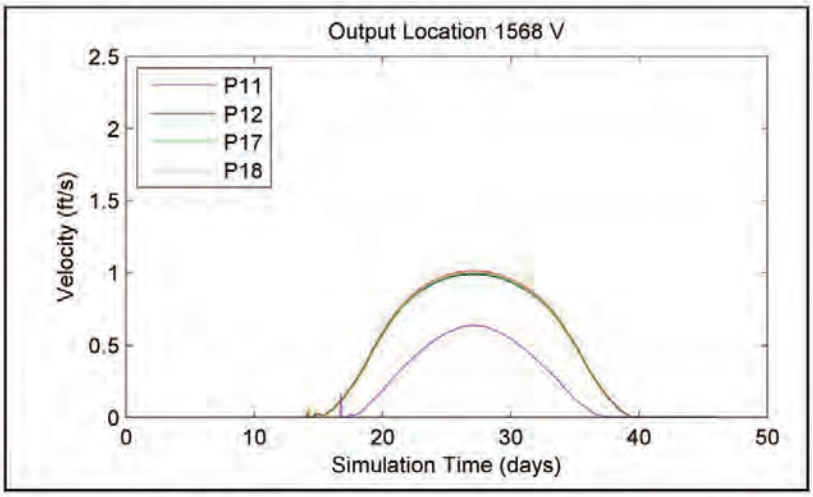


Figure A-85. Node 1568 Velocity Time Series Data for P11,P12,P17,P18

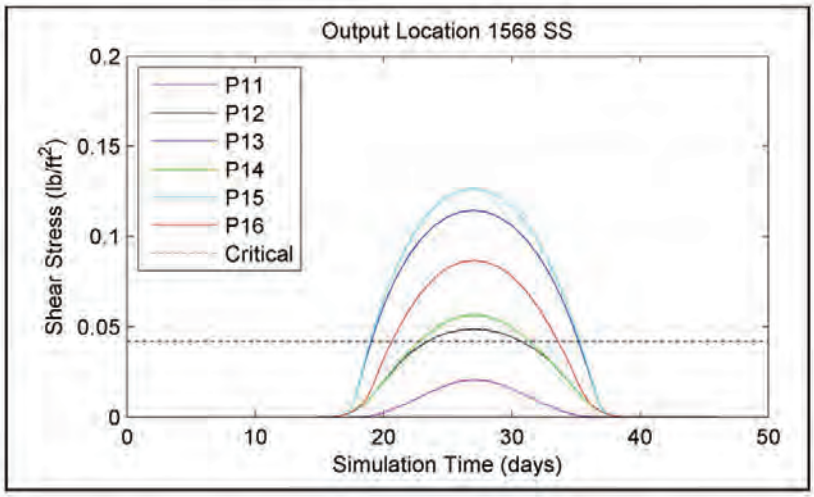


Figure A-86. Node 1568 Shear Stress Time Series Data for P11-P16

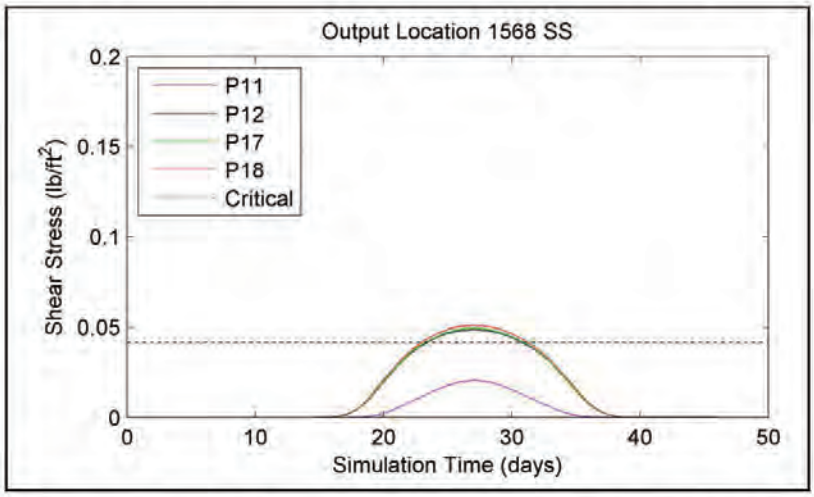


Figure A-87. Node 1568 Shear Stress Time Series Data for P11,P12,P17,P18

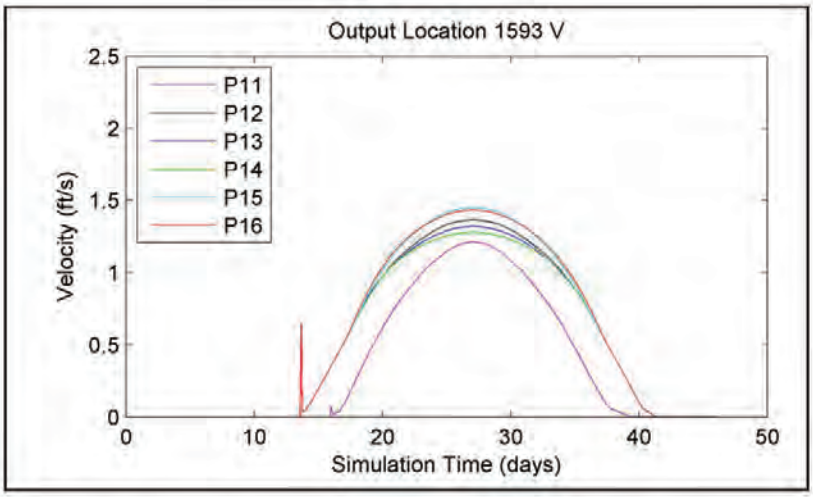


Figure A-88. Node 1593 Velocity Time Series Data for P11-P16

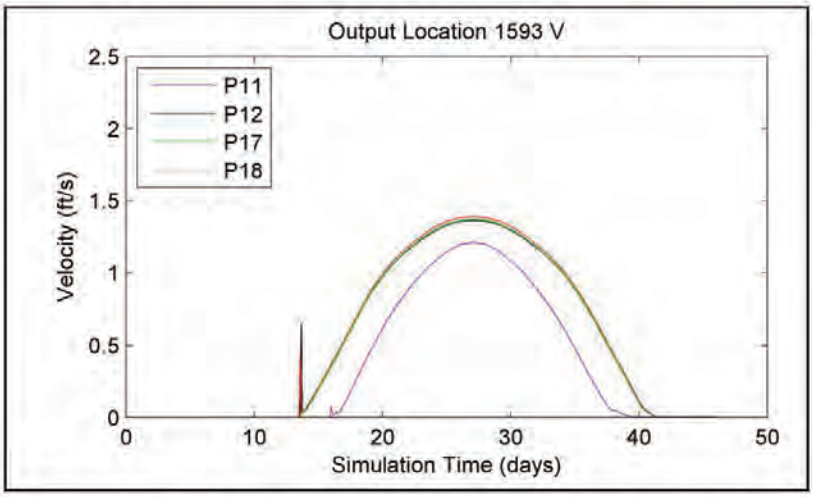


Figure A-89. Node 1593 Velocity Time Series Data for P11,P12,P17,P18

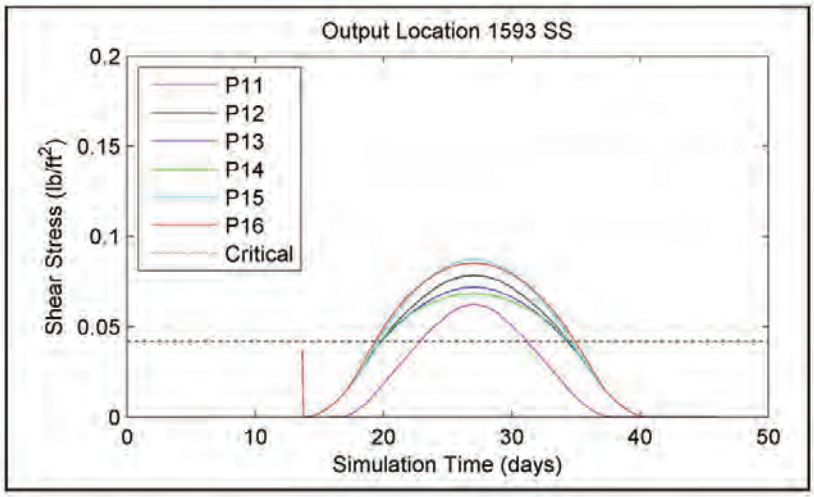


Figure A-90. Node 1593 Shear Stress Time Series Data for P11-P16

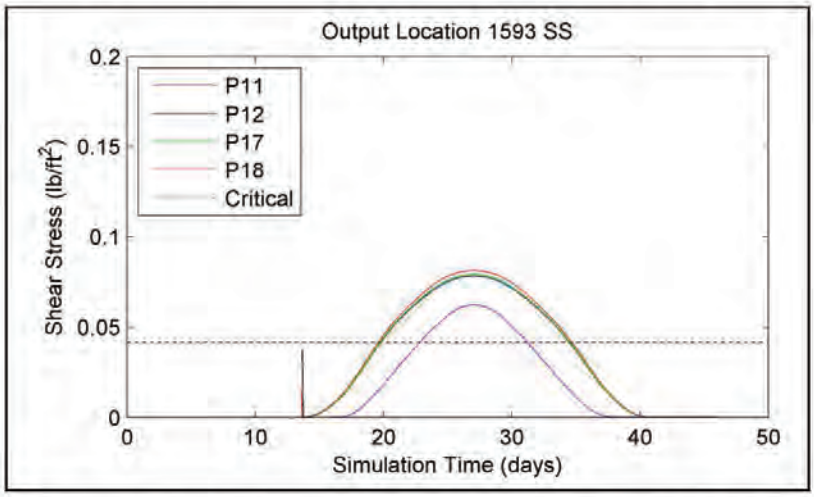


Figure A-91. Node 1593 Shear Stress Time Series Data for P11,P12,P17,P18

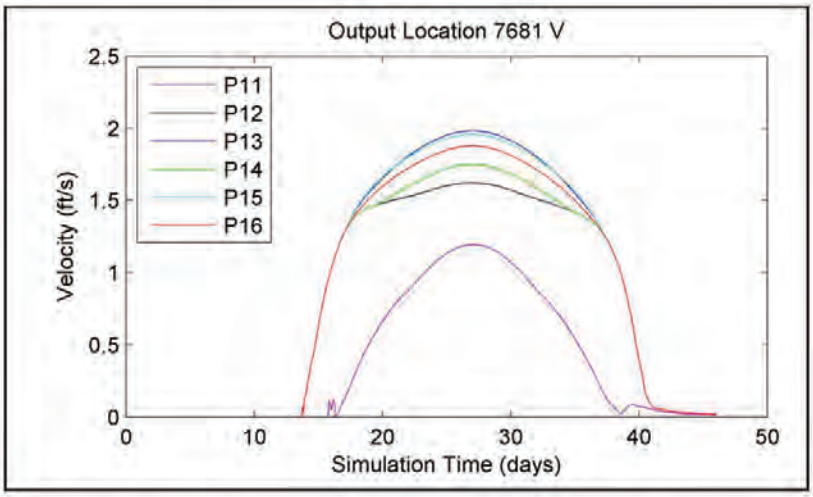


Figure A-92. Node 7681 Velocity Time Series Data for P11-P16

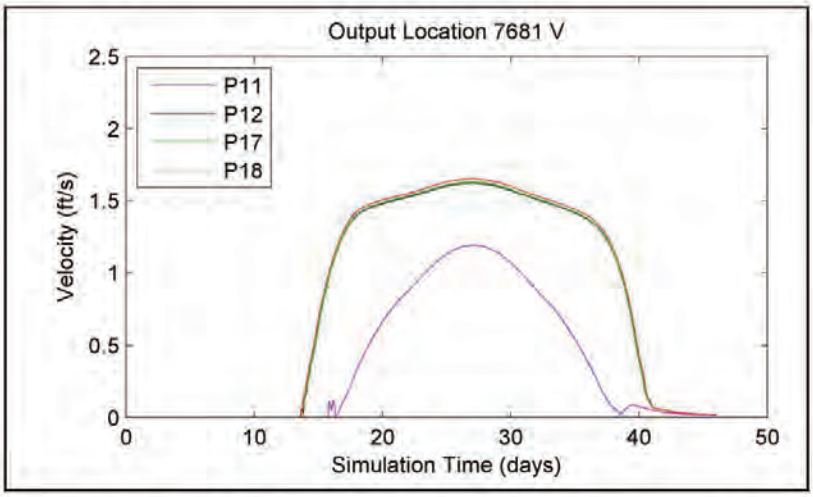


Figure A-93. Node 7681 Velocity Time Series Data for P11,P12,P17,P18

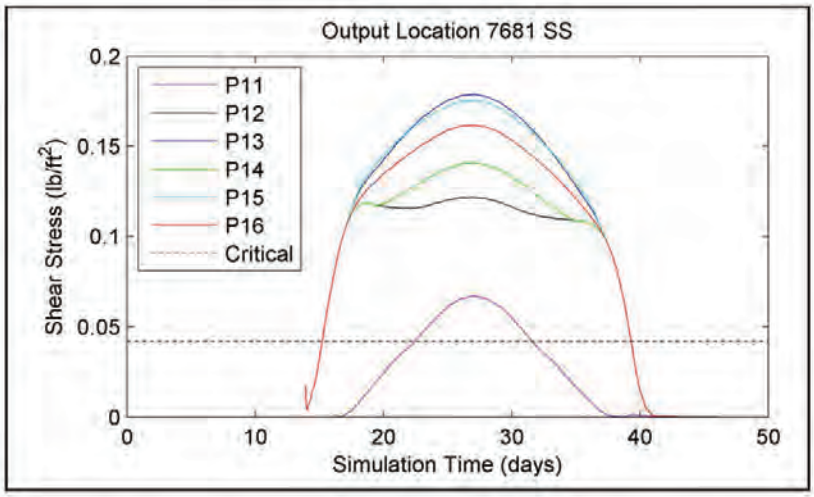


Figure A-94. Node 7681 Shear Stress Time Series Data for P11-P16

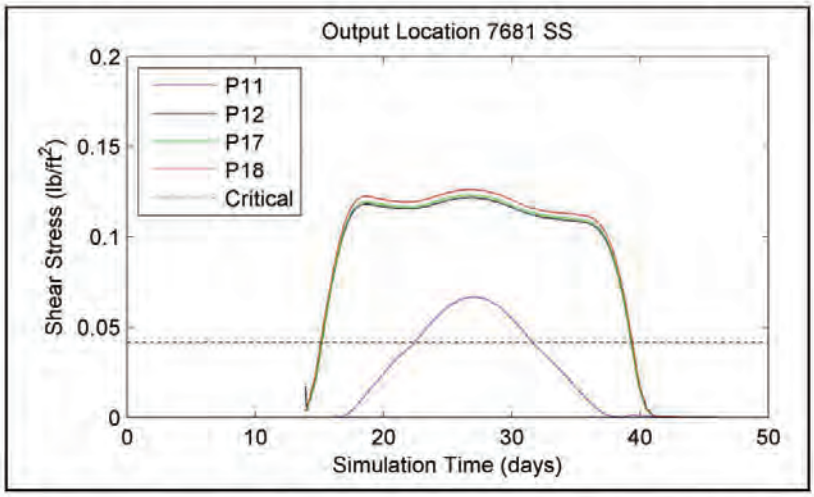


Figure A-95. Node 7681 Shear Stress Time Series Data for P11,P12,P17,P18

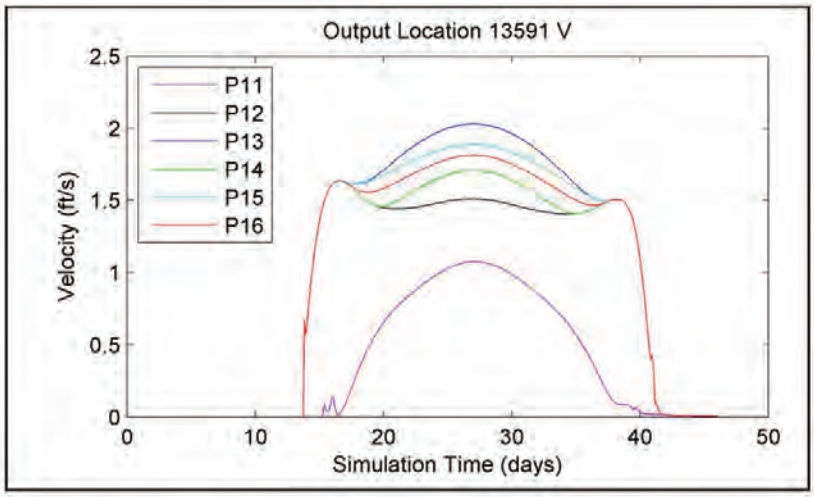


Figure A-96. Node 13591 Velocity Time Series Data for P11-P16

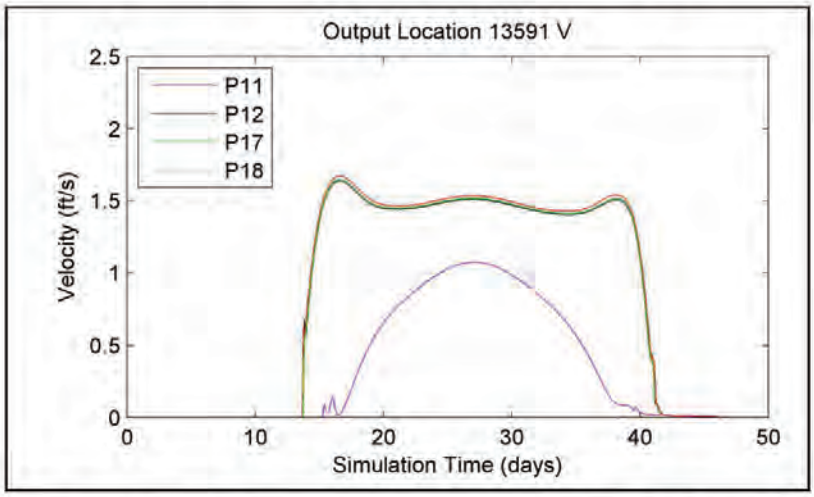


Figure A-97. Node 13591 Velocity Time Series Data for P11,P12,P17,P18

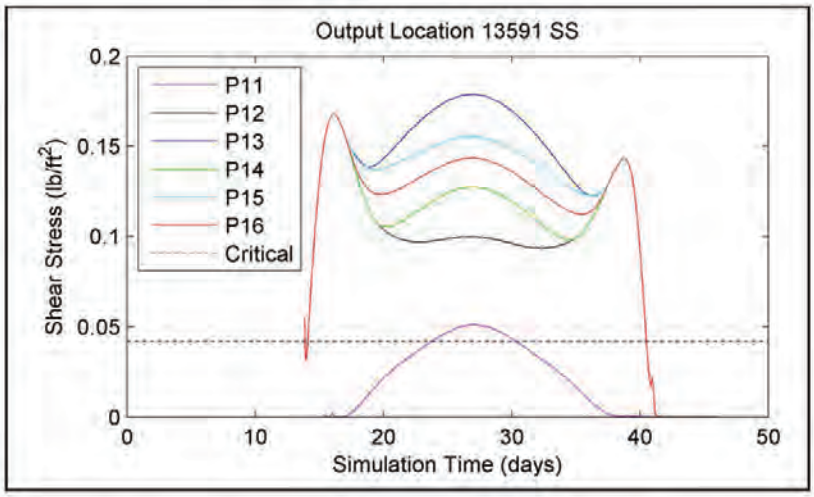


Figure A-98. Node 13591 Shear Stress Time Series Data for P11-P16

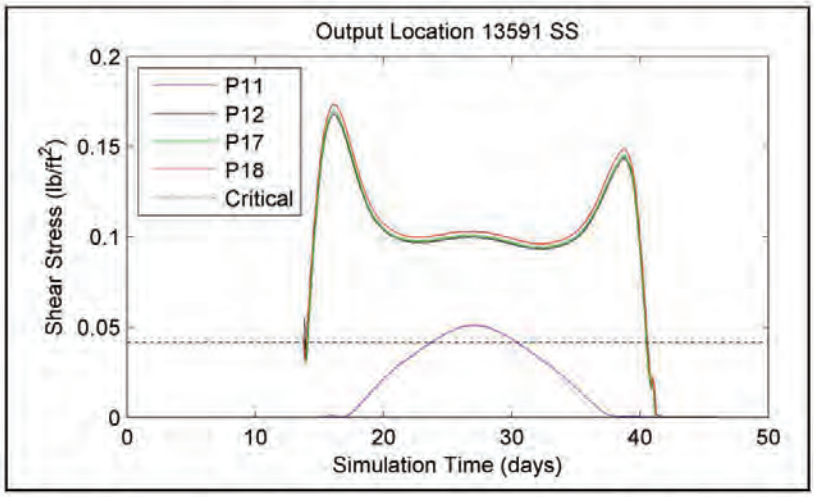


Figure A-99. Node 13591 Shear Stress Time Series Data for P11,P12,P17,P18

A.11 Sediment Transport Capacity

Figures located in A.11 depict the sediment transport capacity results computed utilizing the HEC-RAS Hydraulic Design Function. Results are presented for the Toffaleti Function and the Laursen (Copeland) Function.

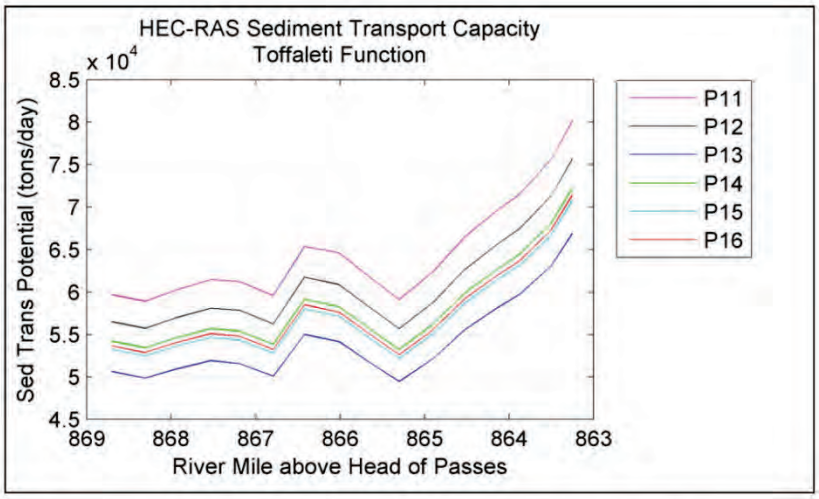


Figure A-100. Toffaleti Sediment Transport Capacity P11-P12

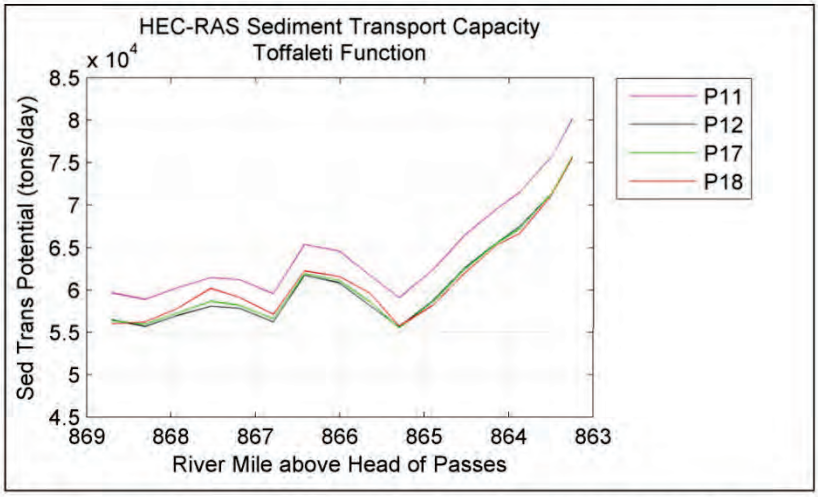


Figure A-101. Toffaleti Sediment Transport Capacity P11,P12,P17,P18

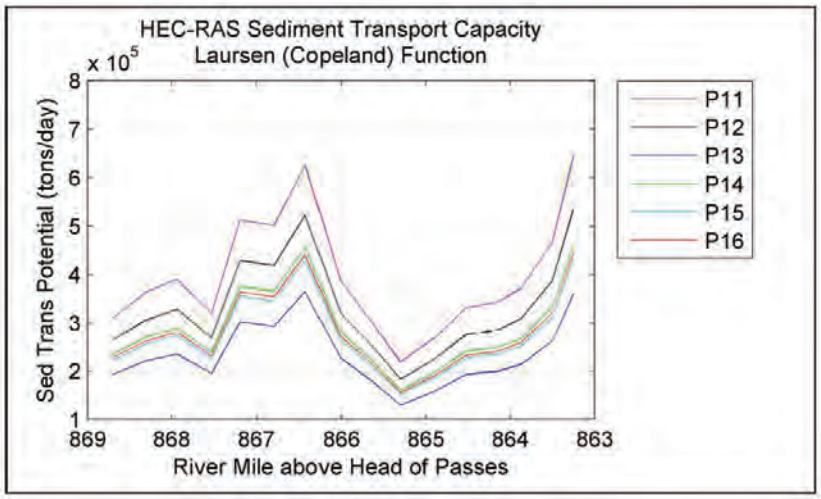


Figure A-102. Laursen-Copeland Sediment Transport Capacity P11-P12

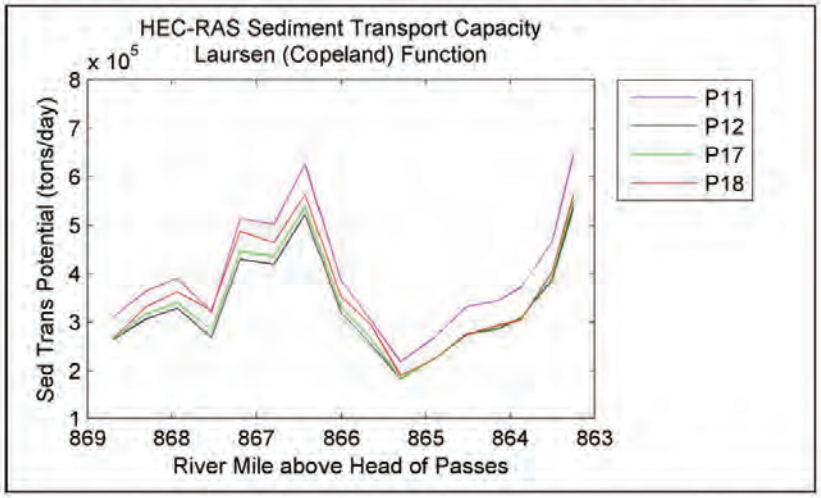


Figure A-103. Laursen-Copeland Sediment Transport Capacity P11,P12,P17,P18

A.12 Calibration of 2D Overbank Region

The 2D flow area was calibrated to the 8 May 2013 Acoustic Doppler Current Profilers (ADCP) survey that measured the flow velocity through the crevasse. The calibration was achieved by adjusting lateral structure weir coefficients and the 2D flow area Manning's n-value. Figures located in A.12 depict the calibration results to the 8 May 2013 ADCP velocity measurement. Figure A-104 displays the 8 May 2013 ADCP velocity measurements. Figure A-105 presents the 8 May 2013 calibrated model velocity. Note that Figure A-105 was created from an earlier version of the MATLAB script that processed the model output data. Note that the magenta line in Figure A-105 represents the model output transect line. The model output transect line compared modeled velocity to ADCP measured velocity. Figure A-106 displays the modeled velocity difference from the measured ADCP velocity. Figure A-107 presents the modeled velocity and ADCP velocity along the output transect line (referenced in Figure A-105). Figure A-108 displays the sensitivity analysis results conducted on the 2D flow area Manning's n-value and the lateral structure weir coefficients. The calibrated lateral structure weir coefficients and Manning's n-value were selected by the simulation having the lowest standard deviation with respect to the ADCP velocity measurement. A lateral structure weir coefficient of 0.6 and overbank Manning's n-value of 0.06 yielded the lowest standard deviation.

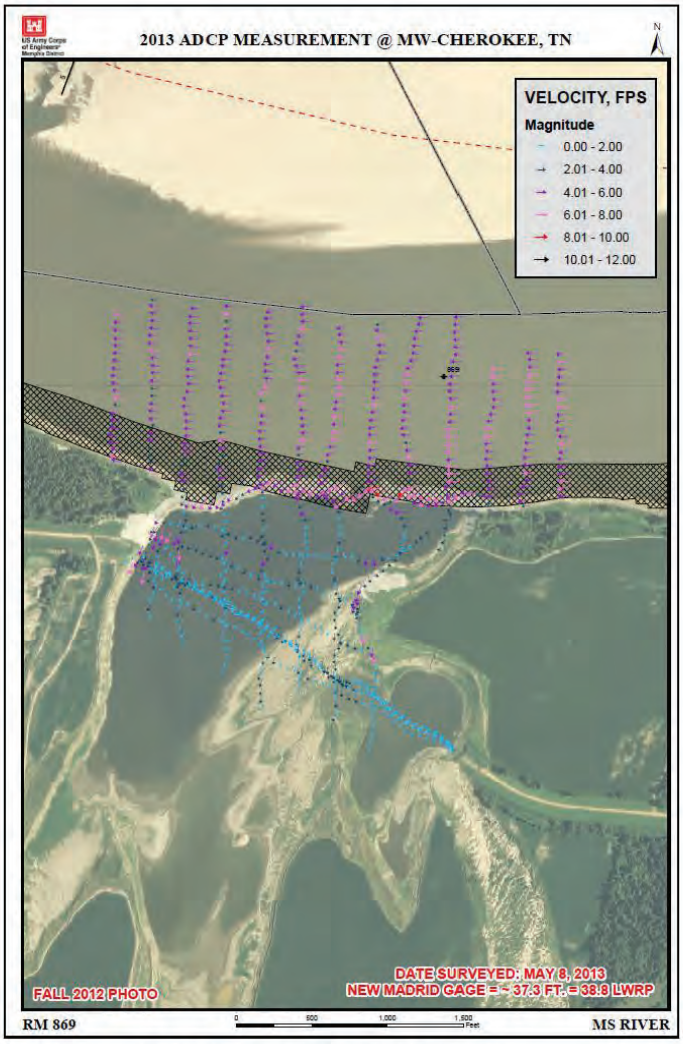


Figure A-104. 08 May 2013 ADCP Velocity Measurement

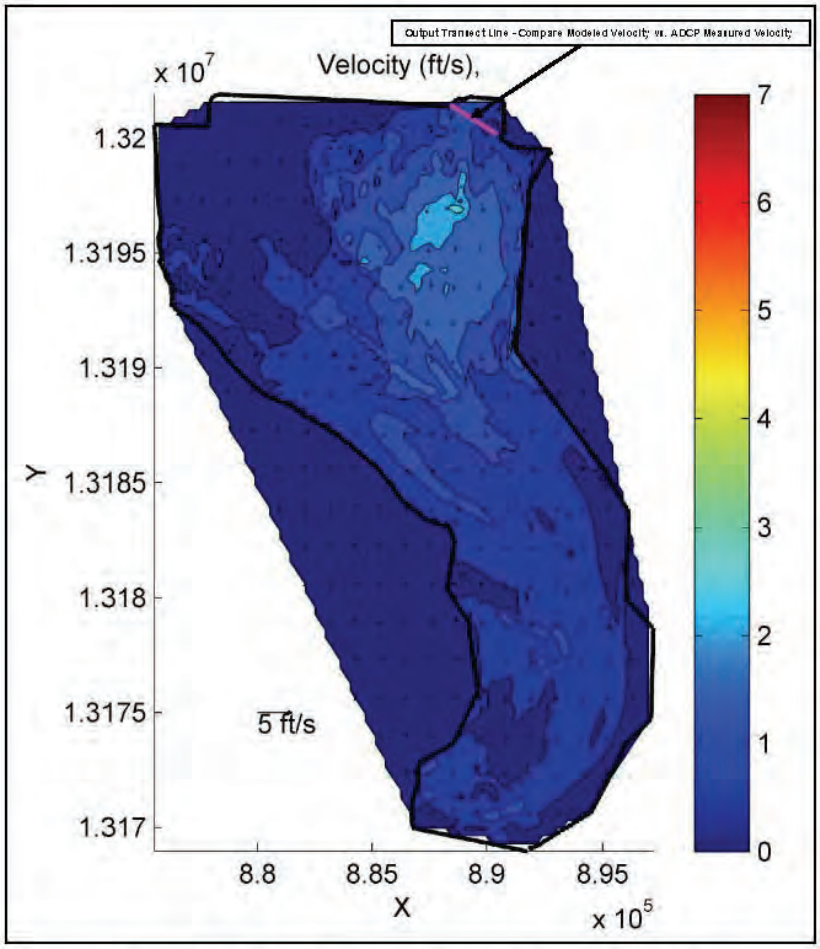


Figure A-105. Modeled Velocity Output - 8 May 2013 1200

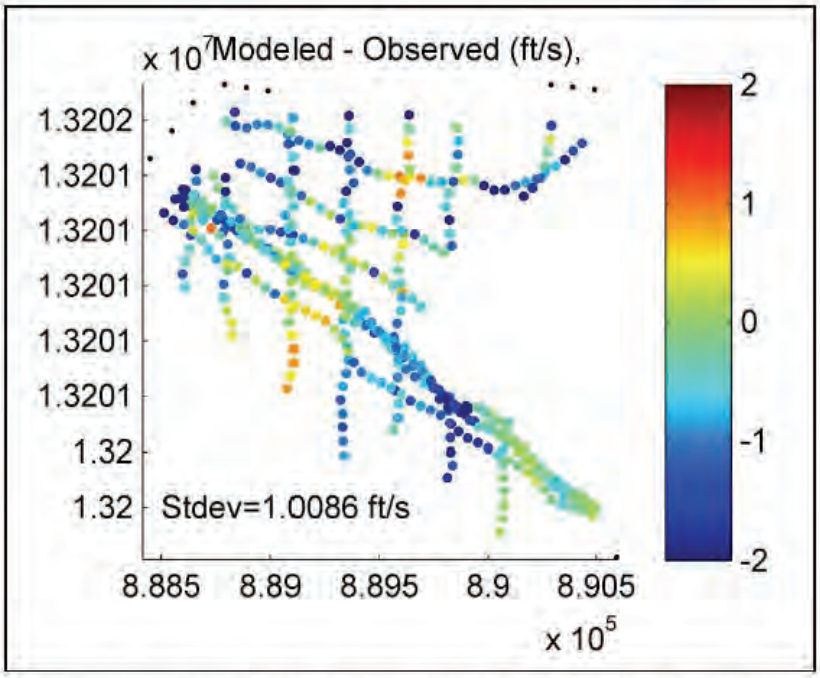


Figure A-106. Modeled Velocity Difference from ADCP Velocity - 8 May 2013 1200

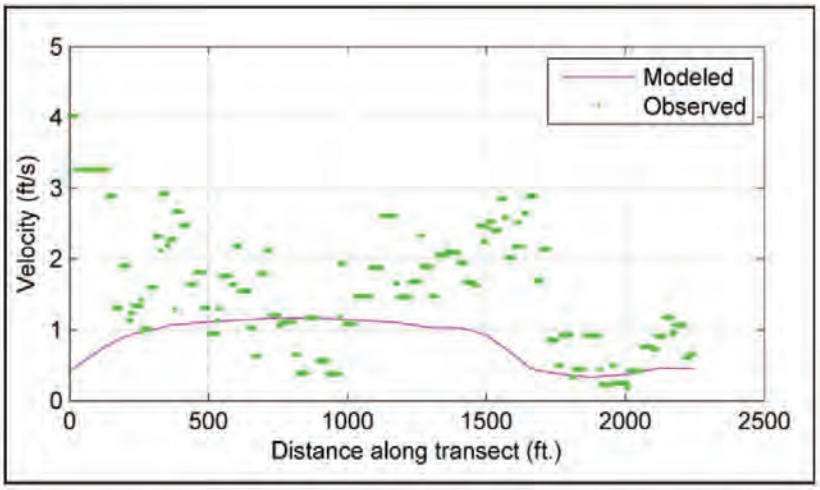


Figure A-107. Modeled vs. ADCP Velocity Along Transect - 8 May 2013 1200

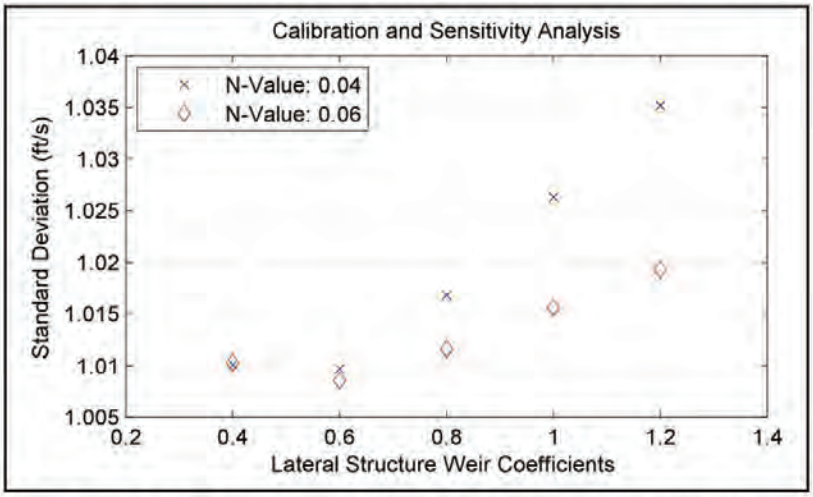


Figure A-108. Calibration and Sensitivity Analysis - 8 May 2013 1200

(this page intentionally blank)

Appendix B. CEERD-HF-RS MFR

Appendix B contains the Memorandum for Record (MFR) Subject: Merriwether-Cherokee Potamology Study from the River Engineering Branch of USACE ERDC Coastal & Hydraulics Laboratory.

CEERD-HFR-S 14 February 2014

Memorandum for Record

Subject: Merriwether-Cherokee Potamology Study

1. During the Mississippi River Flood of 2011, the Sheeps Ridge Road Spur Levee overtopped and crevassed near river mile 869. The crevasse generated significant erosion over more than 140 acres of the floodplain, extending approximately 4,000 feet from the left descending bank of the Mississippi River into Island 13 at depths up to 80 feet below the previous ground elevation. Flow over the left bank of the Mississippi River damaged but did not erode completely through the Merriwether-Cherokee Revetment along the outside of Merriwether Bend. Subsequent deposition of scoured soil and river borne sediments generated sand splays extending two to three miles downstream over Island 13. The Potamology study will assess: (1) the potential for additional overbank scour and cutoff formation, (2) the effects of completed repairs and further alternatives on long-term reach behavior, including diversion-induced sediment deposition in the Mississippi River, and (3) potential impacts to the Tiptonville-Obion Levee (mainline levee) and navigation. Formation of a cutoff along the path of the longest splay would shorten the river by approximately 6 miles.

2. Repairs to date include reconstruction of approximately 2,700 feet of Mississippi River bankline, construction of 1,600 feet of riprap baffle landward of the restored bankline, and placement of dredge fill between the bank and the baffle. On-going and planned repairs include stabilization of the dredge fill with riprap overlaid by a clay blanket that will be planted with trees and placement of articulated concrete mattress along the restored bank. These repairs would allow overflow through the spur levee breech whenever the river exceeds flood stage.

3. The two-dimensional (2D), depth-averaged Adaptive Hydraulics (AdH) program is the Hydraulics, Hydrology, & Coastal Community of Practice preferred software option for 2D numerical hydraulic and sedimentation modeling. AdH has been used to evaluate complex floodplain hydraulics in the Arkansas-White River Cutoff area and the sedimentation impacts of existing and proposed diversions on the Lower Mississippi River. AdH is an appropriate tool for evaluation of short-term hydraulic and sedimentation issues at this site and is recommended for this purpose. Evaluation of long-term (years to decades) sedimentation in the Mississippi River would require usage of a one-dimensional (1D) sedimentation model, such as the MVD HEC-6T regional model, with input from the 2D model.

Page 1 of 3

4. An Adh model can be used to estimate the depth and velocity of flows through the existing spur levee breech, across the floodplain and back into the Mississippi River via sloughs and drainage canals. The computed hydraulics will help identify regions of flow concentration that have greater potential for erosion and head-cut formation. The model will account for super-elevation of the water surface in Merriwether Bend, which may have a significant influence on discharge through the breech. Modeling of proposed alternatives, such as partial removal of the remaining spur levee, will allow assessment of impacts on the flow and sedimentation in both the river and the floodplain.

5. AdH will provide estimates of sediment deposition rates and the longitudinal and lateral distribution of deposits in the Mississippi River downstream of the breech. Typically, the AdH sedimentation model would be used to simulate a period ranging from a single flood hydrograph to a few years. Longer sedimentation simulations will require a 1D model. AdH can provide estimates of the sediment diversion coefficients required by 1D sedimentation models to describe sediment diversions. The 2D AdH model incorporates pseudo-three-dimensional (3D) sedimentation process descriptions that compute sediment diversion coefficient estimates for bed material that compare favorably with 3D models. In contrast, analytical estimates based on Rouse profile predictions typically underestimate the amount of sediment diverted at sites along the Lower Mississippi River.

6. The initial formation of the crevasse and the associated scour include non-hydrostatic, 3D flow and local scour processes that are not fully described by current models. Thus, attempts to validate a model to observed volumes of floodplain erosion and deposition are unlikely to be fully successful. Therefore, the modeling approach for this project should focus on analysis of existing (post-repair) conditions and comparisons to proposed alternatives. Modeling of a pre-formed levee breech would avoid most of the non-hydrostatic processes and may provide some useful insights into formation of the scour hole and subsequent deposition but should be a secondary objective.

7. While the AdH model can be developed from existing datasets and boundary conditions supplied by 1D hydraulic and sedimentation models, field data should be obtained, as opportunities arise, to confirm or adjust model coefficients. Useful field data would include:

   a. ADCP measurements to confirm estimates of discharge through the repaired breech and distribution of flow within the channel and between the channel and the floodplain throughout the study area.

Page 2 of 3

b. water surface profiles through the study area for a wide range of flows, and

c. measurements of suspended- and bed-load.

Because sediment loads are highly variable, reasonable model estimates of sediment transport rates can vary significantly from individual measurements. ADCP back-scatter data can be correlated to suspended load and would provide insight into lateral variations in sediment concentration. This type of information may be particularly useful for model adjustment and circumstantiation in the vicinity of the breech.

8. Specific recommendations regarding data requirements, model limits and selection of initial and boundary conditions for an AdH model were discussed with the Memphis District's Hydraulics and Hydrology staff during the week 6 Jan 2014. A statement of work to provide technical assistance with development of a 2D hydraulic and sedimentation model for the Merriwether-Cherokee Potamology Study has been prepared and was forwarded to the Memphis District on 30 Jan 2014.

HEATH.RONALD.E.1232240209

Digitally signed by HEATH.RONALD.E.1232240209
DN: c=US, o=U.S. Government, ou=DoD, ou=PKI, ou=USA, cn=HEATH.RONALD.E.1232240209
Date: 2014.02.14 12:55:15 -06'00'

Ronald E. Heath
Research Hydraulic Engineer
River Engineering Branch

End of Report

Appendix B: Volumetric Analysis

Appendix B contains data from the volumetric analysis.

Figures B-1 through B-18 depict the spatial plots of the dataset surface comparisons. The dataset surface comparison depicts bed elevation change (feet). Tables B-1 through B-9 lists the tabular output from the dataset surface comparisons.

Figure B-1. Surface difference comparison from 1989 dataset to 1994 dataset (RM 840-860).

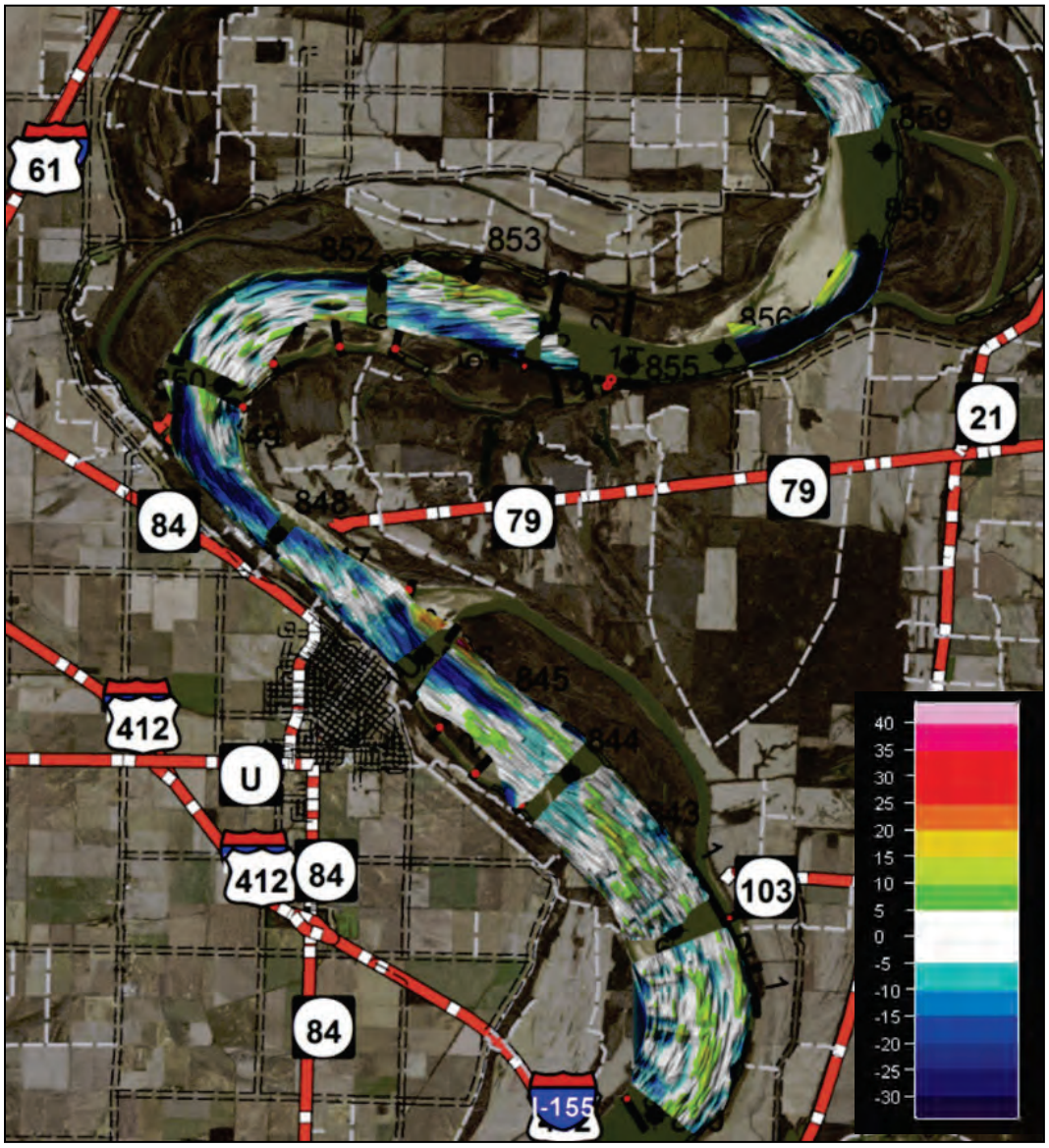


Figure B-2. Surface difference comparison from 1989 dataset to 1994 dataset (RM 860-878).

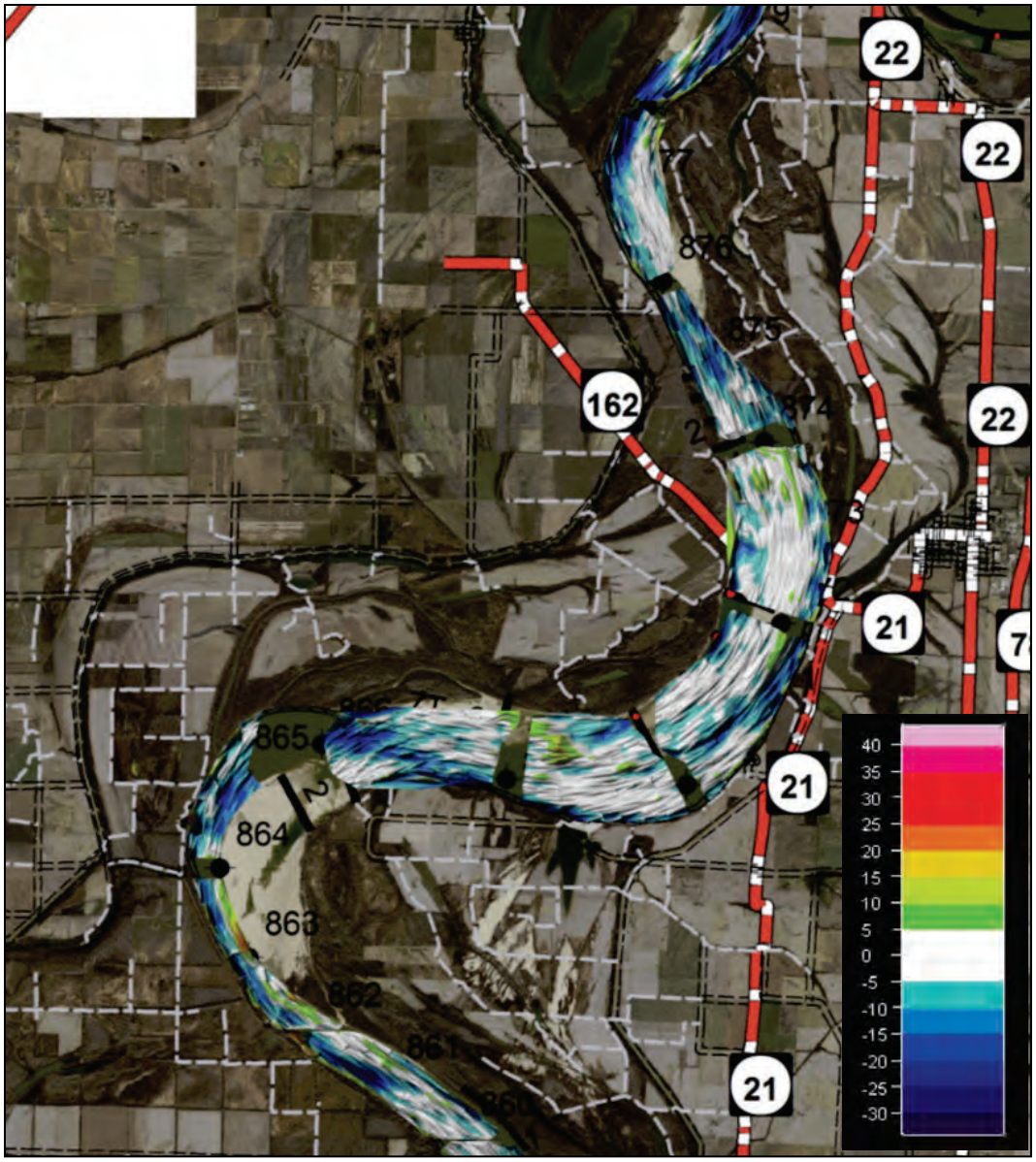


Figure B-3. Surface difference comparison from 1989 dataset to 1994 dataset (RM 878-888).

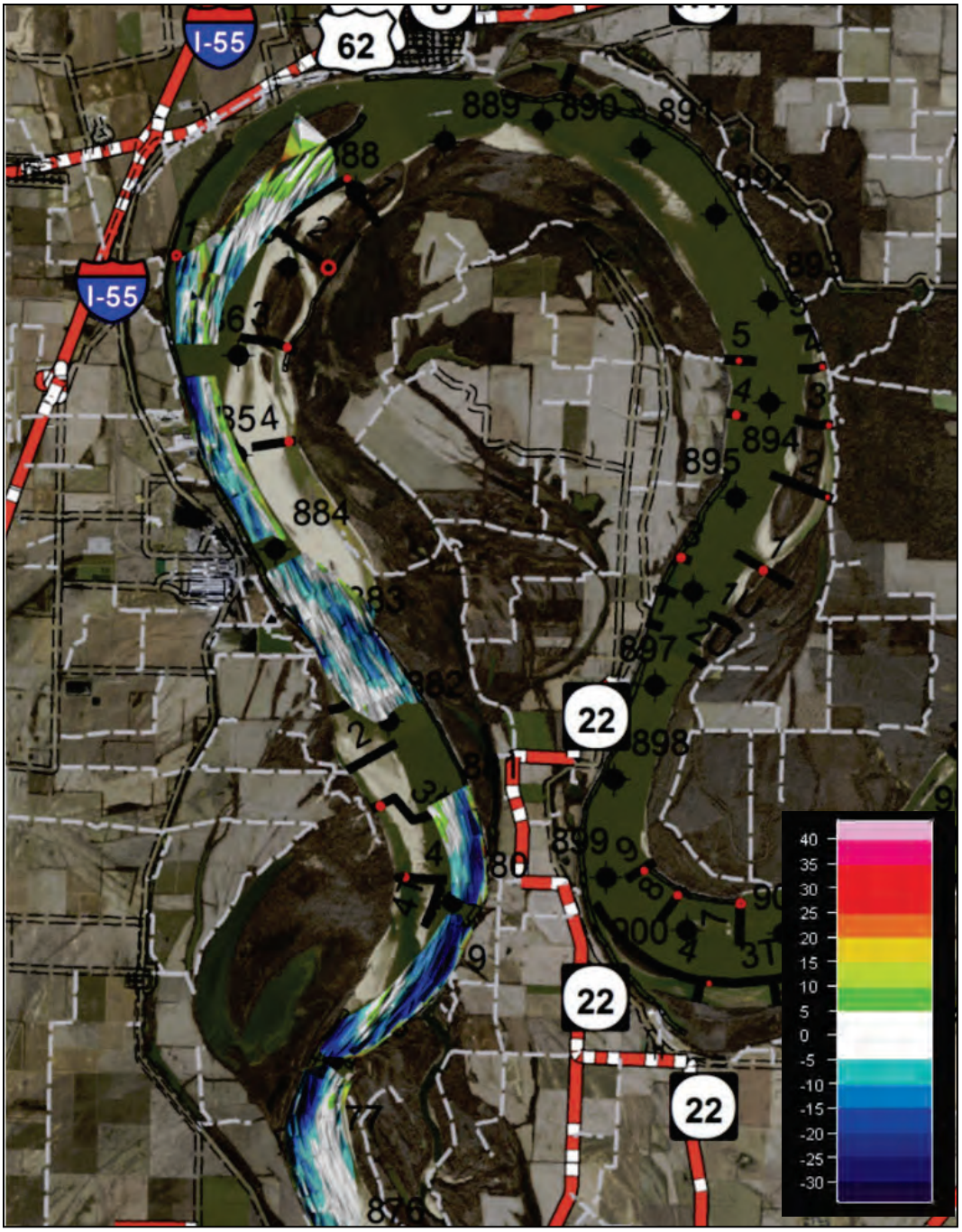


Figure B-4. Surface difference comparison from 1994 dataset to 2004 dataset (RM 840-860).

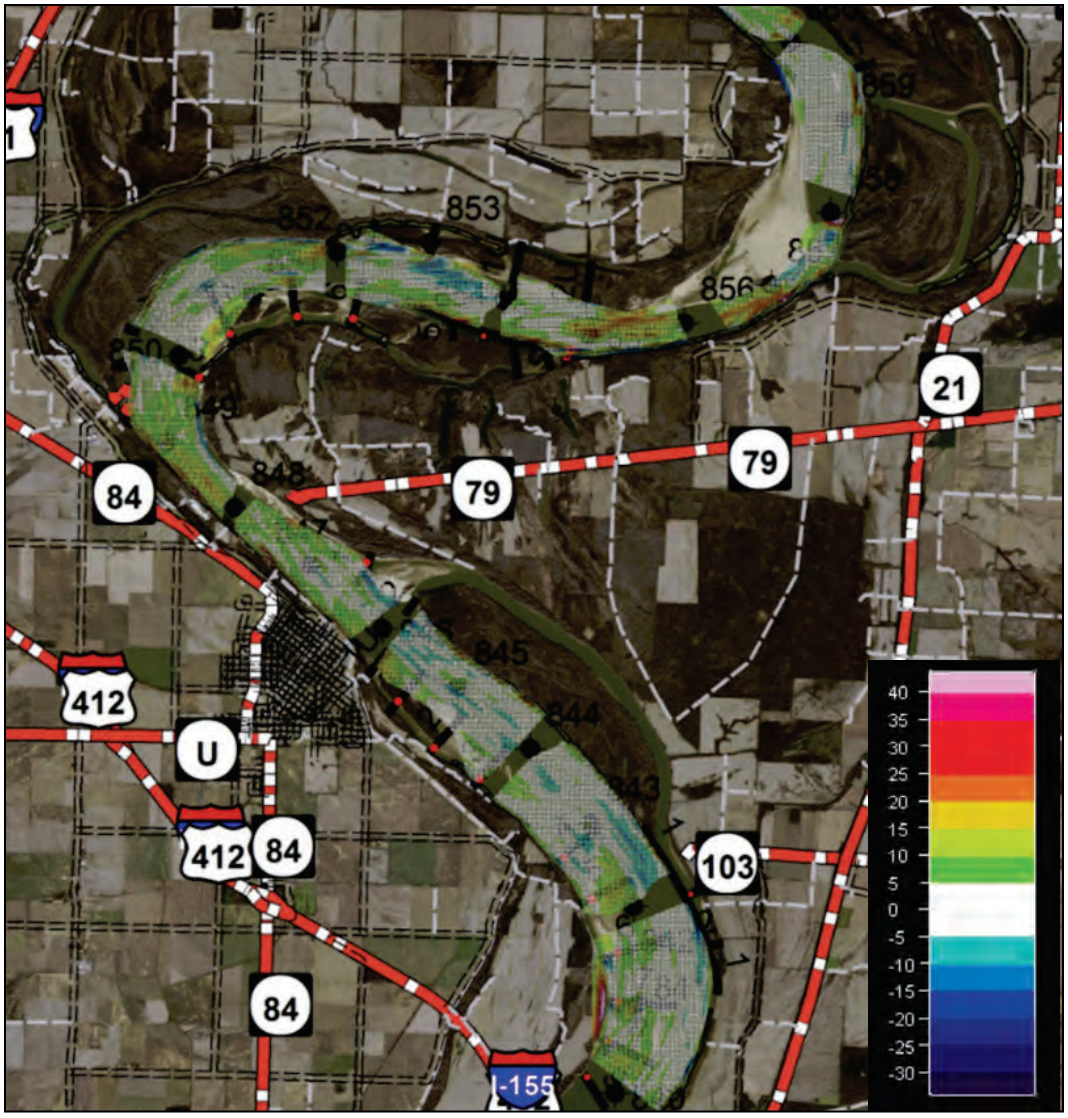


Figure B-5. Surface difference comparison from 1994 dataset to 2004 dataset (RM 860-878).

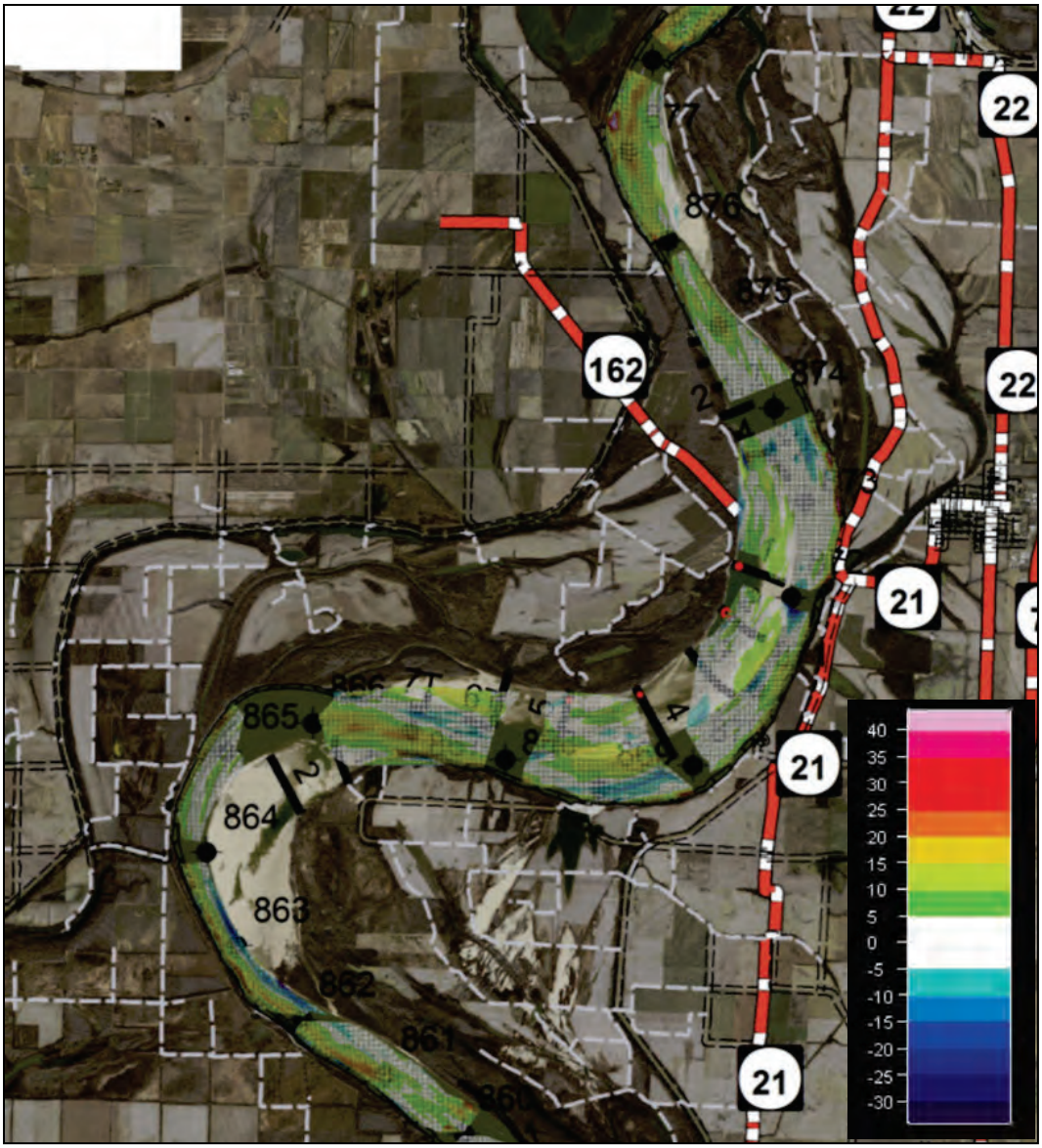


Figure B-6. Surface difference comparison from 1994 dataset to 2004 dataset (RM 878-888).

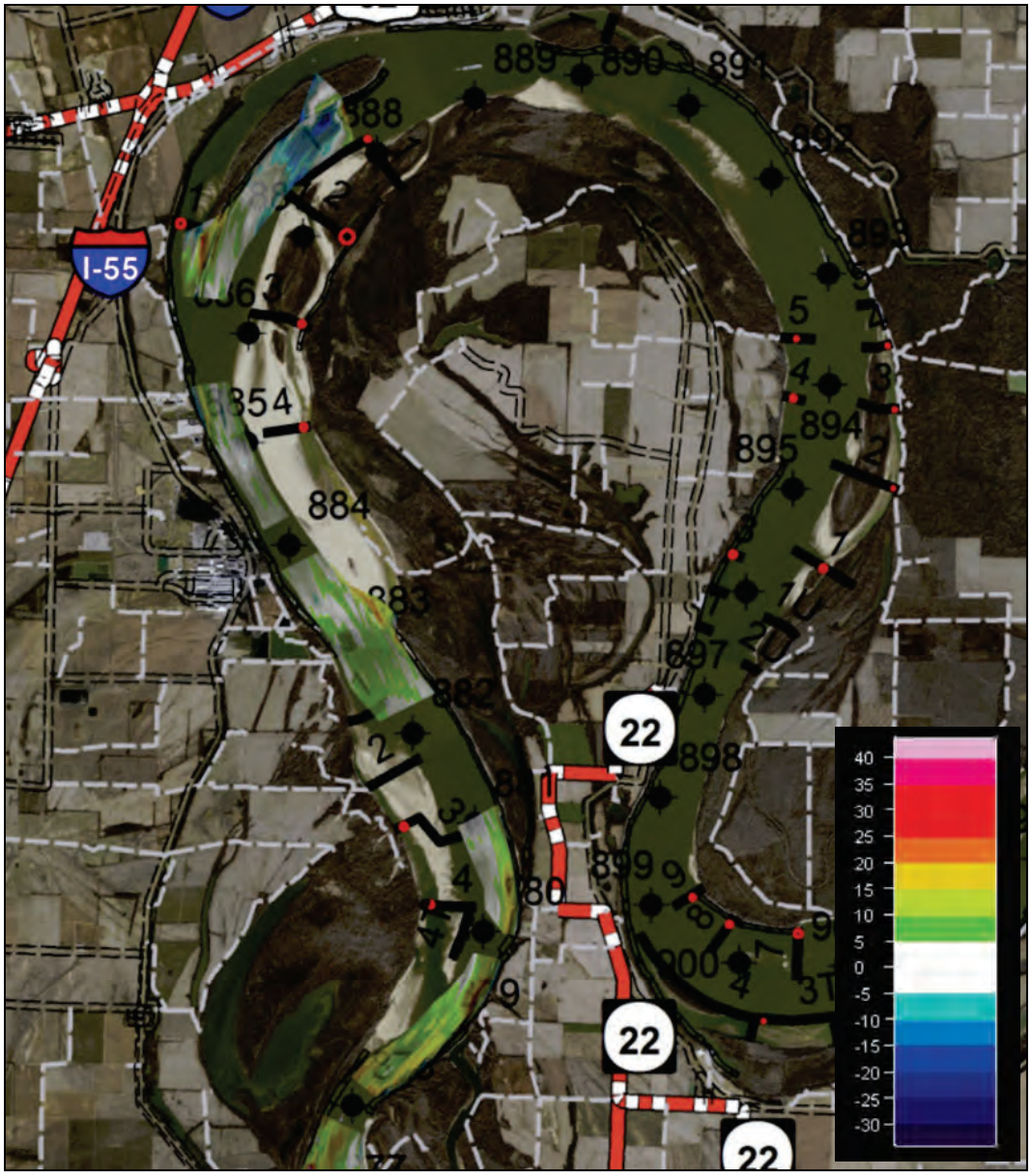


Figure B-7. Surface difference comparison from 2004 dataset to 2009 dataset (RM 840-860).

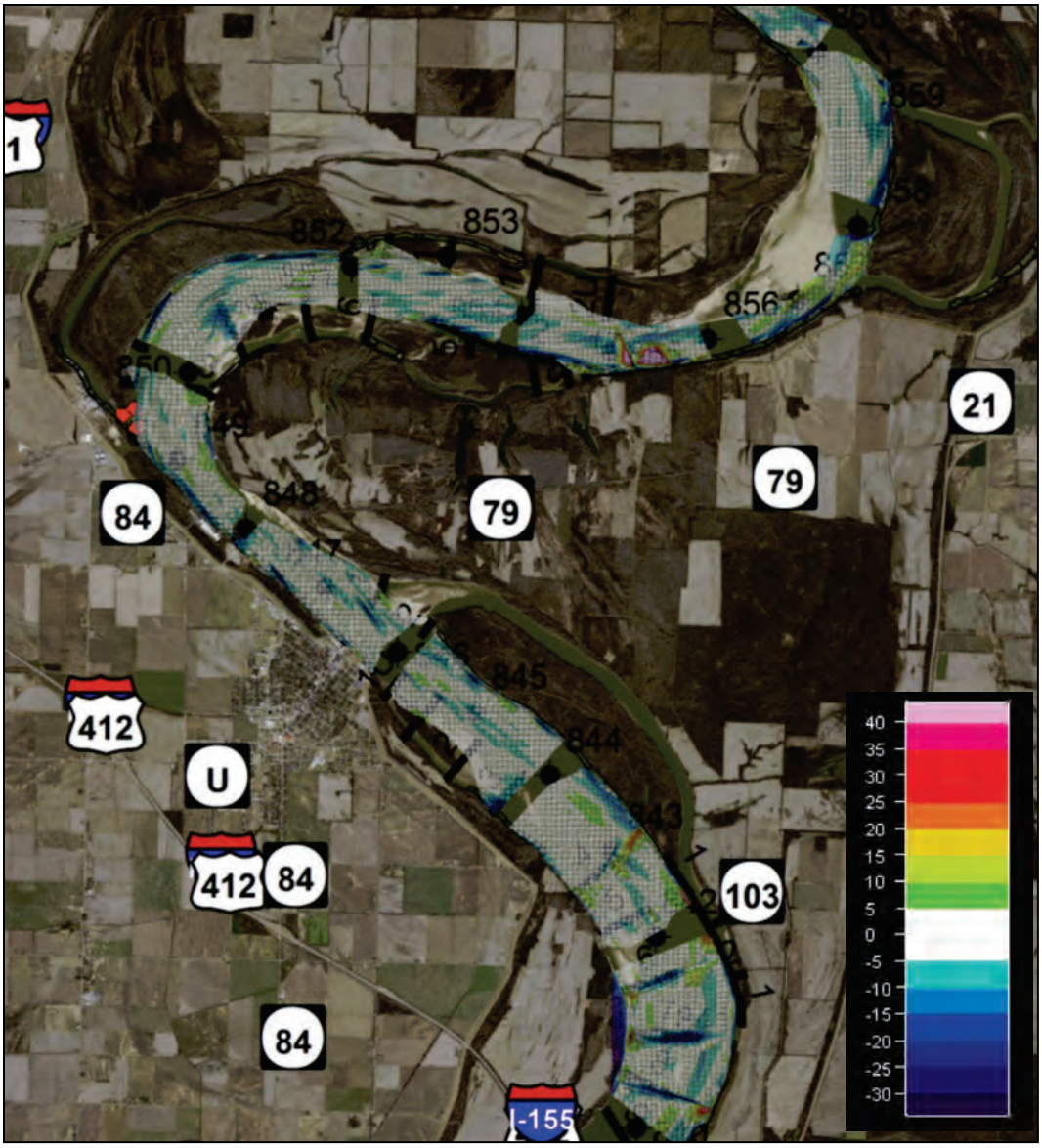


Figure B-8. Surface difference comparison from 2004 dataset to 2009 dataset (RM 860-878).

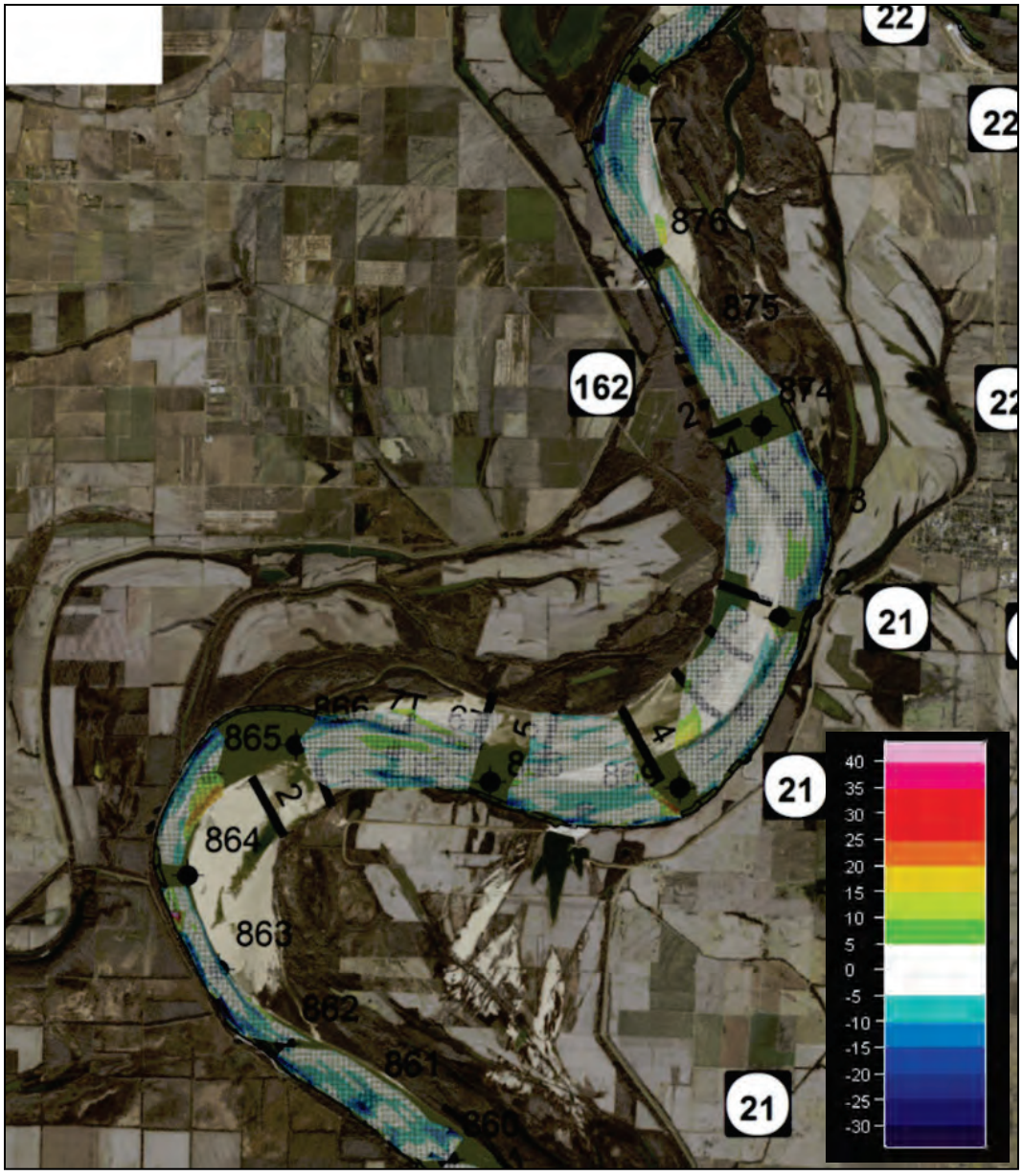


Figure B-9. Surface difference comparison from 2004 dataset to 2009 dataset (RM 878-888).

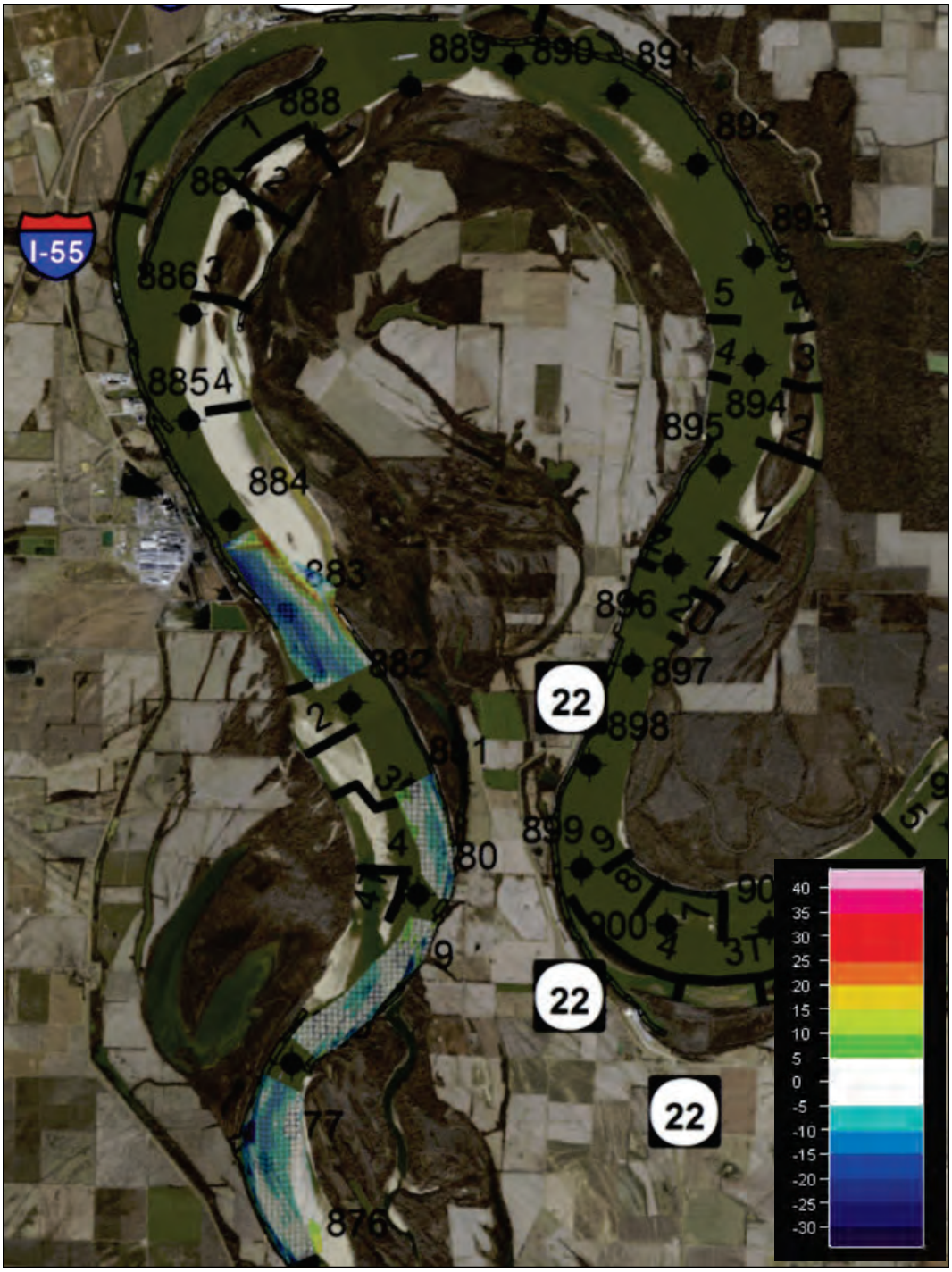


Figure B-10. Surface difference comparison from 2009 dataset to 2010 dataset (RM 840-860).

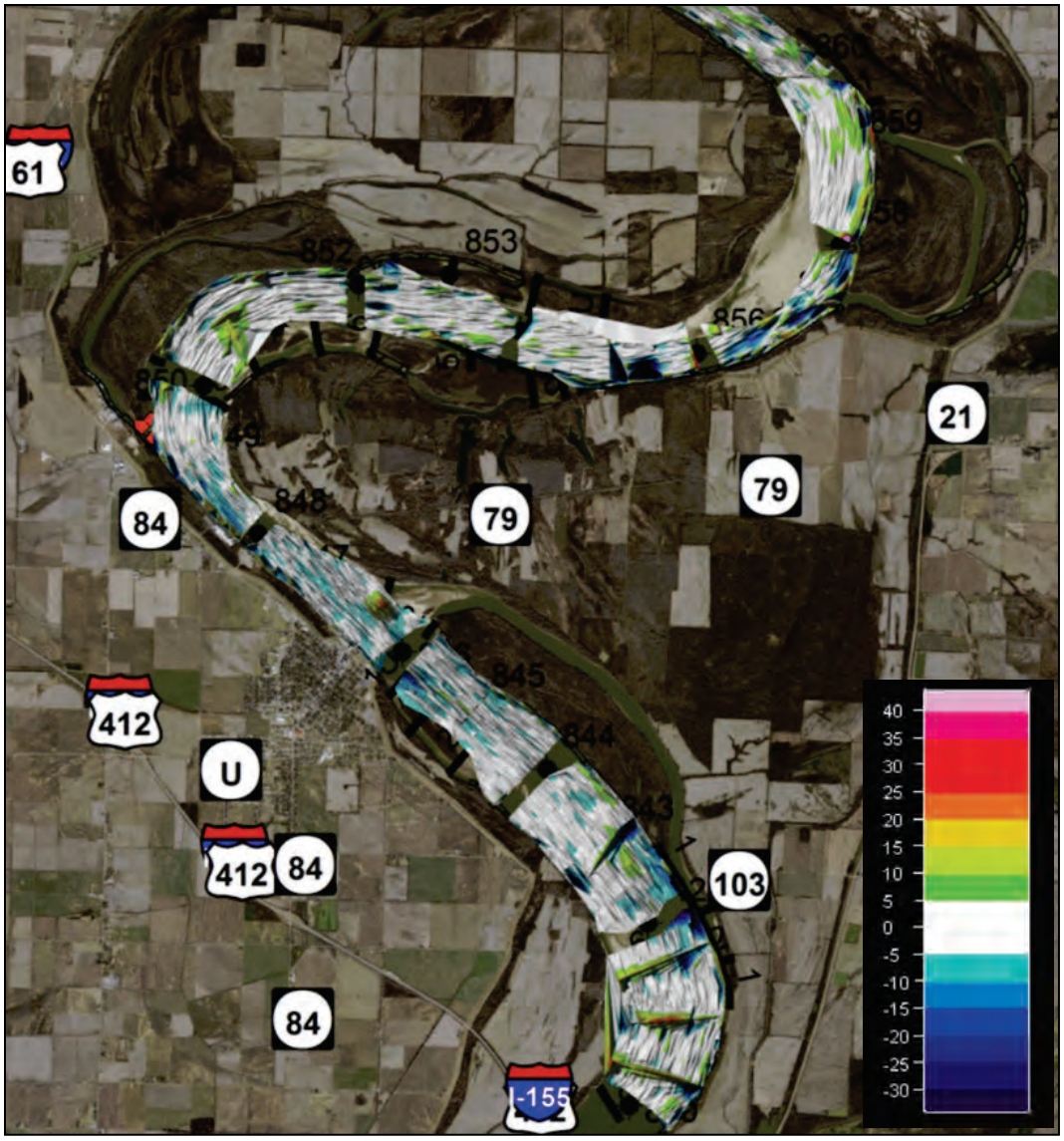


Figure B-11. Surface difference comparison from 2009 dataset to 2010 dataset (RM 860-878).

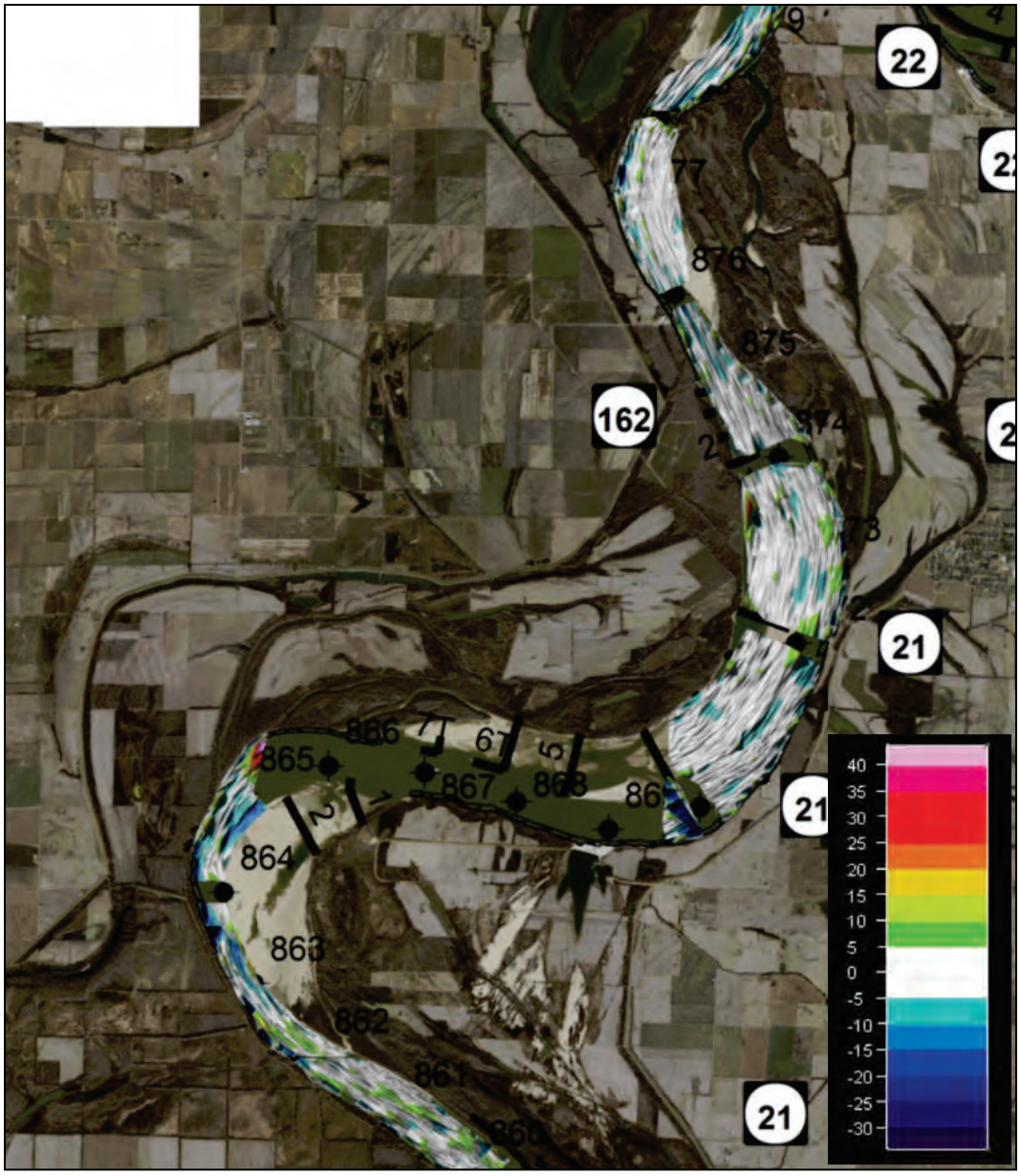


Figure B-12. Surface difference comparison from 2009 dataset to 2010 dataset (RM 878-888).

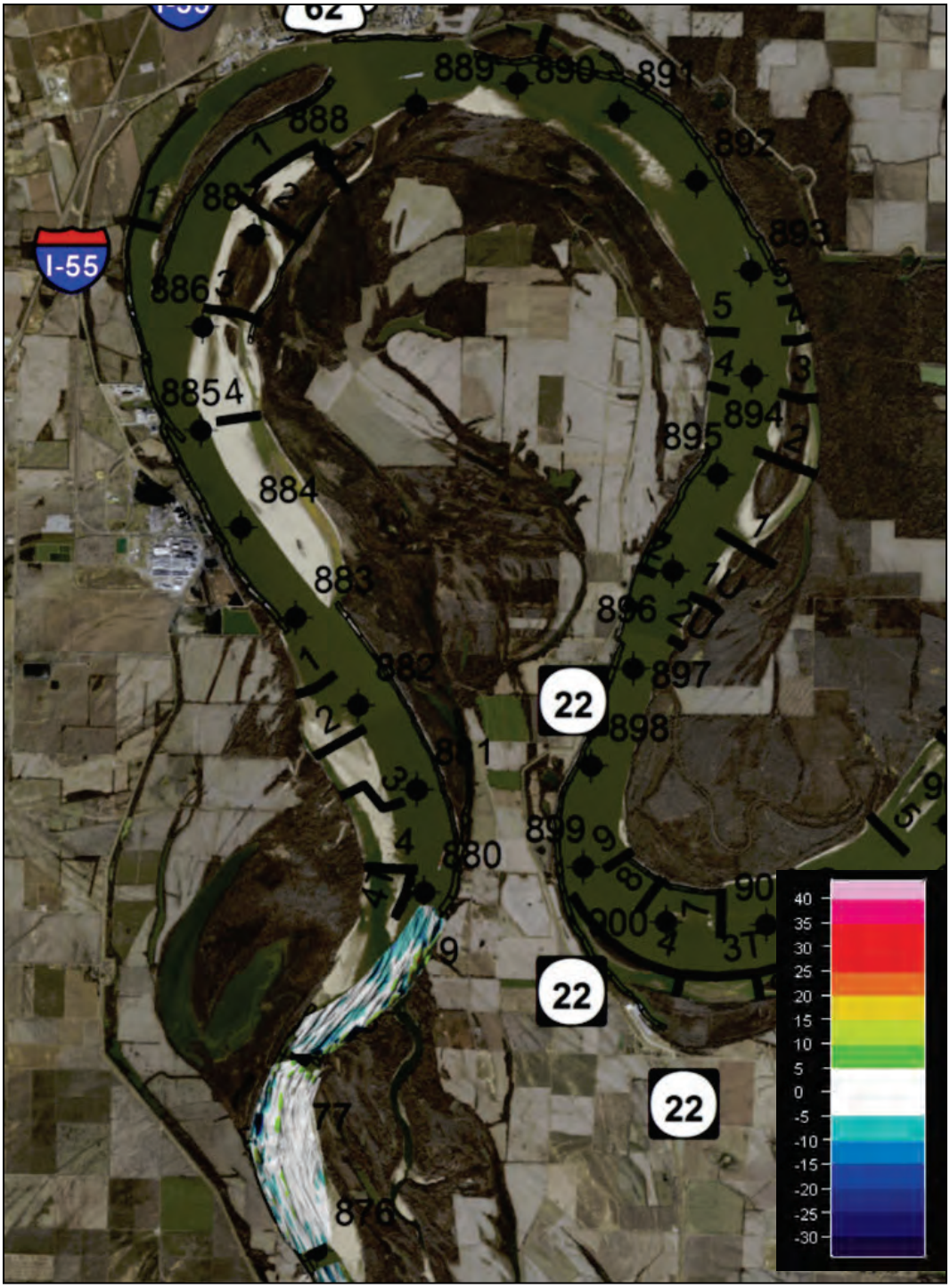


Figure B-13. Surface difference comparison from 2010 dataset to 2013 dataset (RM 840-860).

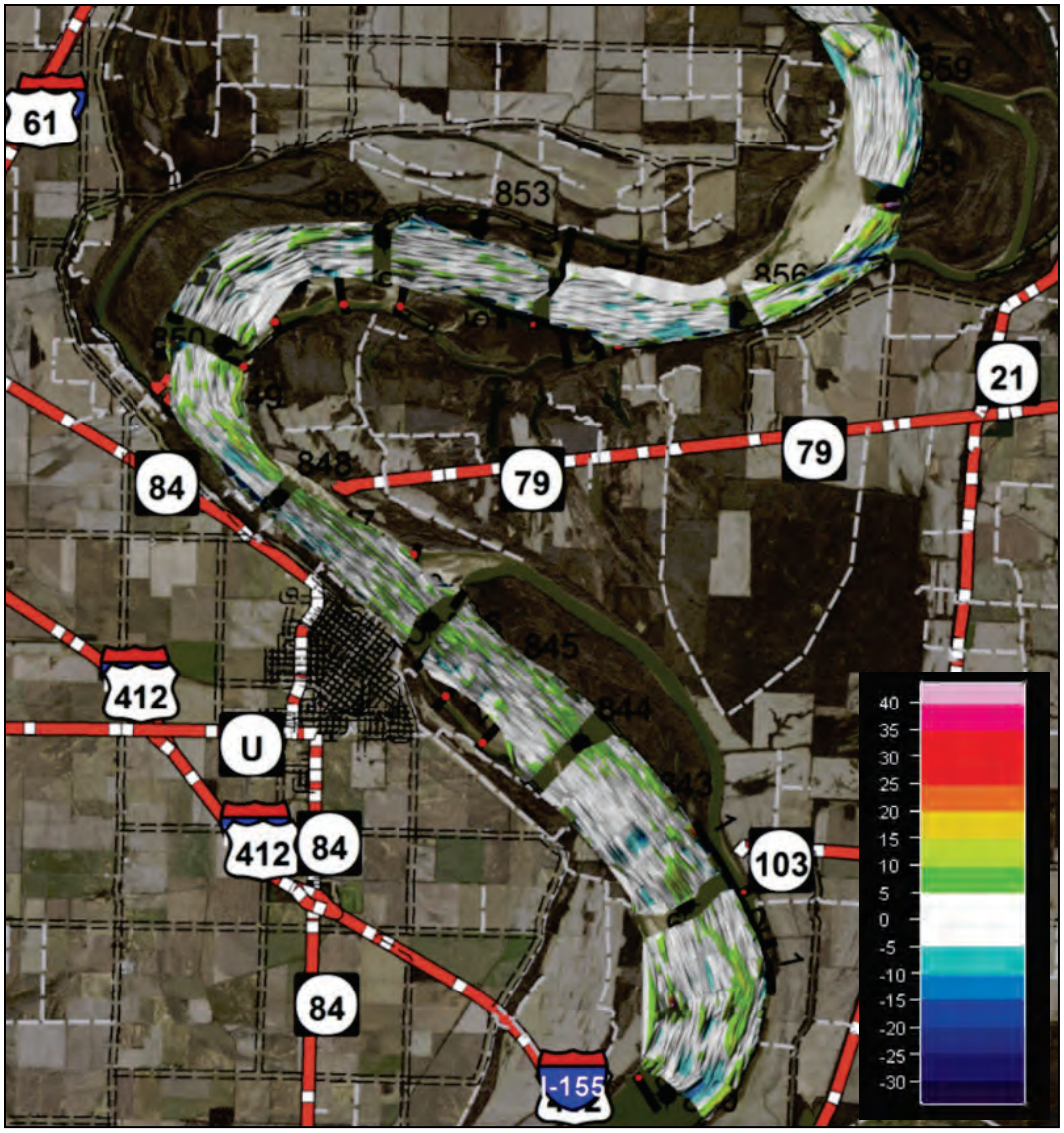


Figure B-14. Surface difference comparison from 2010 dataset to 2013 dataset (RM 860-878).

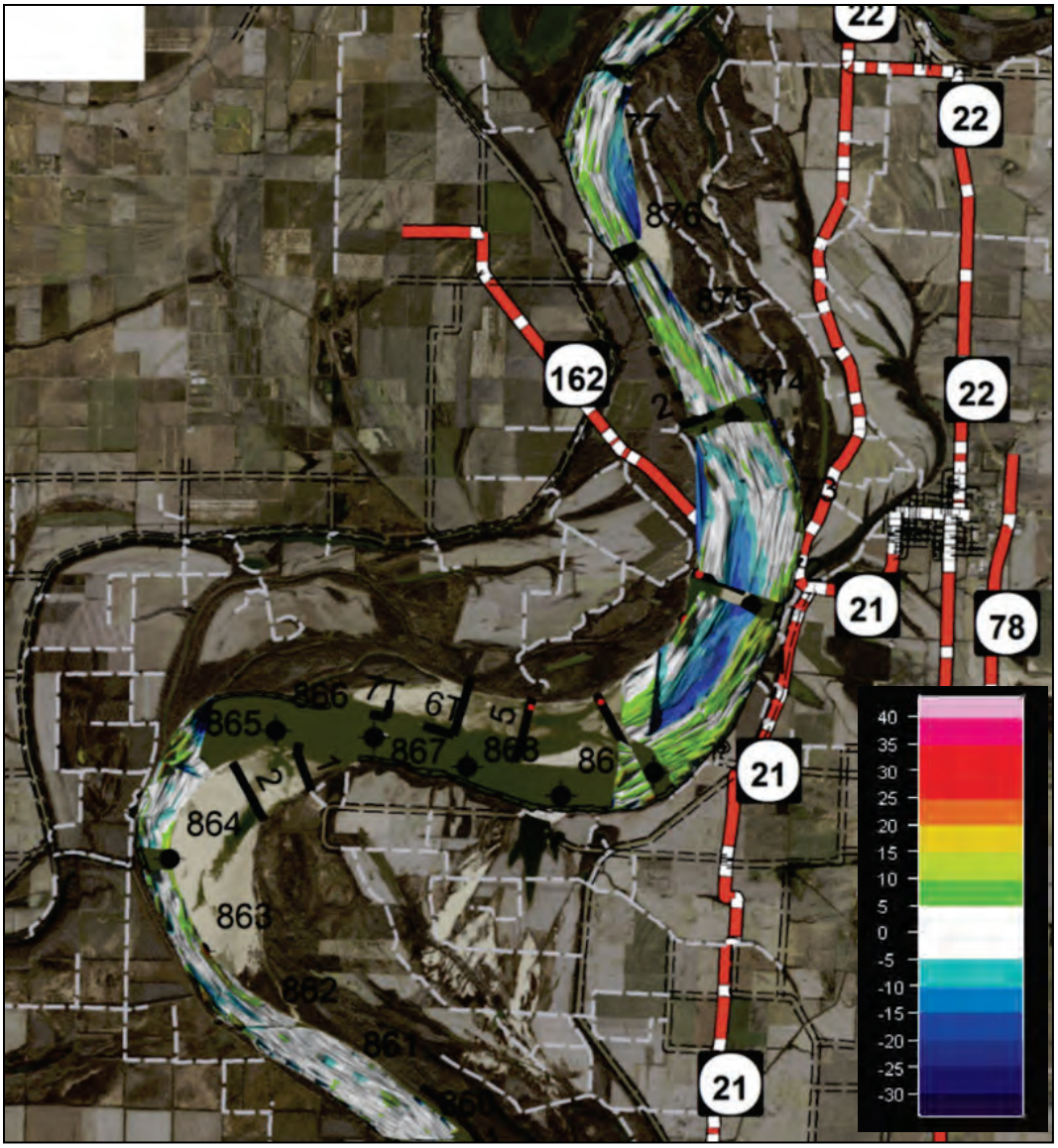


Figure B-15. Surface difference comparison from 2010 dataset to 2013 dataset (RM 878-888).

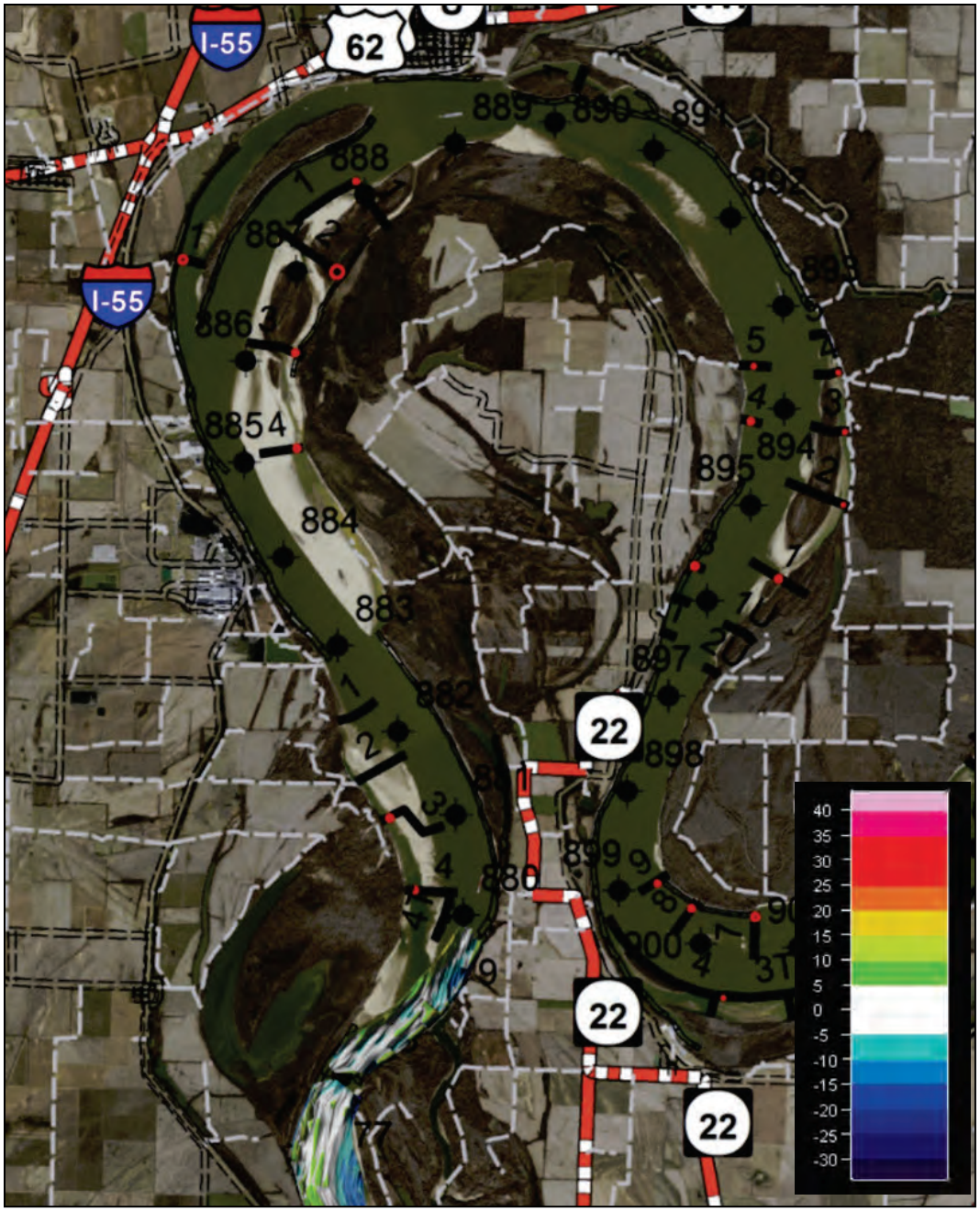


Figure B-16. Surface difference comparison from 1989 dataset to 2013 dataset (RM 840-860).

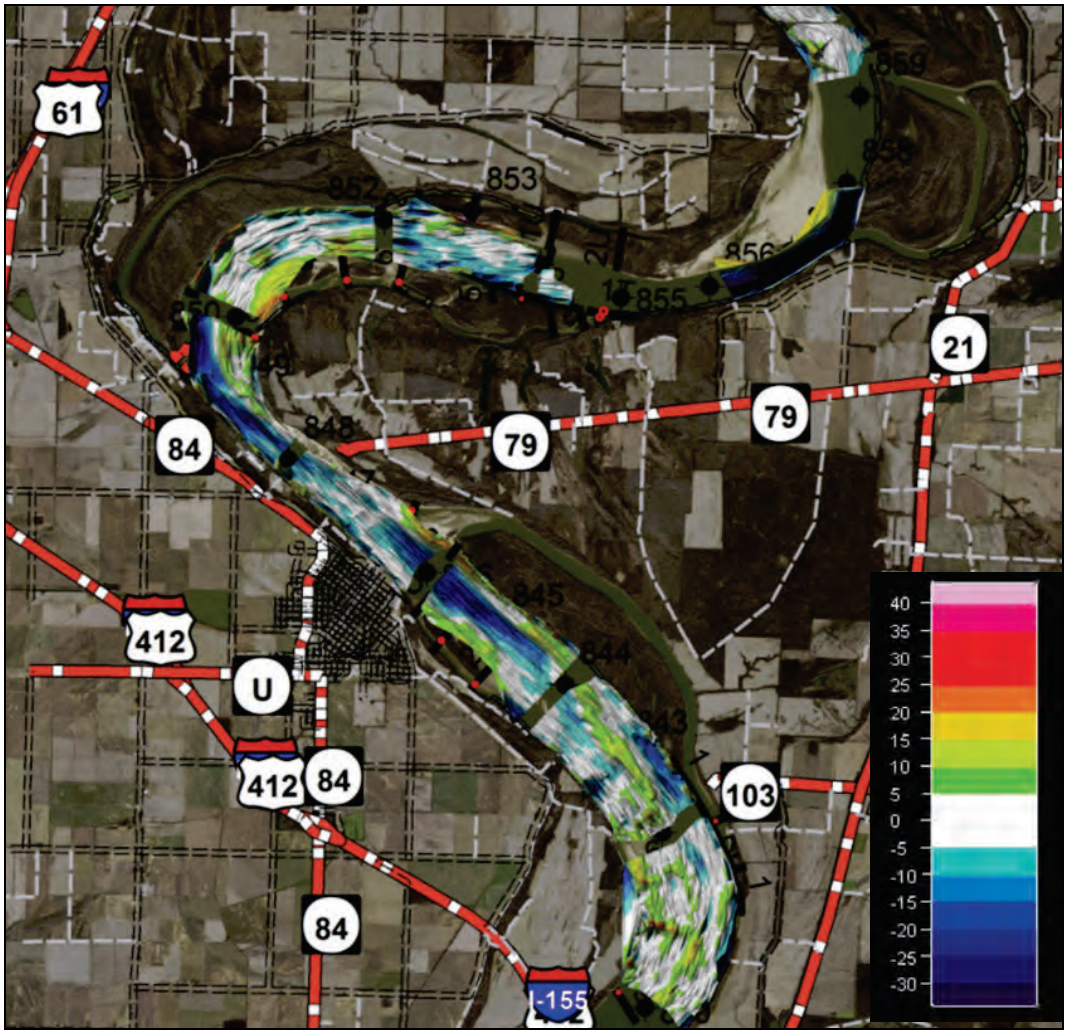


Figure B-17. Surface difference comparison from 1989 dataset to 2013 dataset (RM 860-878).

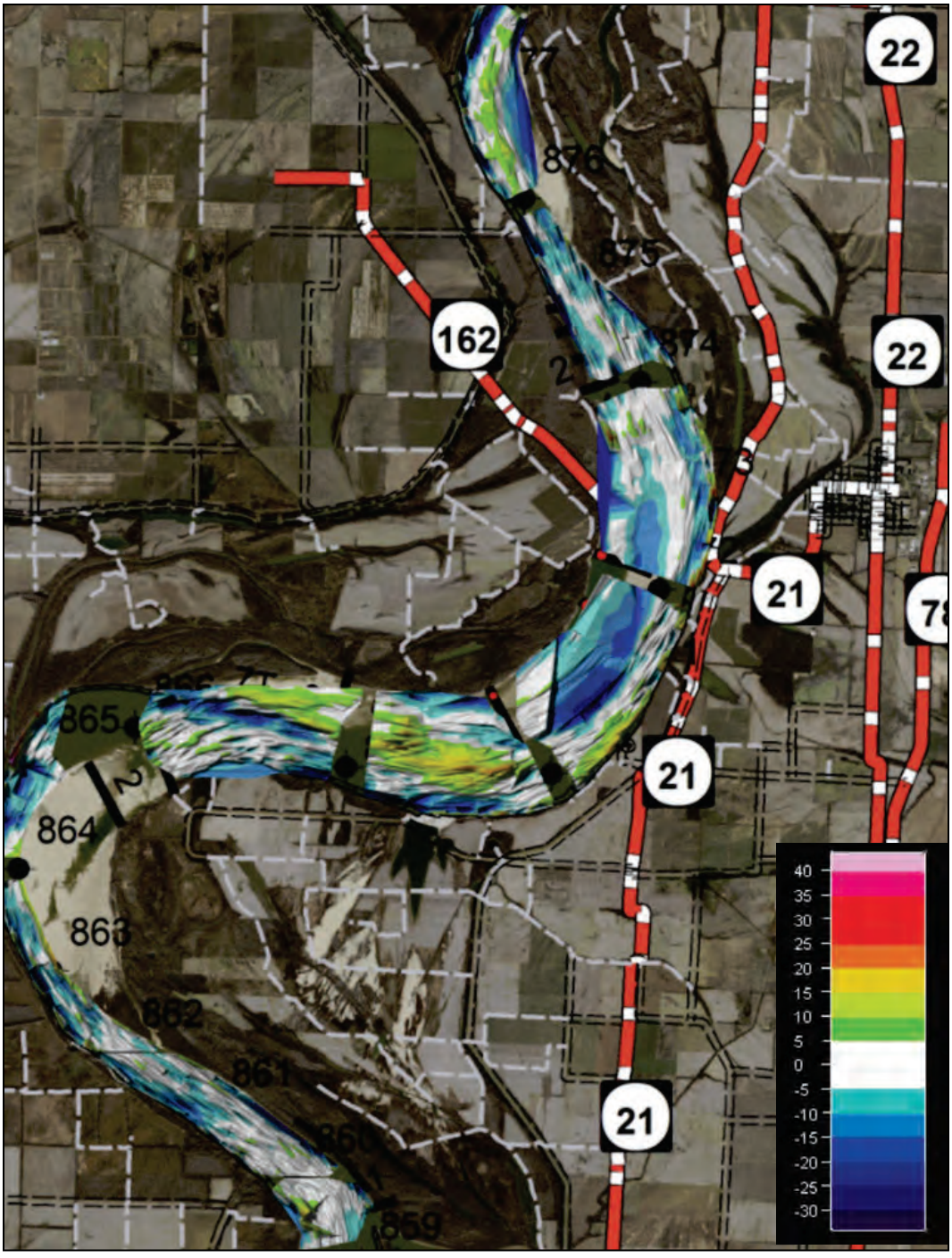


Figure B-18. Surface difference comparison from 1989 dataset to 2013 dataset (RM 878-888).

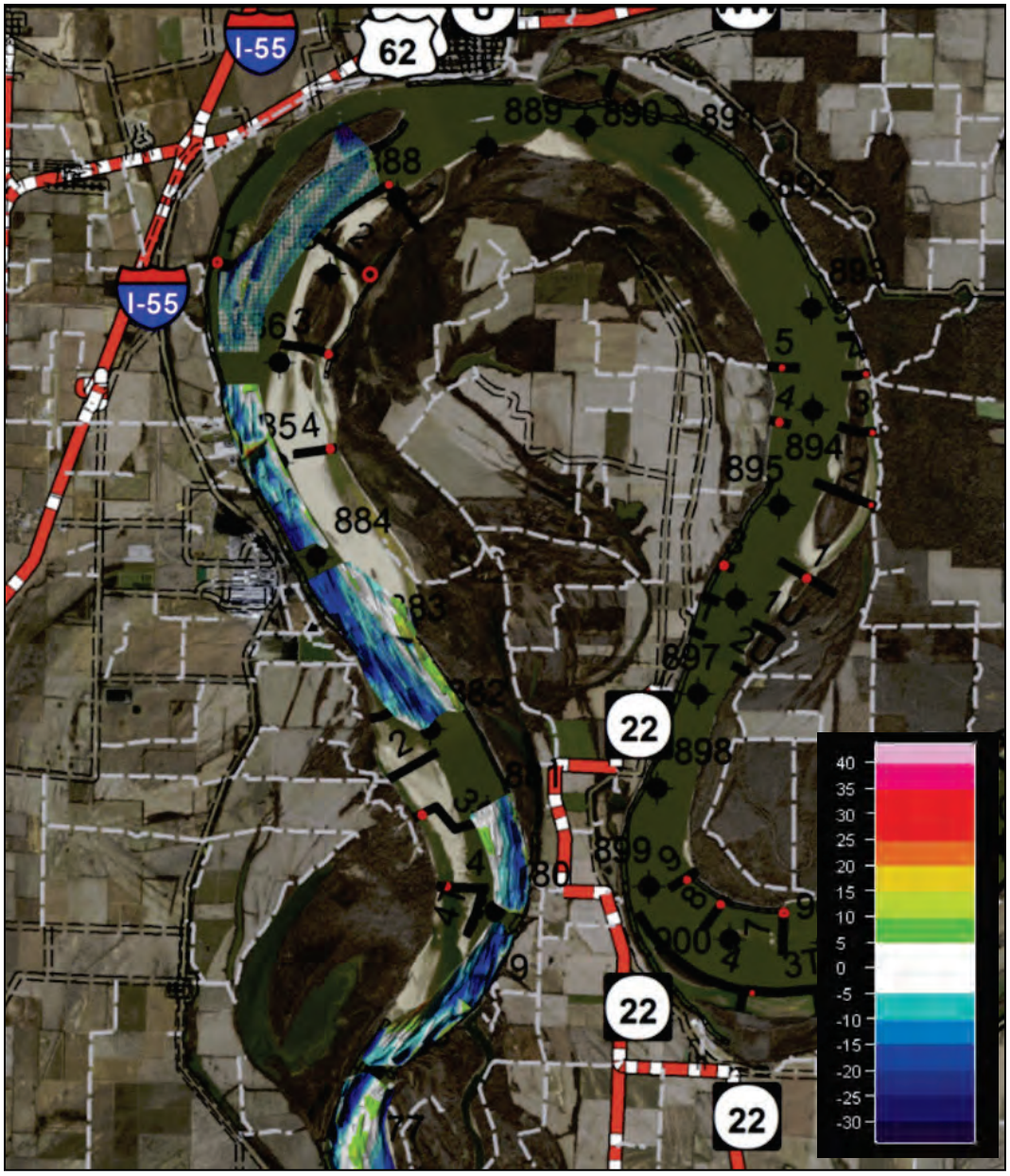


Table B-1. Surface difference comparison from 1989 dataset to 1994 dataset.

U/S RM	D/S RM	Volume Increased (ft^3)	Volume Decreased (ft^3)	Net Volume Change (ft^3)
888	886	107,071,316	-91,271,416	15,799,901
886	884	35,413,005	-112,388,354	-76,975,350
884	882	16,875,897	-171,285,405	-154,409,508
882	880	16,205,107	-113,527,320	-97,322,212
880	878	15,074,166	-256,909,703	-241,835,537
878	876	22,619,234	-181,161,320	-158,542,086
876	874	4,788,027	-182,489,190	-177,701,163
874	872	72,968,066	-167,546,929	-94,578,863
872	870	21,120,573	-265,469,049	-244,348,476
870	868	53,245,694	-178,848,764	-125,603,070
868	866	14,868,019	-325,139,566	-310,271,548
866	864	12,624,798	-141,207,853	-128,583,055
864	862	62,879,148	-92,815,201	-29,936,054
862	860	47,134,954	-155,273,240	-108,138,286
860	858	5,637,728	-42,161,237	-36,523,509
858	856	38,166,772	-762,005,708	-723,838,936
856	854	Dataset could not be compared: Small 1989 Dataset		
854	852	65,884,173	-16,658,644	-100,702,272
852	850	93,326,176	-174,325,764	-80,999,588
850	848	22,369,731	-361,140,127	-338,770,396
848	846	49,028,806	-228,590,411	-179,561,605
846	844	89,158,101	-211,791,842	122,633,741
844	842	96,264,637	-124,981,257	-28,716,619
842	840	127,215,503	-213,035,405	-85,819,903

Table B-2. Surface difference comparison from 1989 dataset to 2013 dataset.

U/S RM	D/S RM	Volume Increased (ft^3)	Volume Decreased (ft^3)	Net Volume Change (ft^3)
888	886	No Data		
886	884	21,135,948	-129,996,461	-108,860,514
884	882	37,563,466	-286,752,681	-249,189,215
882	880	12,415,954	-90,386,510	-77,970,556
880	878	29,459,253	-185,882,740	-156,423,487
878	876	54,539,111	-187,063,749	-132,524,638
876	874	7,734,427	-171,109,328	-163,374,901
874	872	56,649,806	-298,545,962	-241,896,156
872	870	78,577,272	-331,829,504	-253,252,232
870	868	206,435,463	-176,670,839	29,764,625
868	866	99,462,547	-206,081,380	-106,618,833
866	864	38,566,897	-119,610,837	-81,044,040
864	862	25,582,767	-96,694,384	-71,111,617
862	860	16,921,214	-132,137,078	-115,215,864
860	858	20,154,402	-33,449,681	-13,295,279
858	856	62,920,619	-659,311,699	-596,391,080
856	854	Dataset could not be compared: Small 1989 Dataset		
854	852	54,074,924	-16,619,210	-112,544,287
852	850	198,757,521	-92,379,948	106,377,573
850	848	73,953,392	-263,041,830	-189,088,438
848	846	54,445,314	-172,170,746	-117,725,432
846	844	118,250,943	-275,326,134	157,075,192
844	842	131,517,619	-184,921,602	-53,403,983
842	840	207,657,140	-134,070,200	73,586,940

Table B-3. Surface difference comparison from 1994 dataset to 2004 dataset.

U/S RM	D/S RM	Volume Increased (ft^3)	Volume Decreased (ft^3)	Net Volume Change (ft^3)
888	886	60,396,878	-61,044,788	-647,910
886	884	22,938,034	-5,179,639	17,758,395
884	882	93,000,905	-2,691,620	90,309,285
882	880	38,378,391	-1,825,001	36,553,390
880	878	105,551,300	-2,664,169	102,887,131
878	876	160,468,363	-2,675,351	157,793,011
876	874	62,718,278	-3,917,950	58,800,328
874	872	105,370,666	-35,223,618	70,147,048
872	870	99,439,576	-24,315,403	75,124,173
870	868	124,331,334	-33,005,669	91,325,665
868	866	180,839,679	-20,039,712	160,799,967
866	864	38,116,472	-3,102,167	35,014,305
864	862	69,212,542	-30,999,320	38,213,222
862	860	99,449,951	-11,860,465	87,589,486
860	858	46,409,958	-23,021,524	23,388,434
858	856	96,129,225	-10,010,551	86,118,674
856	854	151,467,917	-12,276,471	139,191,446
854	852	67,684,198	-38,653,620	29,030,578
852	850	131,671,921	-14,716,770	116,955,151
850	848	145,537,371	-9,408,393	136,128,978
848	846	104,284,013	-11,038,769	93,245,244
846	844	65,876,042	-38,711,546	27,164,496
844	842	79,788,089	-55,476,182	24,311,907
842	840	164,956,038	-32,423,838	132,532,200

Table B-4. Surface difference comparison from 1994 dataset to 2013 dataset.

U/S RM	D/S RM	Volume Increased (ft^3)	Volume Decreased (ft^3)	Net Volume Change (ft^3)
888	886	No Data		
886	884	102,753,571	-197,501,793	-94,748,222
884	882	22,916,312	-35,366,780	-12,450,468
882	880	36,912,408	-17,167,731	19,744,677
880	878	125,963,600	-40,491,732	85,471,868
878	876	132,888,320	-109,293,816	23,594,504
876	874	70,667,856	-56,248,988	14,418,868
874	872	Erroneous Data		
872	870	Erroneous Data		
870	868	233,452,256	-78,728,454	154,723,802
868	866	277,991,091	-74,328,805	203,662,286
866	864	79,691,281	-32,204,021	47,487,260
864	862	48,558,804	-89,519,962	-40,934,158
862	860	83,219,216	-90,625,925	-7,406,709
860	858	59,390,060	-81,664,560	-22,274,500
858	856	177,061,574	-49,833,192	127,228,381
856	854	132,450,073	-93,289,064	39,161,009
854	852	82,814,124	-94,432,130	-11,618,006
852	850	222,532,504	-35,171,488	187,361,016
850	848	179,447,736	-56,738,251	152,709,485
848	846	116,495,032	-55,669,215	60,825,817
846	844	87,097,796	-118,071,408	-30,973,612
844	842	113,128,638	-137,872,500	-24,743,862
842	840	263,965,975	-77,492,908	186,473,067

Table B-5. Surface difference comparison from 2004 dataset to 2009 dataset.

U/S RM	D/S RM	Volume Increased (ft^3)	Volume Decreased (ft^3)	Net Volume Change (ft^3)
888	886	No Data		
886	884	No Data		
884	882	121,316,078	-46,600,756	74,715,321
882	880	24,284,996	-6,747,665	17,537,331
880	878	28,848,134	-7,909,527	20,938,607
878	876	95,653,194	-6,848,758	88,804,436
876	874	59,968,948	-6,576,266	53,392,682
874	872	98,088,870	-27,395,025	70,693,845
872	870	50,968,639	-29,224,735	21,743,904
870	868	82,760,399	-16,333,861	66,426,539
868	866	77,695,303	-23,975,821	53,719,482
866	864	33,064,703	-35,325,776	-2,261,072
864	862	51,440,765	-15,062,902	36,377,863
862	860	81,793,299	-1,559,429	80,233,870
860	858	77,731,187	-15,068,103	62,663,084
858	856	48,329,486	-31,695,198	16,634,289
856	854	71,871,538	-75,663,356	-3,791,818
854	852	66,920,576	-12,897,158	54,023,417
852	850	86,458,937	-22,684,222	63,774,715
850	848	47,305,199	-21,486,782	25,818,417
848	846	65,708,656	-7,529,565	58,179,090
846	844	71,358,049	-19,582,117	51,775,932
844	842	65,707,303	-63,112,026	2,595,277
842	840	178,936,075	-70,324,167	108,611,908

Table B-6. Surface difference comparison from 2004 dataset to 2013 dataset.

U/S RM	D/S RM	Volume Increased (ft^3)	Volume Decreased (ft^3)	Net Volume Change (ft^3)
888	886	No Data		
886	884	40,742,669	-9,209,234	31,533,435
884	882	160,316,249	-27,093,362	133,222,887
882	880	30,545,521	-4,437,182	26,108,339
880	878	67,407,700	-8,361,761	59,045,940
878	876	130,503,790	-4,056,398	126,447,392
876	874	52,747,842	-7,734,738	45,013,104
874	872	167,196,007	-11,439,057	155,756,949
872	870	158,440,318	-38,722,583	119,717,736
870	868	52,987,387	-43,733,735	9,253,652
868	866	78,969,114	-40,325,215	38,643,898
866	864	32,577,446	-15,111,231	17,466,216
864	862	65,025,008	-6,816,988	58,208,020
862	860	66,063,699	-660,120	65,403,579
860	858	58,935,296	-22,215,546	36,719,750
858	856	50,356,845	-21,927,317	28,429,528
856	854	96,227,328	-10,291,694	85,935,634
854	852	58,597,958	-17,735,821	40,862,137
852	850	51,572,458	-48,919,474	2,652,984
850	848	79,298,261	-34,317,062	44,981,198
848	846	86,657,314	-21,236,942	65,420,372
846	844	76,919,587	-24,695,645	52,223,942
844	842	82,640,888	-39,408,078	43,232,810
842	840	100,282,701	-78,935,785	21,346,915

Table B-7. Surface difference comparison from 2009 dataset to 2010 dataset.

U/S RM	D/S RM	Volume Increased (ft^3)	Volume Decreased (ft^3)	Net Volume Change (ft^3)
888	886	No Data		
886	884	No Data		
884	882	No Data		
882	880	No Data		
880	878	19,625,726	-77,615,147	-57,989,421
878	876	23,669,615	-57,983,010	-34,313,395
876	874	24,394,194	-48,716,742	-24,322,547
874	872	88,376,059	-87,949,422	426,637
872	870	26,107,922	-109,708,272	-83,600,350
870	868	6,307,751	-59,558,810	-53,251,059
868	866	No Data		
866	864	56,082,763	-78,481,391	-22,398,628
864	862	33,919,194	-86,545,089	-52,625,896
862	860	62,256,113	-37,554,628	24,701,486
860	858	113,200,488	-53,813,955	59,386,533
858	856	57,011,033	-106,169,071	-49,158,039
856	854	42,575,932	-160,473,885	-117,897,953
854	852	54,029,603	-48,769,122	5,260,481
852	850	107,192,460	-48,064,481	59,127,978
850	848	25,035,142	-107,465,586	-82,430,444
848	846	29,473,236	-115,798,618	-86,325,382
846	844	15,646,297	-129,481,756	-113,835,459
844	842	40,890,372	-183,724,214	-142,833,842
842	840	167,497,647	-164,573,404	2,924,243

Table B-8. Surface difference comparison from 2009 dataset to 2013 dataset.

U/S RM	D/S RM	Volume Increased (ft^3)	Volume Decreased (ft^3)	Net Volume Change (ft^3)
888	886	No Data		
886	884	No Data		
884	882	50,059,288	-163,637,535	-113,578,247
882	880	22,916,312	-35,366,780	-12,450,468
880	878	28,249,841	-93,753,053	-65,503,212
878	876	45,973,614	-123,128,335	-77,154,721
876	874	59,969,155	-55,662,542	4,306,613
874	872	Erroneous Data		
872	870	Erroneous Data		
870	868	161,556,701	-70,824,966	90,731,735
868	866	102,972,713	-75,844,403	27,128,311
866	864	45,036,557	-80,739,188	-35,702,631
864	862	45,389,614	-73,390,206	-28,000,592
862	860	56,206,709	-3,346,348	22,742,361
860	858	914,684,466	-52,668,065	38,800,401
858	856	99,691,095	-87,430,458	12,260,638
856	854	36,238,268	-181,871,077	-145,632,809
854	852	71,622,822	-50,771,442	2,081,380
852	850	141,976,723	-43,961,784	98,014,940
850	848	60,921,061	-90,632,310	-29,711,249
848	846	59,746,065	-69,908,635	-10,162,570
846	844	66,724,298	-65,553,483	1,170,815
844	842	89,128,473	-152,398,008	-63,269,535
842	840	264,601,270	-149,358,995	115,242,275

Table B-9. Surface difference comparison from 2010 dataset to 2013 dataset.

U/S RM	D/S RM	Volume Increased (ft^3)	Volume Decreased (ft^3)	Net Volume Change (ft^3)
888	886	No Data		
886	884	No Data		
884	882	No Data		
882	880	No Data		
880	878	48,690,619	-56,134,322	-7,443,703
878	876	57,536,028	-100,179,353	-42,643,326
876	874	73,134,051	-44,447,456	28,686,594
874	872	Erroneous Data		
872	870	Erroneous Data		
870	868	33,872,740	-3,792,286	30,080,454
868	866	No Data		
866	864	46,204,070	-59,329,496	-13,125,426
864	862	57,098,327	-32,244,736	24,853,592
862	860	31,769,174	-33,718,447	-1,949,273
860	858	55,933,960	-76,643,704	-20,709,744
858	856	105,987,028	-44,453,107	61,533,920
856	854	38,662,763	-66,304,393	-27,641,630
854	852	52,213,470	-36,597,563	15,615,906
852	850	77,694,725	-38,776,056	38,918,670
850	848	94,260,813	-42,018,413	52,152,401
848	846	96,559,128	-20,317,667	76,241,461
846	844	128,353,941	-13,374,030	114,979,910
844	842	125,800,724	-46,194,778	79,605,946
842	840	178,313,477	-66,327,651	111,985,826

Appendix C: Multidimensional Modeling Analysis

Appendix C contains detailed AdH model output and analysis.

Base condition output

The following sections contain AdH model output and analysis for the base condition.

Hydrodynamic calibration and validation

Depicted below are the Tiptonville (MS116) and Caruthersville (MS117) observed versus modeled WSEL hydrographs for the calibration events (Figures C-1 through C4 and C-11 through C-12). Note that local inflow (rainfall) was not modeled in AdH. During the rising limb of the second peak of calibration Event 2, there was significant local rainfall over the modeled domain that was not included; this accounts for the missing volume in the hydrograph. Refer to Figures C-5 through C-10 for Dec 2013 observed precipitation. Figures C-13 through C-28 depict the observed versus modeled velocity comparison (spatially and graphically).

Figures C-29 and C-30 depict the Tiptonville and Caruthersville WSEL hydrographs for the validation event.

Figure C-1. WSEL calibration—MS116 Event 1.

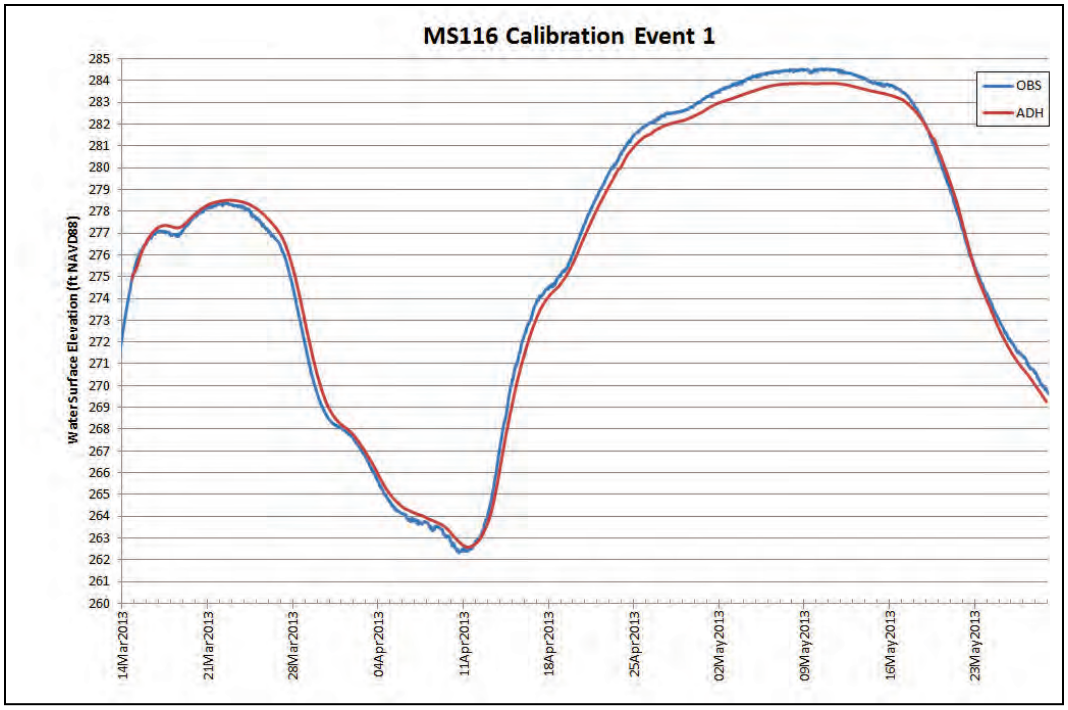


Figure C-2. WSEL calibration—MS117 Event 1.

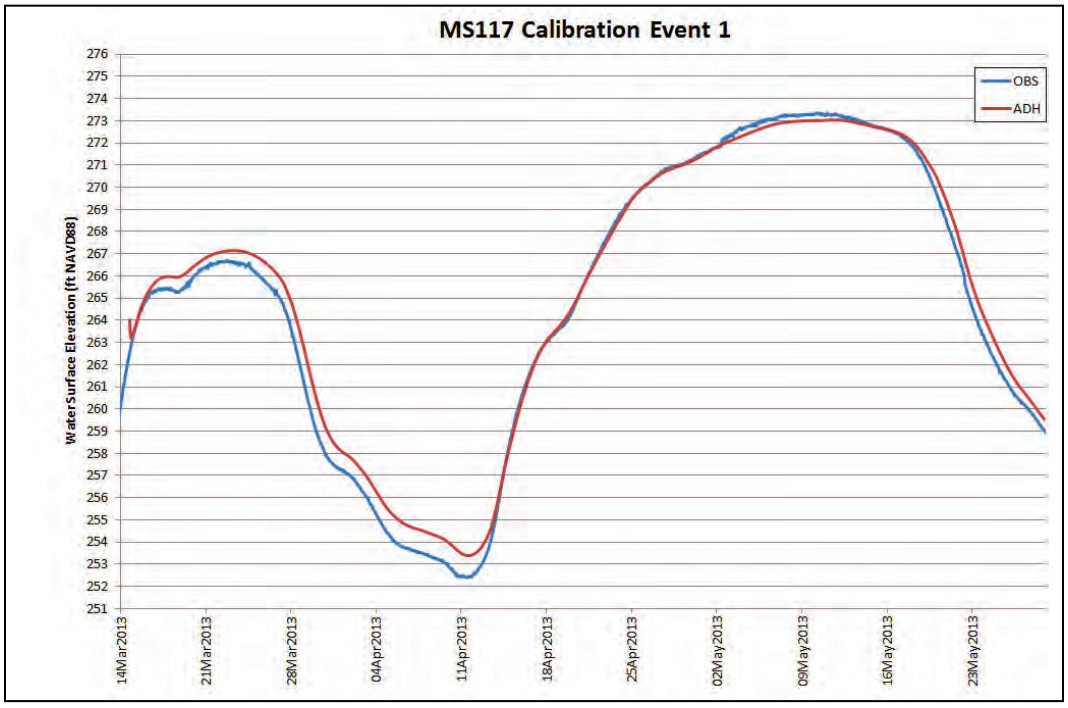


Figure C-3. WSEL calibration—MS116 Event 2.

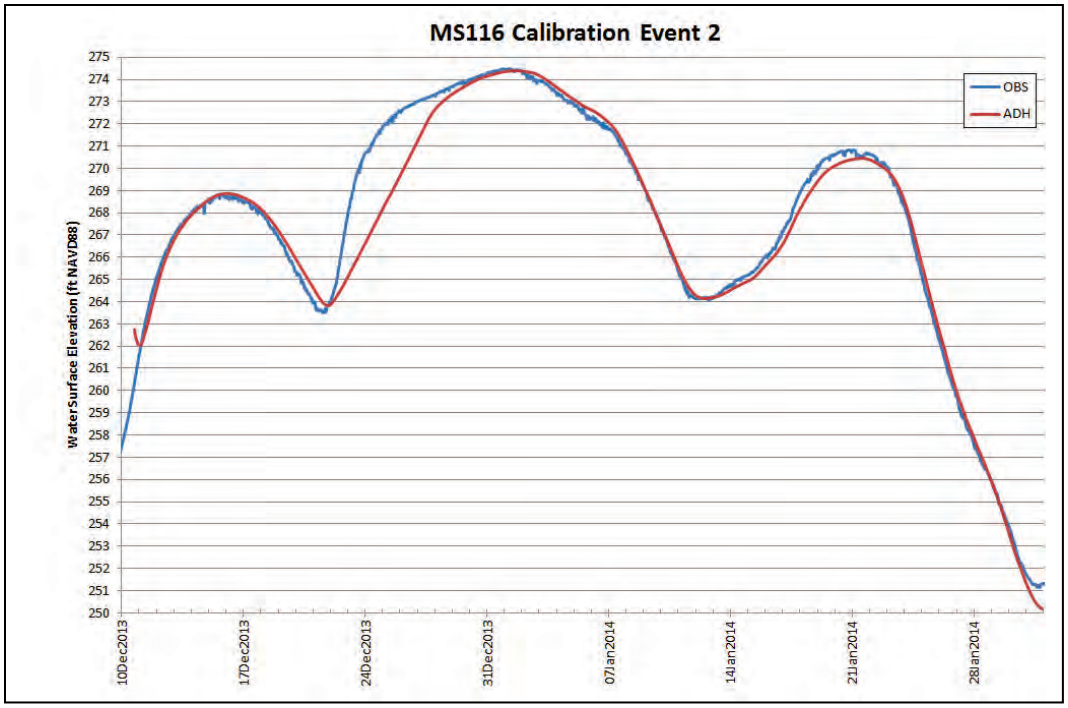


Figure C-4. WSEL calibration—MS117 Event 2.

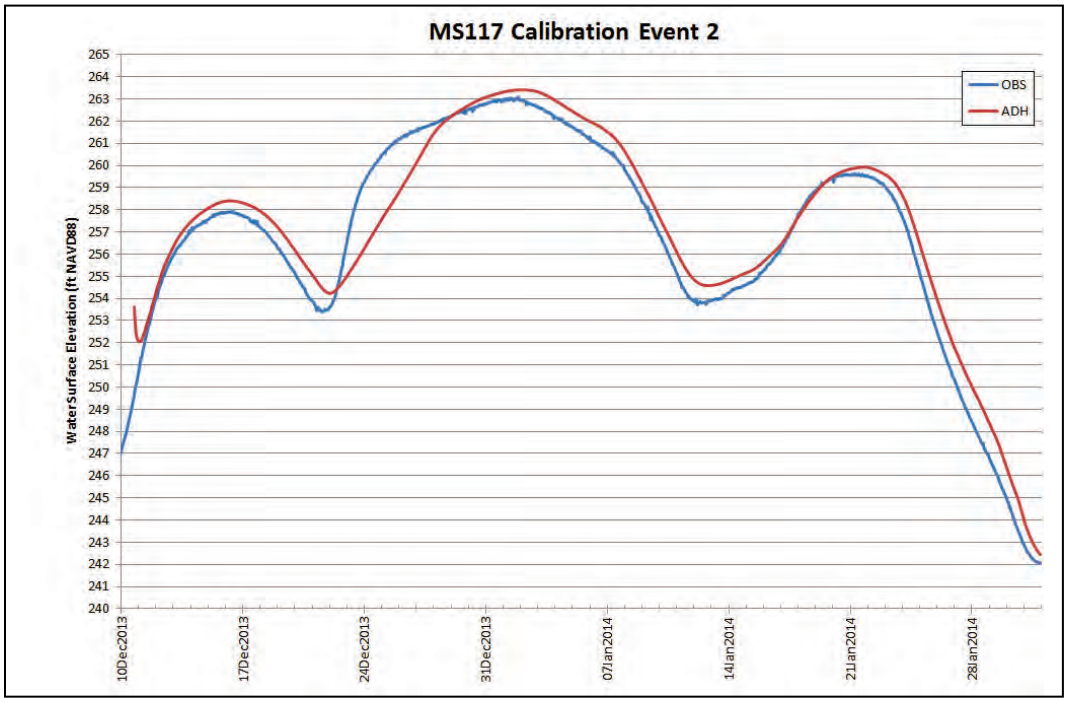


Figure C-5. Dec 2013 observed precipitation.

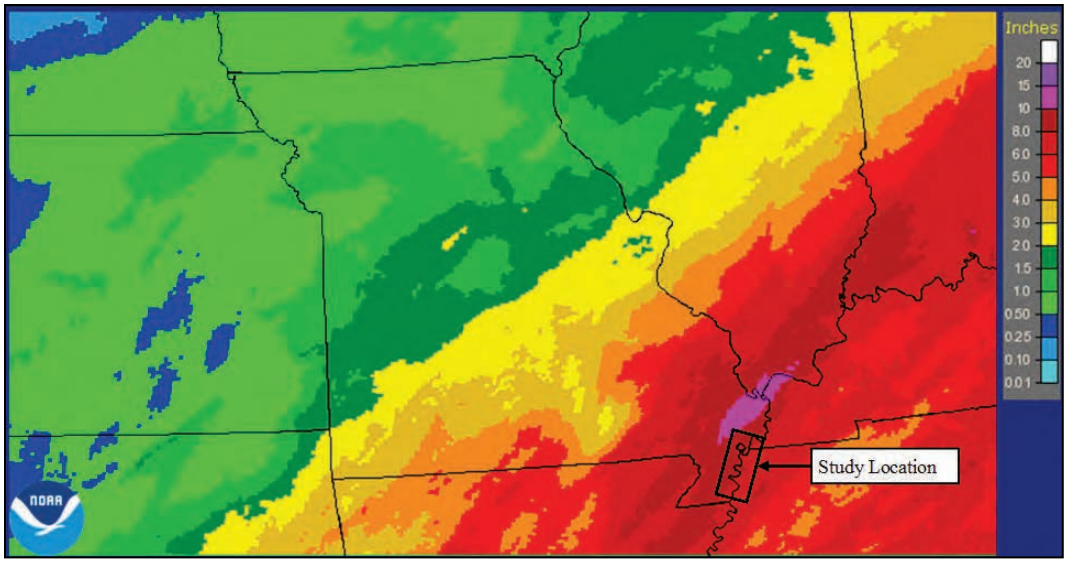


Figure C-6. 20 Dec 2013 observed precipitation.

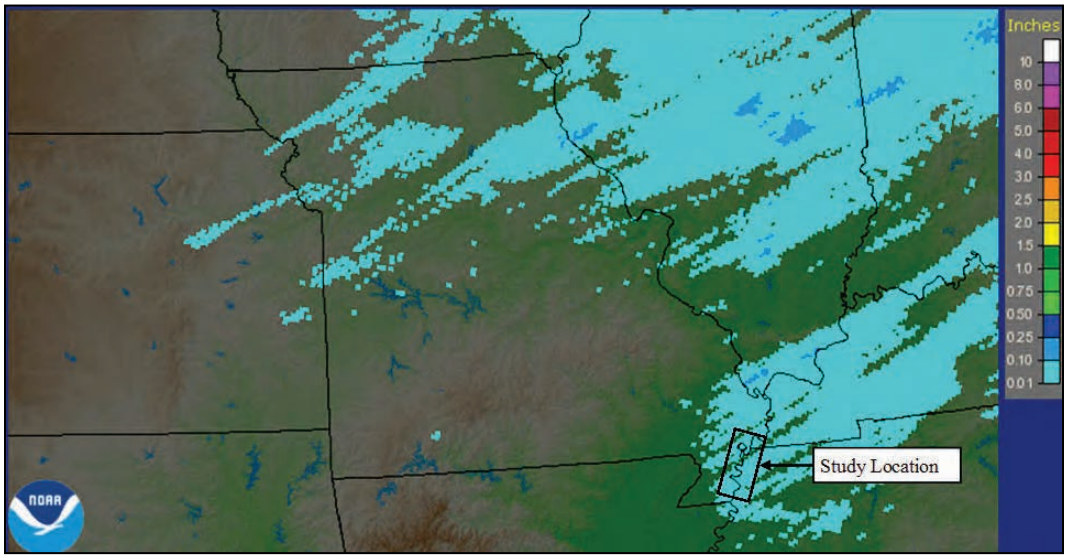


Figure C-7. 21 Dec 2013 observed precipitation.

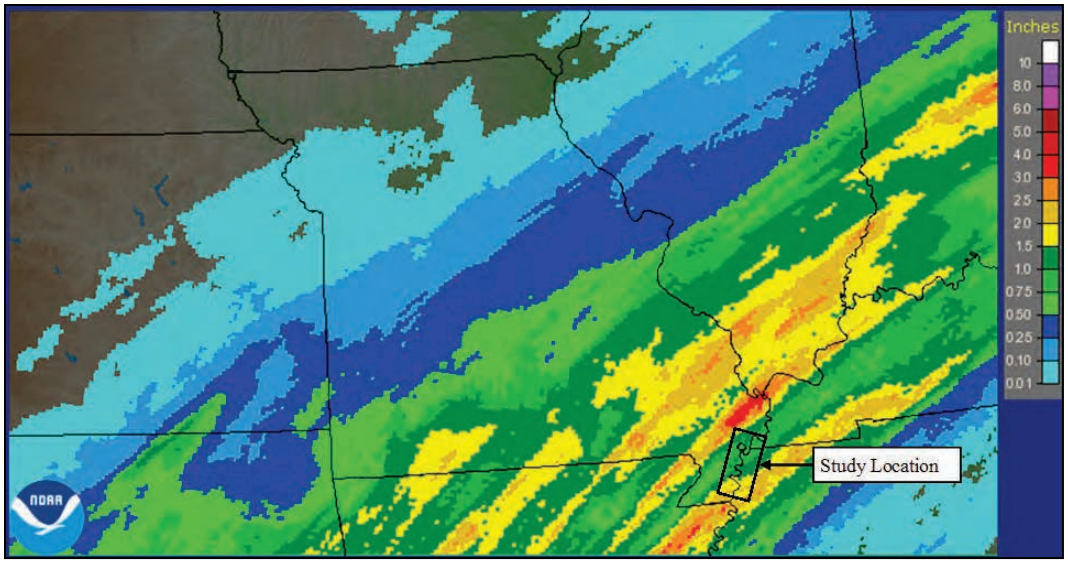


Figure C-8. 22 Dec 2013 observed precipitation.

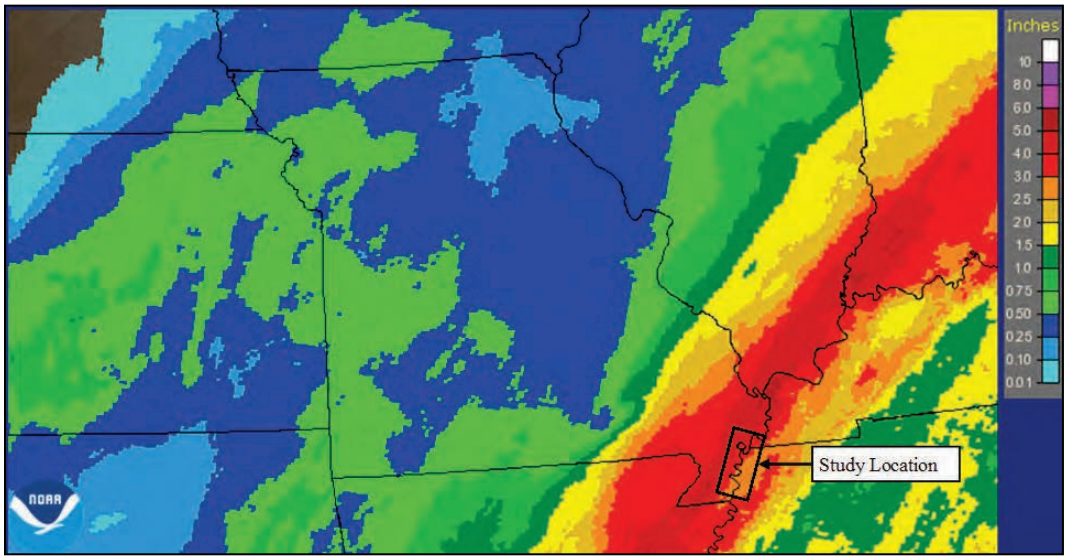


Figure C-9. 23 Dec 2013 observed precipitation.

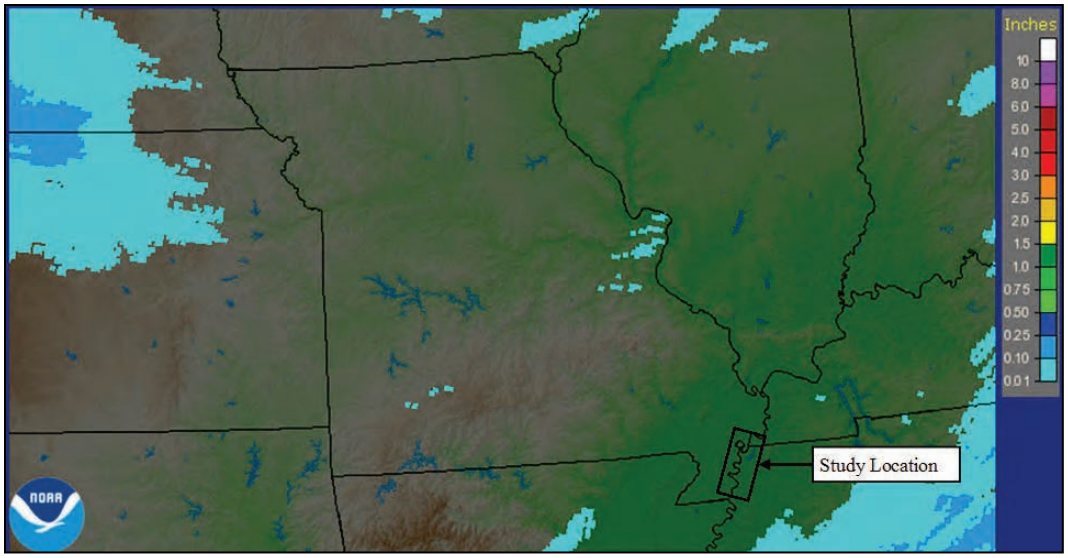


Figure C-10. 24 Dec 2013 observed precipitation.

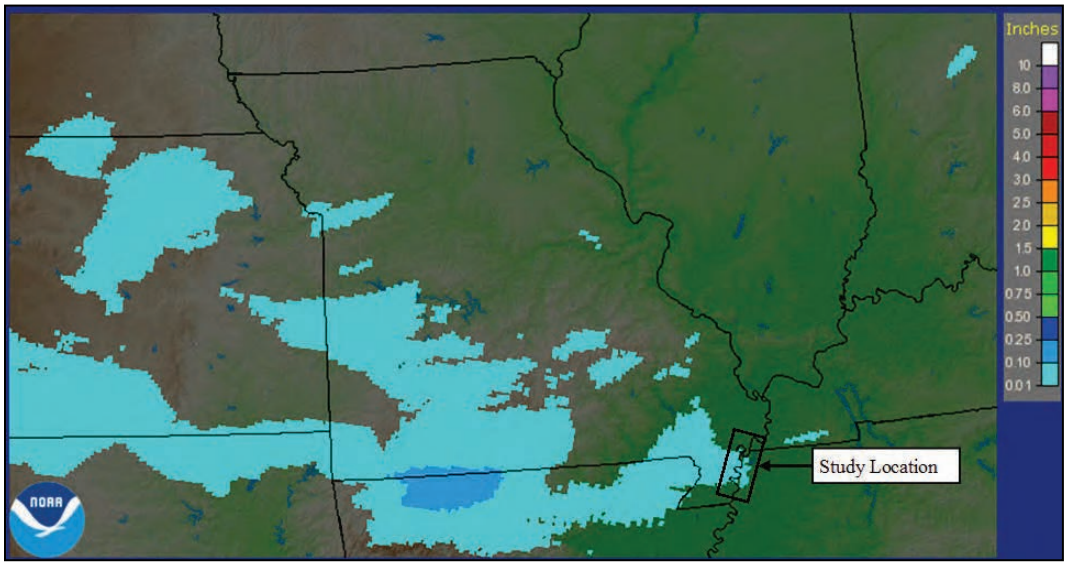


Figure C-11. WSEL calibration—MS116 Event 3.

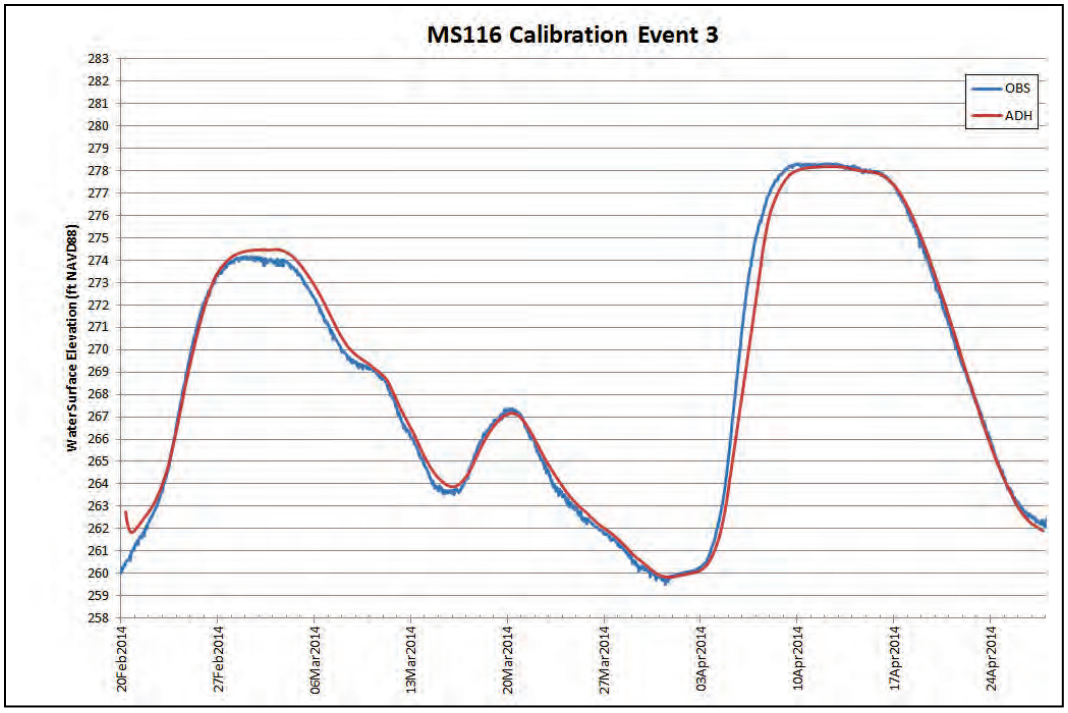


Figure C-12. WSEL calibration—MS117 Event 3.

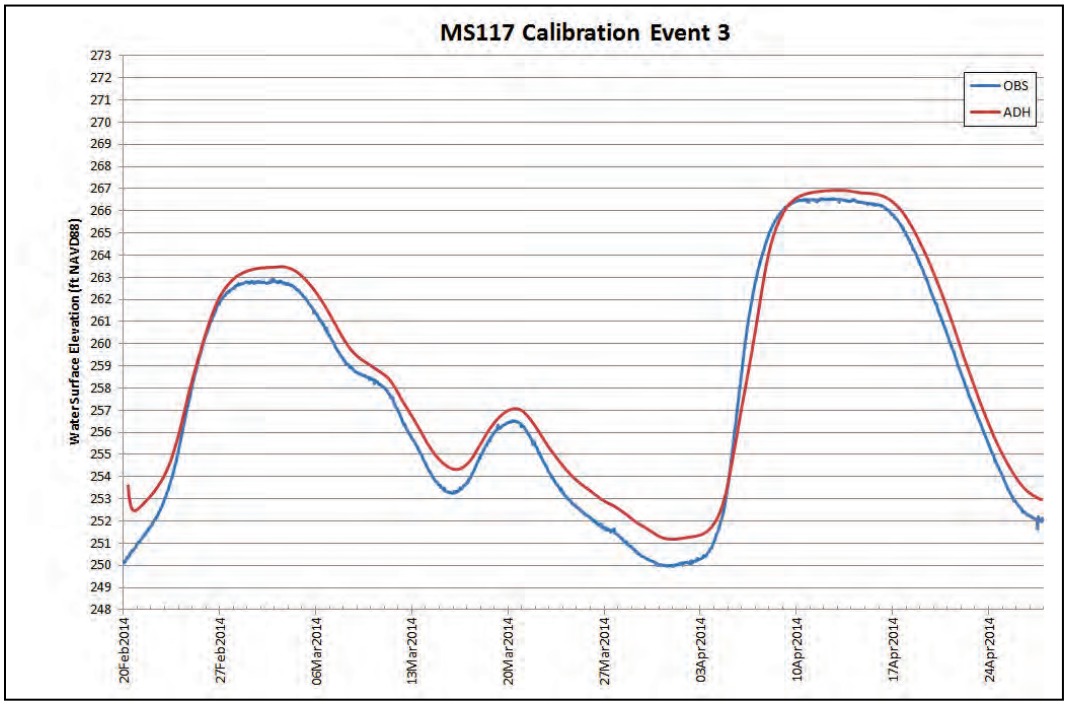


Figure C-13. Velocity calibration—8 May 2013 velocity difference.

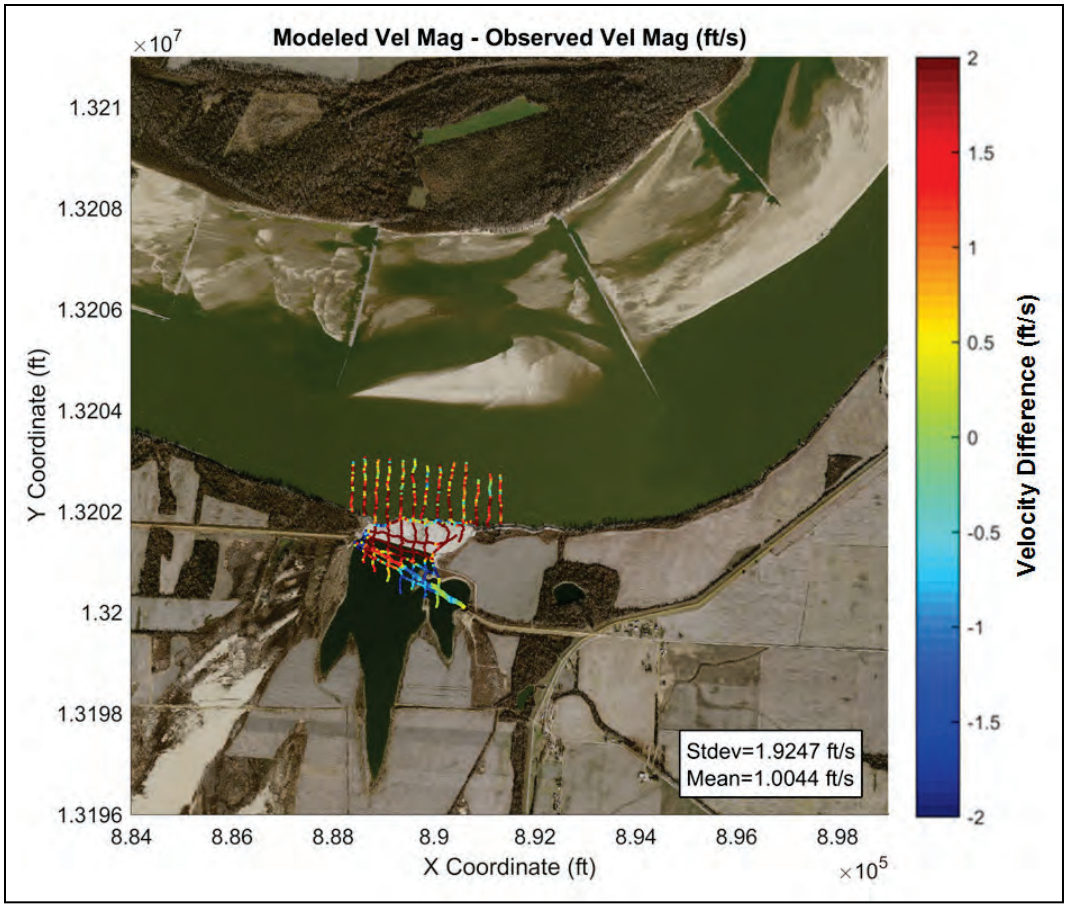


Figure C-14. Velocity calibration—8 May 2013 modeled vs. observed.

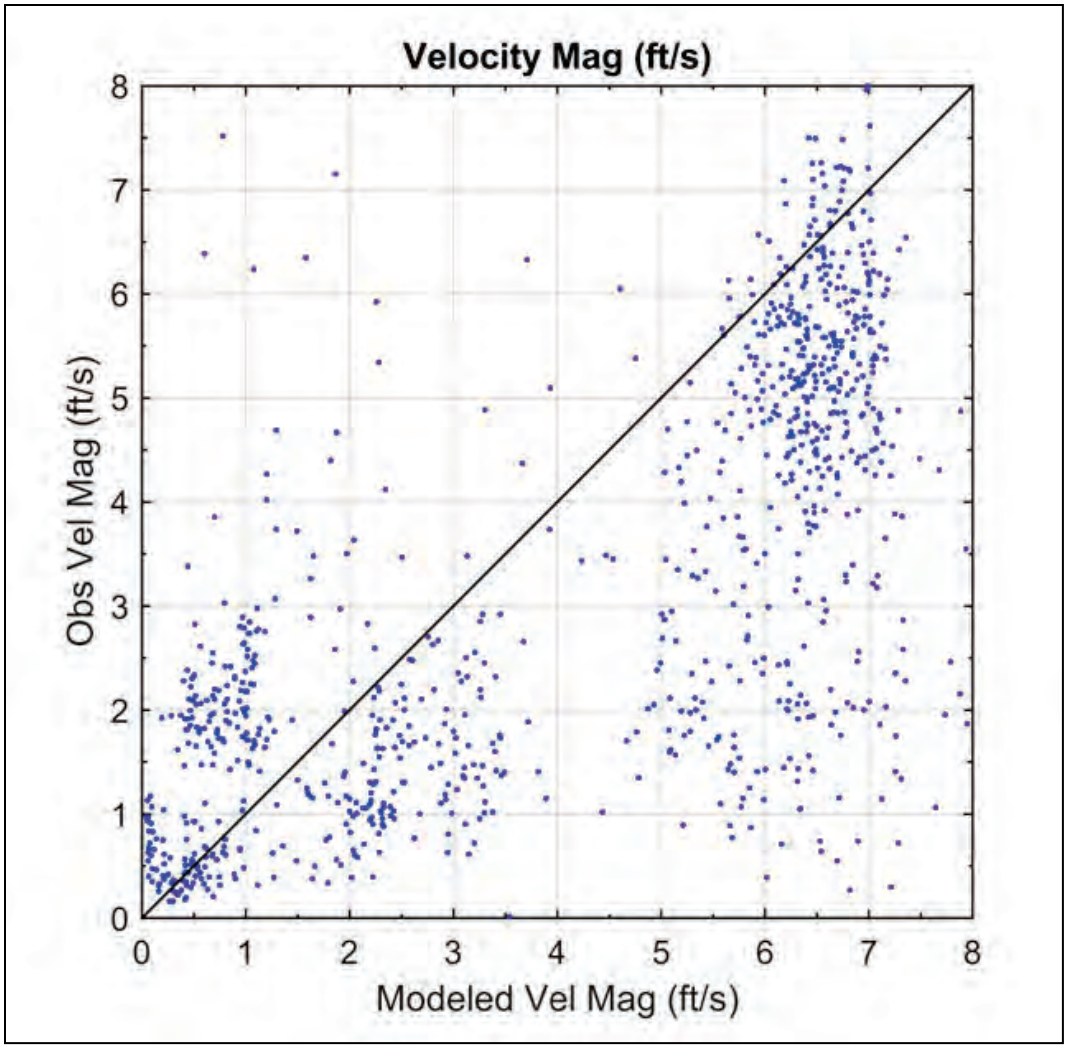


Figure C-15. Velocity calibration—19 Dec 2013 velocity difference.

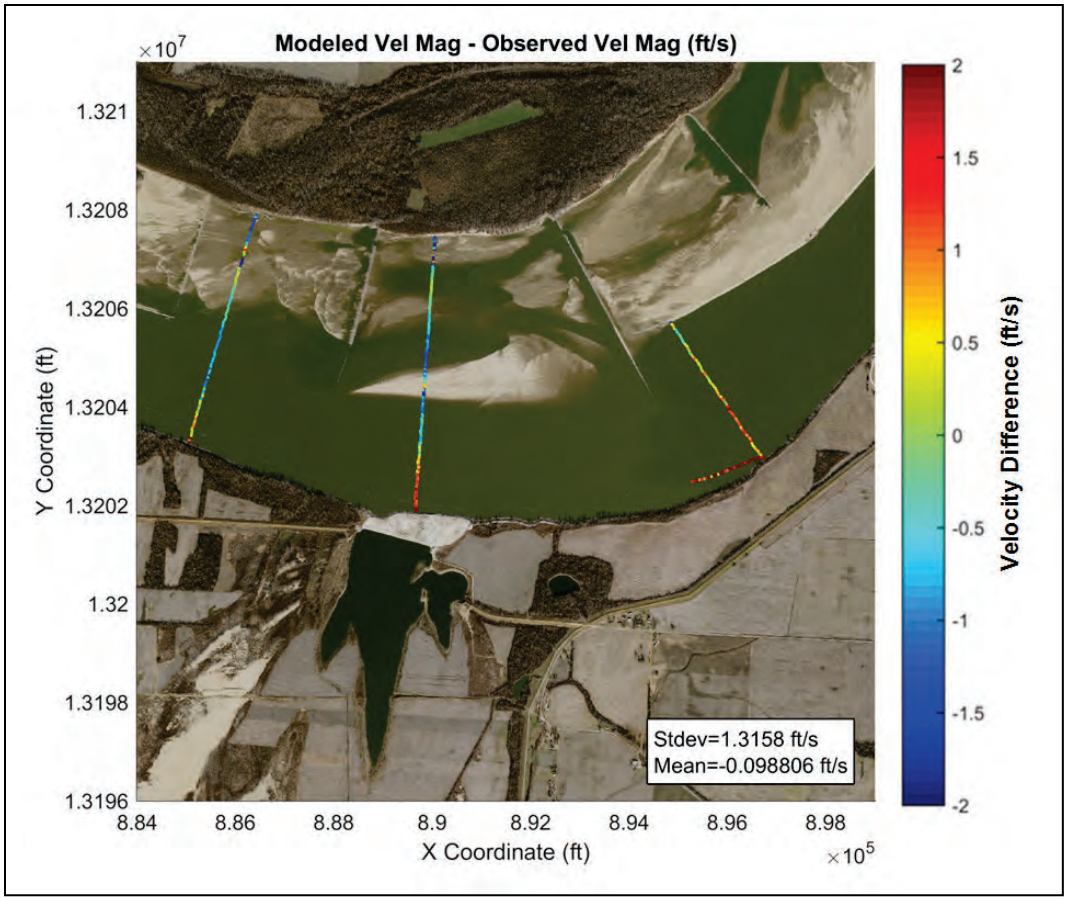


Figure C-16. Velocity calibration—19 Dec 2013 modeled vs. observed.

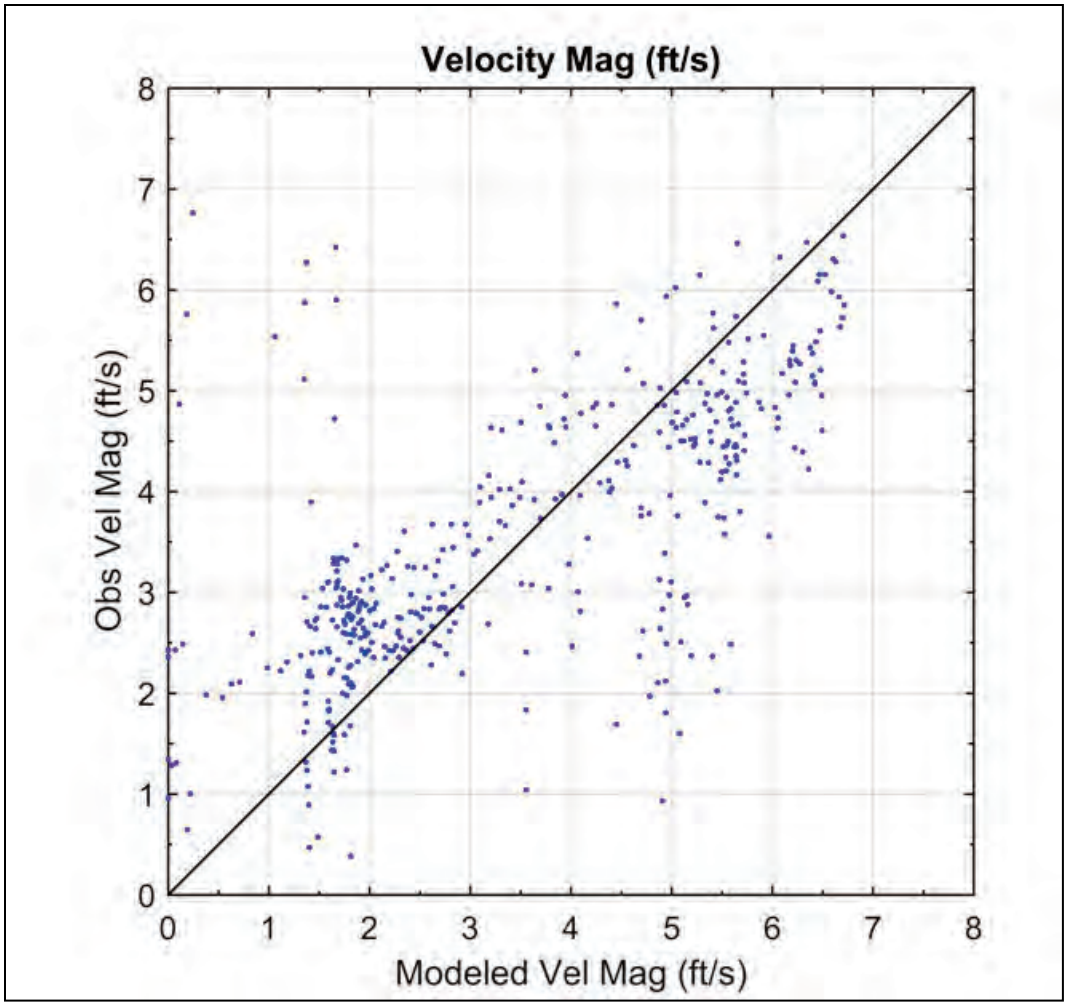


Figure C-17. Velocity calibration—28 Feb 2014 Dataset 1 velocity difference.

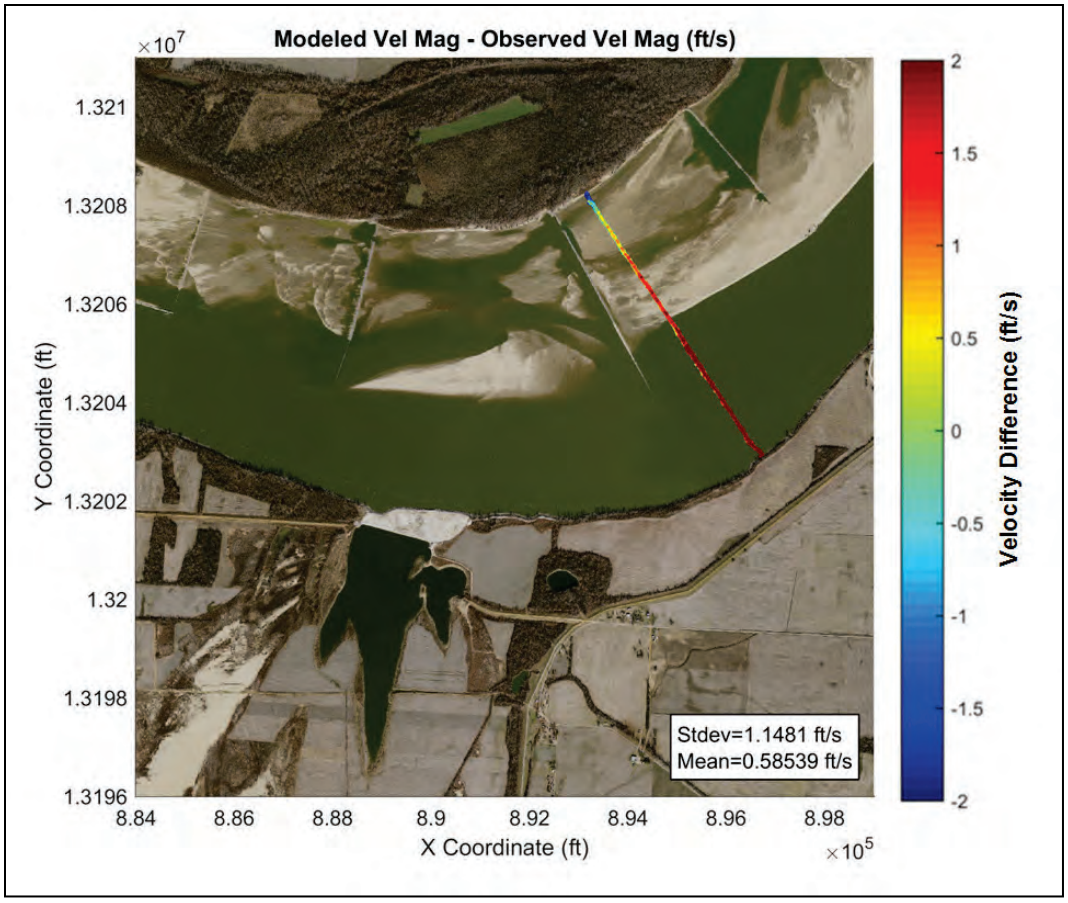


Figure C-18. Velocity calibration—28 Feb 2014 Dataset 1 modeled vs. observed.

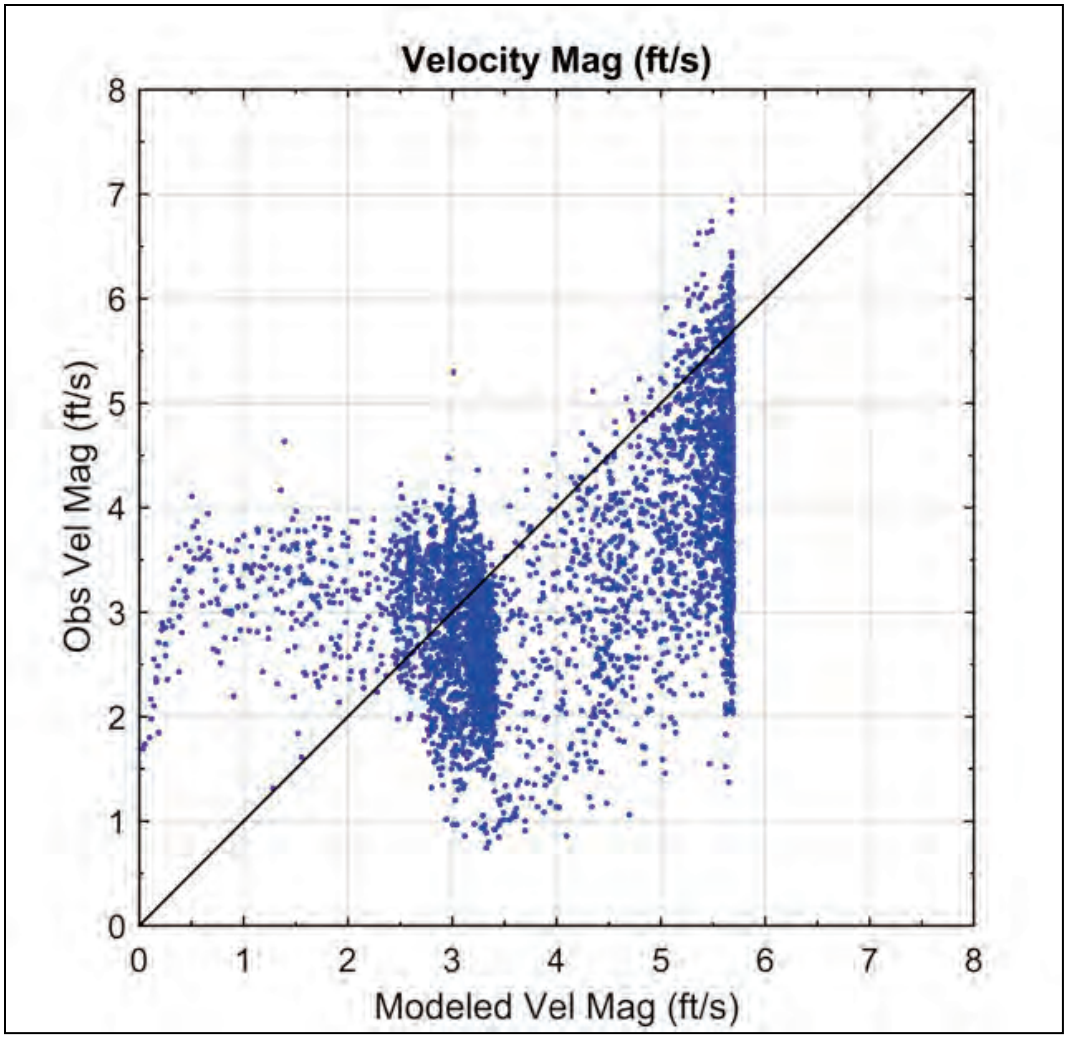


Figure C-19. Velocity calibration—28 Feb 2014 Dataset 2 velocity difference.

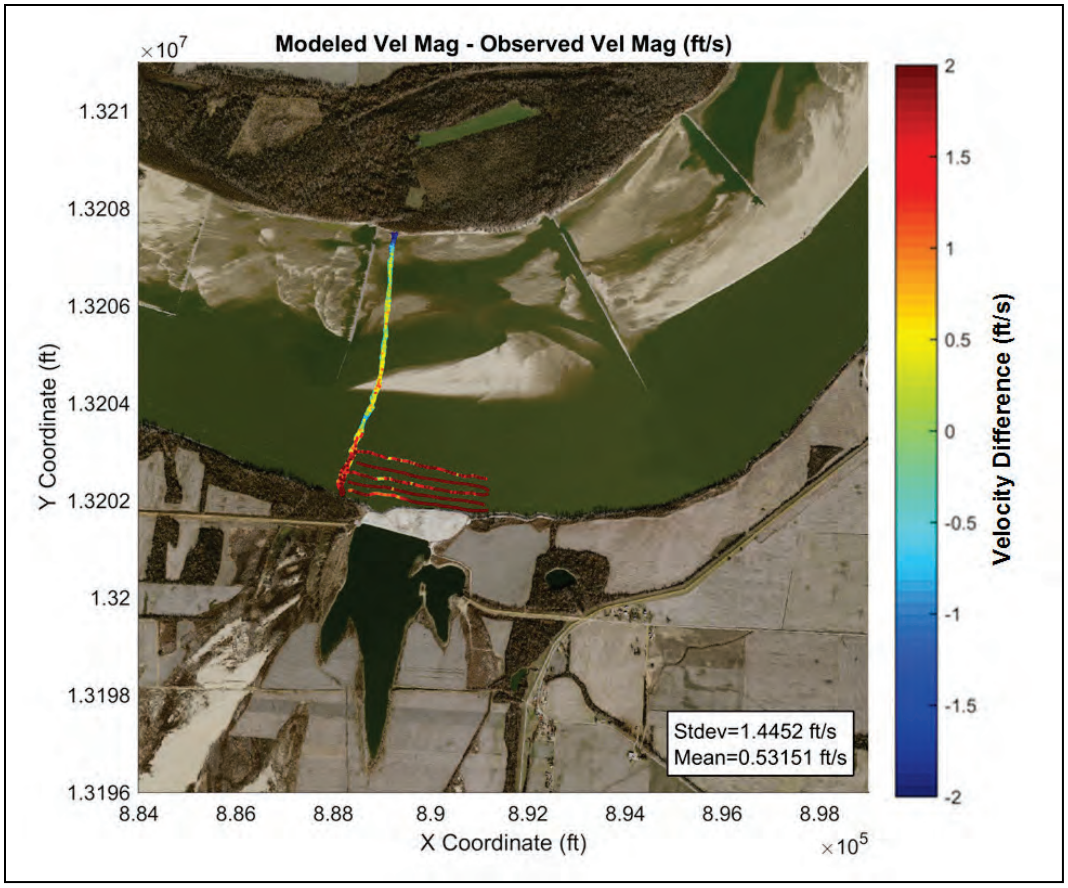


Figure C-20. Velocity calibration—28 Feb 2014 Dataset 2 modeled vs. observed.

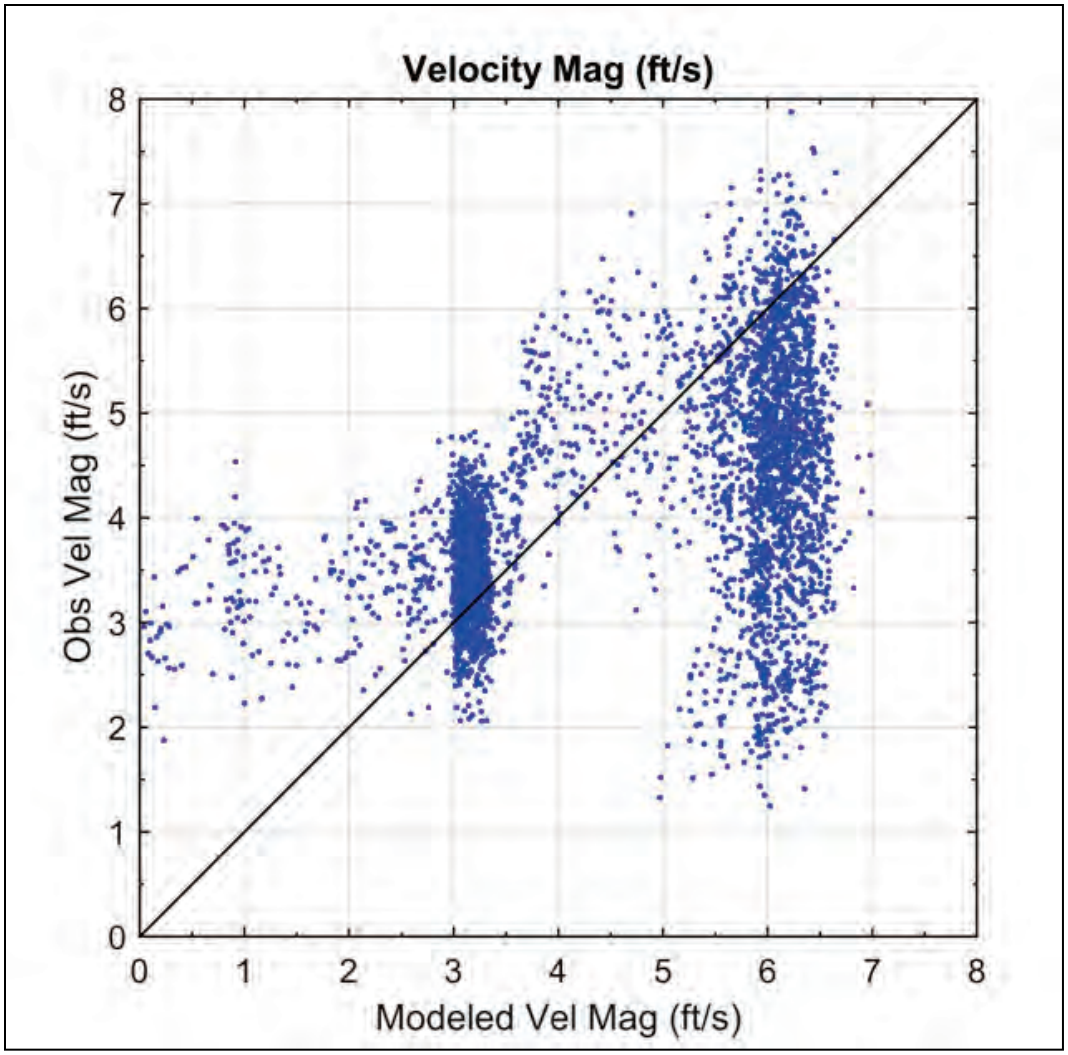


Figure C-21. Velocity calibration—28 Feb 2014 Dataset 3 velocity difference.

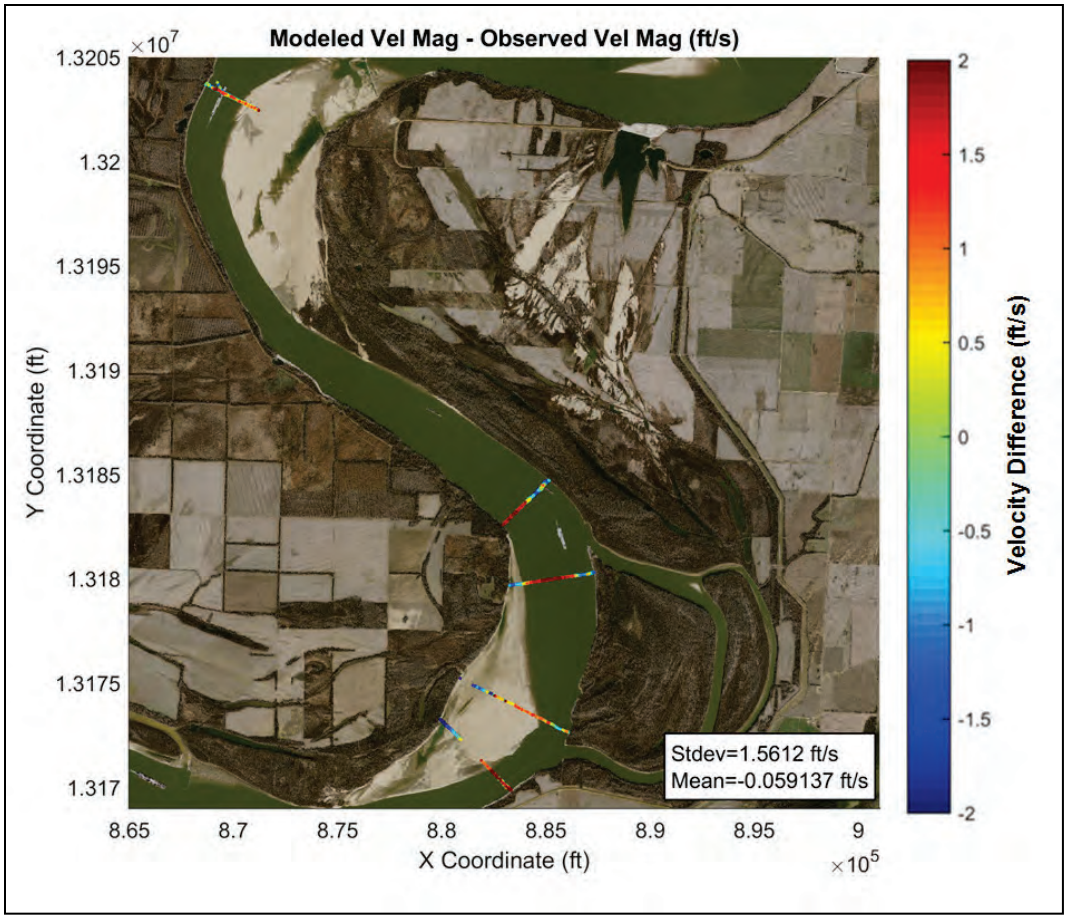


Figure C-22. Velocity calibration—28 Feb 2014 Dataset 3 modeled vs. observed.

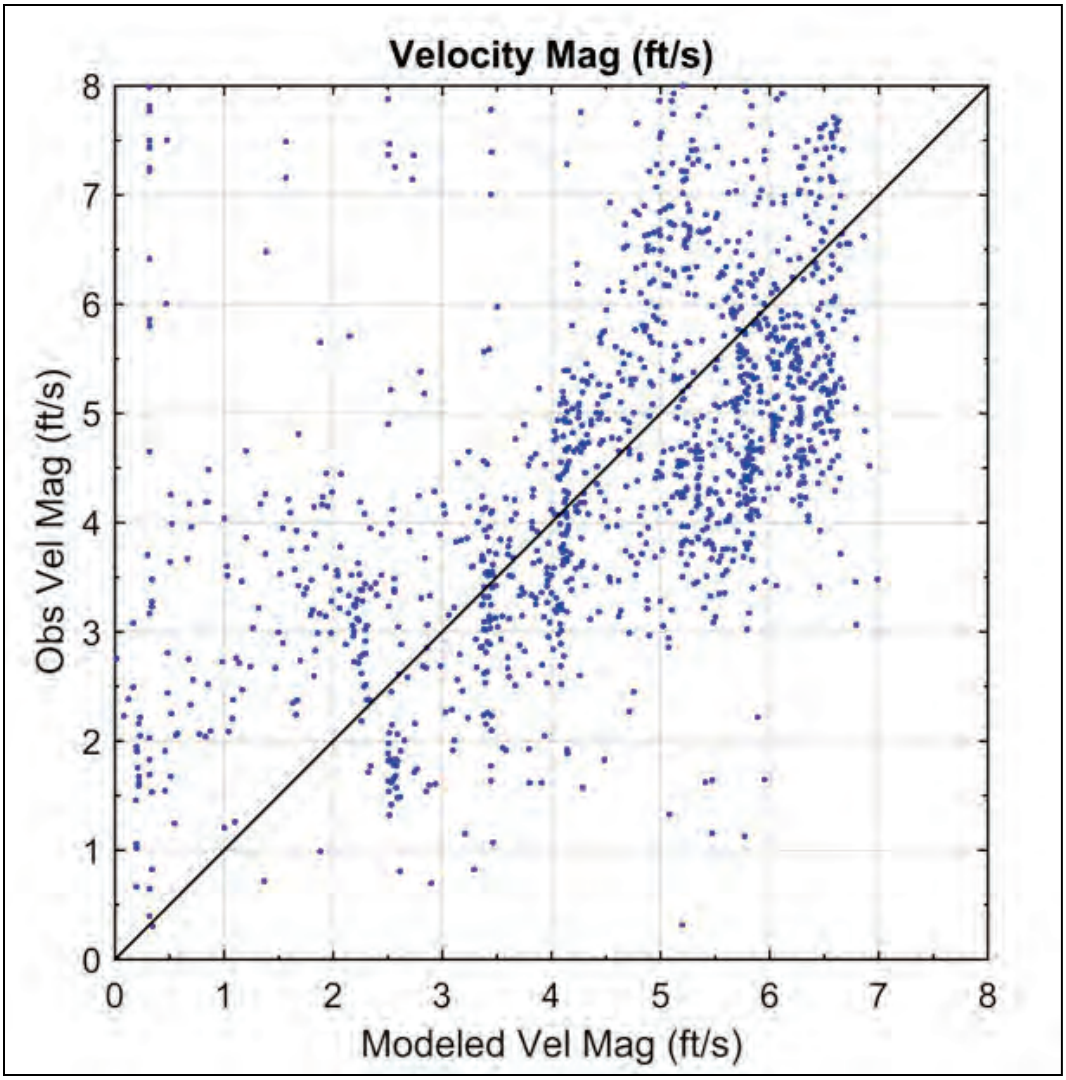


Figure C-23. Velocity calibration—9 Apr 2014 Dataset 1 velocity difference.

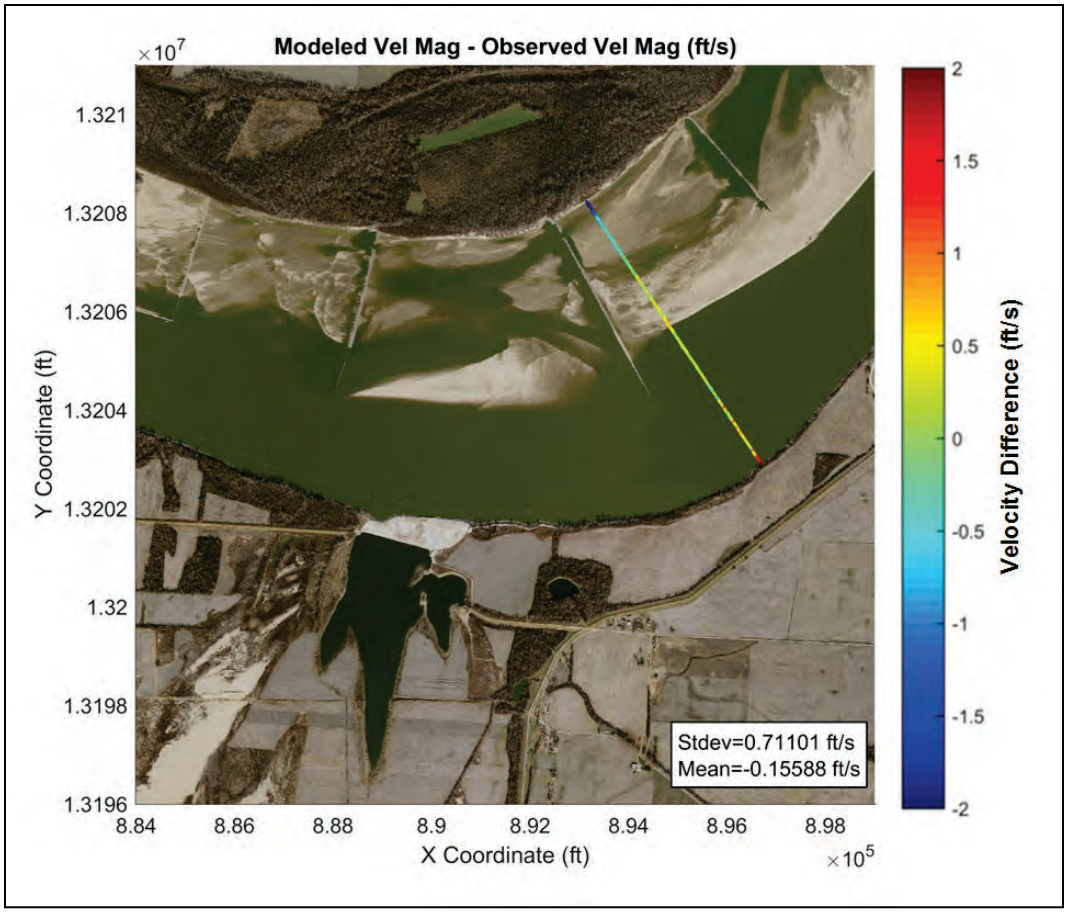


Figure C-24. Velocity calibration—9 Apr 2014 Dataset 1 modeled vs. observed.

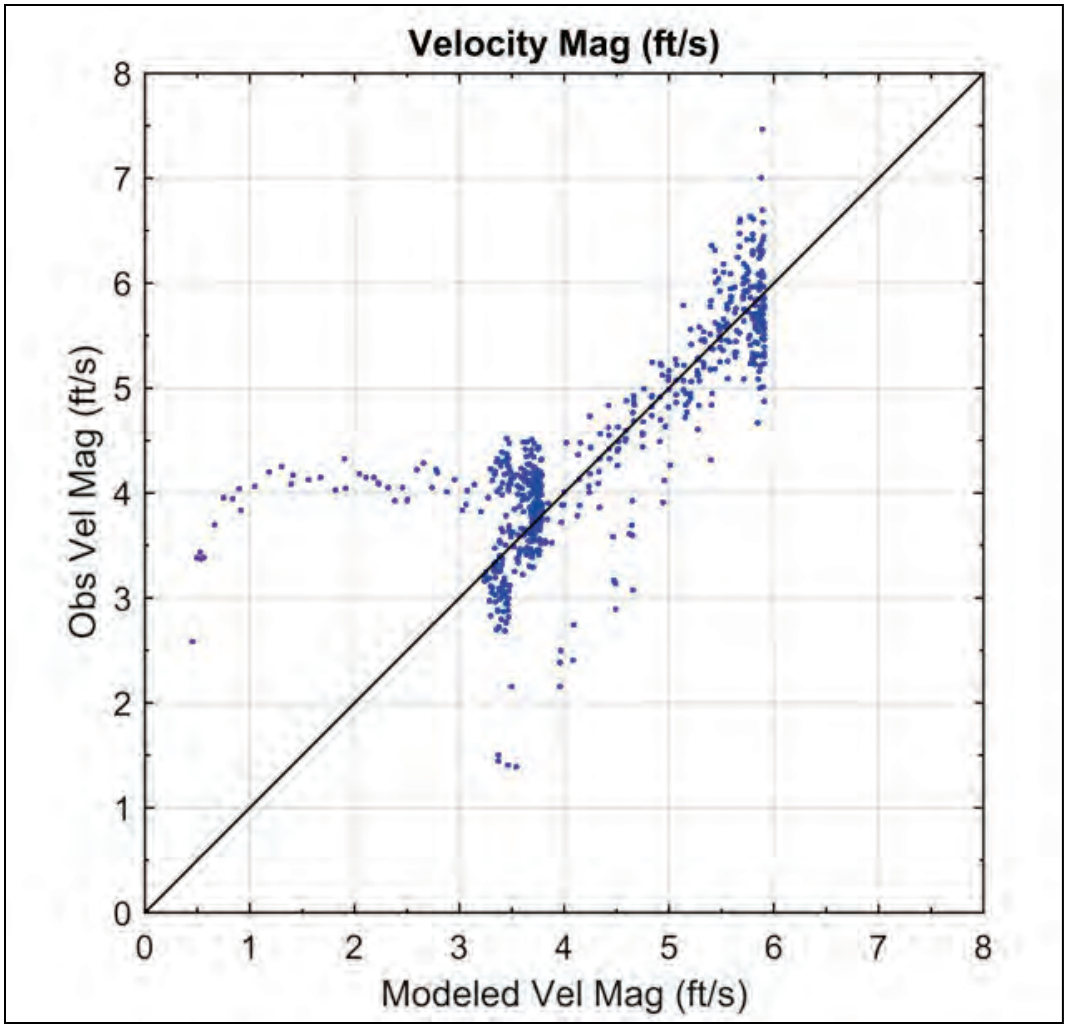


Figure C-25. Velocity calibration—9 Apr 2014 Dataset 2 velocity difference.

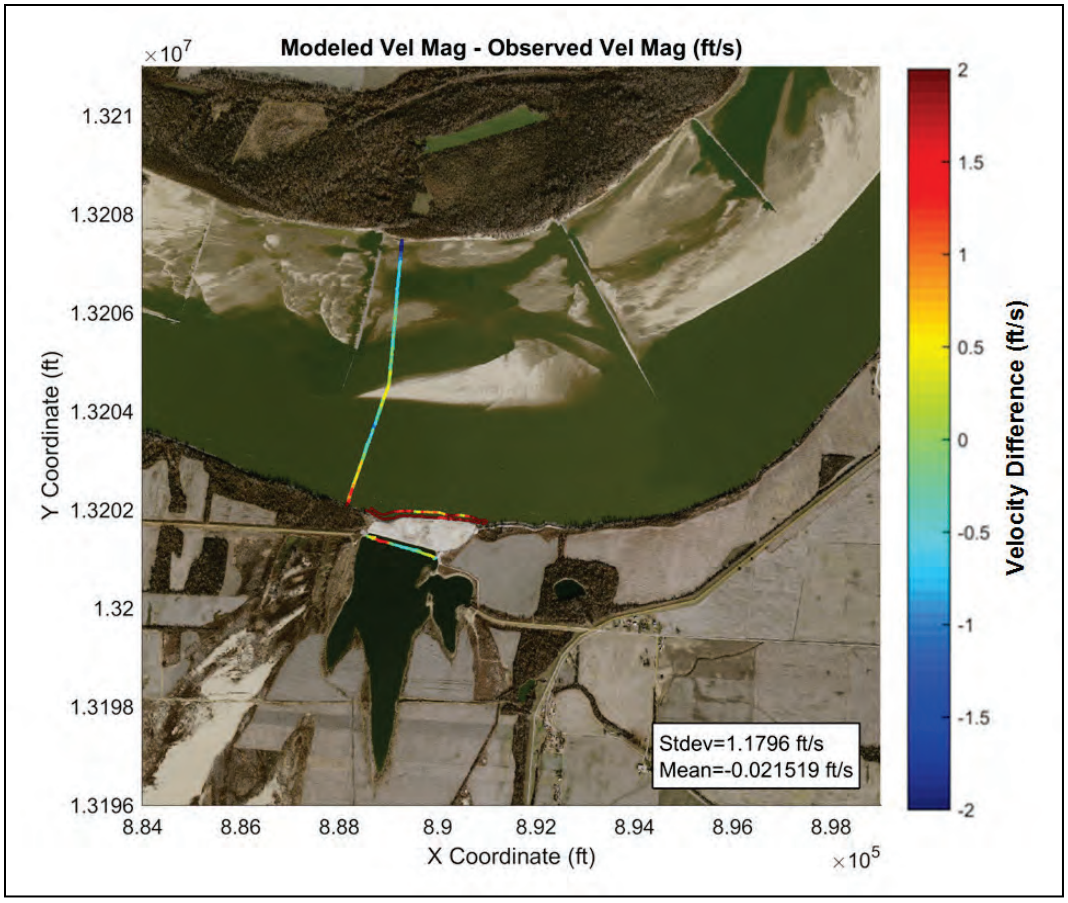


Figure C-26. Velocity calibration—9 Apr 2014 Dataset 2 modeled vs. observed.

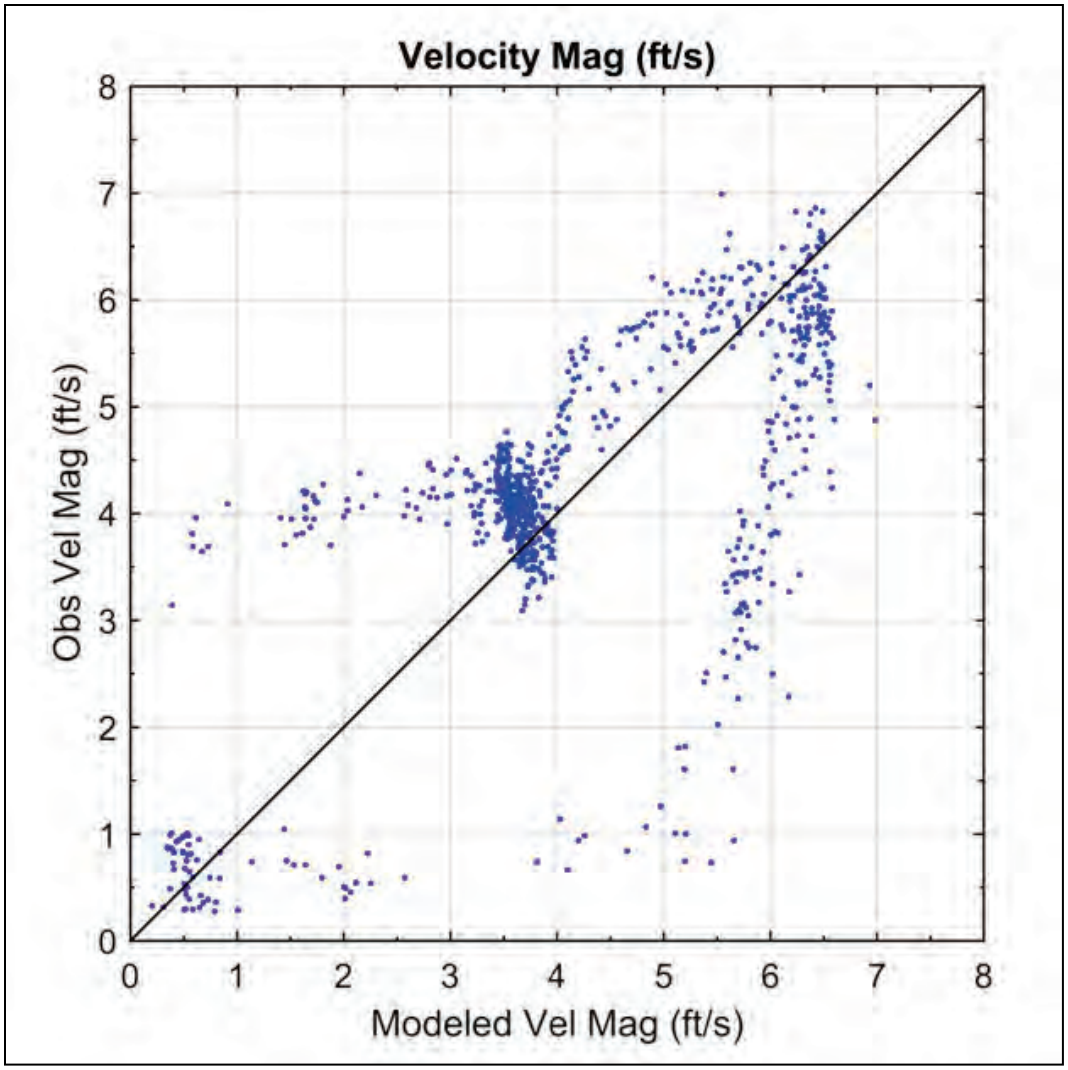


Figure C-27. Velocity calibration—9 Apr 2014 Dataset 3 velocity difference.

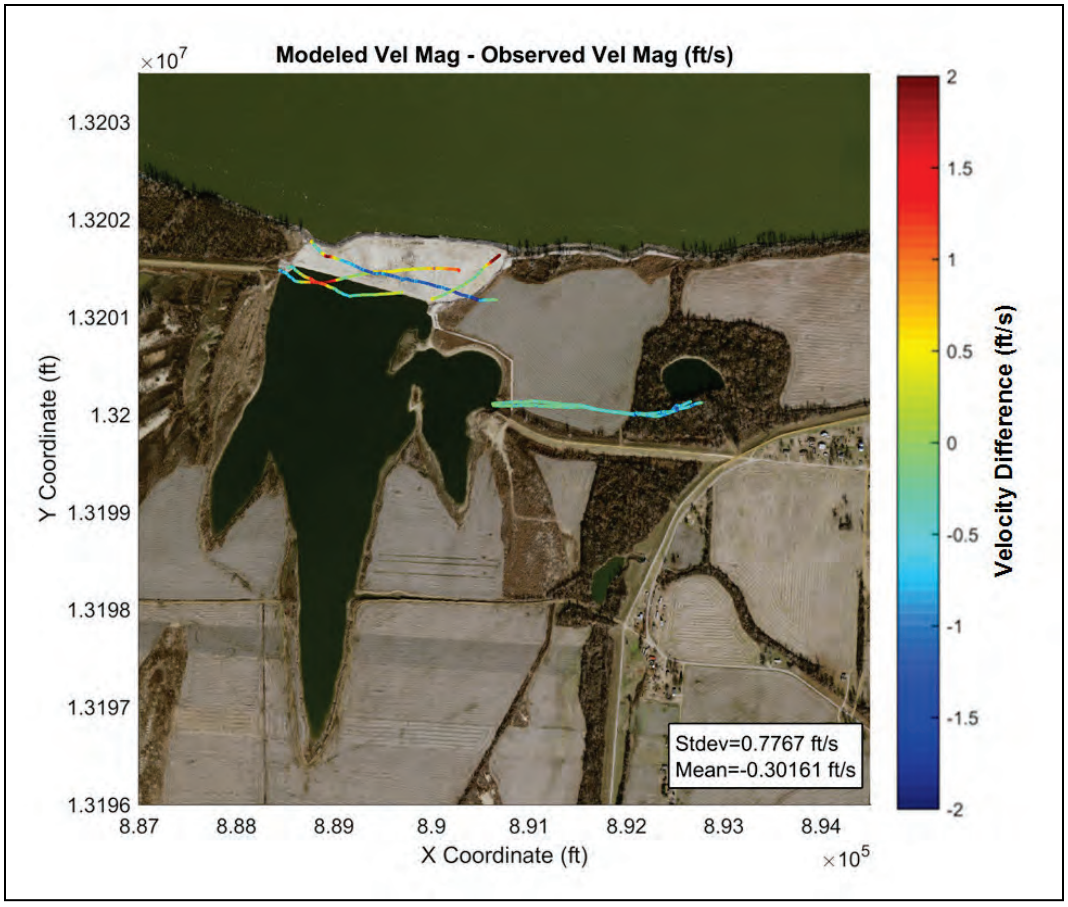


Figure C-28. Velocity calibration—9 Apr 2014 Dataset 3 modeled vs. observed.

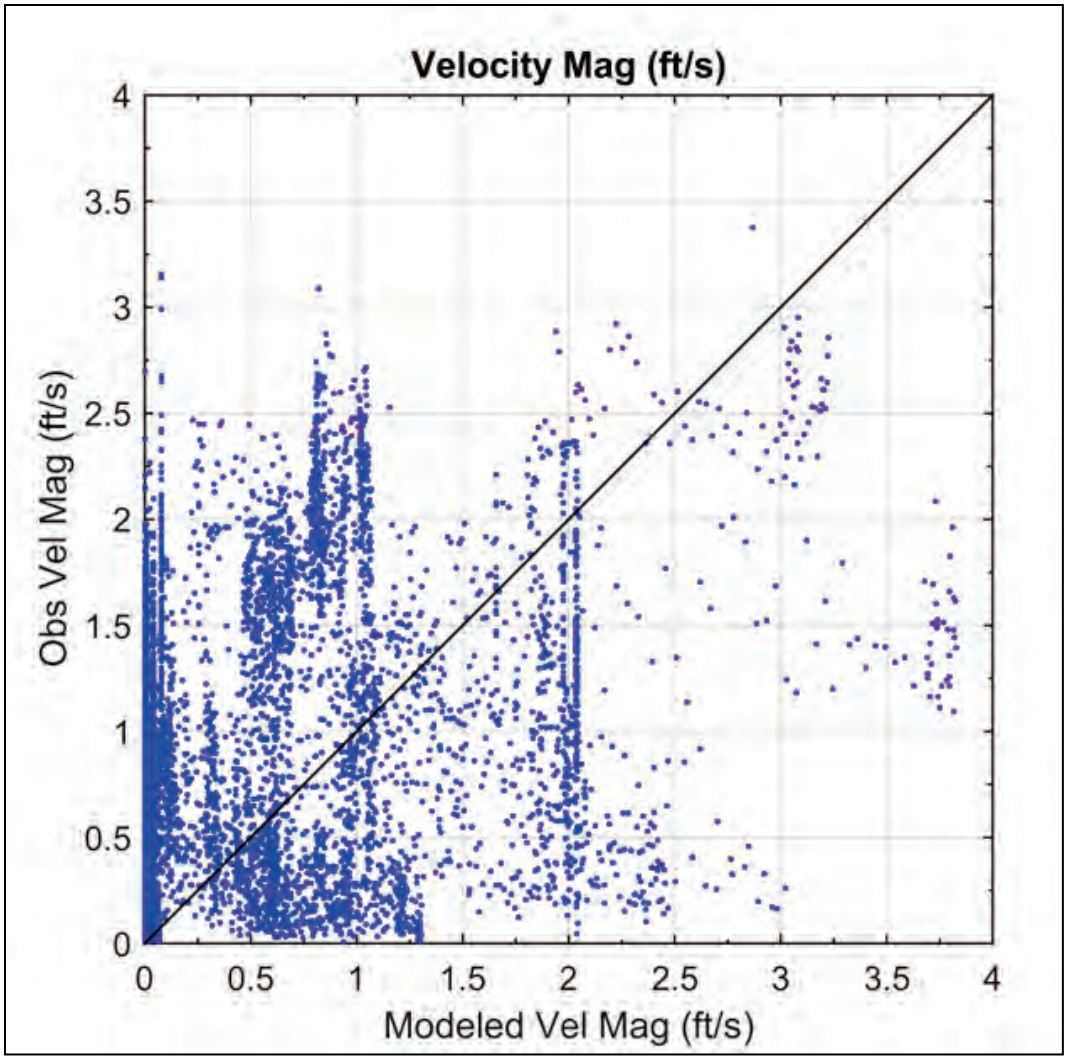


Figure C-29. WSEL validation—MS116.

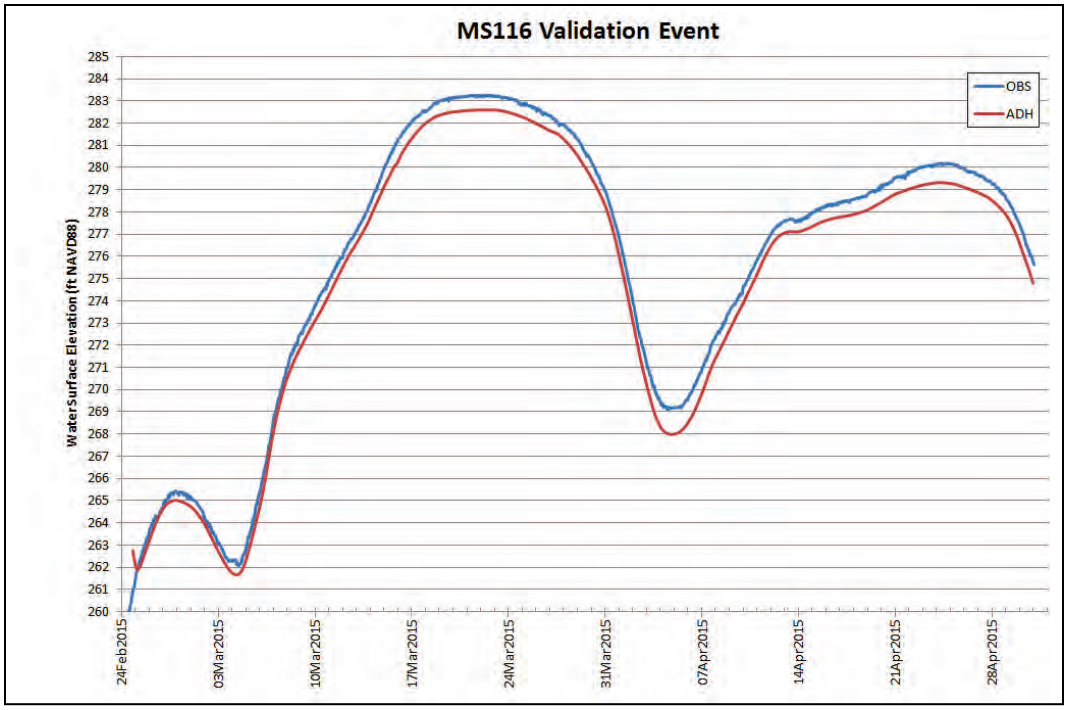
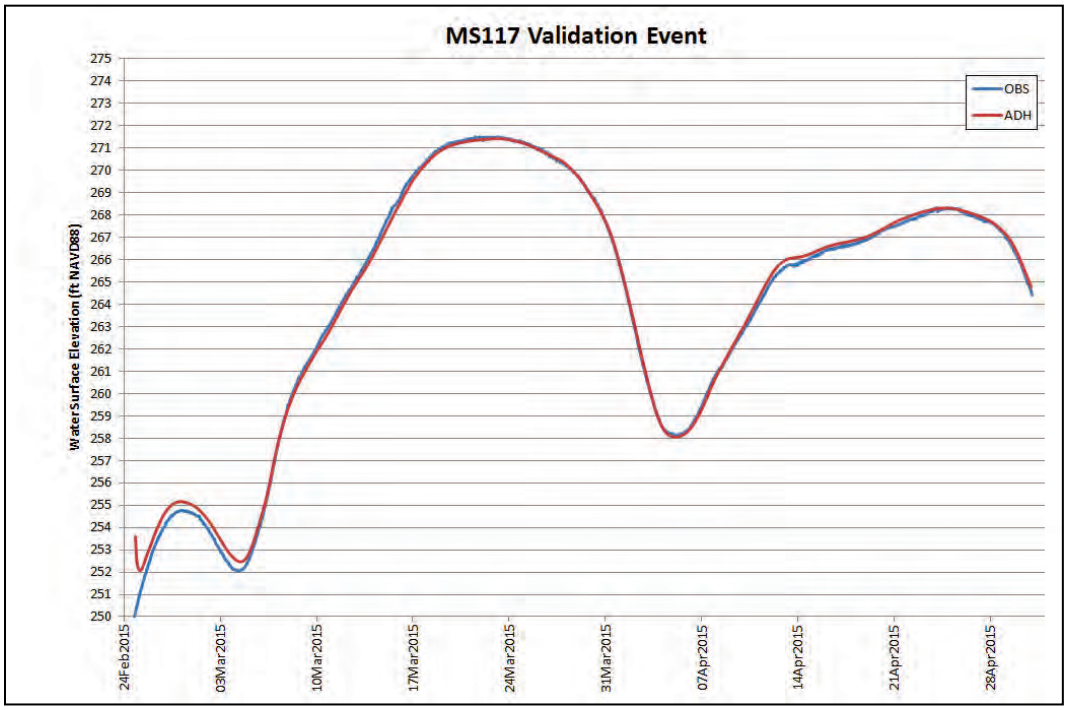


Figure C-30. Water Surface Elevation Validation—MS117



Bed sediment initialization

Figures C-31 through C-40 depict the observed versus modeled bed particle size distribution for the d16, d25, d50, and d75 (spatially and graphically) for the bed sediment initialization.

Figure C-31. Bed sediment initialization—d16 difference.

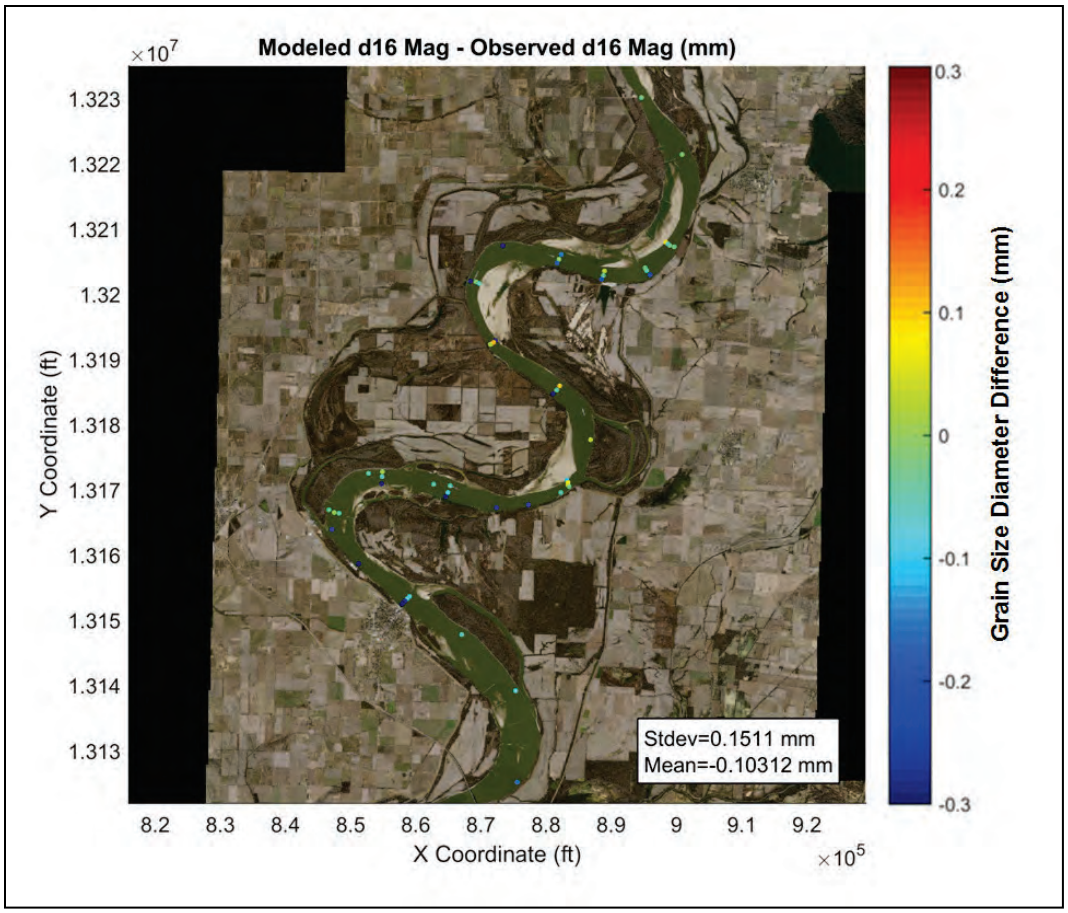


Figure C-32. Bed sediment initialization—d16 modeled vs. observed.

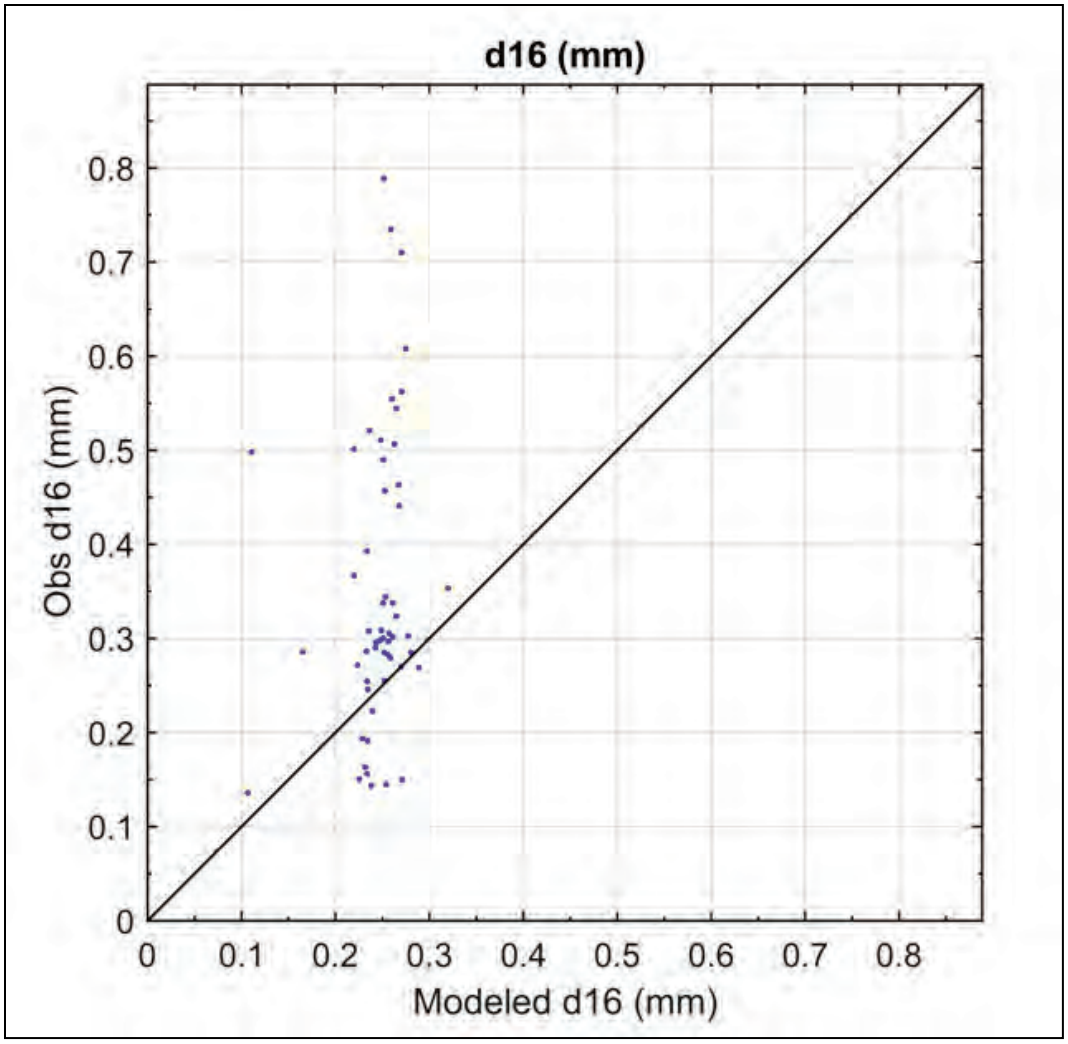


Figure C-33. Bed sediment initialization—d25 difference.

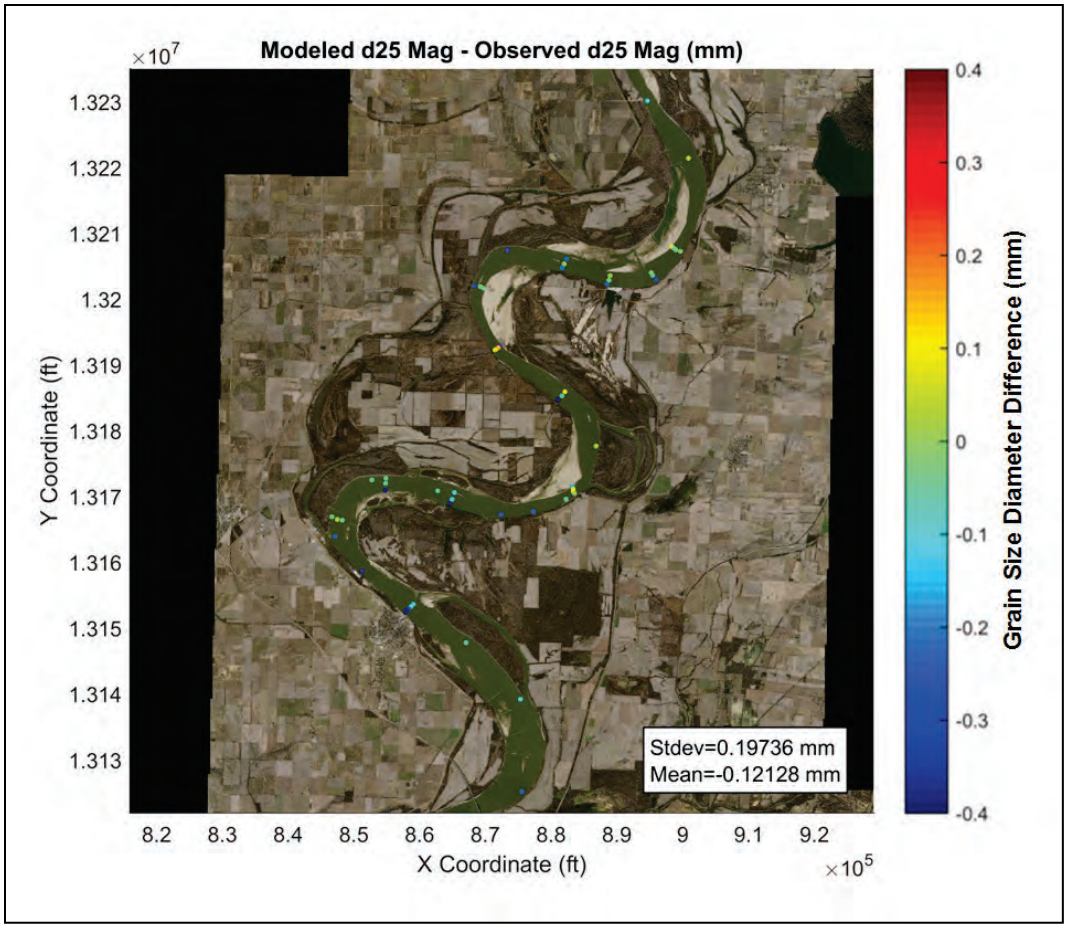


Figure C-34. Bed sediment initialization—d25 modeled vs. observed.

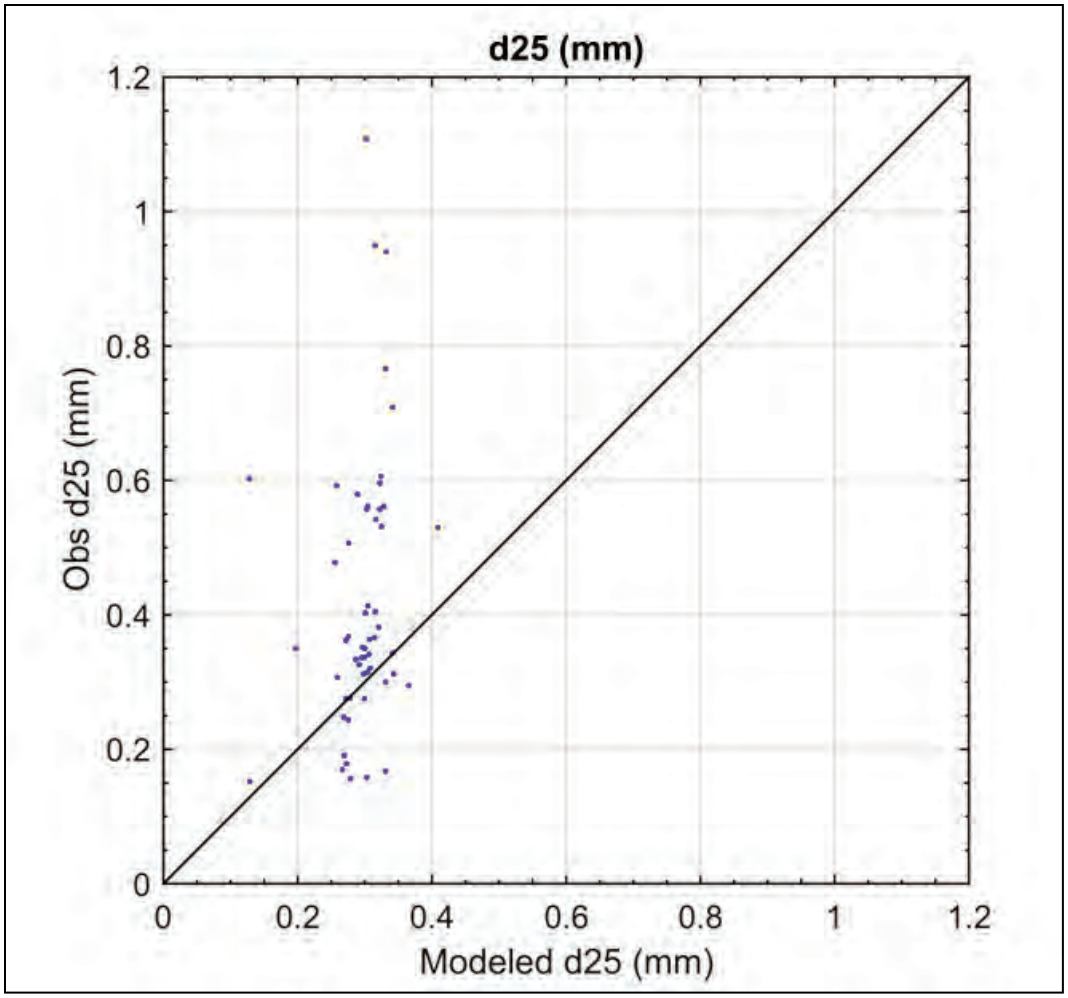


Figure C-35. Bed sediment initialization—d50 difference.

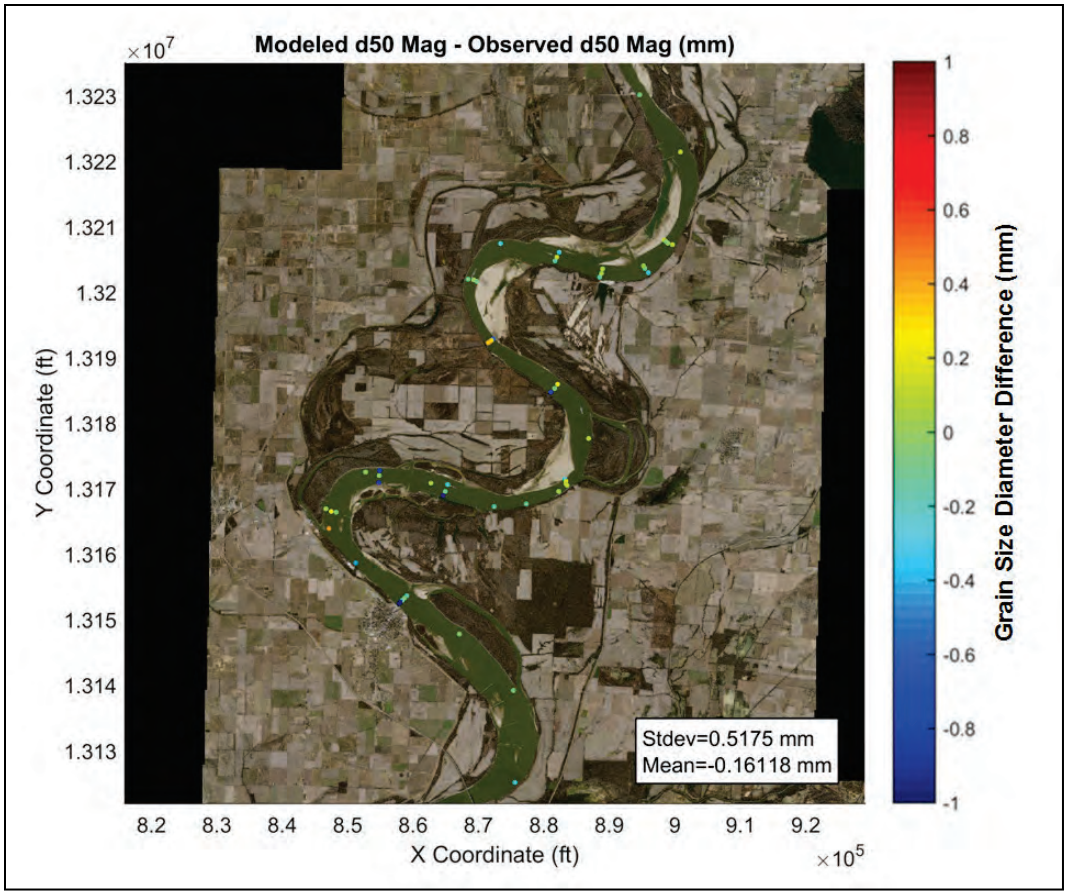


Figure C-36. Bed sediment initialization—d50 modeled vs. observed.

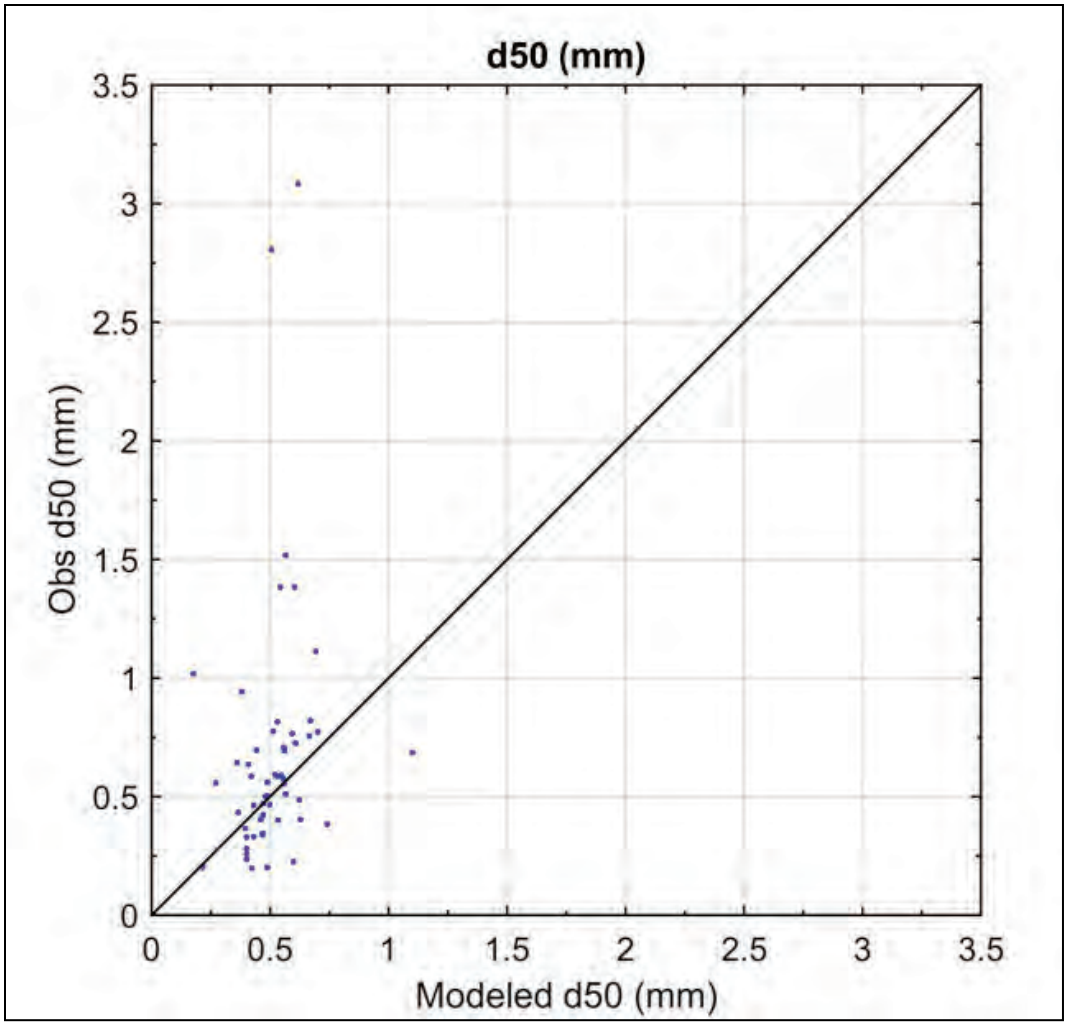


Figure C-37. Bed sediment initialization—d75 difference.

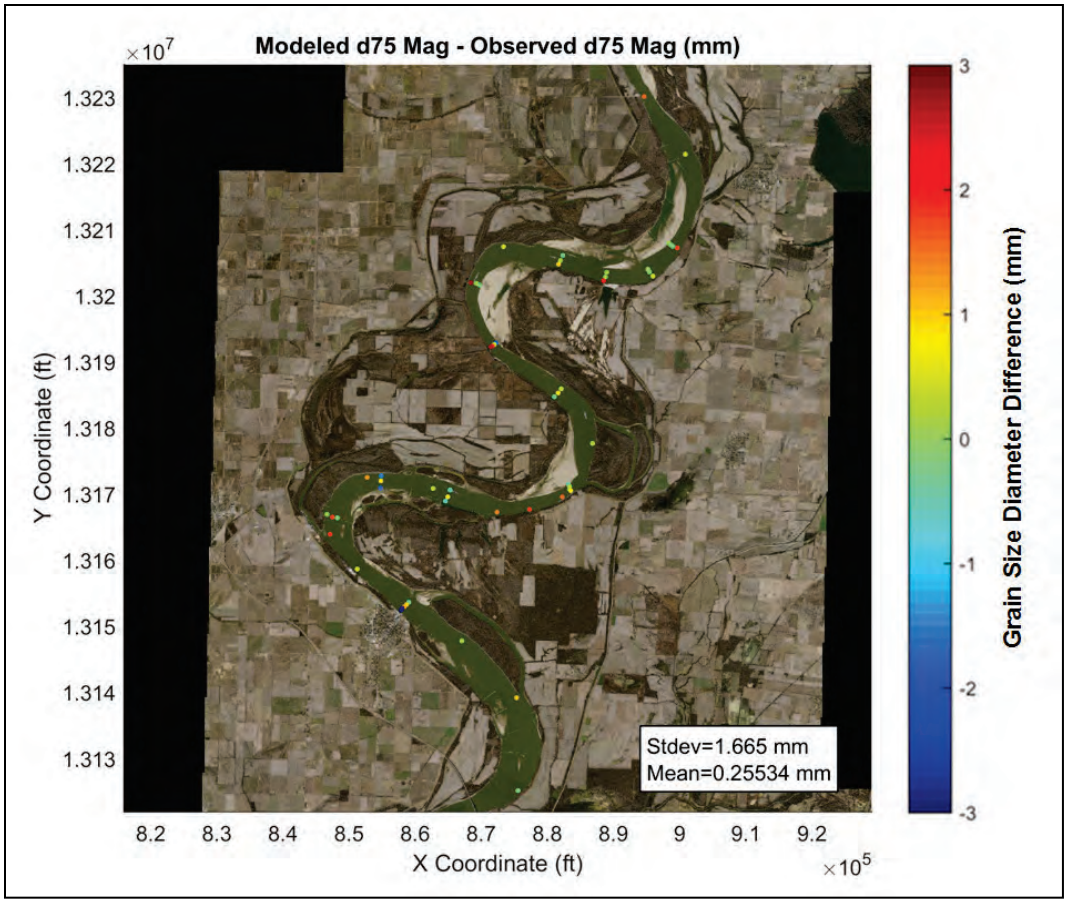


Figure C-38. Bed sediment initialization—d75 modeled vs. observed.

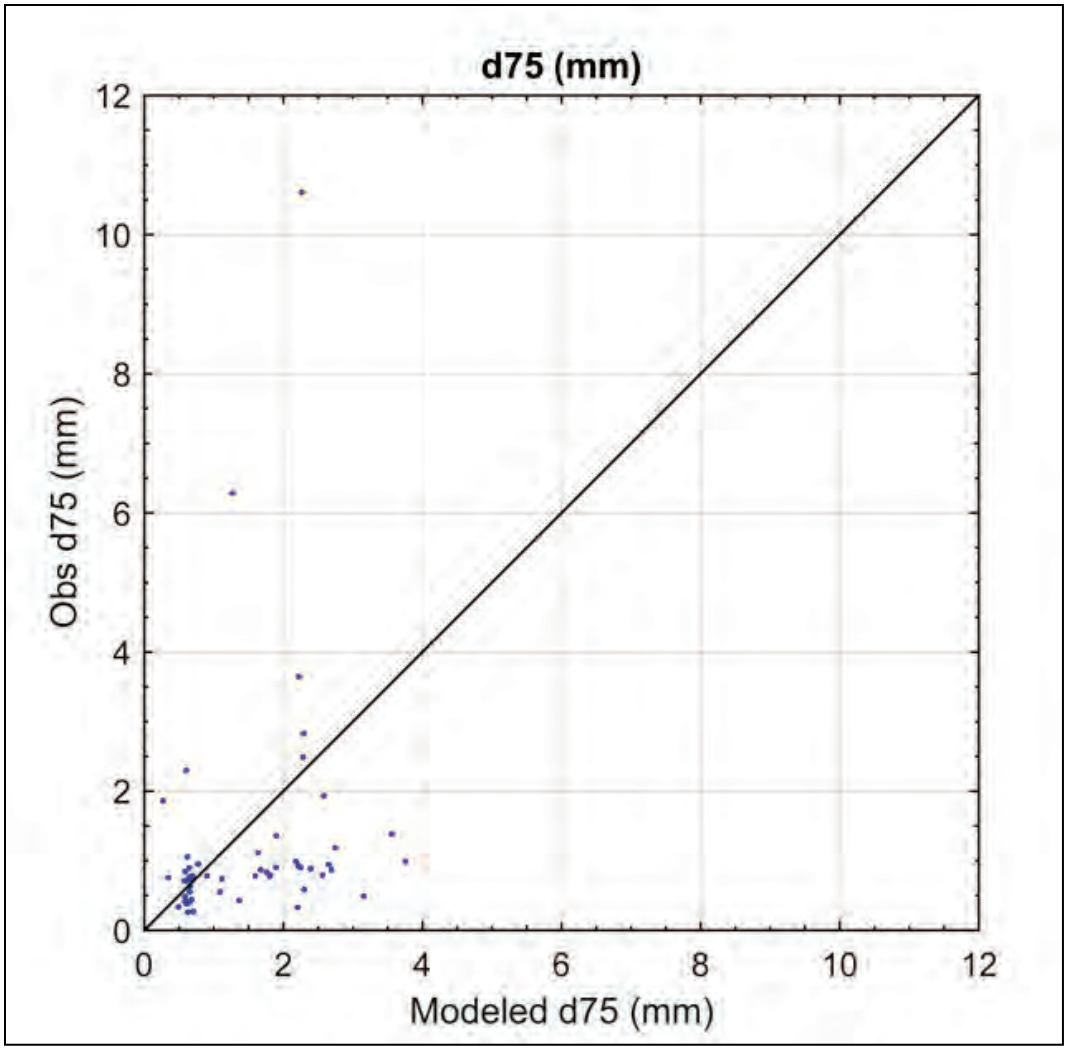


Figure C-39. Bed sediment initialization—d84 difference.

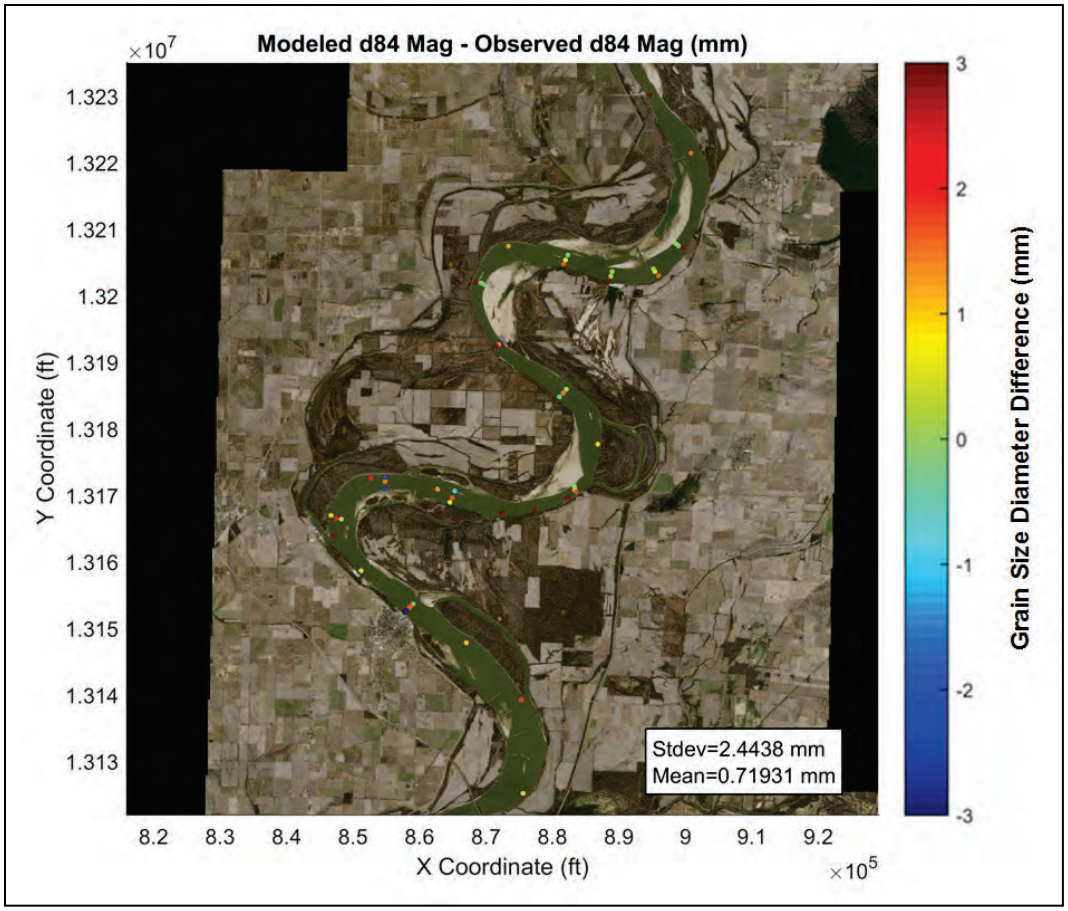
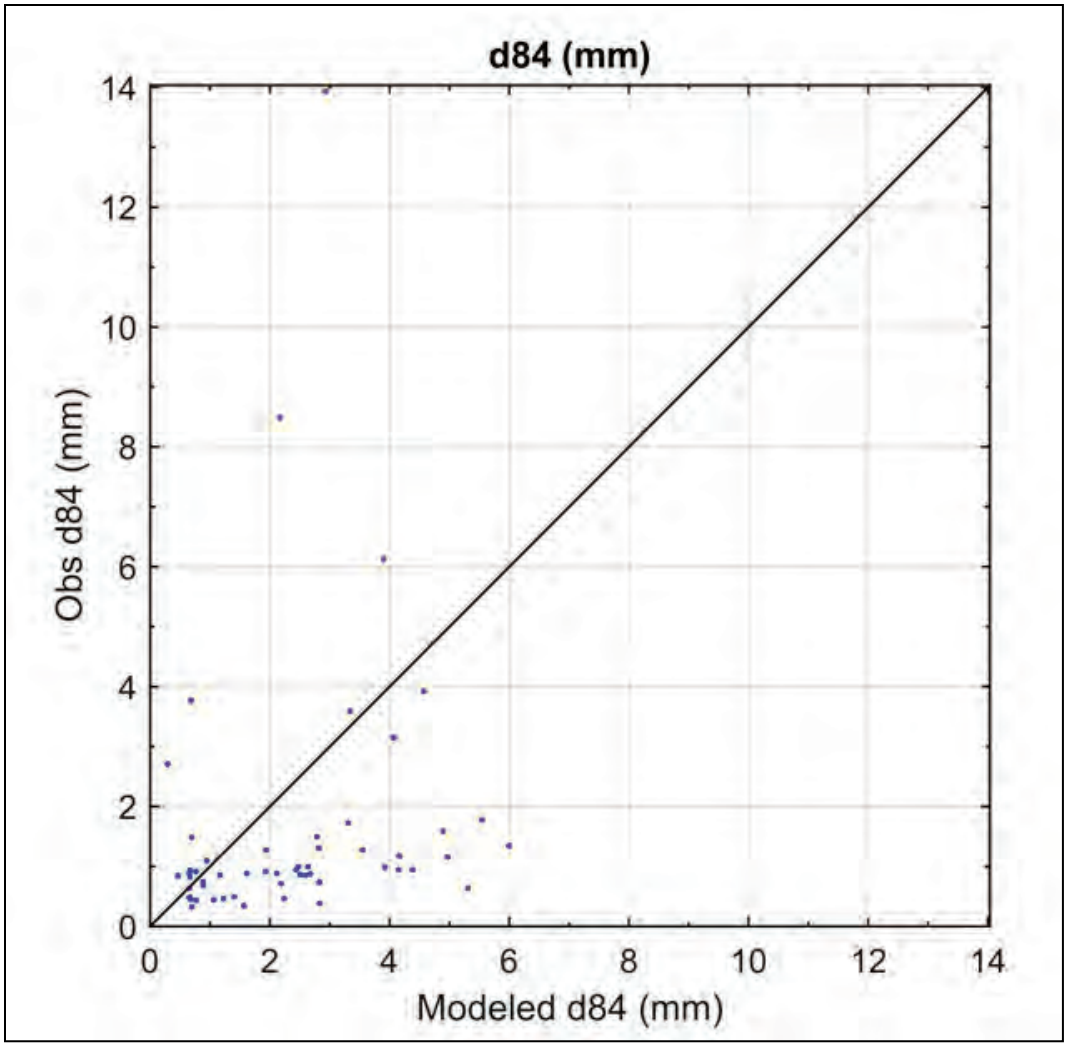


Figure C-40. Bed sediment initialization—d84 modeled vs. observed.



Velocity

The modeled velocity outputs at flows ranging from 400,000 to 2,100,000 cfs are depicted for following locations:

- Entire Model Domain: Figures C-41 through C-55
- Study Overbank: Figures C-56 through C-70
- Study Crevasse: Figures C-71 through C-85.

Figure C-41. Base condition velocity—400,000 cfs (entire model domain).

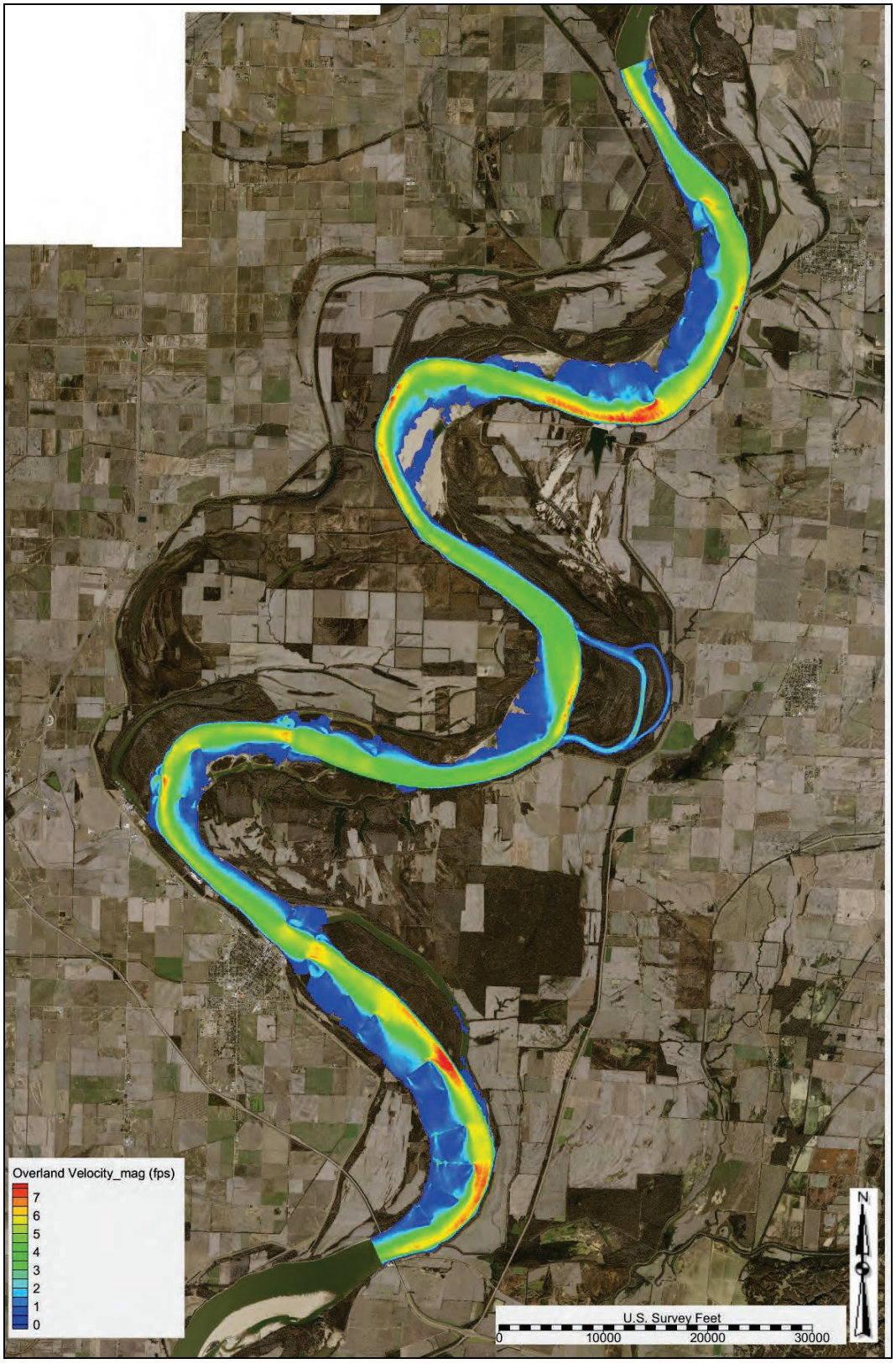


Figure C-42. Base condition velocity—500,000 cfs (entire model domain).

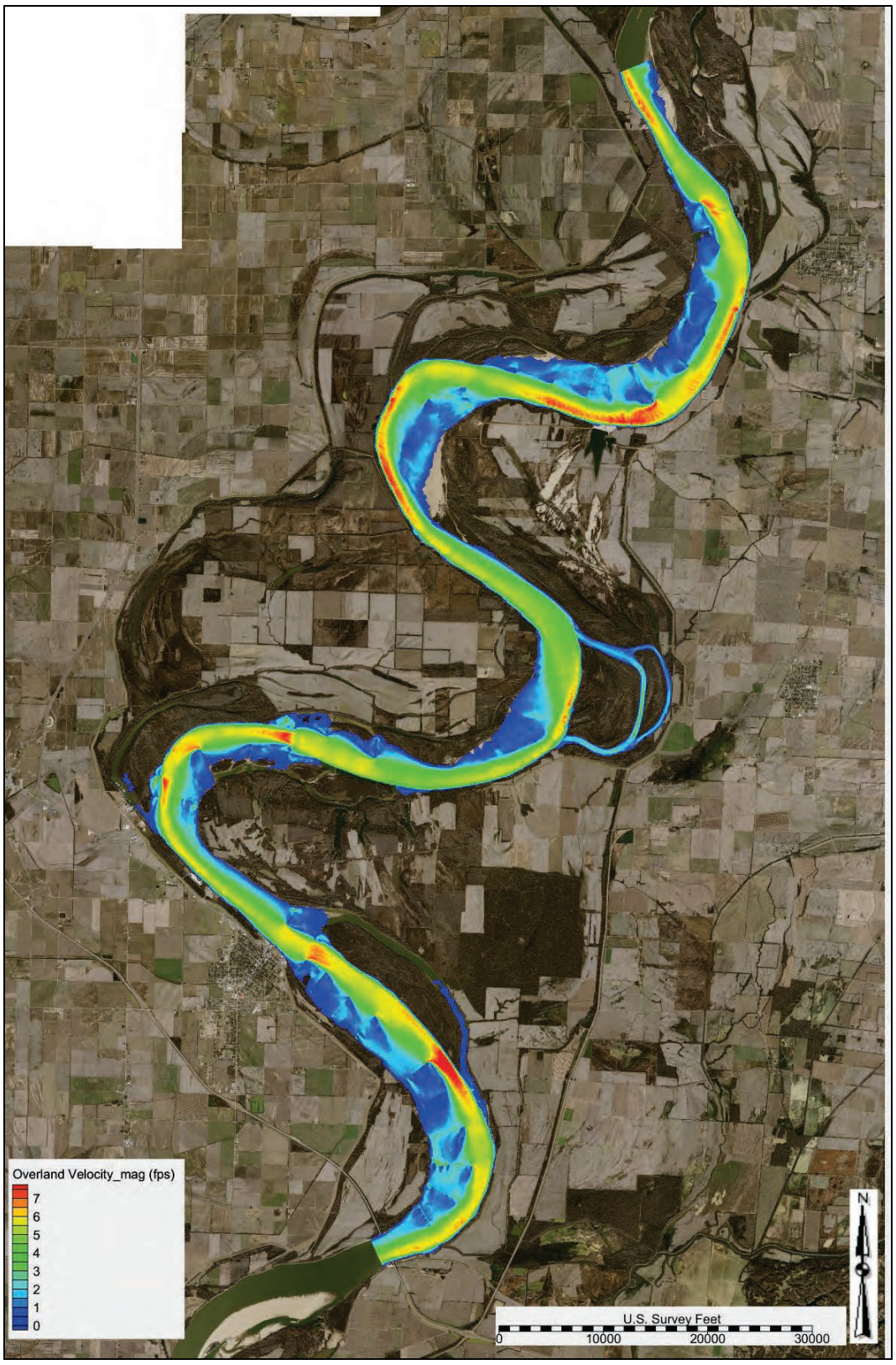


Figure C-43. Base condition velocity—600,000 cfs (entire model domain).

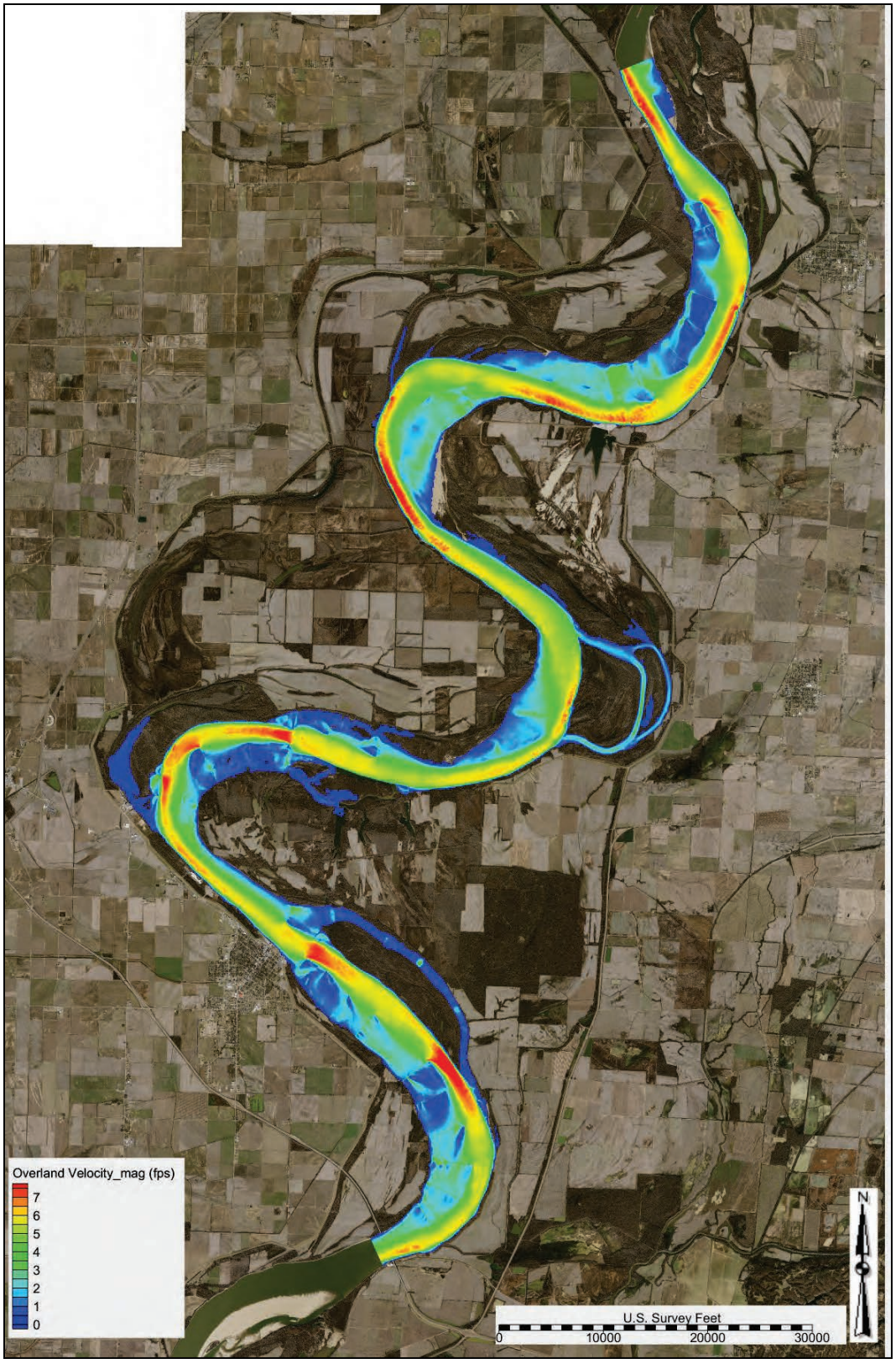


Figure C-44. Base condition velocity—650,000 cfs (entire model domain).

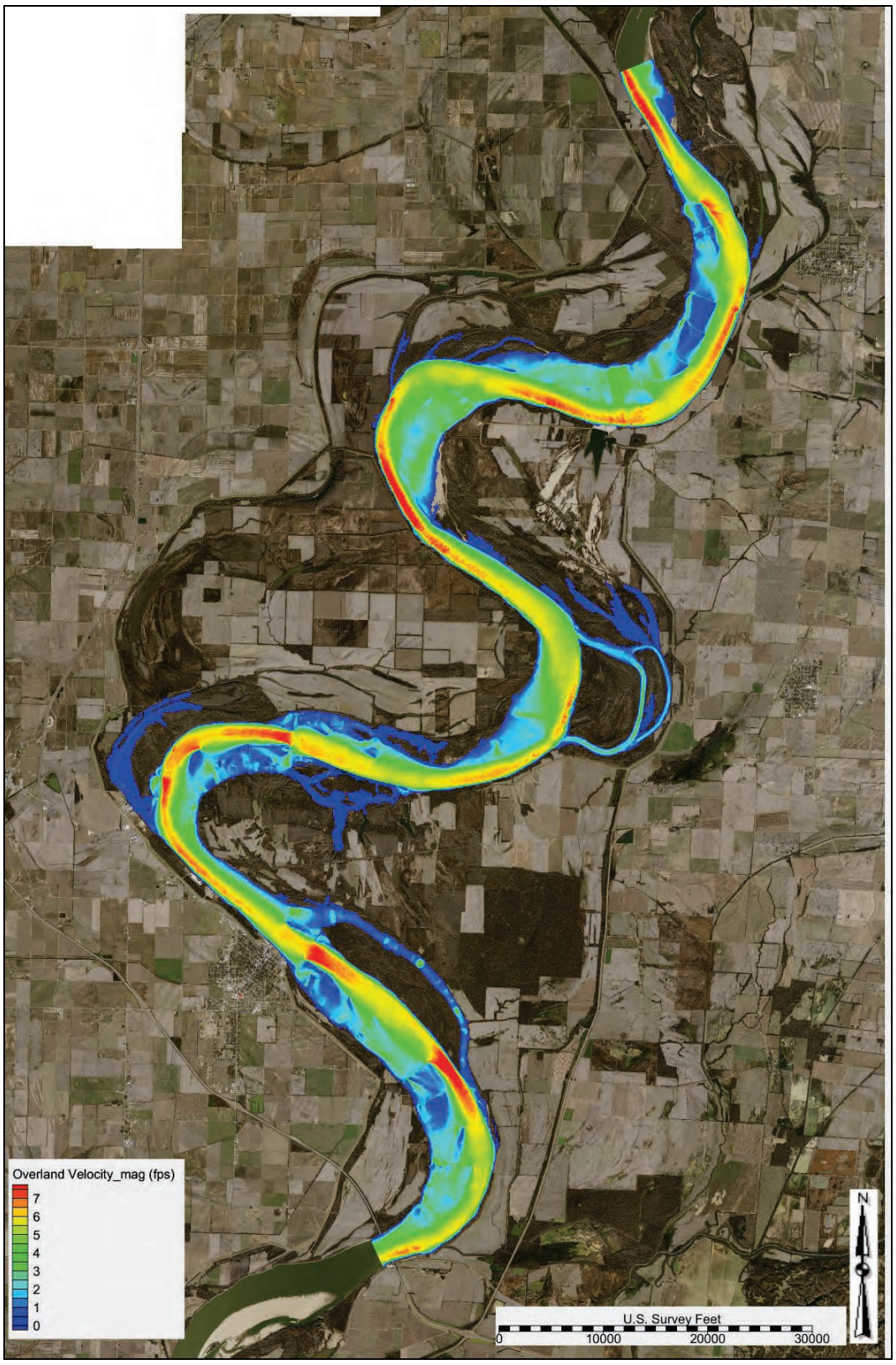


Figure C-45. Base condition velocity—700,000 cfs (entire model domain).

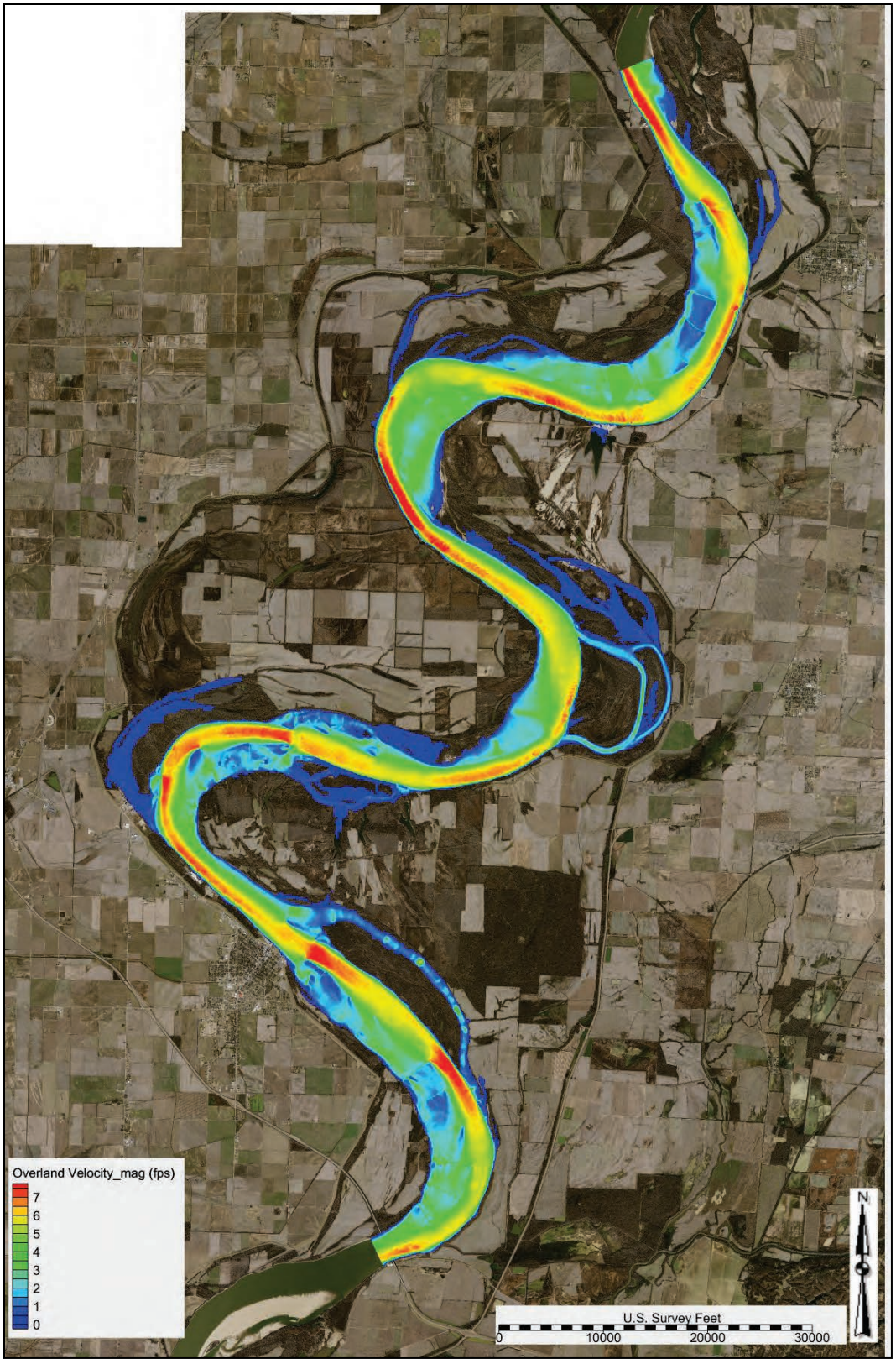


Figure C-46. Base condition velocity—750,000 cfs (entire model domain).

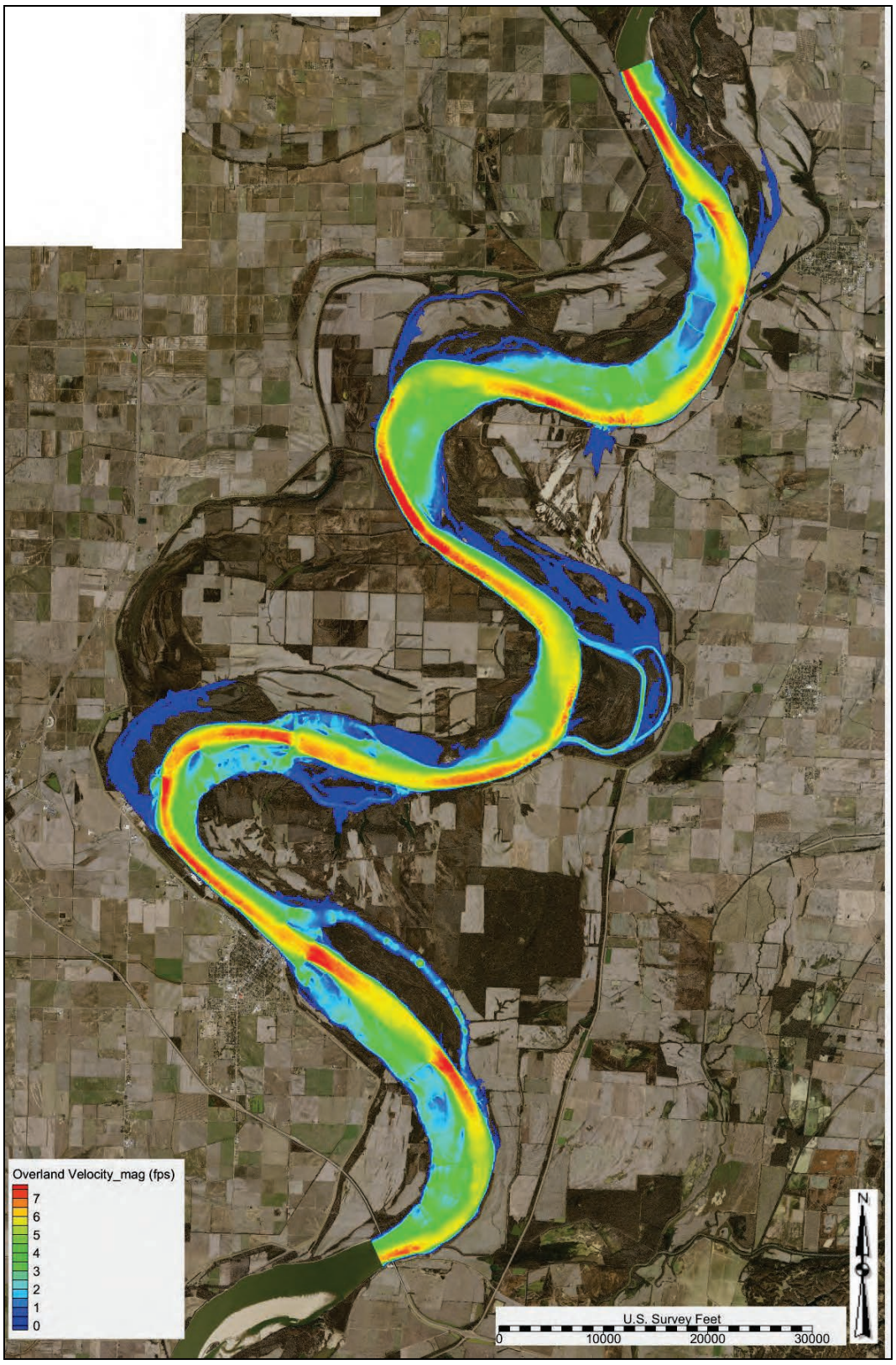


Figure C-47. Base condition velocity—800,000 cfs (entire model domain).

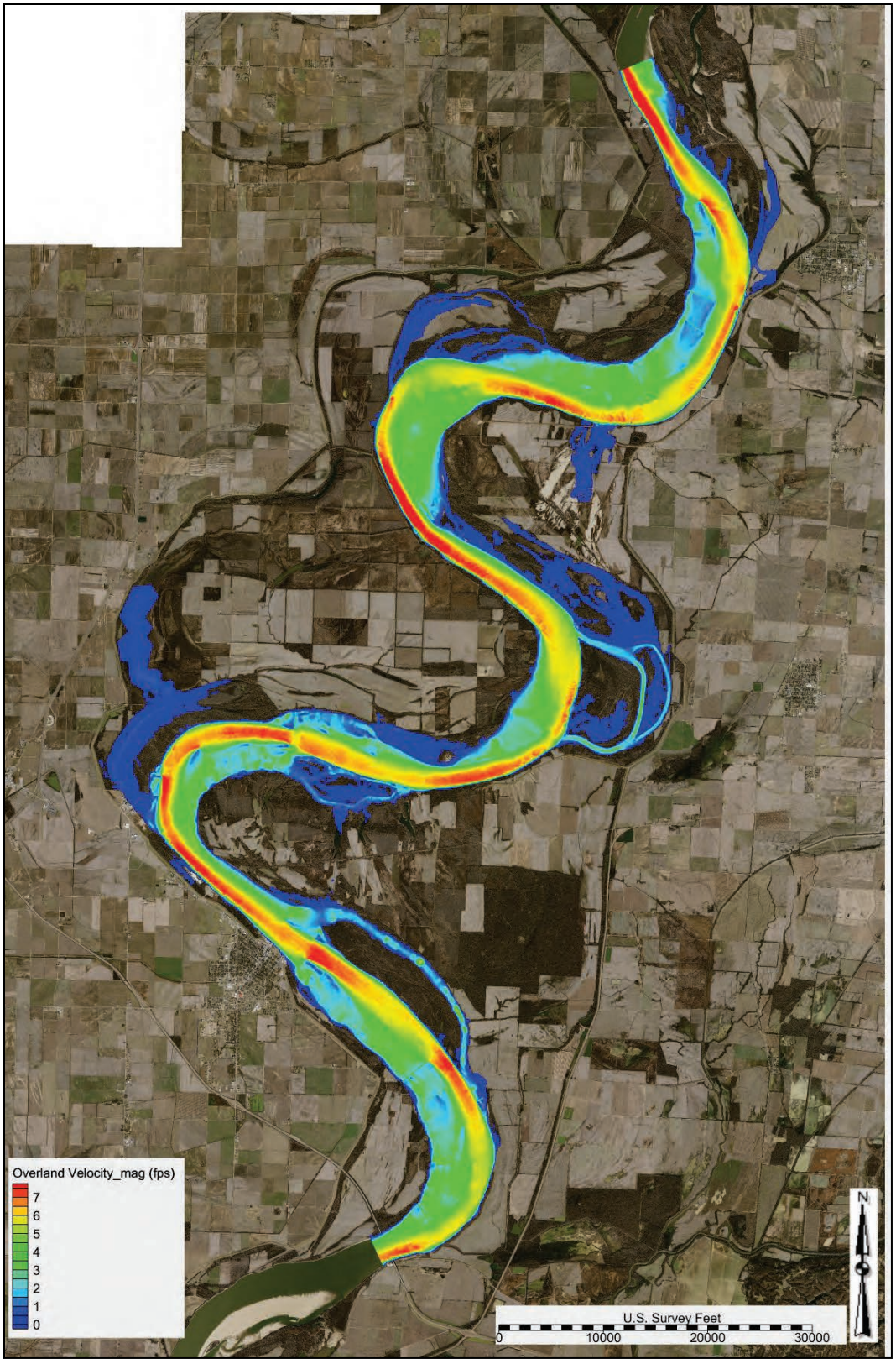


Figure C-48. Base condition velocity—850,000 cfs (entire model domain).

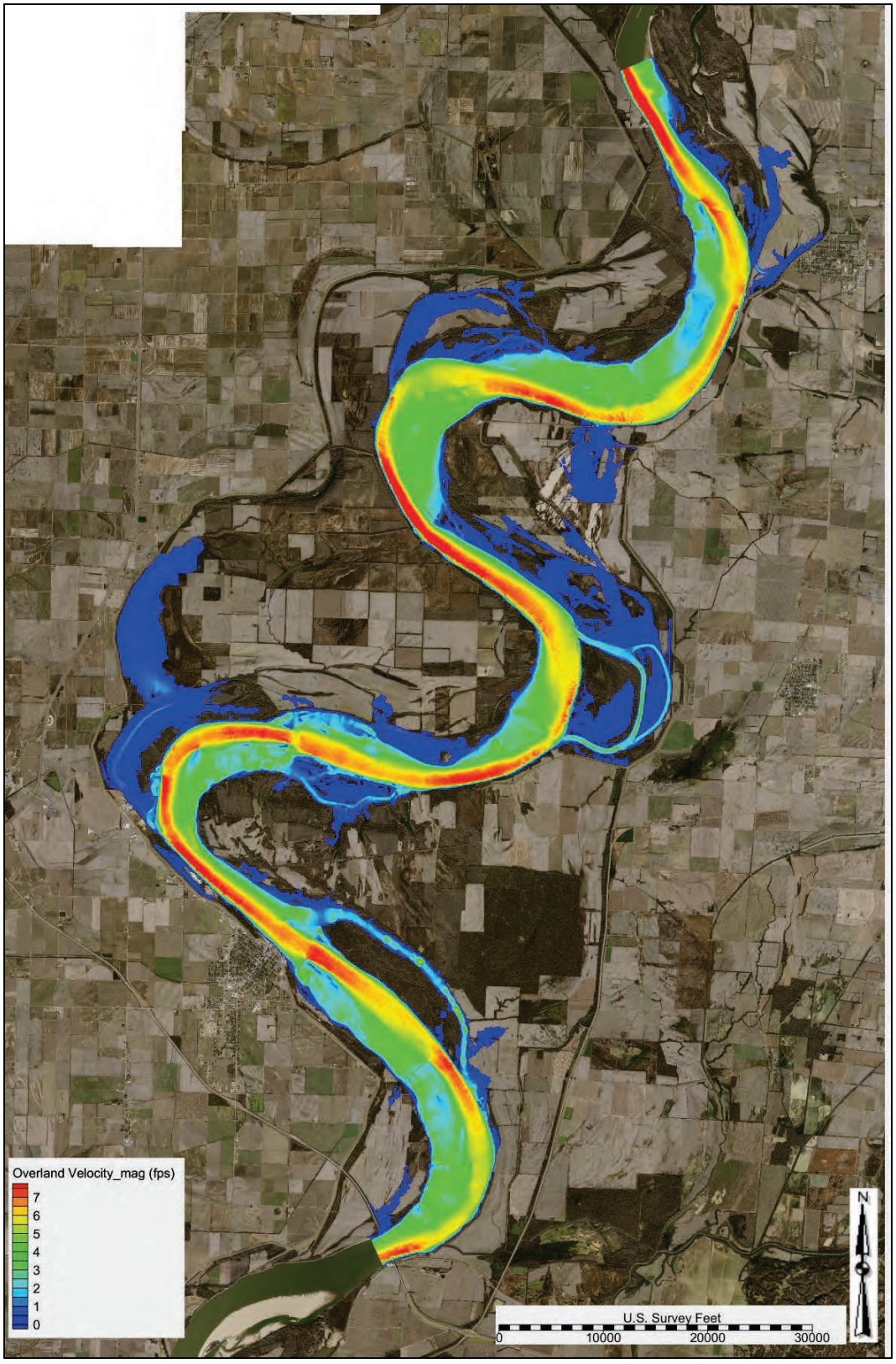


Figure C-49. Base condition velocity—900,000 cfs (entire model domain).

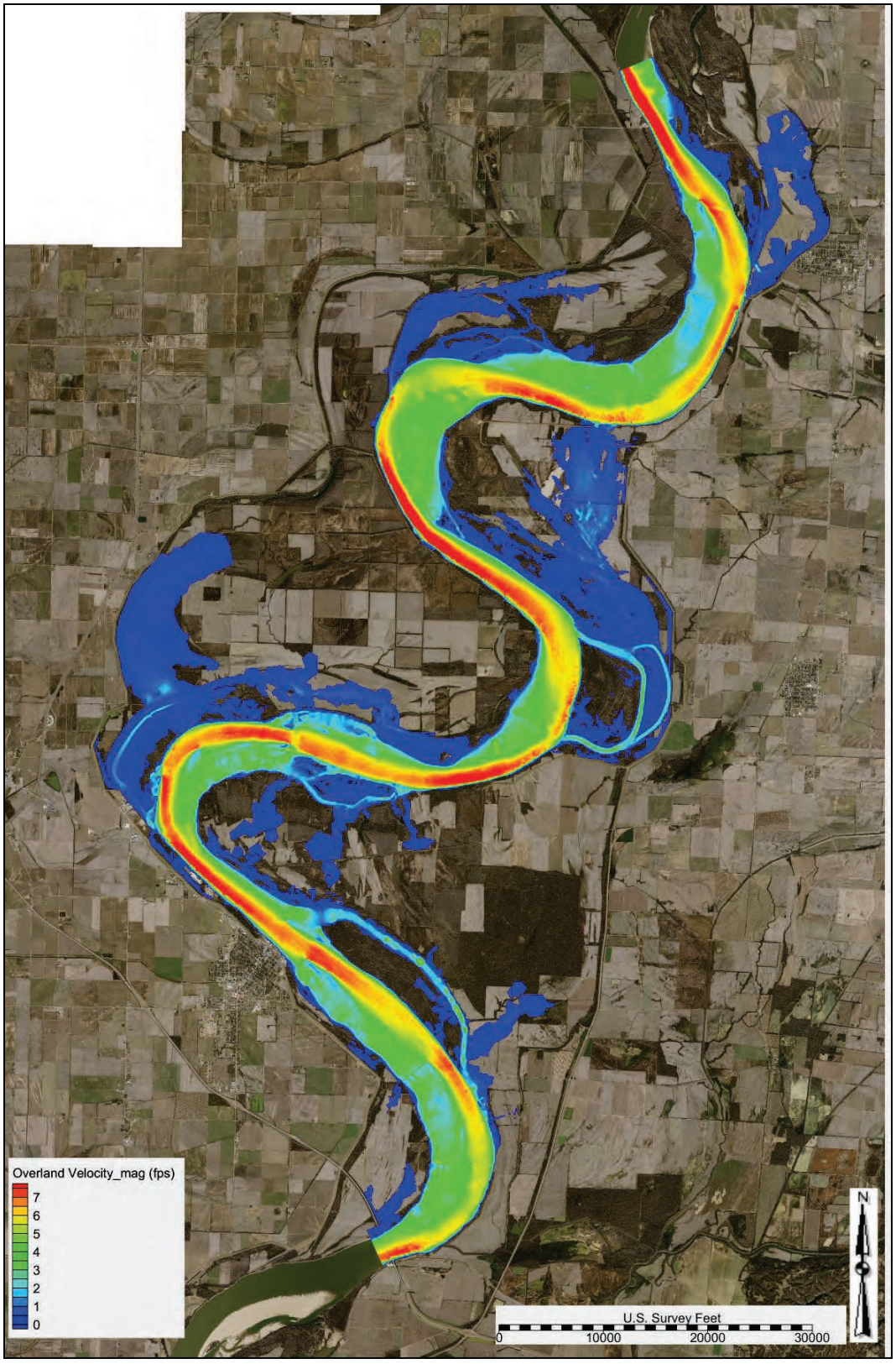


Figure C-50. Base condition velocity—1,100,000 cfs (entire model domain).

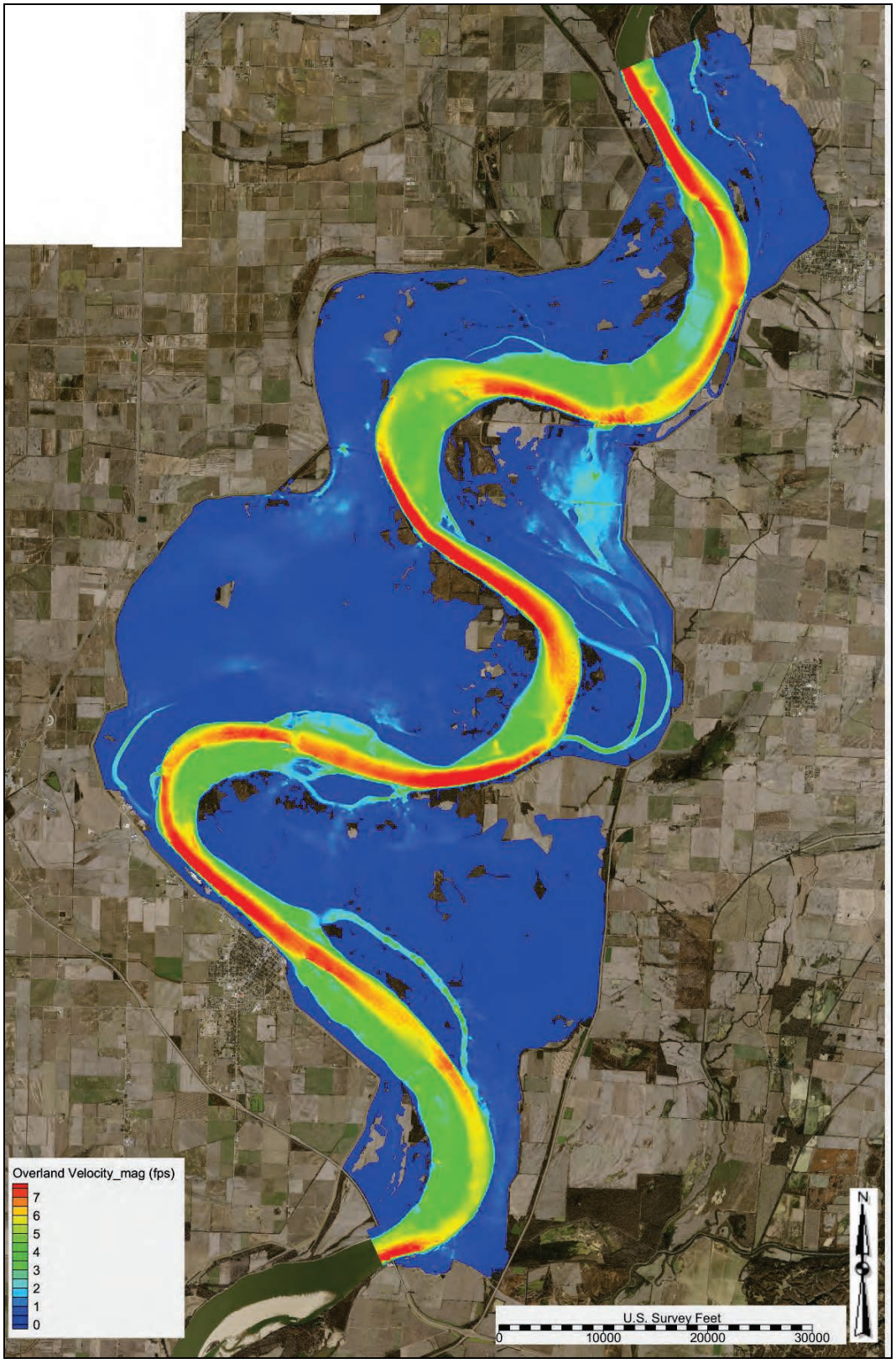


Figure C-51. Base condition velocity—1,300,000 cfs (entire model domain).

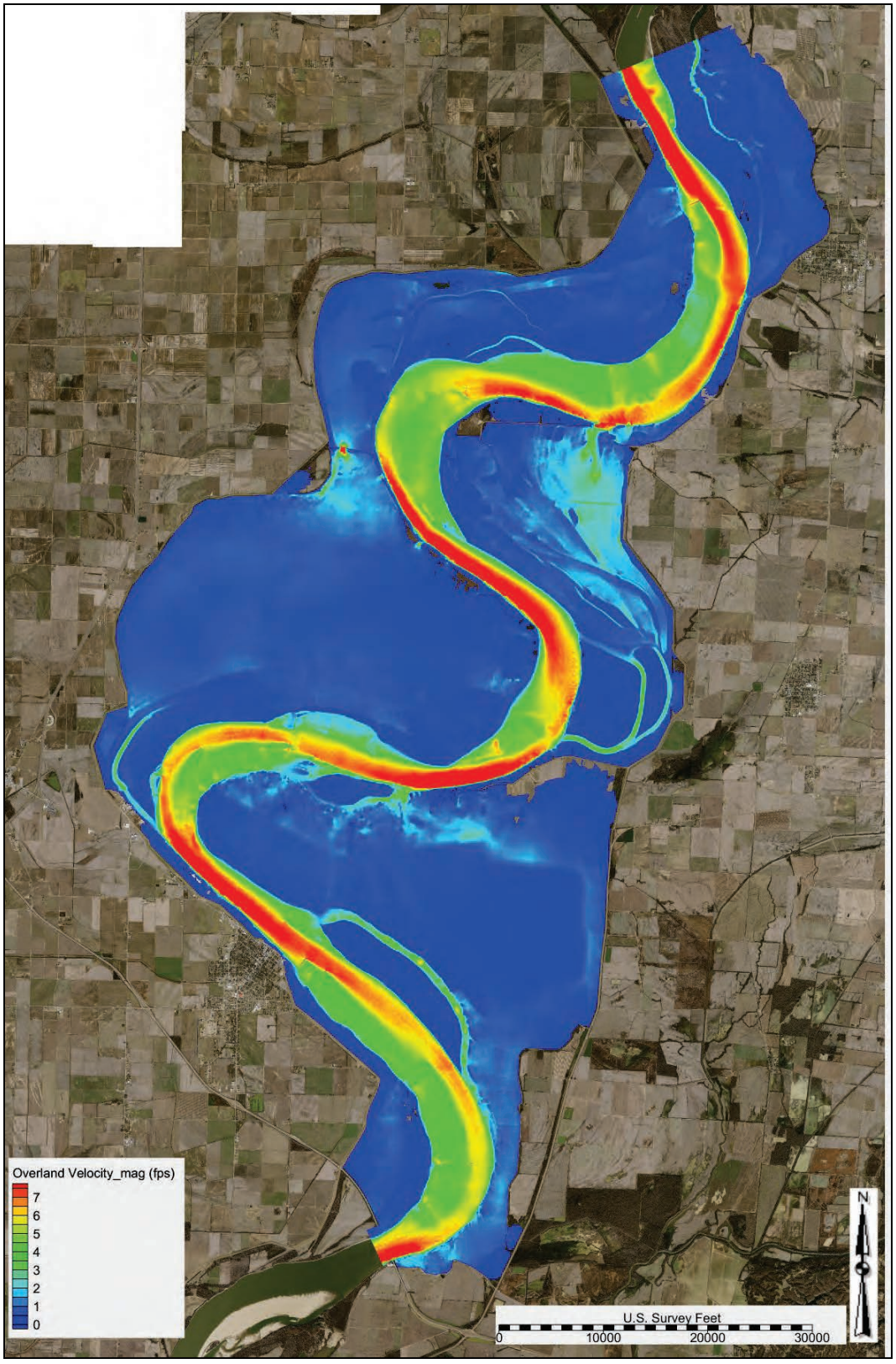


Figure C-52. Base condition velocity—1,500,000 cfs (entire model domain).

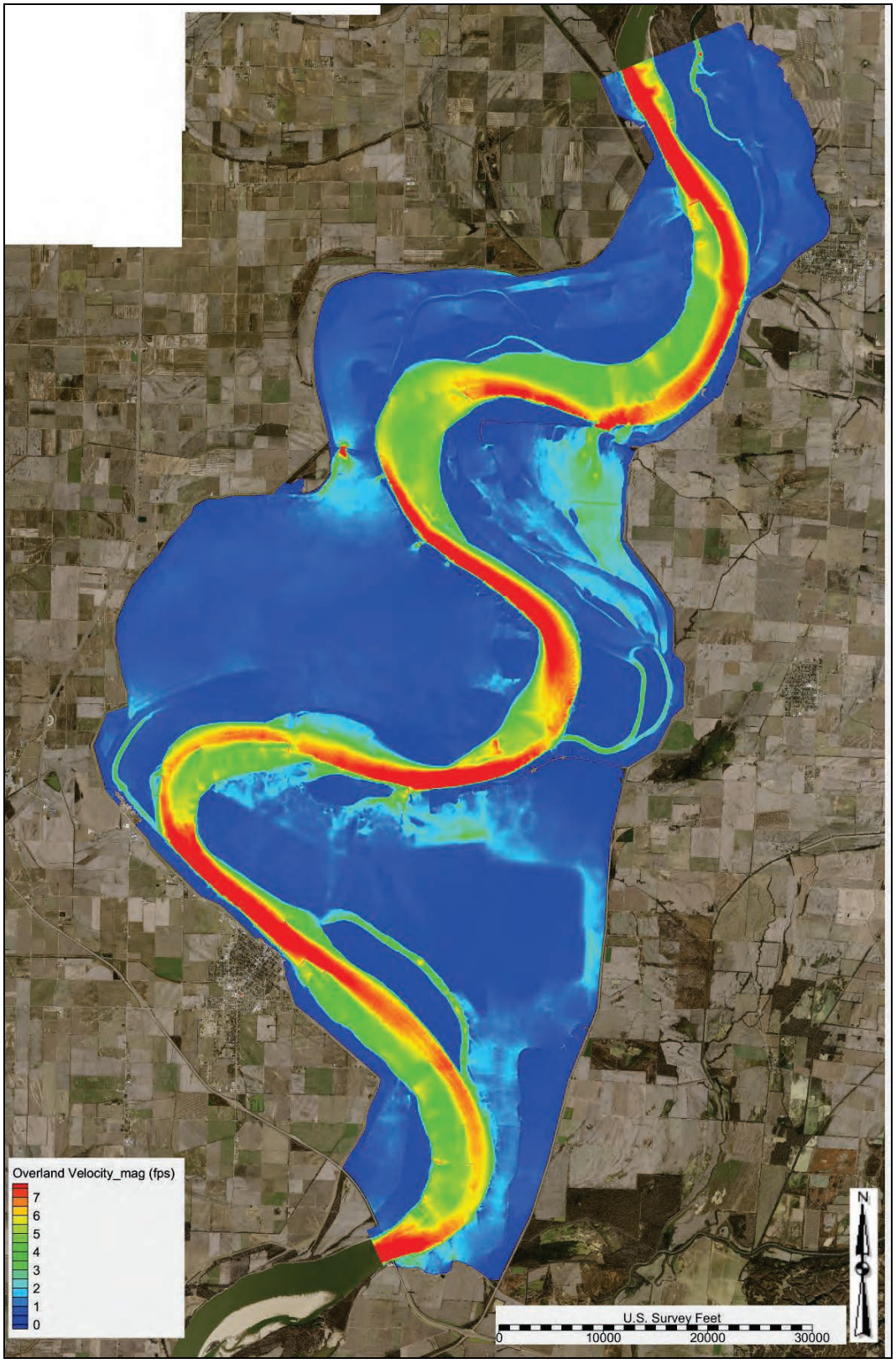


Figure C-53. Base condition velocity—1,700,000 cfs (entire model domain).

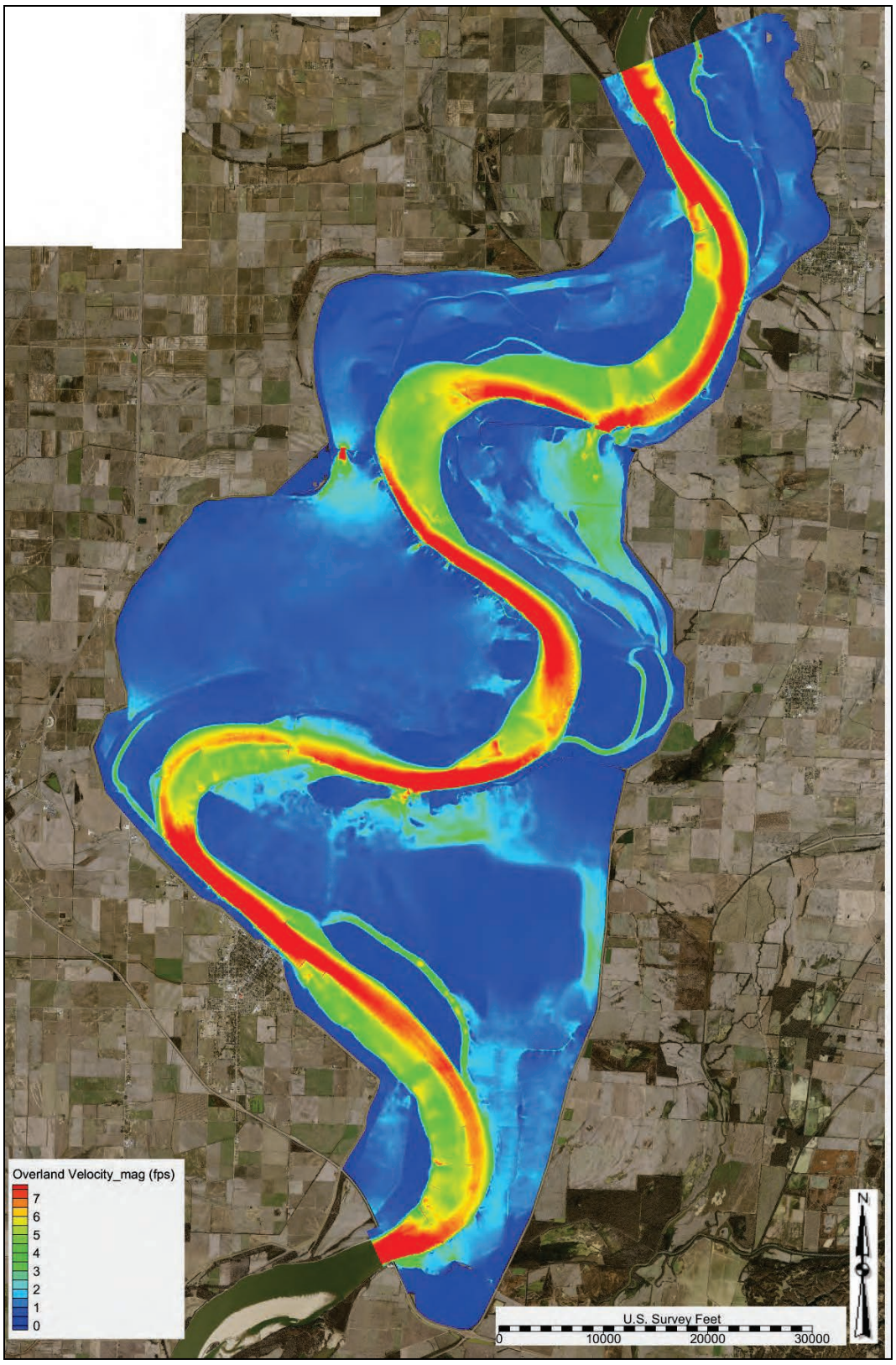


Figure C-54. Base condition velocity—1,900,000 cfs (entire model domain).

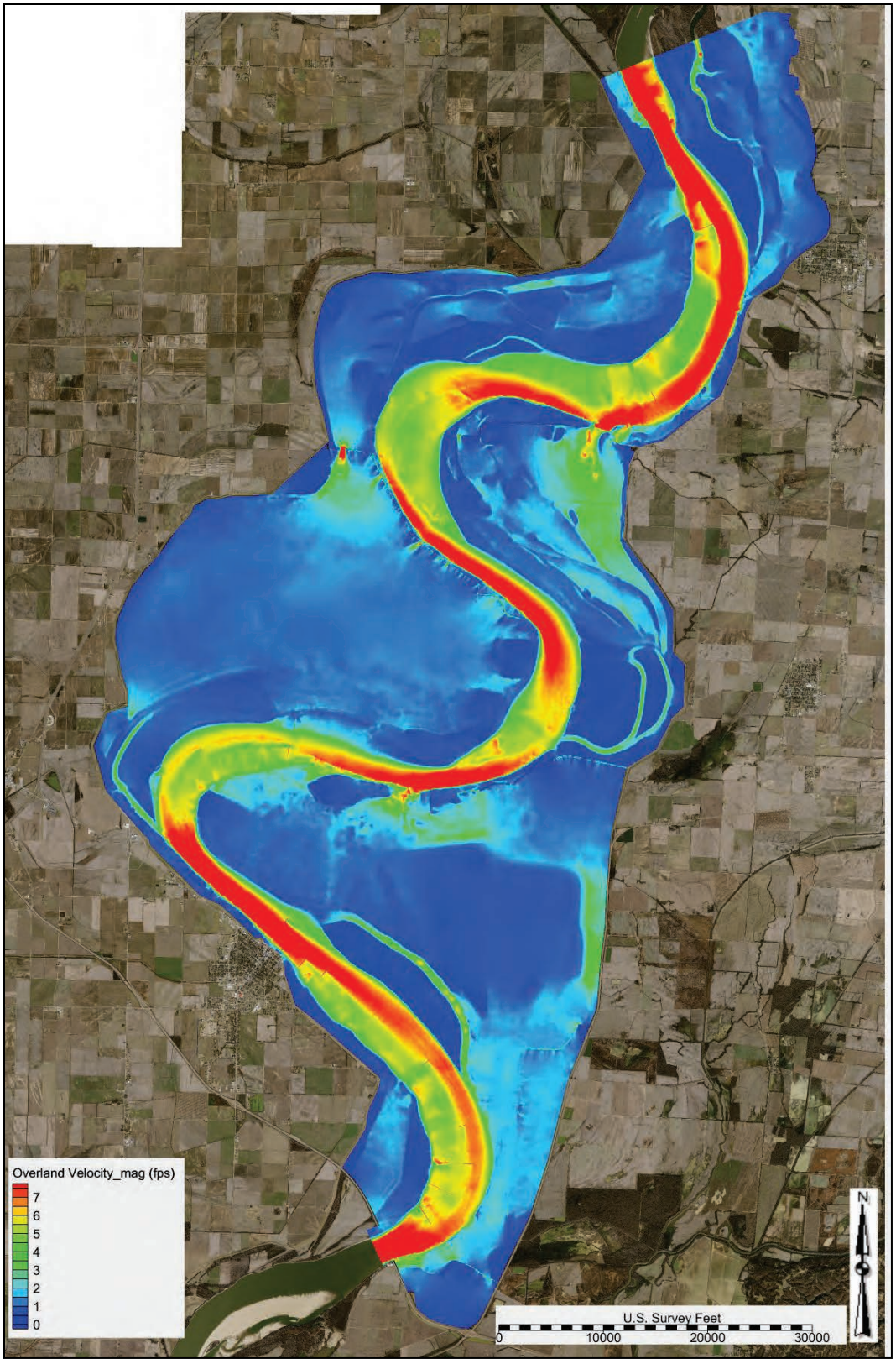


Figure C-55. Base condition velocity—2,100,000 cfs (entire model domain).

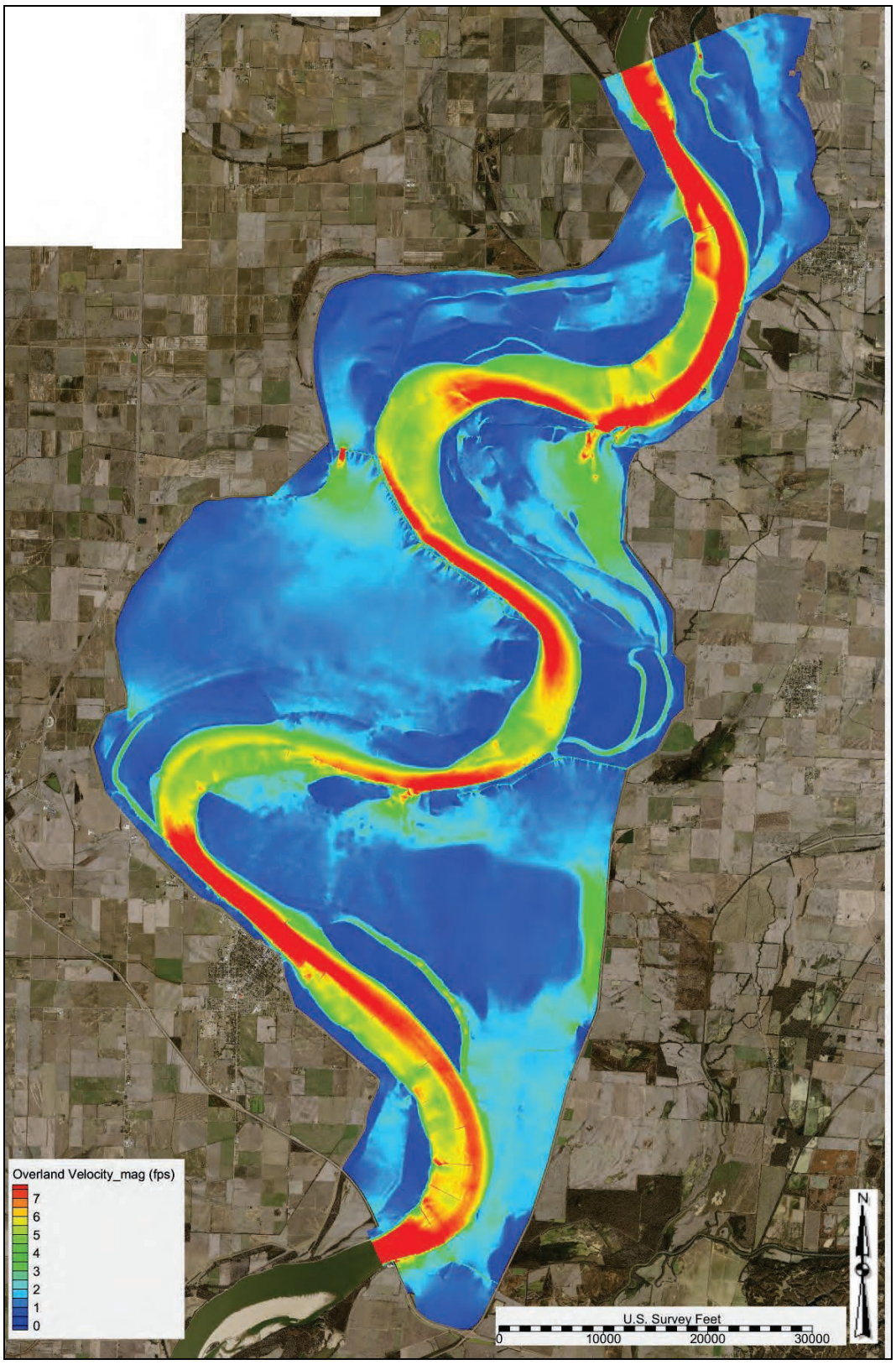


Figure C-56. Base condition velocity—400,000 cfs (study overbank).

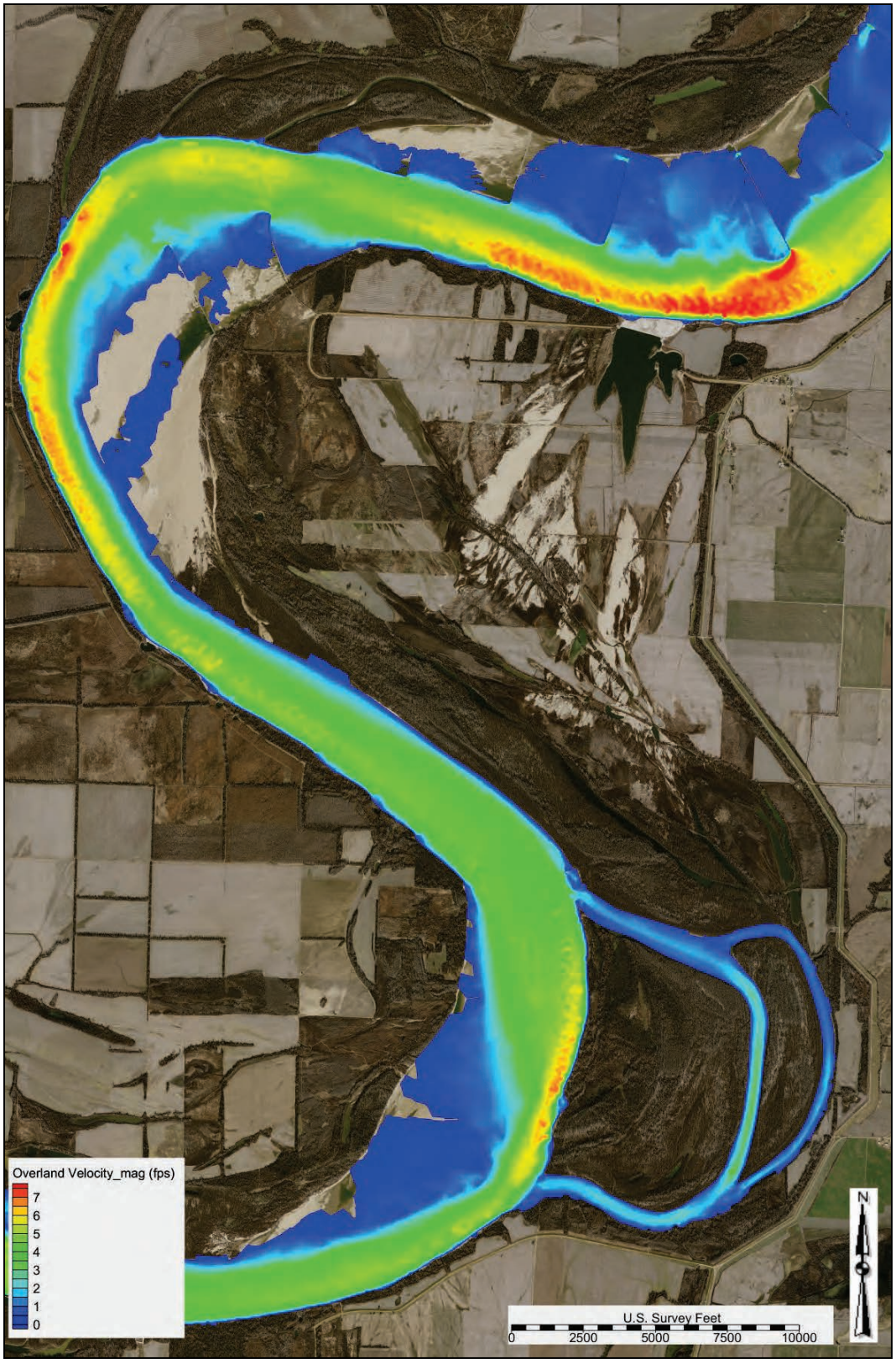


Figure C-57. Base condition velocity—500,000 cfs (study overbank).

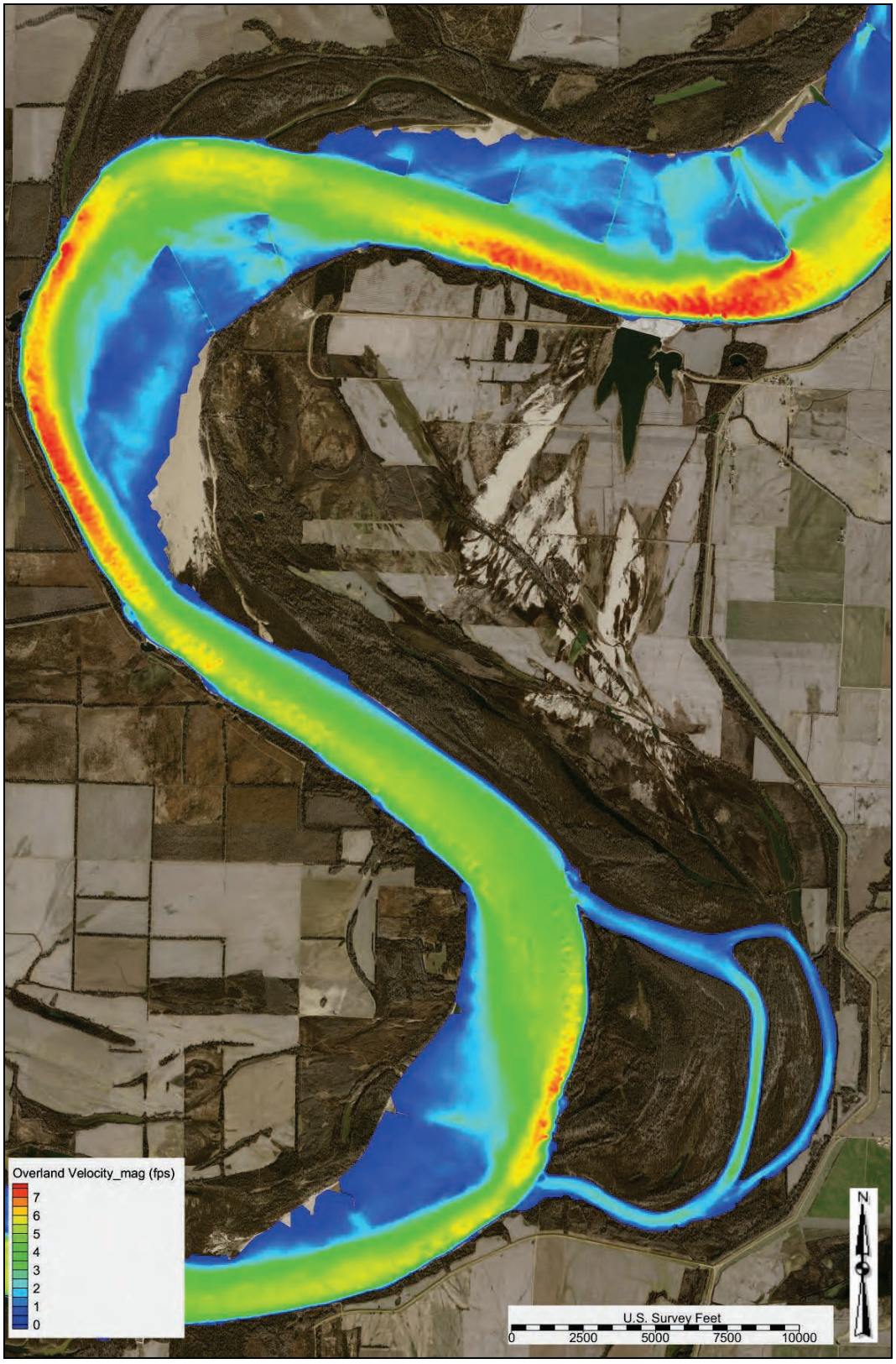


Figure C-58. Base condition velocity—600,000 cfs (study overbank).

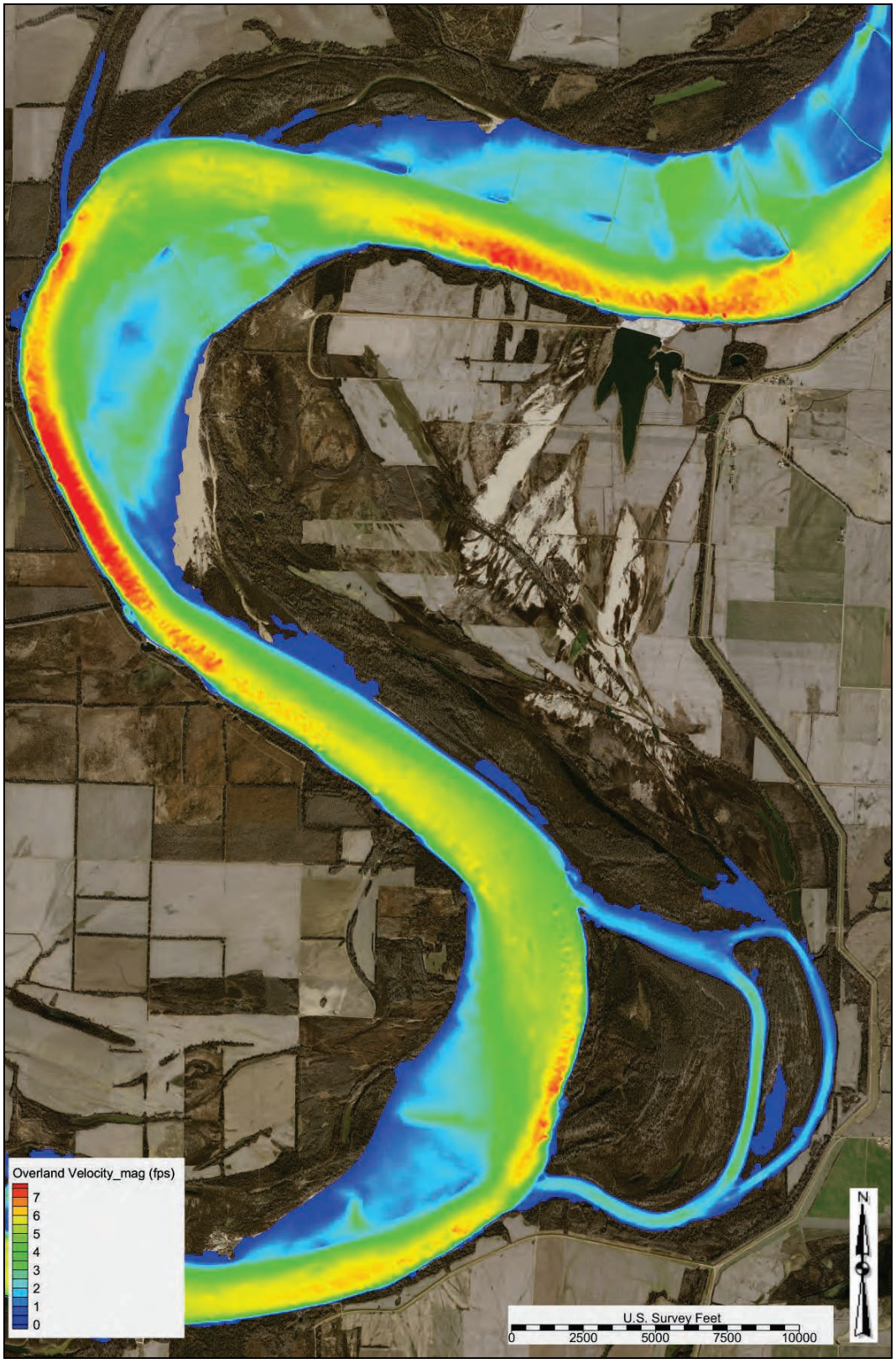


Figure C-59. Base condition velocity—650,000 cfs (study overbank).

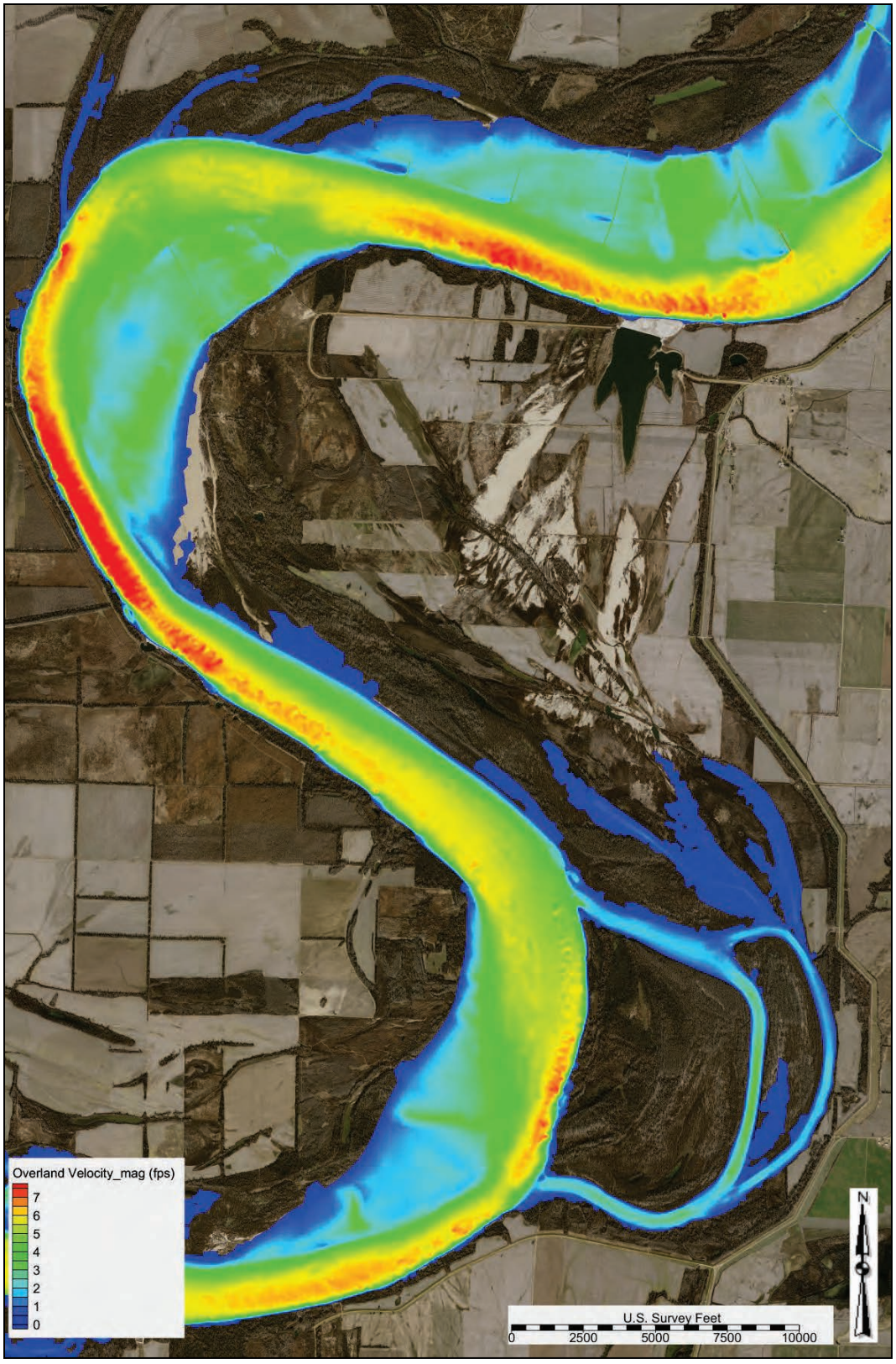


Figure C-60. Base condition velocity—700,000 cfs (study overbank).

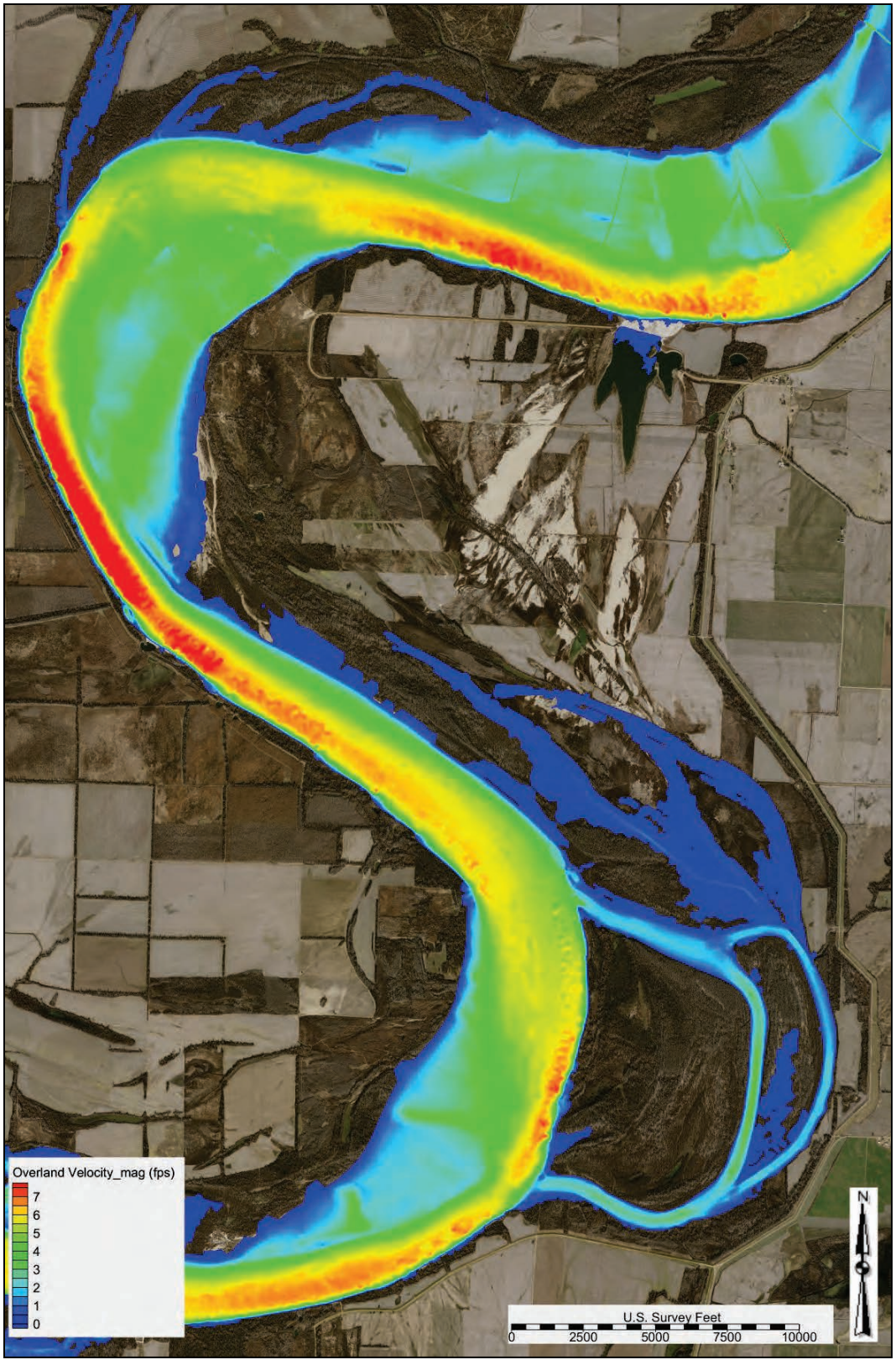


Figure C-61. Base condition velocity—750,00 cfs (study overbank).

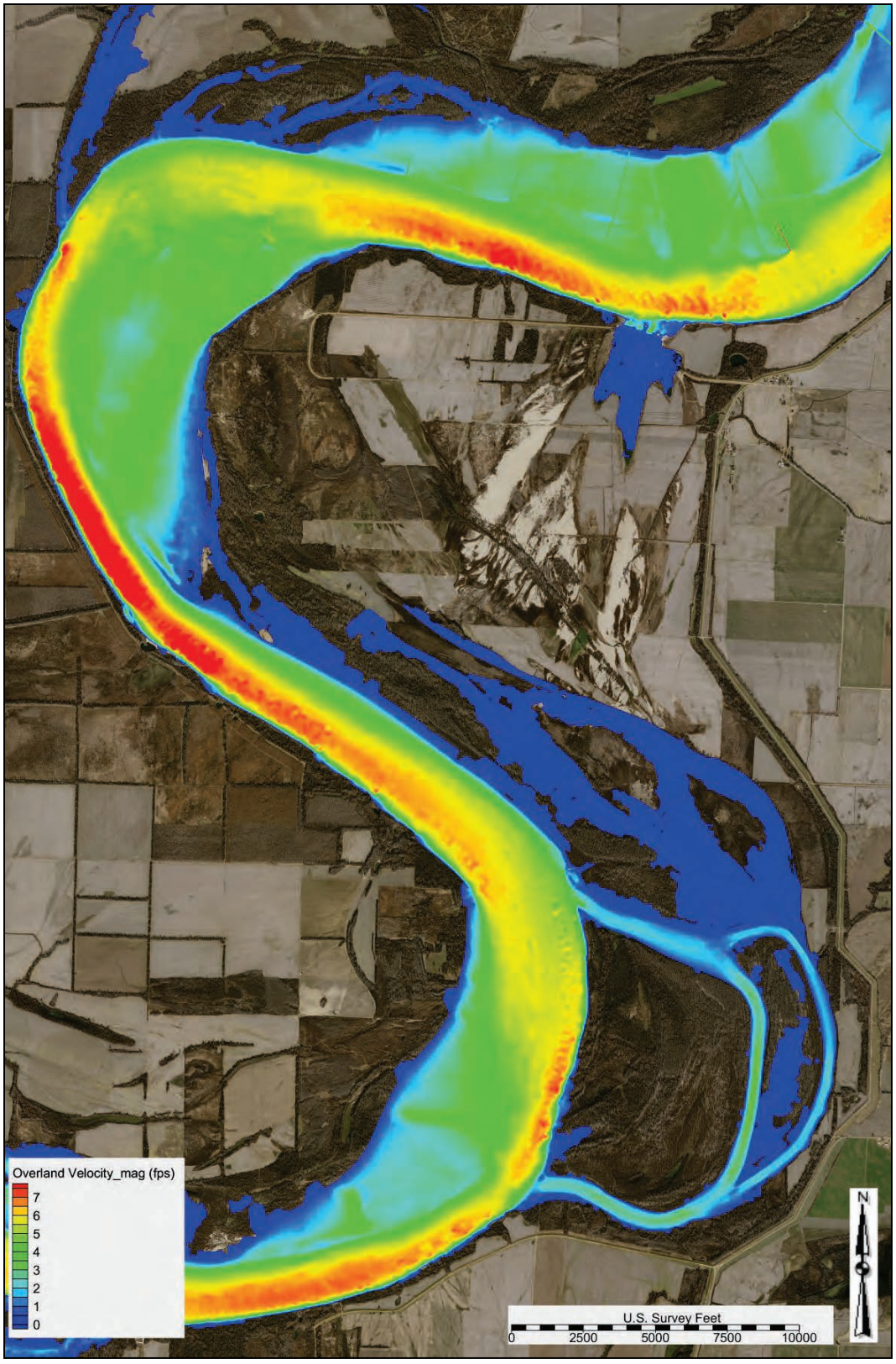


Figure C-62. Base condition velocity—800,000 cfs (study overbank).

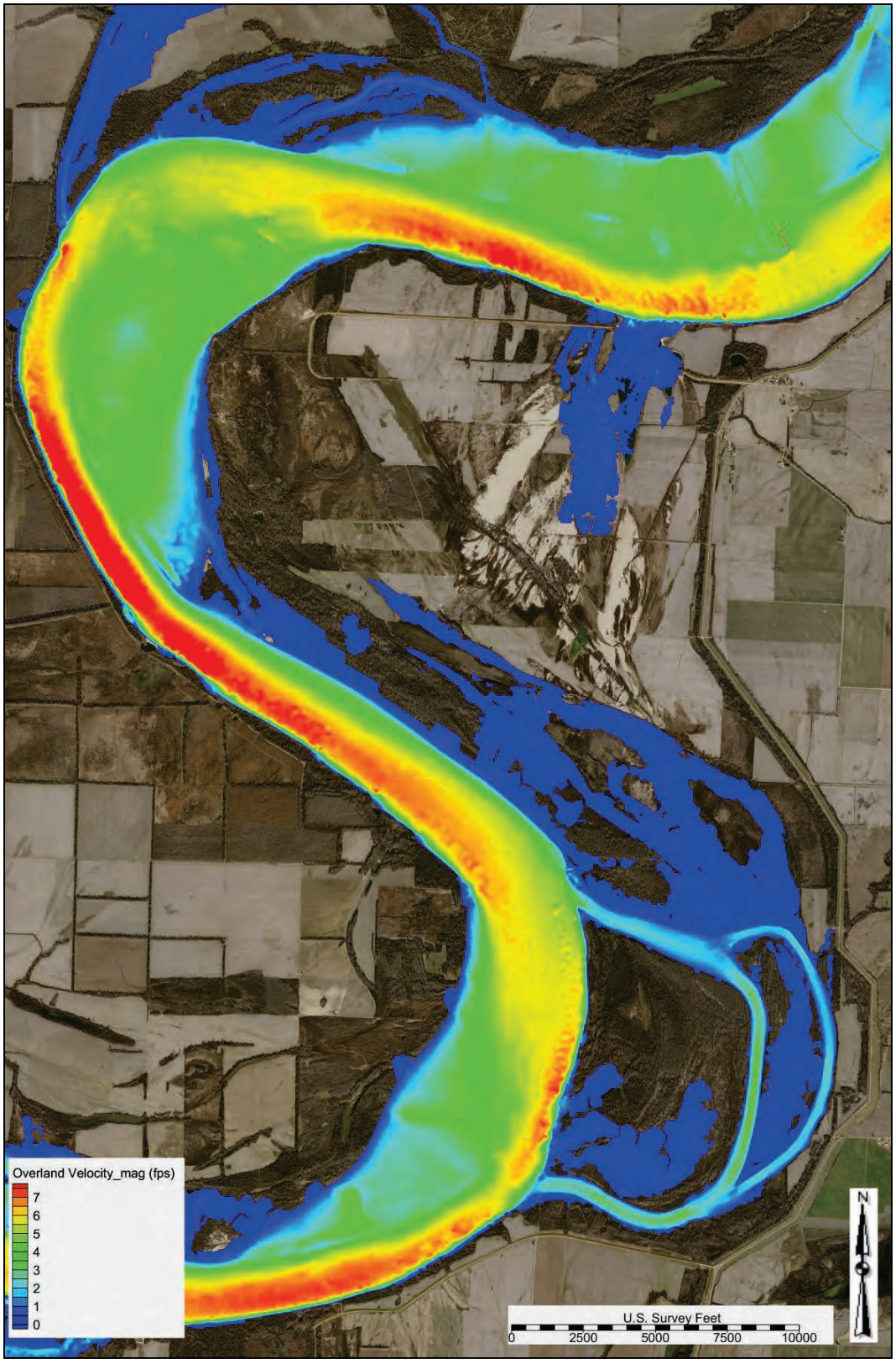


Figure C-63. Base condition velocity—850,000 cfs (study overbank).

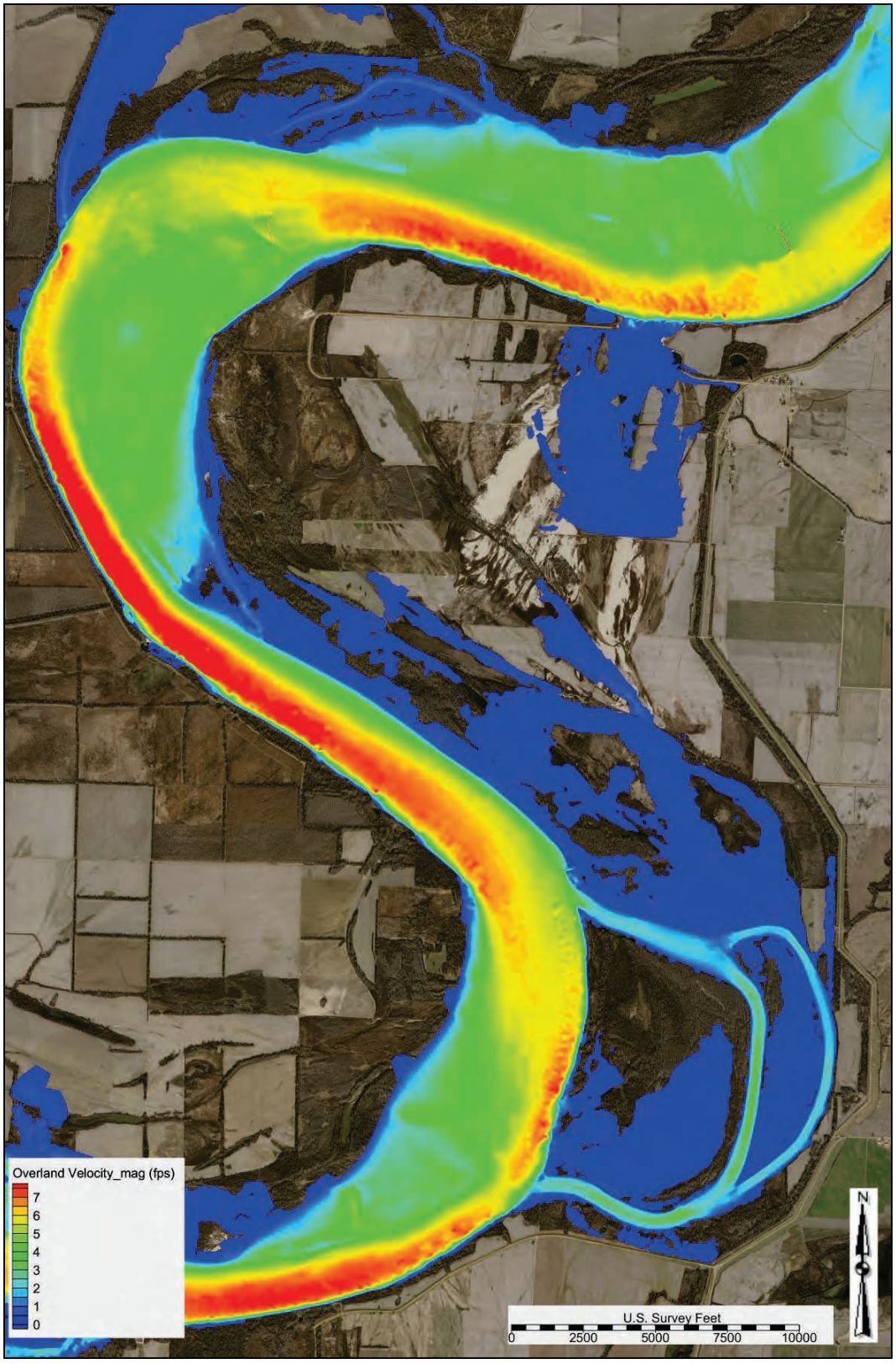


Figure C-64. Base condition velocity—900,000 cfs (study overbank).

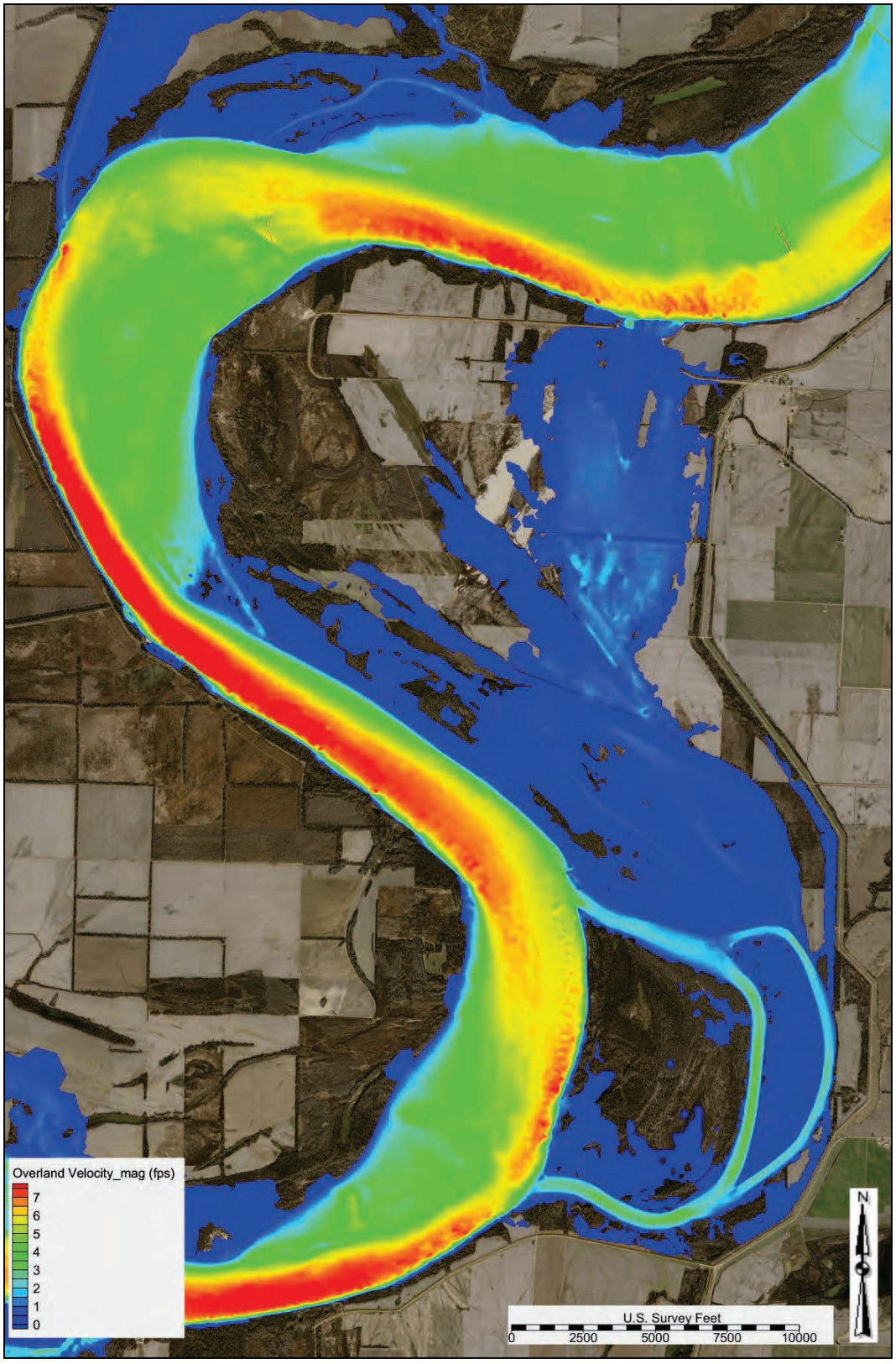


Figure C-65. Base condition velocity—1,100,000 cfs (study overbank).

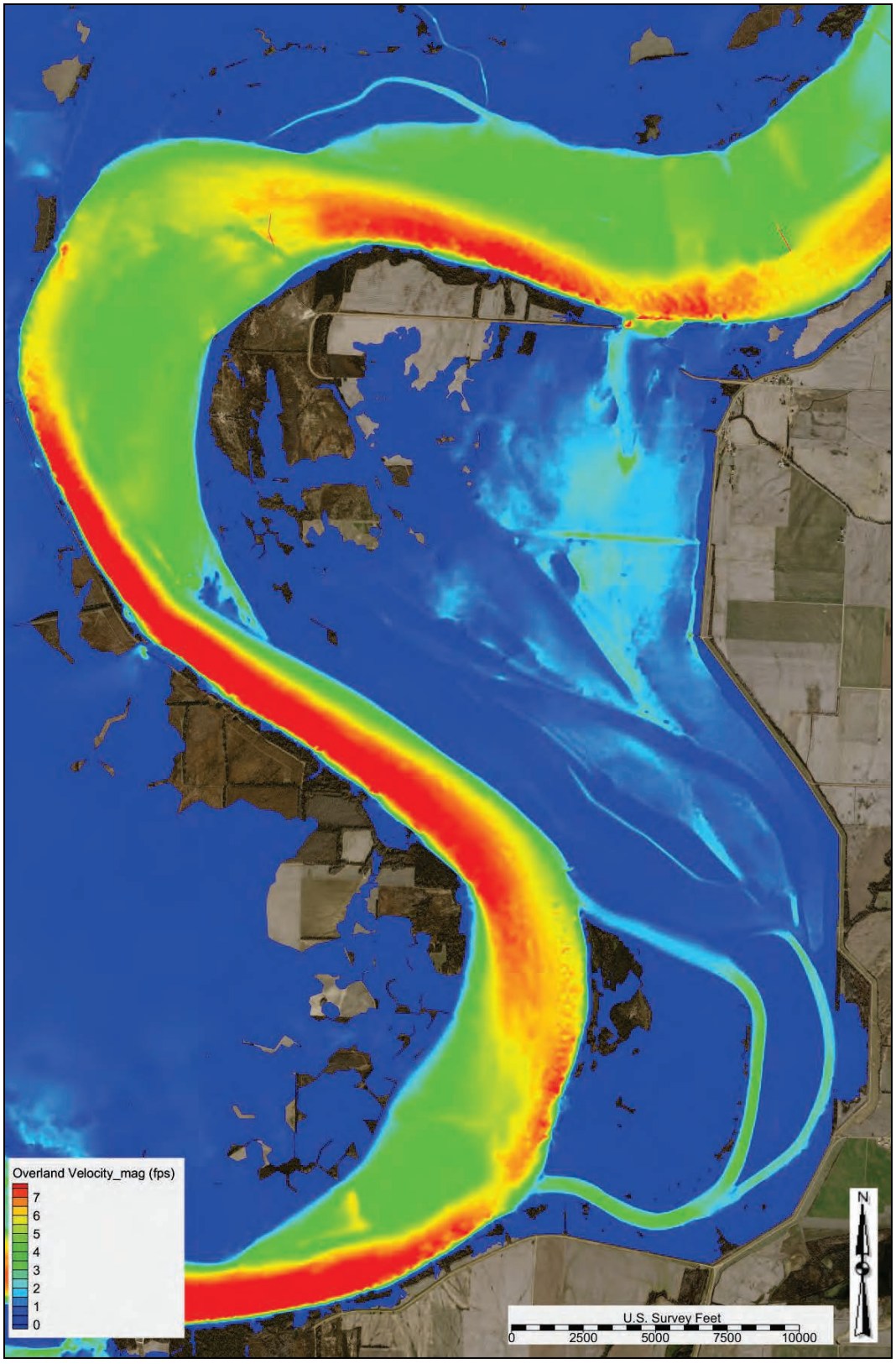


Figure C-66. Base condition velocity—1,300,000 cfs (study overbank).

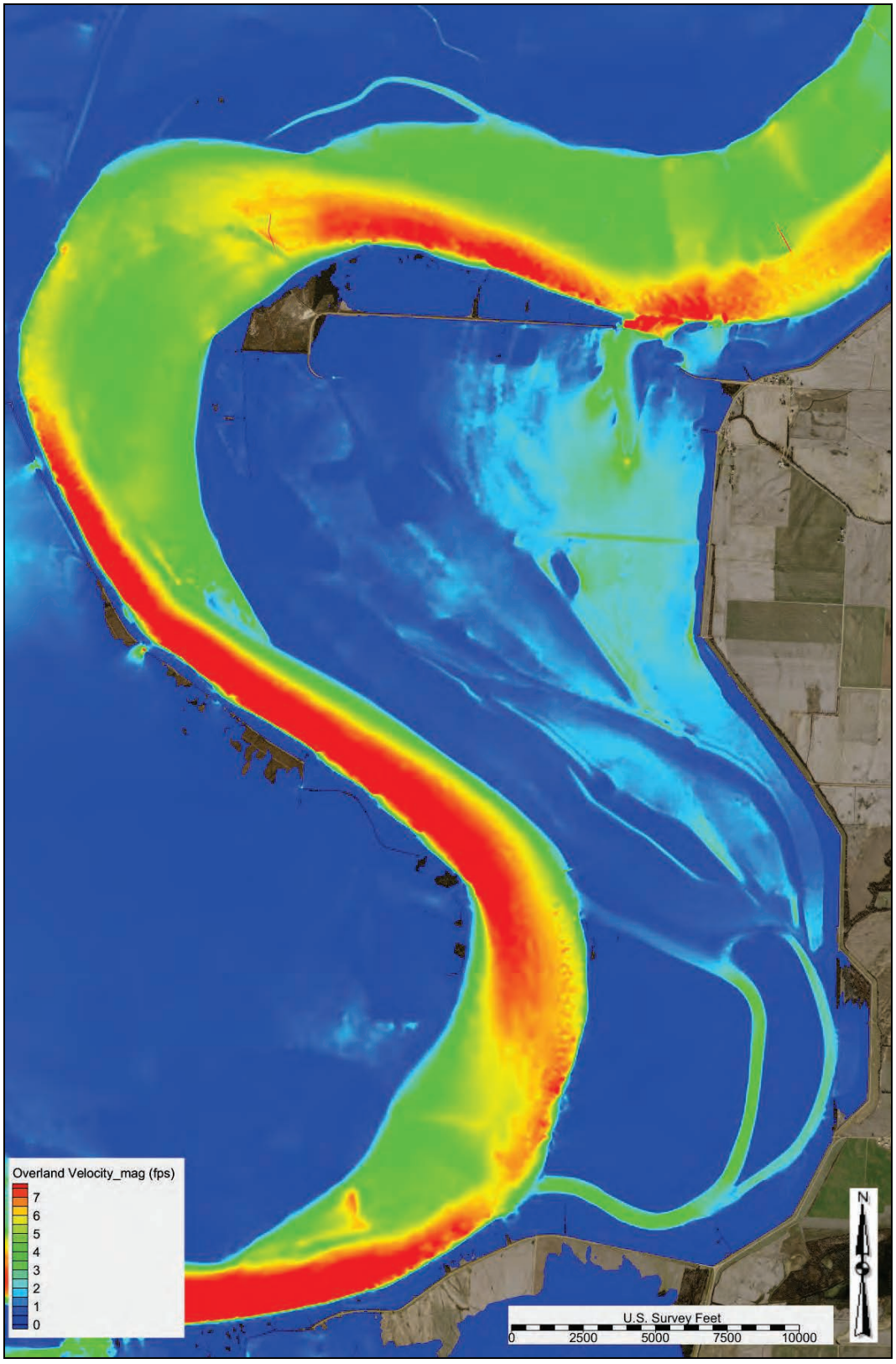


Figure C-67. Base condition velocity—1,500,000 cfs (study overbank).

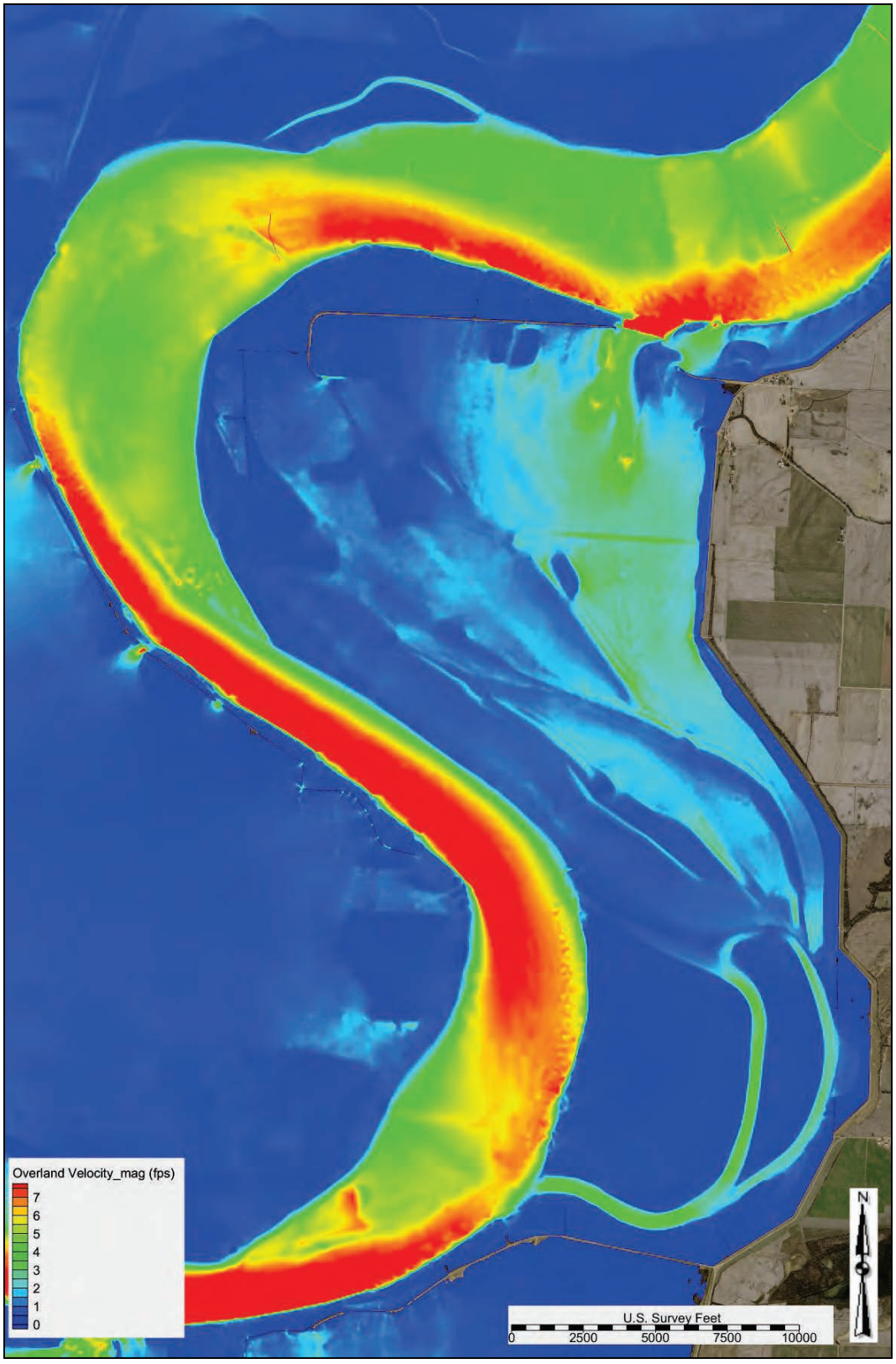


Figure C-68. Base condition velocity—1,700,000 cfs (study overbank).

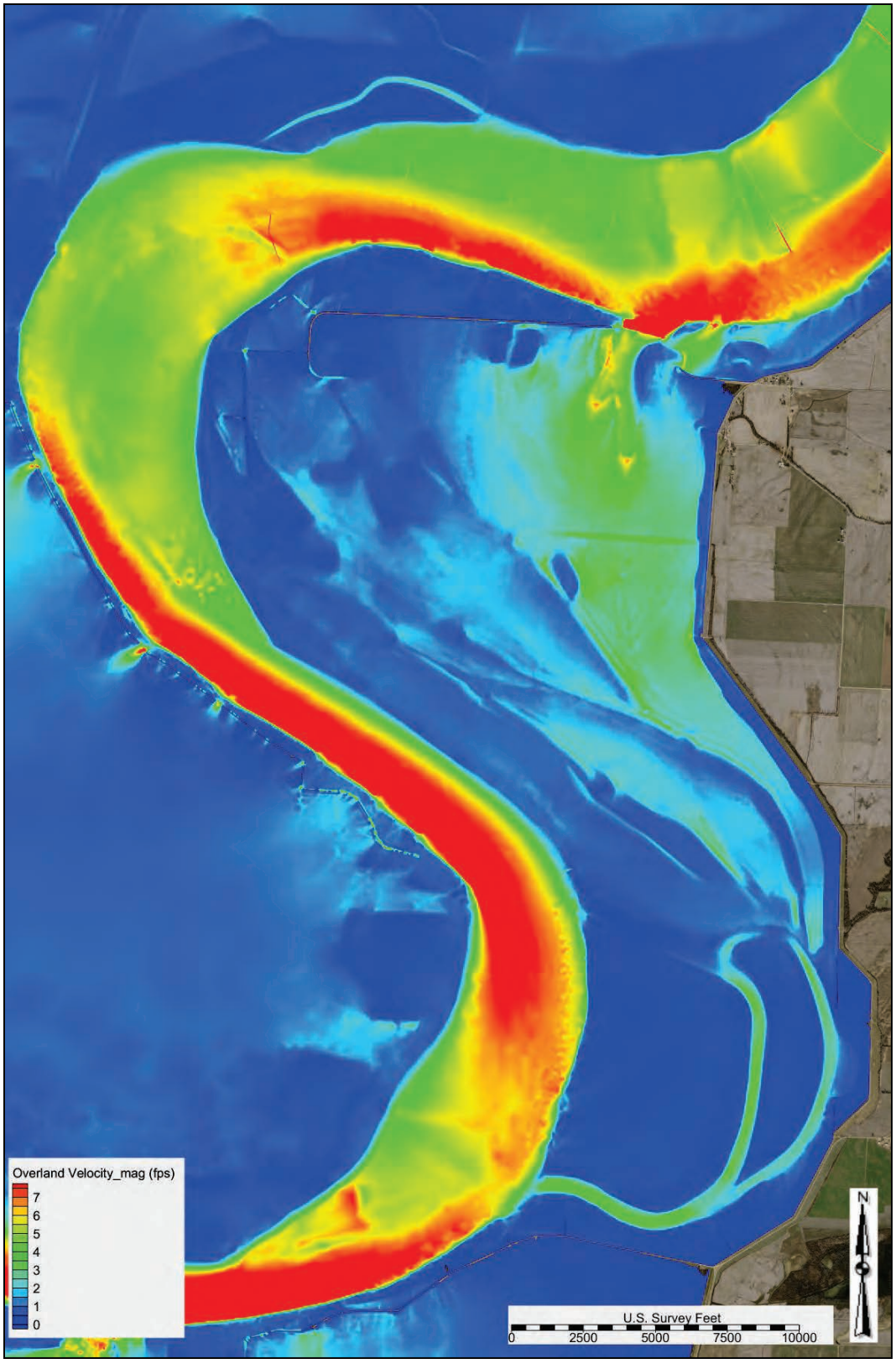


Figure C-69. Base condition velocity—1,900,000 cfs (study overbank).

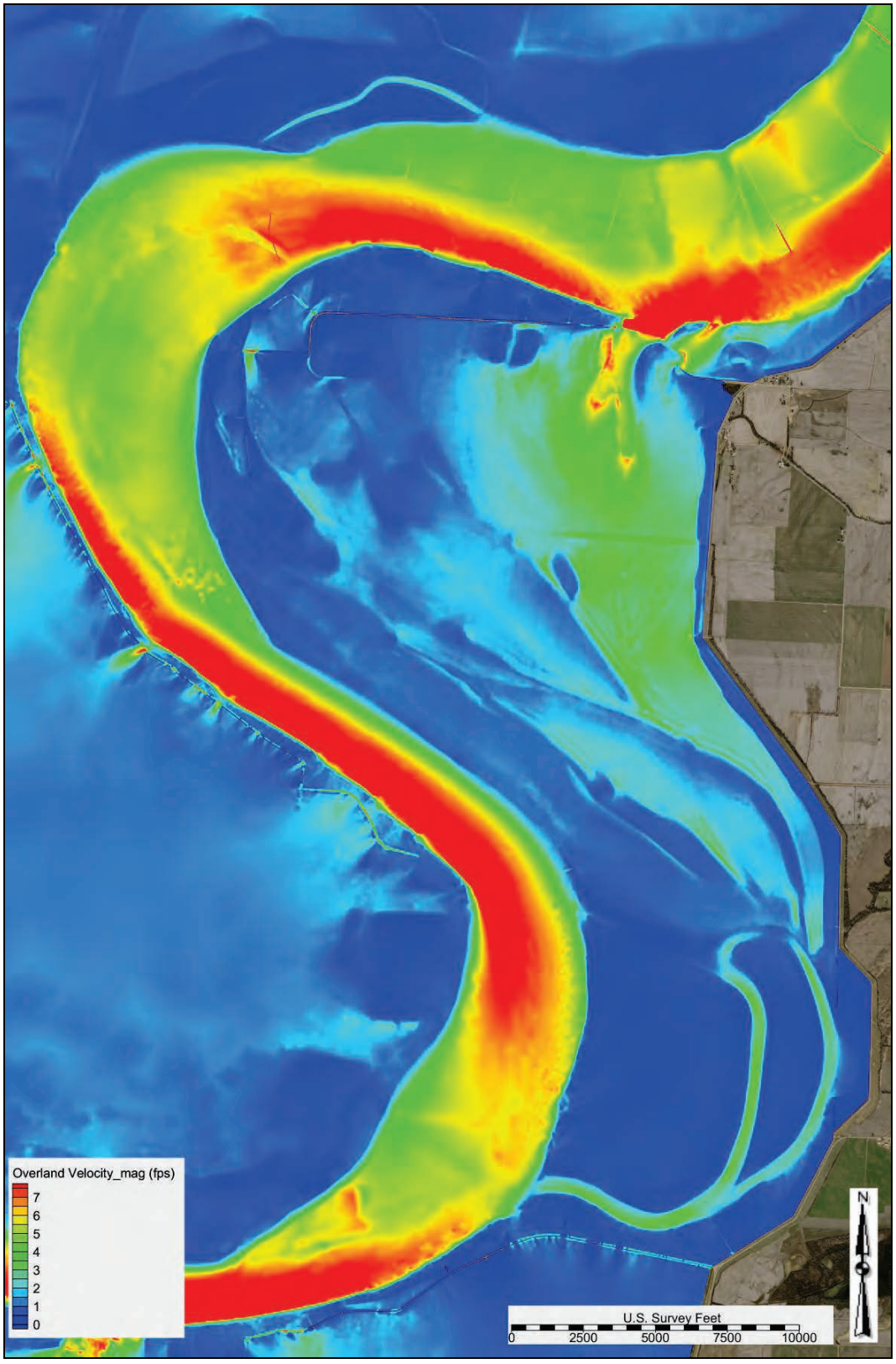


Figure C-70. Base condition velocity—2,100,000 cfs (study overbank).

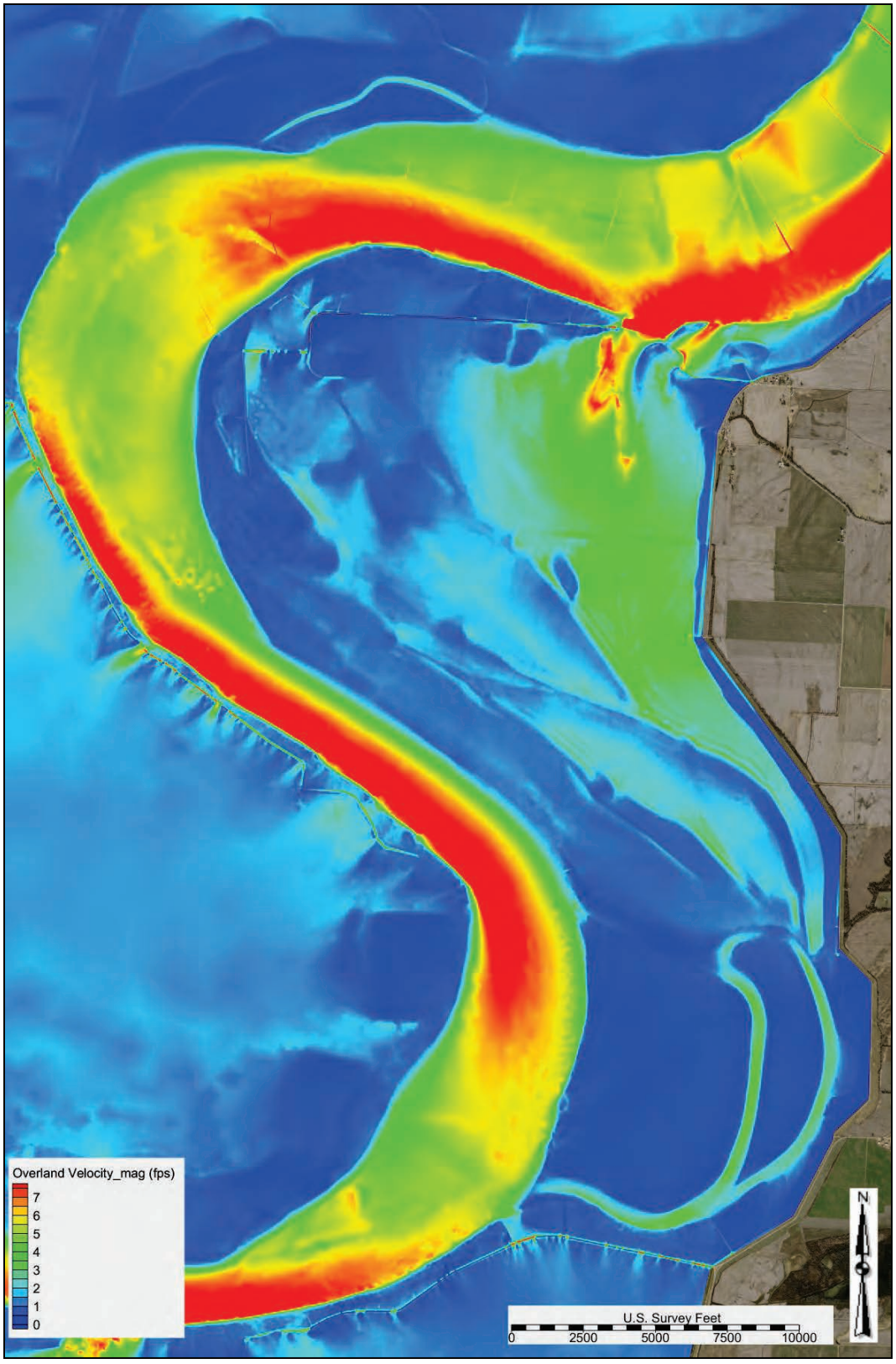


Figure C-71. Base condition velocity—400,000 cfs (study crevasse).

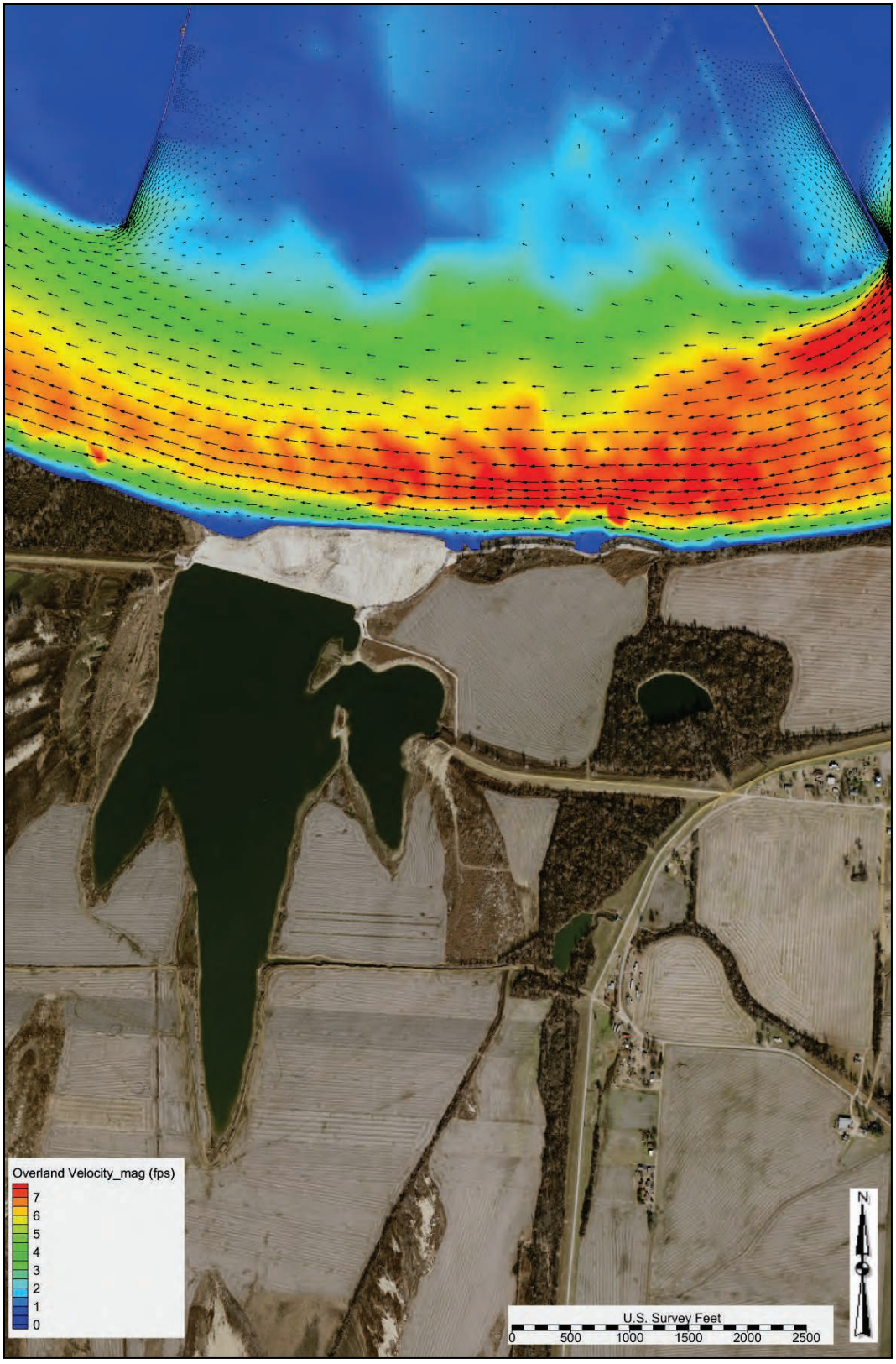


Figure C-72. Base condition velocity—500,000 cfs (study crevasse).

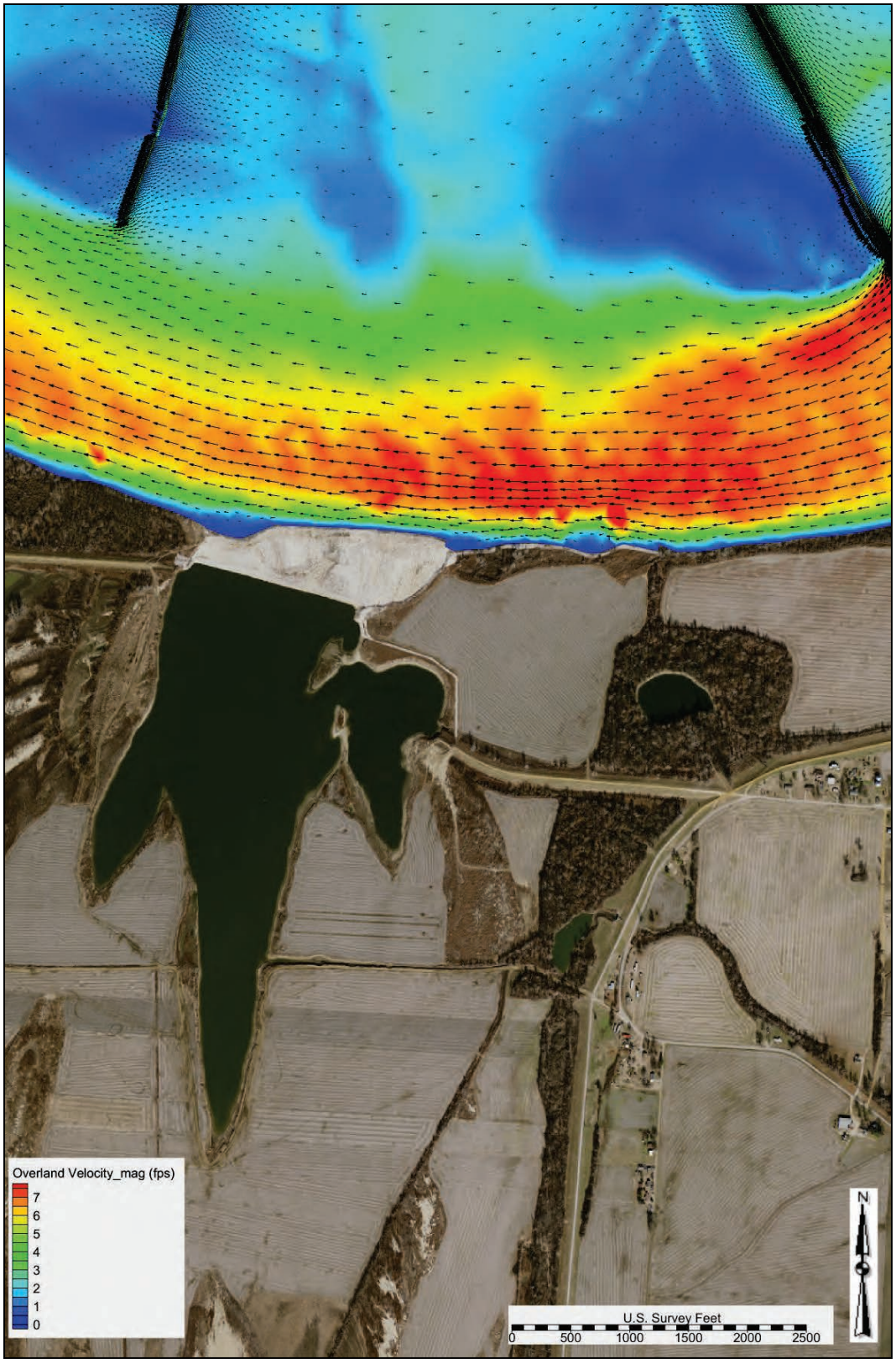


Figure C-73. Base condition velocity—600,000 cfs (study crevasse).

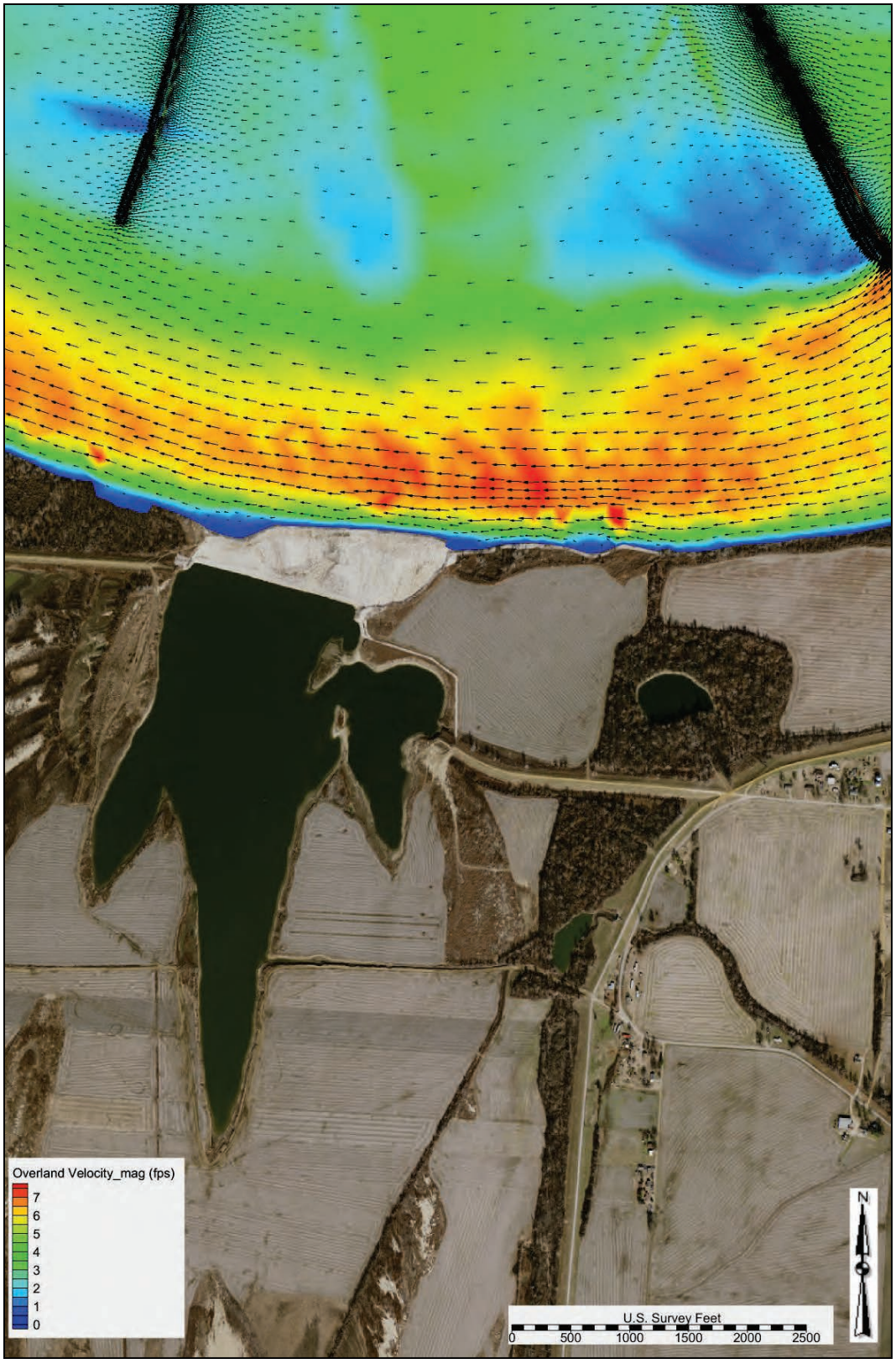


Figure C-74. Base condition velocity—650,000 cfs (study crevasse).

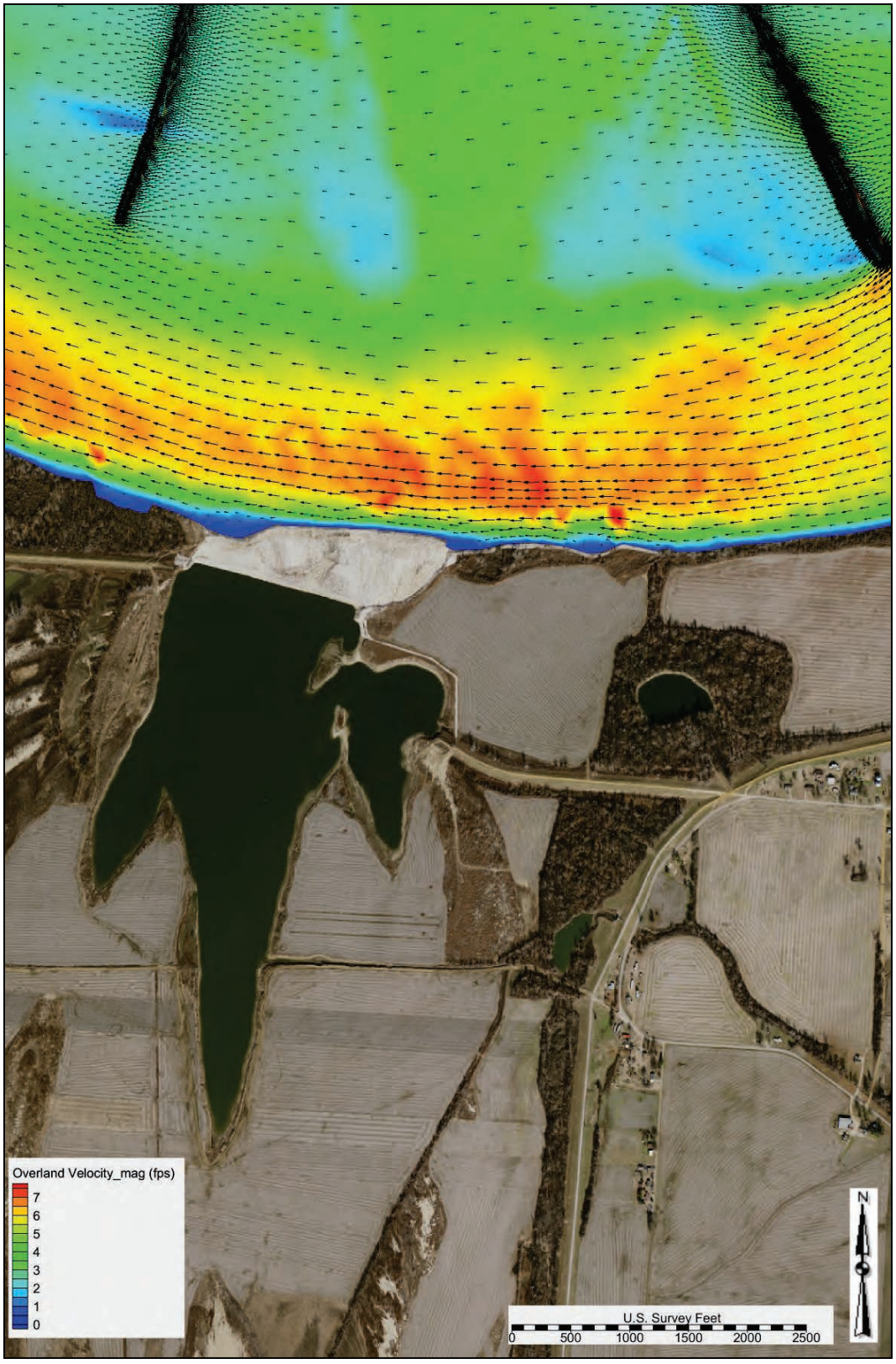


Figure C-75. Base condition velocity—700,000 cfs (study crevasse).

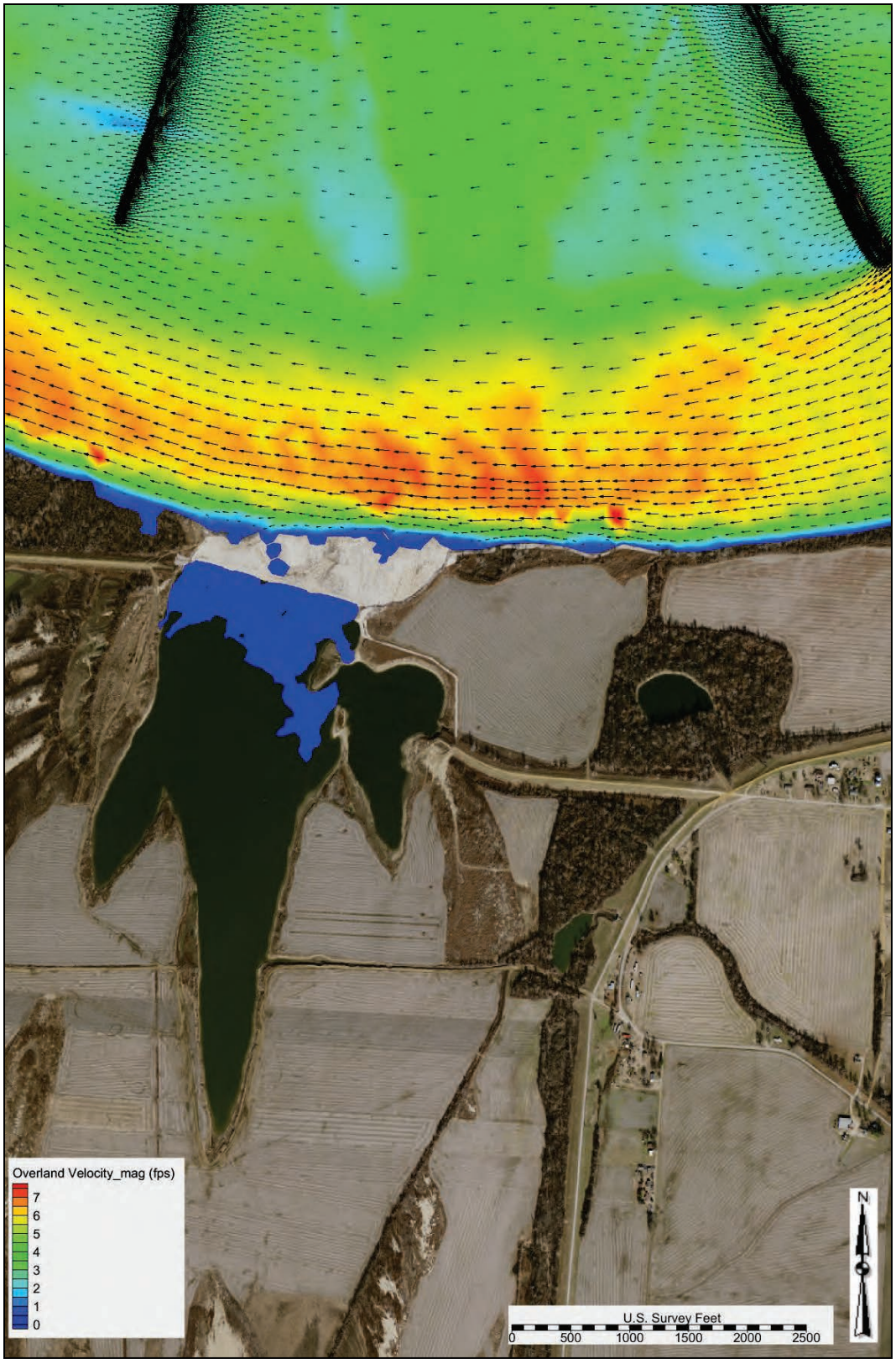


Figure C-76. Base condition velocity—750,000 cfs (study crevasse).

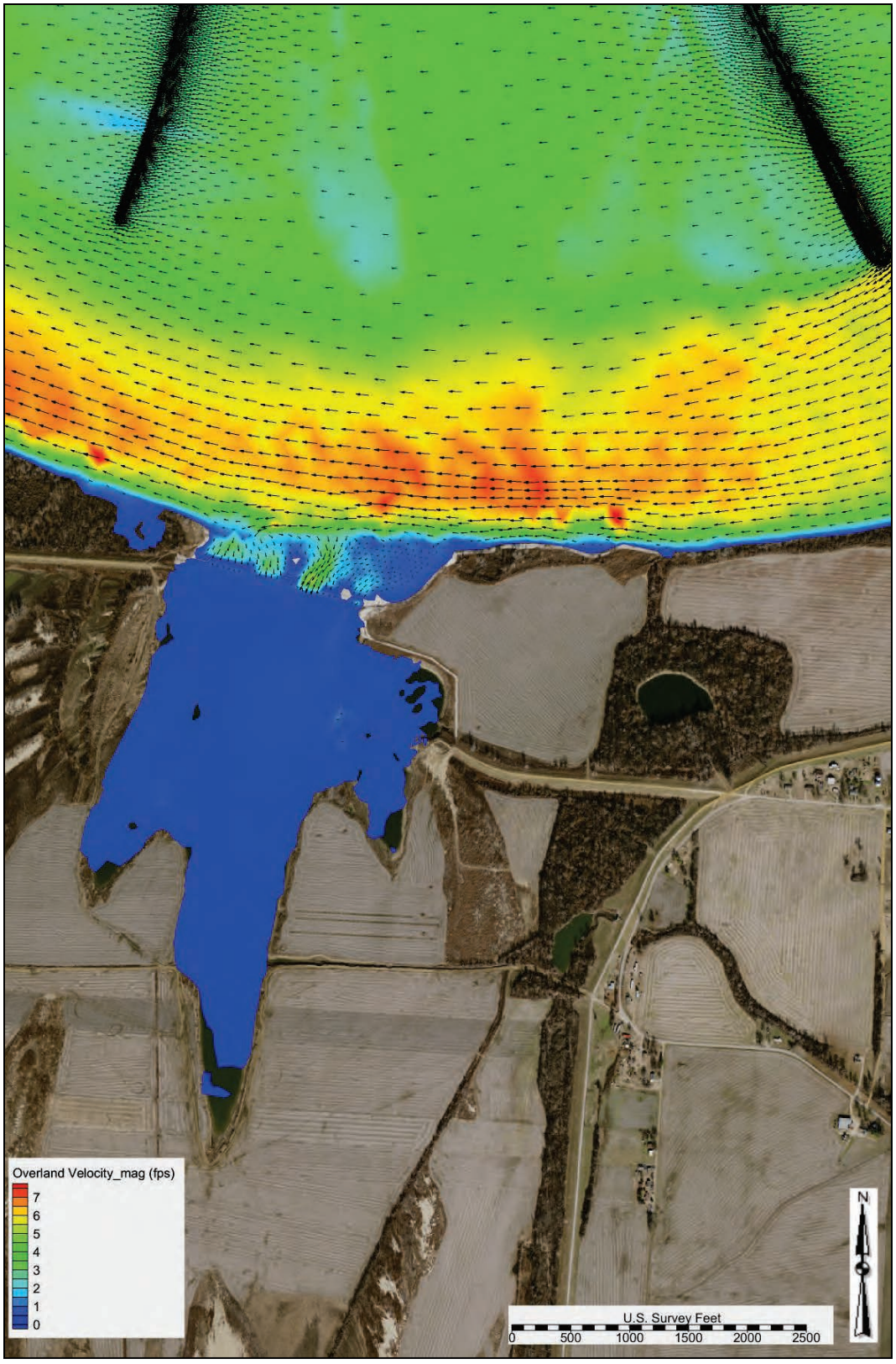


Figure C-77. Base condition velocity—800,000 cfs (study crevasse).

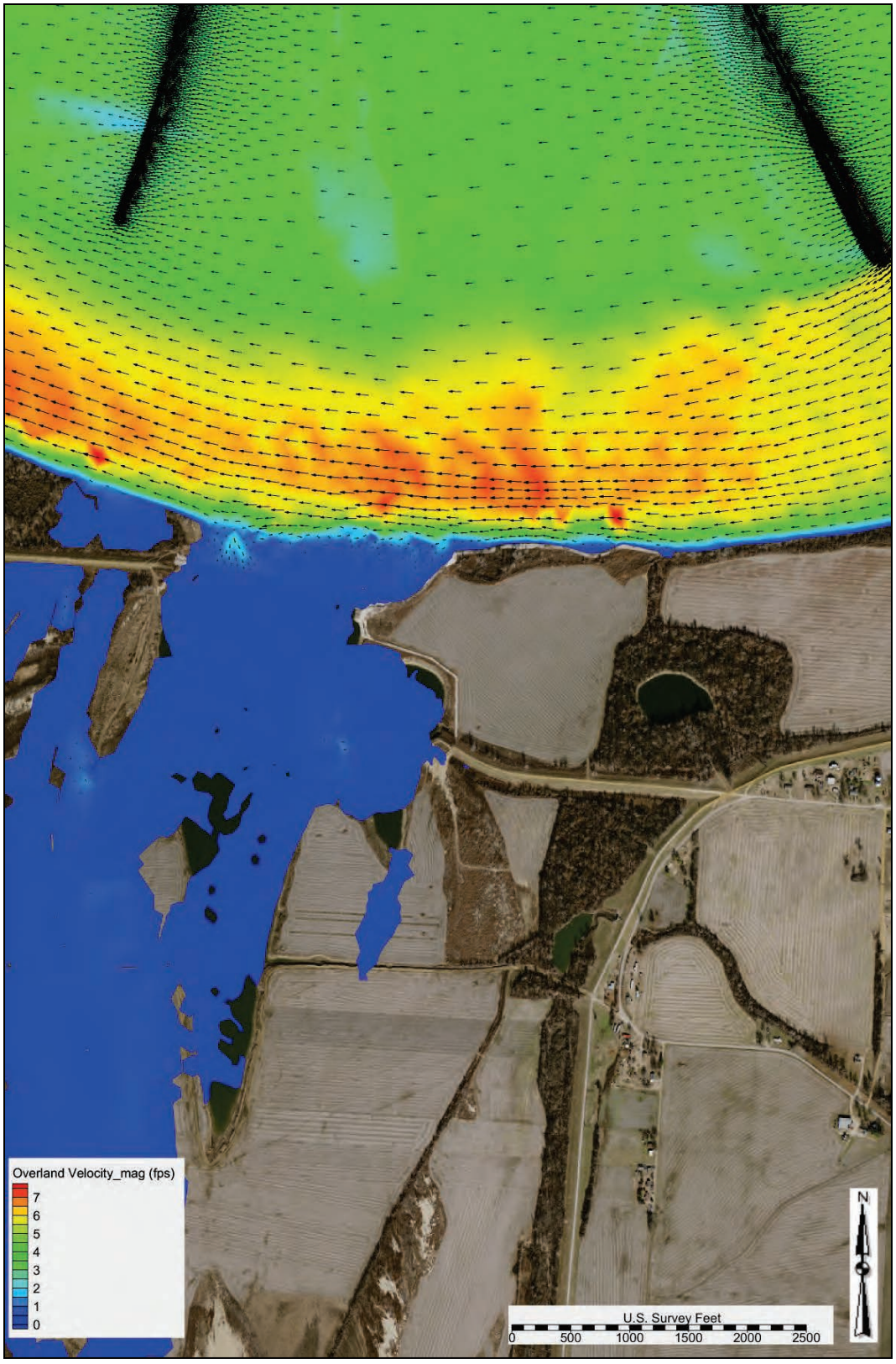


Figure C-78. Base condition velocity—850,000 cfs (study crevasse).

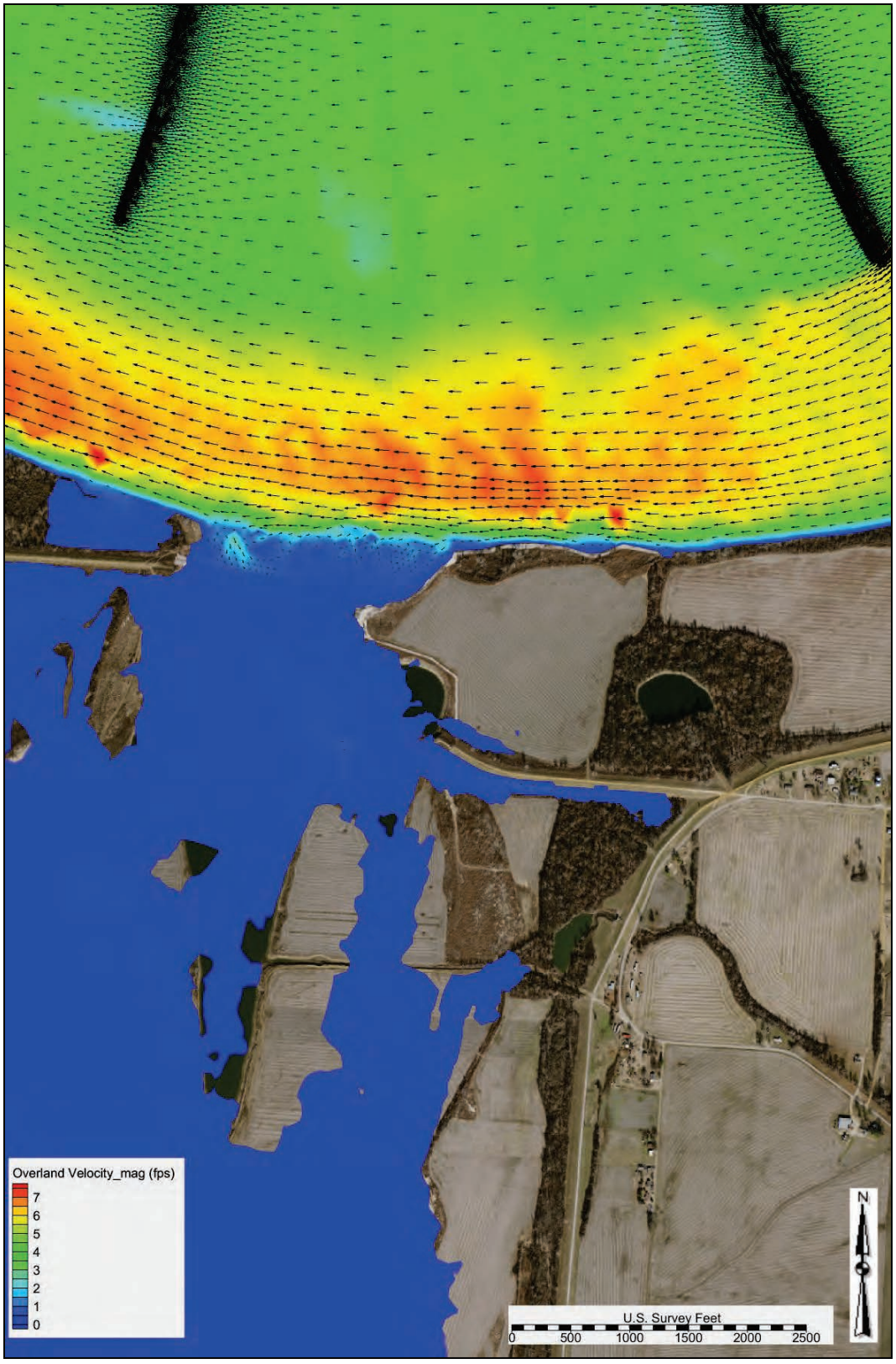


Figure C-79. Base condition velocity—900,000 cfs (study crevasse).

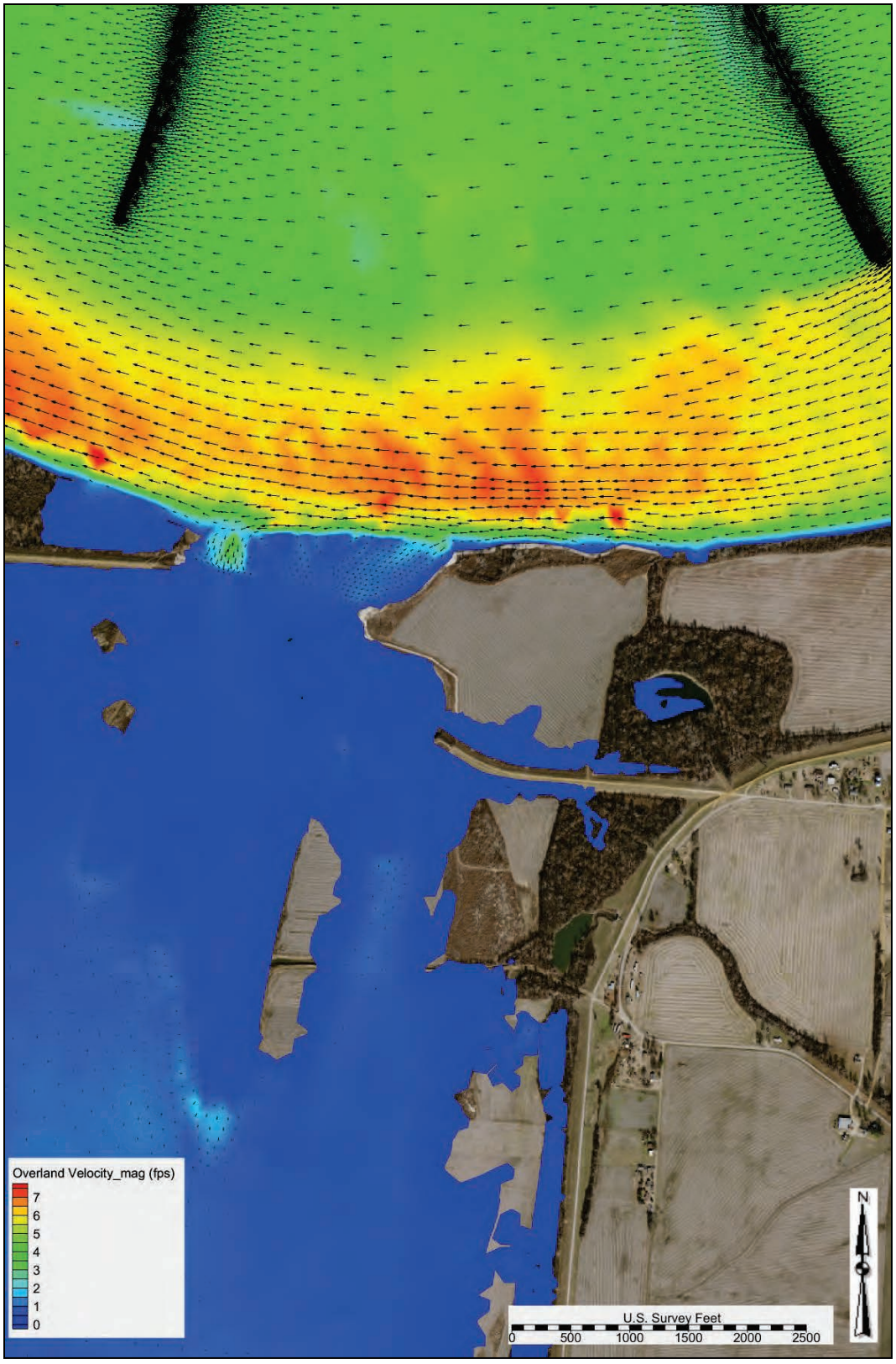


Figure C-80. Base condition velocity—1,100,000 cfs (study crevasse).

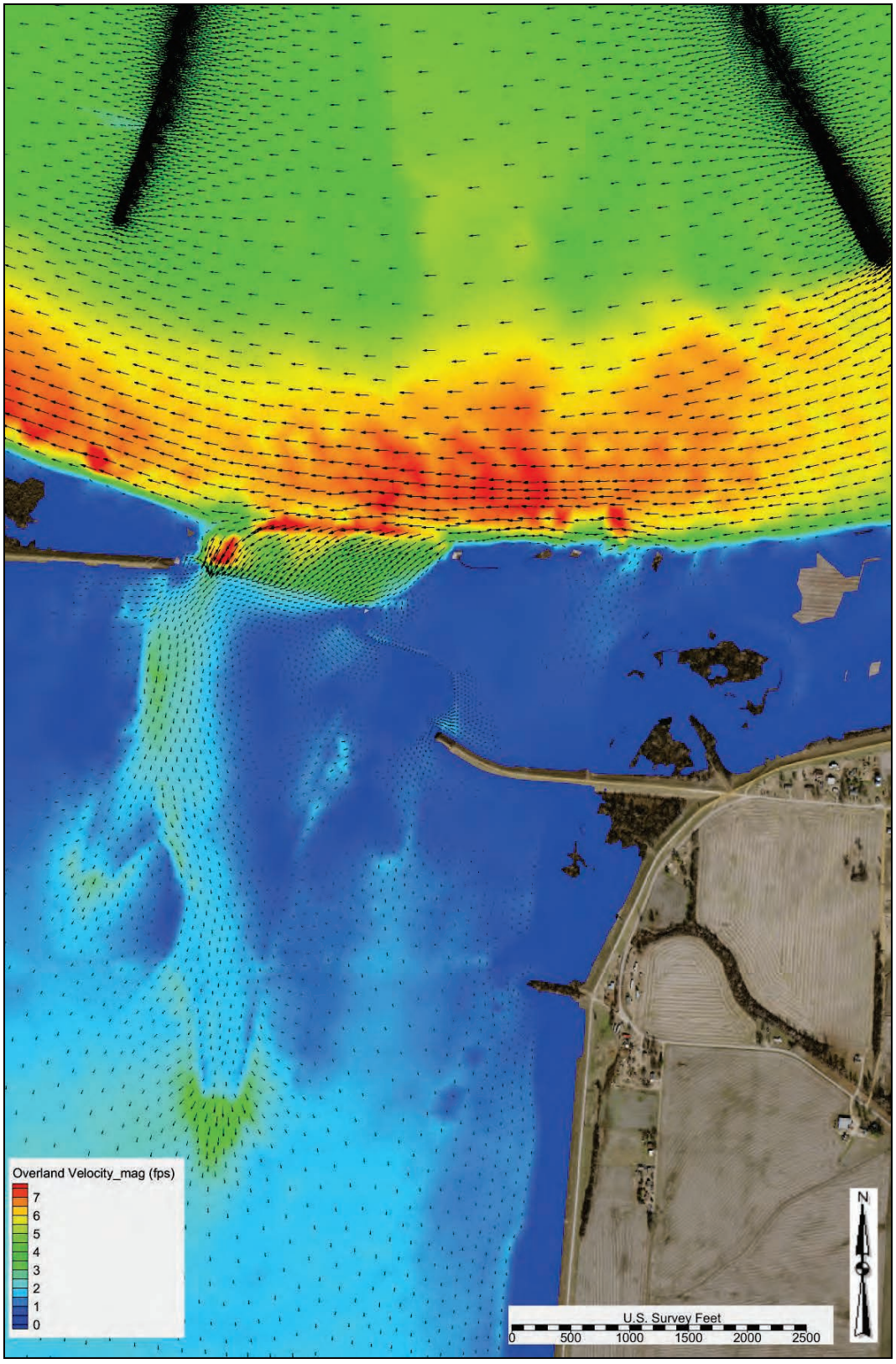


Figure C-81. Base condition velocity—1,300,000 cfs (study crevasse).

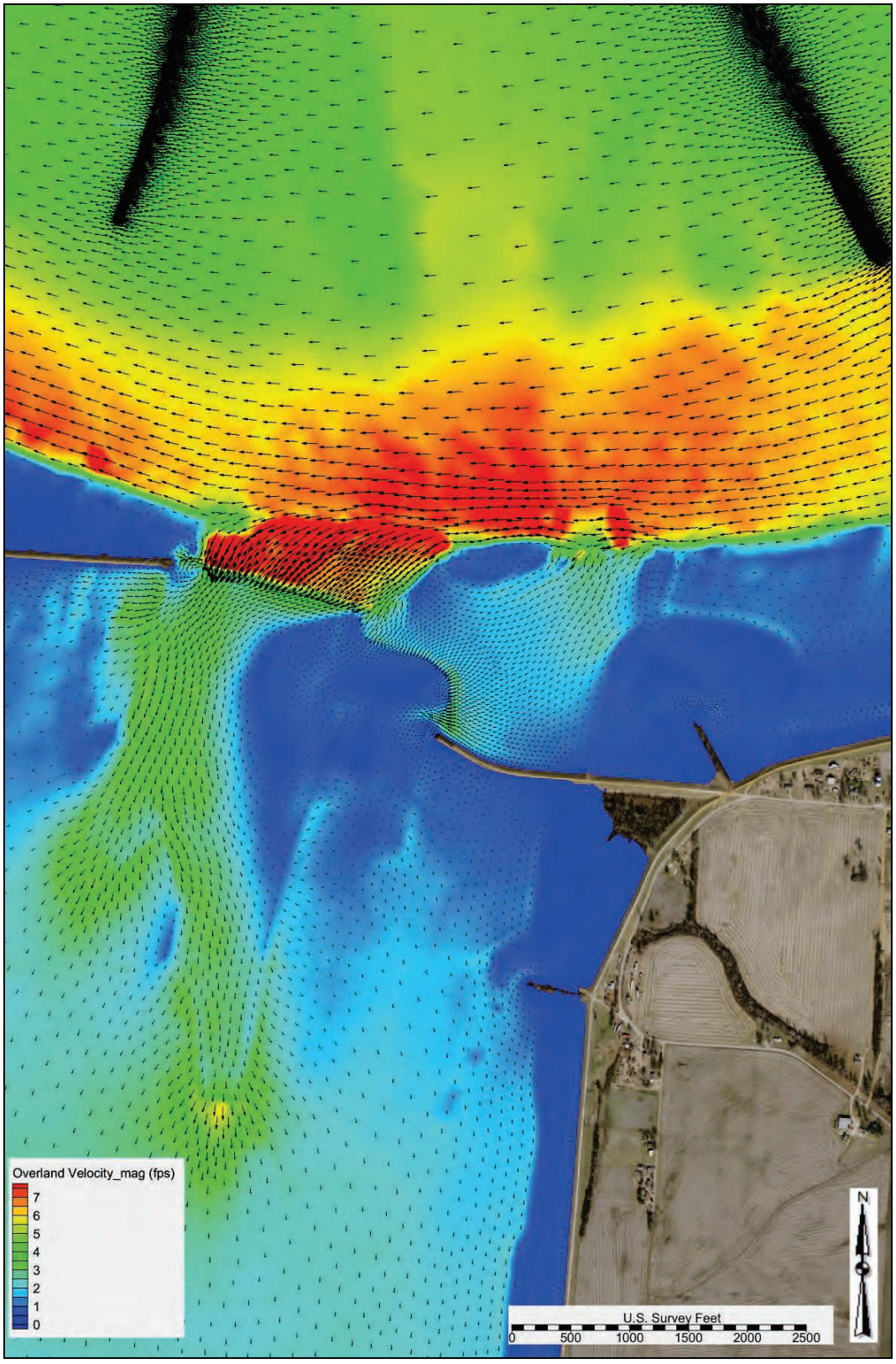


Figure C-82. Base condition velocity—1,500,000 cfs (study crevasse).

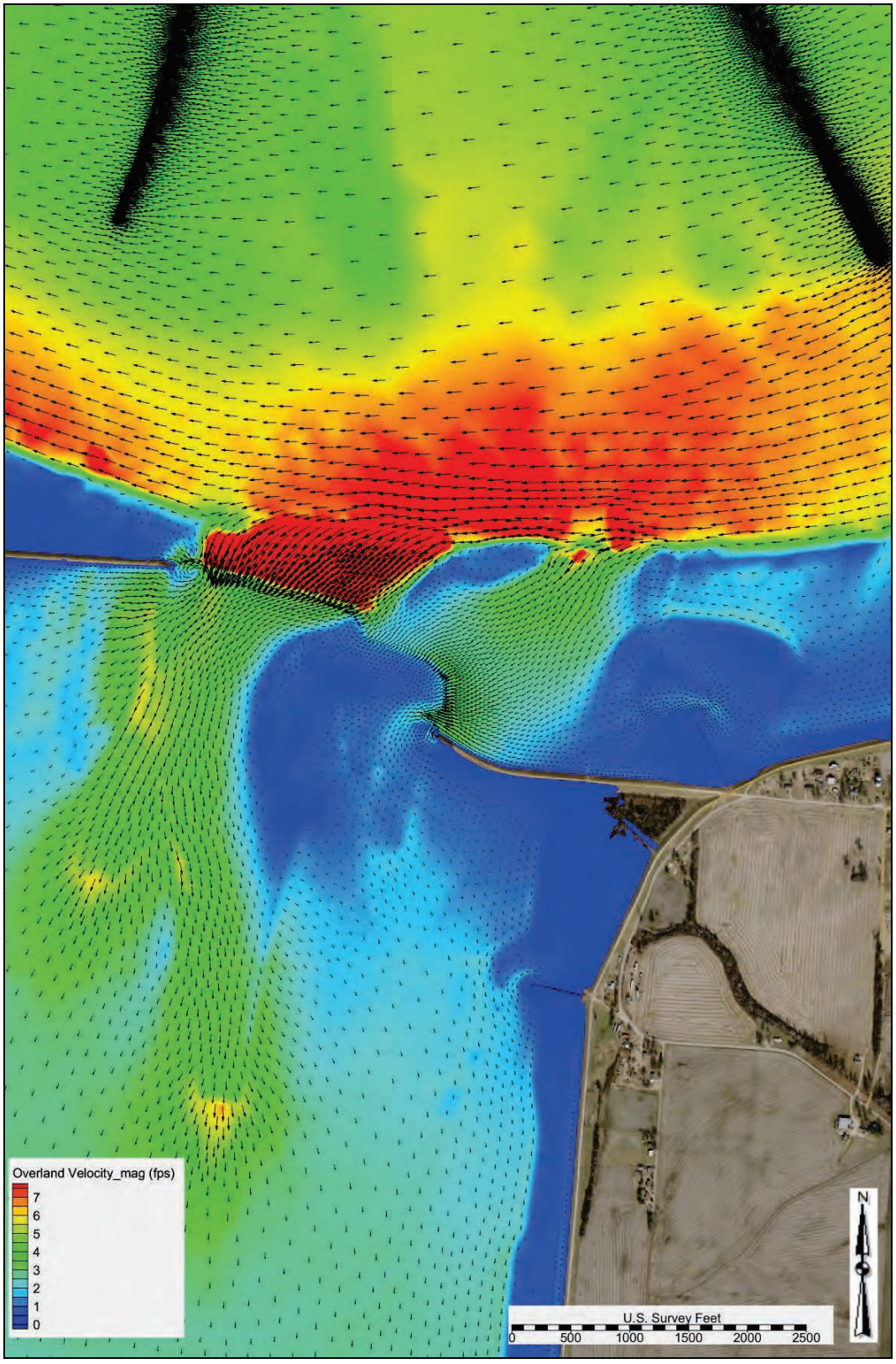


Figure C-83. Base condition velocity—1,700,000 cfs (study crevasse).

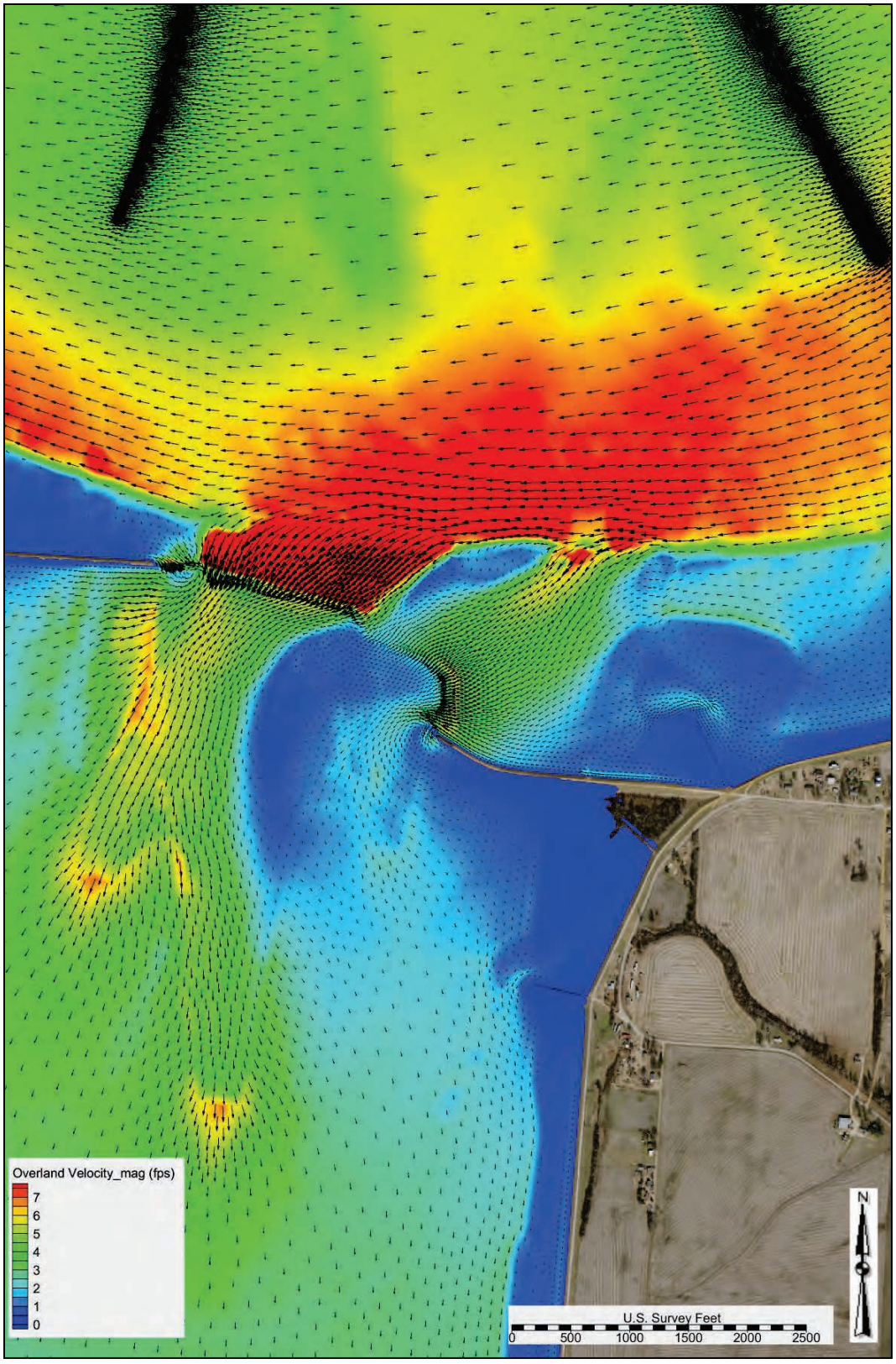


Figure C-84. Base condition velocity—1,900,000 cfs (study crevasse).

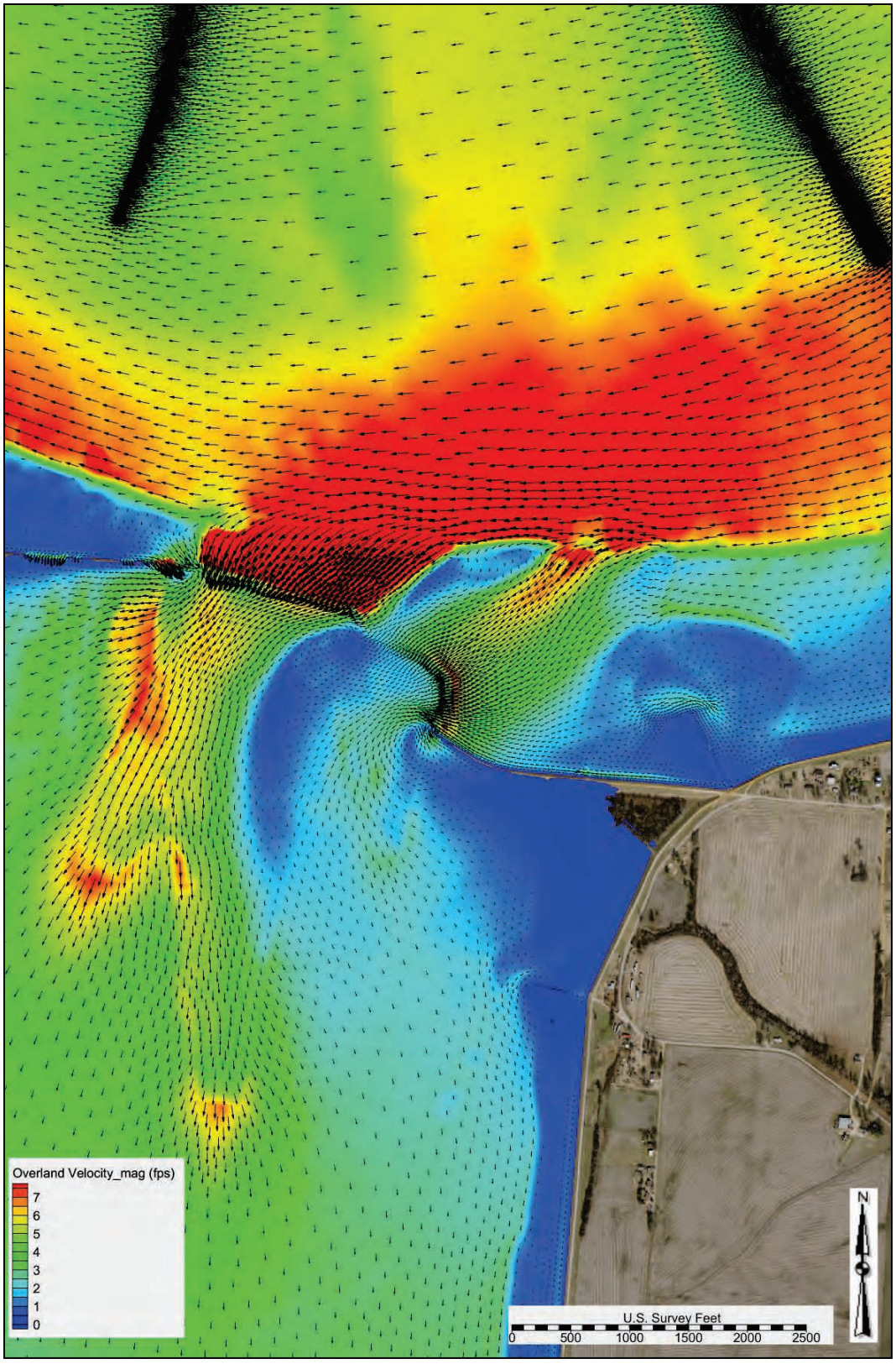
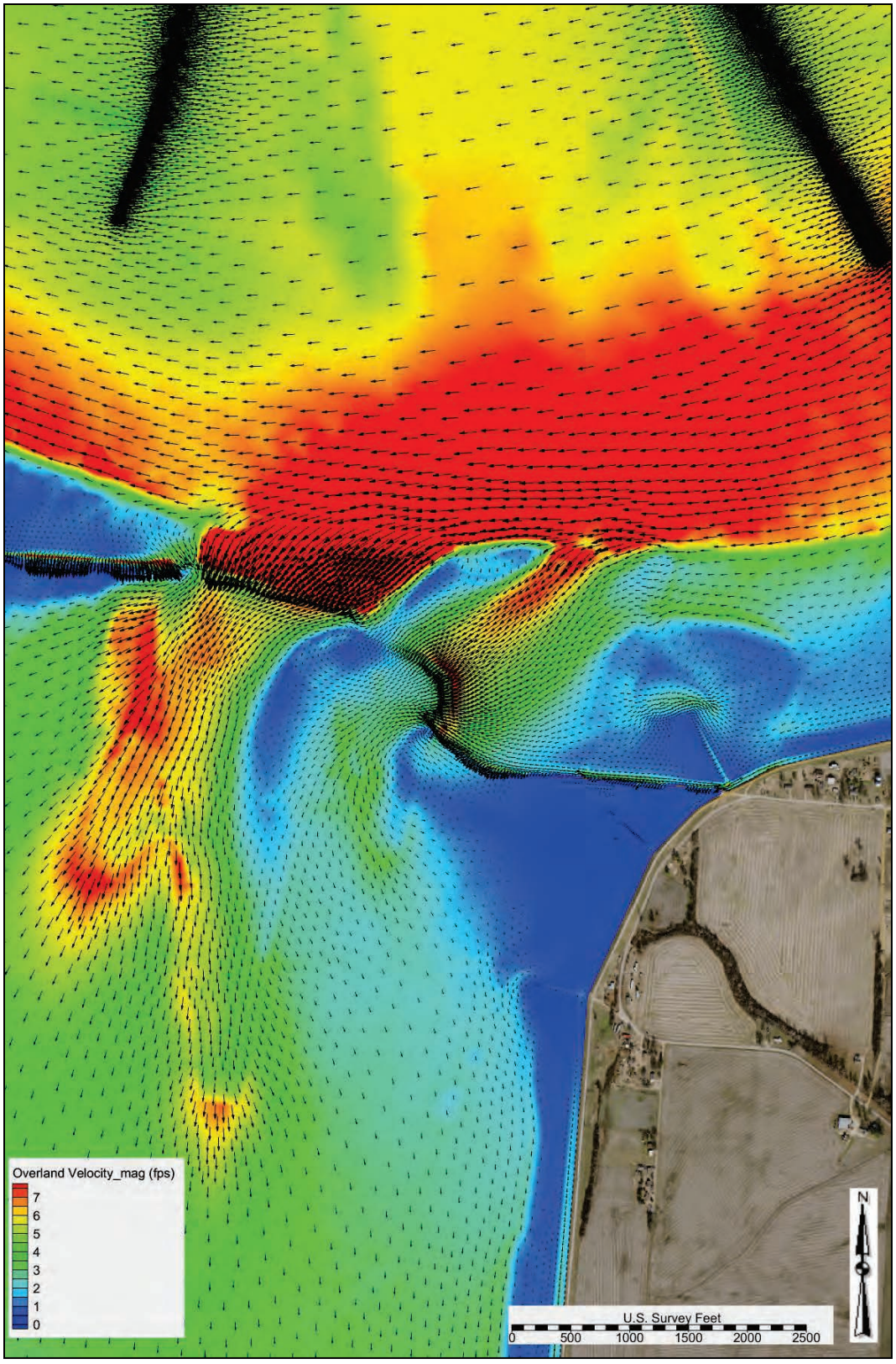


Figure C-85. Base condition velocity—2,100,000 cfs (study crevasse).



Shear stress

The modeled shear stress outputs at flows ranging from 900,000 to 2,100,000 cfs for the study overbank are depicted in Figures C-86 through C-92.

Figure C-86. Base condition shear stress—900,000 cfs (study overbank).

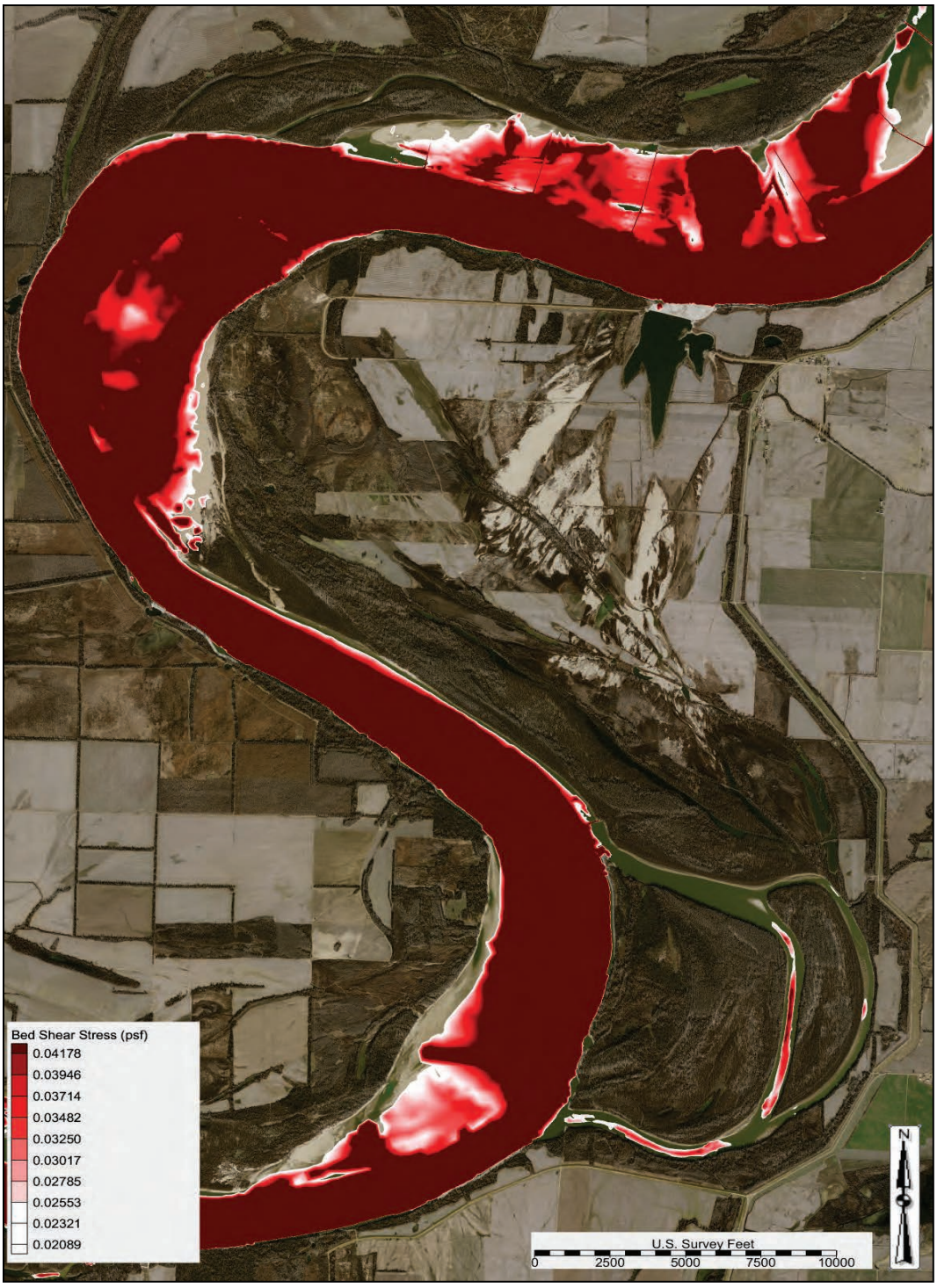


Figure C-87. Base condition shear stress—1,100,000 cfs (study overbank).

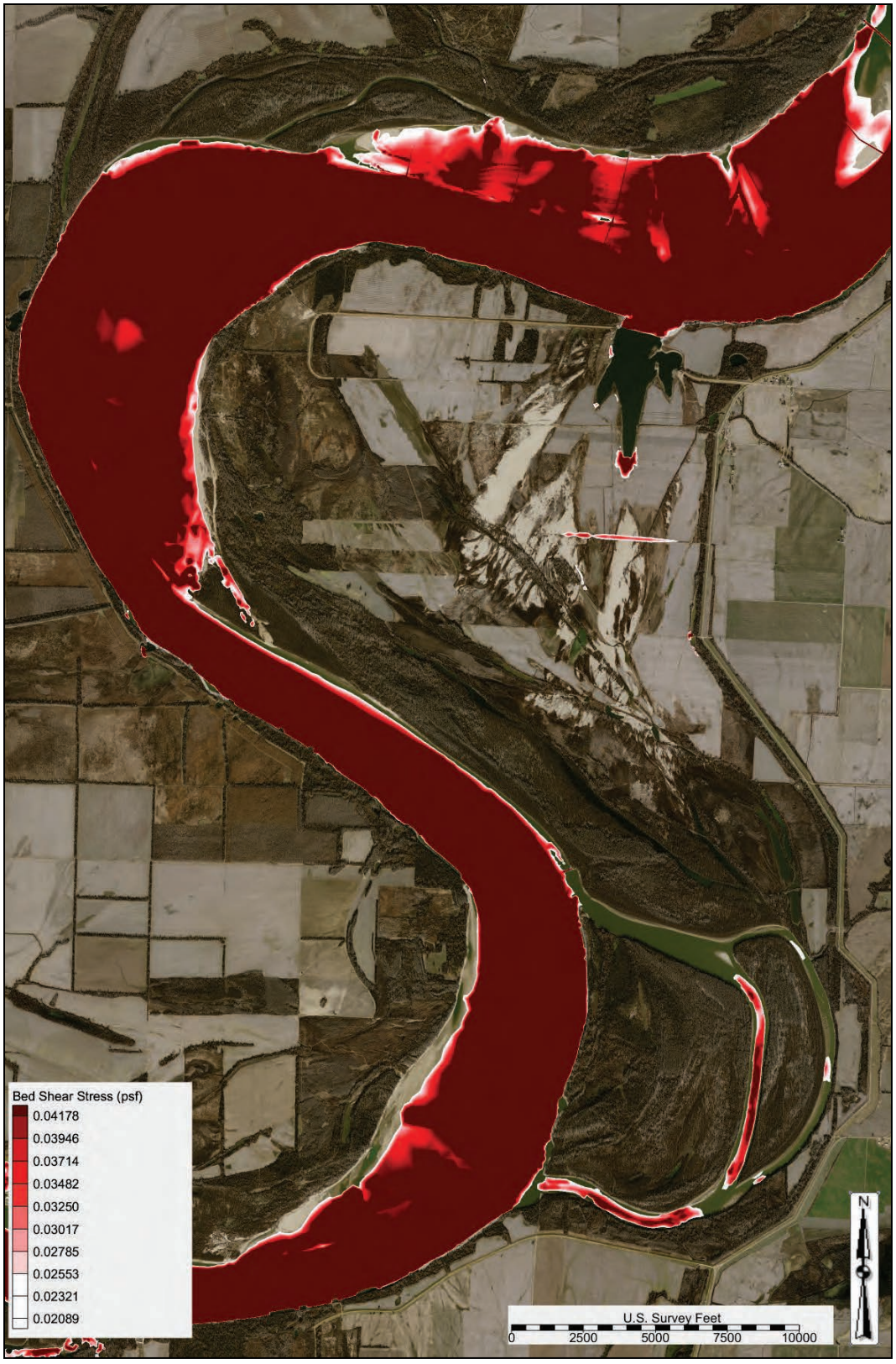


Figure C-88. Base condition shear stress—1,300,000 cfs (study overbank).

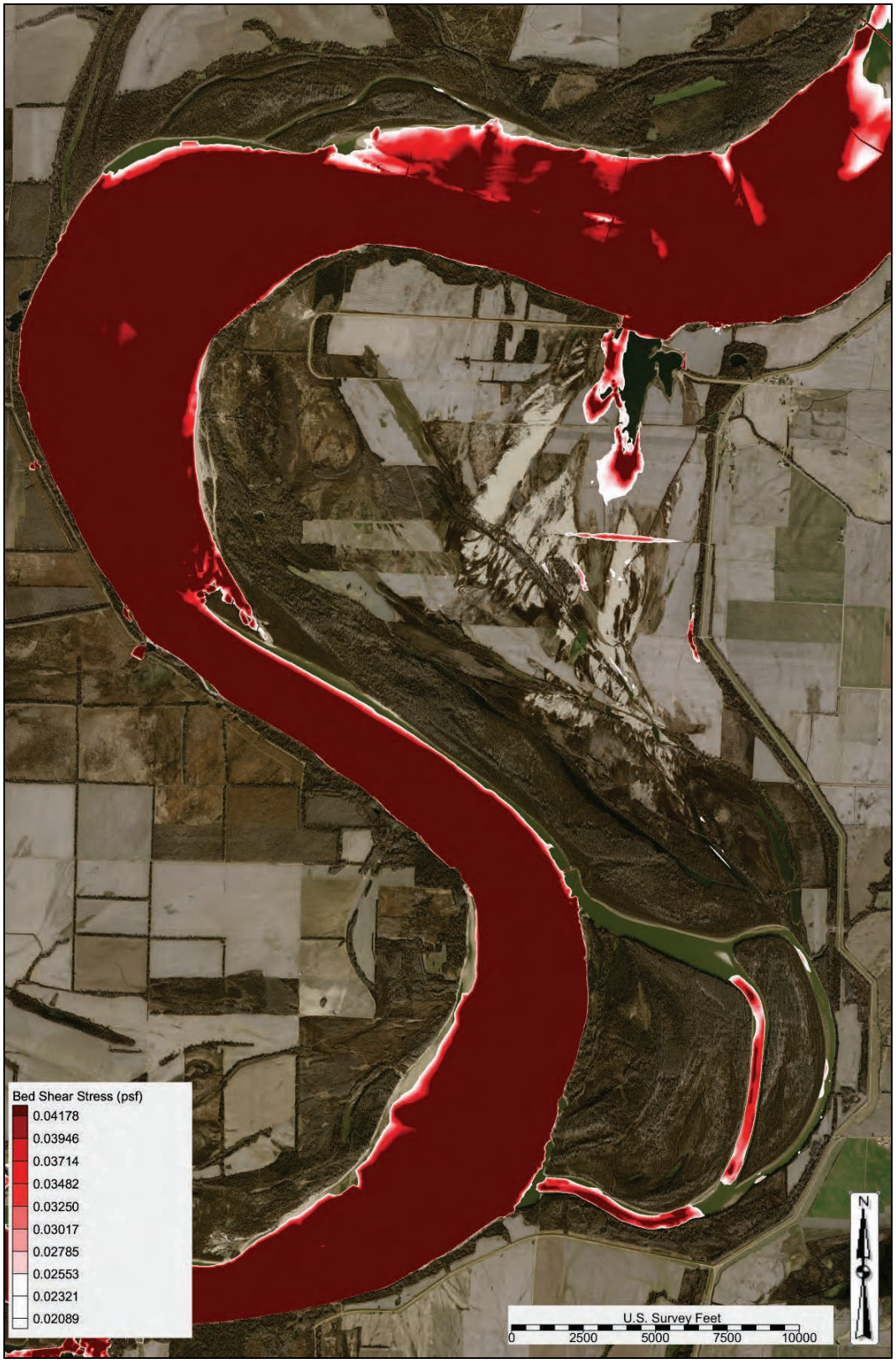


Figure C-89. Base condition shear stress—1,500,000 cfs (study overbank).

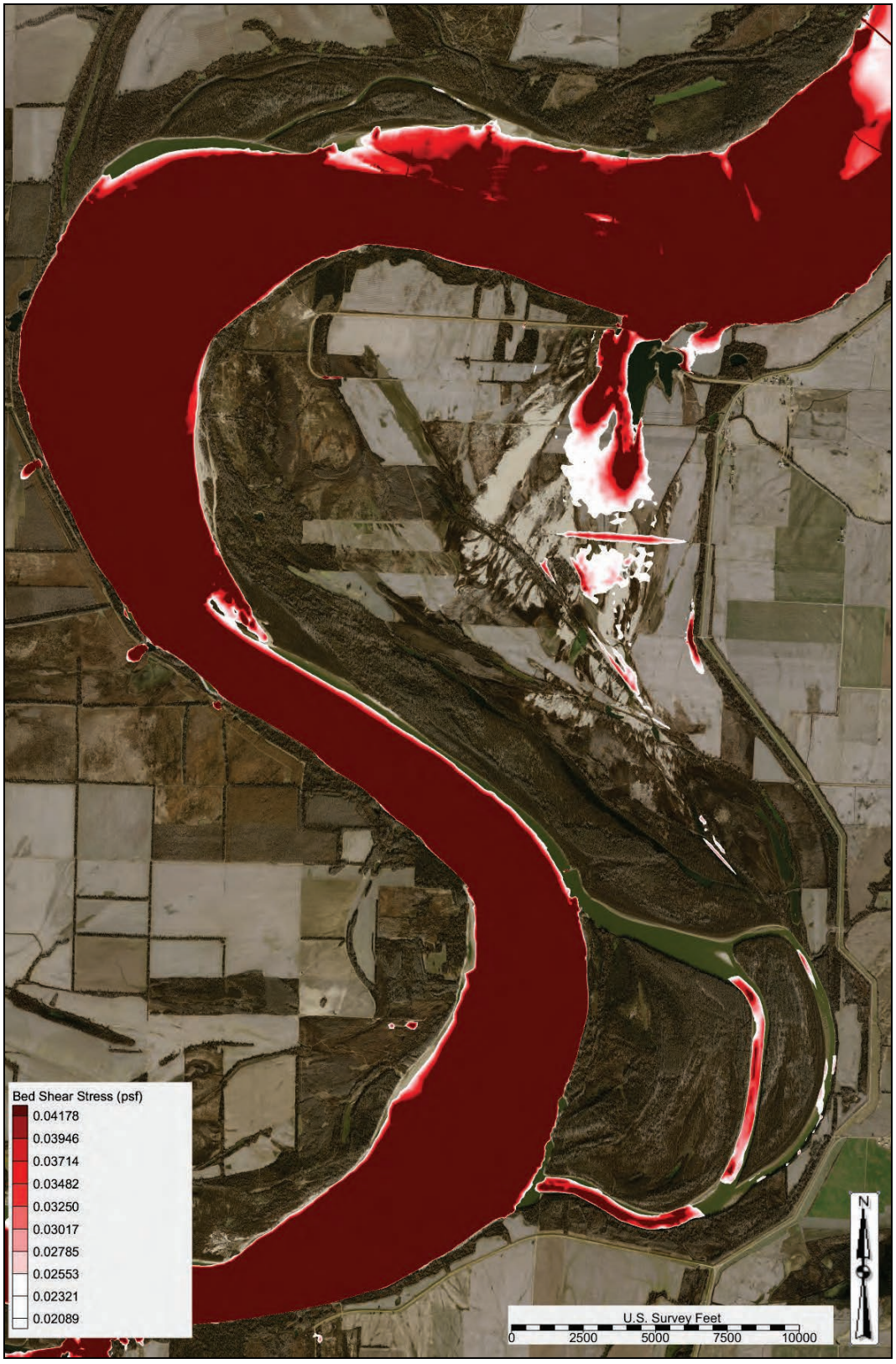


Figure C-90. Base condition shear stress—1,700,000 cfs (study overbank).

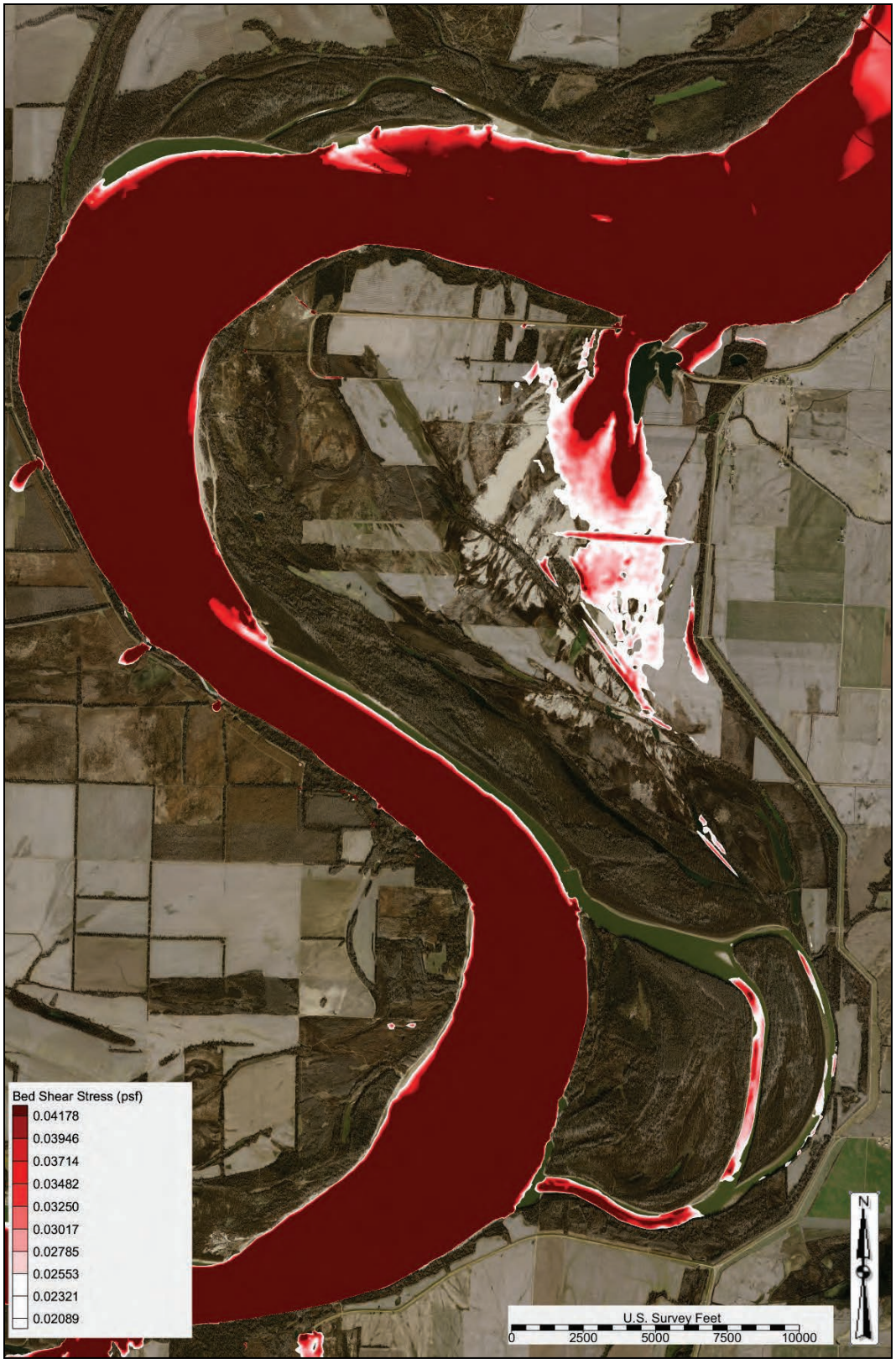


Figure C-91. Base condition shear stress—1,900,000 cfs (study overbank).

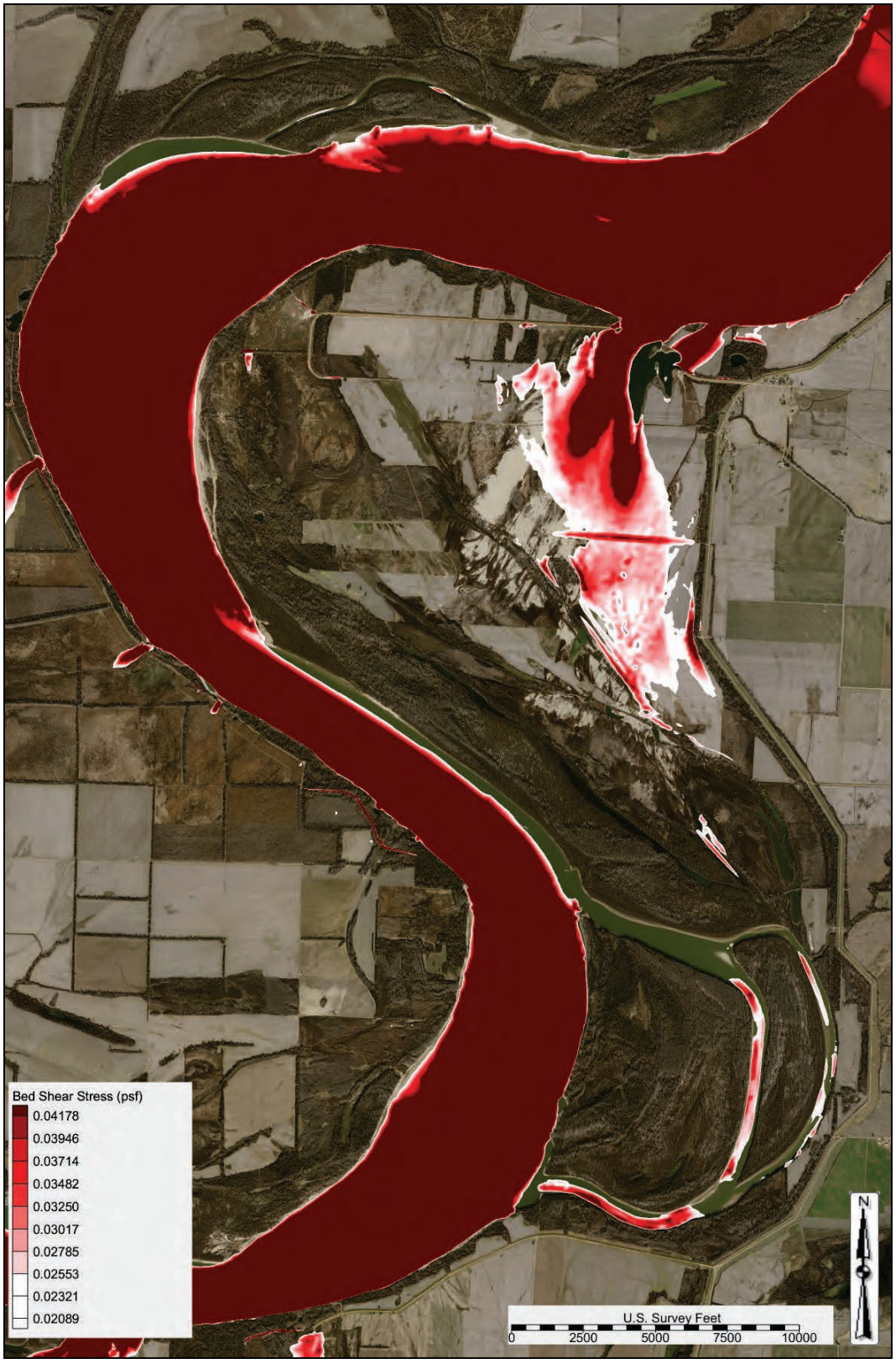
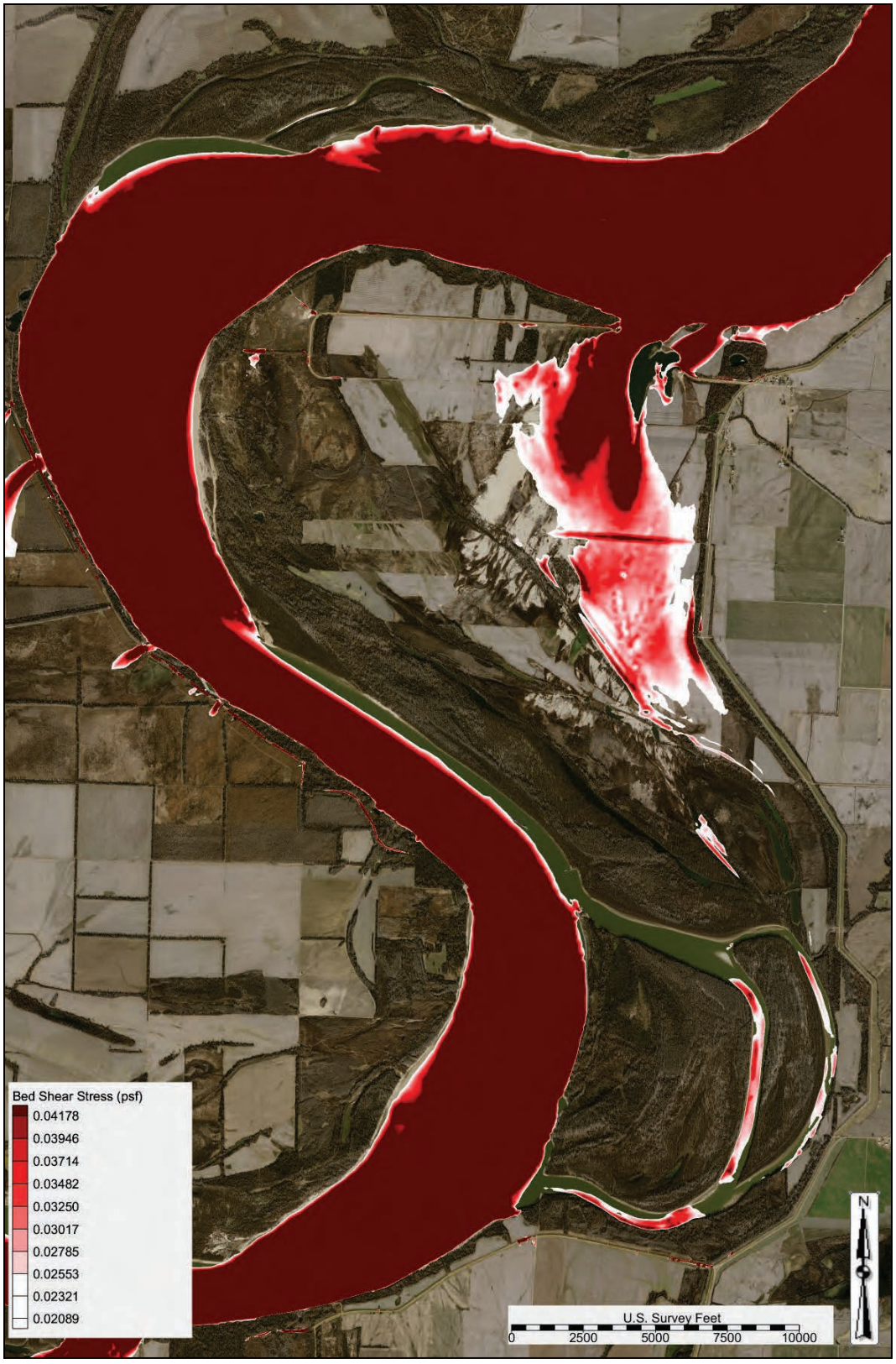


Figure C-92. Base condition shear stress—2,100,000 cfs (study overbank).



Water surface elevation (WSEL)

Figure C-93 depicts the WSEL profiles in the study reach for the following flows: 1,100,000 cfs, 1,500,000 cfs, 1,900,000 cfs, and 2,100,000 cfs.

Figure C-94 depicts the WSEL map at 2,100,000 cfs. Note the super elevation and head differentials that exist in the study reach.

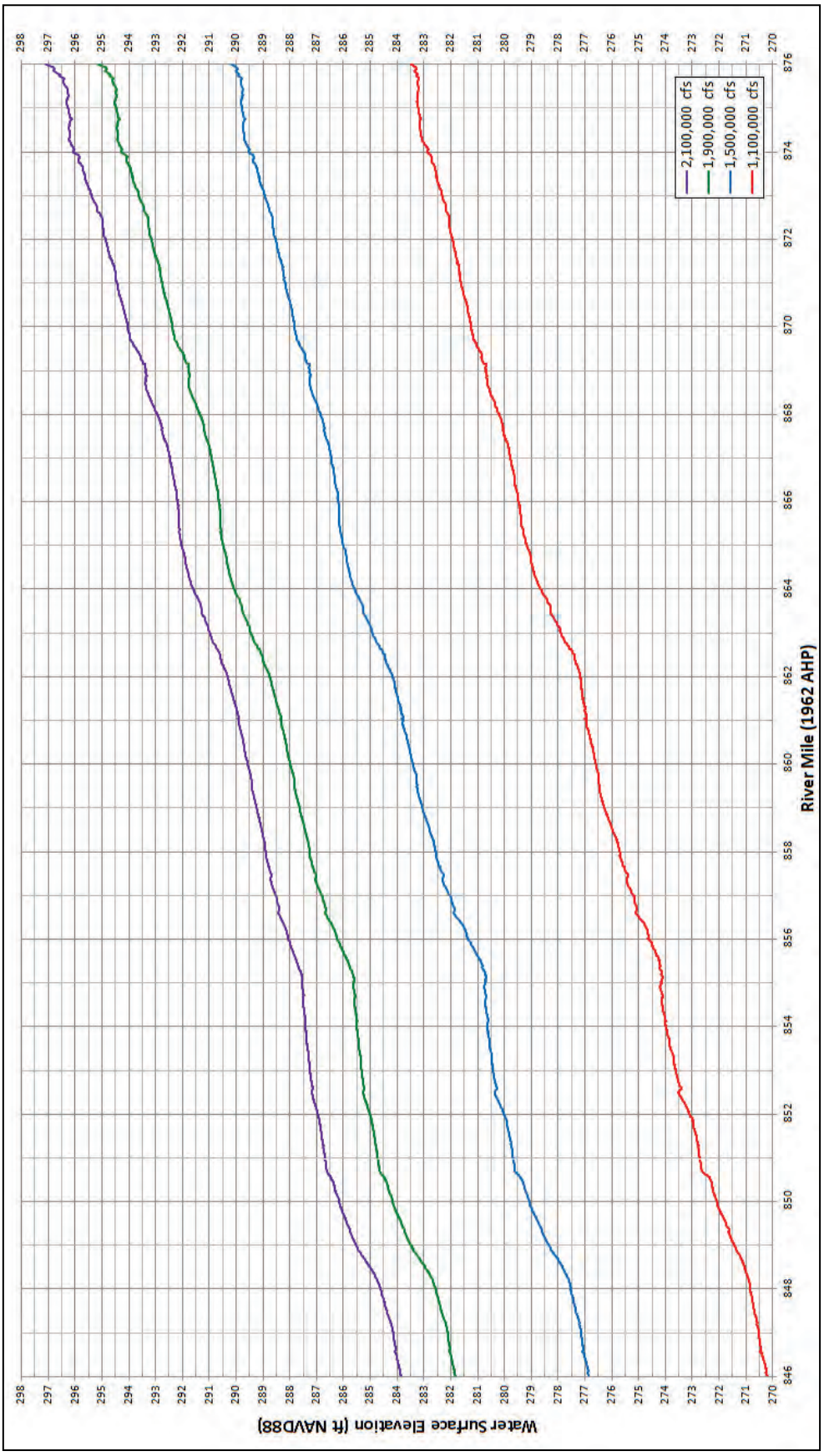
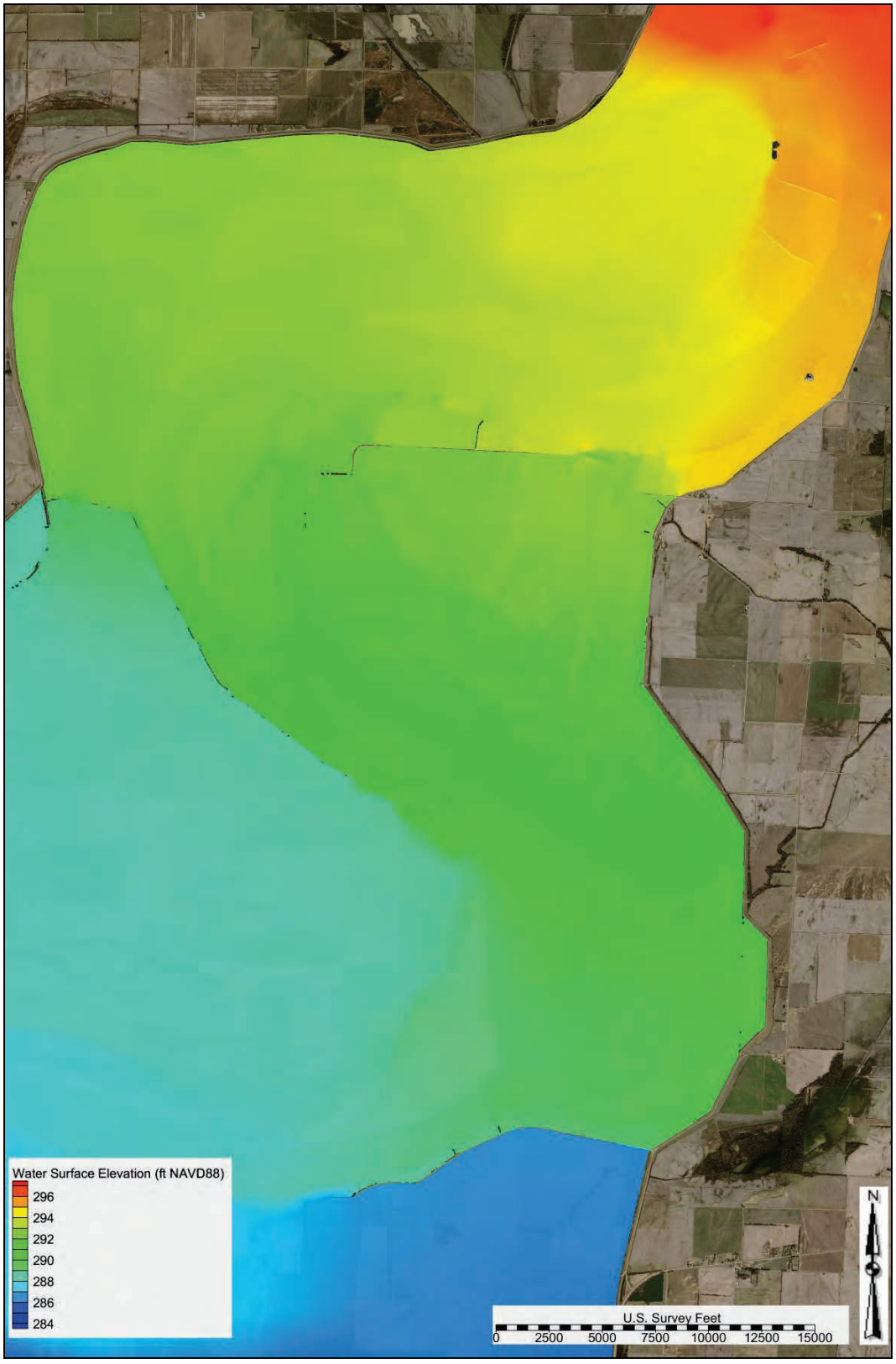


Figure C-93. Base condition WSEL profile.

Figure C-94. Base condition WSEL—2,100,000 cfs (study overbank).



Sediment diversion grain size distribution

Table C-1 lists the sediment diversion grain size distribution for flows ranging from 870,000 cfs to 2,000,000 cfs.

Table C-1. Base condition diversion grain size distribution.

Main Channel Flow US of Crevasse (cfs)	Total Diversion Load Grain Size Fraction Distribution									
	Coarse Silt	Very Fine Sand	Fine Sand	Medium Sand	Coarse Sand	Very Coarse Sand	Very Fine Pebble	Fine Pebble	Medium Pebble	Coarse Pebble
870,000	0.0000	0.9515	0.0480	0.0005	0.0000	0.0000	0.0000	0.0000	0.0000	0.0000
900,000	0.0000	0.8997	0.0989	0.0014	0.0000	0.0000	0.0000	0.0000	0.0000	0.0000
1,000,000	0.0000	0.4120	0.4318	0.1225	0.0276	0.0061	0.0000	0.0000	0.0000	0.0000
1,100,000	0.0000	0.2140	0.4010	0.2550	0.1086	0.0207	0.0005	0.0001	0.0000	0.0000
1,200,000	0.0002	0.1465	0.3366	0.3105	0.1584	0.0408	0.0051	0.0011	0.0006	0.0001
1,300,000	0.0004	0.1170	0.3029	0.3458	0.1853	0.0415	0.0035	0.0025	0.0011	0.0002
1,400,000	0.0006	0.1048	0.2688	0.3546	0.2127	0.0511	0.0026	0.0031	0.0015	0.0002
1,500,000	0.0018	0.1092	0.2812	0.3580	0.2000	0.0422	0.0026	0.0021	0.0025	0.0003
1,600,000	0.0011	0.1008	0.2790	0.3724	0.1976	0.0403	0.0030	0.0014	0.0040	0.0005
1,700,000	0.0011	0.0944	0.2724	0.3795	0.2022	0.0400	0.0033	0.0012	0.0051	0.0007
1,800,000	0.0011	0.0881	0.2651	0.3884	0.2074	0.0404	0.0038	0.0013	0.0032	0.0011
1,900,000	0.0007	0.0860	0.2635	0.3932	0.2080	0.0392	0.0040	0.0015	0.0023	0.0015
2,000,000	0.0009	0.0786	0.2514	0.4041	0.2147	0.0408	0.0043	0.0015	0.0018	0.0020
2,100,000	0.0010	0.0790	0.2529	0.4014	0.2145	0.0401	0.0050	0.0017	0.0018	0.0027

Closure structure failure output

The following sections contain AdH model output and analysis for the closure structure failure scenario.

Shear stress

The modeled shear stress outputs at flows ranging from 900,000 to 2,100,000 cfs for the study overbank are depicted in Figures C-95 through C-101.

Figure C-95. Closure structure failure shear stress—900,000 cfs (study overbank).



Figure C-96. Closure structure failure shear stress—1,100,000 cfs (study overbank).

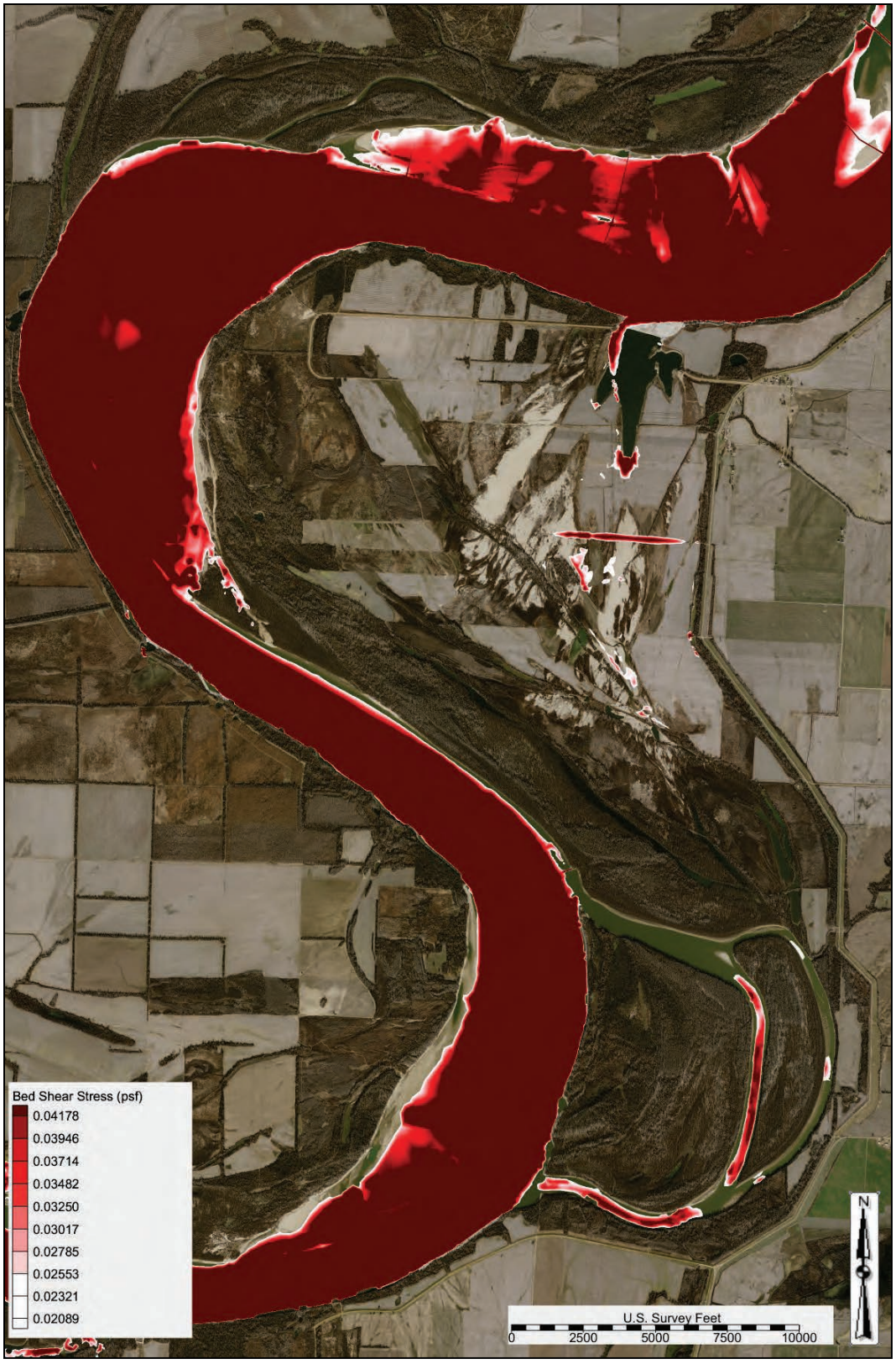


Figure C-97. Closure structure failure shear stress—1,300,000 cfs (study overbank).

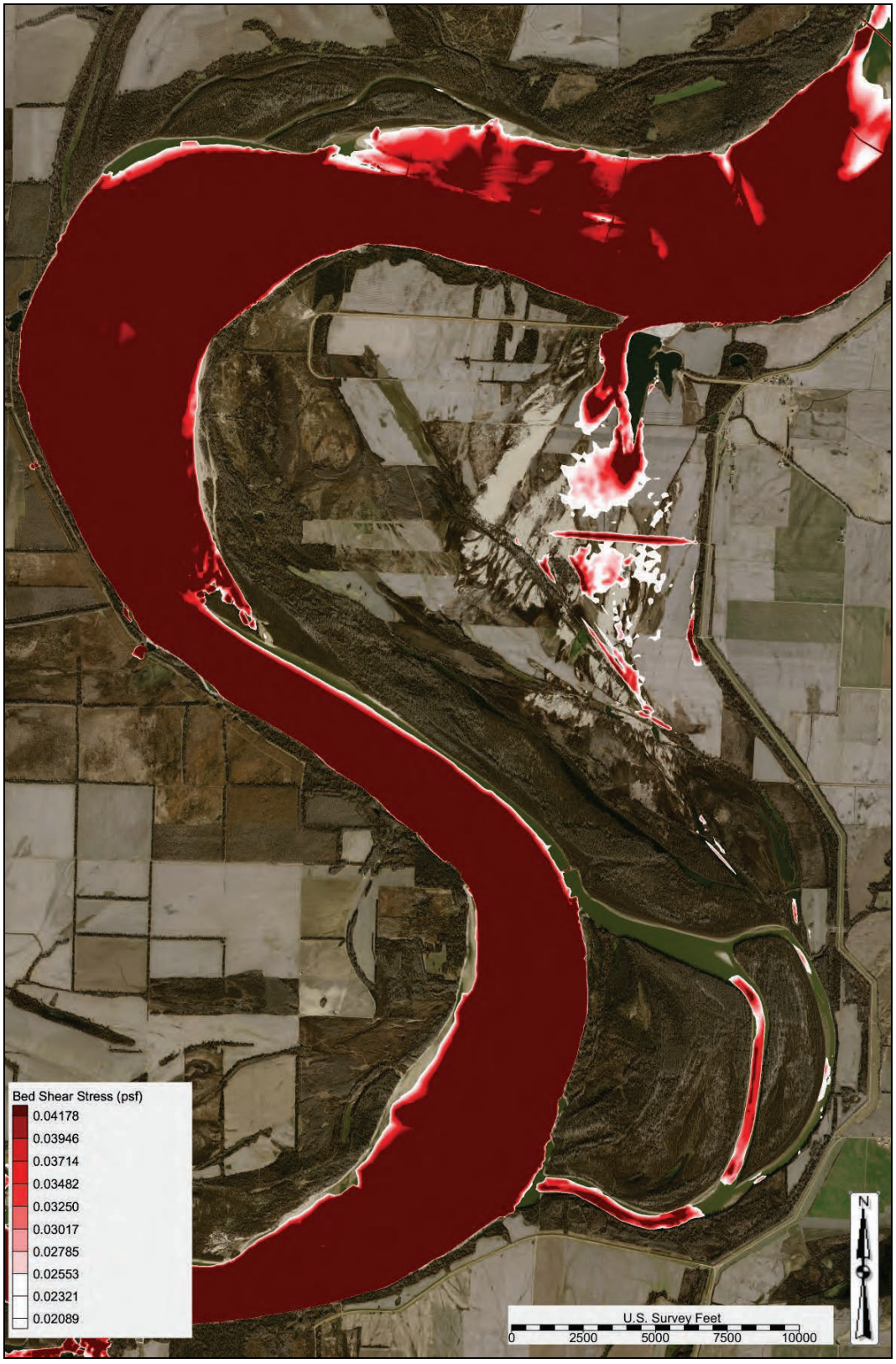


Figure C-98. Closure structure failure shear stress—1,500,000 cfs (study overbank).

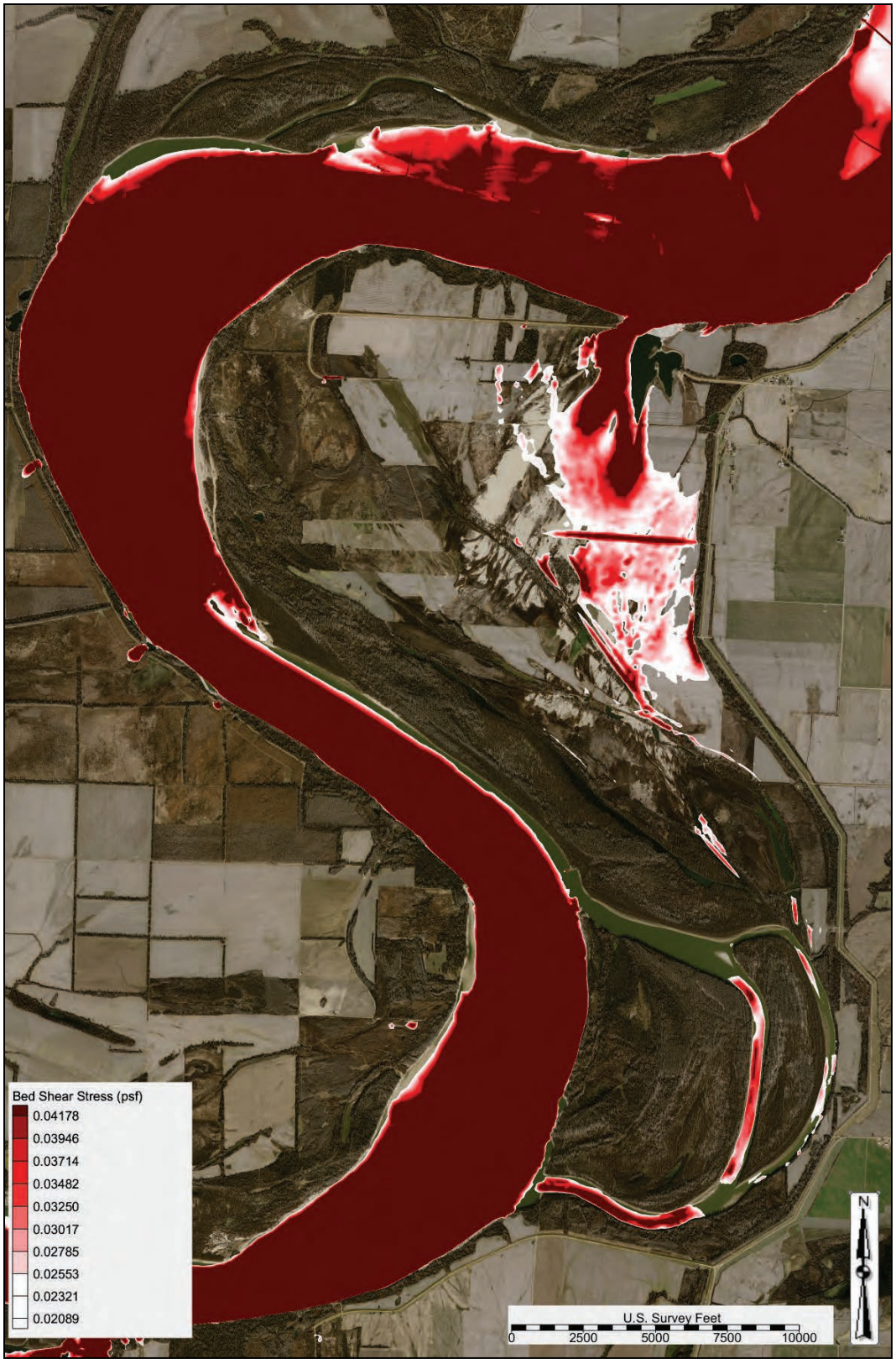


Figure C-99. Closure structure failure shear stress—1,700,000 cfs (study overbank).

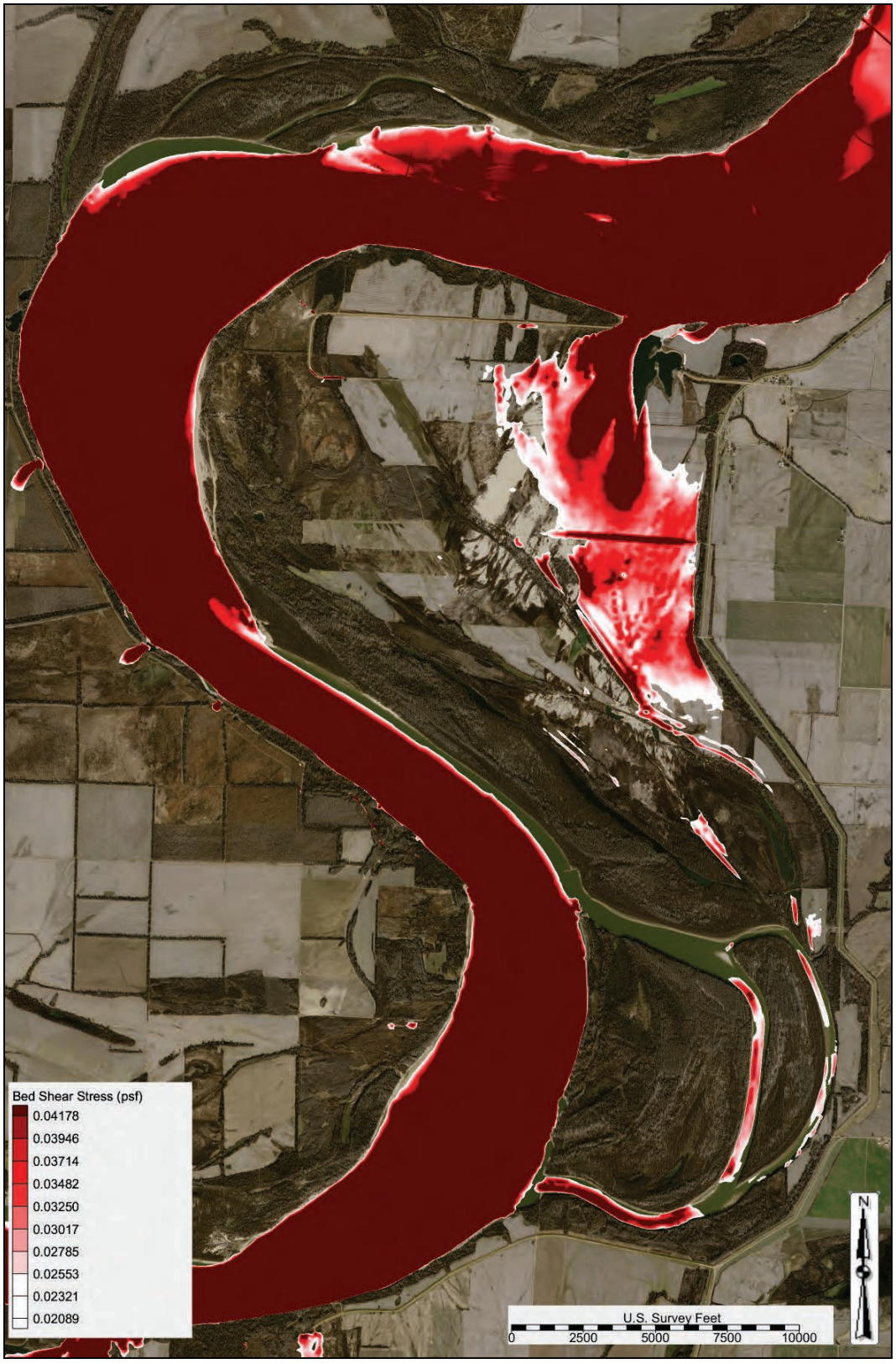


Figure C-100. Closure structure failure shear stress—1,900,000 cfs (study overbank).

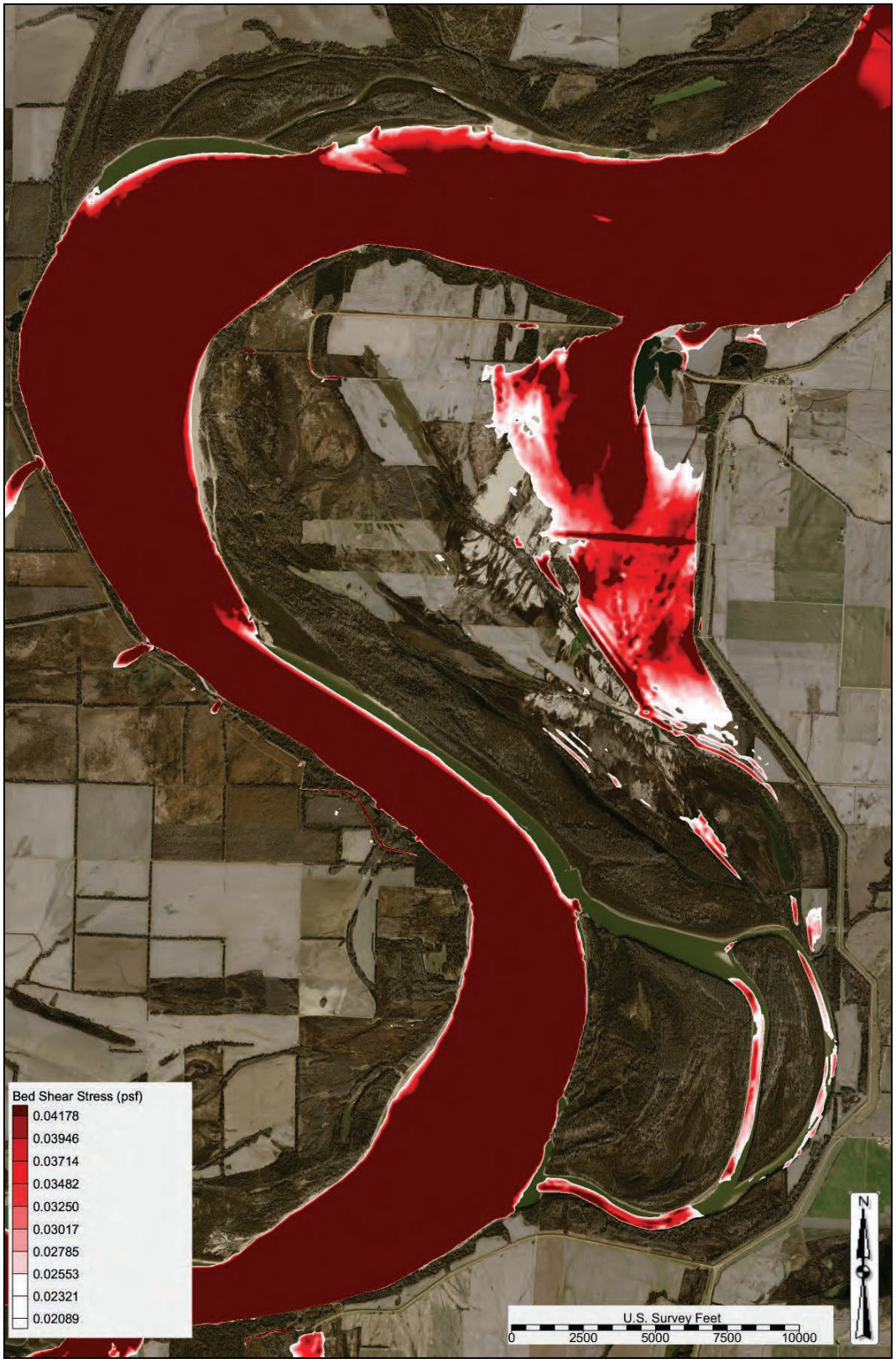
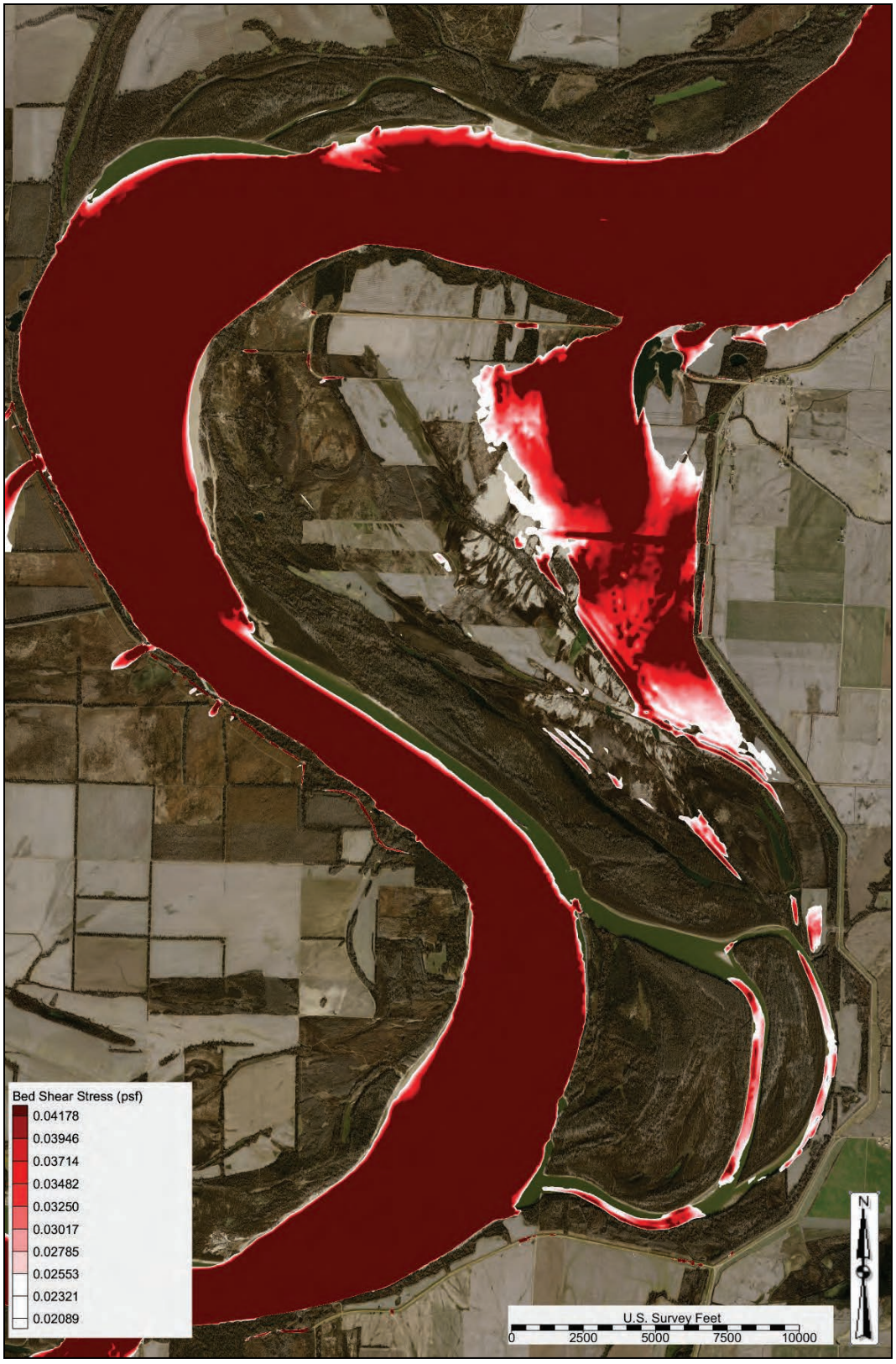


Figure C-101. Closure structure failure shear stress—2,100,000 cfs (study overbank).



Shear stress difference comparison

The modeled shear stress difference plots compared to the base condition output for flows ranging from 900,000 through 2,100,000 cfs are depicted in Figures C-102 through C-108. A positive shear stress difference (+ value and red and orange) indicated an increased shear stress compared to the base condition. A negative shear stress difference (- value and blue) indicated a decreased shear stress compared to the base condition. A zero shear stress difference (zero value and white) indicated that the alternative had no change in shear stress.

Figure C-102. Closure structure failure shear stress difference—900,000 cfs.

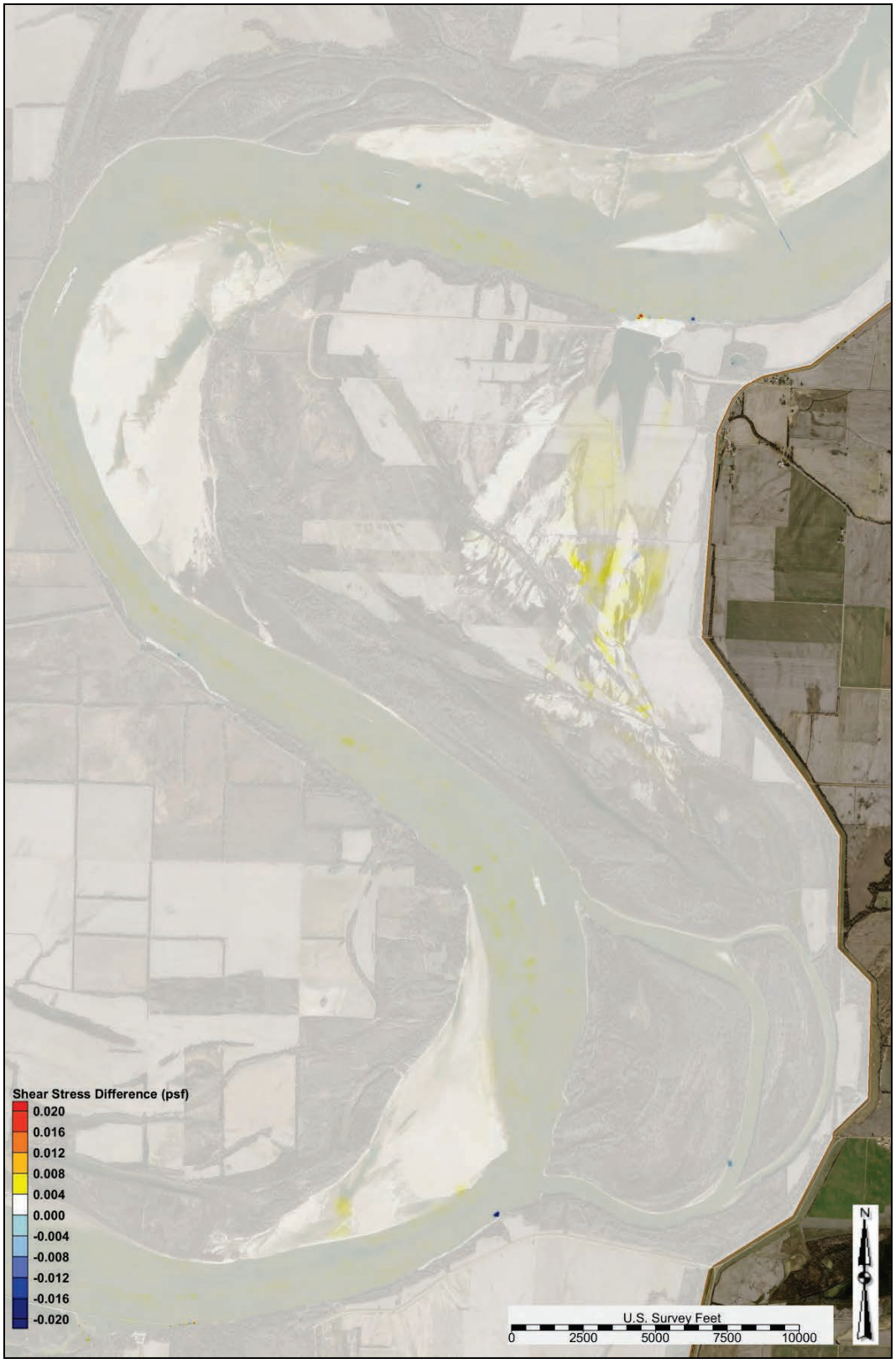


Figure C-103. Closure structure failure shear stress difference—1,100,000 cfs.

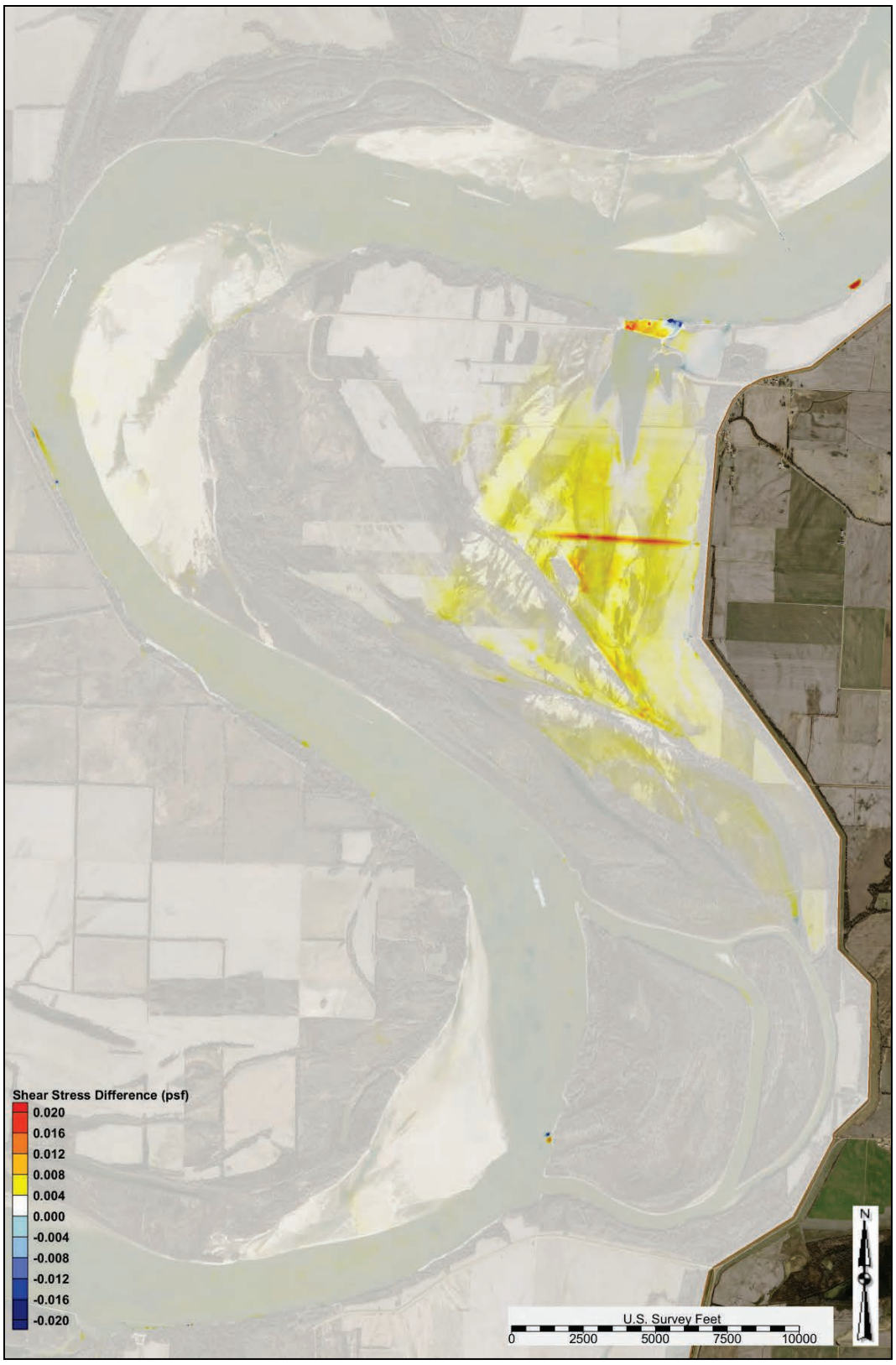


Figure C-104. Closure structure failure shear stress difference—1,300,000 cfs.

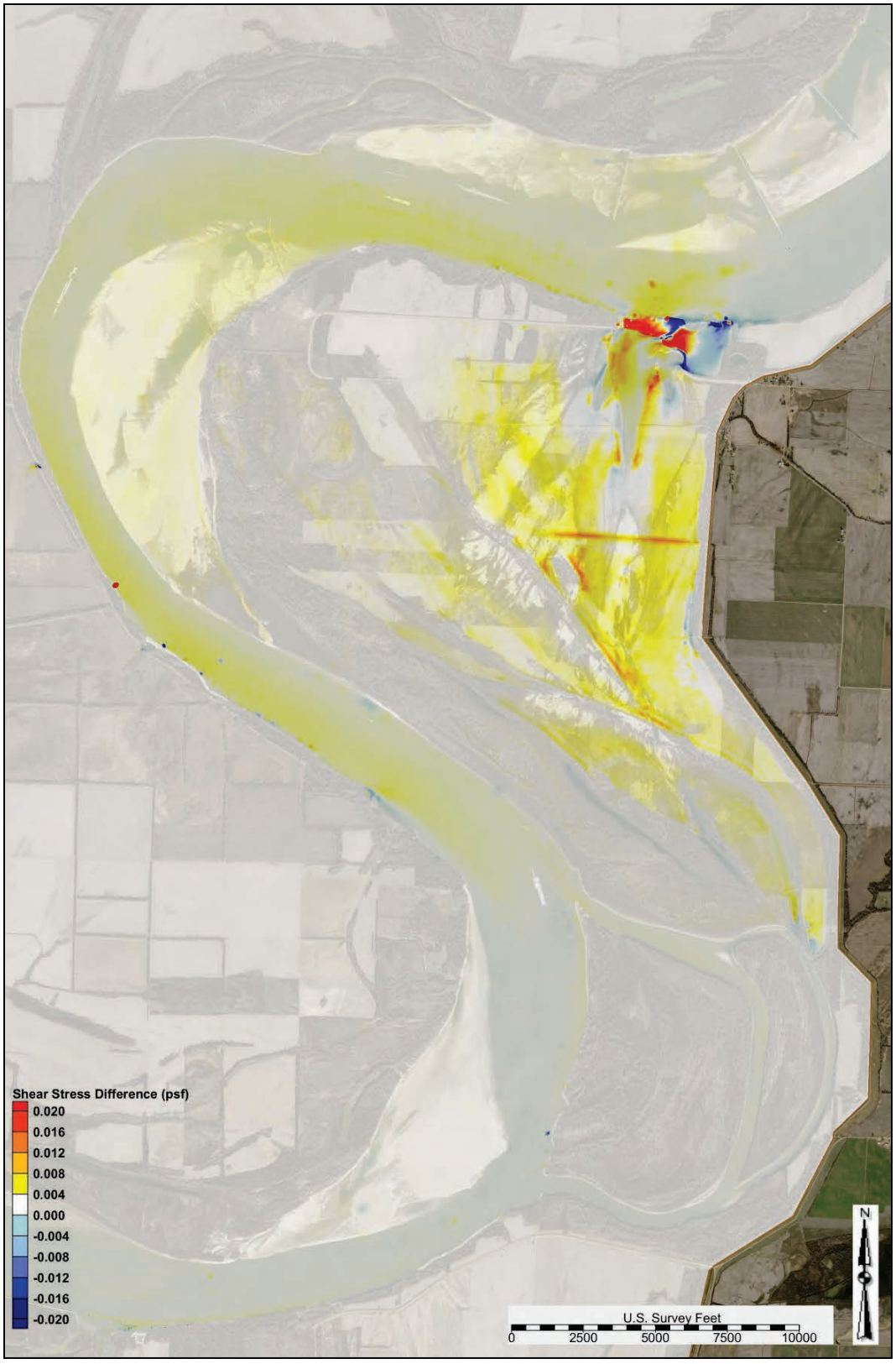


Figure C-105. Closure structure failure shear stress difference—1,500,000 cfs.

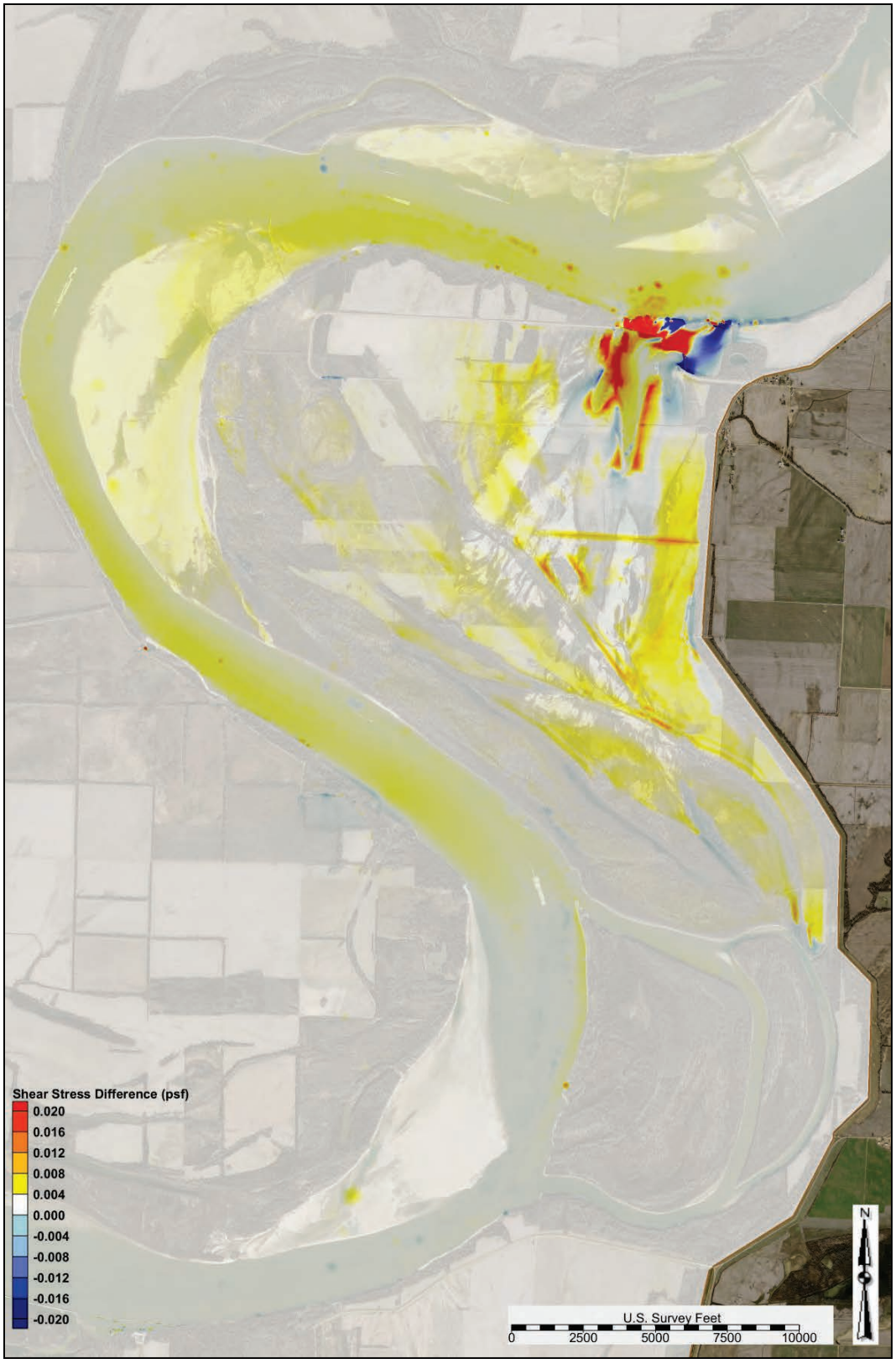


Figure C-106. Closure structure failure shear stress difference—1,700,000 cfs.

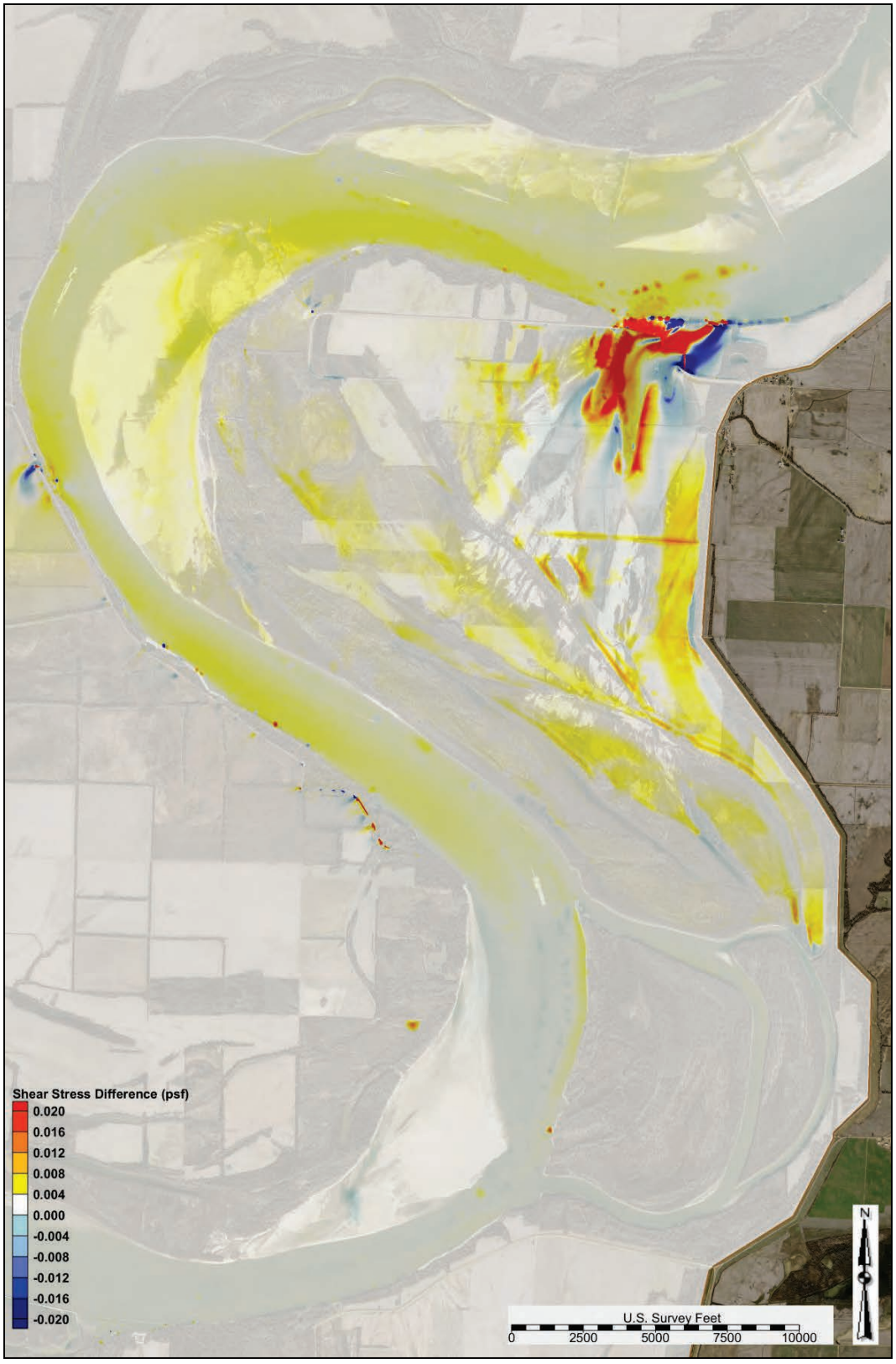


Figure C-107. Closure structure failure shear stress difference—1,900,000 cfs.

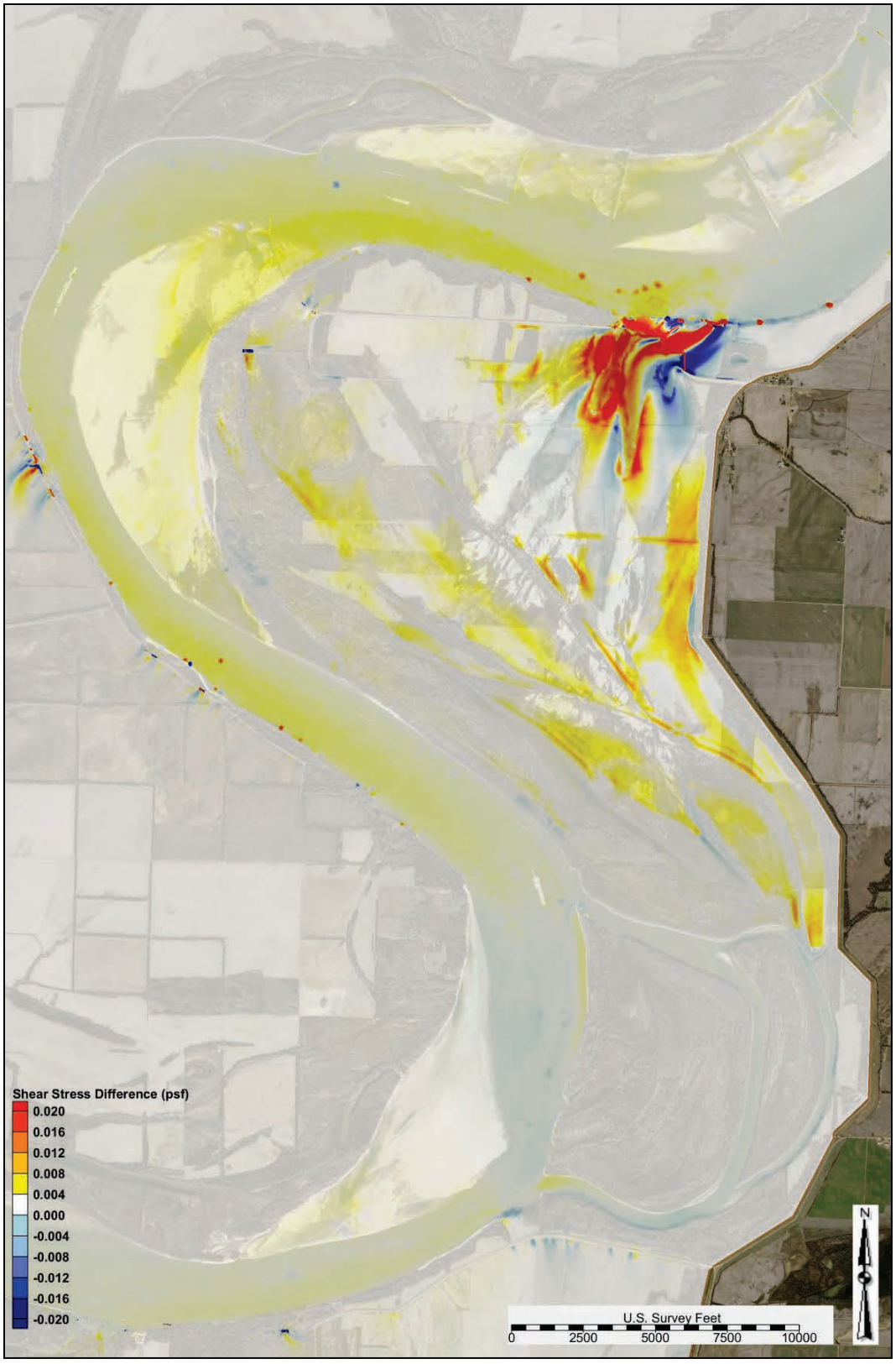
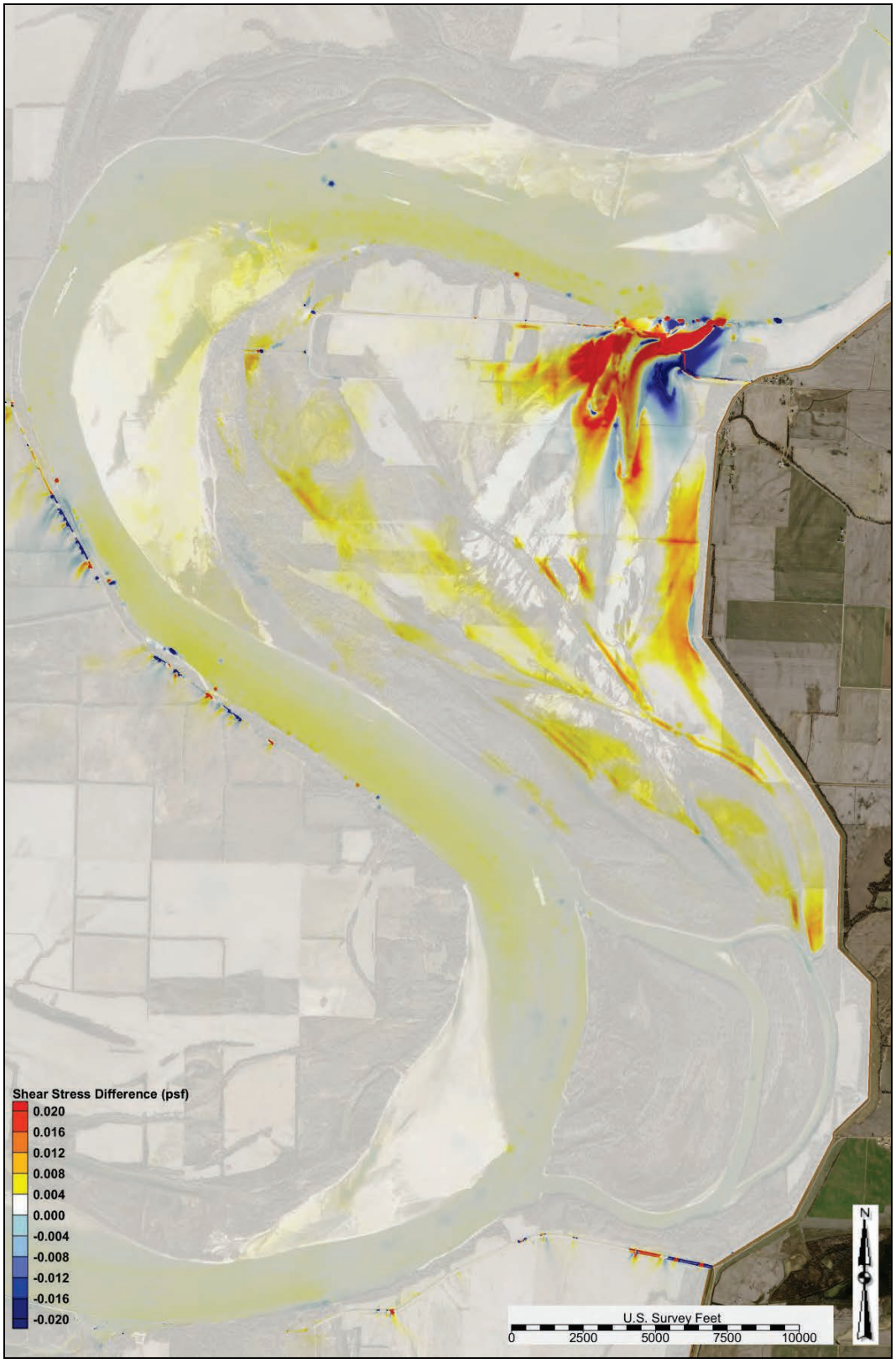


Figure C-108. Closure structure failure shear stress difference—2,100,000 cfs.



WSEL

Figure C-109 depicts the WSEL profiles in the study reach for the following flows: 1,100,000 cfs, 1,500,000 cfs, 1,900,000 cfs, and 2,100,000 cfs.

Figures C-110 through C-113 depict the WSEL profile compared to the base condition for the following flows: 1,100,000 cfs, 1,500,000 cfs, 1,900,000 cfs, and 2,100,000 cfs.

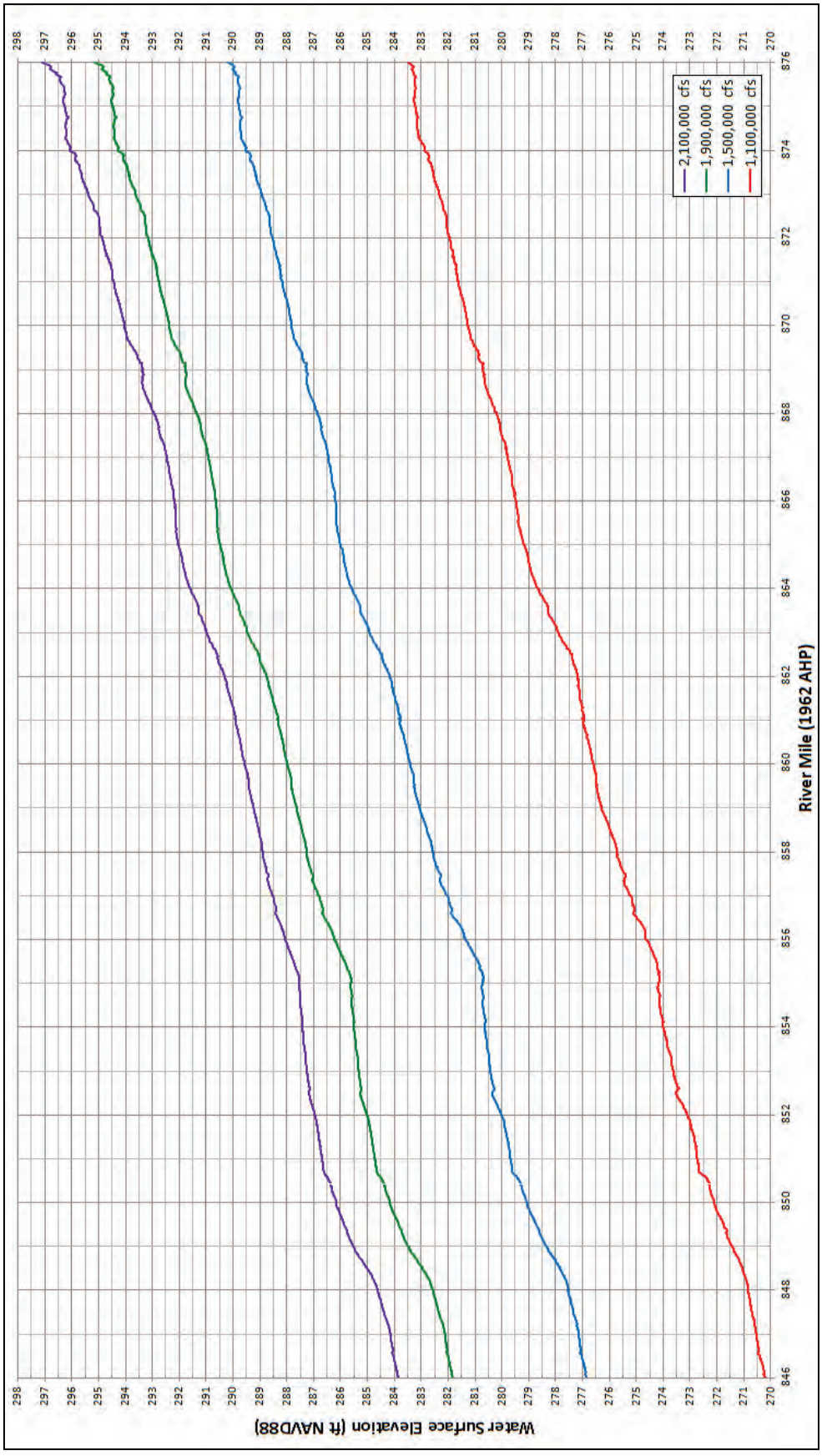


Figure C-109. Closure structure failure WSEL profile.

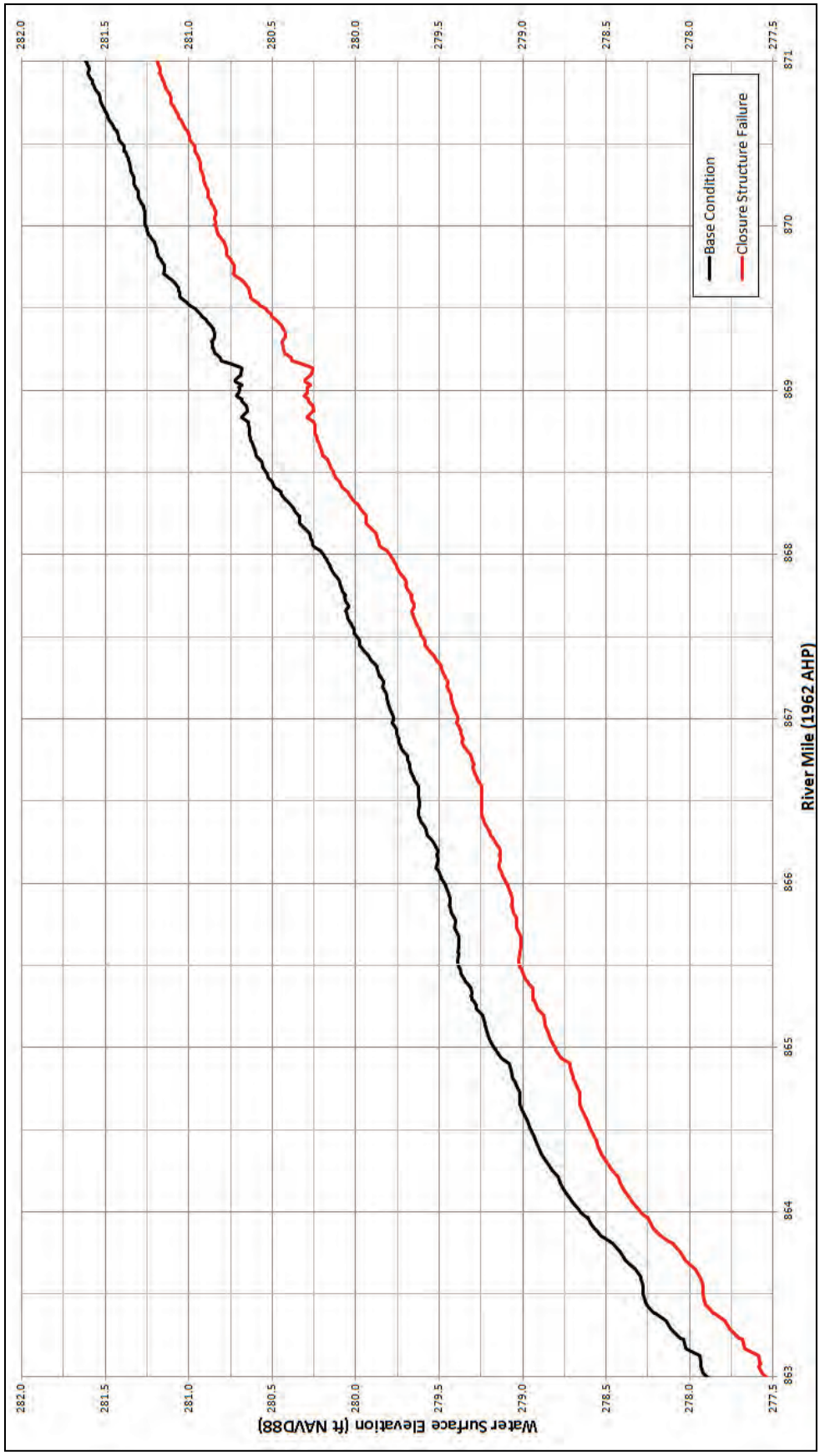


Figure C-110. Closure structure failure vs. base condition WSEL profile 1,100,000 cfs.

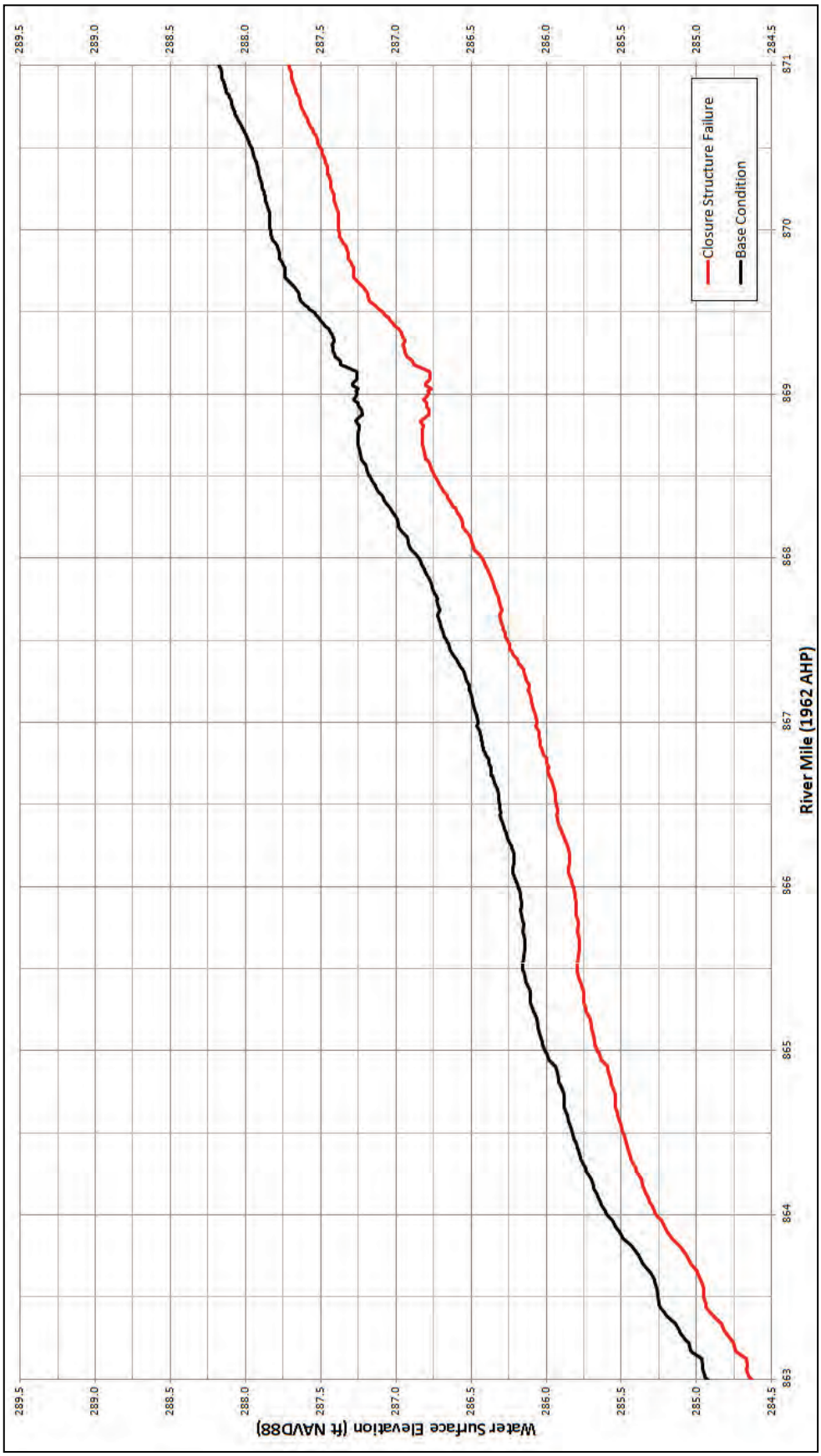


Figure C-111. Closure structure failure vs. base condition WSEL profile 1,500,000 cfs.

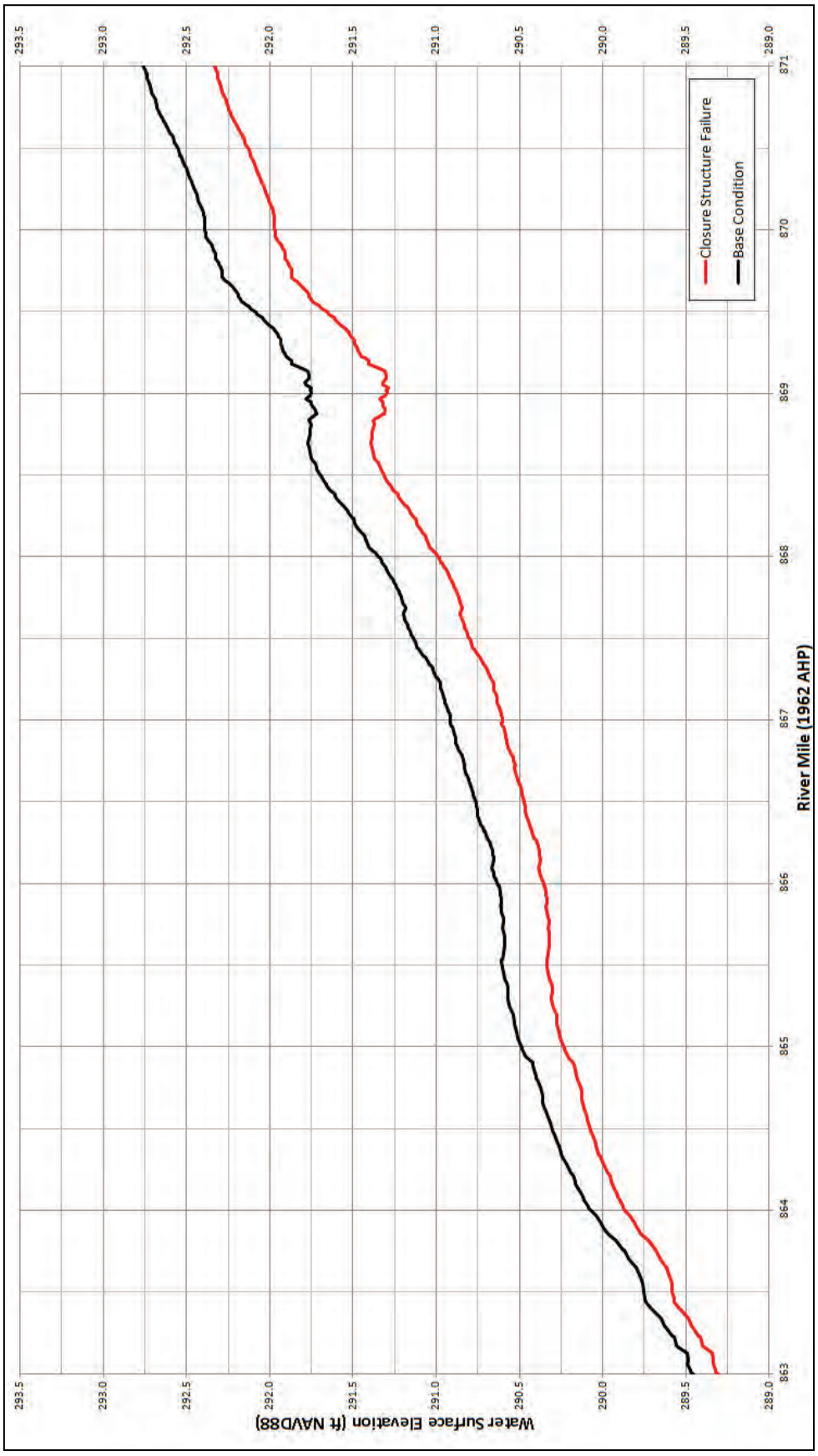


Figure C-112. Closure structure failure vs. base condition WSEL profile 1,900,000 cfs.

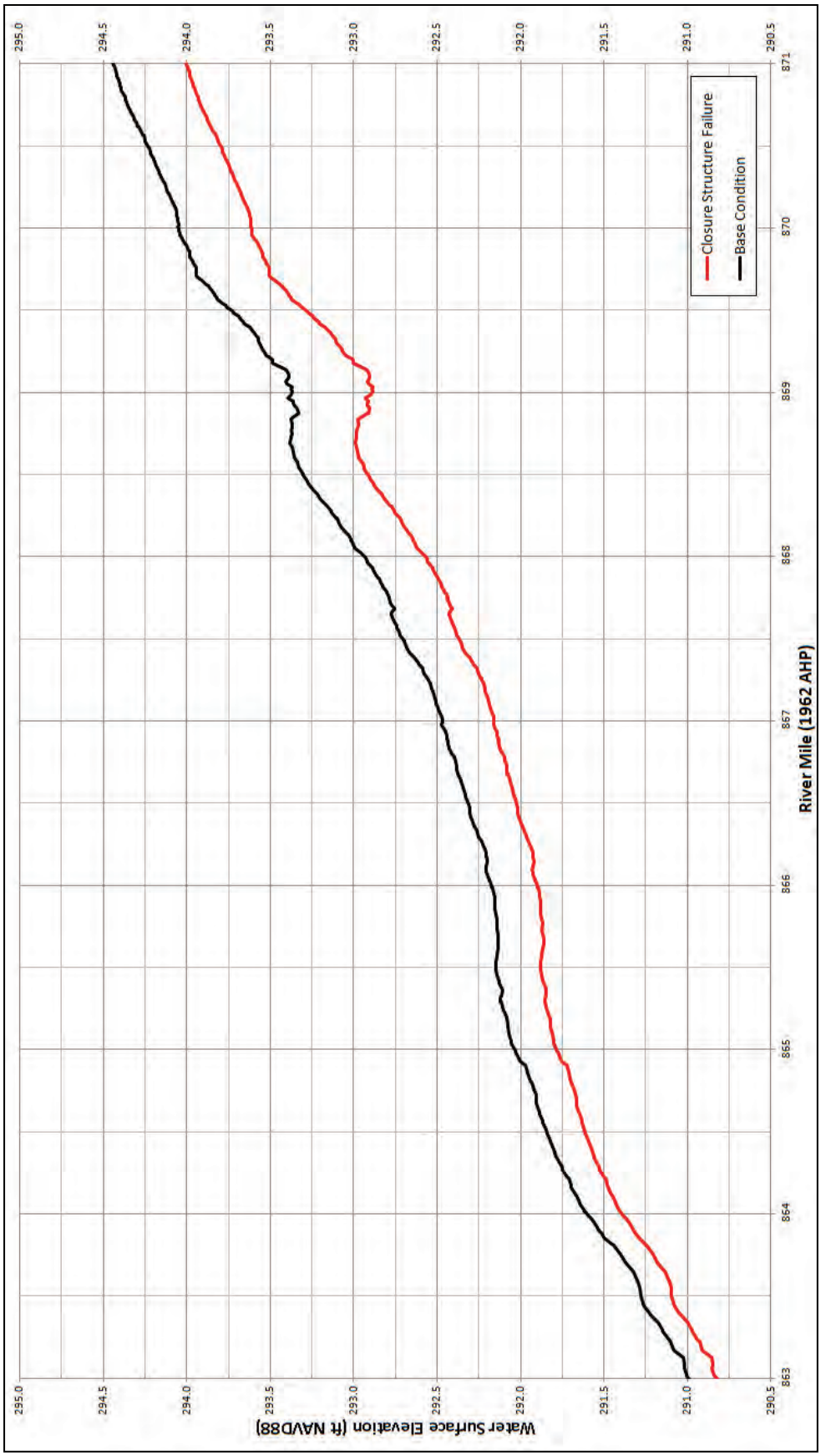


Figure C-113. Closure structure failure vs. base condition WSEL profile 2,100,000 cfs.

Sediment diversion grain size distribution

Table C-2 lists the sediment diversion grain size distribution for flows ranging from 870,000 cfs to 2,000,000 cfs.

Table C-2. Closure structure failure diversion grain size distribution.

Main Channel Flow US of Crevasse (cfs)	Total Diversion Load Grain Size Fraction Distribution									
	Coarse Silt	Very Fine Sand	Fine Sand	Medium Sand	Coarse Sand	Very Coarse Sand	Very Fine Pebble	Fine Pebble	Medium Pebble	Coarse Pebble
870000	0.0000	0.6362	0.3222	0.0356	0.0052	0.0008	0.0000	0.0000	0.0000	0.0000
900000	0.0000	0.5841	0.3585	0.0506	0.0062	0.0006	0.0000	0.0000	0.0000	0.0000
1000000	0.0000	0.2778	0.4517	0.1841	0.0733	0.0131	0.0001	0.0000	0.0000	0.0000
1100000	0.0000	0.1018	0.2793	0.3477	0.2071	0.0563	0.0063	0.0010	0.0004	0.0000
1200000	0.0000	0.0808	0.2150	0.3586	0.2614	0.0694	0.0070	0.0056	0.0019	0.0003
1300000	0.0000	0.0682	0.1956	0.3664	0.2790	0.0764	0.0059	0.0040	0.0040	0.0005
1400000	0.0000	0.0618	0.1858	0.3655	0.2865	0.0801	0.0088	0.0031	0.0075	0.0009
1500000	0.0000	0.0585	0.1871	0.3724	0.2832	0.0765	0.0117	0.0043	0.0048	0.0014
1600000	0.0000	0.0540	0.1852	0.3821	0.2837	0.0727	0.0099	0.0059	0.0046	0.0019
1700000	0.0000	0.0526	0.1835	0.3861	0.2837	0.0718	0.0094	0.0050	0.0054	0.0025
1800000	0.0000	0.0494	0.1786	0.3919	0.2864	0.0708	0.0098	0.0043	0.0057	0.0031
1900000	0.0000	0.0473	0.1751	0.3968	0.2883	0.0695	0.0102	0.0044	0.0047	0.0037
2000000	0.0000	0.0455	0.1710	0.3990	0.2922	0.0699	0.0102	0.0045	0.0039	0.0037
2100000	0.0000	0.0454	0.1729	0.4048	0.2877	0.0662	0.0110	0.0046	0.0039	0.0034

Alternative 1 output

The following sections contain AdH model output and analysis for Alternative 1.

Shear stress

The modeled shear stress outputs at flows ranging from 900,000 to 2,100,000 cfs for the study overbank are depicted in Figures C-114 through C-120.

Figure C-114. Alternative 1 shear stress—900,000 cfs (study overbank).



Figure C-115. Alternative 1 shear stress—1,100,000 cfs (study overbank).

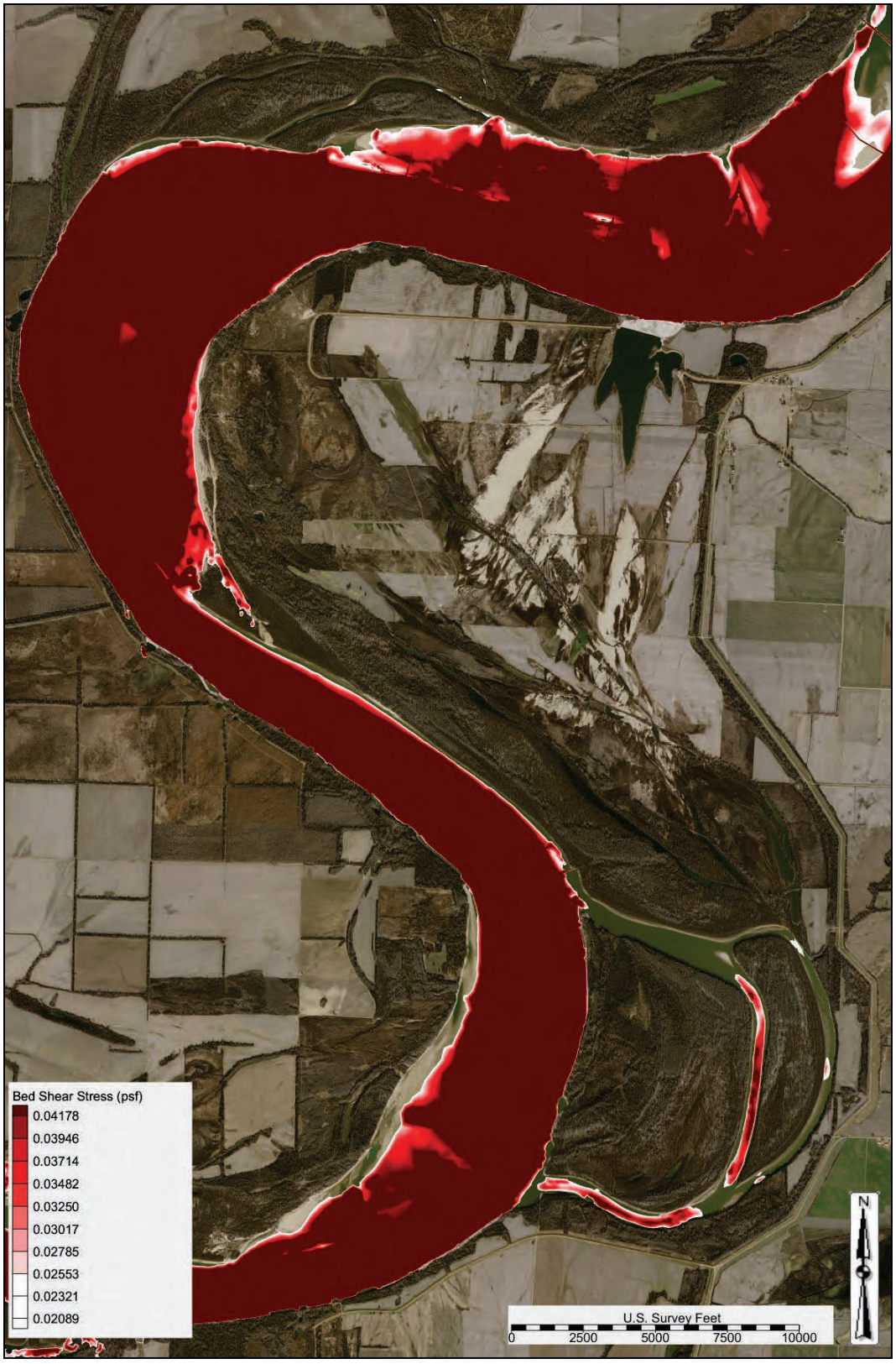


Figure C-116. Alternative 1 shear stress—1,300,000 cfs (study overbank).

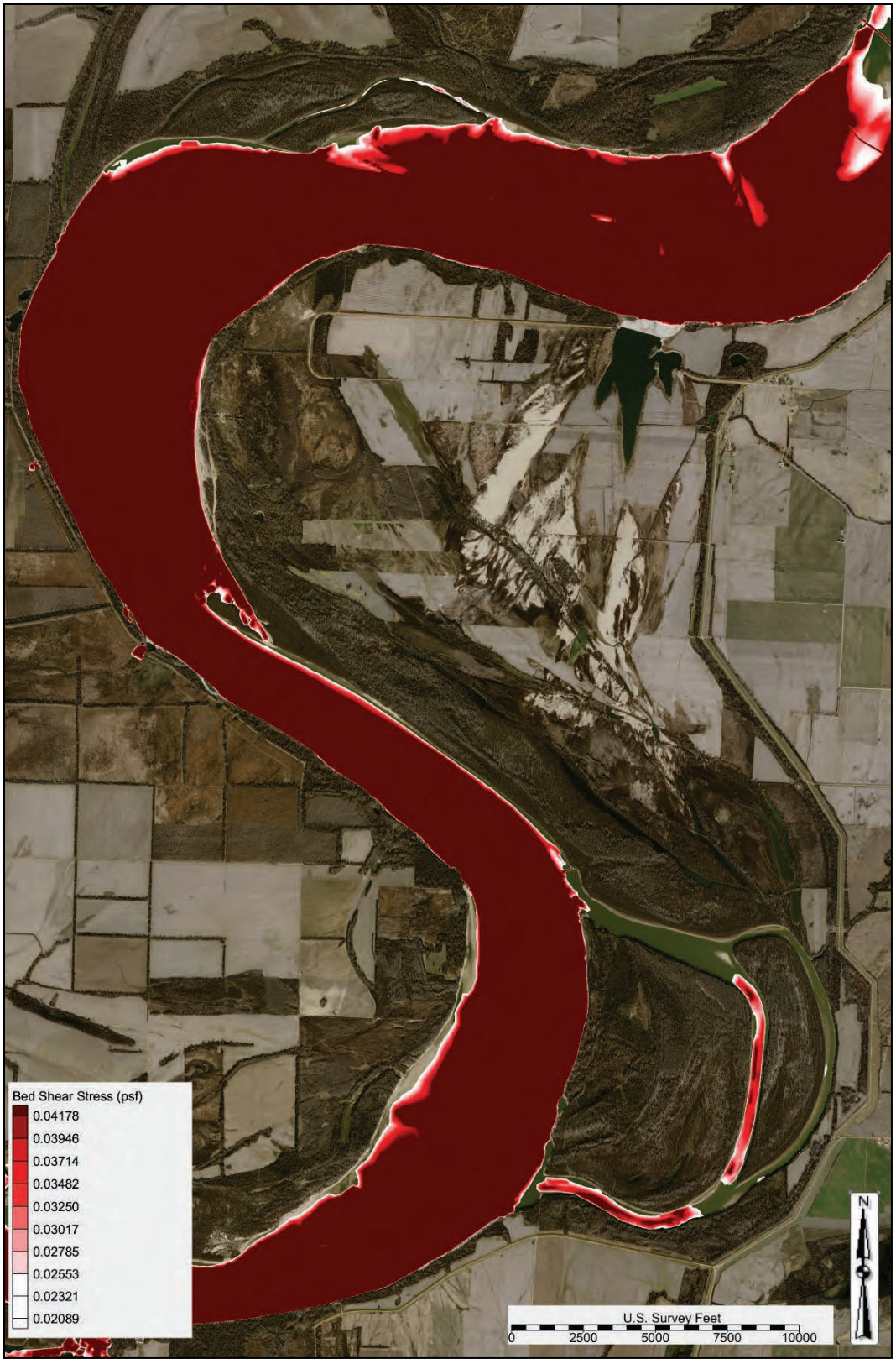


Figure C-117. Alternative 1 shear stress—1,500,000 cfs (study overbank).

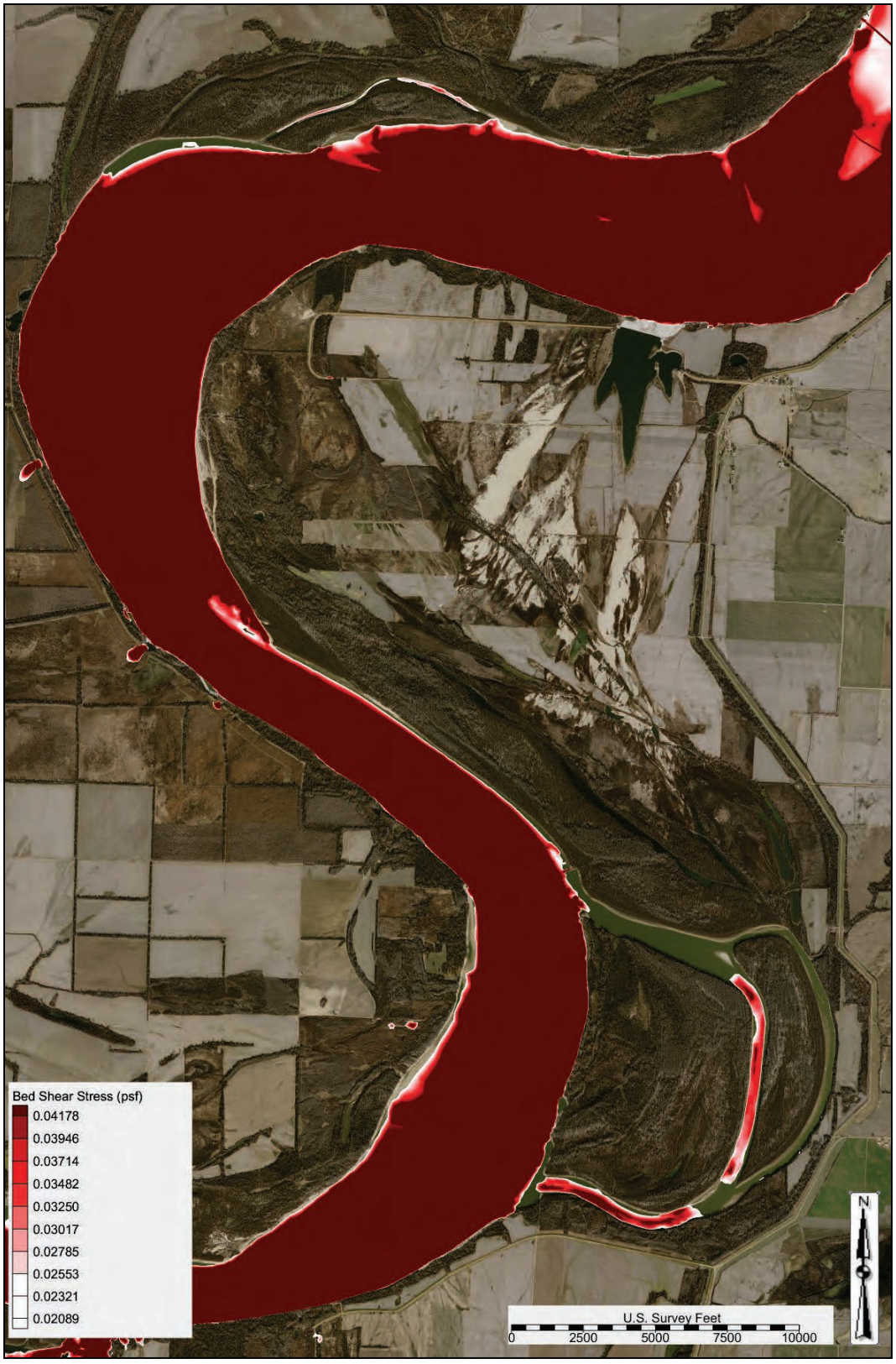


Figure C-118. Alternative 1 shear stress—1,700,000 cfs (study overbank).



Figure C-119. Alternative 1 shear stress—1,900,000 cfs (study overbank).



Figure C-120. Alternative 1 shear stress—2,100,000 cfs (study overbank).



Shear stress difference comparison

The modeled shear stress difference plots compared to the base condition output for flows ranging from 900,000 to 2,100,000 cfs are depicted in Figures C-121 through C-127. A positive shear stress difference (+ value and red and orange) indicated an increased shear stress compared to the base condition. A negative shear stress difference (- value and blue) indicated a decreased shear stress compared to the base condition. A zero shear stress difference (zero value and white) indicated that the alternative had no change in shear stress.

Figure C-121. Alternative 1 shear stress difference—900,000 cfs.

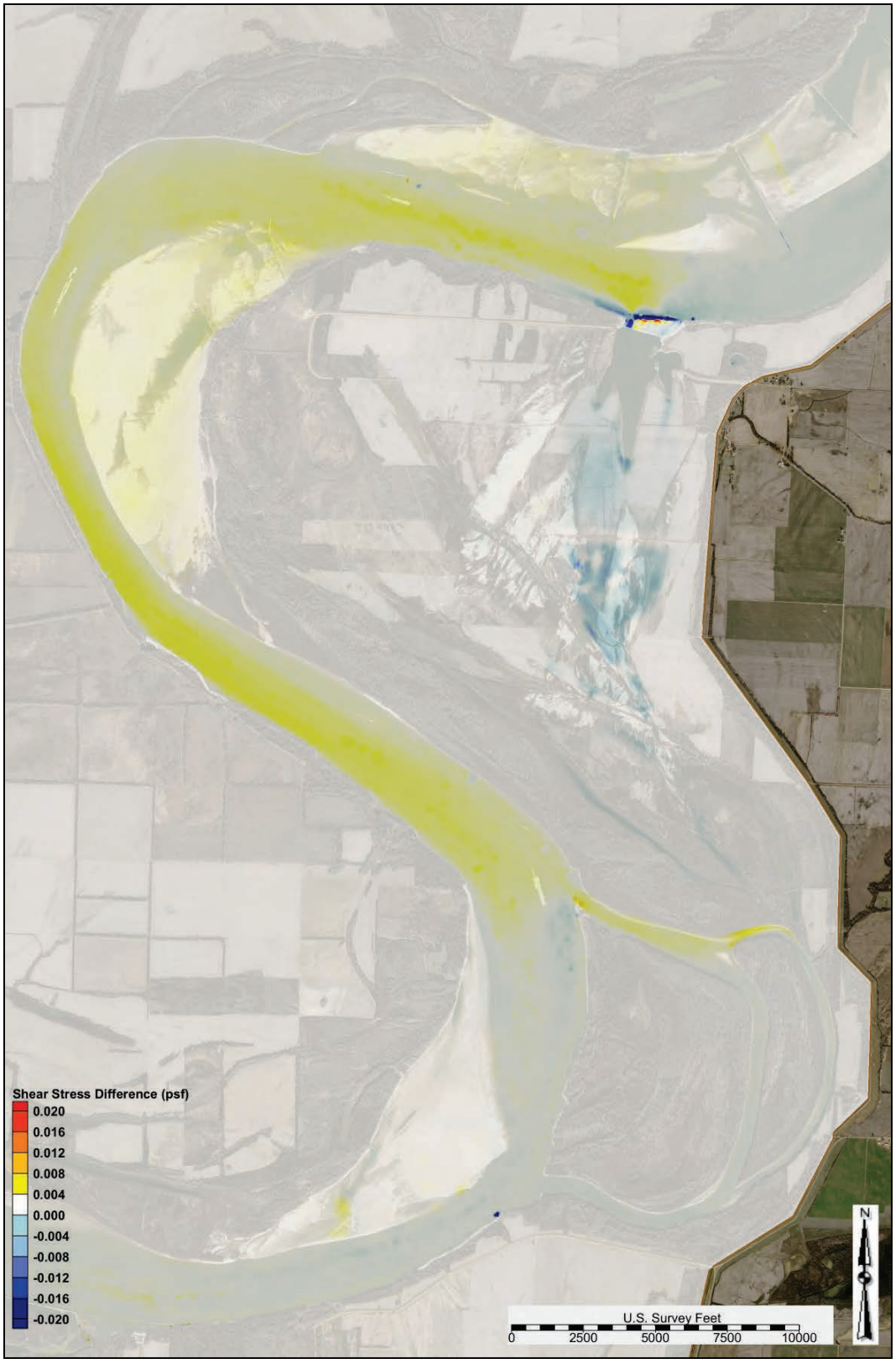


Figure C-122. Alternative 1 shear stress difference—1,100,000 cfs.

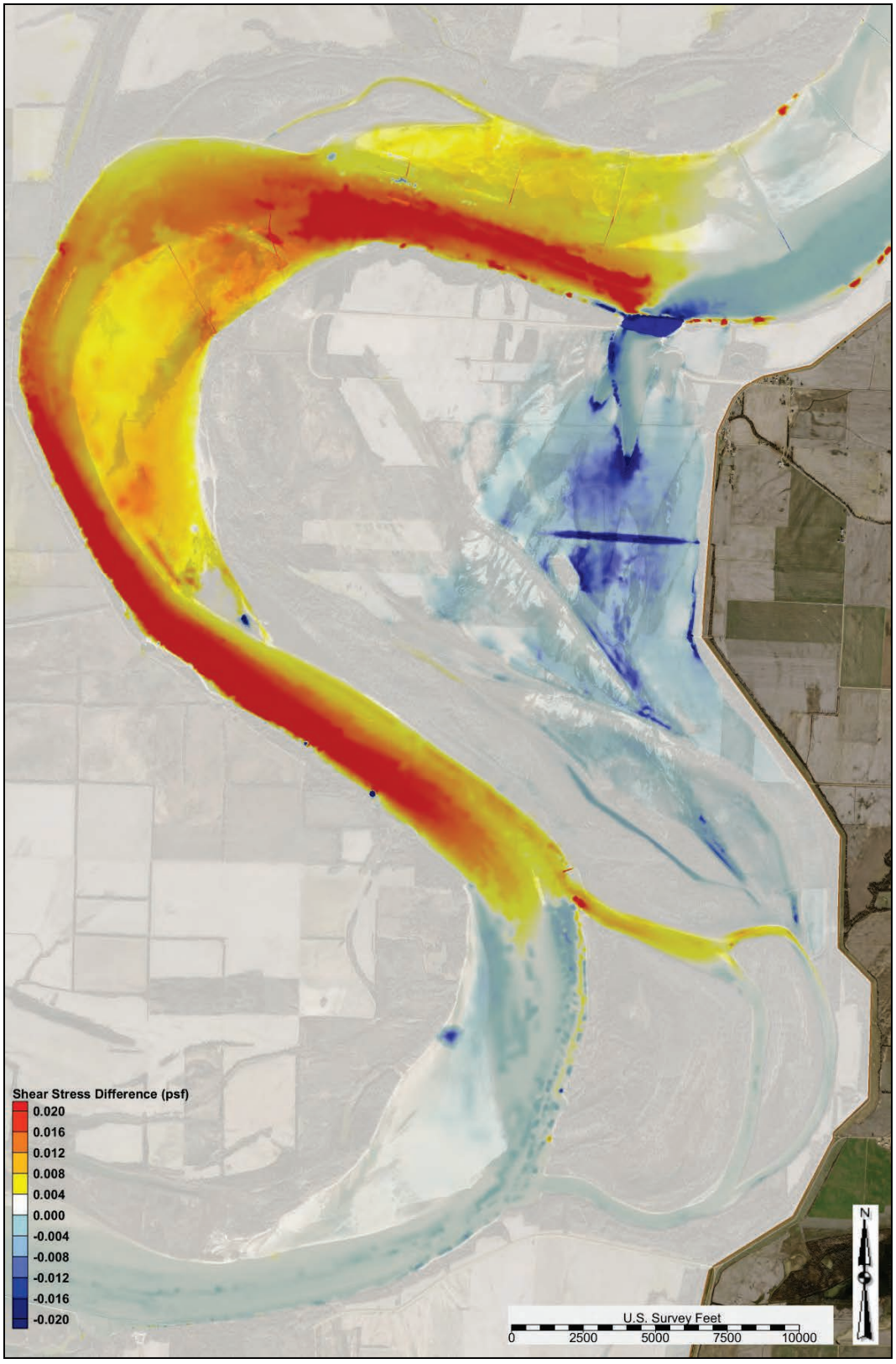


Figure C-123. Alternative 1 shear stress difference—1,300,000 cfs.

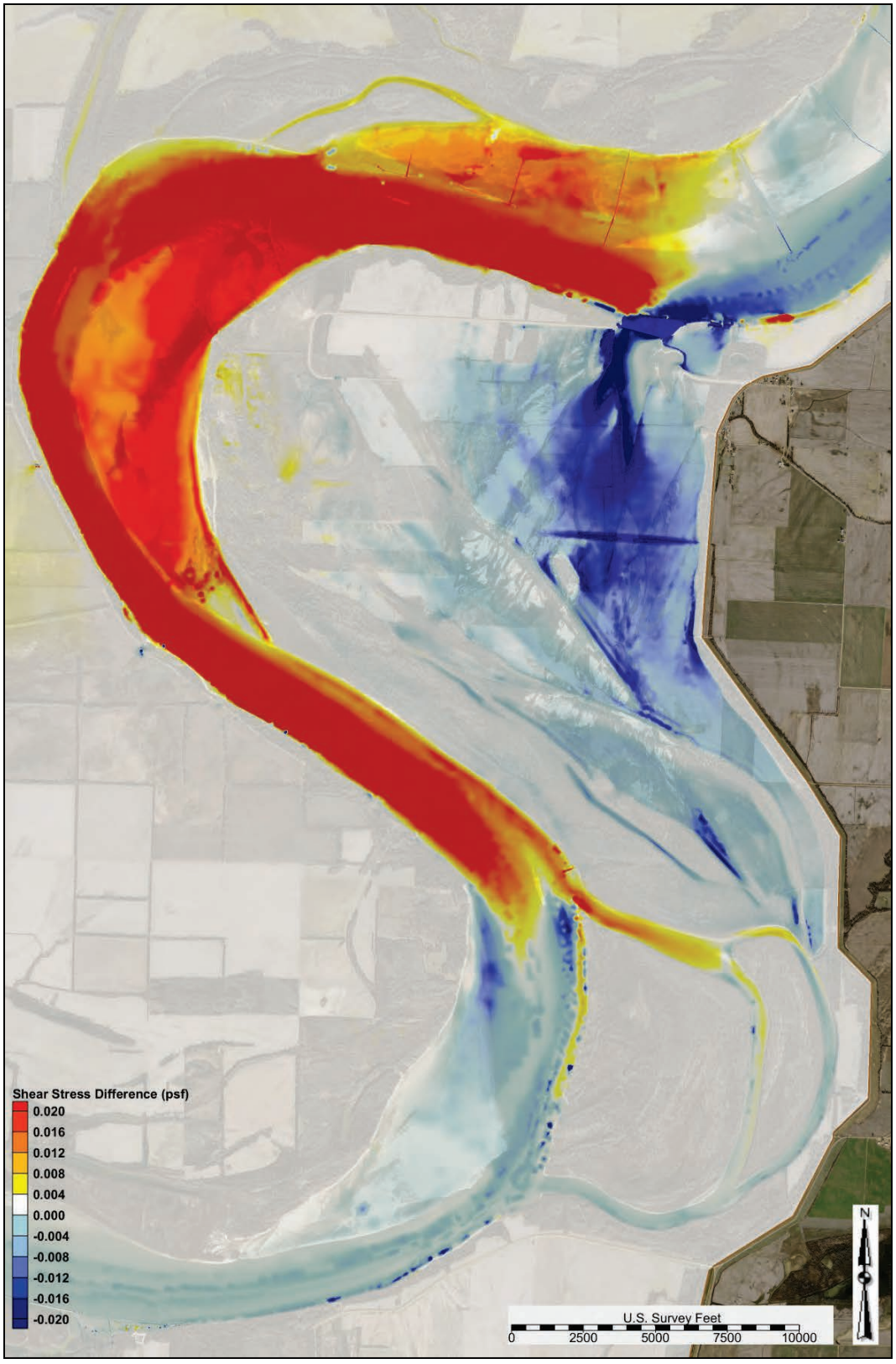


Figure C-124. Alternative 1 shear stress difference—1,500,000 cfs.

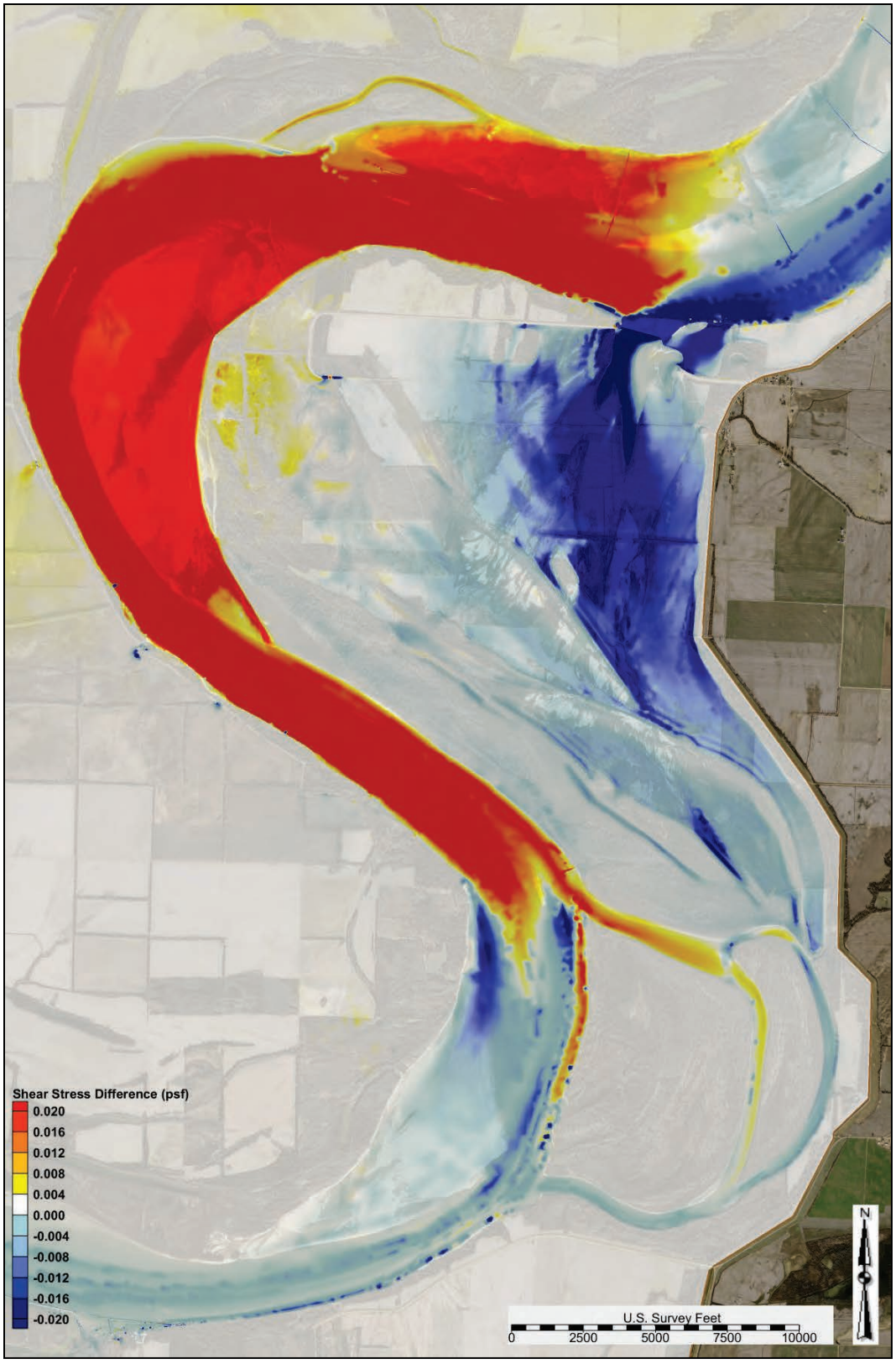


Figure C-125. Alternative 1 shear stress difference—1,700,000 cfs.

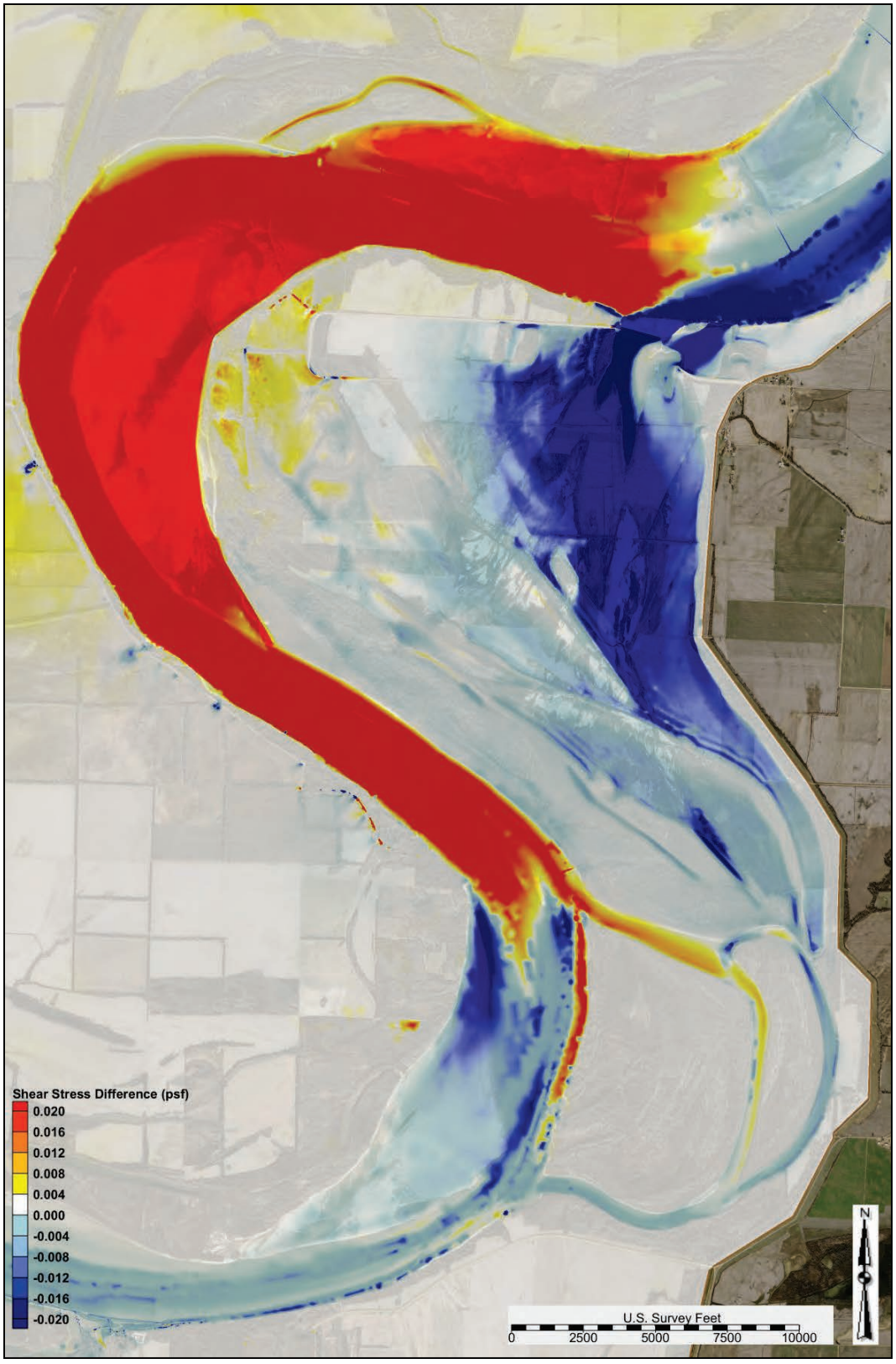


Figure C-126. Alternative 1 shear stress difference—1,900,000 cfs.

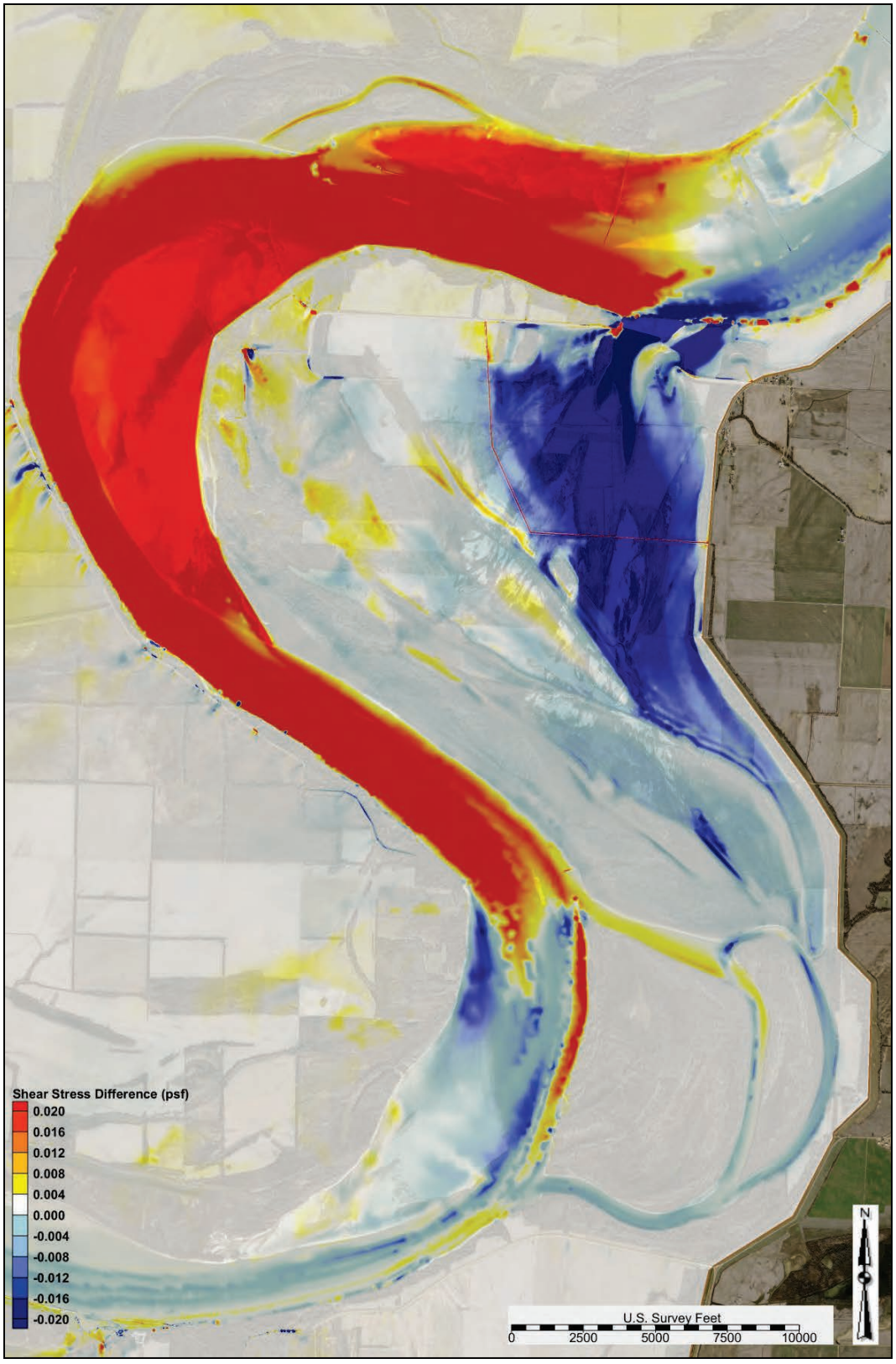
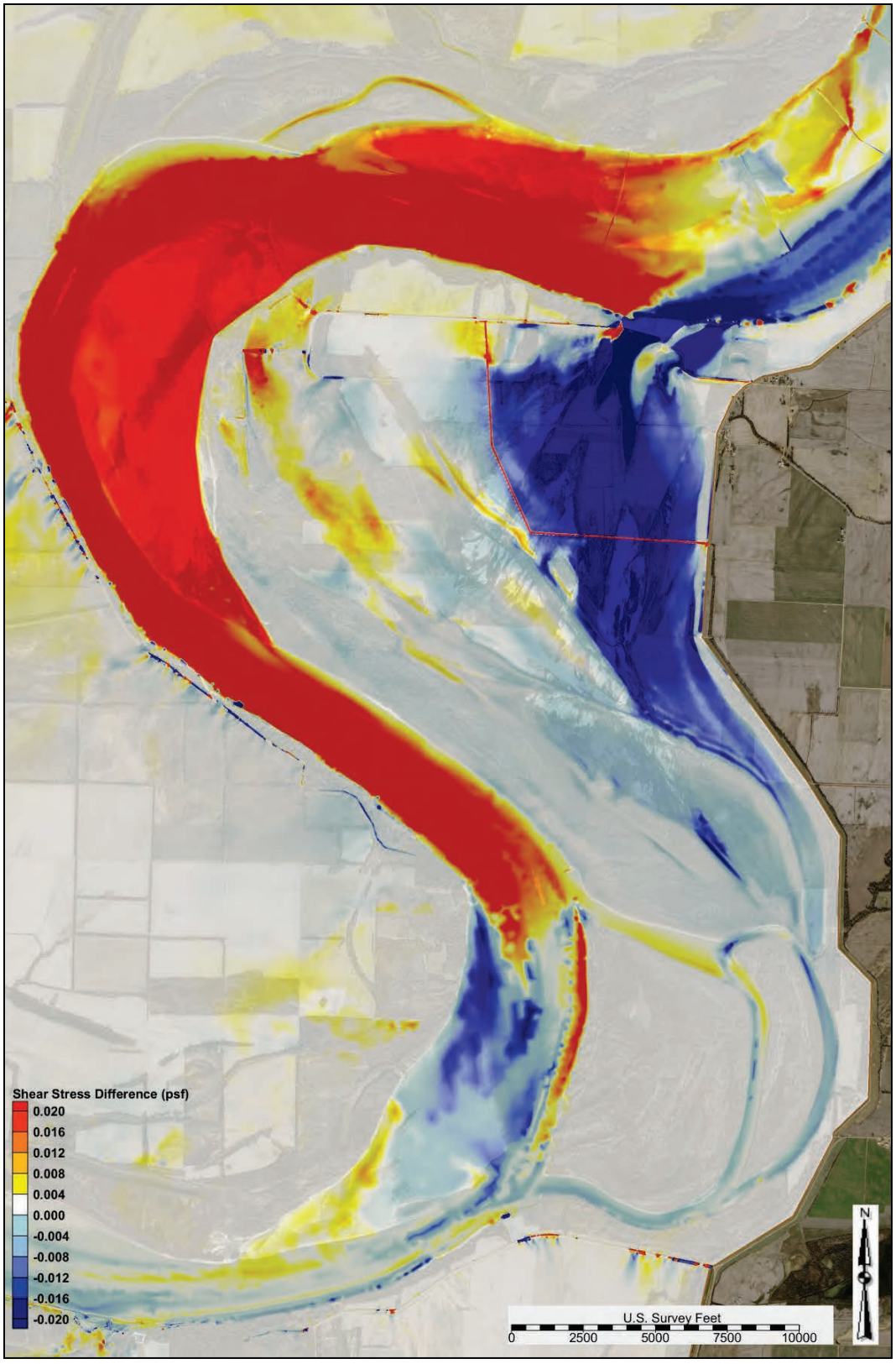


Figure C-127. Alternative 1 shear stress difference—2,100,000 cfs.



WSEL

Figure C-128 depicts the WSEL profiles in the study reach for the following flows: 1,100,000 cfs, 1,500,000 cfs, 1,900,000 cfs, and 2,100,000 cfs.

Sediment diversion grain size distribution

Table C-3 lists the sediment diversion grain size distribution for flows ranging from 870,000 cfs to 2,000,000 cfs.

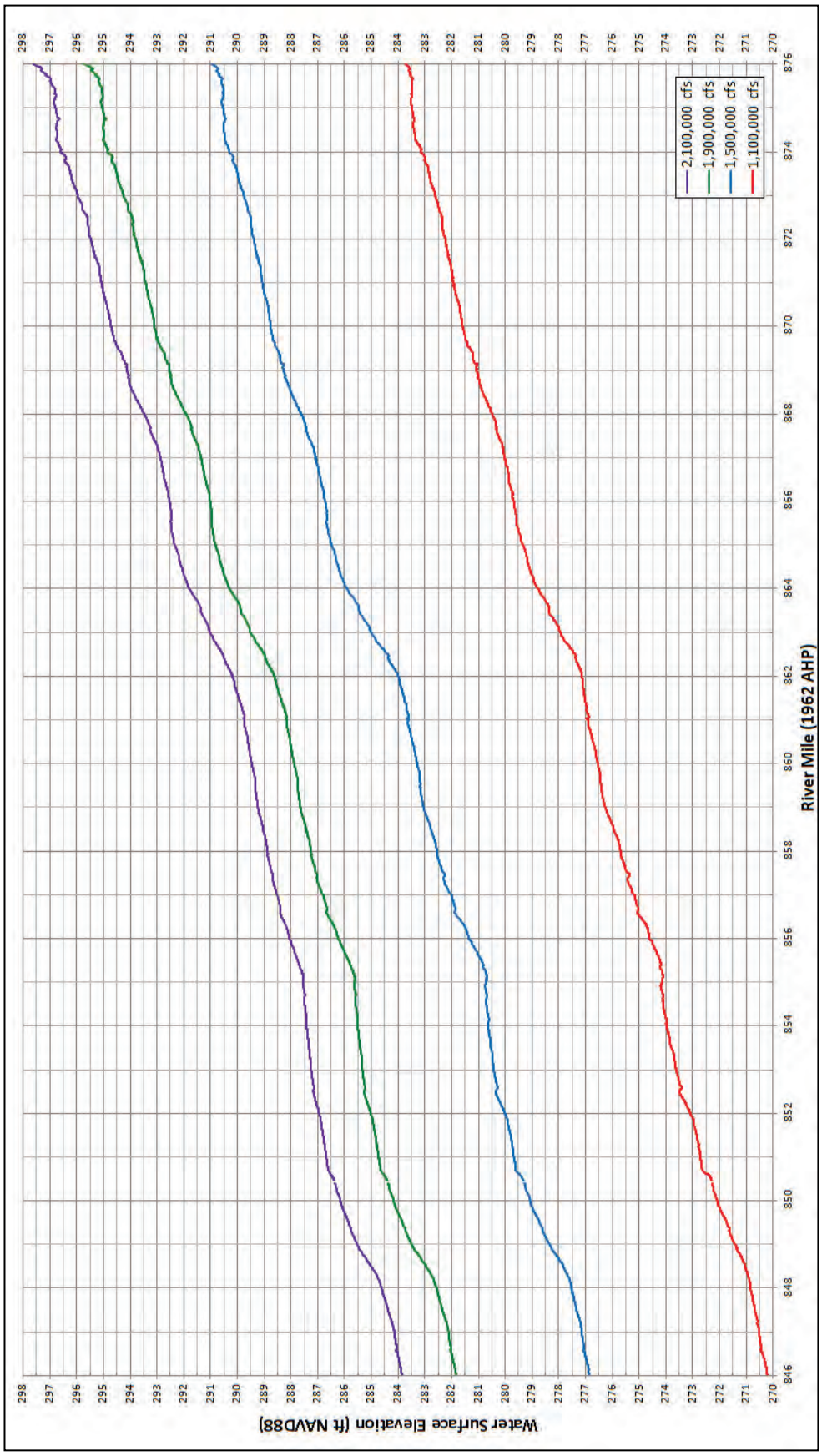


Figure C-128. Alternative 1 WSEL.

Table C-3. Alternative 1 diversion grain size distribution.

Main Channel Flow US of Crevasse (cfs)	Total Diversion Load Grain Size Fraction Distribution									
	Coarse Silt	Very Fine Sand	Fine Sand	Medium Sand	Coarse Sand	Very Coarse Sand	Very Fine Pebble	Fine Pebble	Medium Pebble	Coarse Pebble
870,000	-	-	-	-	-	-	-	-	-	-
900,000	-	-	-	-	-	-	-	-	-	-
1,000,000	-	-	-	-	-	-	-	-	-	-
1,100,000	-	-	-	-	-	-	-	-	-	-
1,200,000	-	-	-	-	-	-	-	-	-	-
1,300,000	-	-	-	-	-	-	-	-	-	-
1,400,000	-	-	-	-	-	-	-	-	-	-
1,500,000	-	-	-	-	-	-	-	-	-	-
1,600,000	-	-	-	-	-	-	-	-	-	-
1,700,000	-	-	-	-	-	-	-	-	-	-
1,800,000	0.0065	0.8987	0.0943	0.0006	0.0000	0.0000	0.0000	0.0000	0.0000	0.0000
2,000,000	0.0139	0.1184	0.2875	0.3152	0.2093	0.0526	0.0000	0.0000	0.0026	0.0005
2,100,000	0.0133	0.1189	0.2917	0.3667	0.1403	0.0663	0.0000	0.0000	0.0023	0.0005

- no diverted sediment

Alternative 2 output

The following sections contain AdH model output and analysis for Alternative 2.

Shear stress

The modeled shear stress outputs at flows ranging from 900,000 to 2,100,000 cfs for the study overbank are depicted in Figures C-129 through C-135.

Figure C-129. Alternative 2 shear stress—900,000 cfs (study overbank).



Figure C-130. Alternative 2 shear stress—1,100,000 cfs (study overbank).

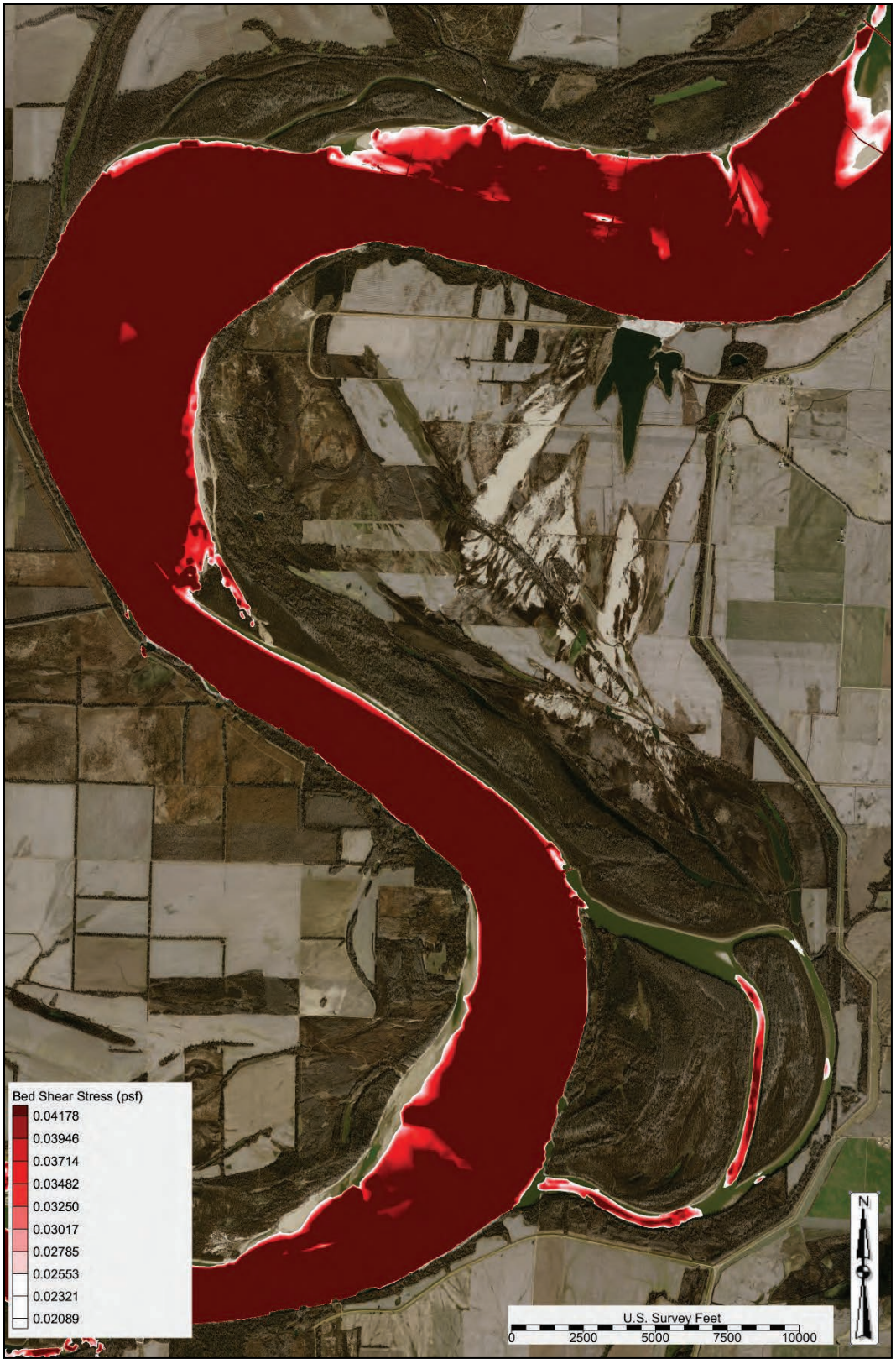


Figure C-131. Alternative 2 shear stress—1,300,000 cfs (study overbank).



Figure C-132. Alternative 2 shear stress—1,500,000 cfs (study overbank).

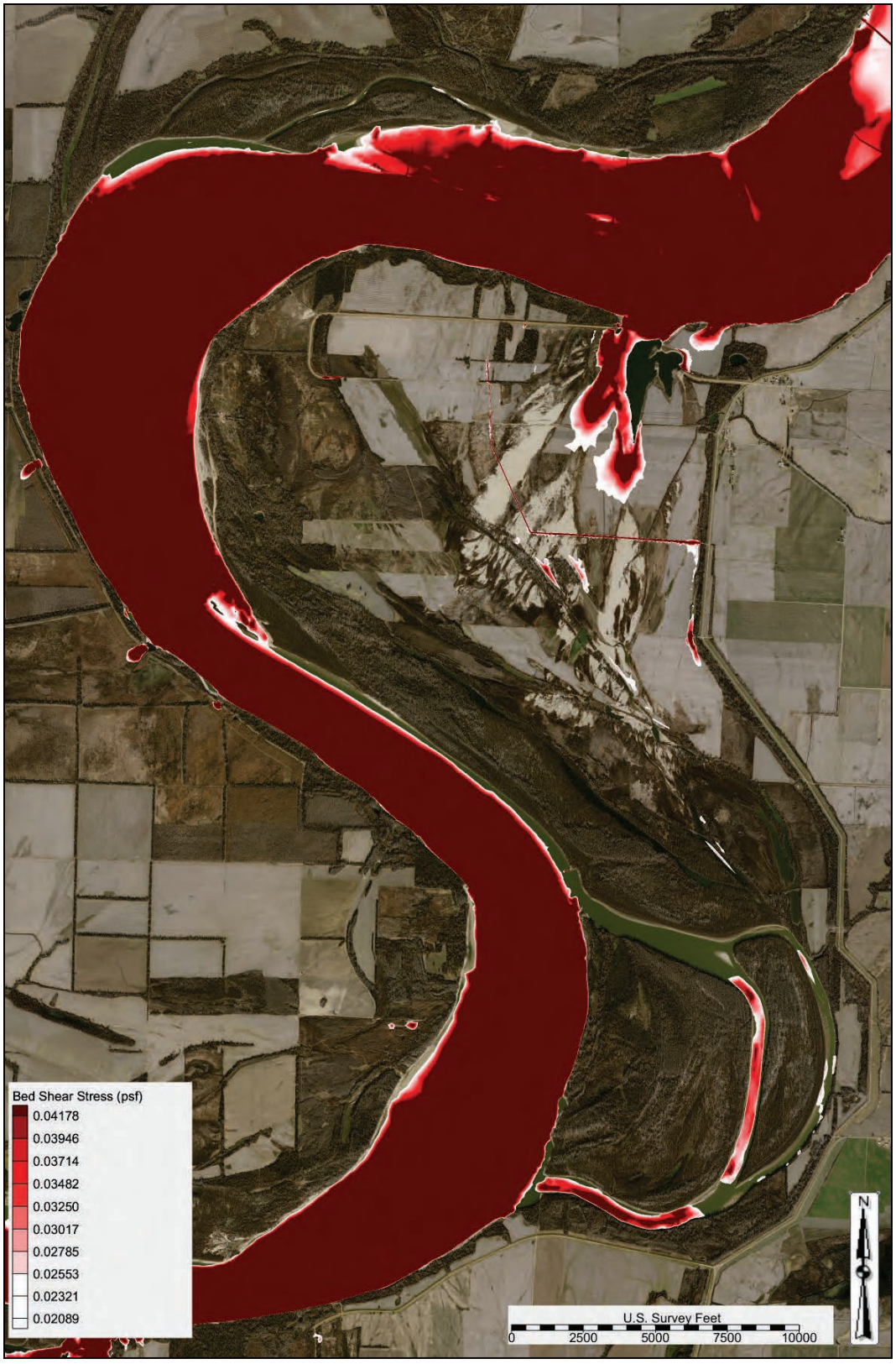


Figure C-133. Alternative 2 shear stress—1,700,000 cfs (study overbank).

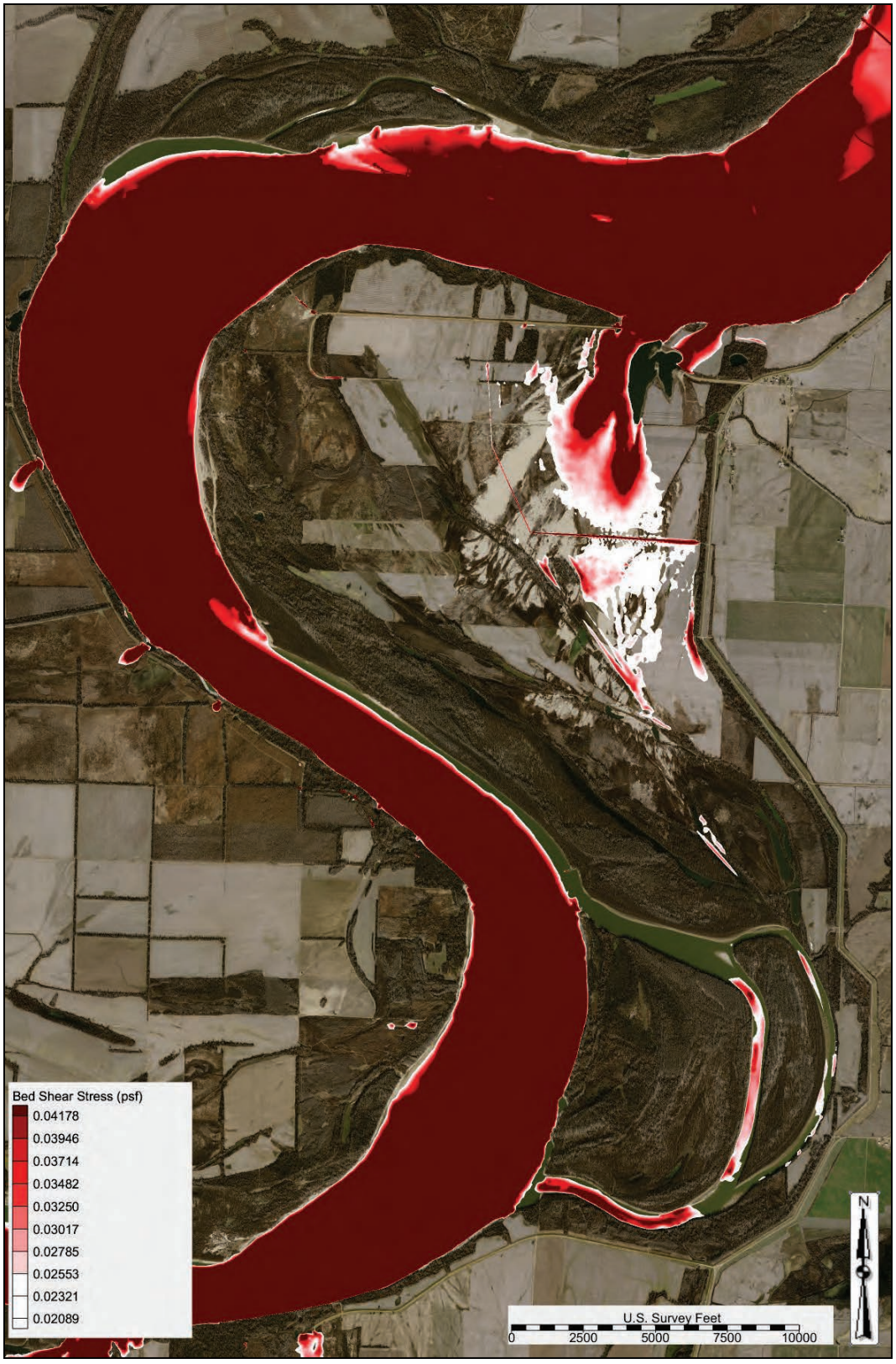
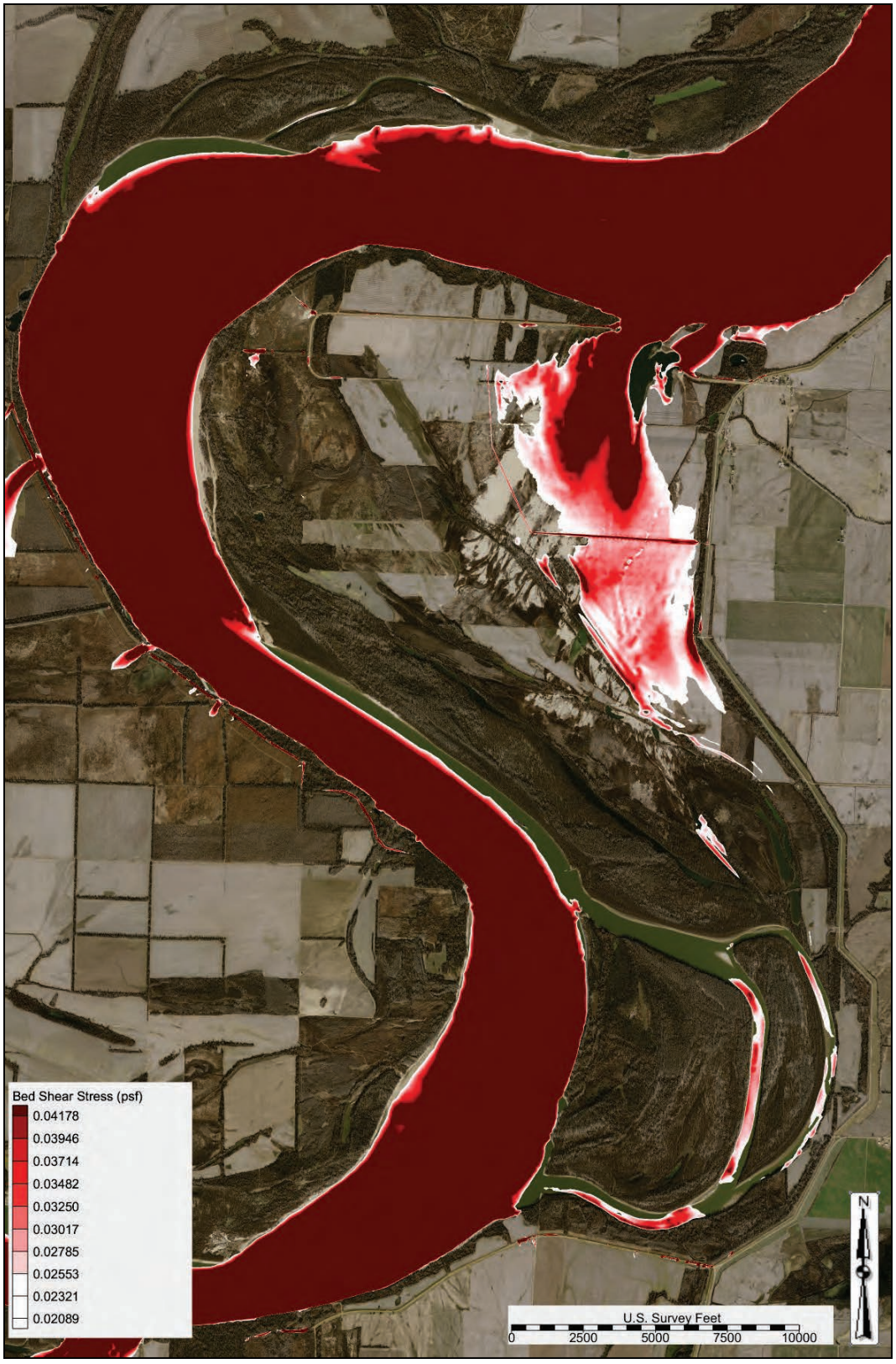


Figure C-134. Alternative 2 shear stress—1,900,000 cfs (study overbank).



Figure C-135. Alternative 2 shear stress—2,100,000 cfs (study overbank).



Shear stress difference comparison

The modeled shear stress difference plots compared to the base condition output for flows ranging from 900,000 to 2,100,000 cfs are depicted in Figures C-136 through C-142. A positive shear stress difference (+ value and red and orange) indicated an increased shear stress compared to the base condition. A negative shear stress difference (- value and blue) indicated a decreased shear stress compared to the base condition. A zero shear stress difference (zero value and white) indicated that the alternative had no change in shear stress.

Figure C-136. Alternative 2 shear stress difference—900,000 cfs.

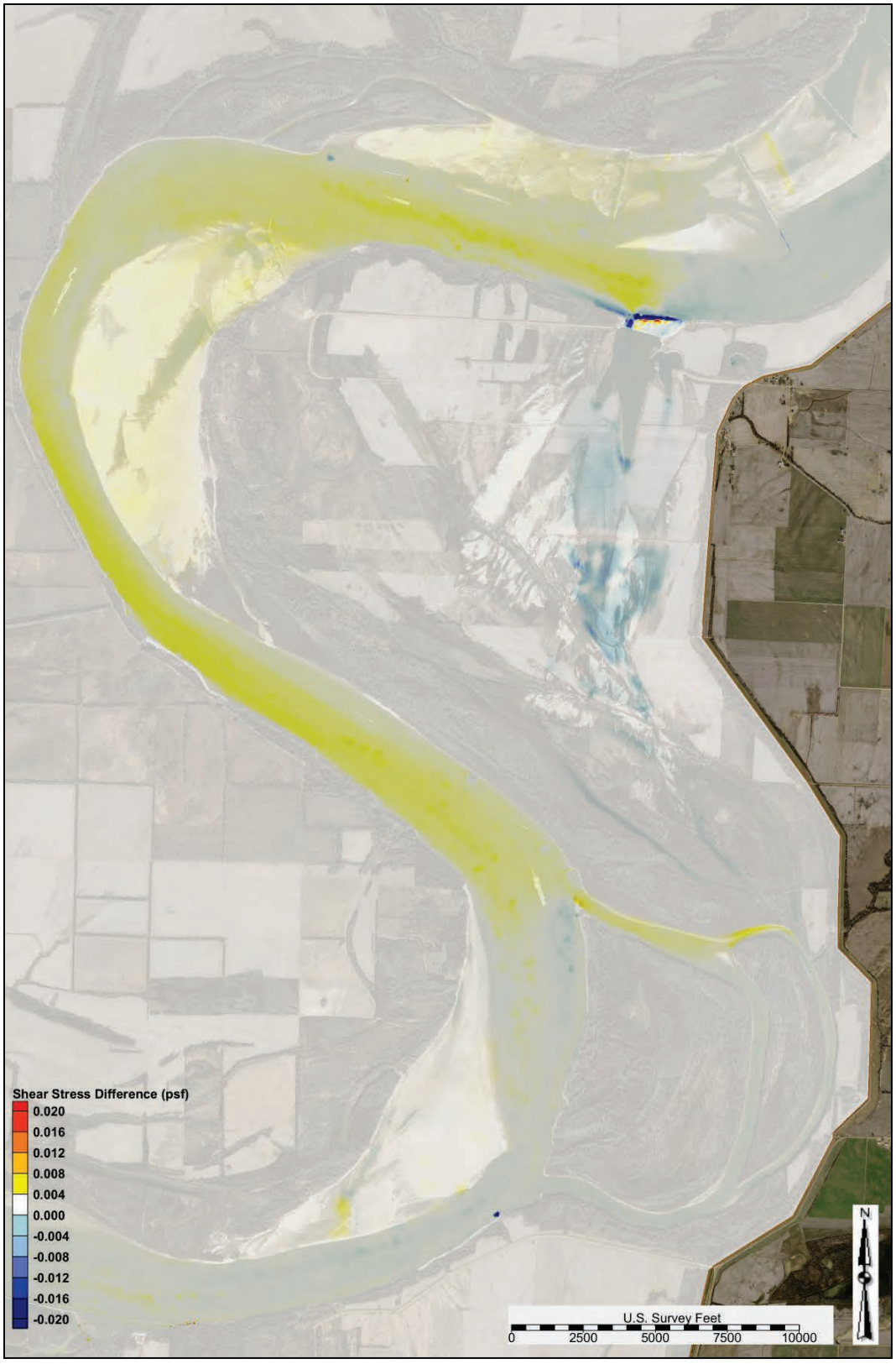


Figure C-137. Alternative 2 shear stress difference—1,100,000 cfs.

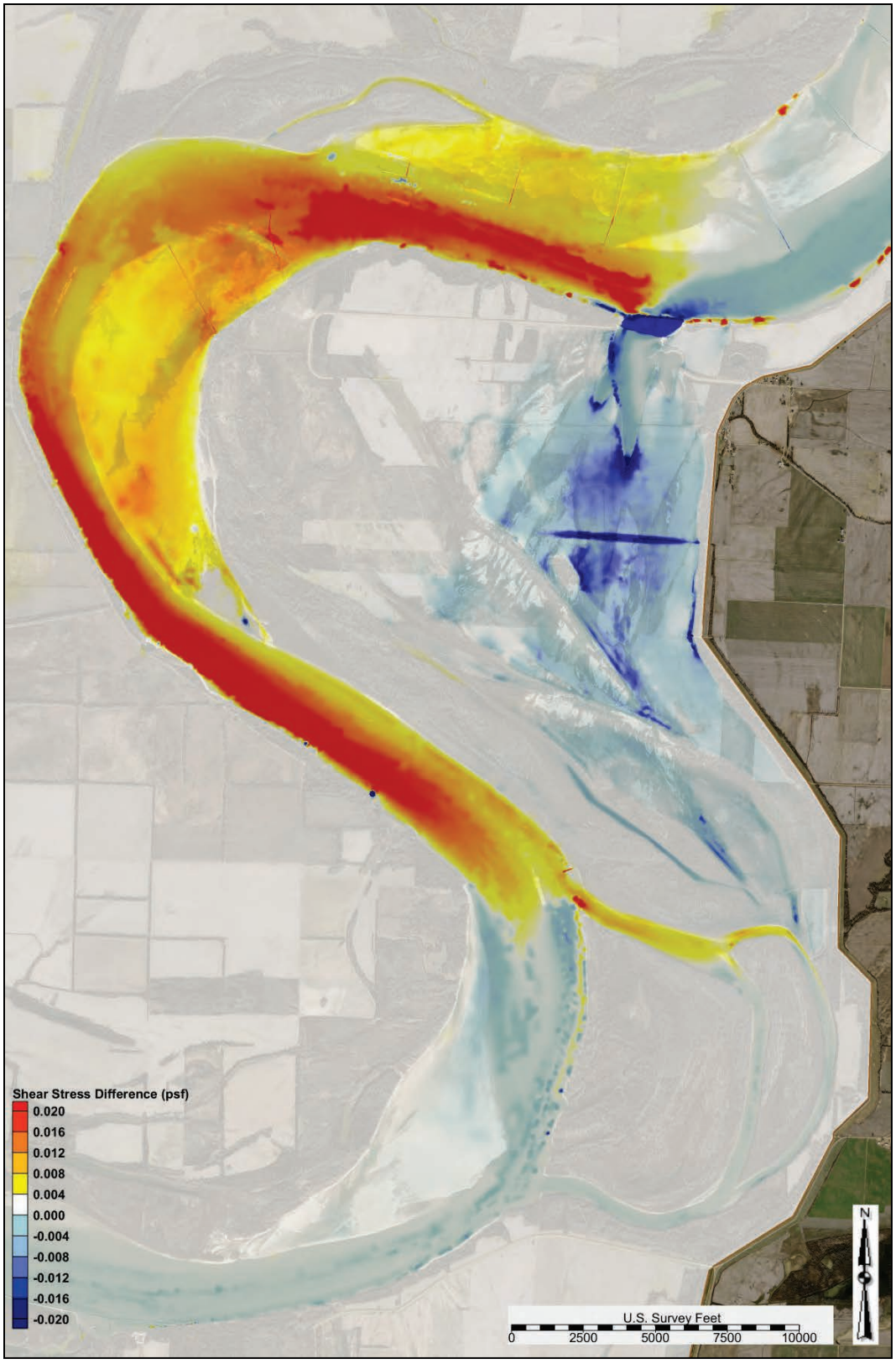


Figure C-138. Alternative 2 shear stress difference—1,300,000 cfs.

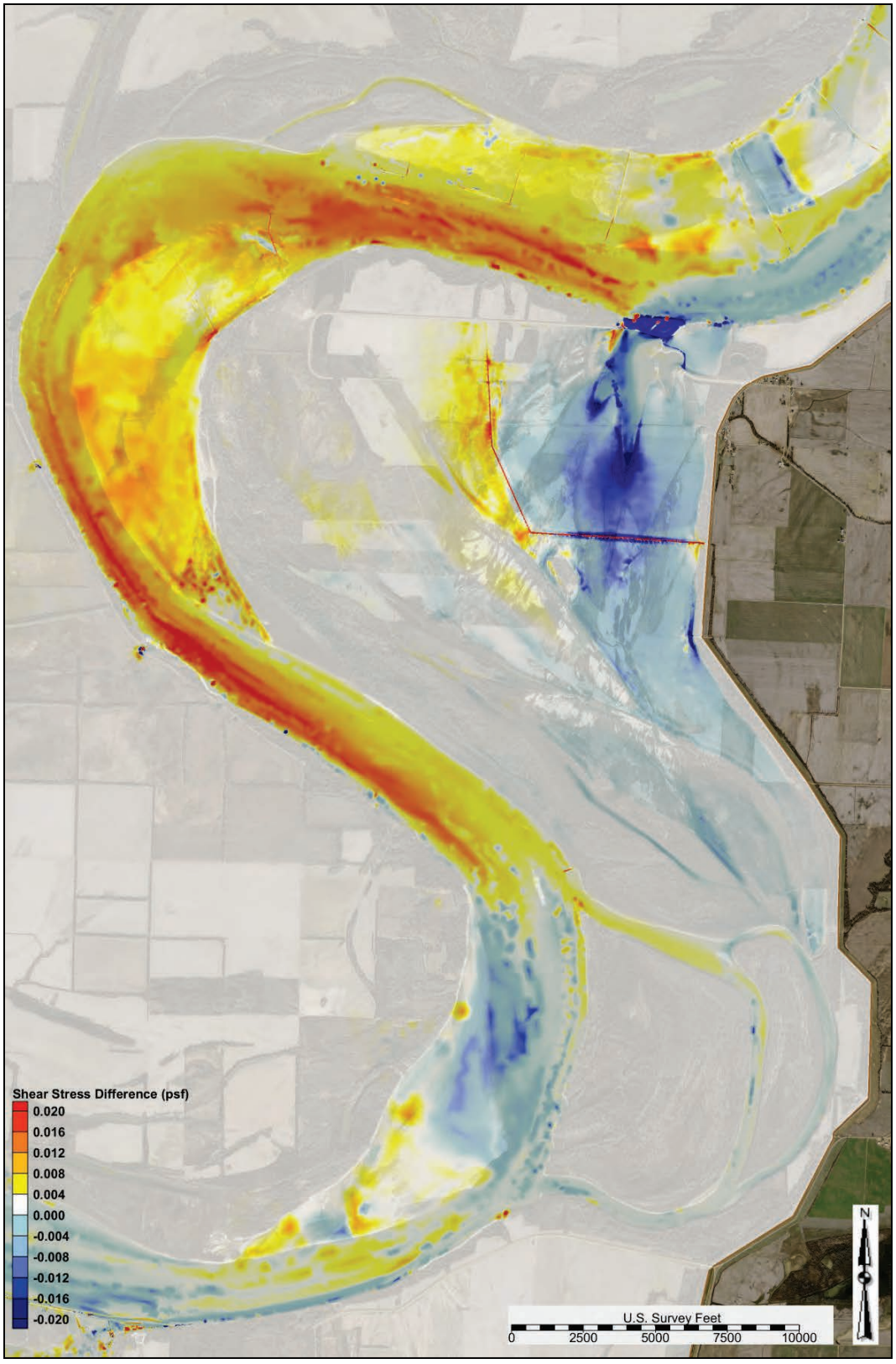


Figure C-139. Alternative 2 shear stress difference—1,500,000 cfs.

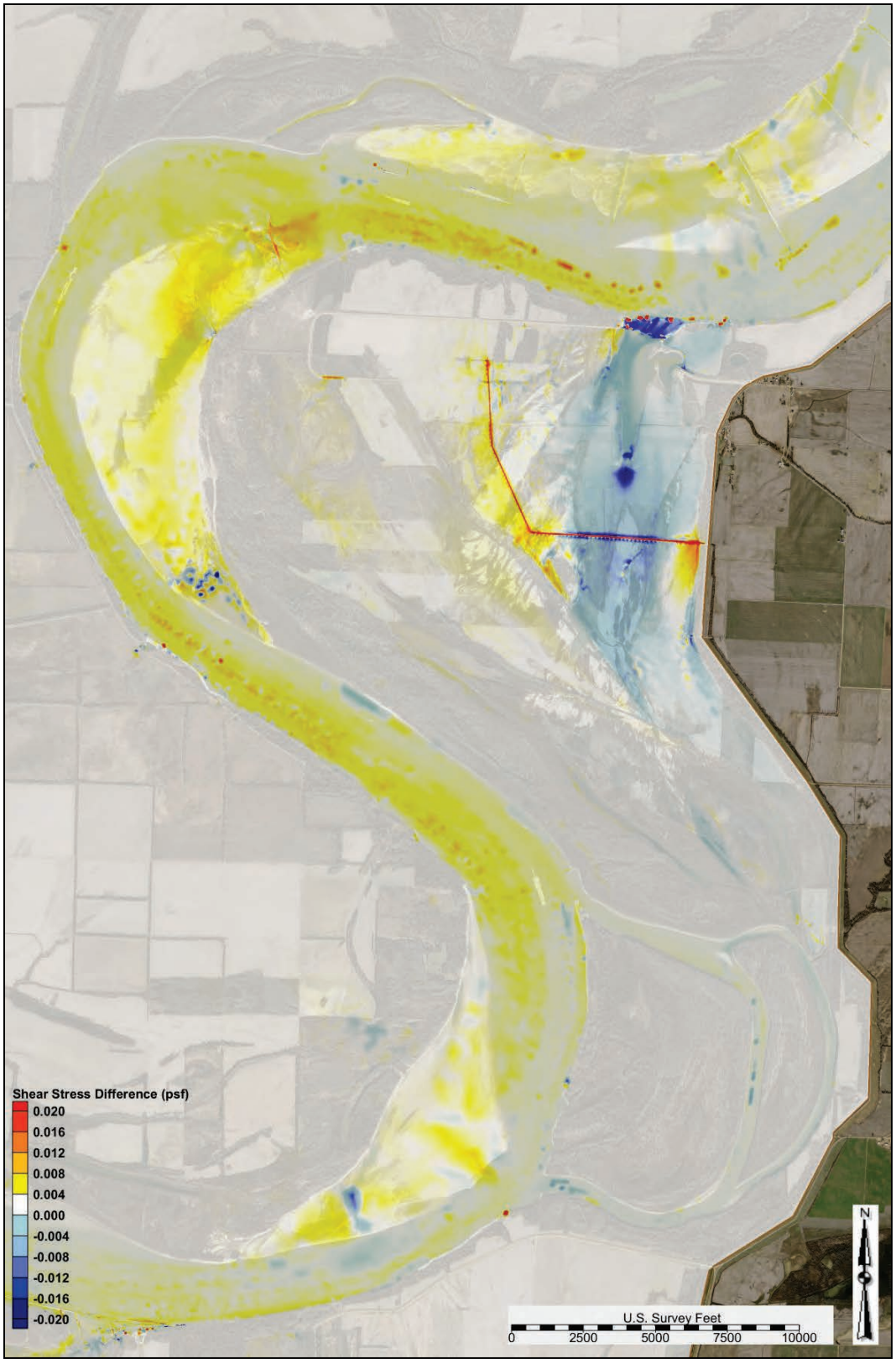


Figure C-140. Alternative 2 shear stress difference—1,700,000 cfs.

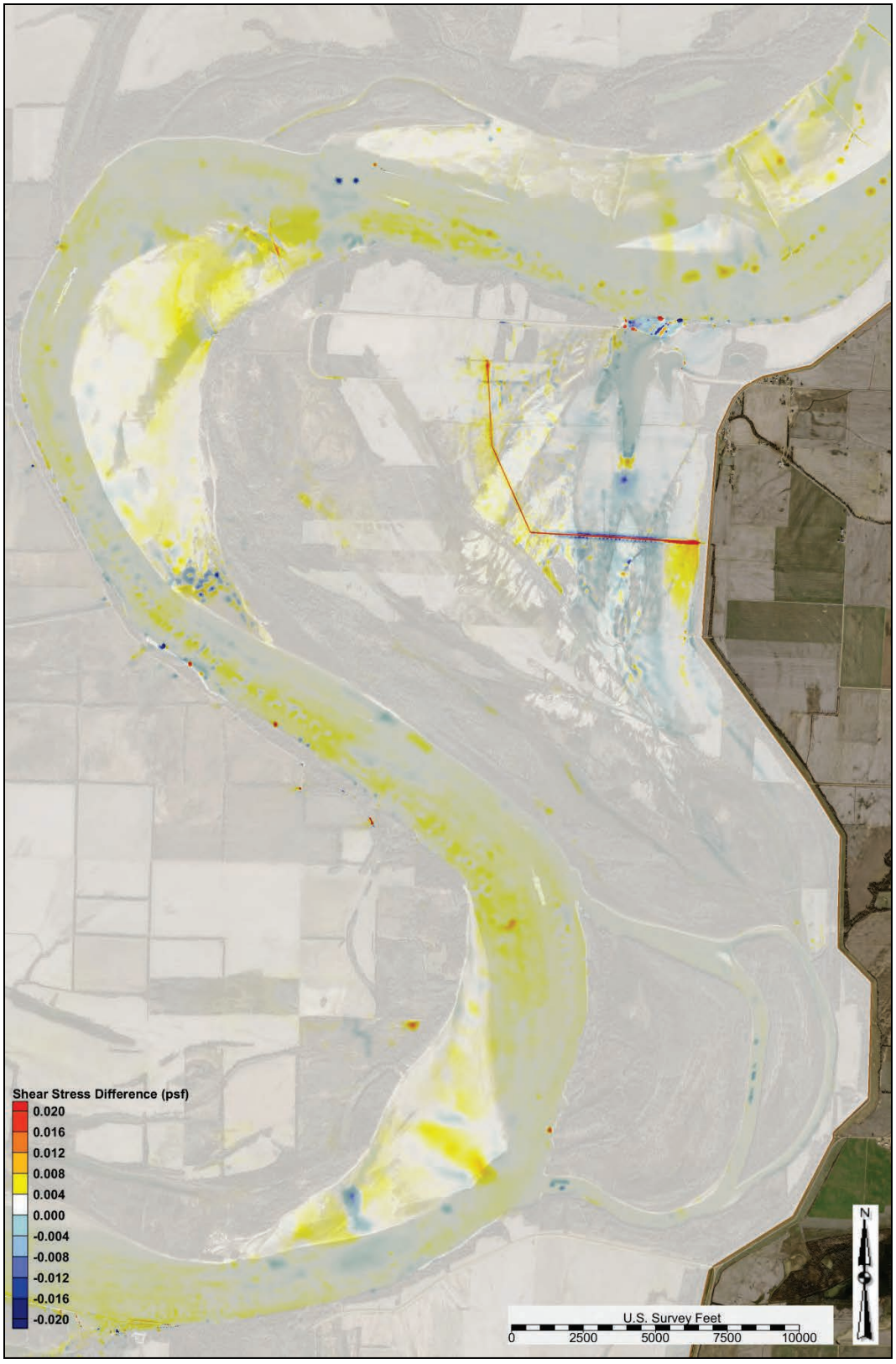


Figure C-141. Alternative 2 shear stress difference—1,900,000 cfs.

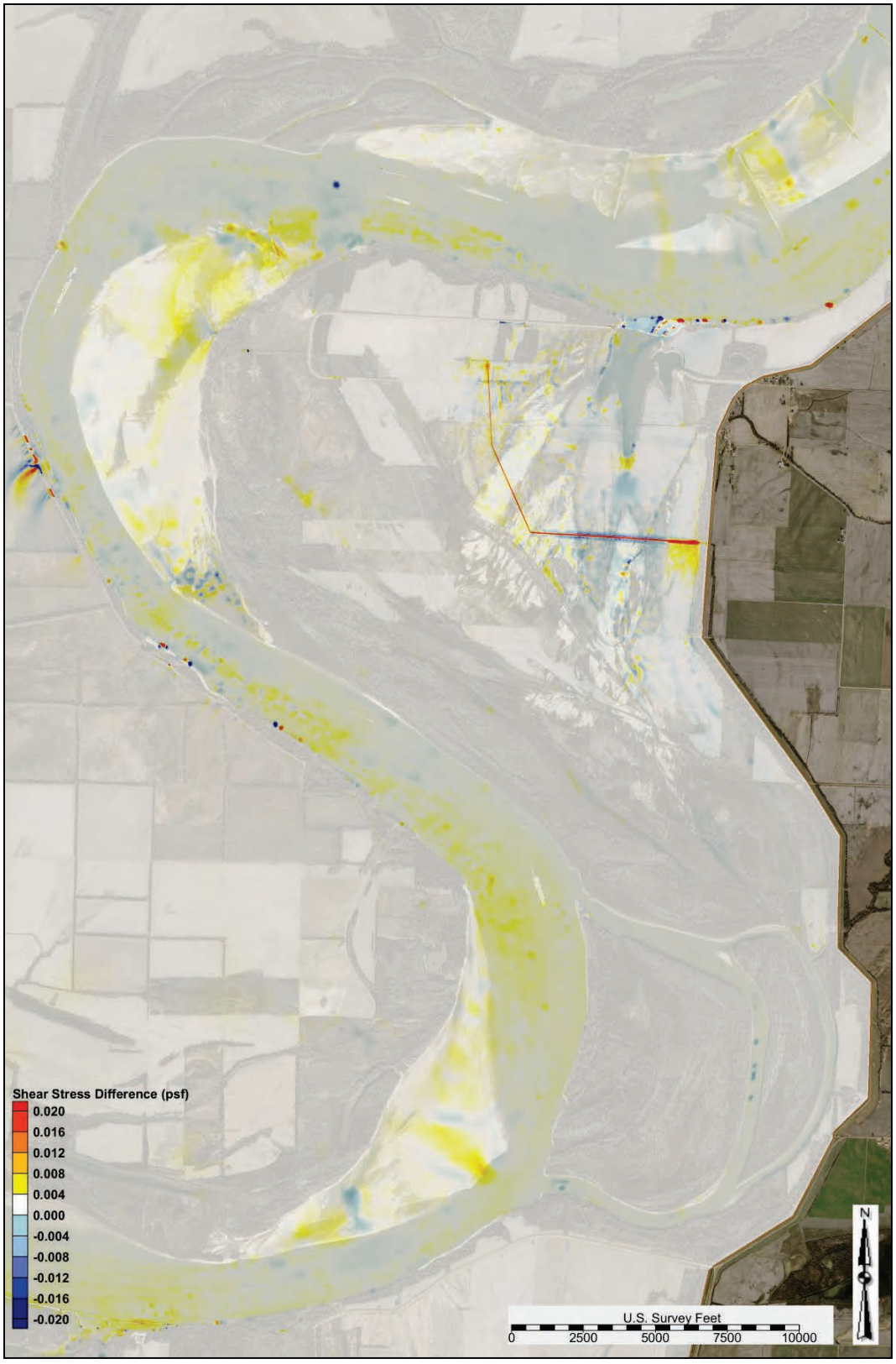
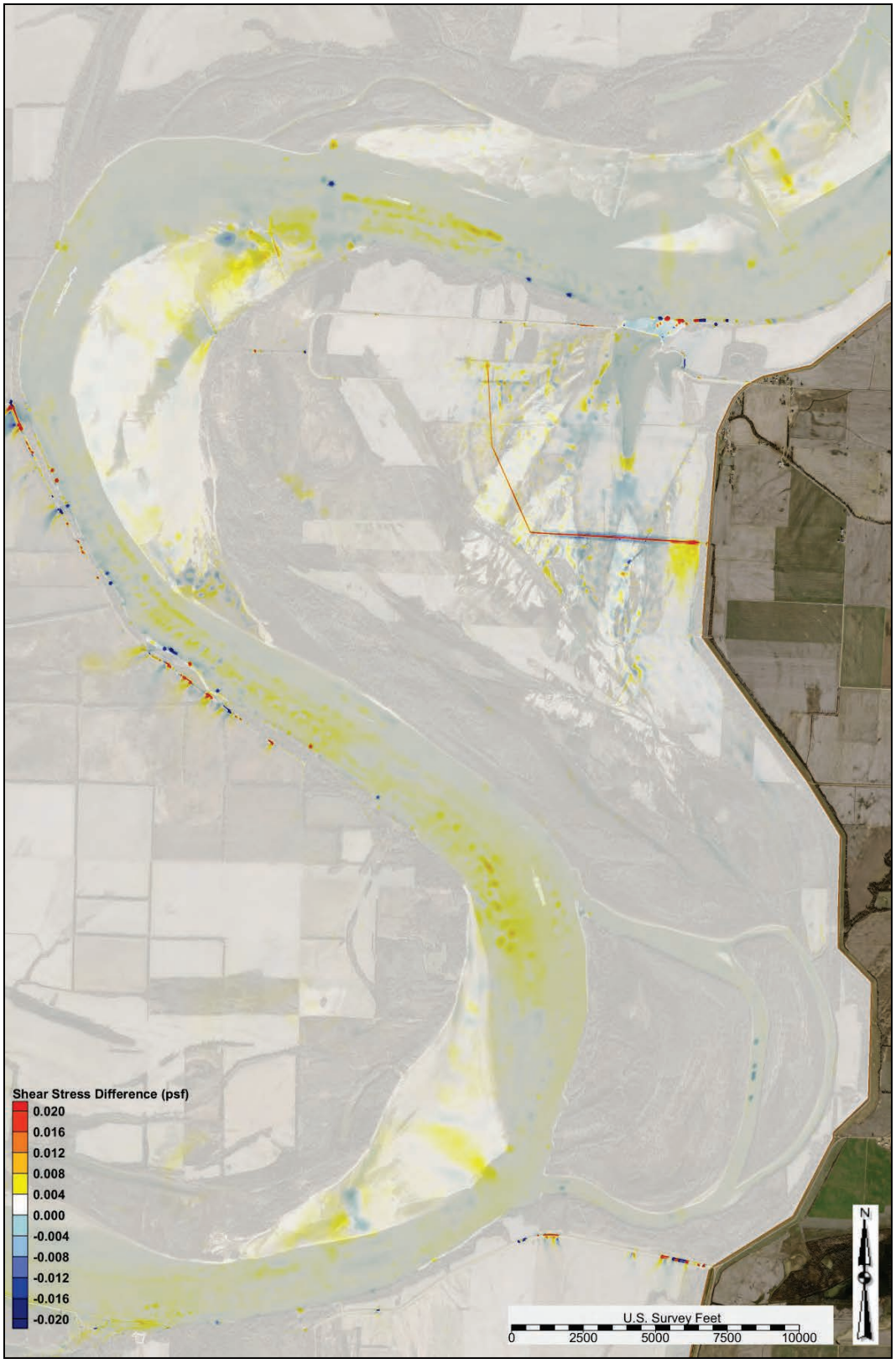


Figure C-142. Alternative 2 shear stress difference—2,100,000 cfs.



WSEL

Figure C-143 depicts the water surface elevation profiles in the study reach for the following flows: 1,100,000 cfs, 1,500,000 cfs, 1,900,000 cfs, and 2,100,000 cfs.

Sediment diversion grain size distribution

Table C-4 lists the sediment diversion grain size distribution for flows ranging from 870,000 cfs to 2,000,000 cfs.

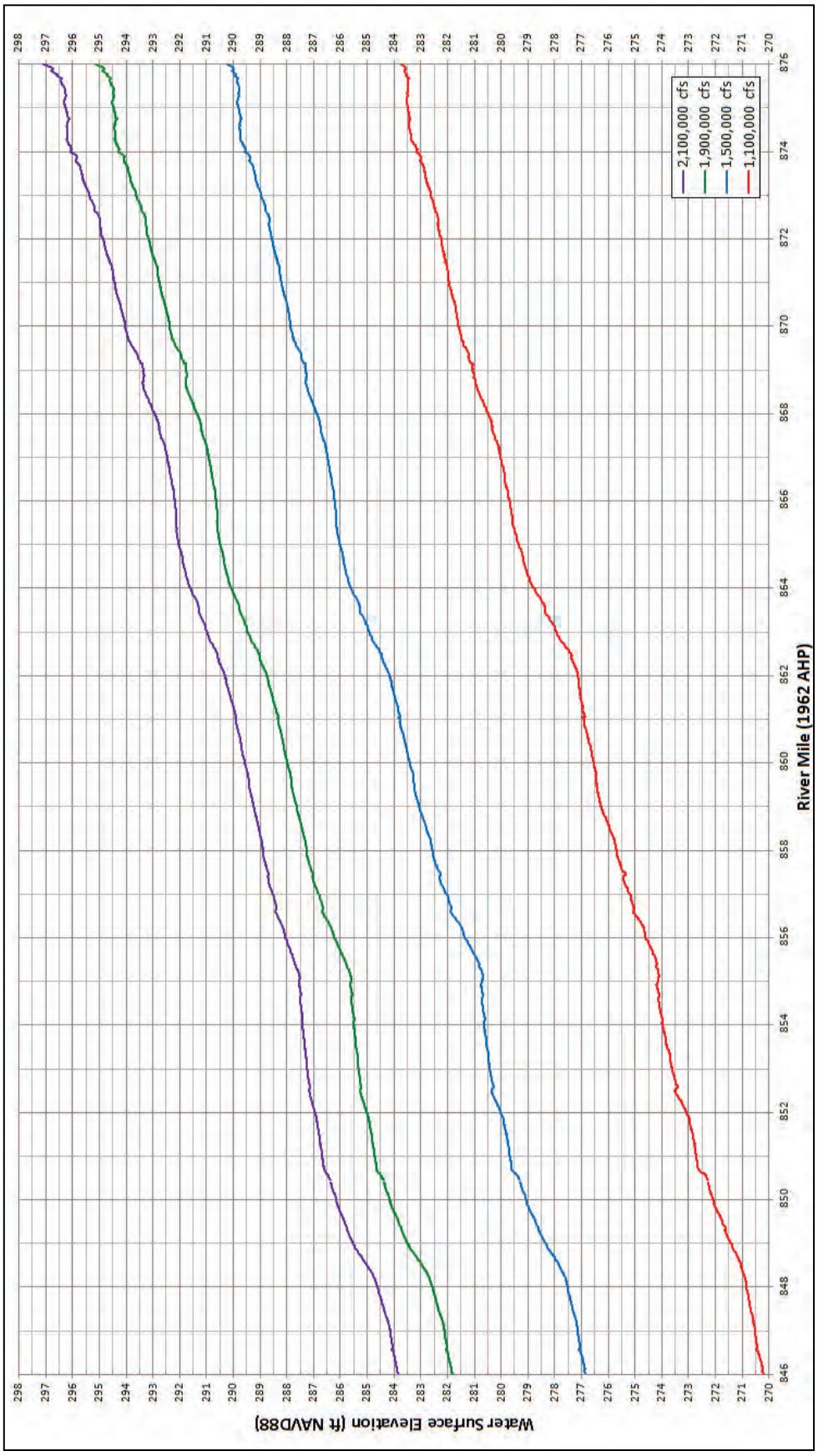


Figure C-143. Alternative 2 WSEL profile.

Table C-4. Alternative 2 diversion grain size distribution.

Main Channel Flow US of Crevasse (cfs)	Total Diversion Load Grain Size Fraction Distribution									
	Coarse Silt	Very Fine Sand	Fine Sand	Medium Sand	Coarse Sand	Very Coarse Sand	Very Fine Pebble	Fine Pebble	Medium Pebble	Coarse Pebble
870,000	-	-	-	-	-	-	-	-	-	-
1,000,000	-	-	-	-	-	-	-	-	-	-
1,100,000	-	-	-	-	-	-	-	-	-	-
1,200,000	0.0000	0.2850	0.4297	0.1935	0.0719	0.0196	0.0003	0.0001	0.0000	0.0000
1,300,000	0.0002	0.1551	0.2888	0.2703	0.2053	0.0607	0.0148	0.0031	0.0015	0.0003
1,400,000	0.0002	0.0985	0.2546	0.3698	0.2154	0.0535	0.0033	0.0030	0.0014	0.0003
1,500,000	0.0005	0.0996	0.2665	0.3609	0.2140	0.0508	0.0026	0.0028	0.0020	0.0003
1,600,000	0.0010	0.1038	0.2863	0.3682	0.1925	0.0394	0.0030	0.0015	0.0038	0.0005
1,700,000	0.0012	0.0963	0.2771	0.3777	0.1976	0.0393	0.0034	0.0013	0.0054	0.0007
1,800,000	0.0011	0.0891	0.2671	0.3875	0.2052	0.0402	0.0038	0.0013	0.0035	0.0011
1,900,000	0.0008	0.0852	0.2630	0.3938	0.2083	0.0395	0.0040	0.0015	0.0025	0.0015
2,000,000	0.0009	0.0791	0.2547	0.4032	0.2113	0.0409	0.0043	0.0016	0.0020	0.0020
2,100,000	0.0009	0.0798	0.2545	0.4000	0.2135	0.0404	0.0049	0.0017	0.0018	0.0025

- no diverted sediment

Alternative 3 output

The following sections contain AdH model output and analysis for Alternative 3.

Shear stress

The modeled shear stress outputs at flows ranging from 900,000 to 2,100,000 cfs for the study overbank are depicted in Figures C-144 through C-150.

Figure C-144. Alternative 3 shear stress—900,000 cfs (study overbank).



Figure C-145. Alternative 3 shear stress—1,100,000 cfs (study overbank).

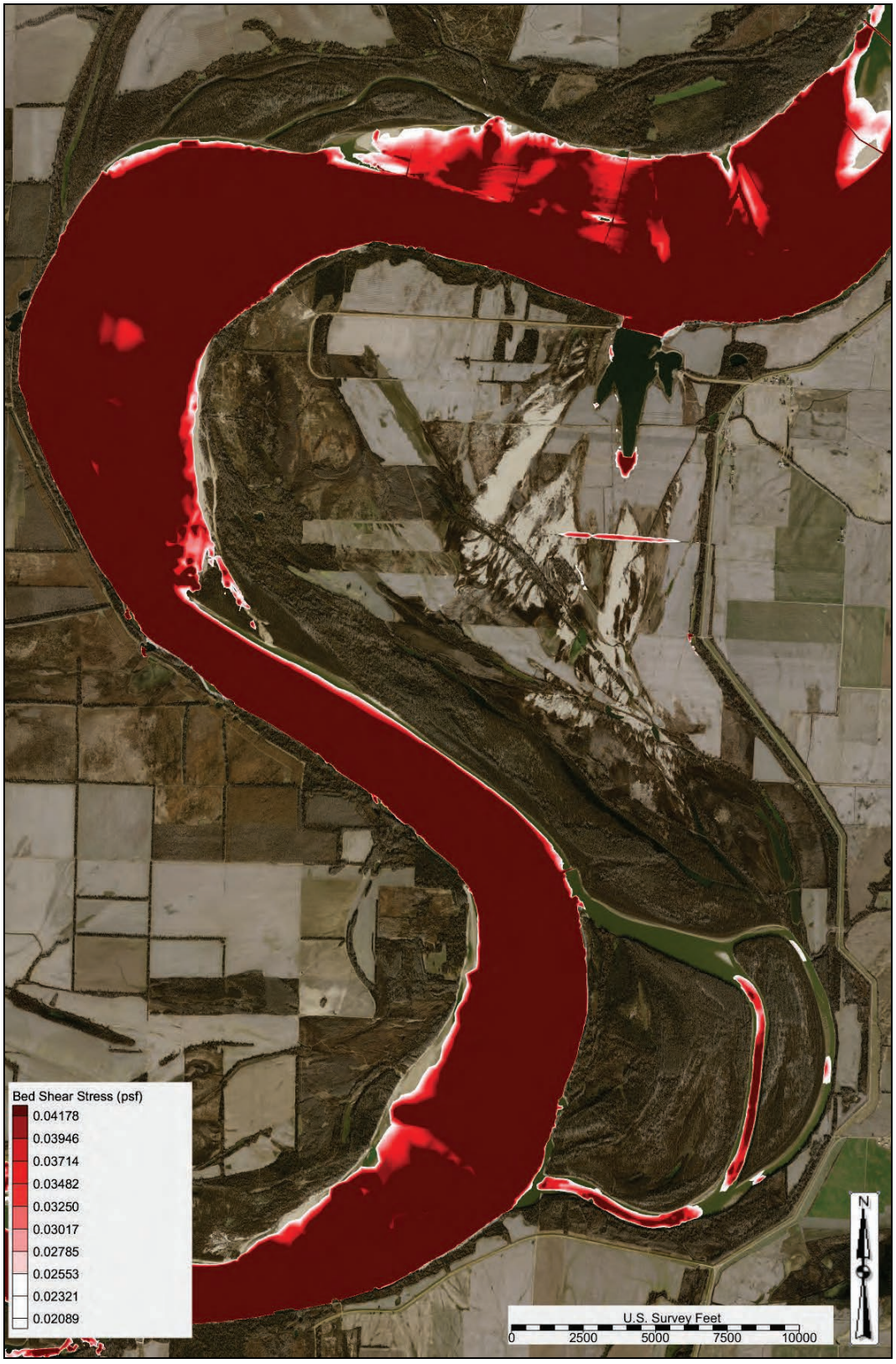


Figure C-146. Alternative 3 shear stress—1,300,000 cfs (study overbank).

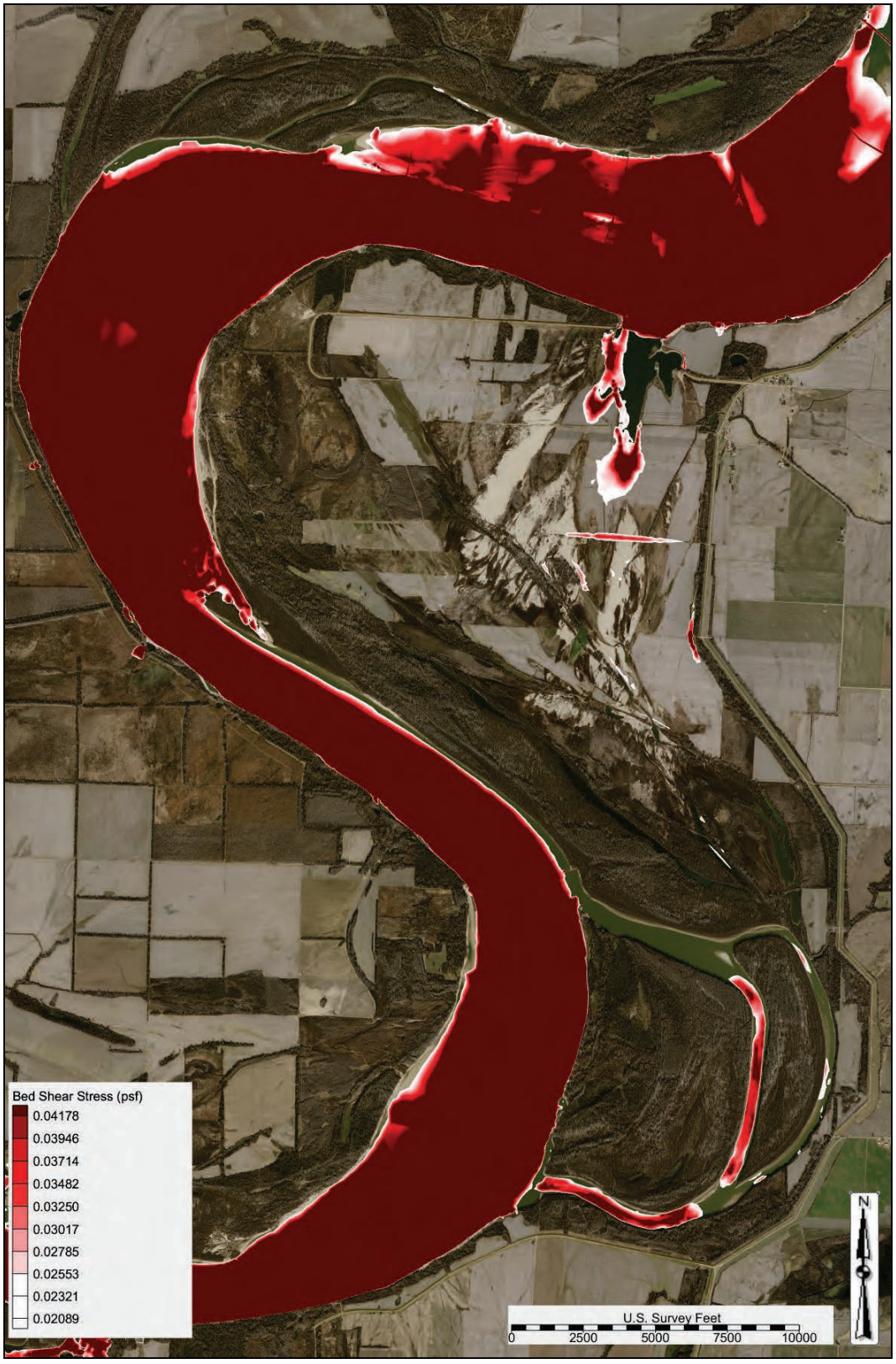


Figure C-147. Alternative 3 shear stress—1,500,000 cfs (study overbank).

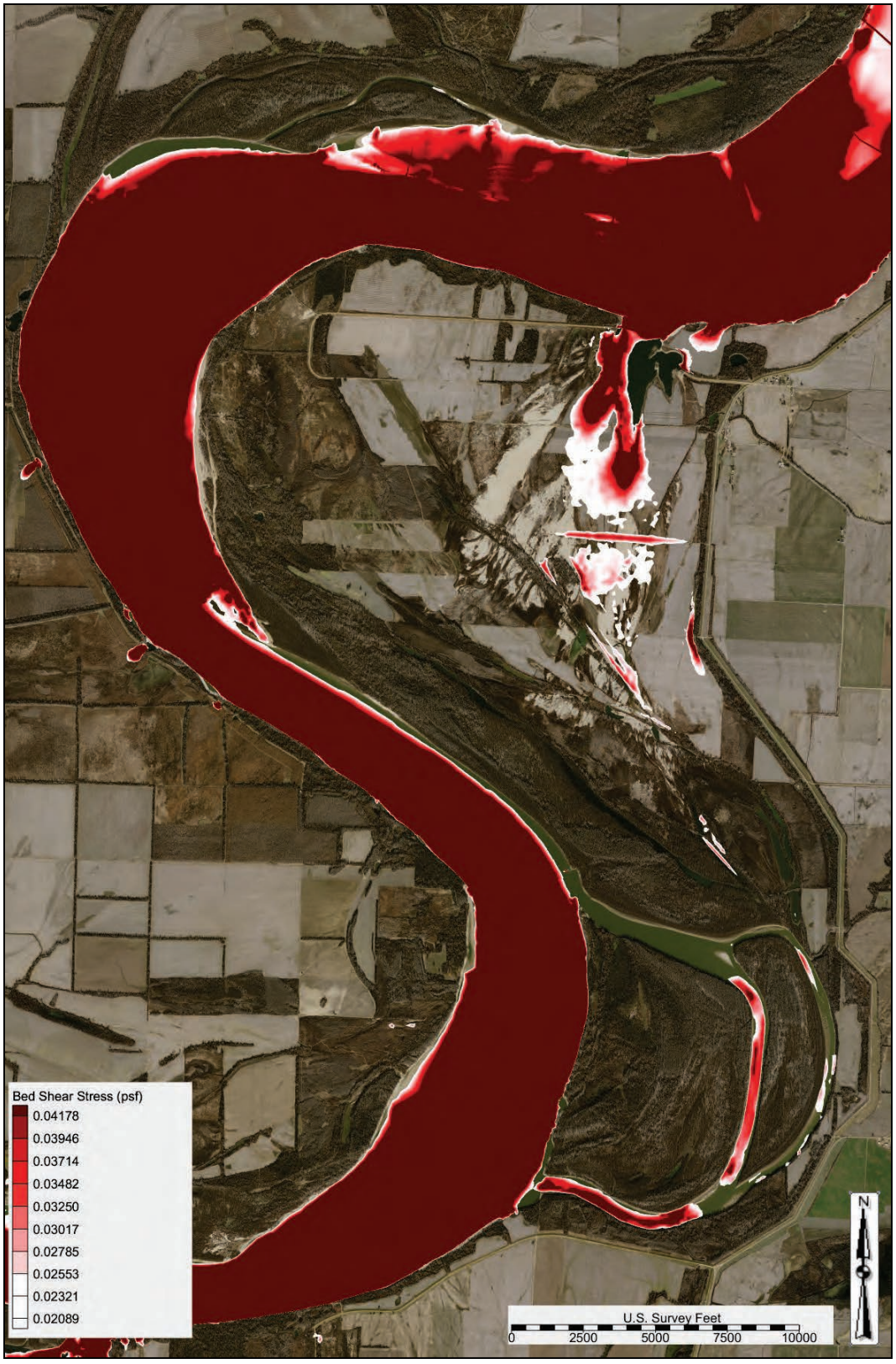


Figure C-148. Alternative 3 shear stress—1,700,000 cfs (study overbank).

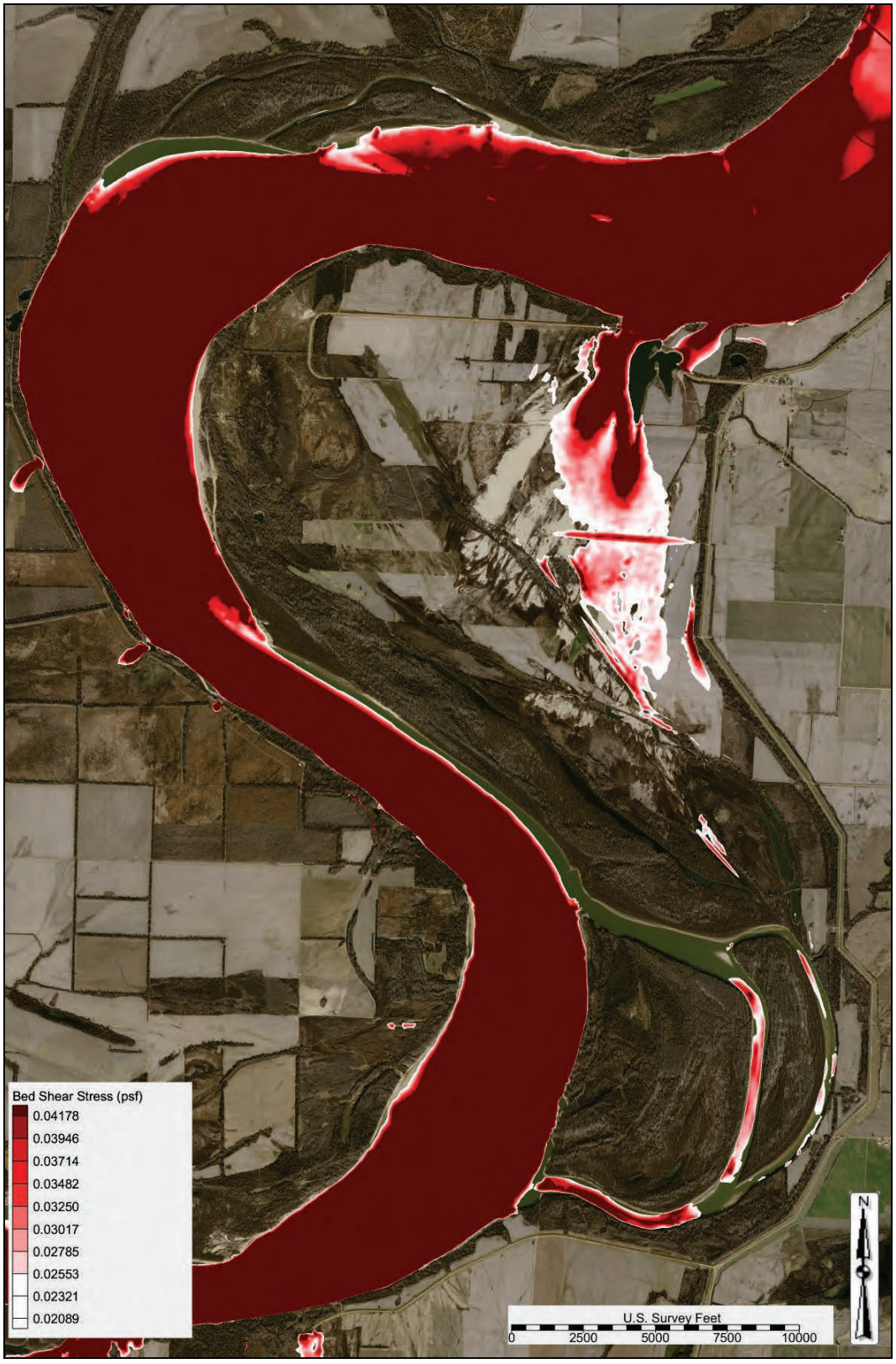


Figure C-149. Alternative 3 shear stress—1,900,000 cfs (study overbank).

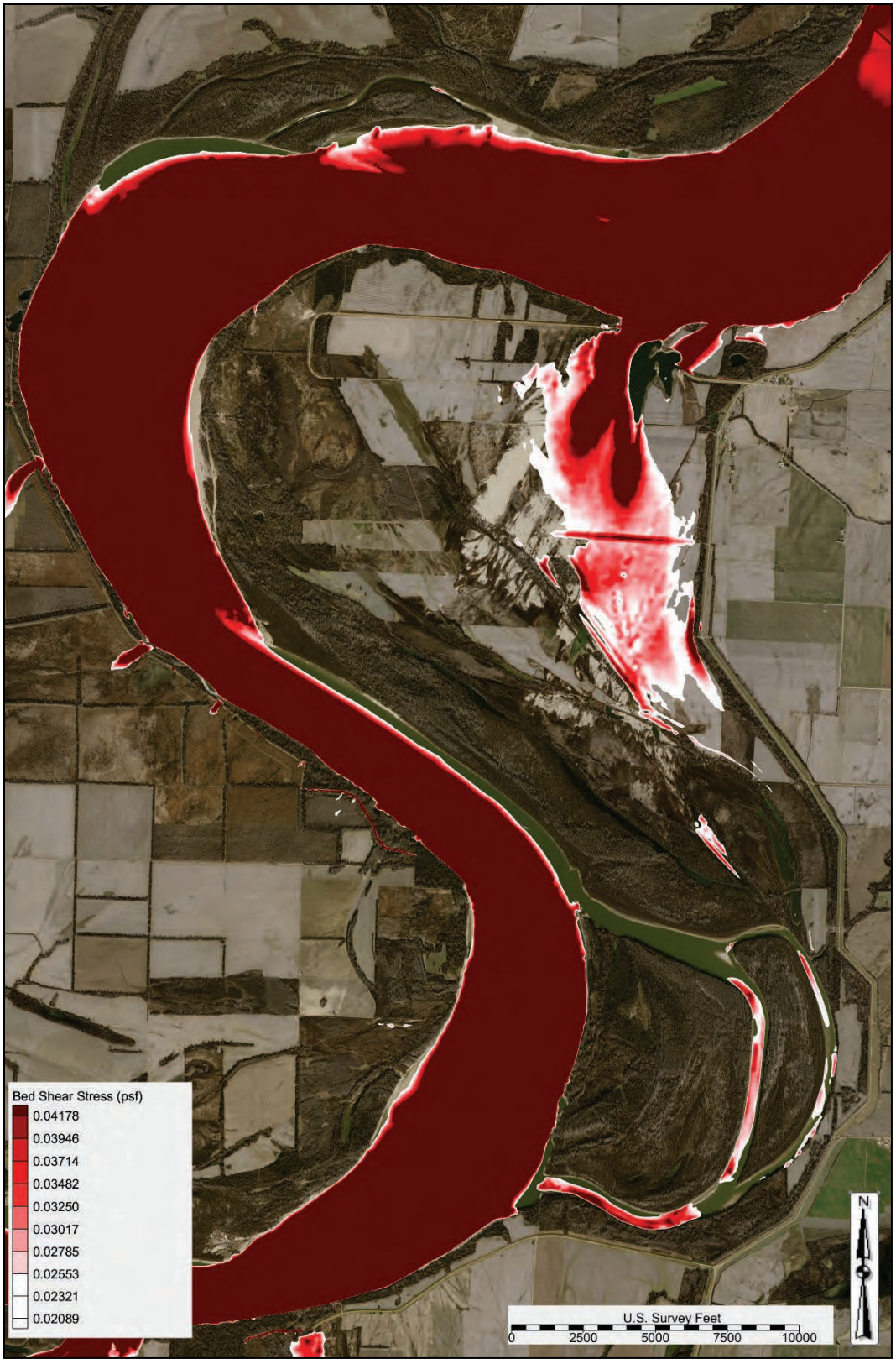
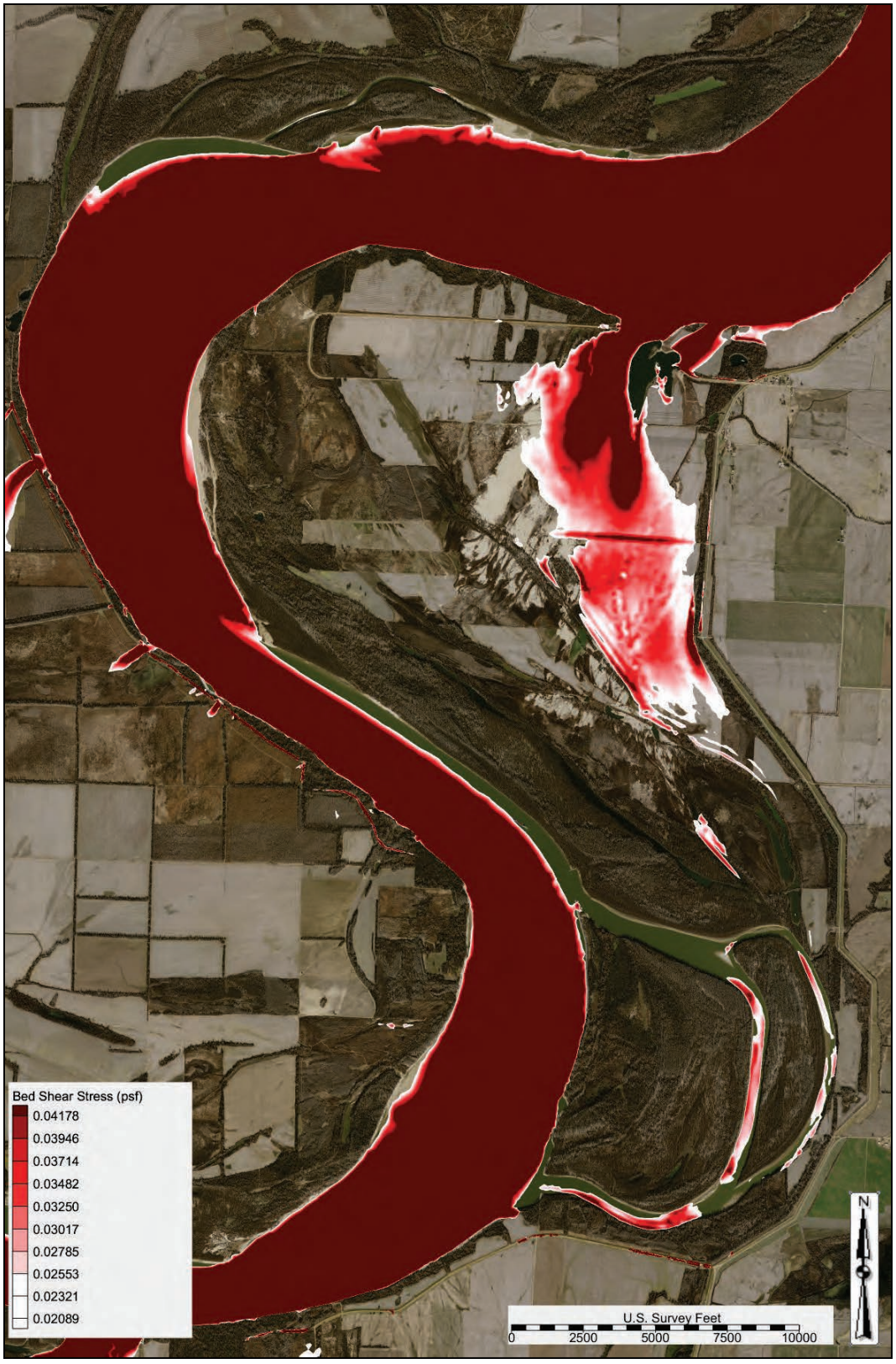


Figure C-150. Alternative 3 shear stress—2,100,000 cfs (study overbank).



Shear stress difference comparison

The modeled shear stress difference plots compared to the base condition output for flows ranging from 900,000 to 2,100,000 cfs are depicted in Figures C-151 through C-157. A positive shear stress difference (+ value and red and orange) indicated an increased shear stress compared to the base condition. A negative shear stress difference (- value and blue) indicated a decreased shear stress compared to the base condition. A zero shear stress difference (zero value and white) indicated that the alternative had no change in shear stress.

Figure C-151. Alternative 3 shear stress difference—900,000 cfs.

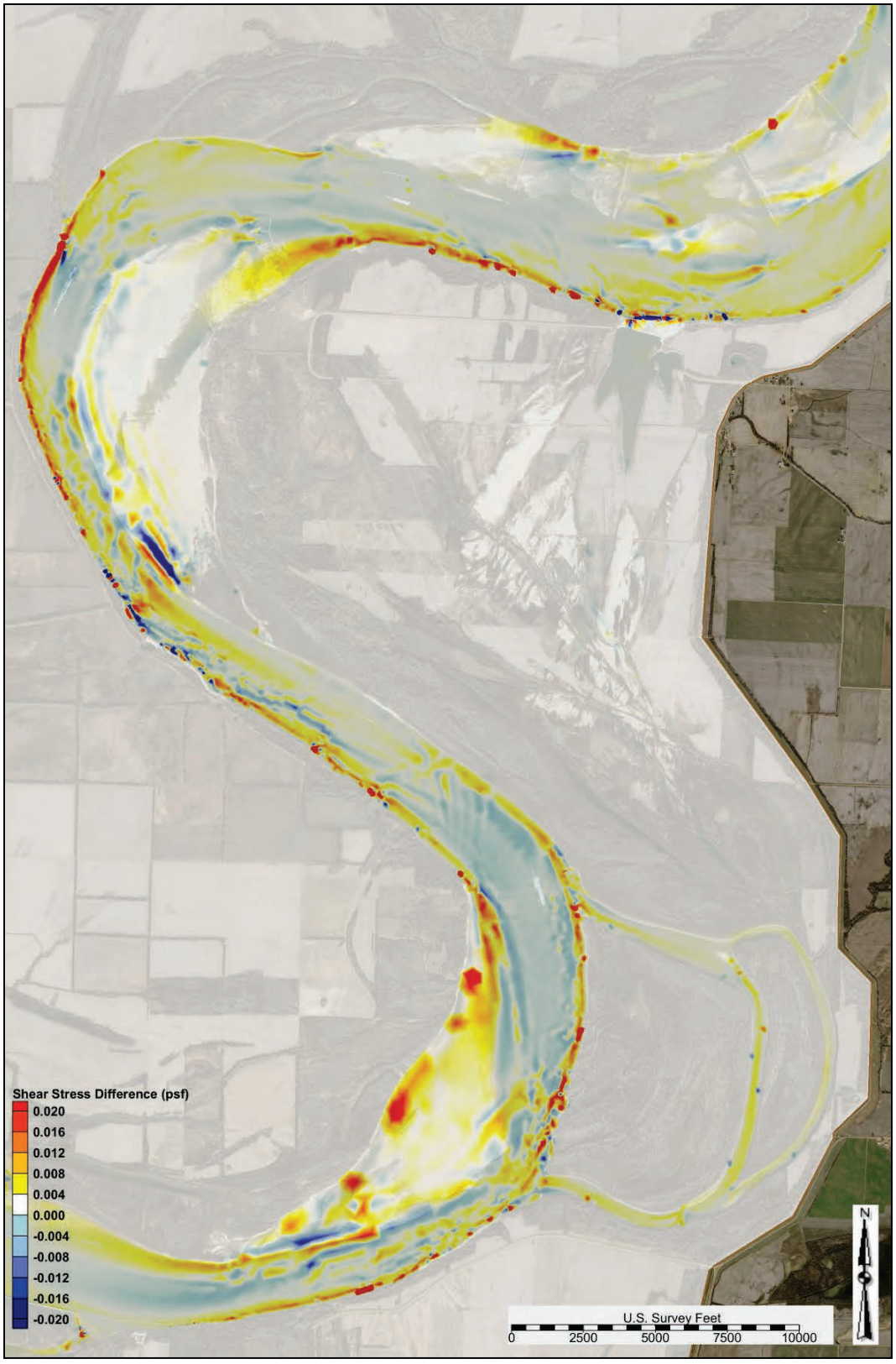


Figure C-152. Alternative 3 shear stress difference—1,100,000 cfs.

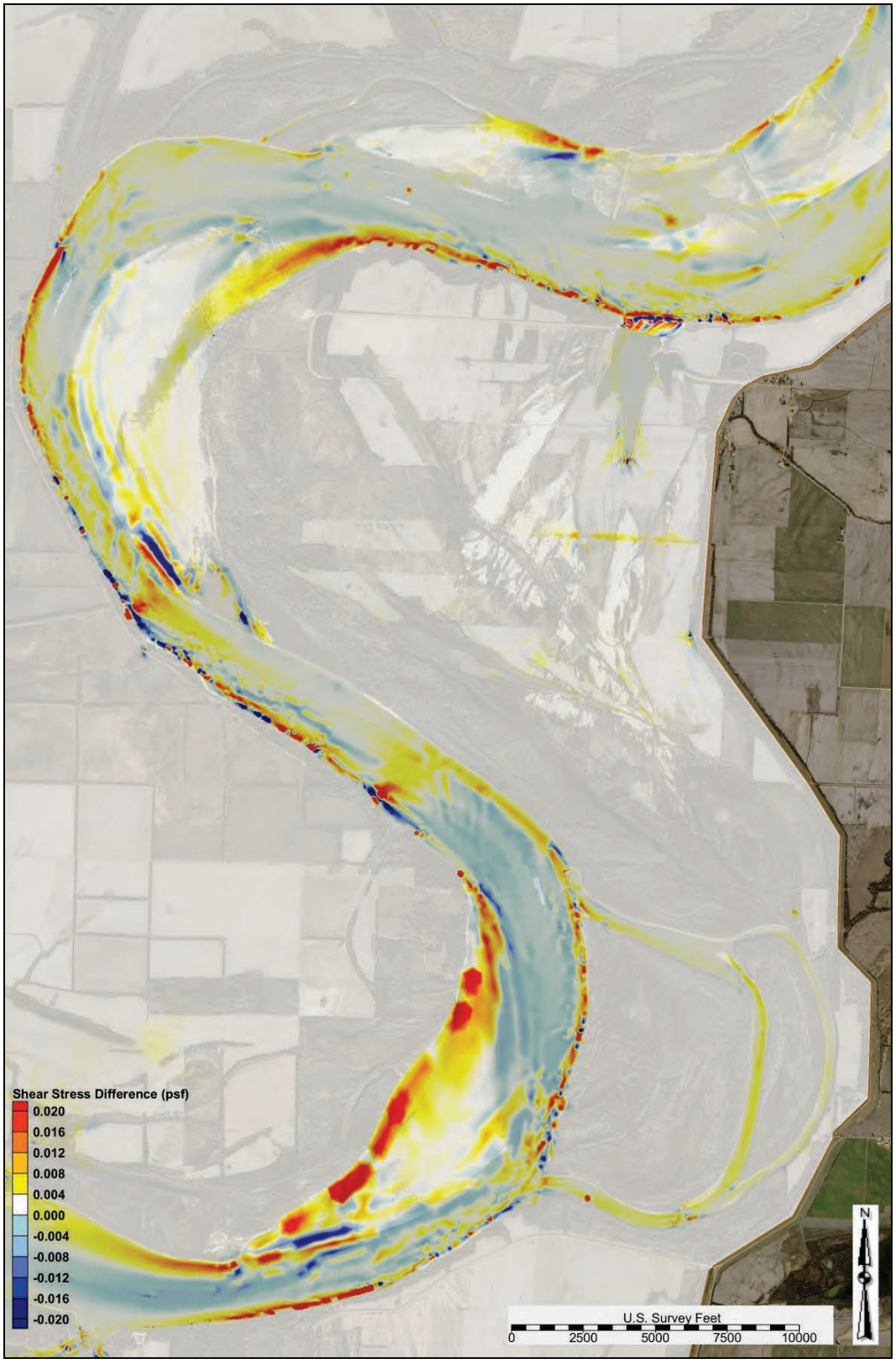


Figure C-153. Alternative 3 shear stress difference—1,300,000 cfs.

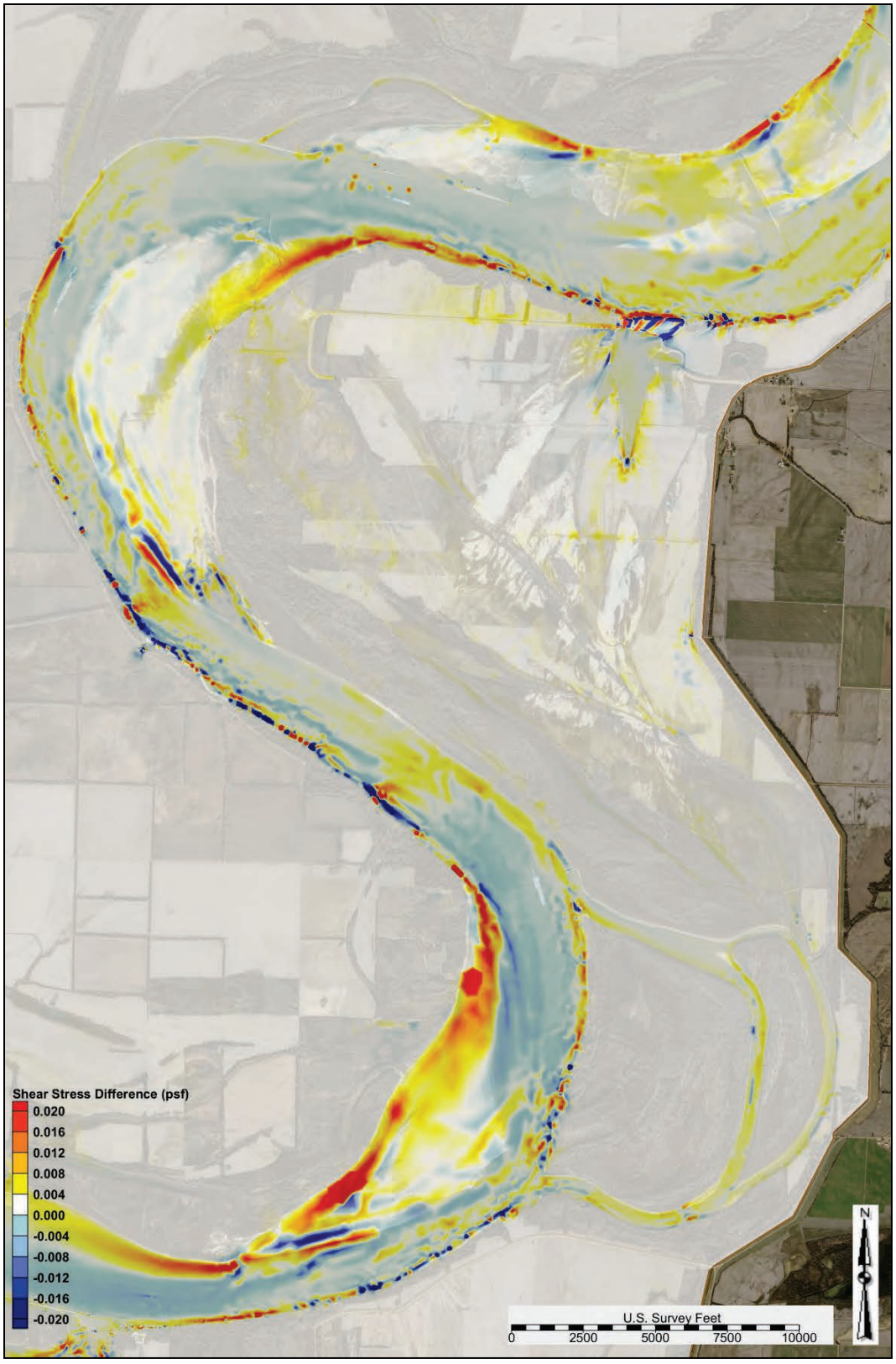


Figure C-154. Alternative 3 shear stress difference—1,500,000 cfs.

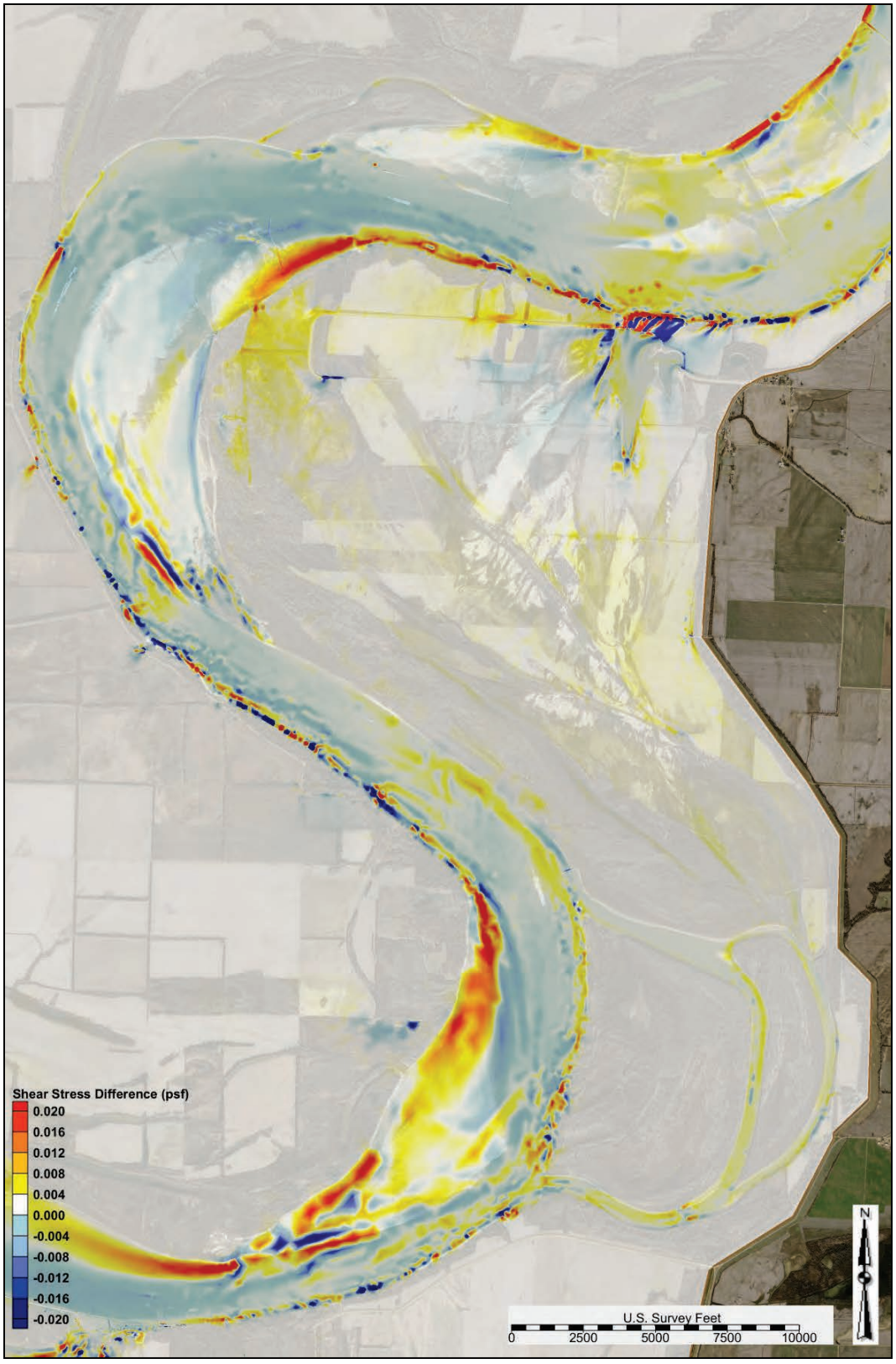


Figure C-155. Alternative 3 shear stress difference—1,700,000 cfs.

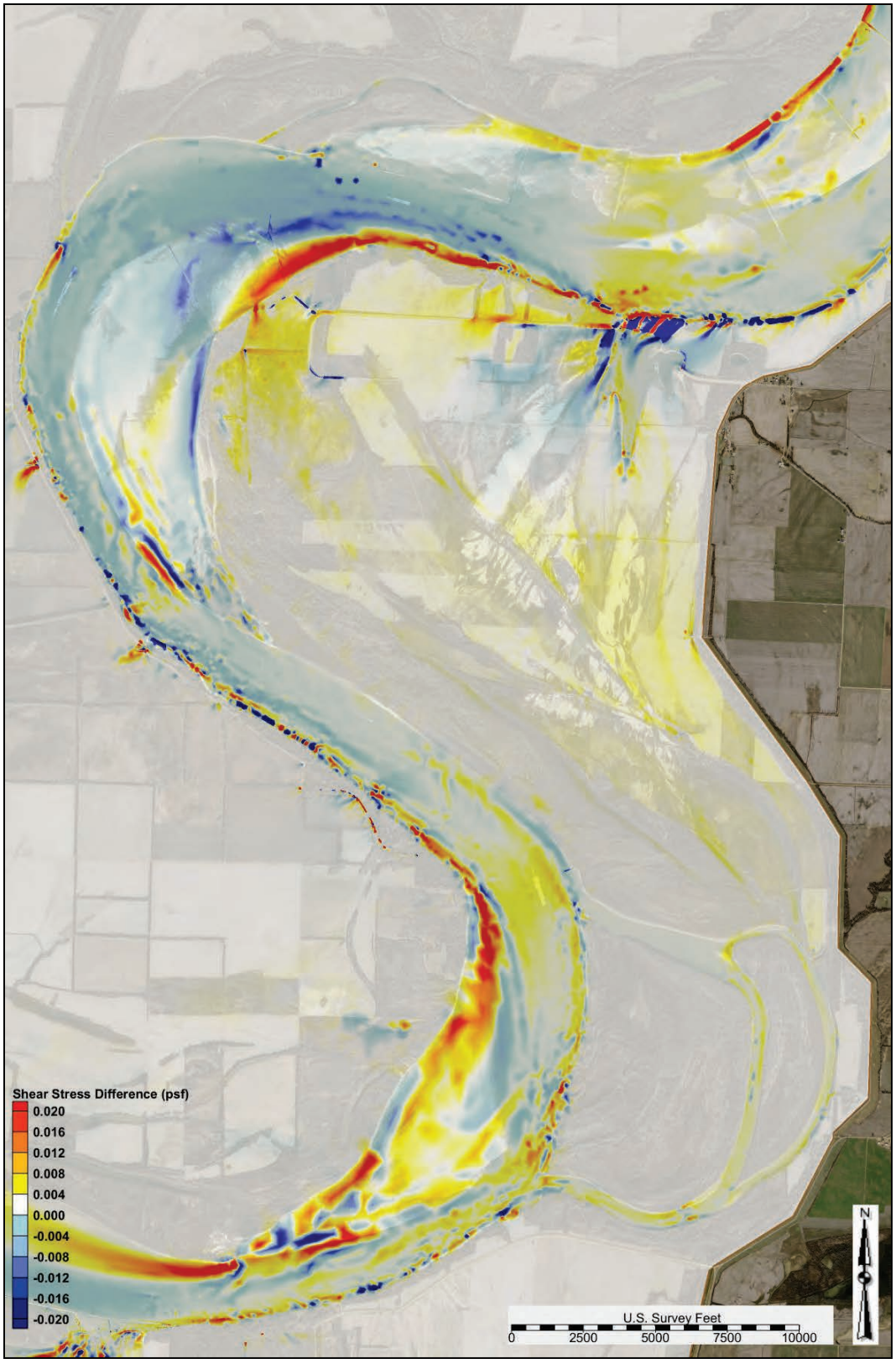


Figure C-156. Alternative 3 shear stress difference—1,900,000 cfs.

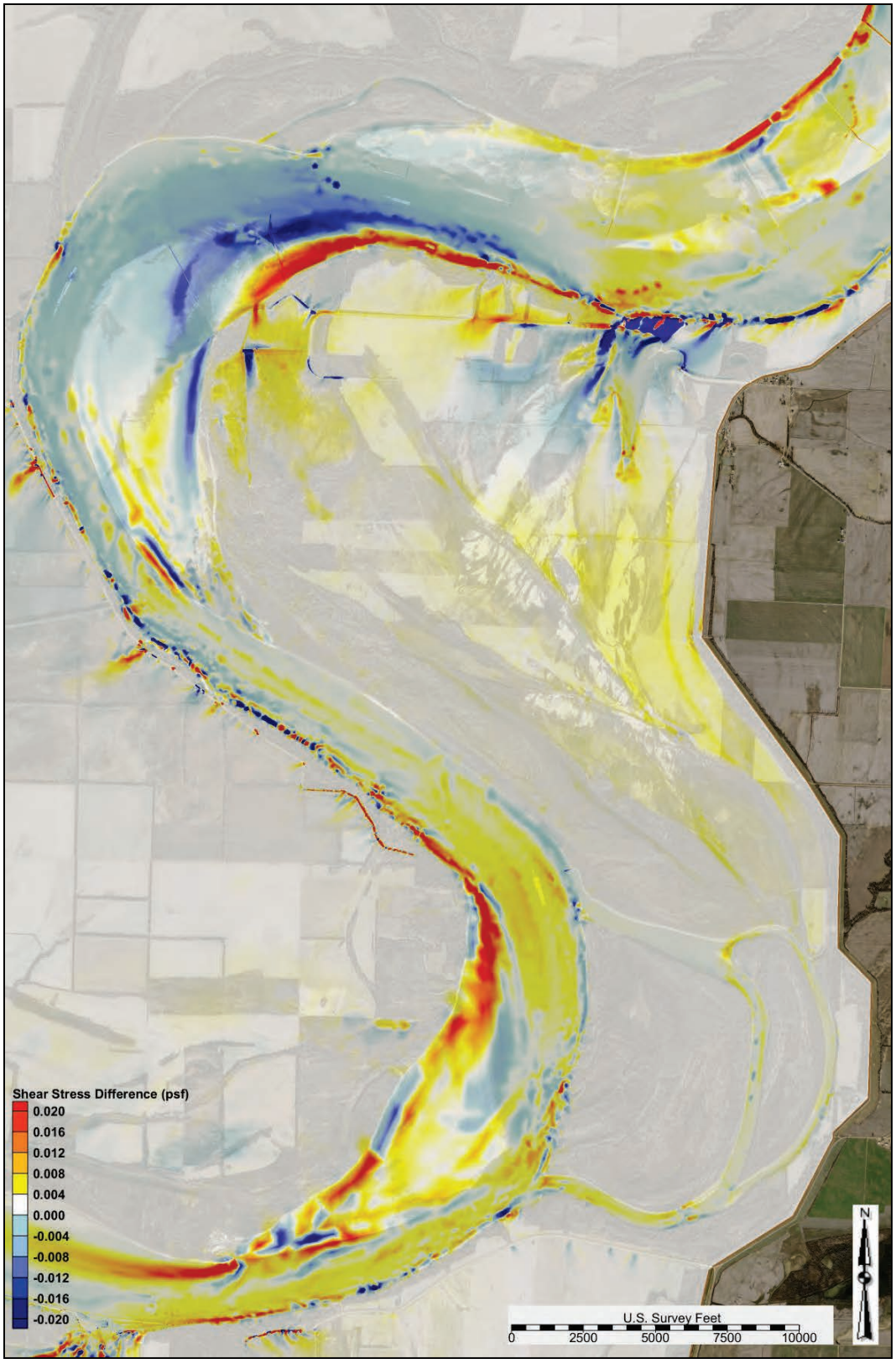
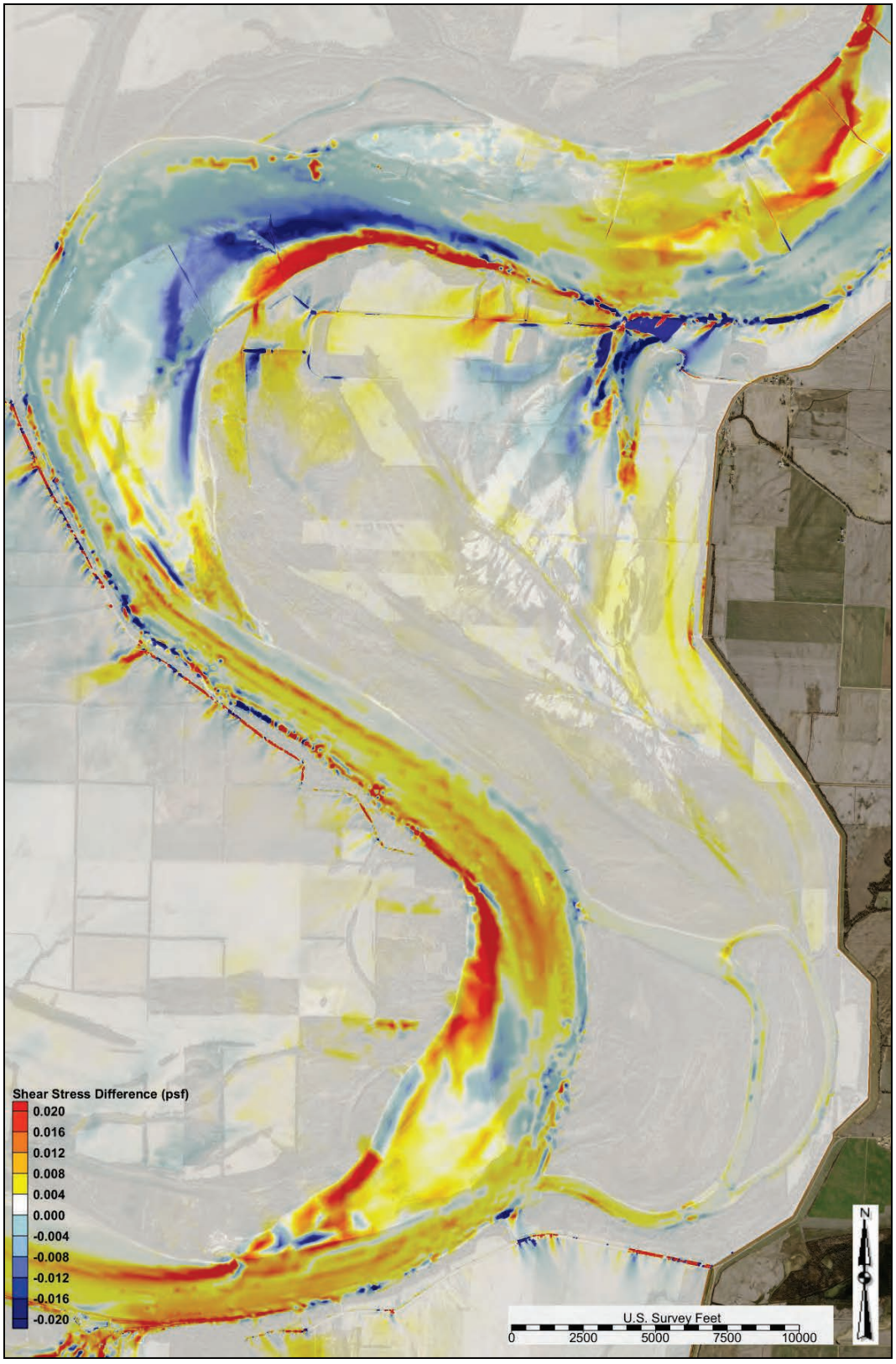


Figure C-157. Alternative 3 shear stress difference—2,100,000 cfs.



WSEL

Figure C-158 depicts the WSEL profiles in the study reach for the following flows: 1,100,000 cfs, 1,500,000 cfs, 1,900,000 cfs, and 2,100,000 cfs.

Sediment diversion grain size distribution

Table C-5 lists the sediment diversion grain size distribution for flows ranging from 870,000 cfs to 2,000,000 cfs.

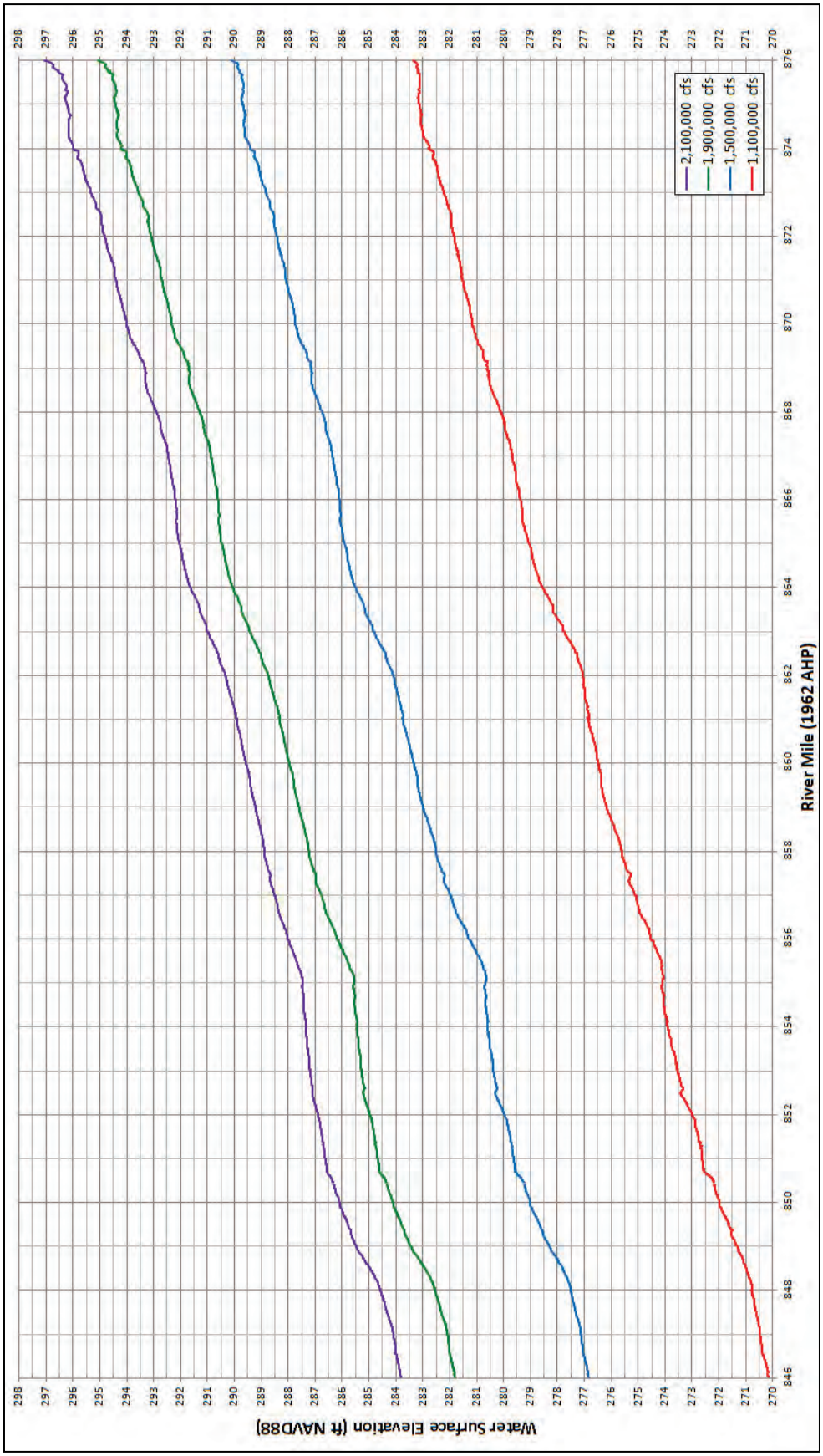


Figure C-158. Alternative 3 WSEL.

Table C-5. Alternative 3 diversion grain size distribution.

Main Channel Flow US of Crevasse (cfs)	Total Diversion Load Grain Size Fraction Distribution									
	Coarse Silt	Very Fine Sand	Fine Sand	Medium Sand	Coarse Sand	Very Coarse Sand	Very Fine Pebble	Fine Pebble	Medium Pebble	Coarse Pebble
870,000	0.0000	0.9830	0.0170	0.0000	0.0000	0.0000	0.0000	0.0000	0.0000	0.0000
900,000	0.0000	0.9304	0.0686	0.0010	0.0000	0.0000	0.0000	0.0000	0.0000	0.0000
1,000,000	0.0000	0.4552	0.4289	0.0965	0.0170	0.0023	0.0000	0.0000	0.0000	0.0000
1,100,000	0.0000	0.2073	0.4006	0.2604	0.1086	0.0224	0.0005	0.0001	0.0001	0.0000
1,200,000	0.0003	0.2043	0.3795	0.2459	0.1284	0.0332	0.0069	0.0011	0.0005	0.0000
1,300,000	0.0005	0.1125	0.3041	0.3558	0.1807	0.0401	0.0033	0.0020	0.0008	0.0001
1,400,000	0.0006	0.1079	0.2779	0.3534	0.2050	0.0479	0.0027	0.0031	0.0013	0.0002
1,500,000	0.0009	0.1084	0.2851	0.3566	0.1978	0.0432	0.0029	0.0022	0.0025	0.0003
1,600,000	0.0011	0.1015	0.2810	0.3683	0.1974	0.0410	0.0033	0.0016	0.0042	0.0005
1,700,000	0.0012	0.0958	0.2762	0.3767	0.1993	0.0399	0.0035	0.0015	0.0051	0.0008
1,800,000	0.0017	0.1006	0.2804	0.3723	0.1932	0.0402	0.0042	0.0019	0.0043	0.0012
1,900,000	0.0013	0.0947	0.2640	0.3725	0.2113	0.0458	0.0045	0.0019	0.0026	0.0014
2,000,000	0.0071	0.0953	0.2594	0.3720	0.2056	0.0480	0.0052	0.0023	0.0032	0.0020
2,100,000	0.0019	0.1083	0.2882	0.3885	0.1982	0.0014	0.0054	0.0024	0.0030	0.0027

Alternative 4 output

The following sections contain AdH model output and analysis for Alternative 4.

Shear stress

The modeled shear stress outputs at flows ranging from 900,000 to 2,100,000 cfs for the study overbank are depicted in Figures C-159 through C-165.

Figure C-159. Alternative 4 shear stress—900,000 cfs (study overbank).



Figure C-160. Alternative 4 shear stress—1,100,000 cfs (study overbank).

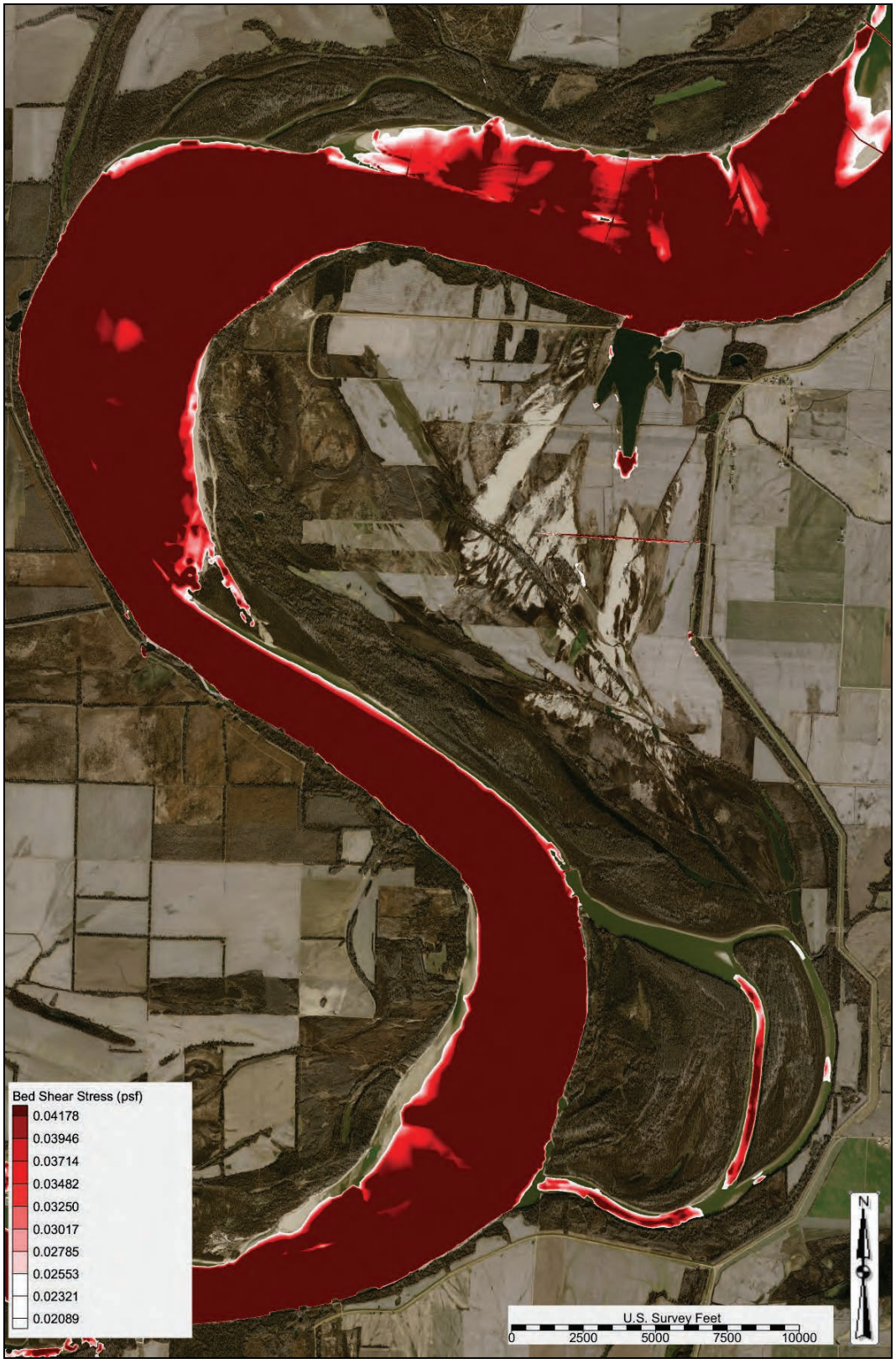


Figure C-161. Alternative 4 shear stress—1,300,000 cfs (study overbank).

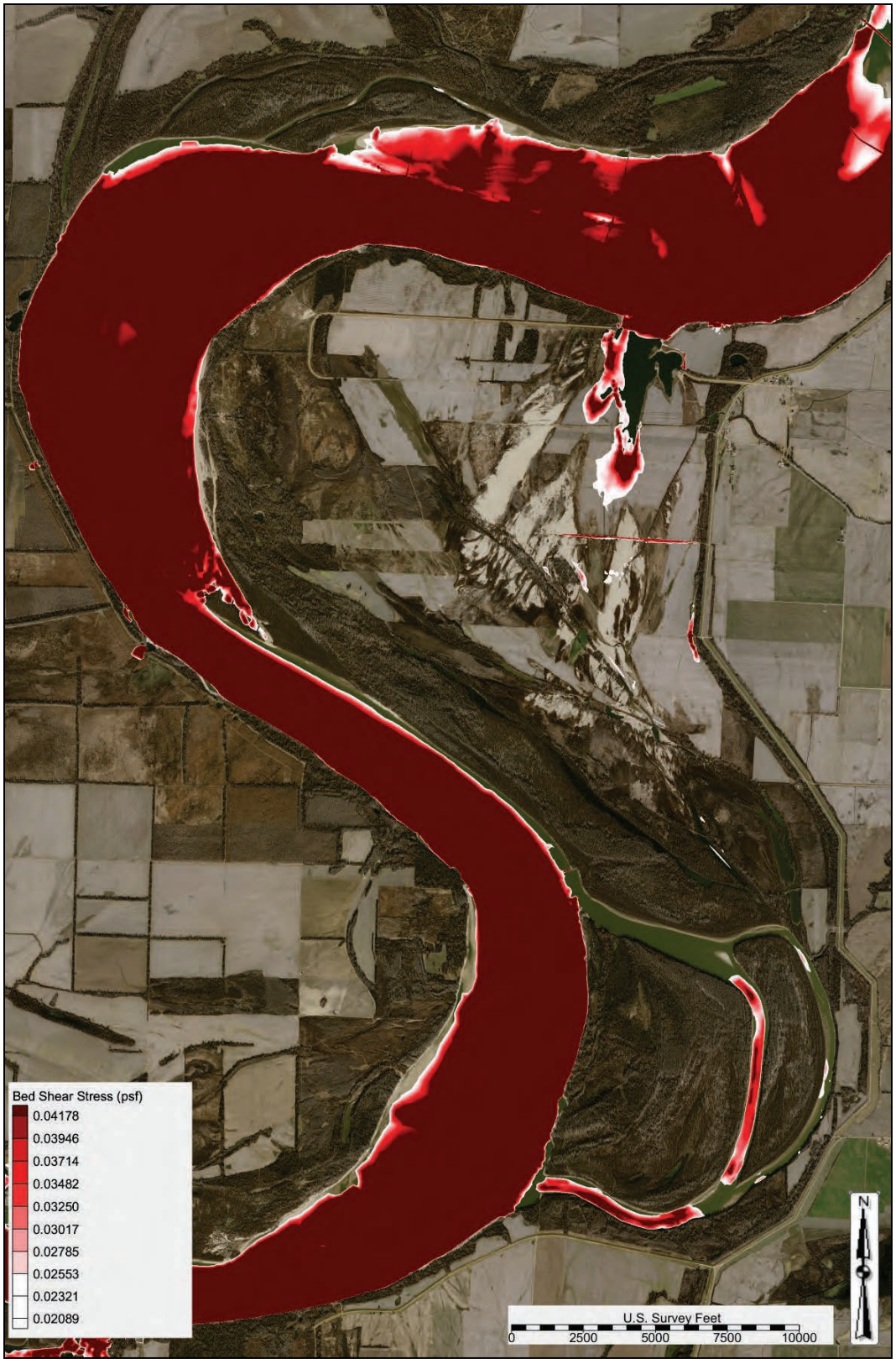


Figure C-162. Alternative 4 shear stress—1,500,000 cfs (study overbank).

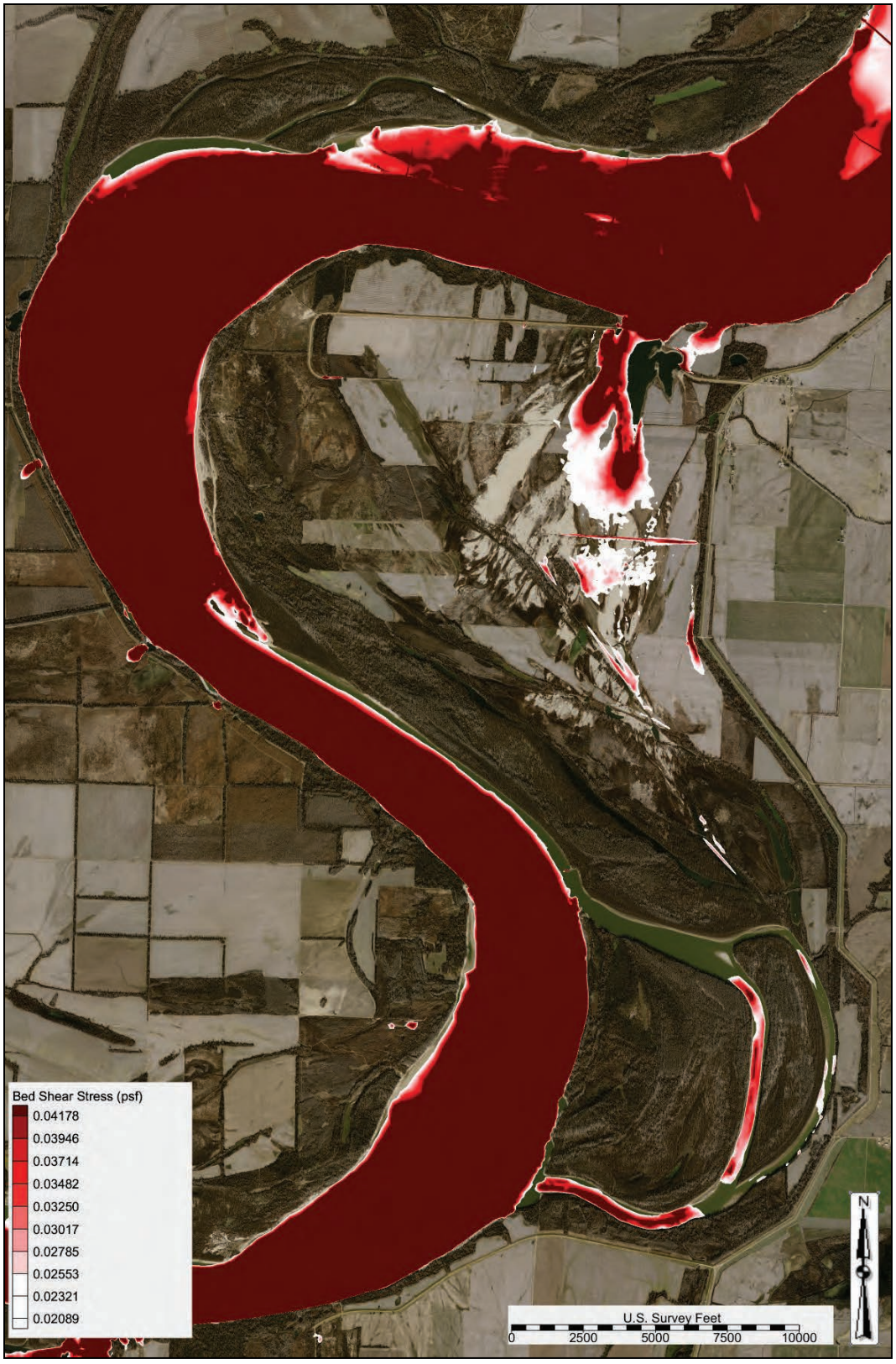


Figure C-163. Alternative 4 shear stress—1,700,000 cfs (study overbank).

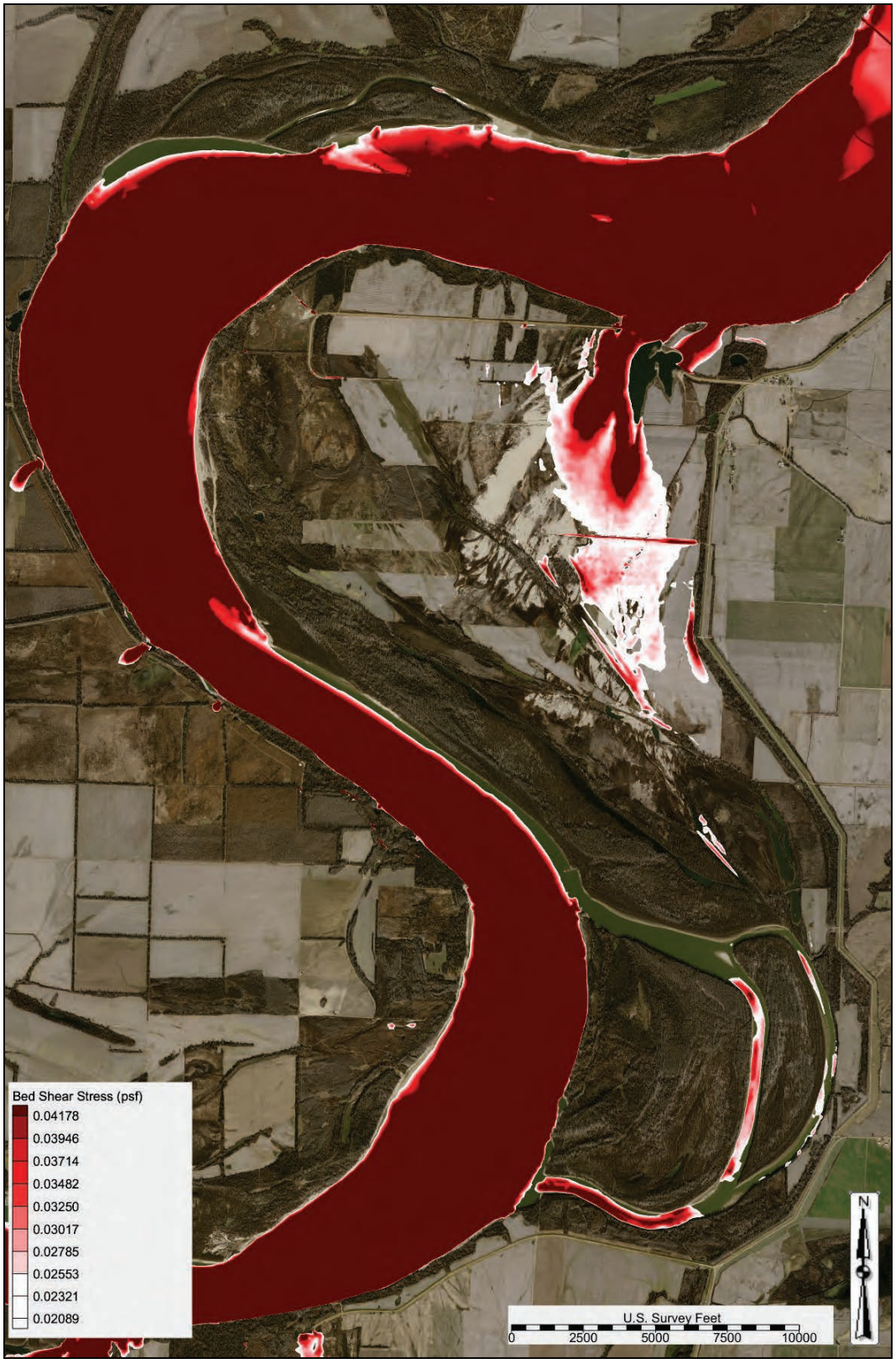


Figure C-164. Alternative 4 shear stress—1,900,000 cfs (study overbank).

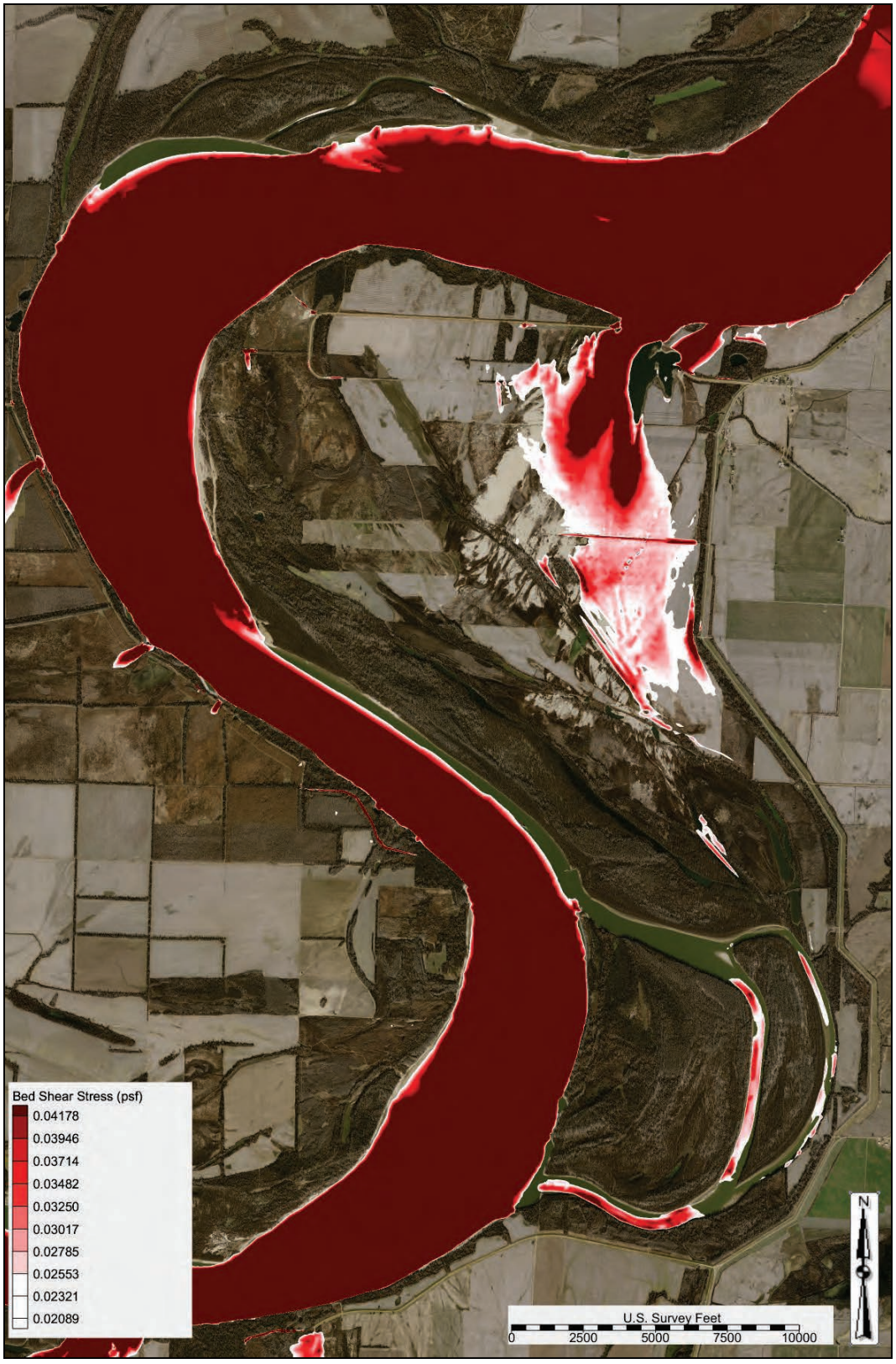
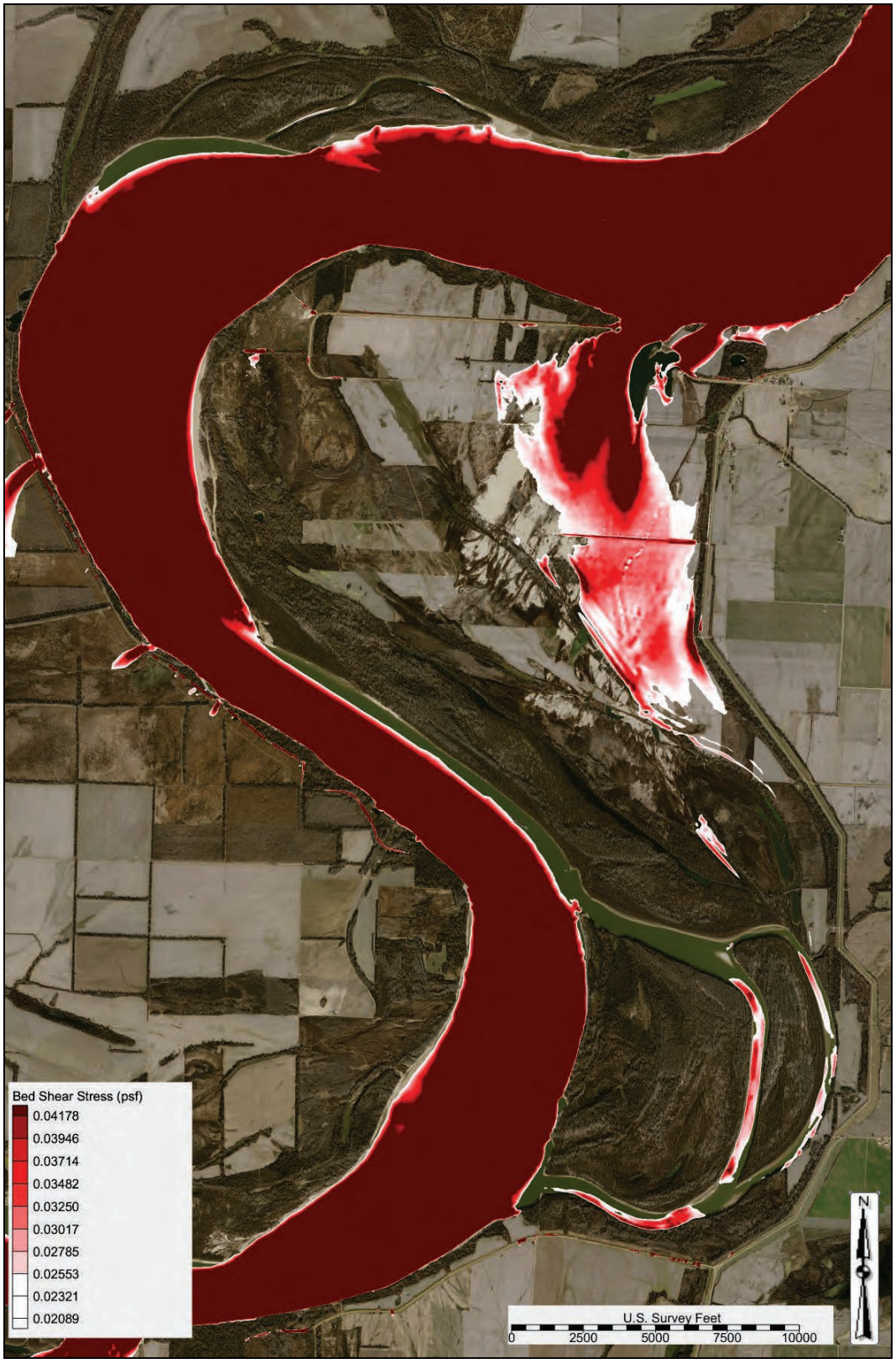


Figure C-165. Alternative 4 shear stress—2,100,000 cfs (study overbank).



Shear stress difference comparison

The modeled shear stress difference plots compared to the base condition output for flows ranging from 900,000 to 2,100,000 cfs are depicted in Figures C-166 through C-172. A positive shear stress difference (+ value and red and orange) indicated an increased shear stress compared to the base condition. A negative shear stress difference (- value and blue) indicated a decreased shear stress compared to the base condition. A zero shear stress difference (zero value and white) indicated that the alternative had no change in shear stress.

Figure C-166. Alternative 4 shear stress difference—900,000 cfs.

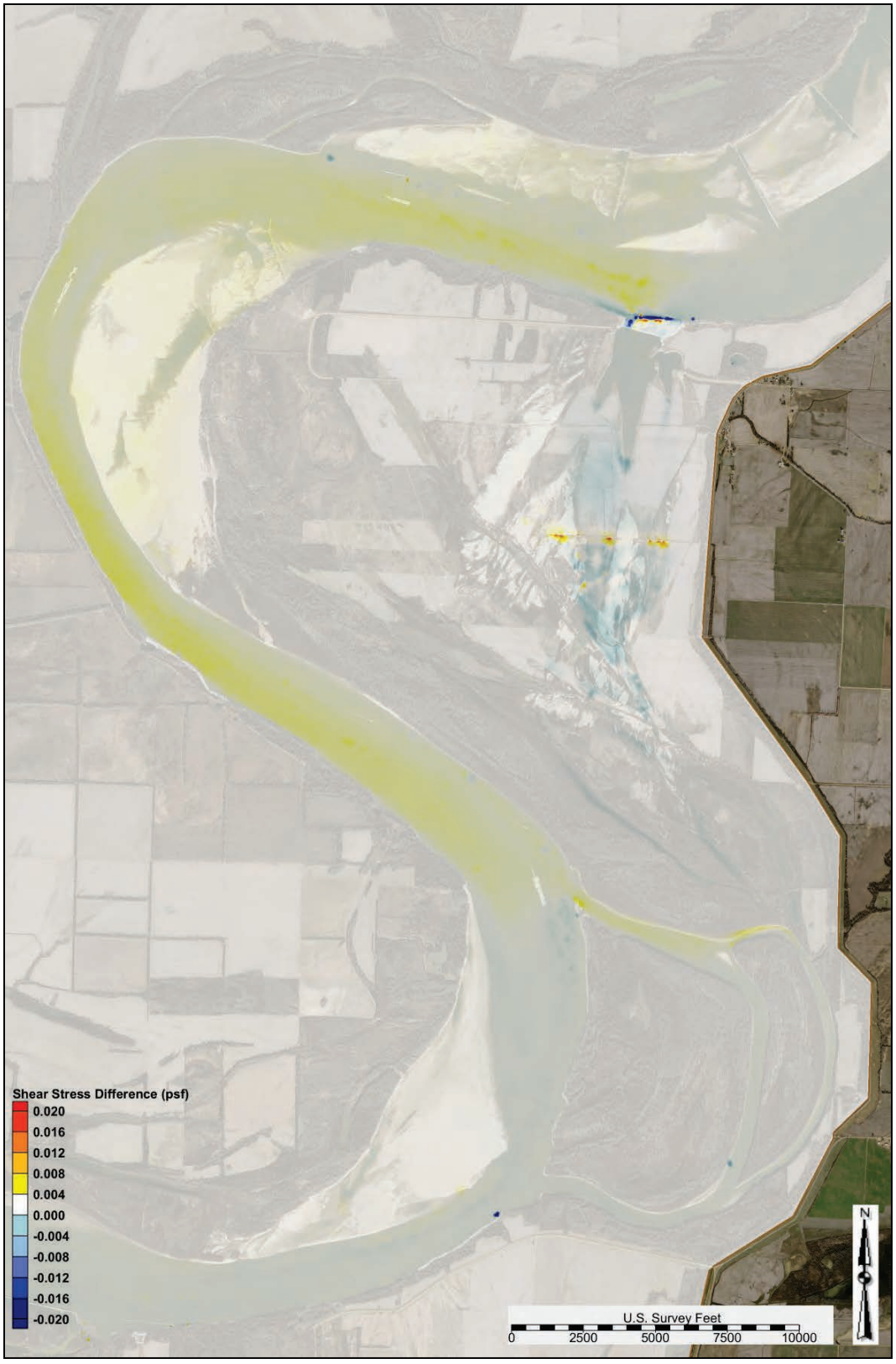


Figure C-167. Alternative 4 shear stress difference—1,100,000 cfs.

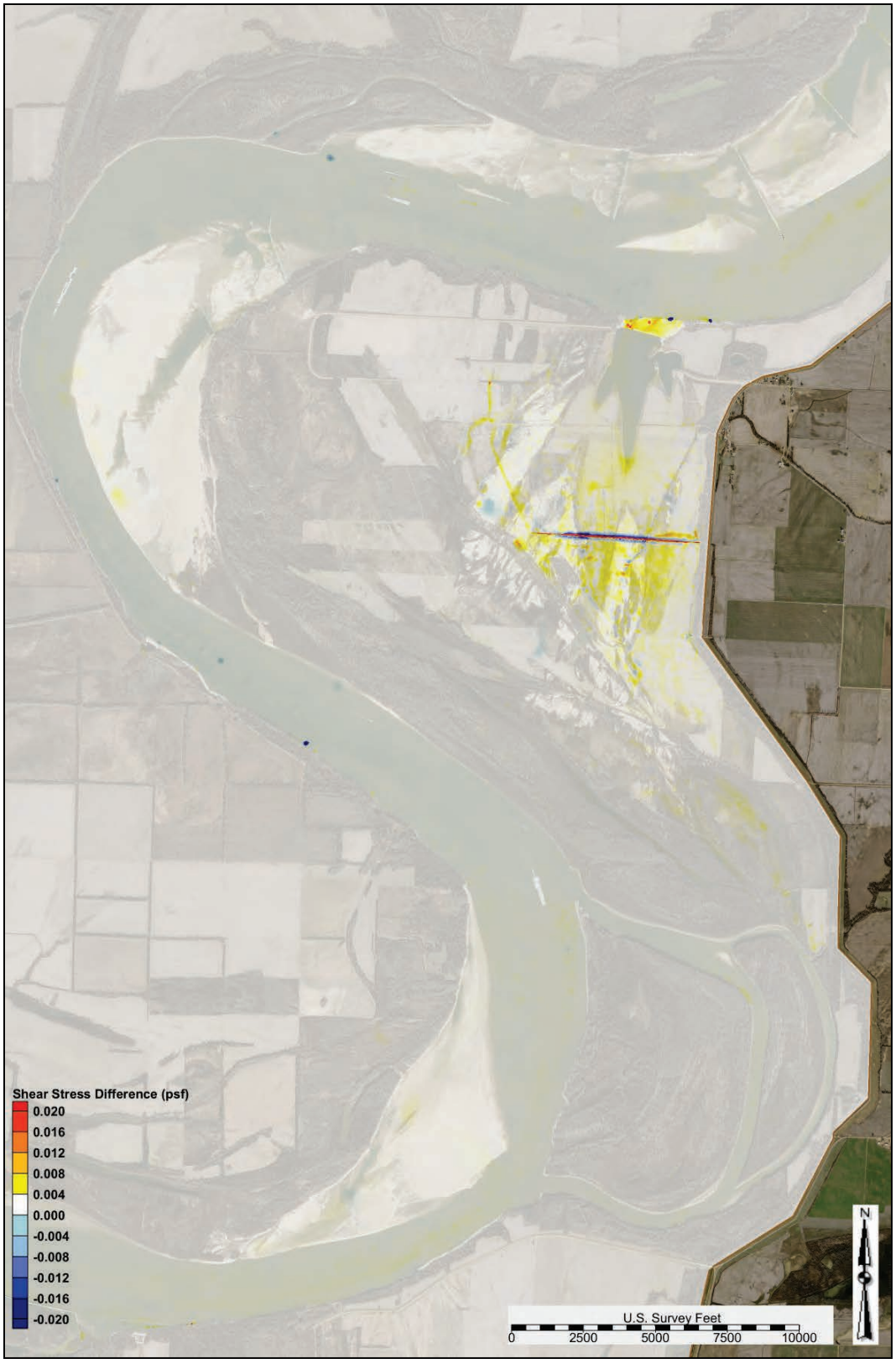


Figure C-168. Alternative 4 shear stress difference—1,300,000 cfs.

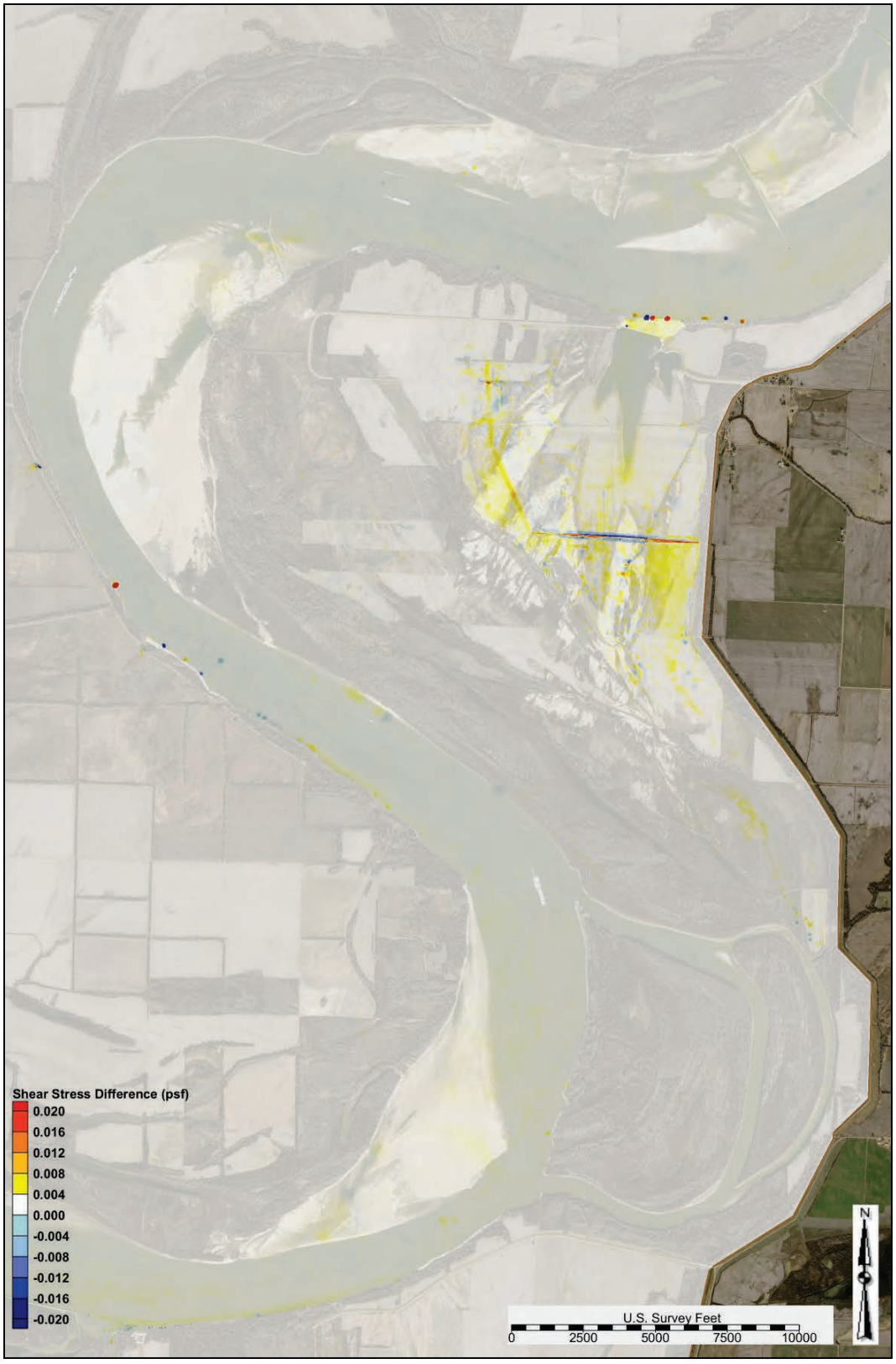


Figure C-169. Alternative 4 shear stress difference—1,500,000 cfs.

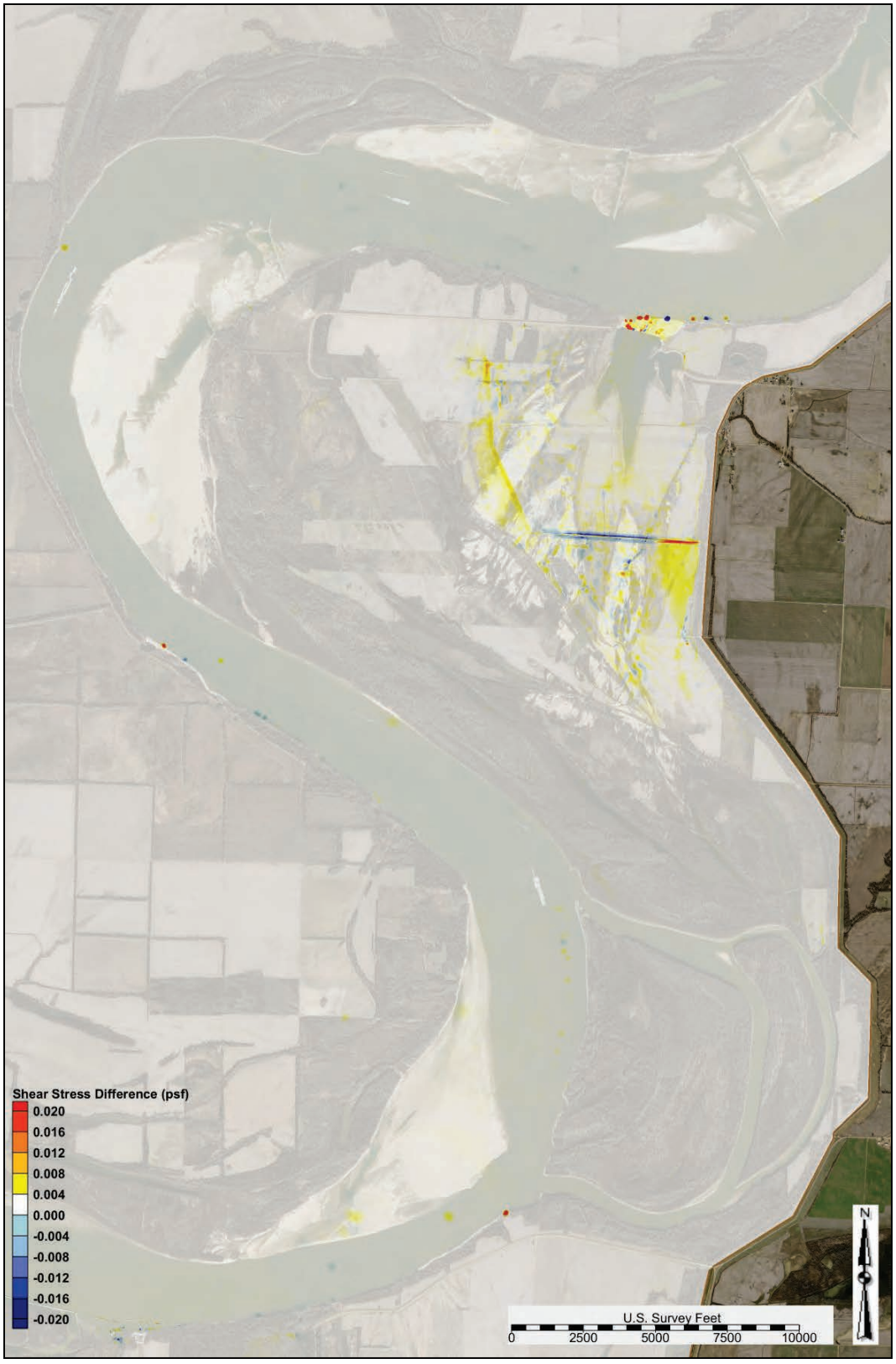


Figure C-170. Alternative 4 shear stress difference—1,700,000 cfs.

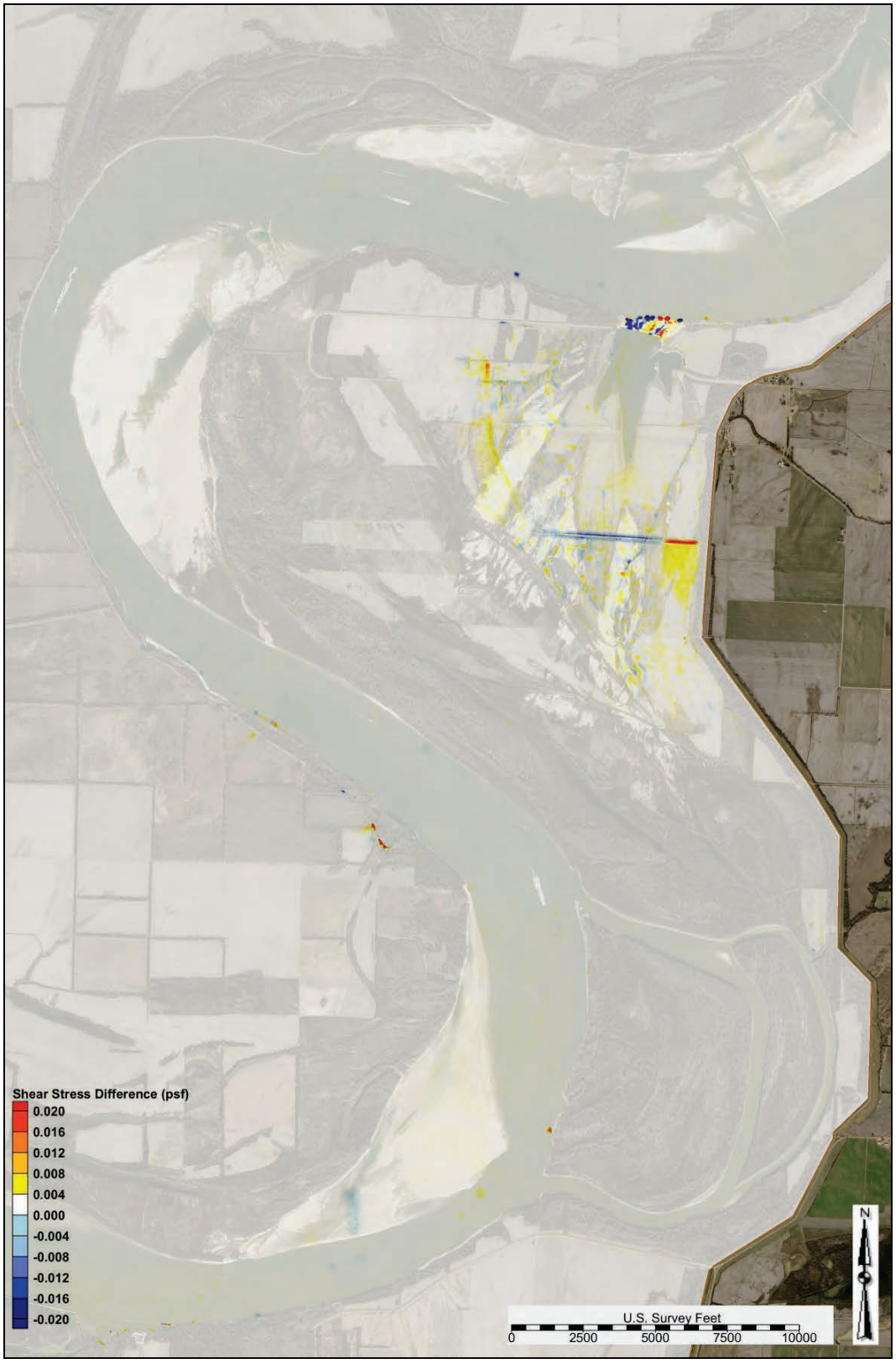


Figure C-171. Alternative 4 shear stress difference—1,900,000 cfs.

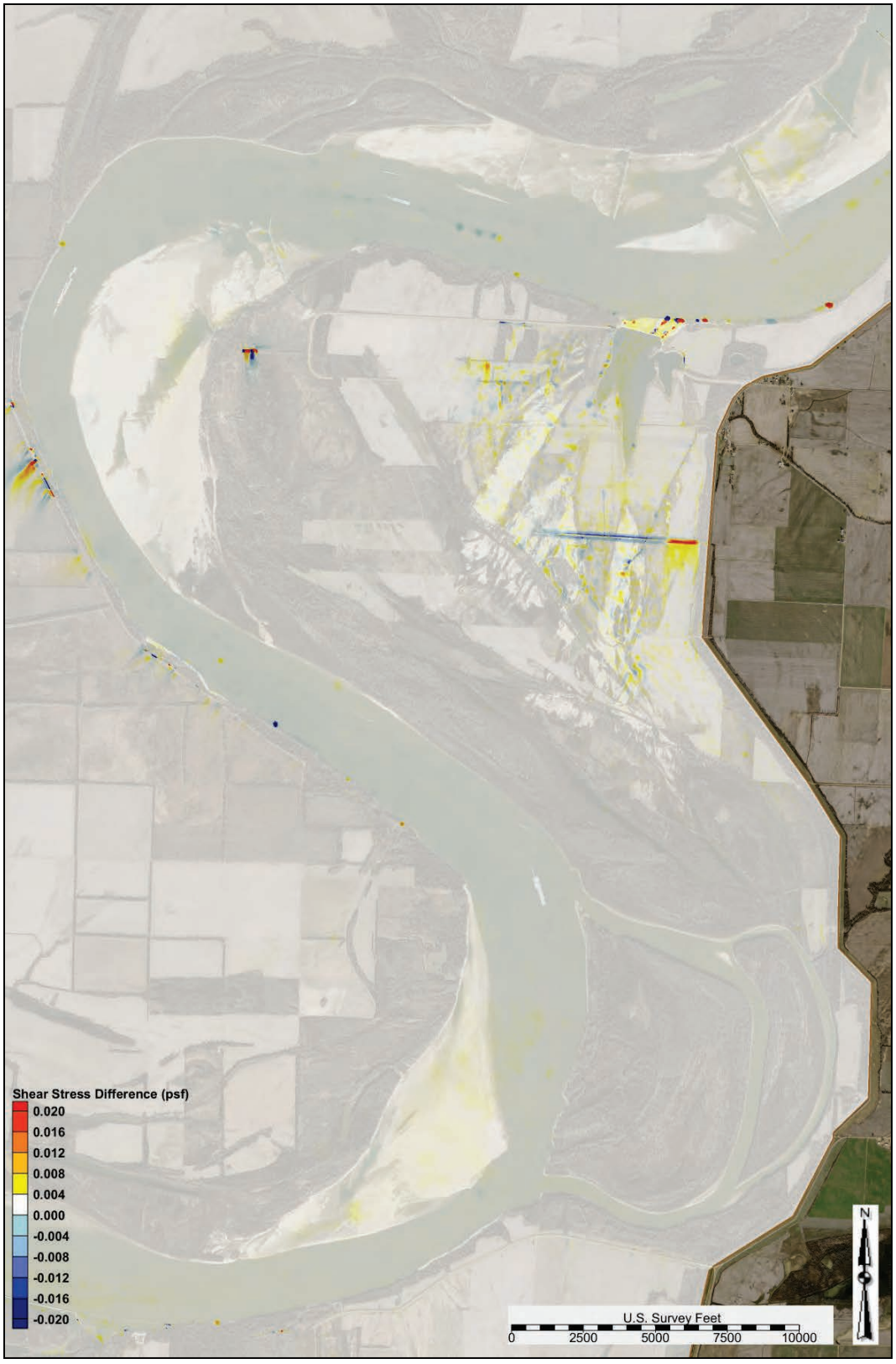
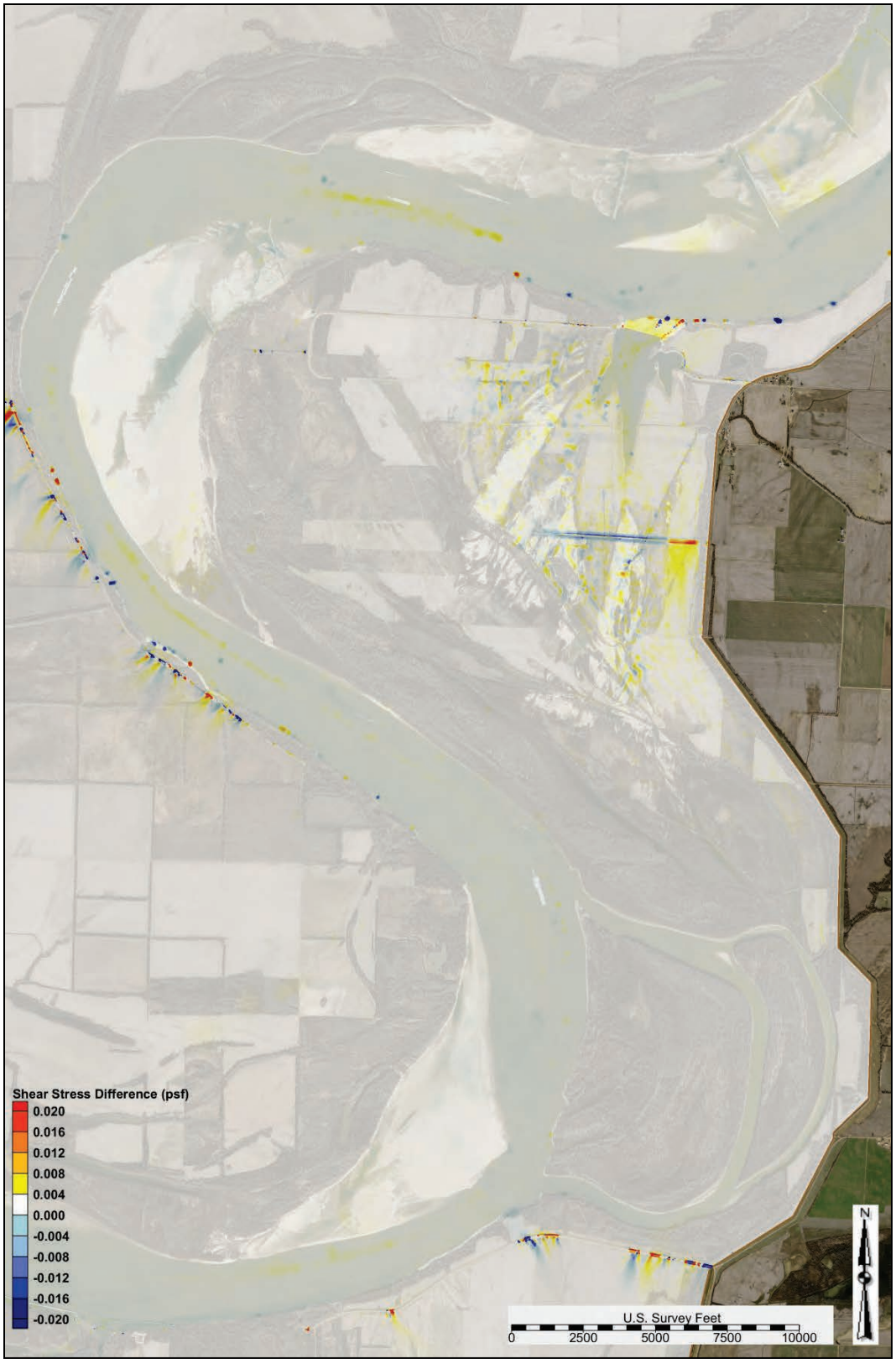


Figure C-172. Alternative 4 shear stress difference—2,100,000 cfs.



WSEL

Figure C-173 depicts the water surface elevation profiles in the study reach for the following flows: 1,100,000 cfs, 1,500,000 cfs, 1,900,000 cfs, and 2,100,000 cfs.

Sediment diversion grain size distribution

Table C-6 lists the sediment diversion grain size distribution for flows ranging from 870,000 cfs to 2,000,000 cfs.

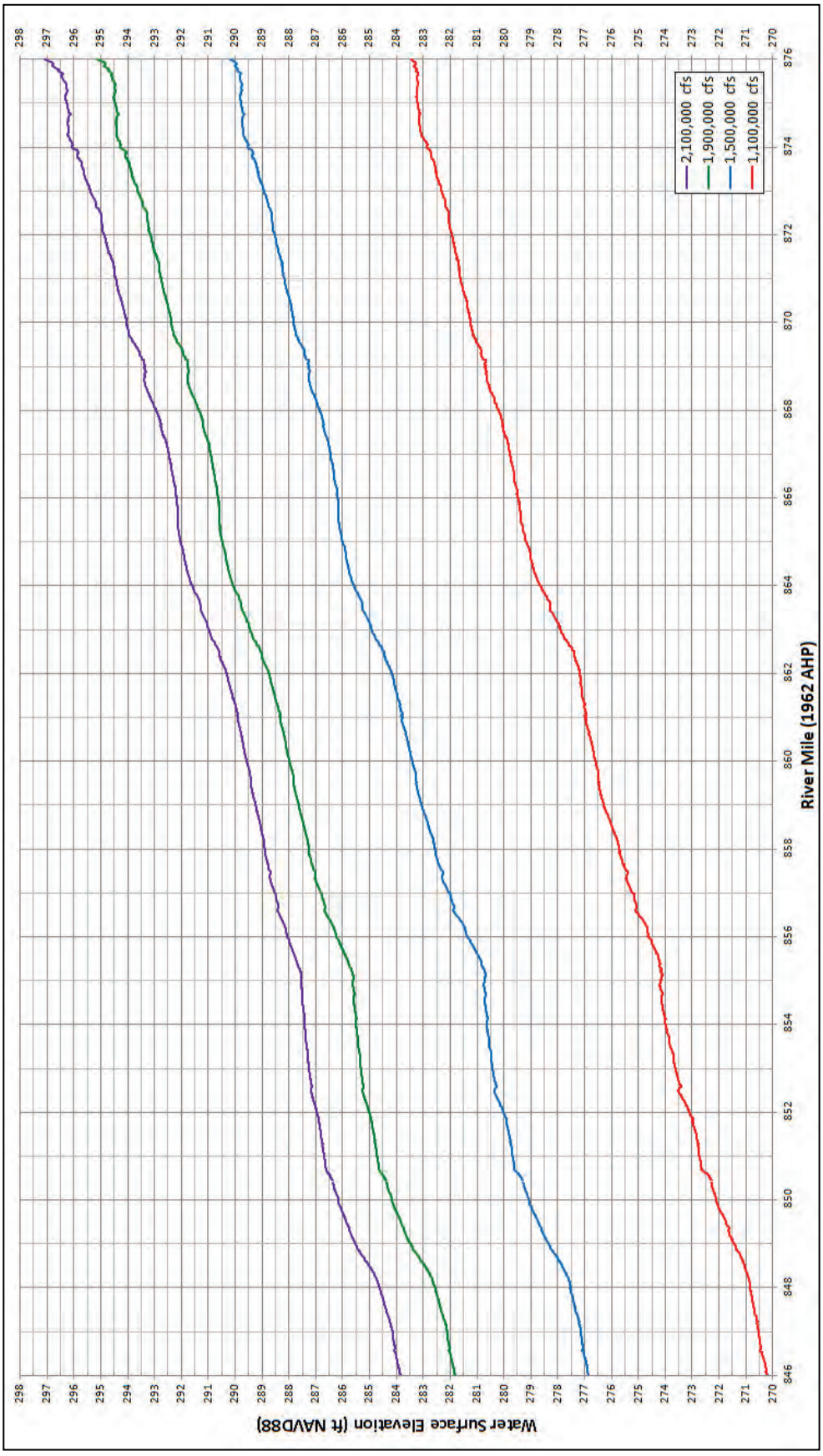


Figure C-173. Alternative 4 WSEL profile.

Table C-6. Alternative 4 diversion grain size distribution.

Main Channel Flow US of Crevasse (cfs)	Total Diversion Load Grain Size Fraction Distribution									
	Coarse Silt	Very Fine Sand	Fine Sand	Medium Sand	Coarse Sand	Very Coarse Sand	Very Fine Pebble	Fine Pebble	Medium Pebble	Coarse Pebble
870,000	0.0000	0.9484	0.0509	0.0007	0.0000	0.0000	0.0000	0.0000	0.0000	0.0000
1,000,000	0.0000	0.4232	0.4303	0.1151	0.0258	0.0057	0.0000	0.0000	0.0000	0.0000
1,100,000	0.0000	0.2171	0.3992	0.2535	0.1083	0.0212	0.0005	0.0001	0.0001	0.0000
1,200,000	0.0002	0.1449	0.3398	0.3140	0.1549	0.0394	0.0050	0.0011	0.0006	0.0001
1,300,000	0.0004	0.1148	0.3001	0.3480	0.1877	0.0419	0.0034	0.0025	0.0011	0.0002
1,400,000	0.0006	0.1074	0.2699	0.3531	0.2110	0.0505	0.0026	0.0031	0.0015	0.0002
1,500,000	0.0013	0.1097	0.2812	0.3585	0.1997	0.0419	0.0027	0.0021	0.0026	0.0003
1,600,000	0.0013	0.0998	0.2794	0.3728	0.1976	0.0402	0.0030	0.0014	0.0041	0.0005
1,700,000	0.0014	0.0933	0.2700	0.3804	0.2043	0.0403	0.0034	0.0012	0.0050	0.0007
1,800,000	0.0009	0.0883	0.2656	0.3883	0.2072	0.0402	0.0038	0.0013	0.0032	0.0011
1,900,000	0.0008	0.0851	0.2620	0.3941	0.2090	0.0396	0.0041	0.0015	0.0023	0.0015
2,000,000	0.0006	0.0799	0.2548	0.4017	0.2130	0.0403	0.0042	0.0015	0.0018	0.0020
2,100,000	0.0006	0.0786	0.2516	0.4039	0.2146	0.0406	0.0045	0.0015	0.0016	0.0024

Alternative 5 output

The following sections contain AdH model output and analysis for Alternative 5.

Shear stress

The modeled shear stress outputs at flows ranging from 900,000 to 2,100,000 cfs for the study overbank are depicted in Figures C-174 through C-180.

Figure C-174. Alternative 5 shear stress—900,000 cfs (study overbank).



Figure C-175. Alternative 5 shear stress—1,100,000 cfs (study overbank).

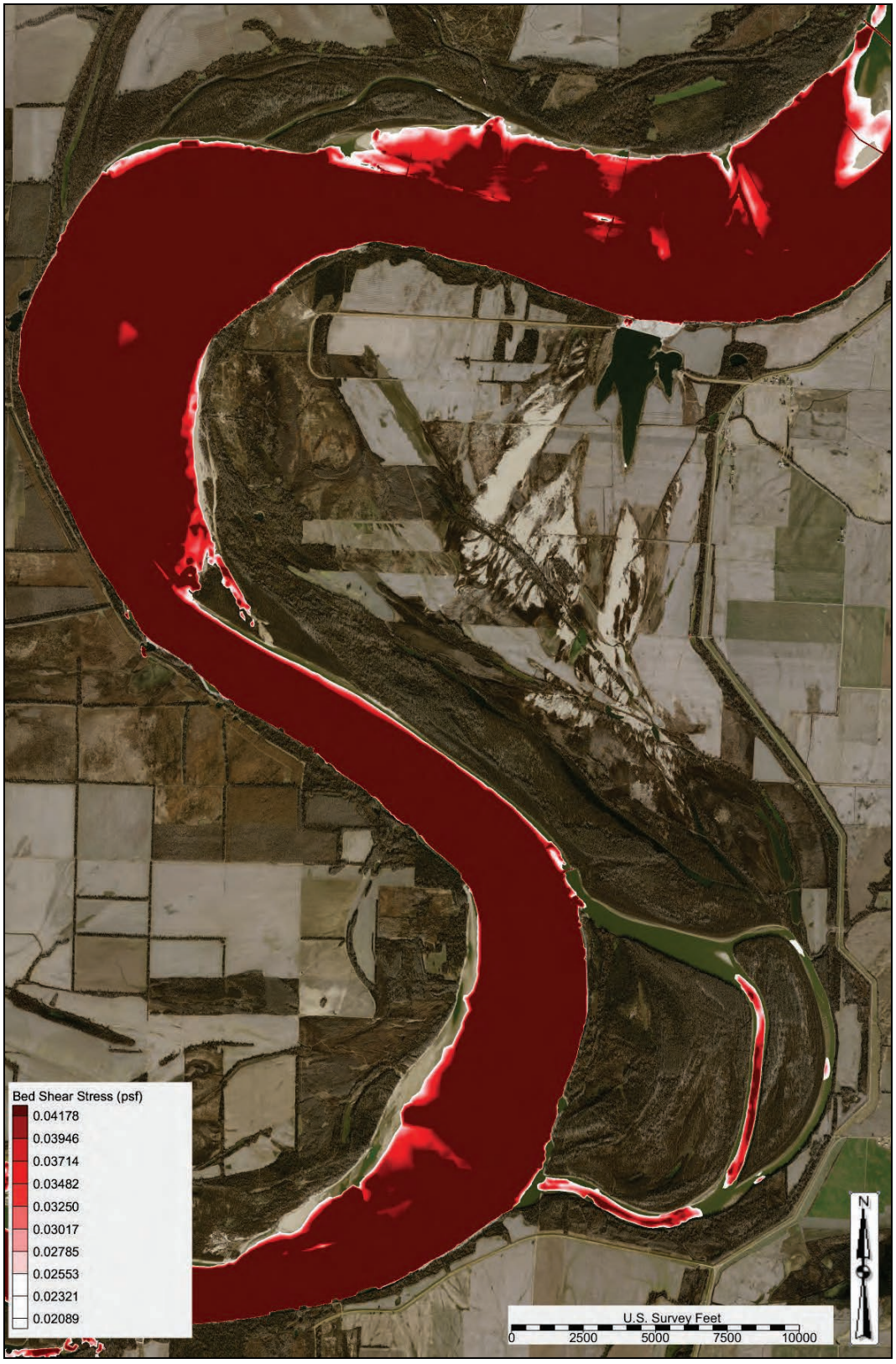


Figure C-176. Alternative 5 shear stress—1,300,000 cfs (study overbank).



Figure C-177. Alternative 5 shear stress—1,500,000 cfs (study overbank).

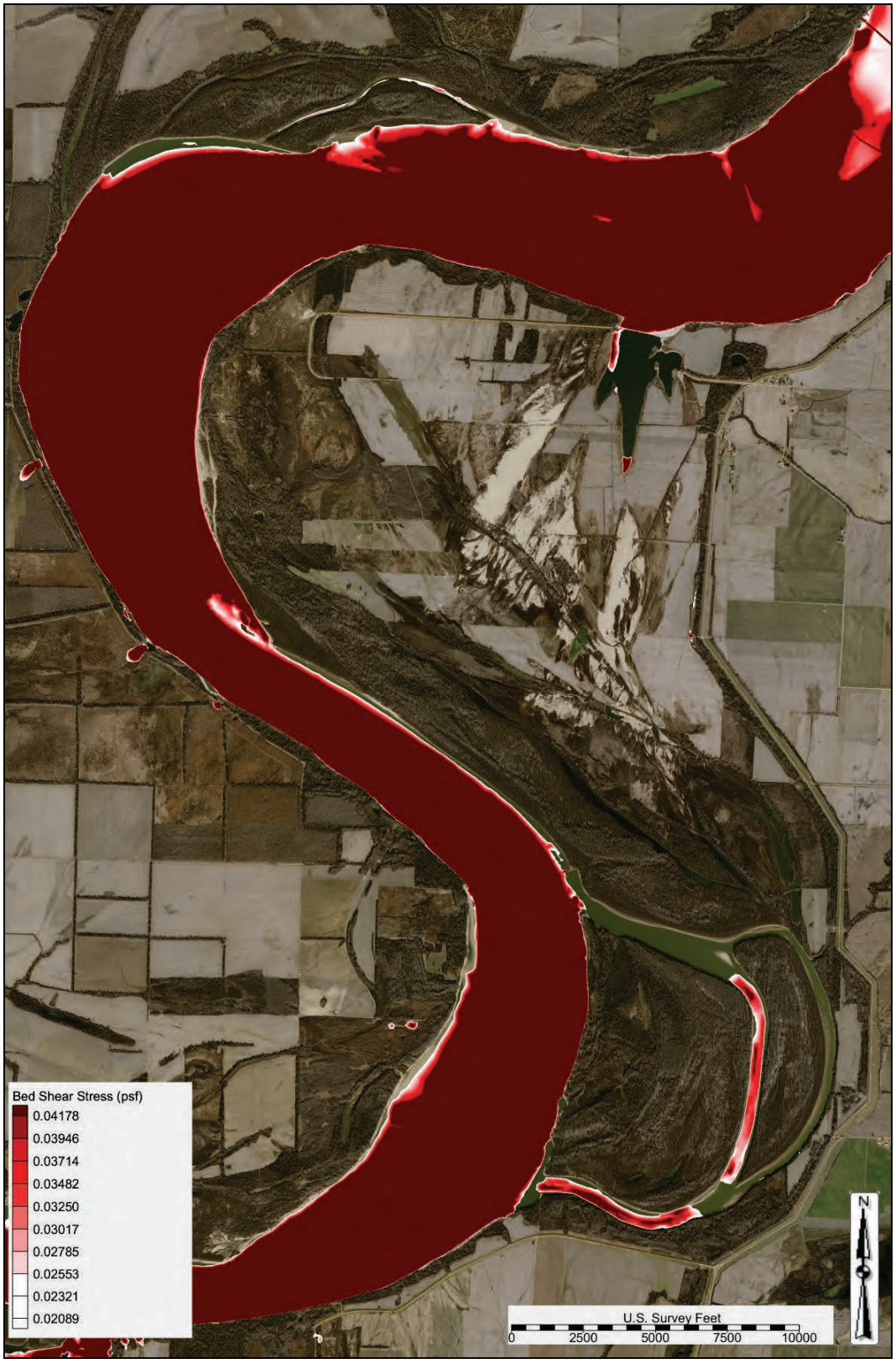


Figure C-178. Alternative 5 shear stress—1,700,000 cfs (study overbank).



Figure C-179. Alternative 5 shear stress—1,900,000 cfs (study overbank).



Figure C-180. Alternative 5 shear stress—2,100,000 cfs (study overbank).



Shear stress difference comparison

The modeled shear stress difference plots compared to the base condition output for flows ranging from 900,000 to 2,100,000 cfs are depicted in Figures C-181 through C-187. A positive shear stress difference (+ value and red and orange) indicated an increased shear stress compared to the base condition. A negative shear stress difference (- value and blue) indicated a decreased shear stress compared to the base condition. A zero shear stress difference (zero value and white) indicated that the alternative had no change in shear stress.

Figure C-181. Alternative 5 shear stress difference—900,000 cfs.

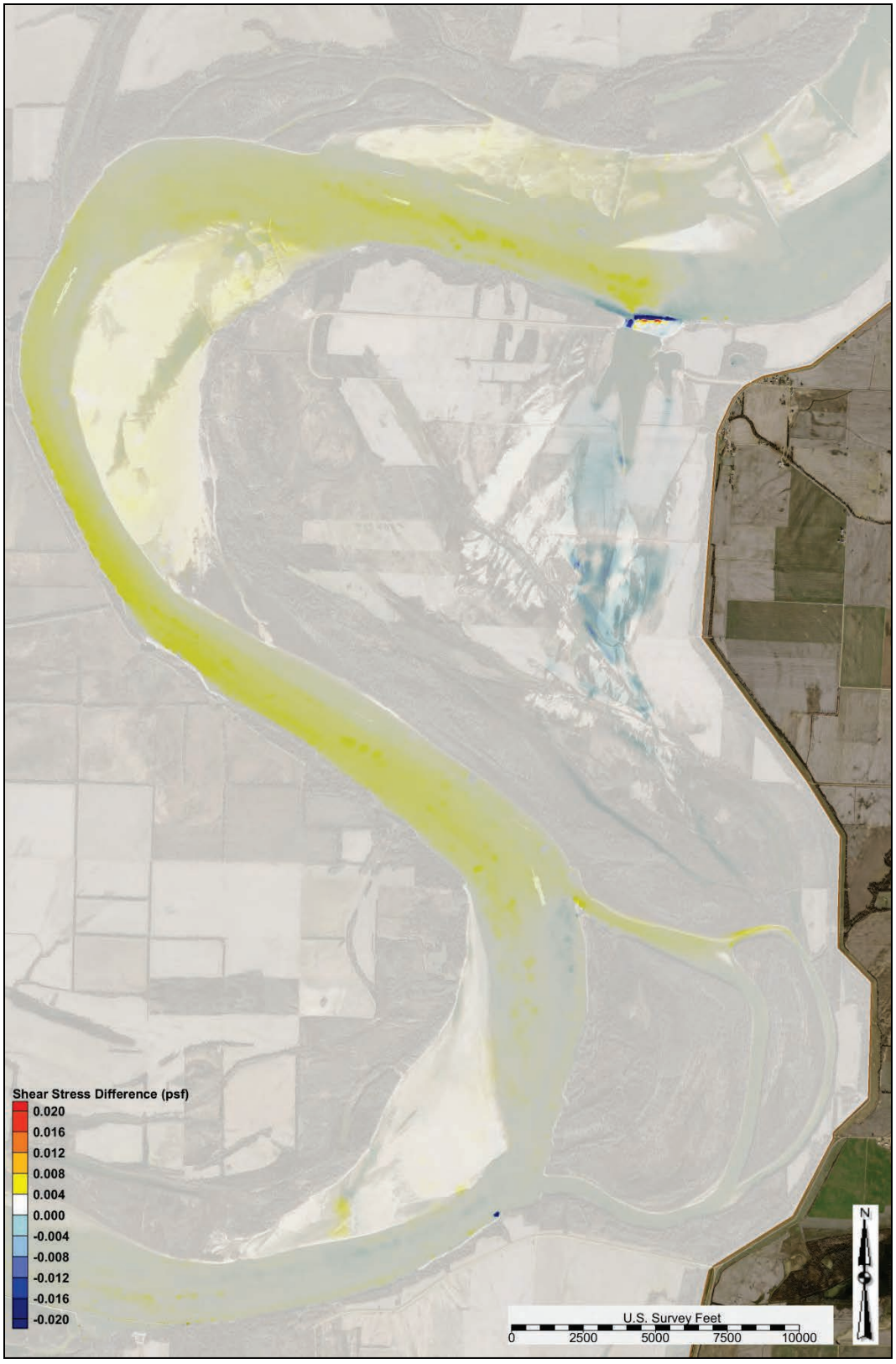


Figure C-182. Alternative 5 shear stress difference—1,100,000 cfs.

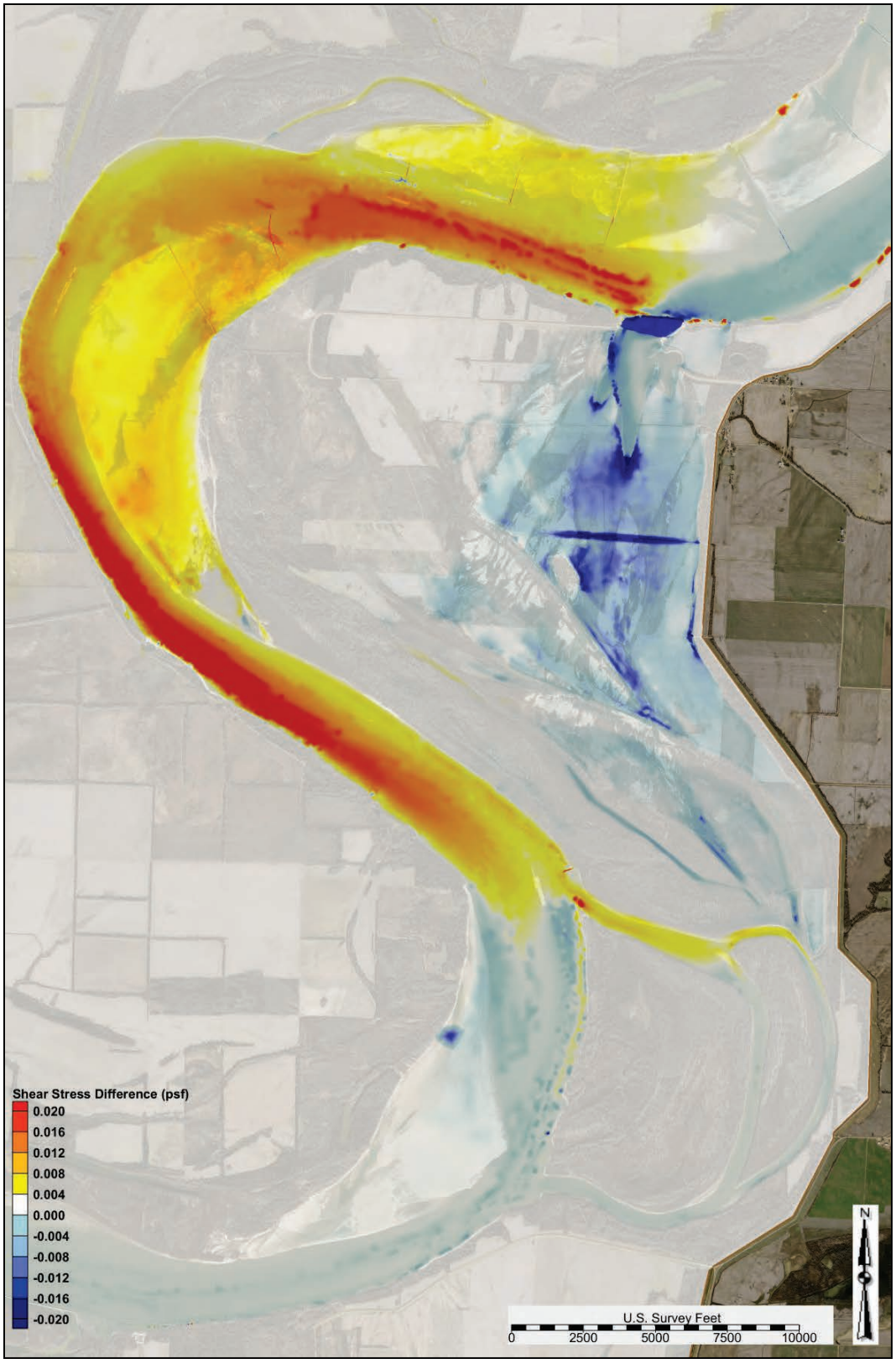


Figure C-183. Alternative 5 shear stress difference—1,300,000 cfs.

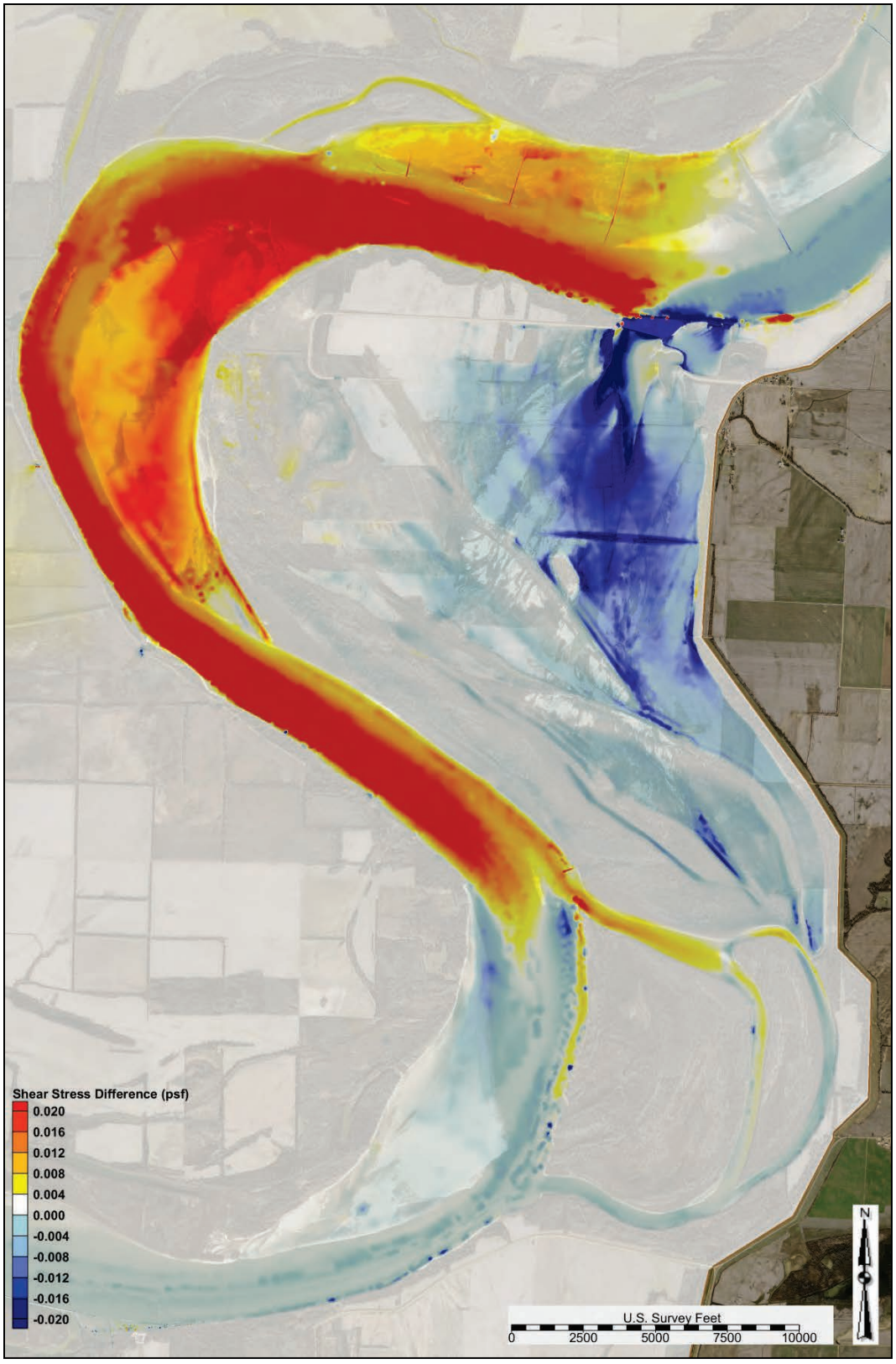


Figure C-184. Alternative 5 shear stress difference—1,500,000 cfs.

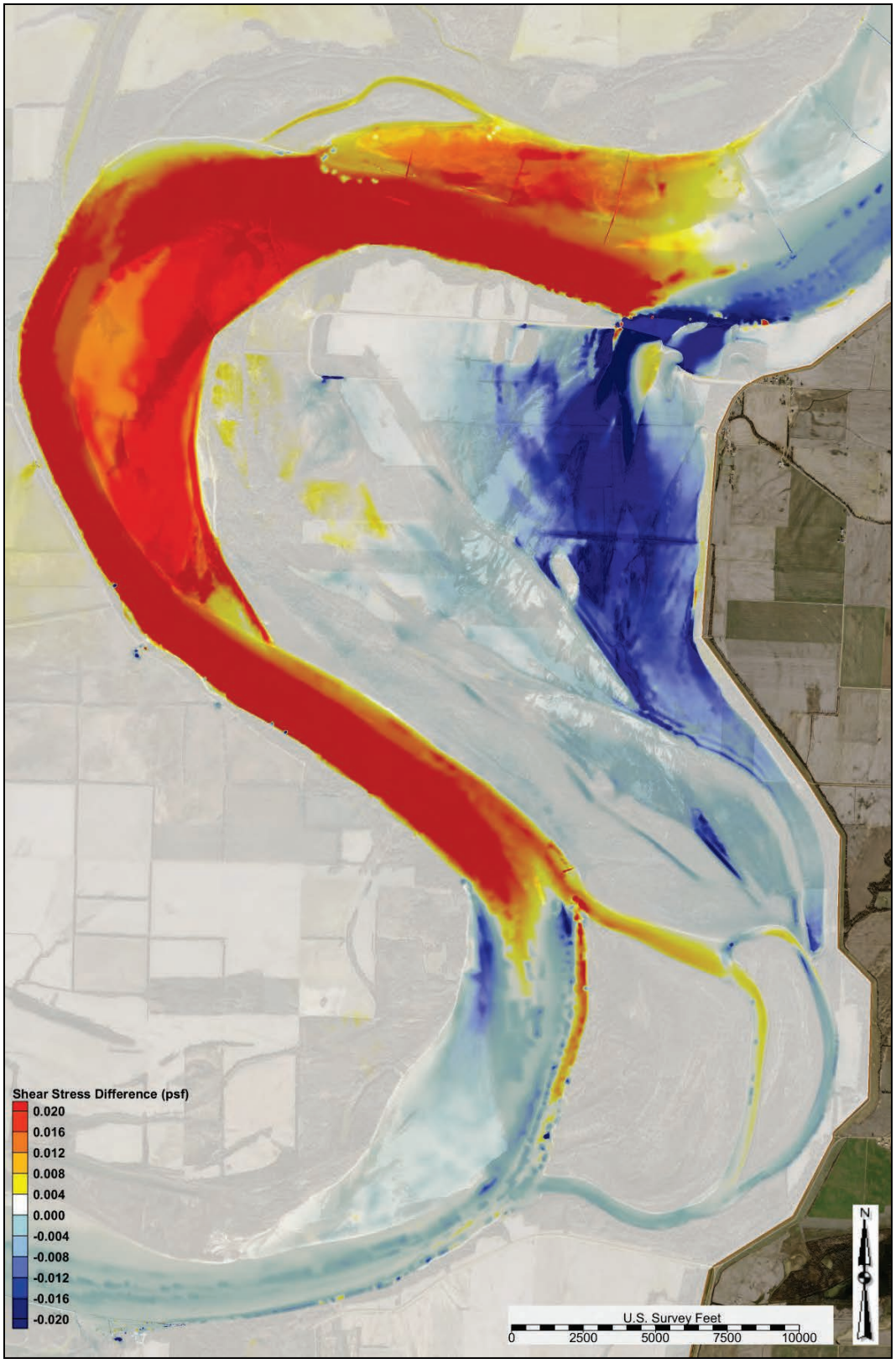


Figure C-185. Alternative 5 shear stress difference—1,700,000 cfs.

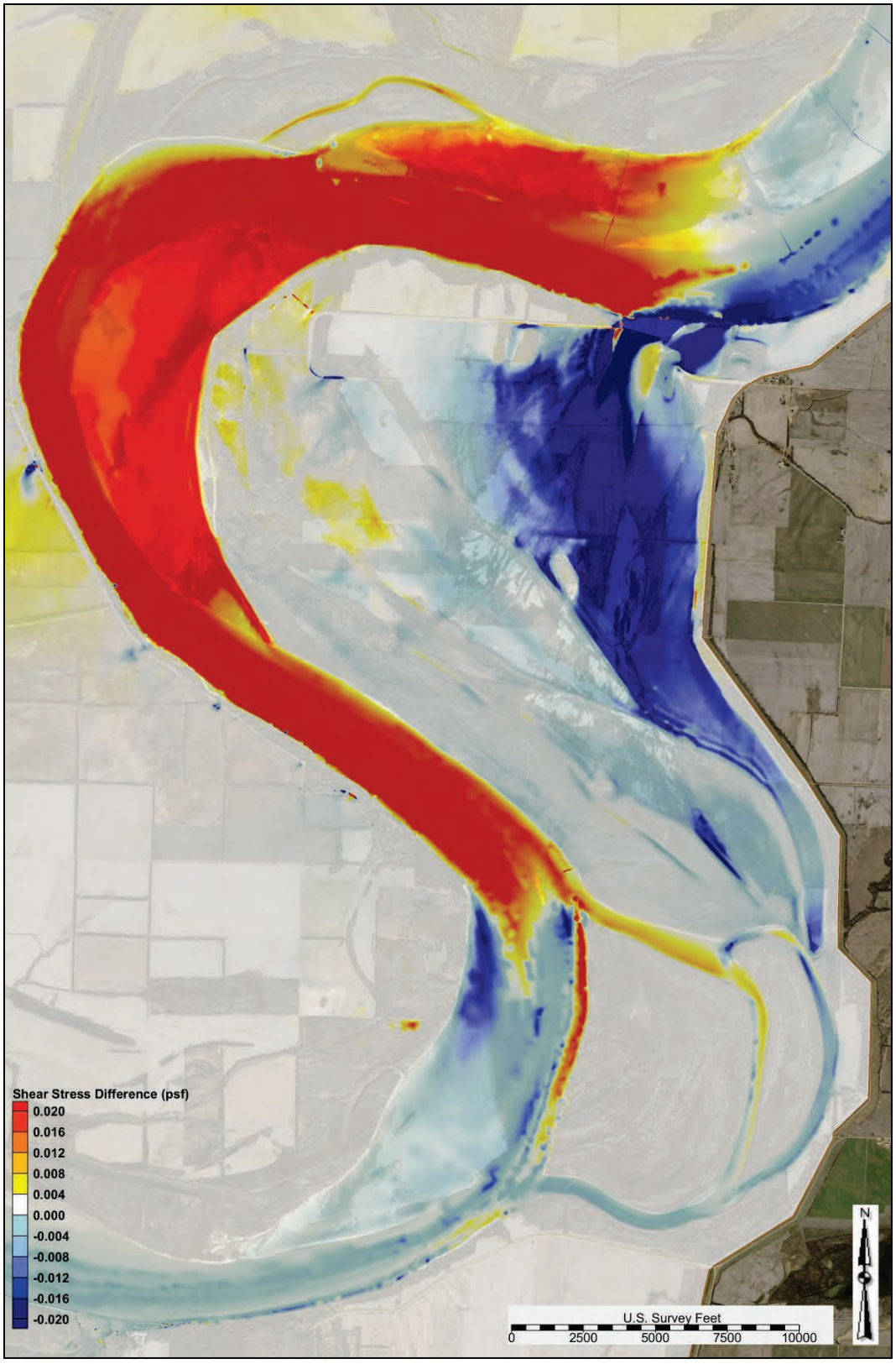


Figure C-186. Alternative 5 shear stress difference—1,900,000 cfs.

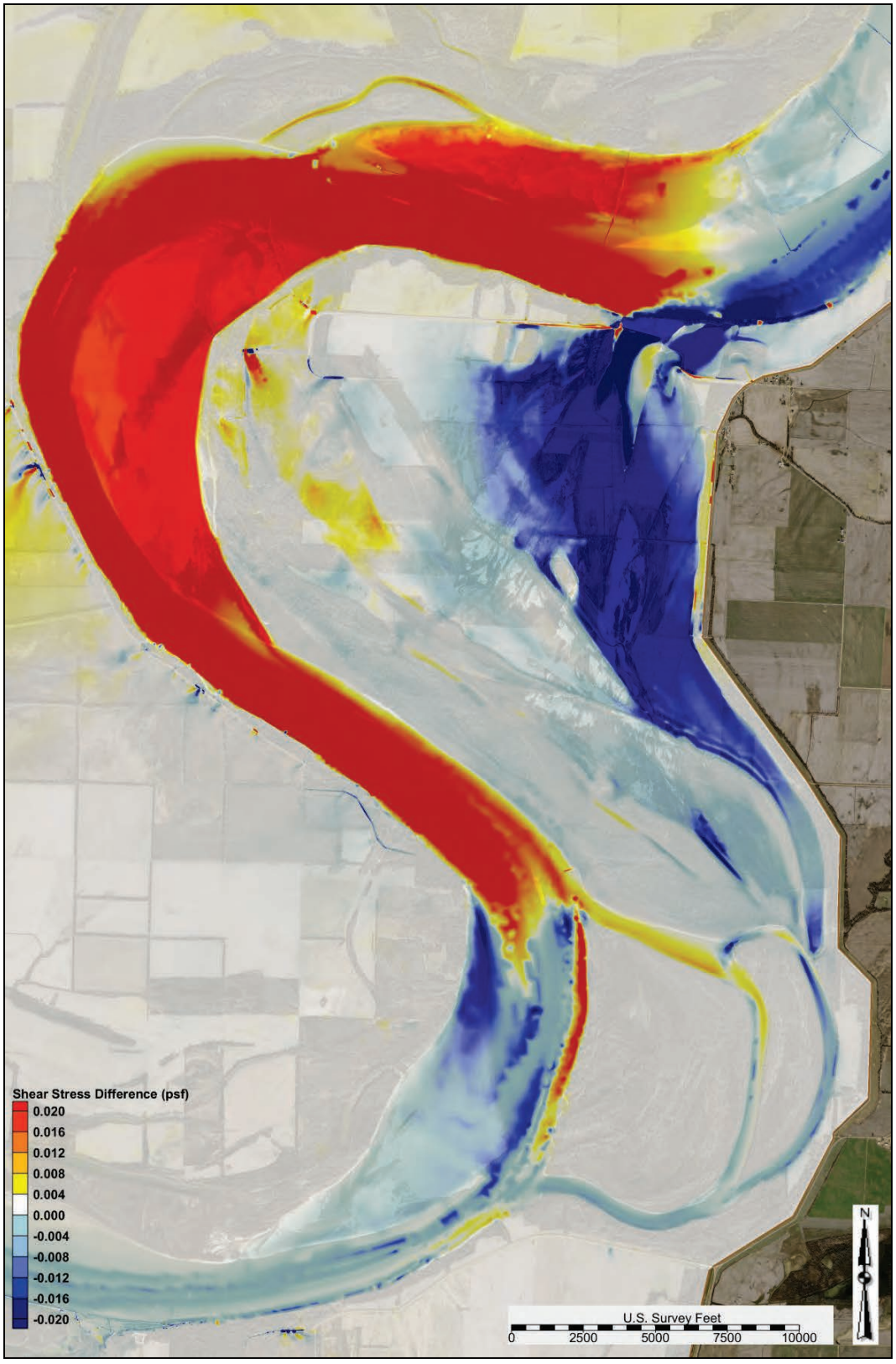
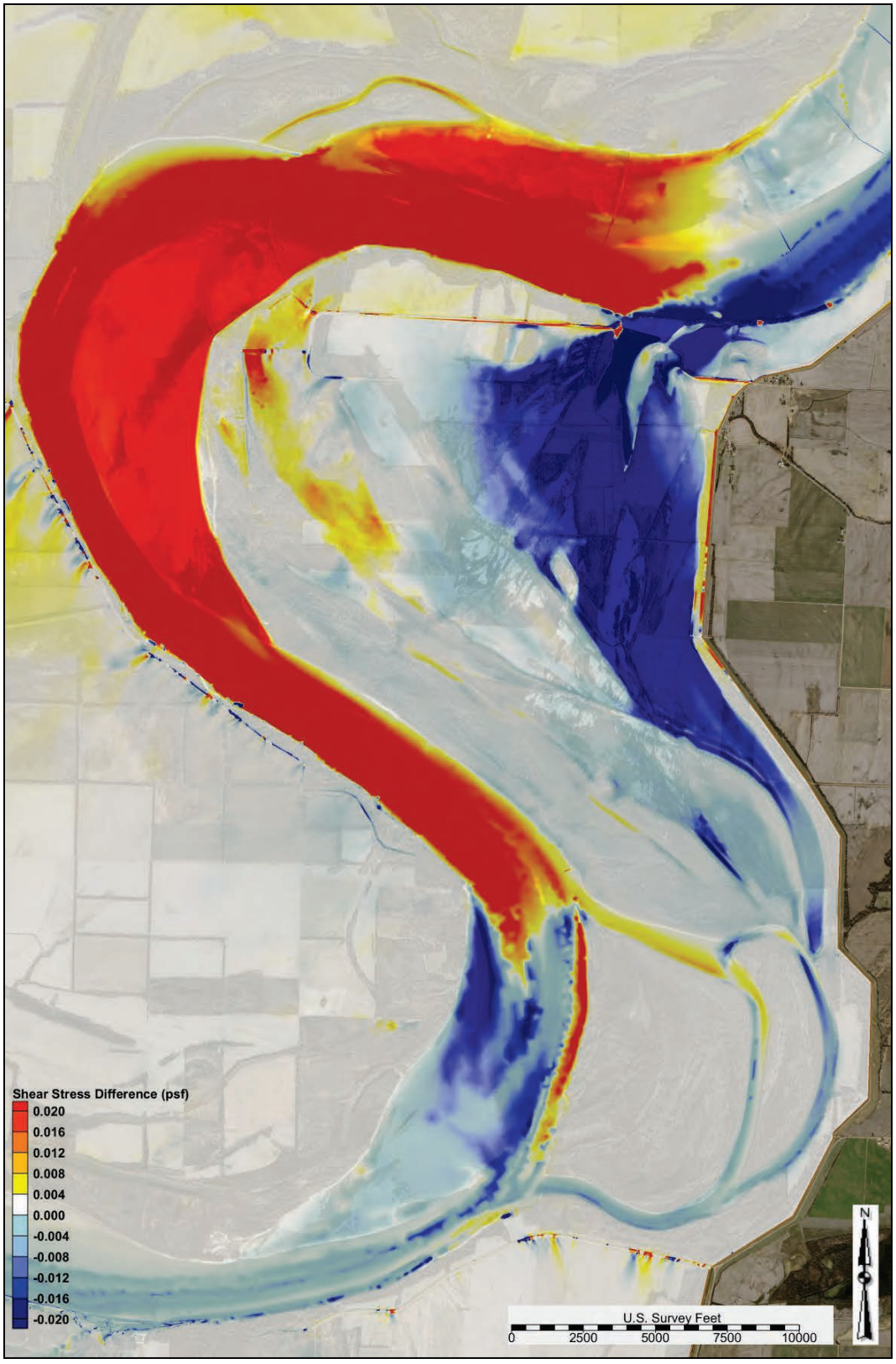


Figure C-187. Alternative 5 shear stress difference—2,100,000 cfs.



WSEL

Figure C-188 depicts the water surface elevation profiles in the study reach for the following flows: 1,100,000 cfs, 1,500,000 cfs, 1,900,000 cfs, and 2,100,000 cfs.

Sediment diversion grain size distribution

Table C-7 lists the sediment diversion grain size distribution for flows ranging from 870,000 cfs to 2,000,000 cfs.

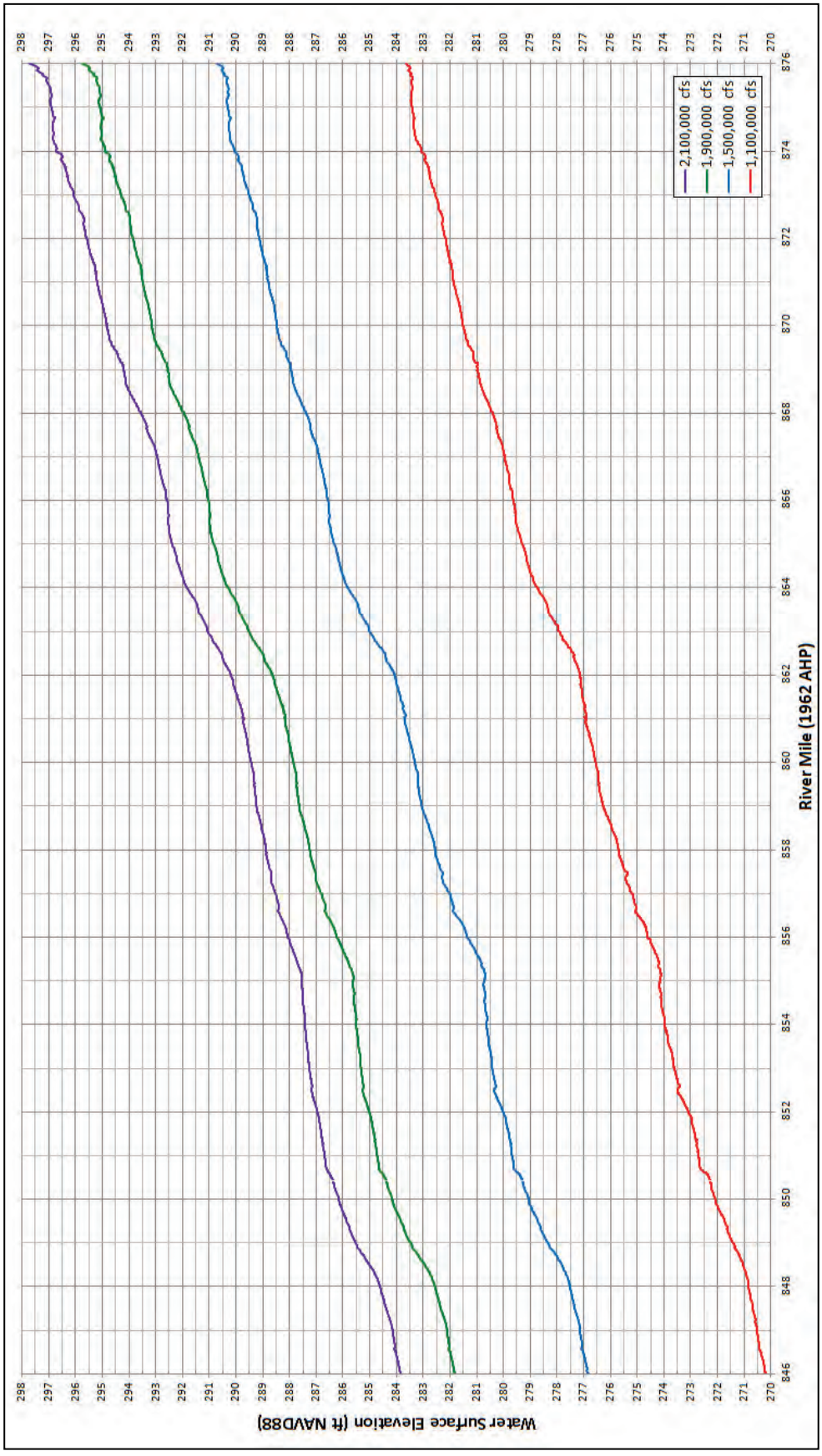


Figure C-188. Alternative 5 WSEL profile.

Table C-7. Alternative 5 diversion grain size distribution.

Main Channel Flow US of Crevasse (cfs)	Total Diversion Load Grain Size Fraction Distribution									
	Coarse Silt	Very Fine Sand	Fine Sand	Medium Sand	Coarse Sand	Very Coarse Sand	Very Fine Pebble	Fine Pebble	Medium Pebble	Coarse Pebble
870,000	0.0000	0.9863	0.0137	0.0000	0.0000	0.0000	0.0000	0.0000	0.0000	0.0000
1,000,000	0.0000	0.8533	0.1402	0.0047	0.0011	0.0008	0.0000	0.0000	0.0000	0.0000
1,100,000	0.0000	0.6640	0.2982	0.0335	0.0036	0.0007	0.0000	0.0000	0.0000	0.0000
1,200,000	0.0000	0.4405	0.4171	0.1120	0.0245	0.0059	0.0000	0.0000	0.0000	0.0000
1,300,000	0.0000	0.2547	0.4757	0.2061	0.0536	0.0099	0.0001	0.0000	0.0000	0.0000
1,400,000	0.0000	0.1834	0.4162	0.2720	0.1042	0.0234	0.0006	0.0001	0.0000	0.0000
1,500,000	0.0000	0.1438	0.3607	0.3181	0.1393	0.0338	0.0034	0.0006	0.0002	0.0000
1,600,000	0.0000	0.1333	0.3315	0.3254	0.1638	0.0336	0.0101	0.0017	0.0006	0.0001
1,700,000	0.0000	0.1230	0.3161	0.3395	0.1731	0.0363	0.0068	0.0038	0.0013	0.0002
1,800,000	0.0000	0.1173	0.3061	0.3460	0.1782	0.0378	0.0059	0.0066	0.0021	0.0002
1,900,000	0.0000	0.1138	0.2969	0.3527	0.1810	0.0386	0.0053	0.0082	0.0032	0.0003
2,000,000	0.0000	0.1034	0.2693	0.3566	0.2077	0.0471	0.0057	0.0057	0.0041	0.0004
2,100,000	0.0000	0.1110	0.3030	0.3818	0.1443	0.0325	0.0089	0.0084	0.0091	0.0010

Alternative 6 output

The following sections contain AdH model output and analysis for Alternative 6.

Shear stress

The modeled shear stress outputs at flows ranging from 900,000 to 2,100,000 cfs for the study overbank are depicted in Figures C-189 through C-195.

Figure C-189. Alternative 6 shear stress—900,000 cfs (study overbank).



Figure C-190. Alternative 6 shear stress—1,100,000 cfs (study overbank).

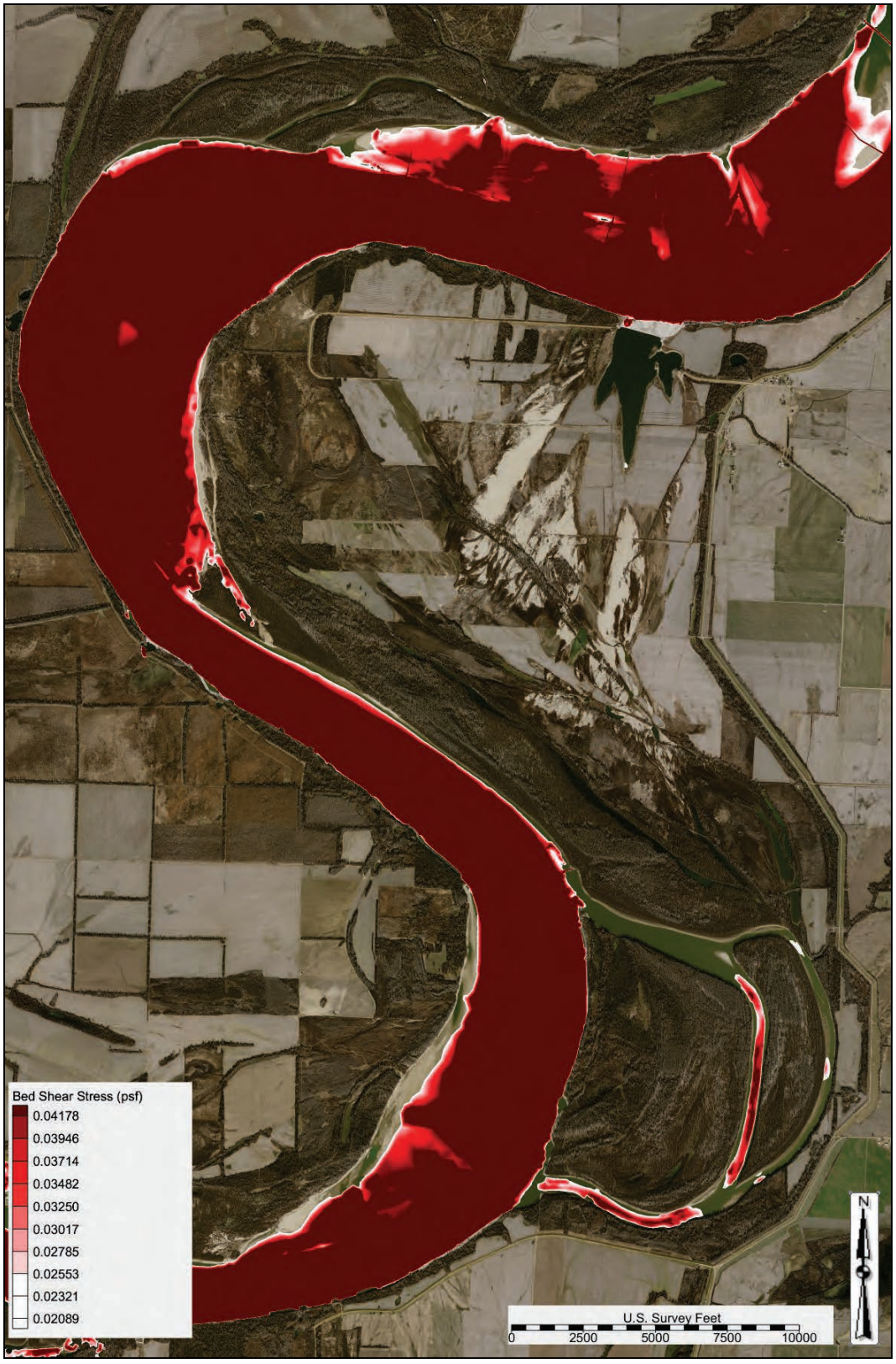


Figure C-191. Alternative 6 shear stress—1,300,000 cfs (study overbank).



Figure C-192. Alternative 6 shear stress—1,500,000 cfs (study overbank).

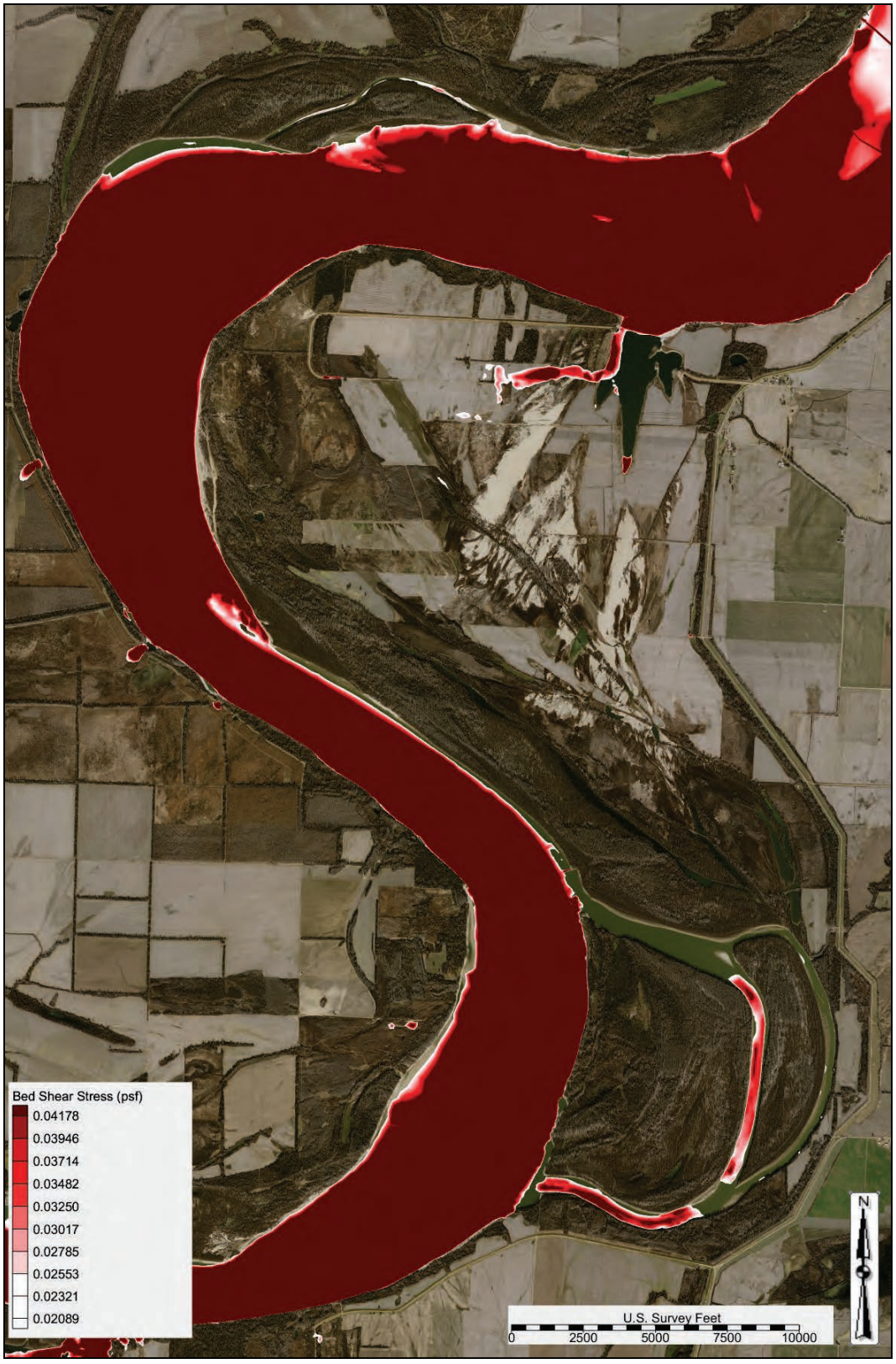


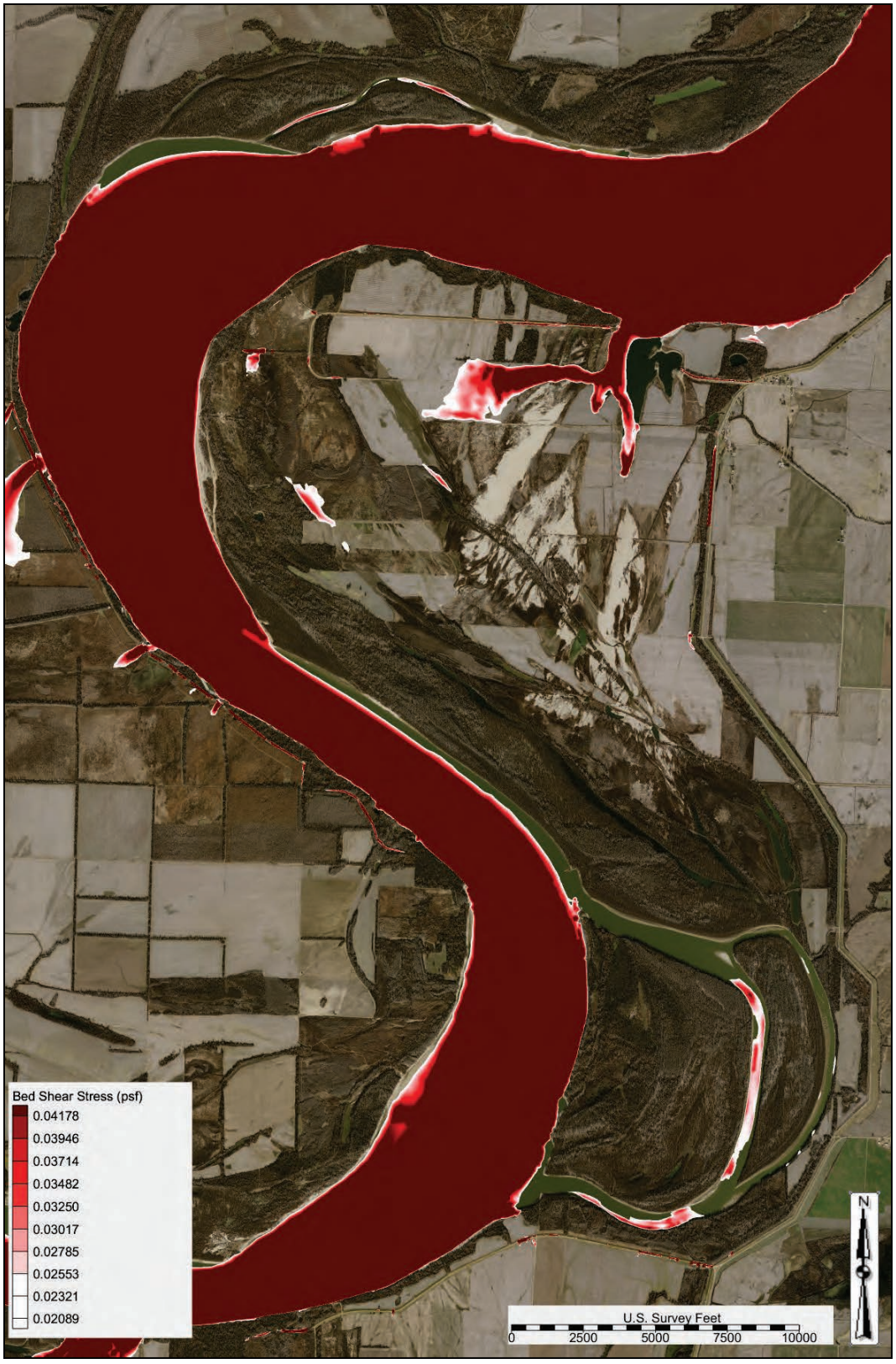
Figure C-193. Alternative 6 shear stress—1,700,000 cfs (study overbank).



Figure C-194. Alternative 6 shear stress—1,900,000 cfs (study overbank).



Figure C-195. Alternative 6 shear stress—2,100,000 cfs (study overbank).



Shear stress difference comparison

The modeled shear stress difference plots compared to the base condition output for flows ranging from 900,000 to 2,100,000 cfs are depicted in Figures C-196 through C-202. A positive shear stress difference (+ value and red and orange) indicated an increased shear stress compared to the base condition. A negative shear stress difference (- value and blue) indicated a decreased shear stress compared to the base condition. A zero shear stress difference (zero value and white) indicated that the alternative had no change in shear stress.

Figure C-196. Alternative 6 shear stress difference—900,000 cfs.

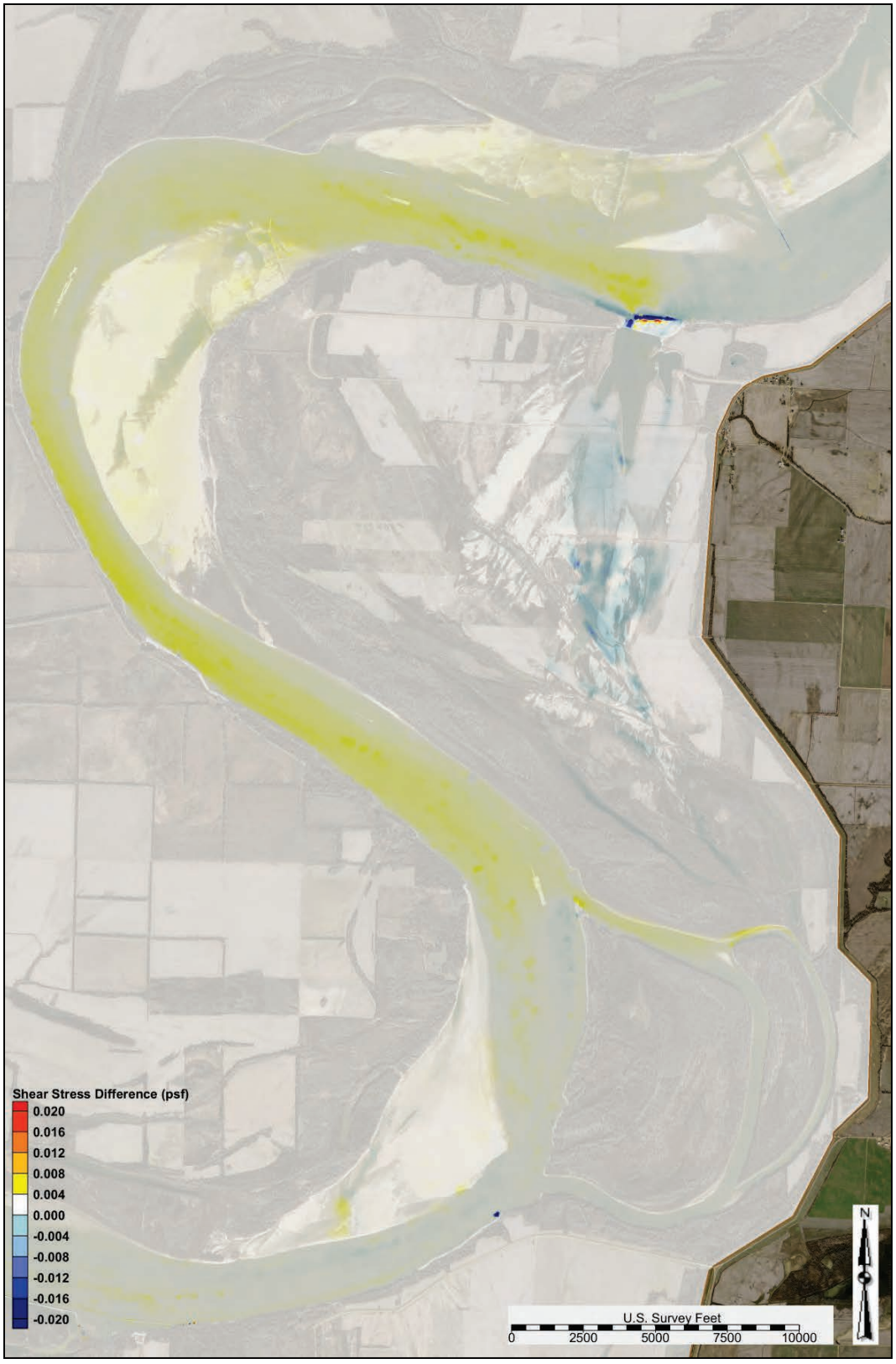


Figure C-197. Alternative 6 shear stress difference—1,100,000 cfs.

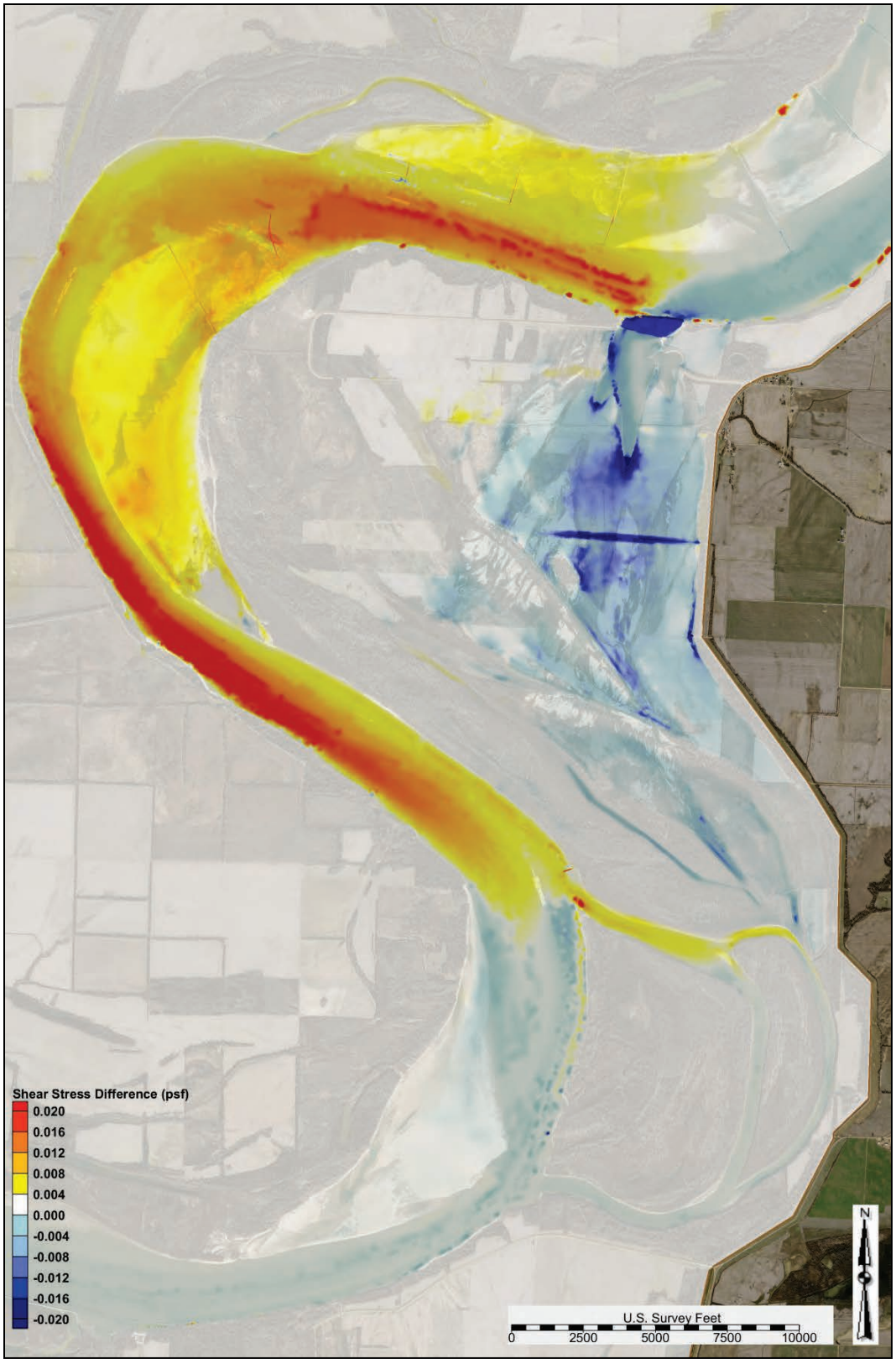


Figure C-198. Alternative 6 shear stress difference—1,300,000 cfs.

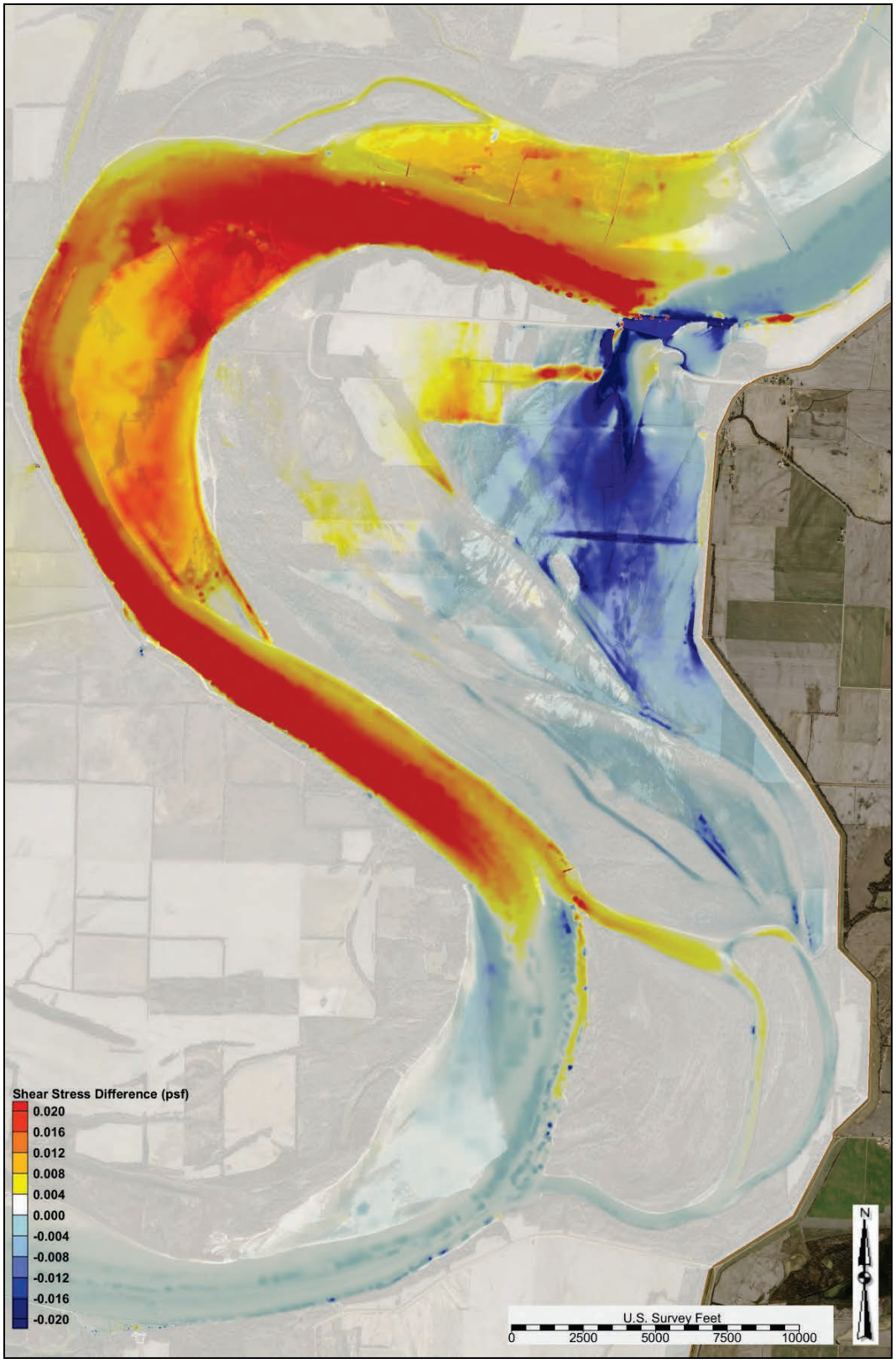


Figure C-199. Alternative 6 shear stress difference—1,500,000 cfs.

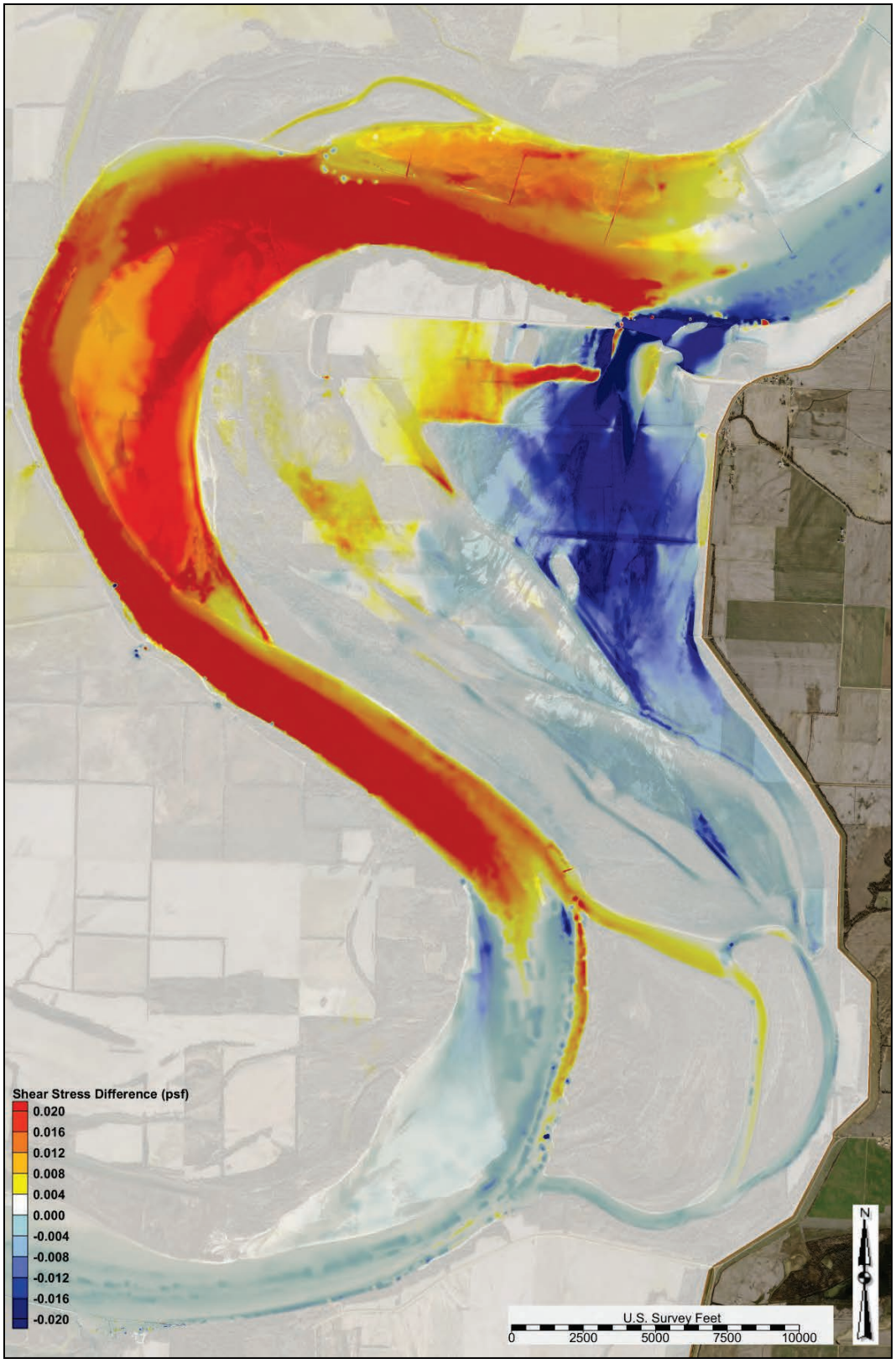


Figure C-200. Alternative 6 shear stress difference—1,700,000 cfs.

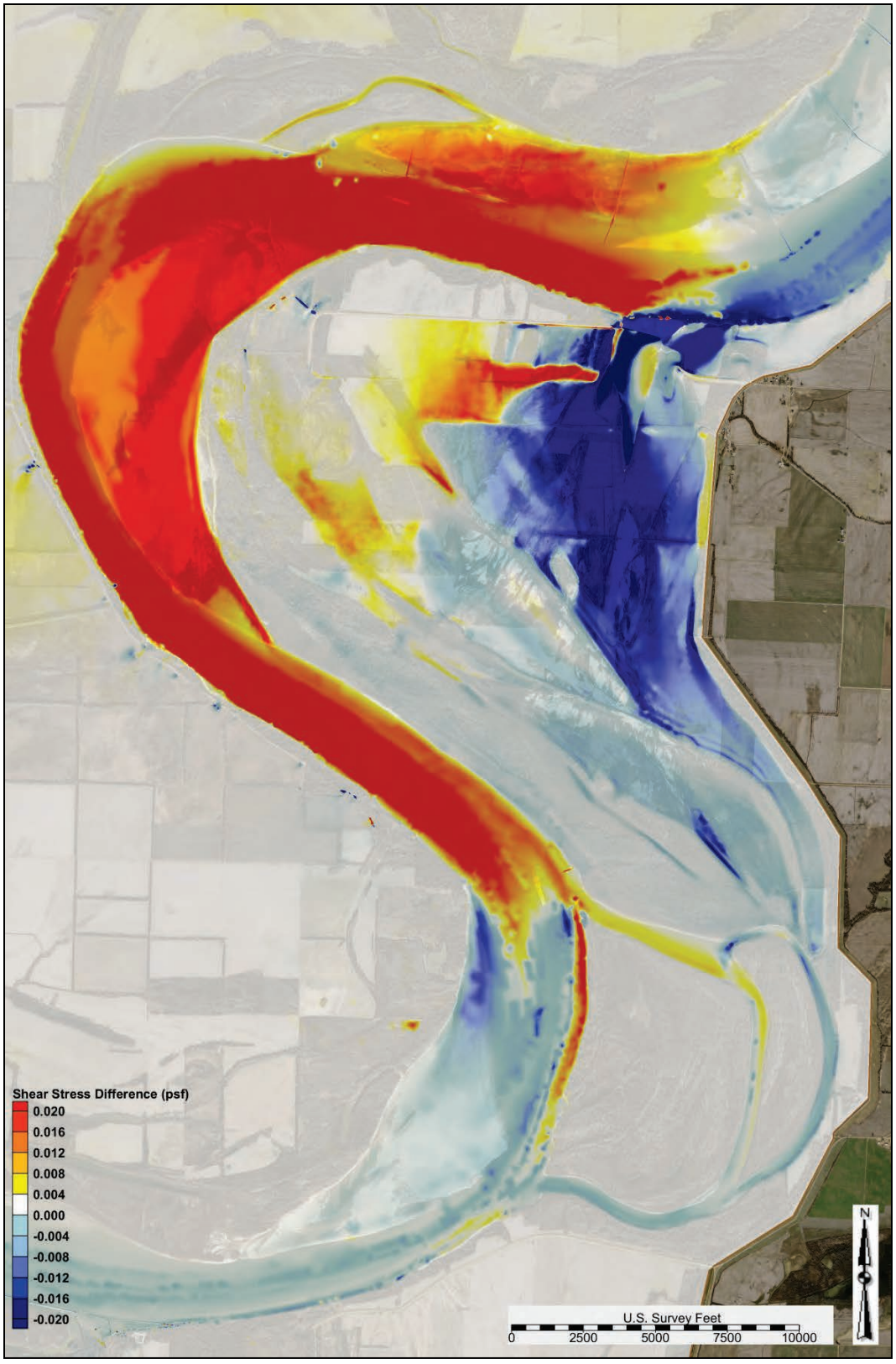


Figure C-201. Alternative 6 shear stress difference—1,900,000 cfs.

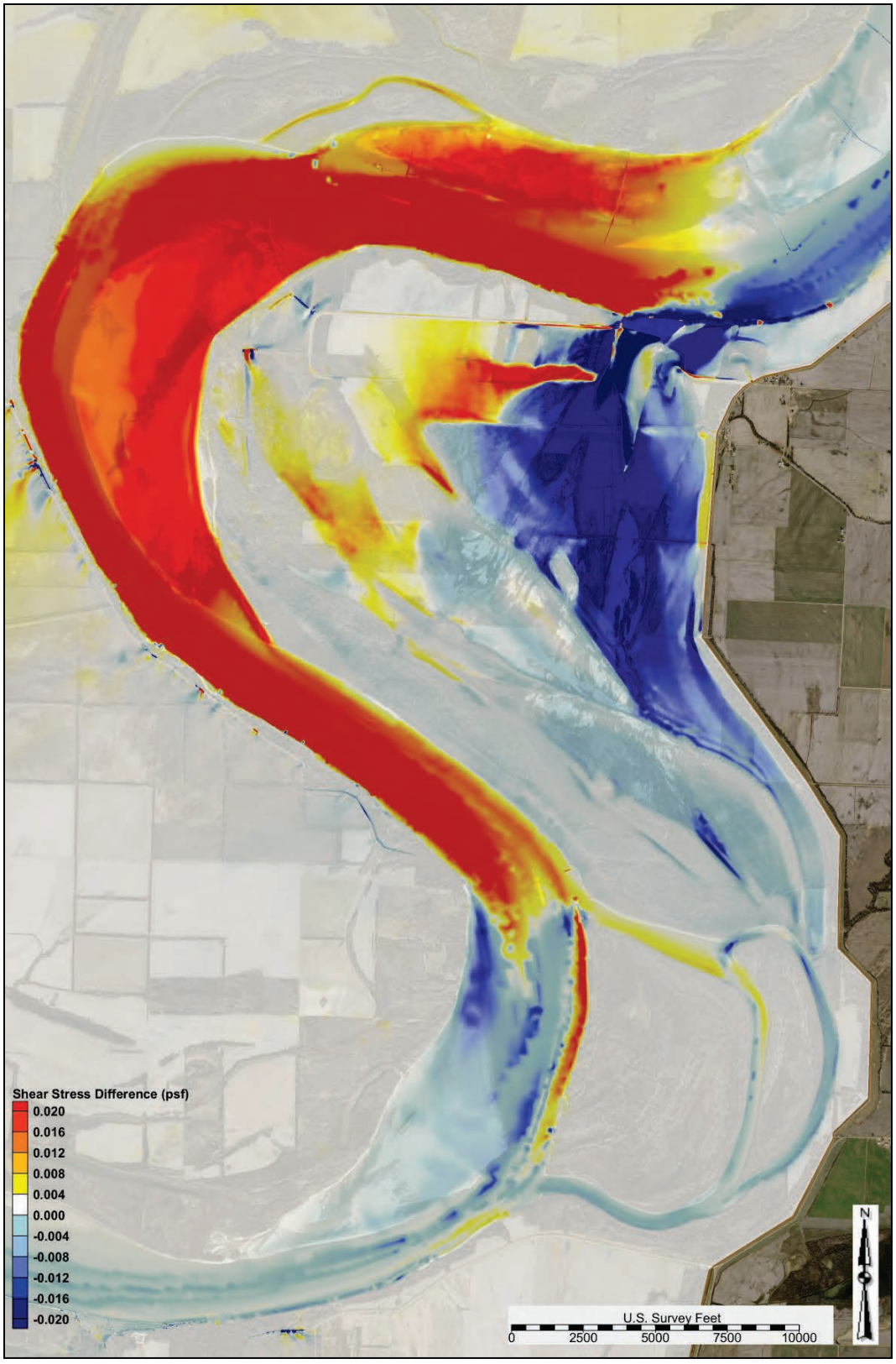
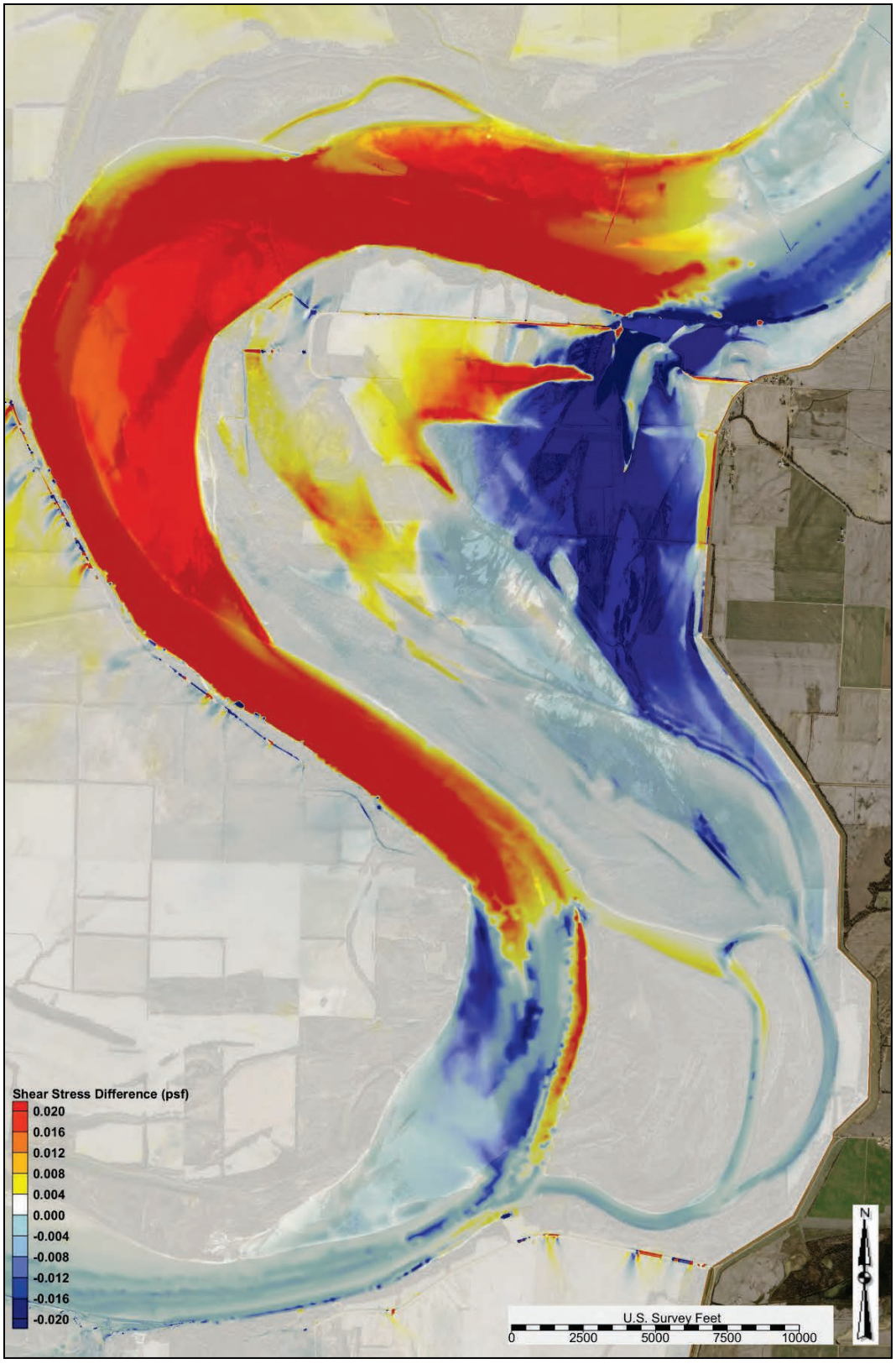


Figure C-202. Alternative 6 shear stress difference—2,100,000 cfs.



WSEL

Figure C-203 depicts the WSEL profiles in the study reach for the following flows: 1,100,000 cfs, 1,500,000 cfs, 1,900,000 cfs, and 2,100,000 cfs.

Sediment diversion grain size distribution

Table C-8 lists the sediment diversion grain size distribution for flows ranging from 870,000 cfs to 2,000,000 cfs.

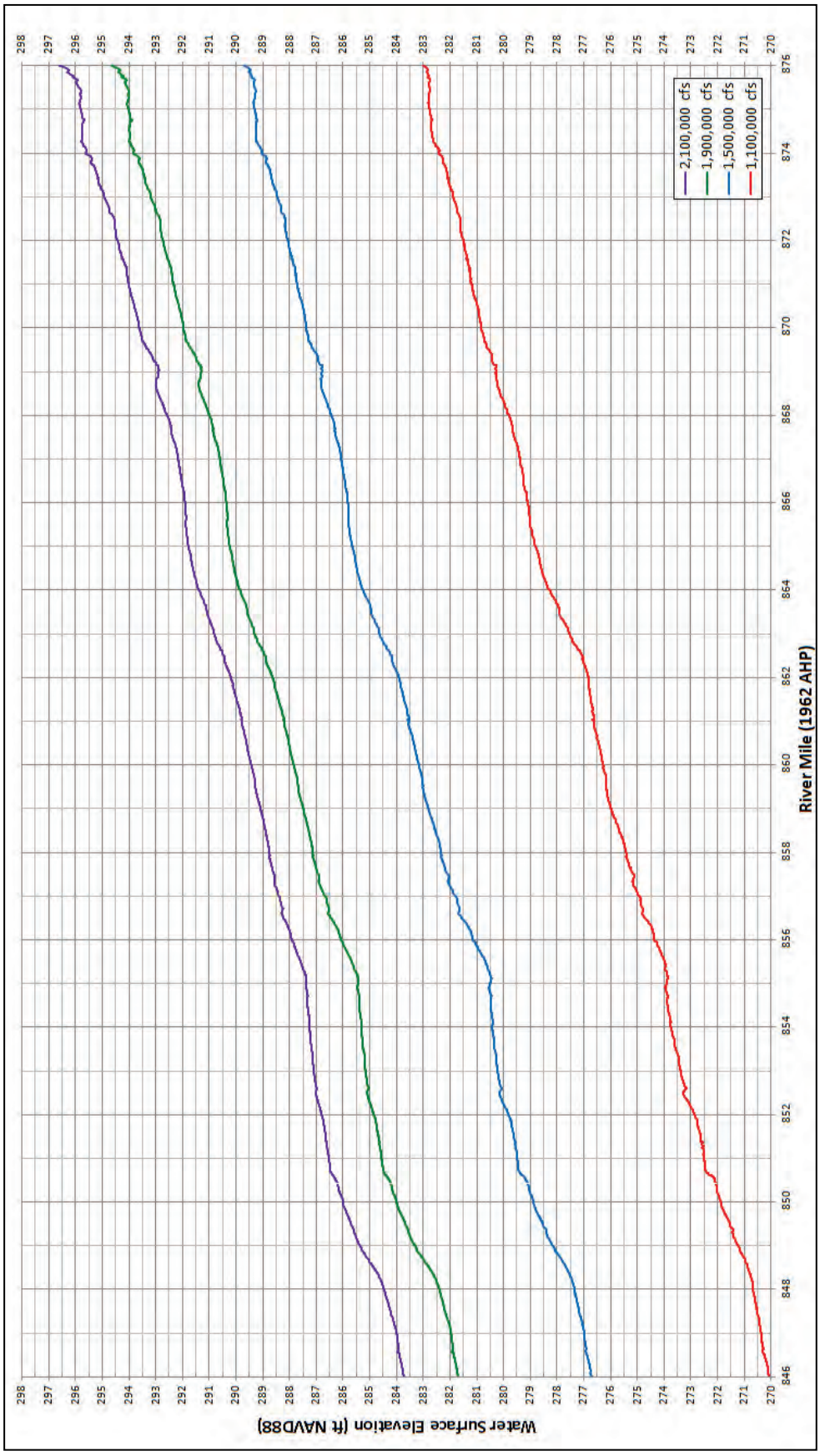


Figure C-203. Alternative 6 WSEL profile.

Table C-8. Alternative 6 diversion grain size distribution.

Main Channel Flow US of Crevasse (cfs)	Total Diversion Load Grain Size Fraction Distribution									
	Coarse Silt	Very Fine Sand	Fine Sand	Medium Sand	Coarse Sand	Very Coarse Sand	Very Fine Pebble	Fine Pebble	Medium Pebble	Coarse Pebble
870,000	0.0000	0.9879	0.0121	0.0000	0.0000	0.0000	0.0000	0.0000	0.0000	0.0000
1,000,000	0.0000	0.8249	0.1672	0.0065	0.0008	0.0005	0.0000	0.0000	0.0000	0.0000
1,100,000	0.0000	0.5594	0.3675	0.0625	0.0088	0.0017	0.0000	0.0000	0.0000	0.0000
1,200,000	0.0000	0.3322	0.4661	0.1524	0.0411	0.0083	0.0000	0.0000	0.0000	0.0000
1,300,000	0.0000	0.1908	0.4124	0.2666	0.1060	0.0232	0.0008	0.0002	0.0000	0.0000
1,400,000	0.0000	0.1357	0.3383	0.3221	0.1566	0.0387	0.0067	0.0013	0.0006	0.0000
1,500,000	0.0000	0.1191	0.3140	0.3405	0.1741	0.0376	0.0089	0.0040	0.0015	0.0002
1,600,000	0.0000	0.1078	0.3006	0.3522	0.1823	0.0399	0.0058	0.0080	0.0030	0.0004
1,700,000	0.0000	0.1015	0.2881	0.3610	0.1910	0.0403	0.0047	0.0075	0.0053	0.0006
1,800,000	0.0000	0.0985	0.2793	0.3649	0.1984	0.0412	0.0046	0.0043	0.0078	0.0009
1,900,000	0.0000	0.0956	0.2732	0.3692	0.2006	0.0421	0.0045	0.0031	0.0106	0.0012
2,000,000	0.0000	0.0973	0.2739	0.3697	0.1974	0.0412	0.0048	0.0028	0.0114	0.0016
2,100,000	0.0000	0.1018	0.2737	0.3677	0.1970	0.0409	0.0052	0.0027	0.0090	0.0020

Alternatives compared to base condition

WSEL

Figures C-204 through C-207 depict the water surface elevation profiles compared to the base condition for the following flows: 1,100,000 cfs, 1,500,000 cfs, 1,900,000 cfs, and 2,100,000 cfs.

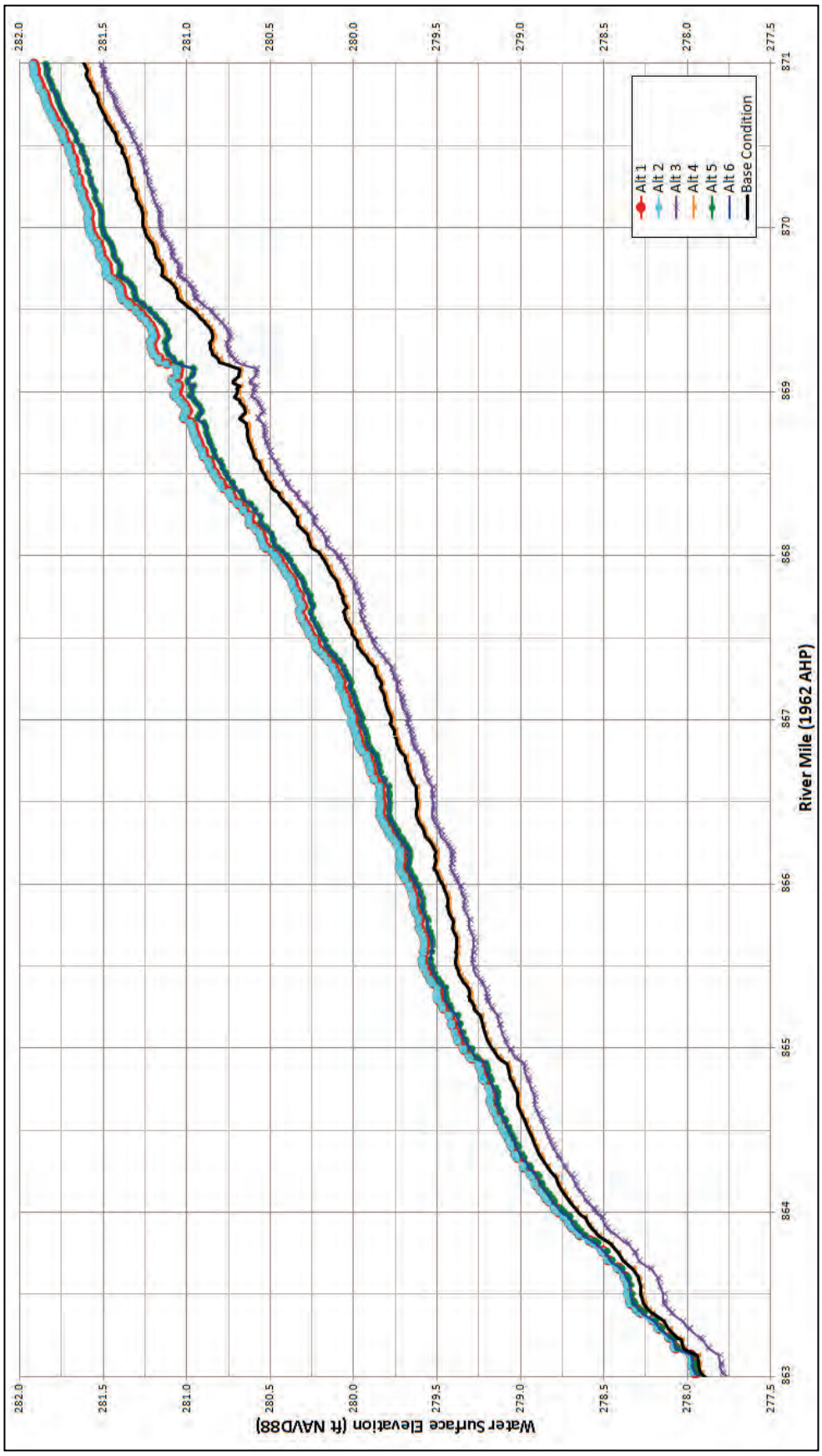


Figure C-204. Alternatives vs. base condition WSEL profile 1,100,000 cfs.

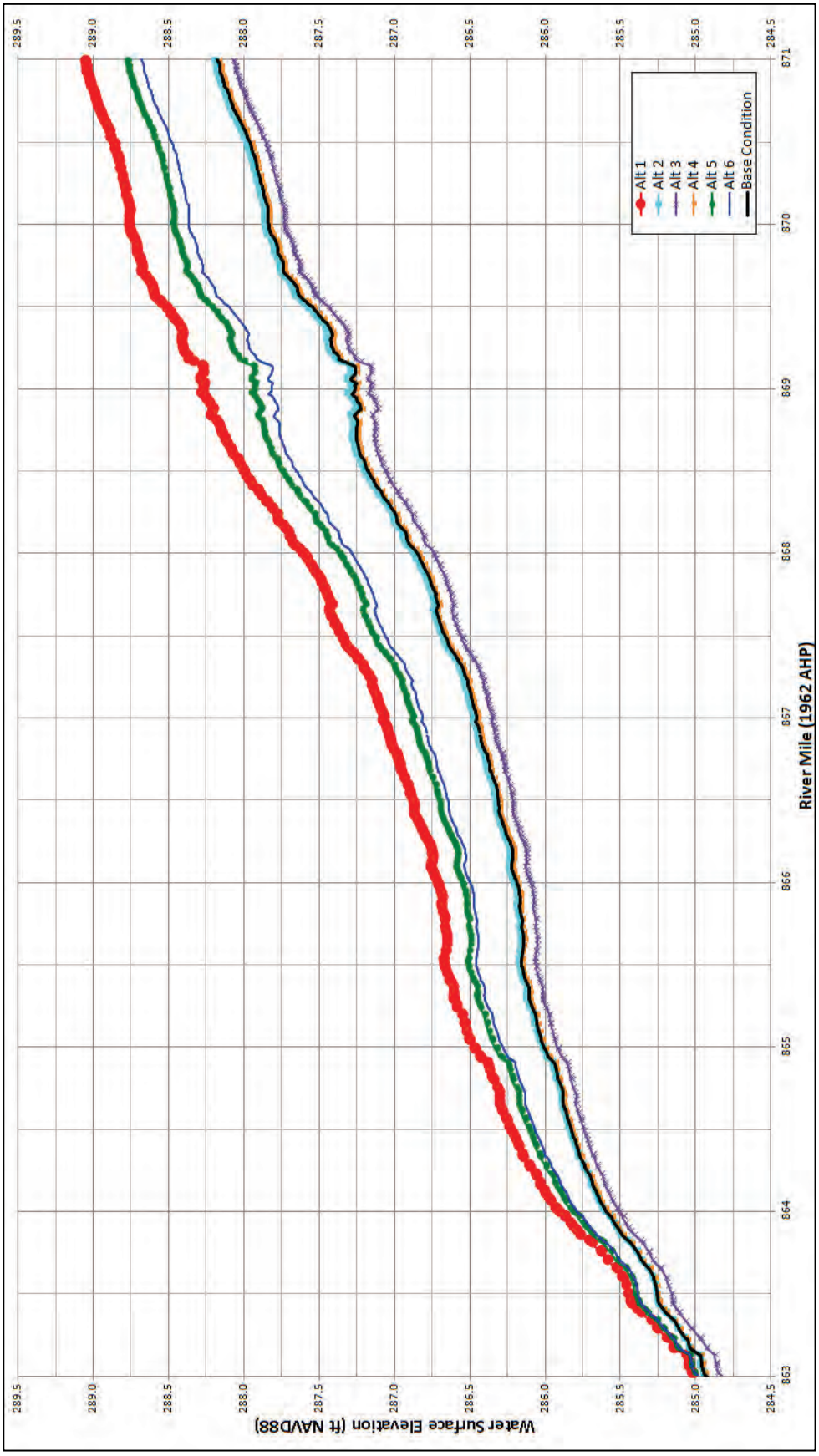


Figure C-205. Alternatives vs. base condition WSEL profile 1,500,000 cfs.

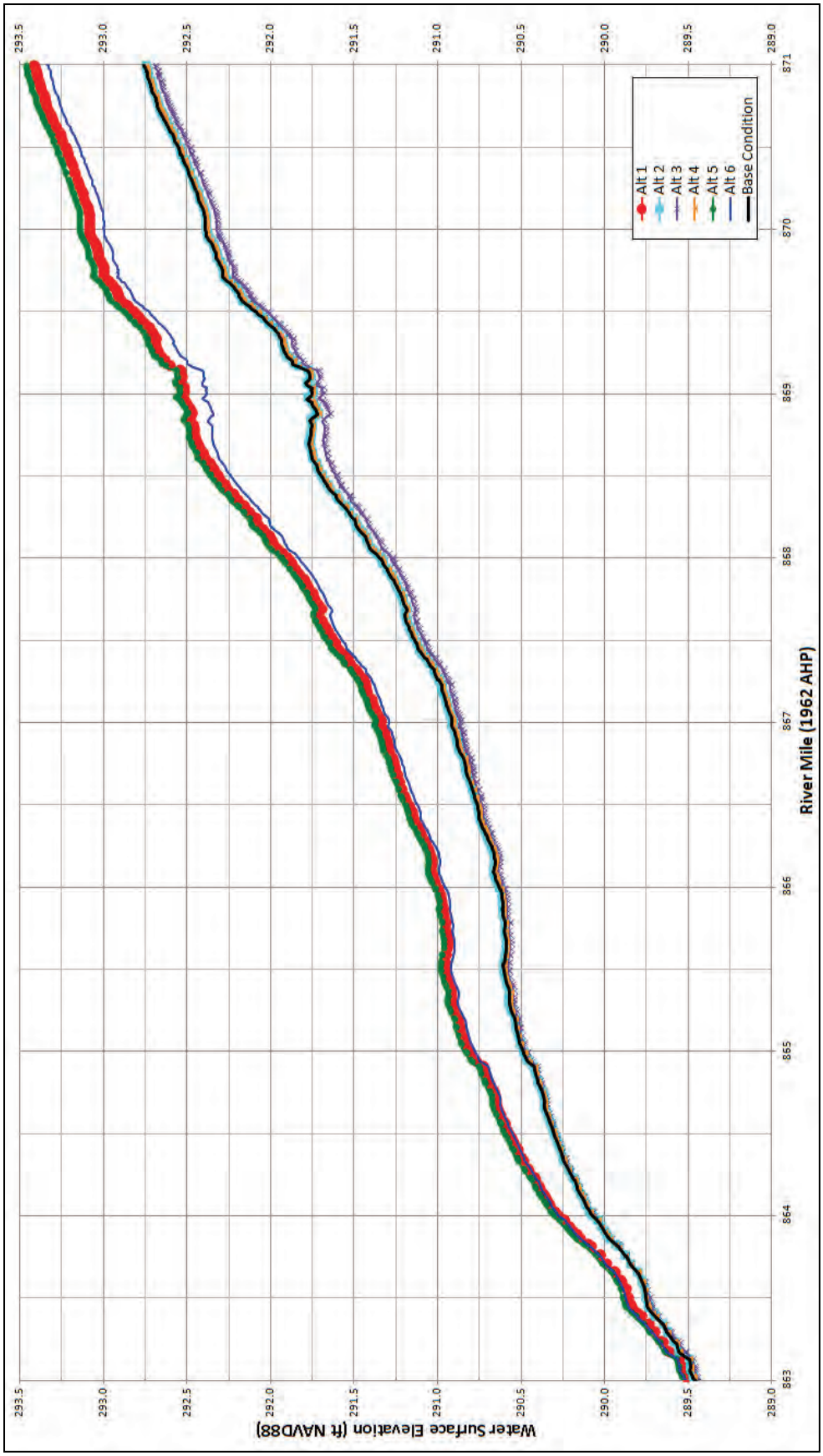


Figure C-206. Alternatives vs. base condition WSEL profile 1,900,000 cfs.

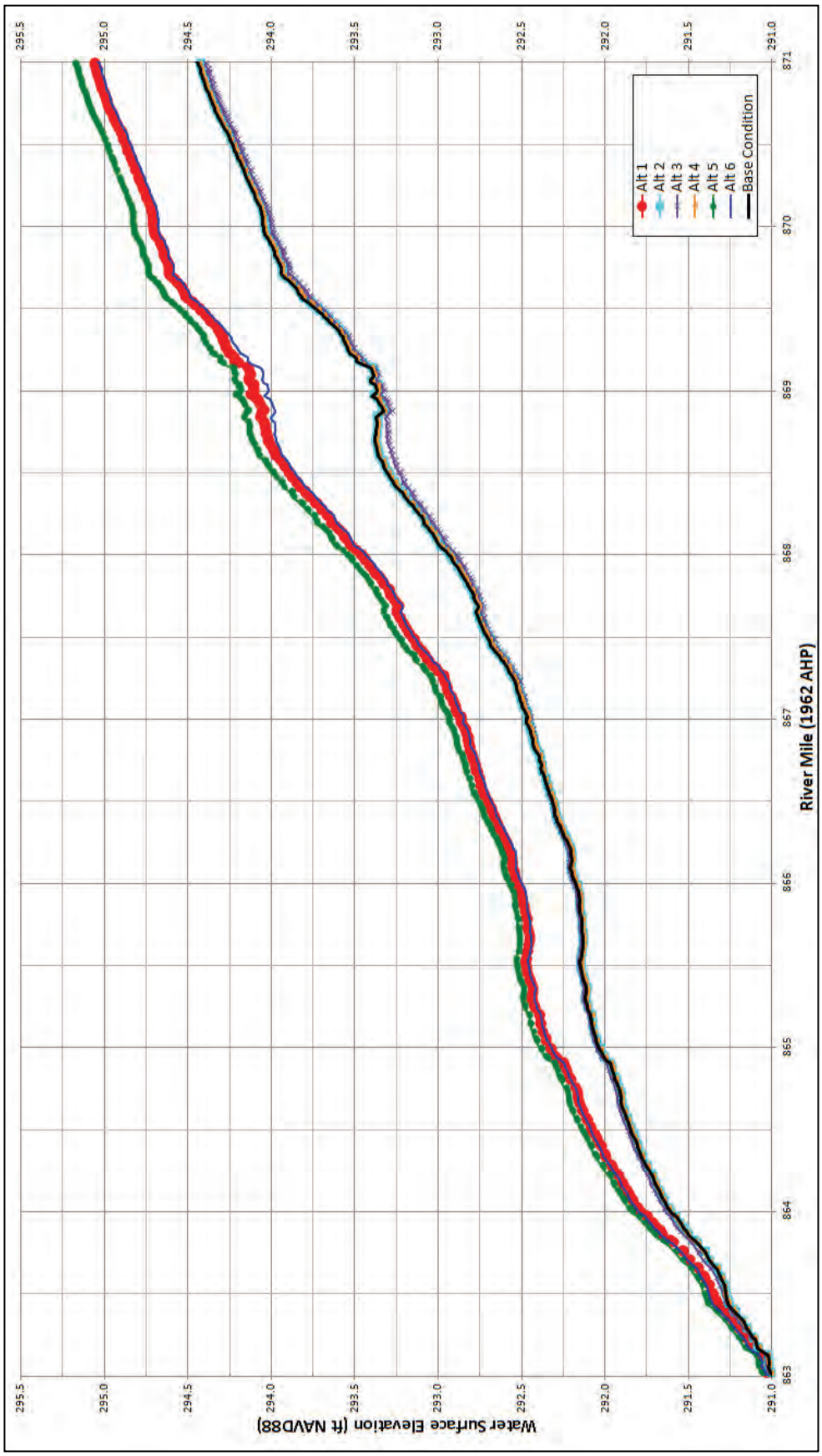


Figure C-207. Alternatives vs. base condition WSEL profile 2,100,000 cfs.

Local Scour Countermeasure 1 output

The following sections contain AdH model output and analysis for Local Scour Countermeasure 1.

Shear stress

The modeled shear stress outputs at flows ranging from 900,000-2,100,000 cfs for the study overbank are depicted in Figures C-208 through C-214.

Figure C-208. Local Scour Countermeasure 1 shear stress—900,000 cfs (study overbank).



Figure C-209. Local Scour Countermeasure 1 shear stress—1,100,000 cfs (study overbank).

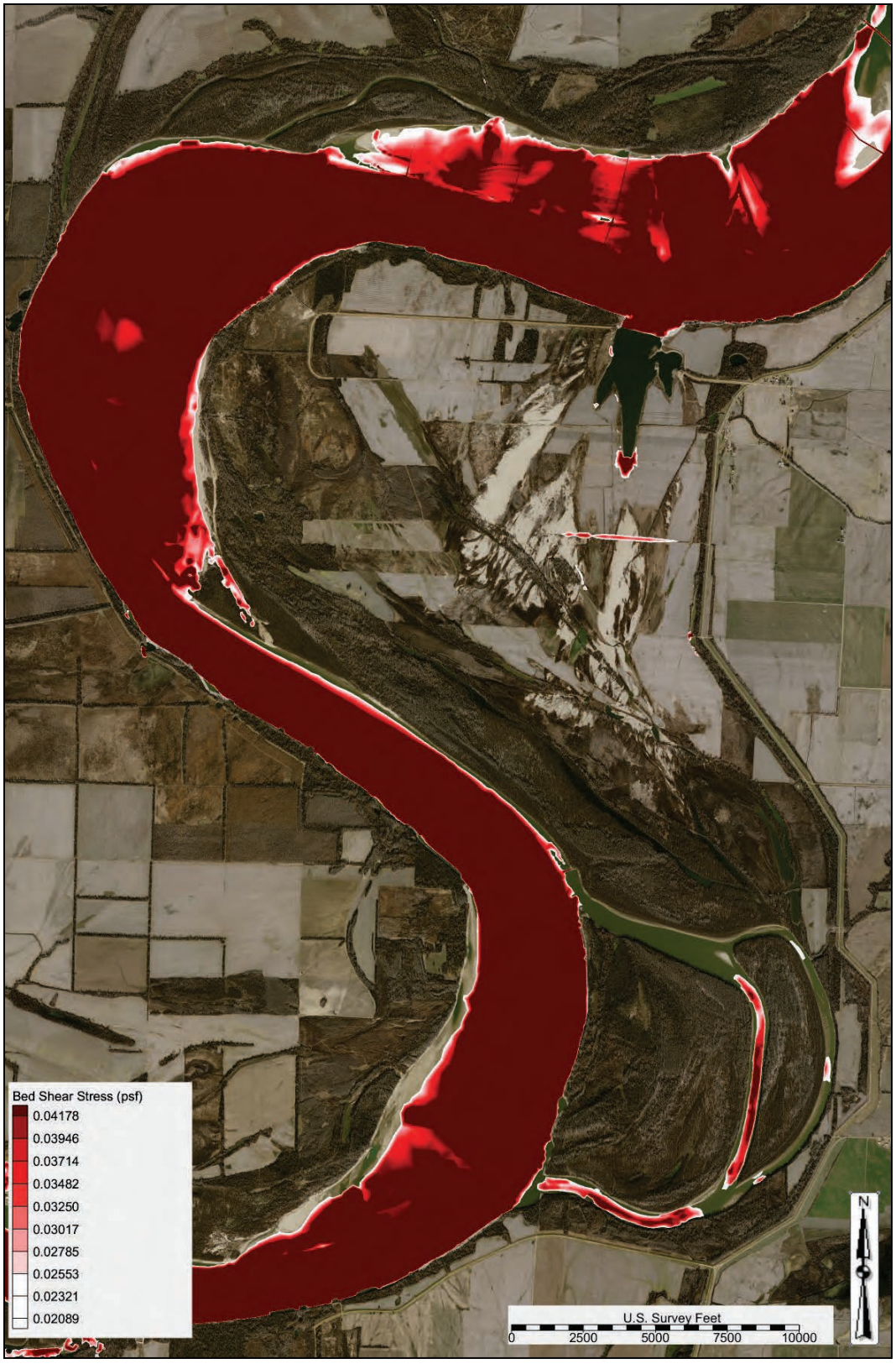


Figure C-210. Local Scour Countermeasure 1 shear stress—1,300,000 cfs (study overbank).

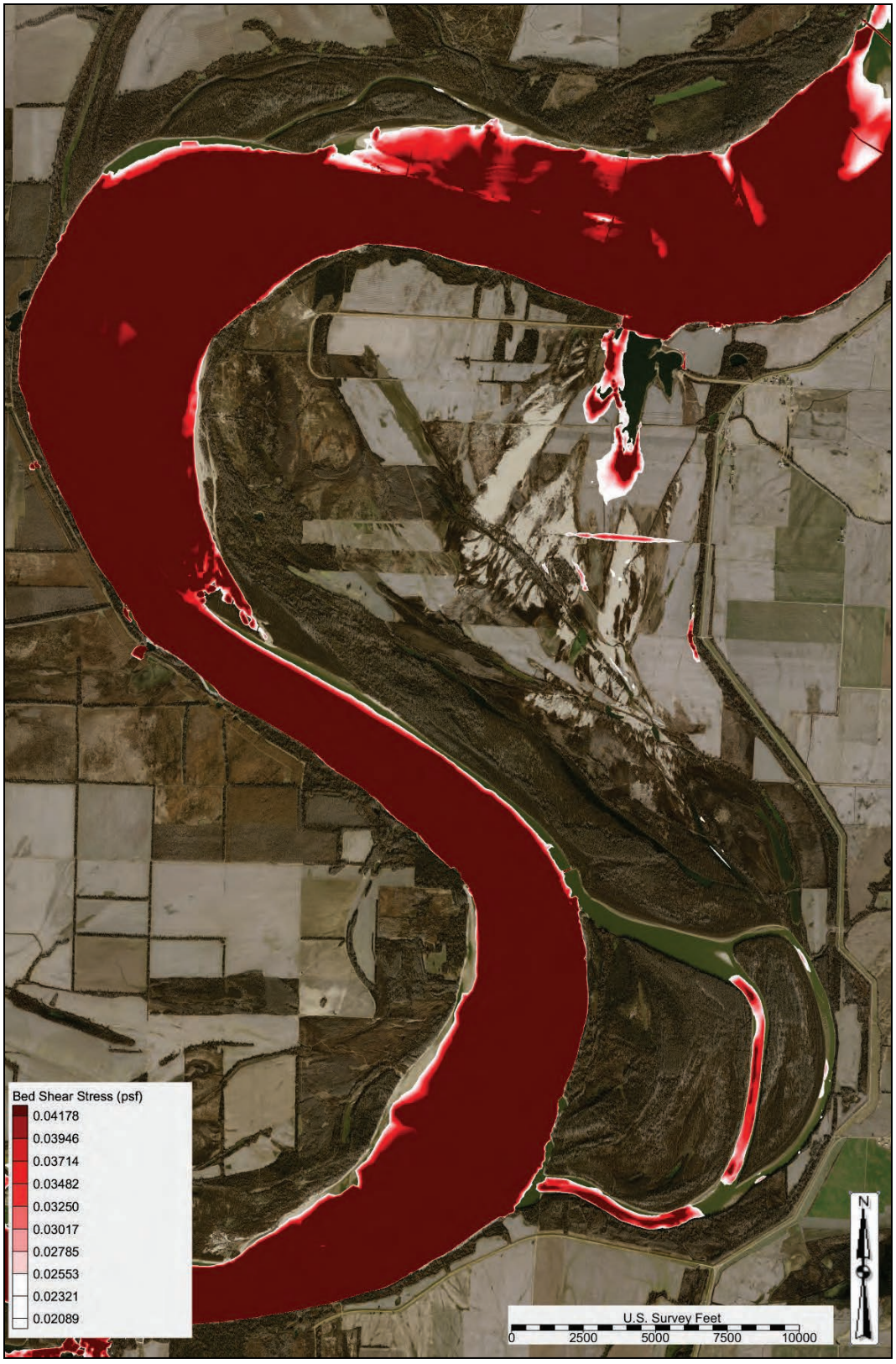


Figure C-211. Local Scour Countermeasure 1 shear stress—1,500,000 cfs (study overbank).

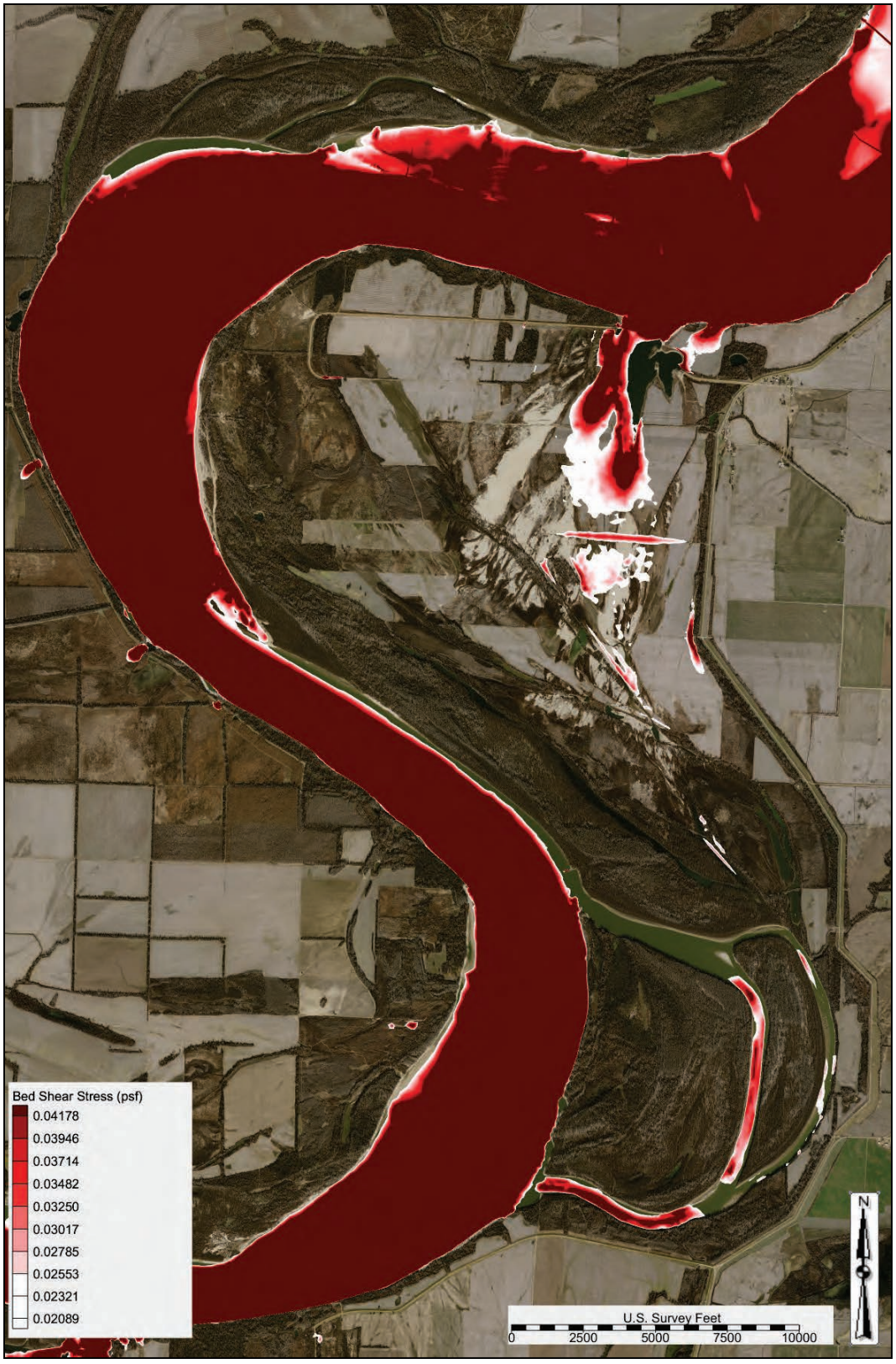


Figure C-212. Local Scour Countermeasure 1 shear stress—1,700,000 cfs (study overbank).

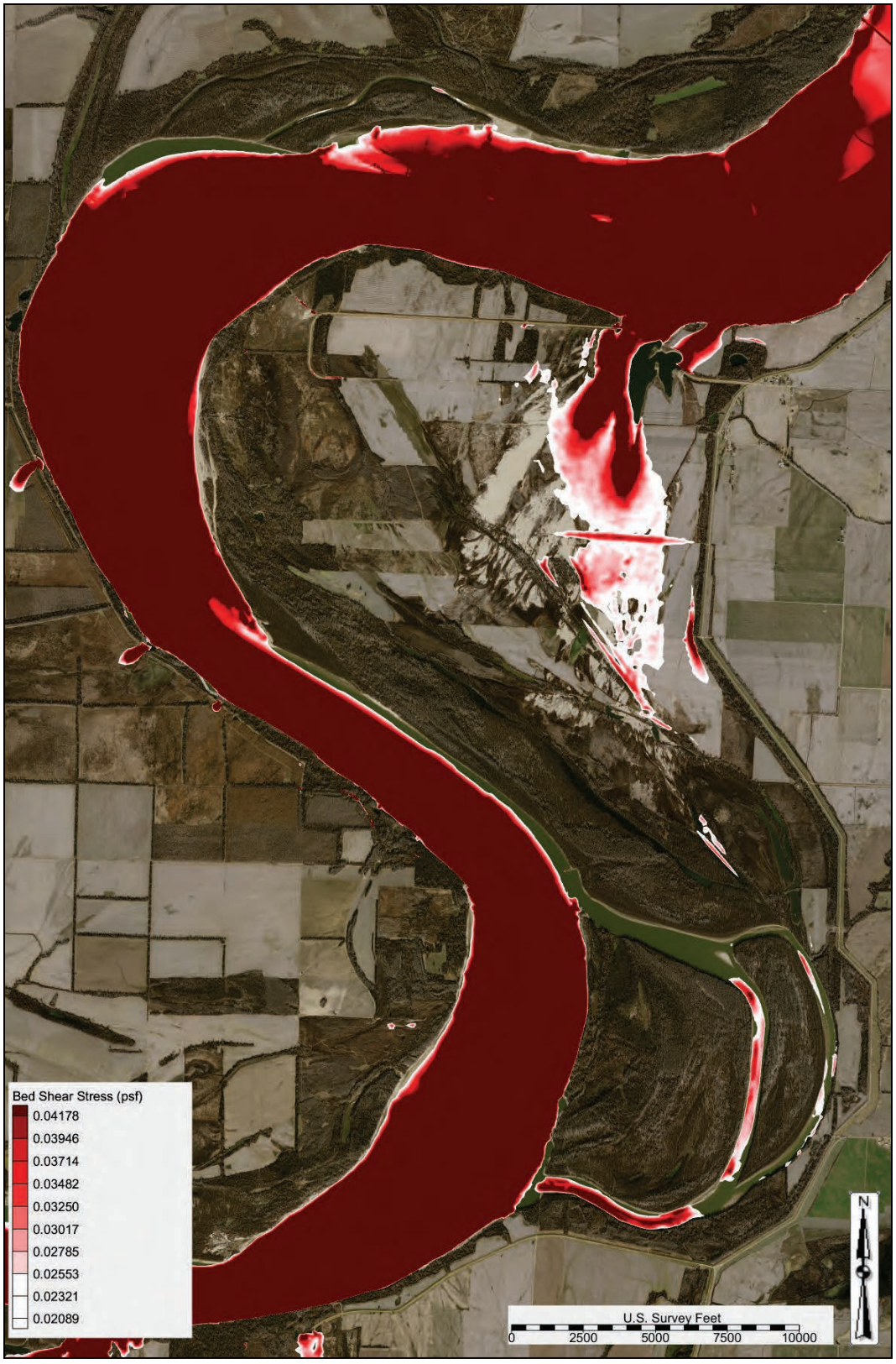


Figure C-213. Local Scour Countermeasure 1 shear stress—1,900,000 cfs (study overbank).

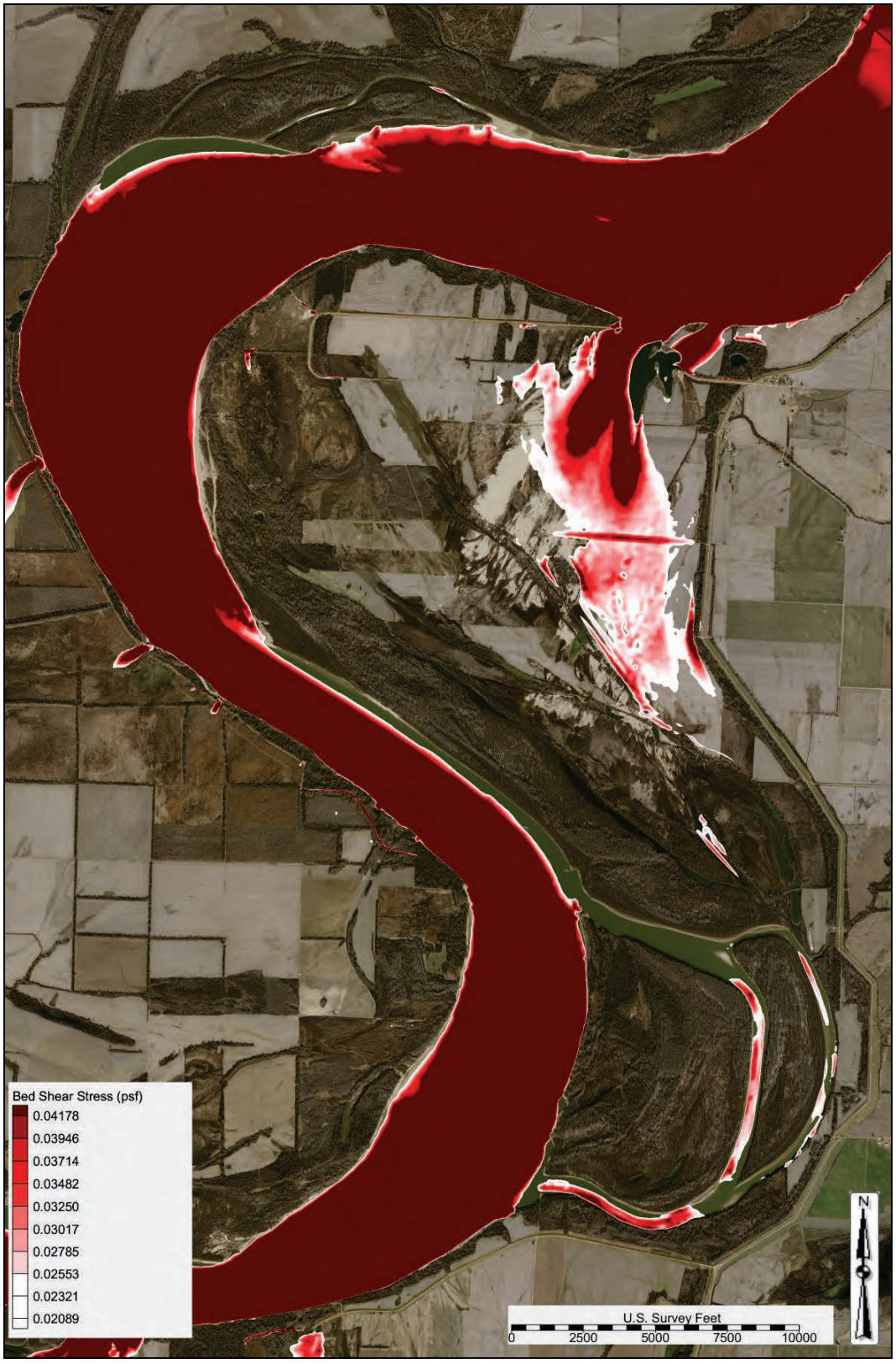
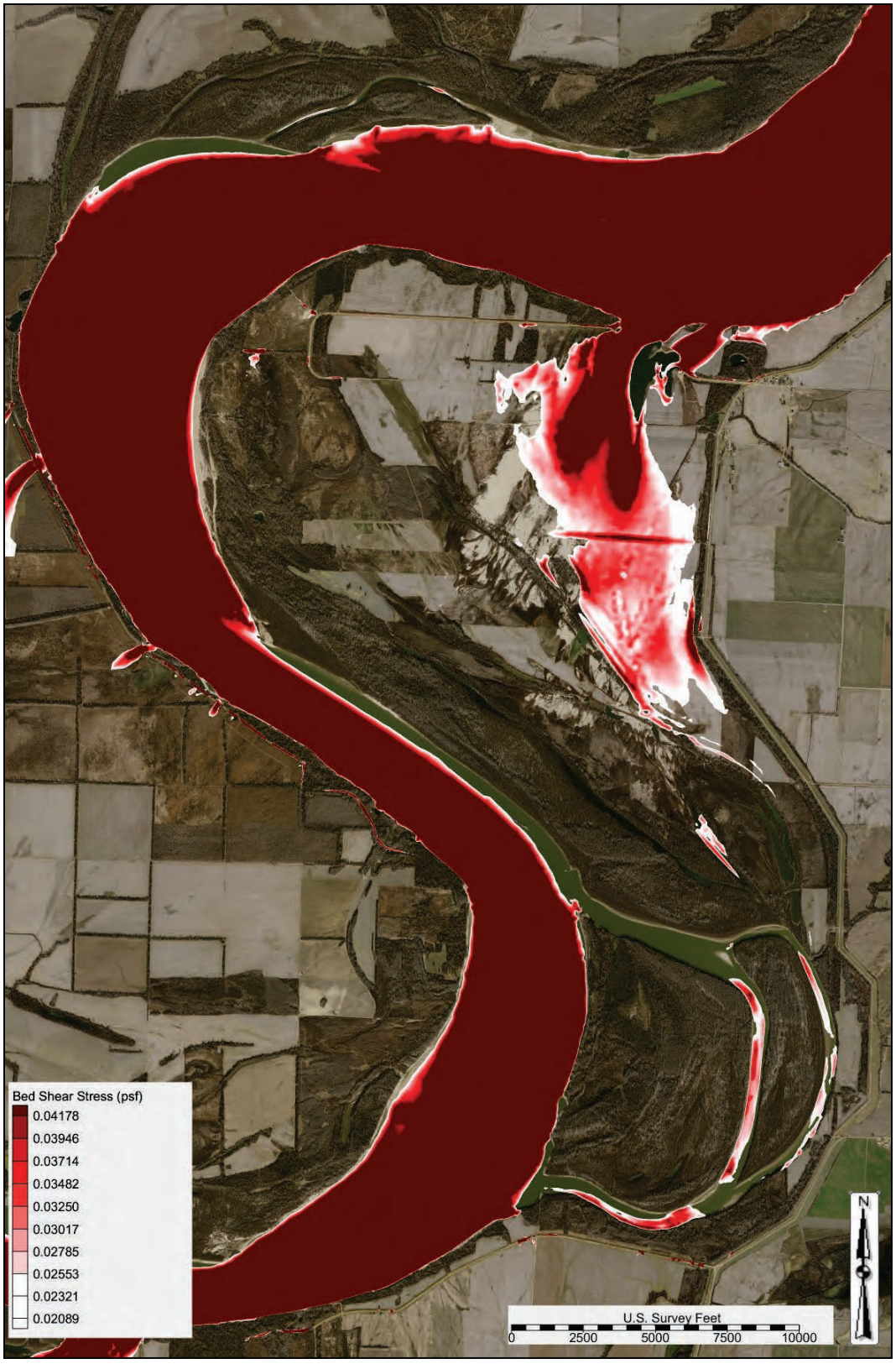


Figure C-214. Local Scour Countermeasure 1 shear stress—2,100,000 cfs (study overbank).



Shear stress difference comparison

The modeled shear stress difference plots compared to the base condition output for flows ranging from 900,000 to 2,100,000 cfs are depicted in Figures C-215 through C-221. A positive shear stress difference (+ value and red and orange) indicated an increased shear stress compared to the base condition. A negative shear stress difference (- value and blue) indicated a decreased shear stress compared to the base condition. A zero shear stress difference (zero value and white) indicated that the alternative had no change in shear stress.

Figure C-215. Local Scour Countermeasure 1 shear stress difference—900,000 cfs.



Figure C-216. Local Scour Countermeasure 1 shear stress difference—1,100,000 cfs.

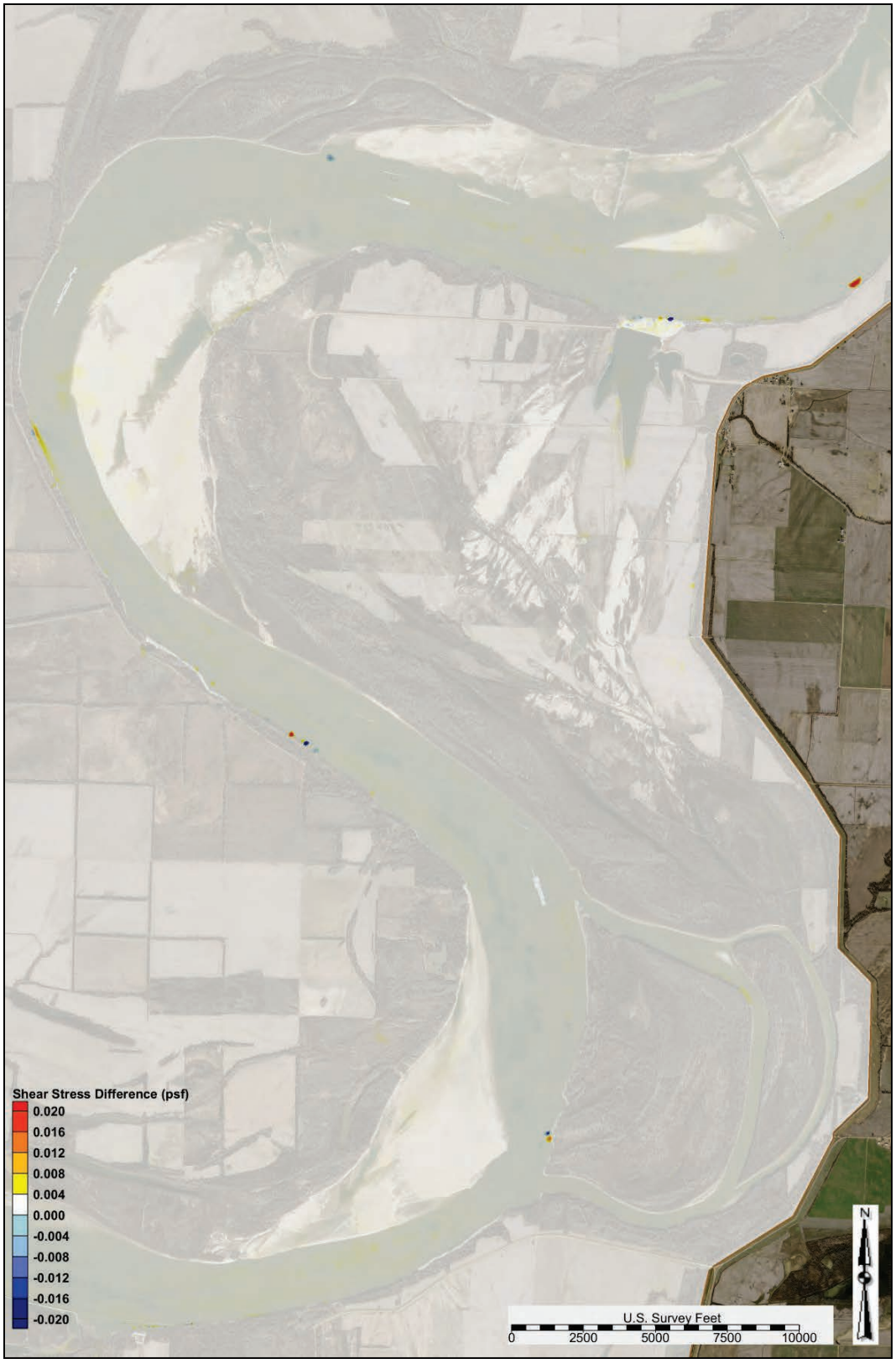


Figure C-217. Local Scour Countermeasure 1 shear stress difference—1,300,000 cfs.

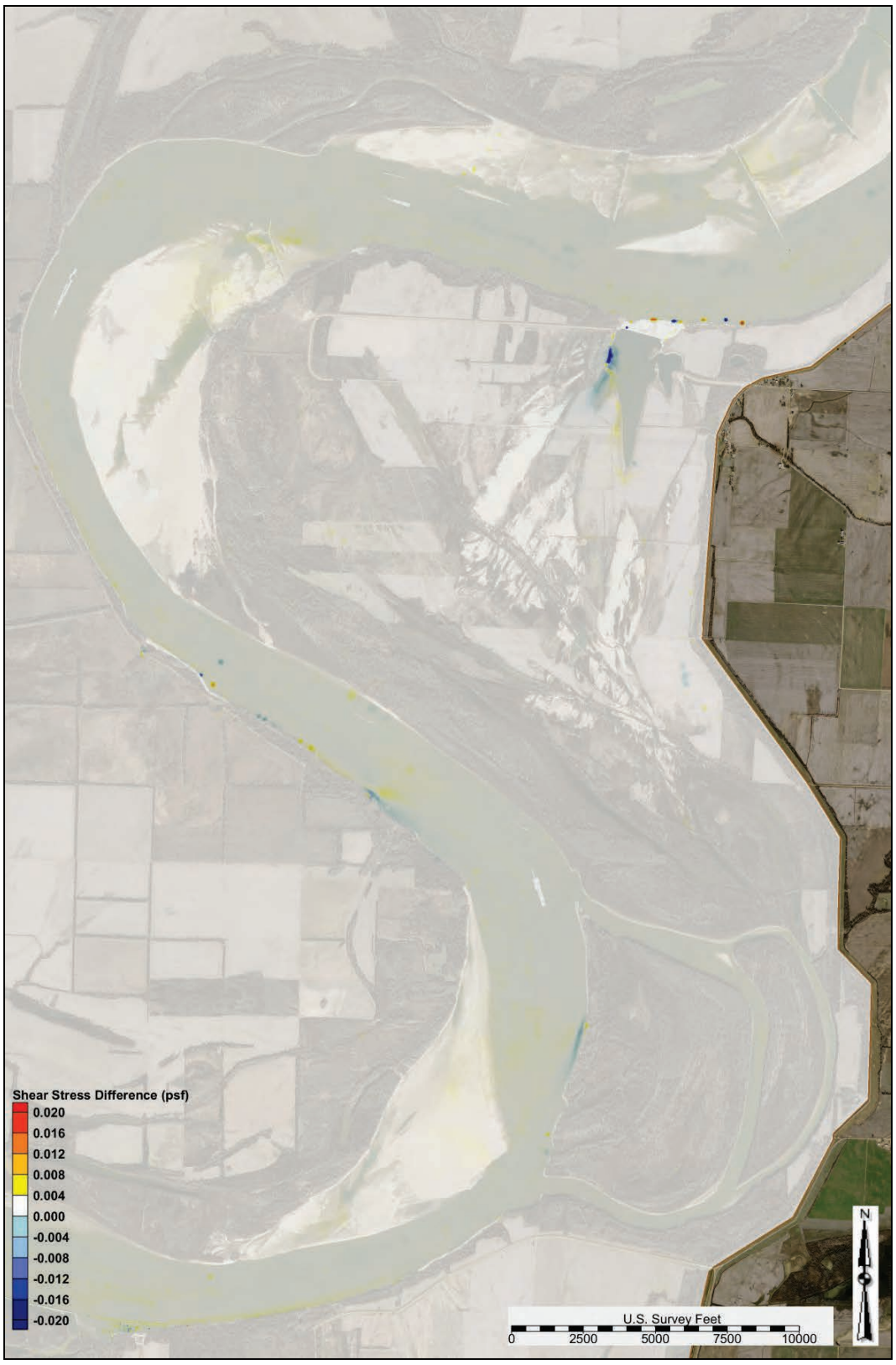


Figure C-218. Local Scour Countermeasure 1 shear stress difference—1,500,000 cfs.

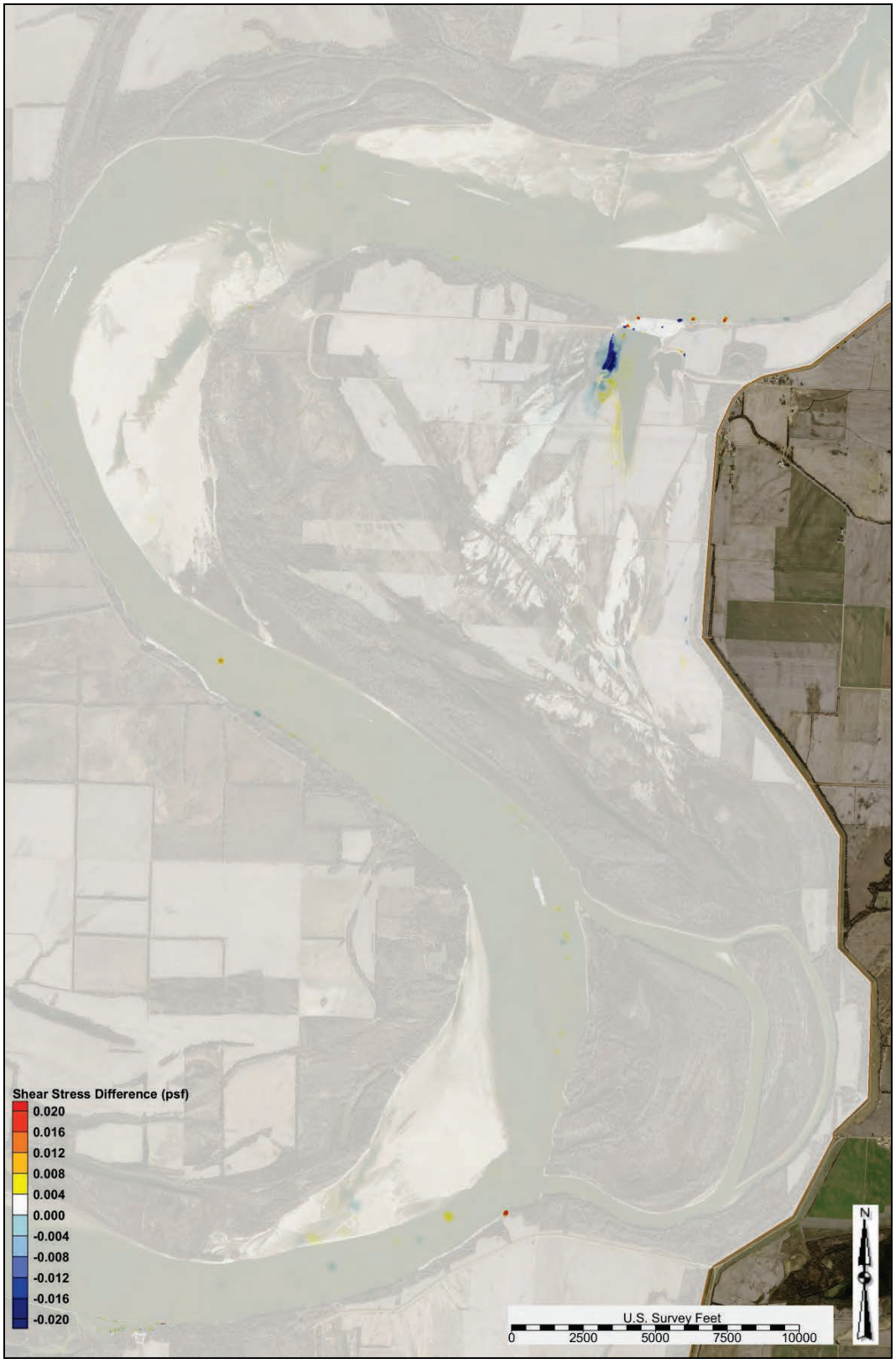


Figure C-219. Local Scour Countermeasure 1 shear stress difference—1,700,000 cfs.

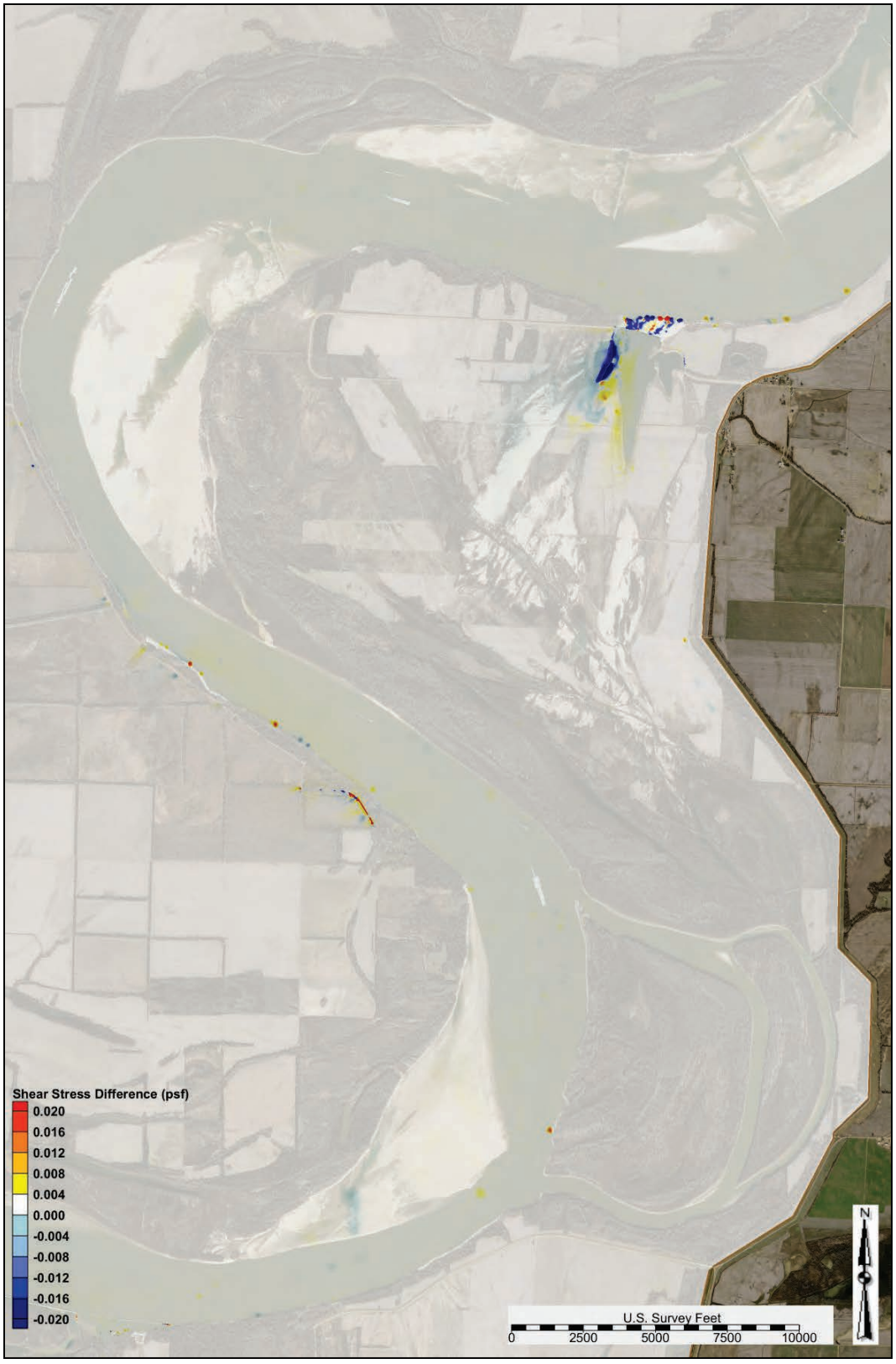


Figure C-220. Local Scour Countermeasure 1 shear stress difference—1,900,000 cfs.

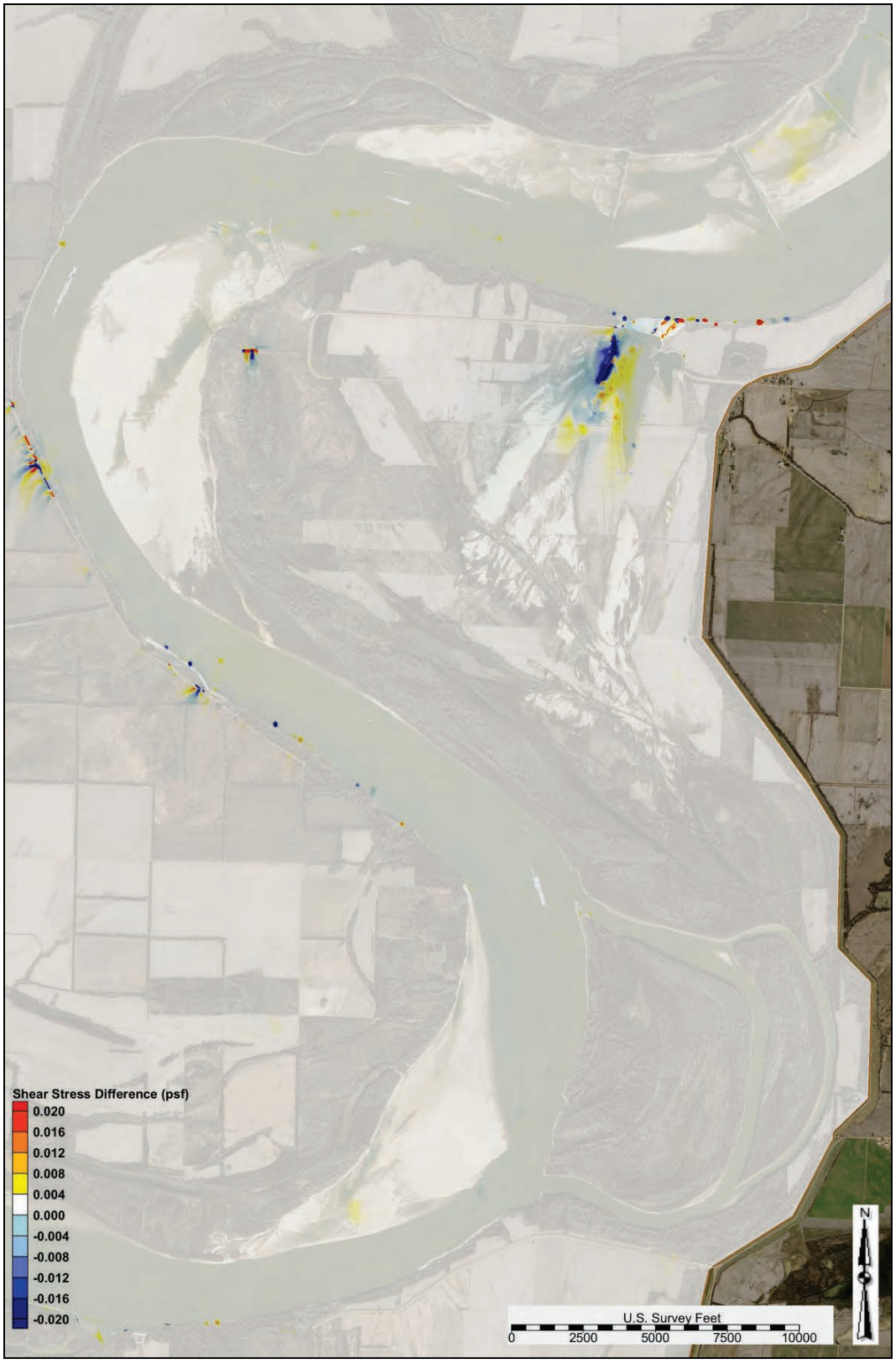
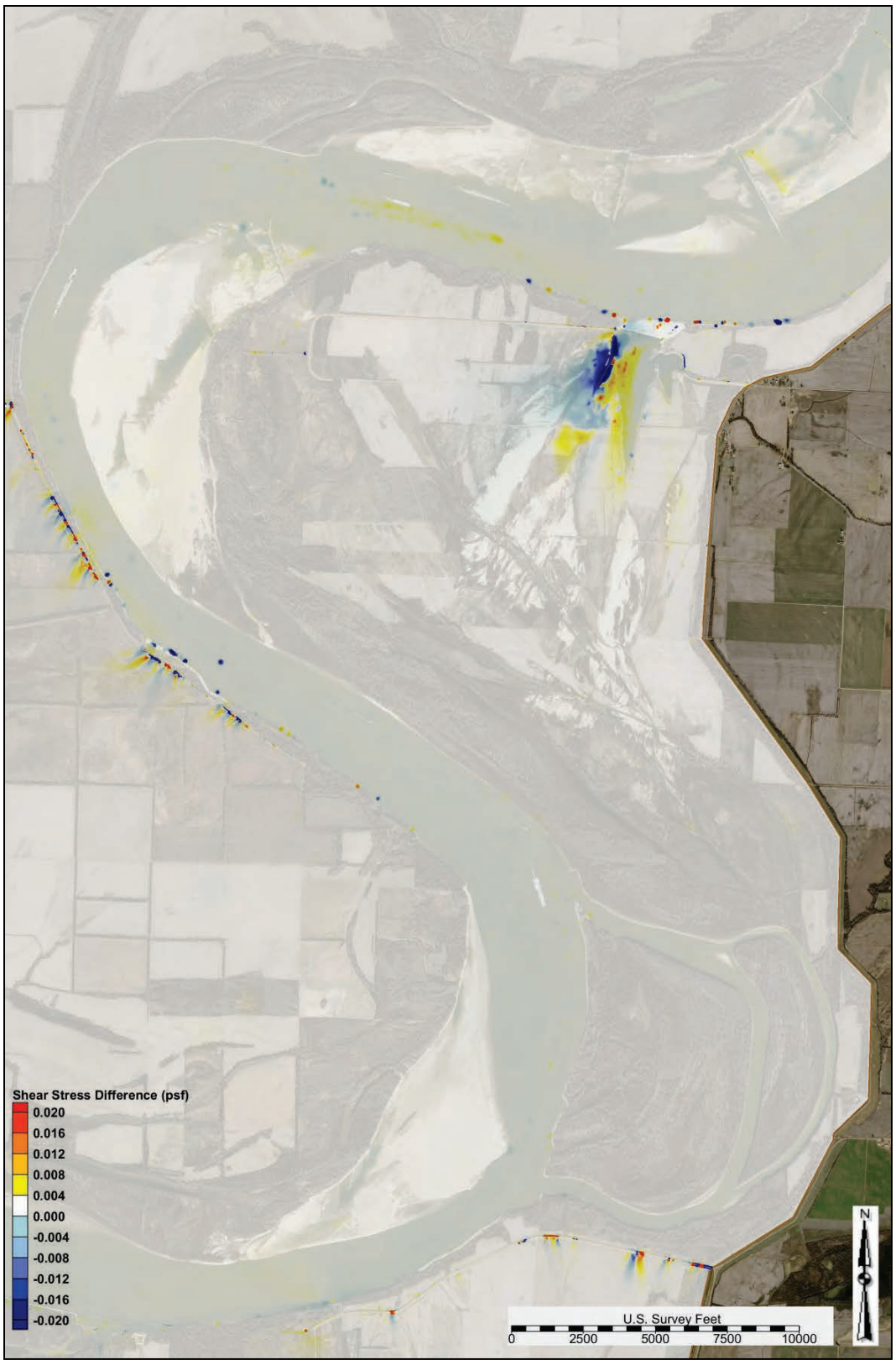


Figure C-221. Local Scour Countermeasure 1 shear stress difference—2,100,000 cfs.



WSEL

Figure C-222 depicts the water surface elevation profiles in the study reach for the following flows: 1,100,000 cfs, 1,500,000 cfs, 1,900,000 cfs, and 2,100,000 cfs.

Sediment diversion grain size distribution

Table C-9 lists the sediment diversion grain size distribution for flows ranging from 870,000 cfs to 2,000,000 cfs.

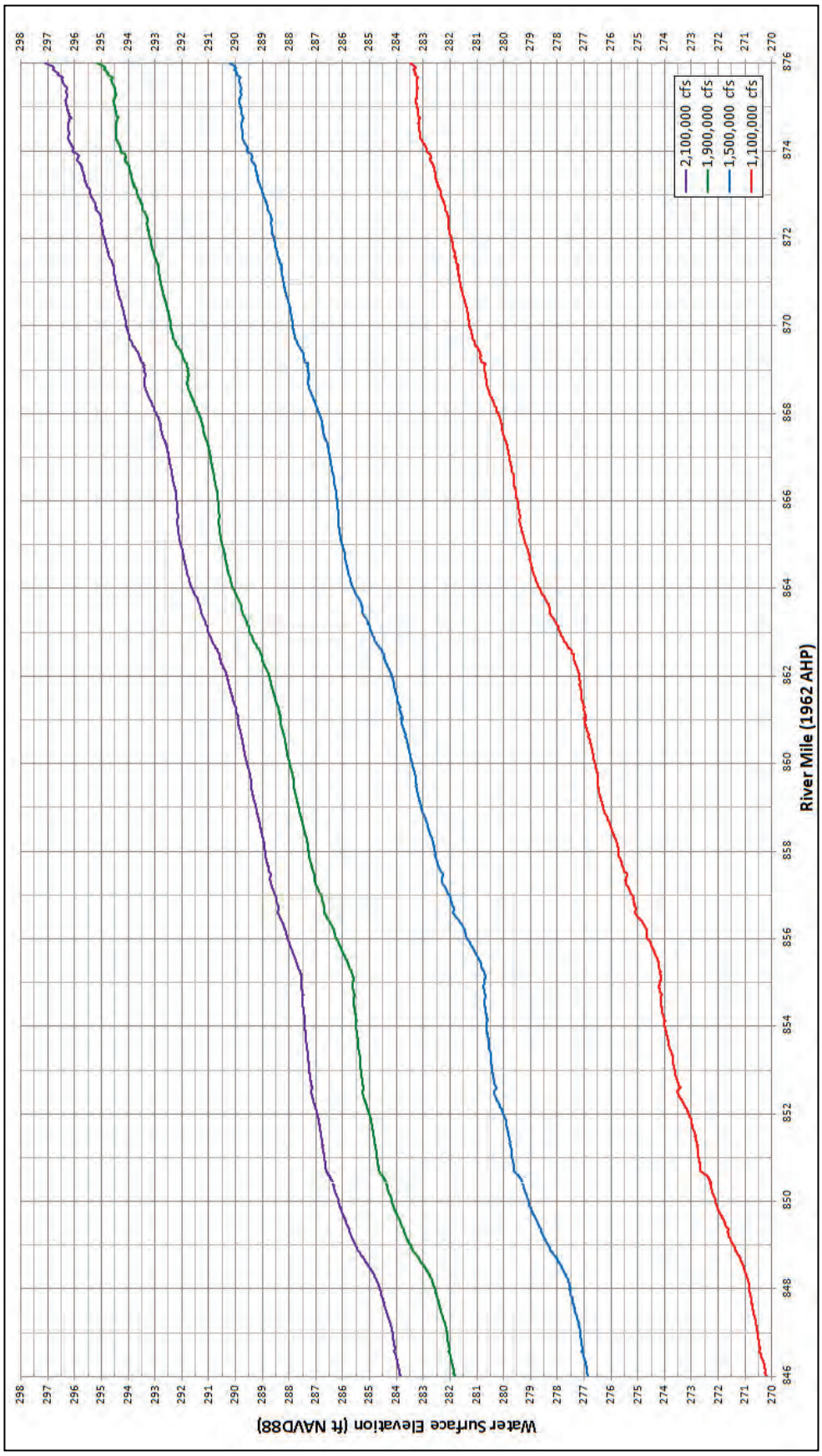


Figure C-222. Local Scour Countermeasure 1 WSEL profile.

Table C-9. Local Scour Countermeasure 1 diversion grain size distribution.

Main Channel Flow US of Crevasse (cfs)	Total Diversion Load Grain Size Fraction Distribution									
	Coarse Silt	Very Fine Sand	Fine Sand	Medium Sand	Coarse Sand	Very Coarse Sand	Very Fine Pebble	Fine Pebble	Medium Pebble	Coarse Pebble
870,000	0.0000	0.9516	0.0479	0.0005	0.0000	0.0000	0.0000	0.0000	0.0000	0.0000
900,000	0.0000	0.9012	0.0976	0.0012	0.0000	0.0000	0.0000	0.0000	0.0000	0.0000
1,000,000	0.0000	0.4139	0.4315	0.1212	0.0274	0.0060	0.0000	0.0000	0.0000	0.0000
1,100,000	0.0000	0.2232	0.4053	0.2504	0.1016	0.0190	0.0004	0.0001	0.0000	0.0000
1,200,000	0.0003	0.1924	0.4069	0.2725	0.1045	0.0207	0.0019	0.0005	0.0003	0.0000
1,300,000	0.0005	0.1422	0.3627	0.3379	0.1349	0.0212	0.0000	0.0003	0.0002	0.0000
1,400,000	0.0007	0.1285	0.3222	0.3586	0.1603	0.0292	0.0002	0.0002	0.0001	0.0000
1,500,000	0.0011	0.1271	0.3201	0.3622	0.1621	0.0264	0.0005	0.0002	0.0003	0.0000
1,600,000	0.0013	0.1135	0.3110	0.3741	0.1701	0.0280	0.0009	0.0003	0.0007	0.0001
1,700,000	0.0011	0.1068	0.3025	0.3801	0.1767	0.0292	0.0013	0.0004	0.0016	0.0001
1,800,000	0.0010	0.1000	0.2939	0.3898	0.1816	0.0293	0.0018	0.0005	0.0019	0.0003
1,900,000	0.0008	0.0960	0.2898	0.3951	0.1844	0.0296	0.0023	0.0005	0.0012	0.0004
2,000,000	0.0007	0.0881	0.2780	0.4076	0.1897	0.0308	0.0027	0.0007	0.0010	0.0007
2,100,000	0.0005	0.0871	0.2784	0.3999	0.1956	0.0312	0.0038	0.0009	0.0011	0.0014

Local Scour Countermeasure 2 output

The following sections contain AdH model output and analysis for Local Scour Countermeasure 2.

Shear Stress

The modeled shear stress outputs at flows ranging from 900,000 to 2,100,000 cfs for the study overbank are depicted in Figures C-223 through C-229.

Figure C-223. Local Scour Countermeasure 2 shear stress—900,000 cfs (study overbank).



Figure C-224. Local Scour Countermeasure 2 shear stress—1,100,000 cfs (study overbank).

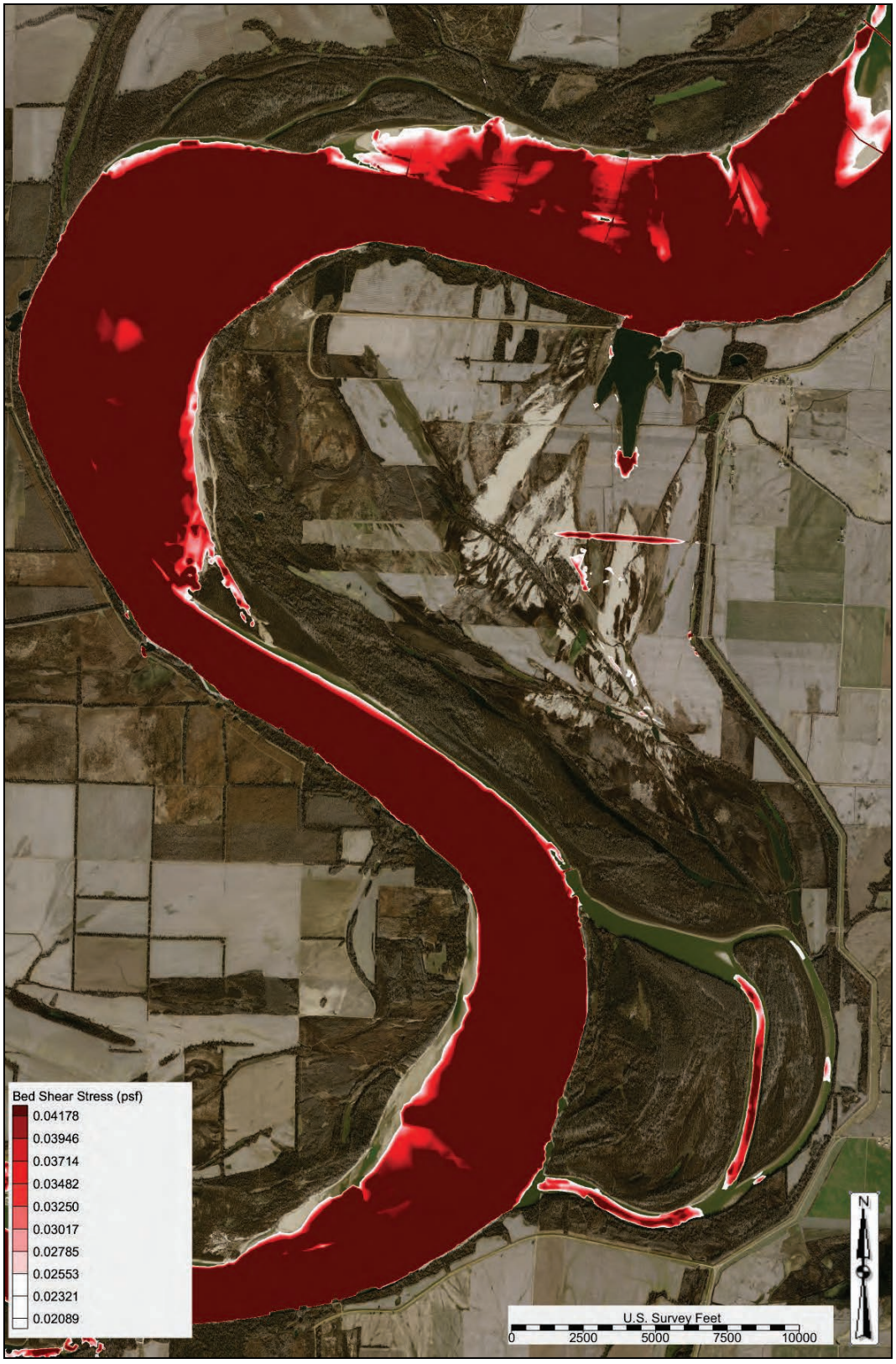


Figure C-225. Local Scour Countermeasure 2 shear stress—1,300,000 cfs (study overbank).

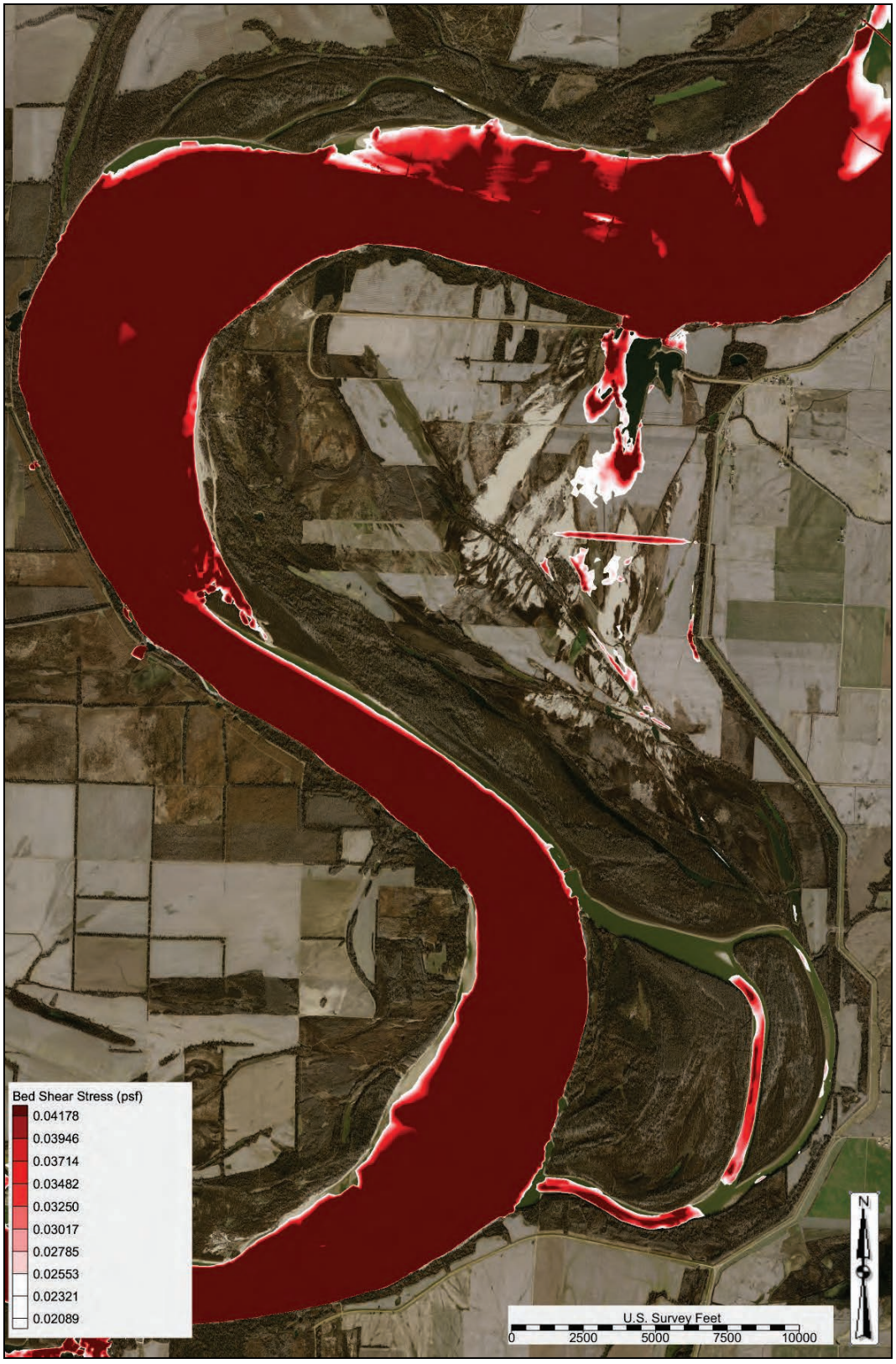


Figure C-226. Local Scour Countermeasure 2 shear stress—1,500,000 cfs (study overbank).

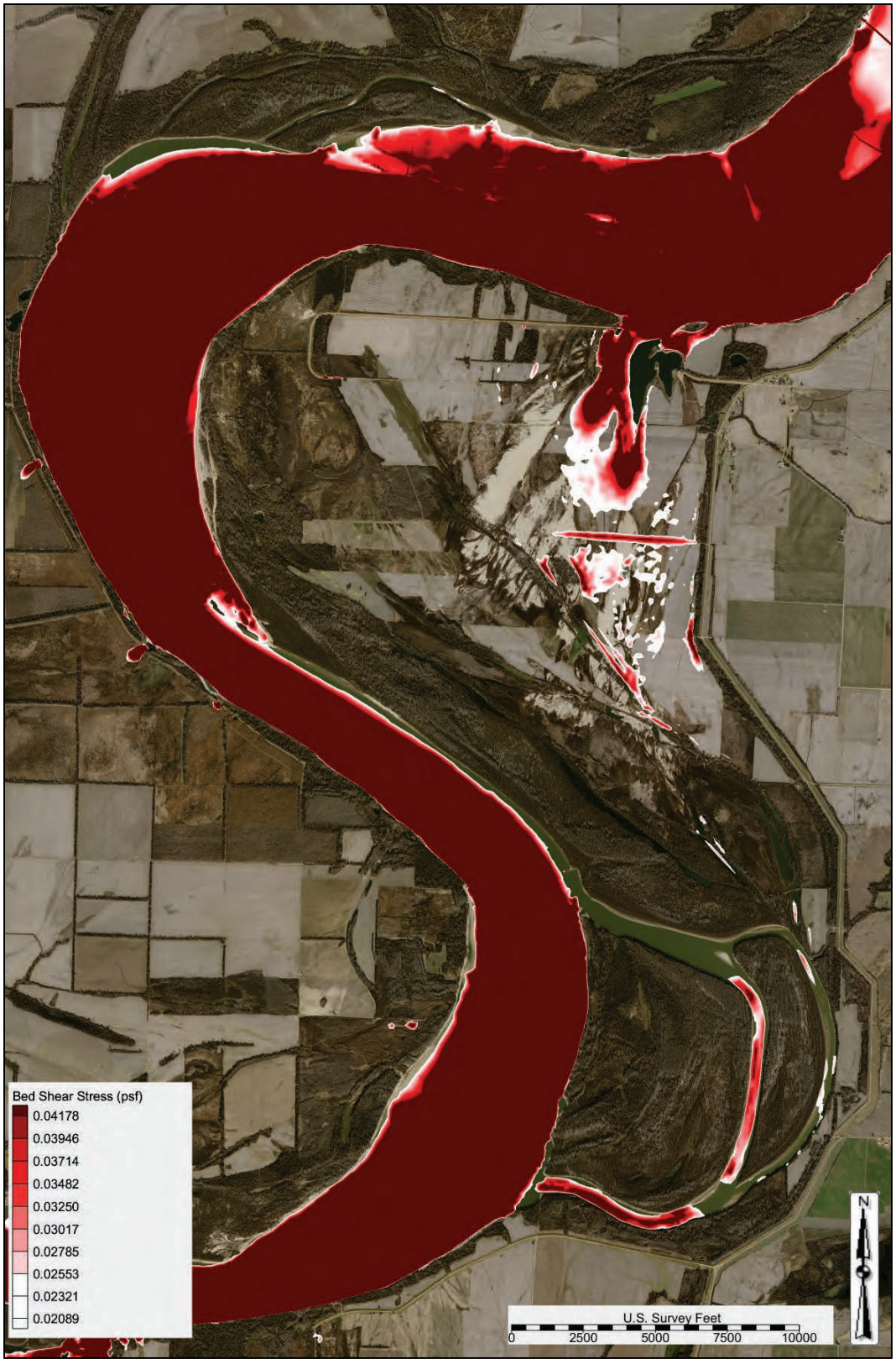


Figure C-227. Local Scour Countermeasure 2 shear stress—1,700,000 cfs (study overbank).

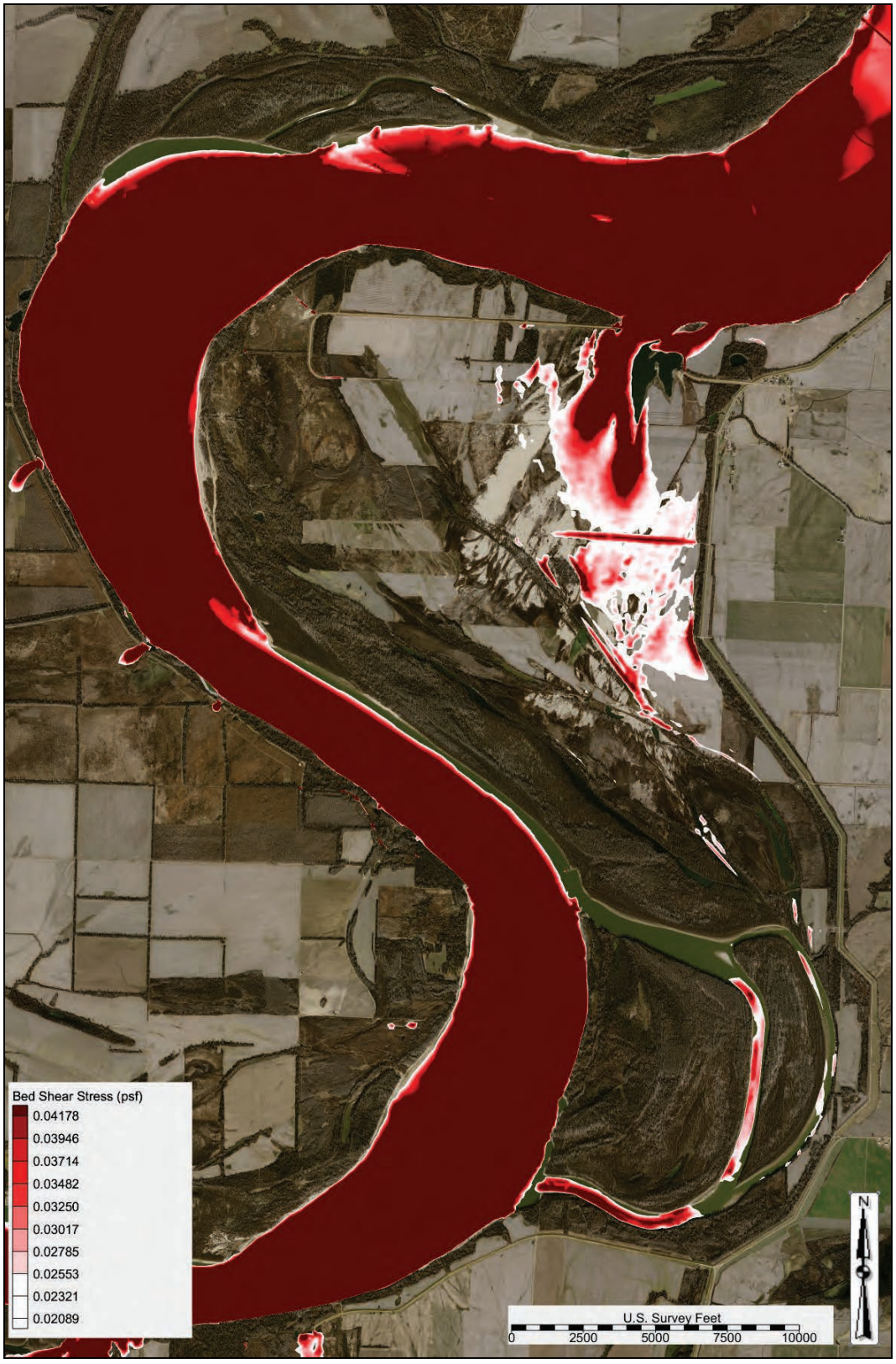


Figure C-228. Local Scour Countermeasure 2 shear stress—1,900,000 cfs (study overbank).

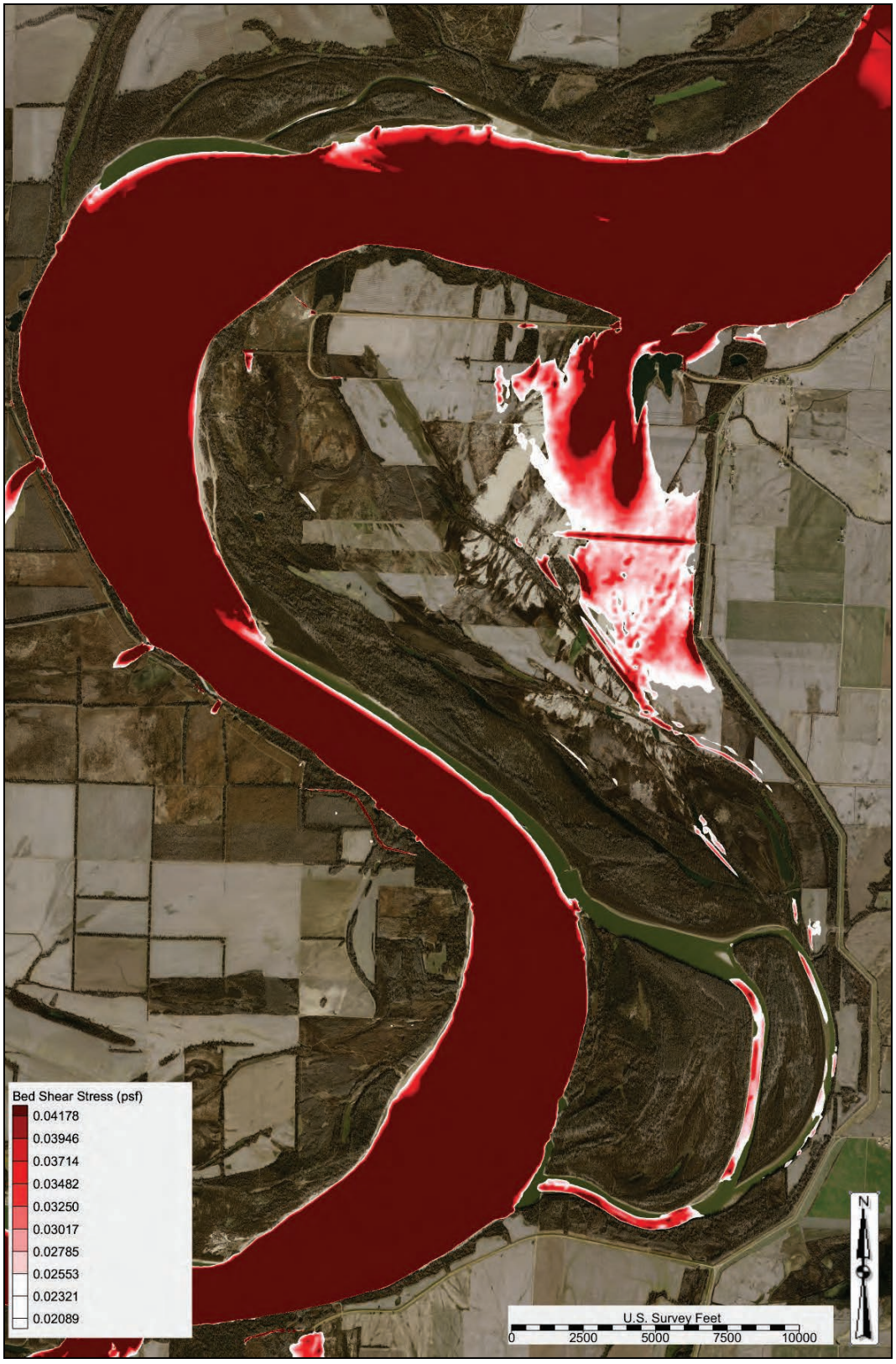
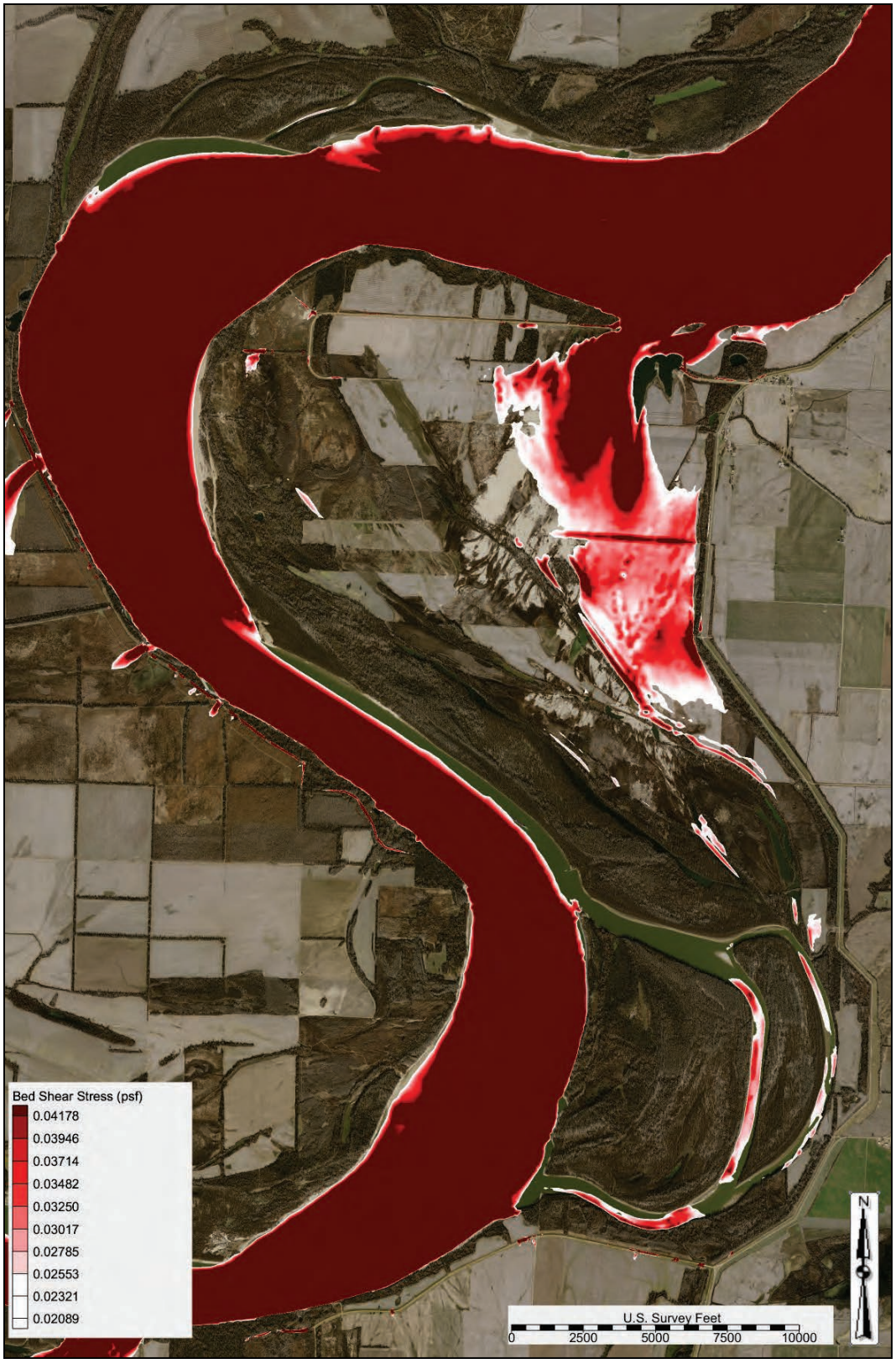


Figure C-229. Local Scour Countermeasure 2 shear stress—2,100,000 cfs (study overbank).



Shear stress difference comparison

The modeled shear stress difference plots compared to the base condition output for flows ranging from 900,000 to 2,100,000 cfs are depicted in Figures C-230 through C-236. A positive shear stress difference (+ value and red and orange) indicated an increased shear stress compared to the base condition. A negative shear stress difference (- value and blue) indicated a decreased shear stress compared to the base condition. A zero shear stress difference (zero value and white) indicated that the alternative had no change in shear stress.

Figure C-230. Local Scour Countermeasure 2 shear stress difference—900,000 cfs.

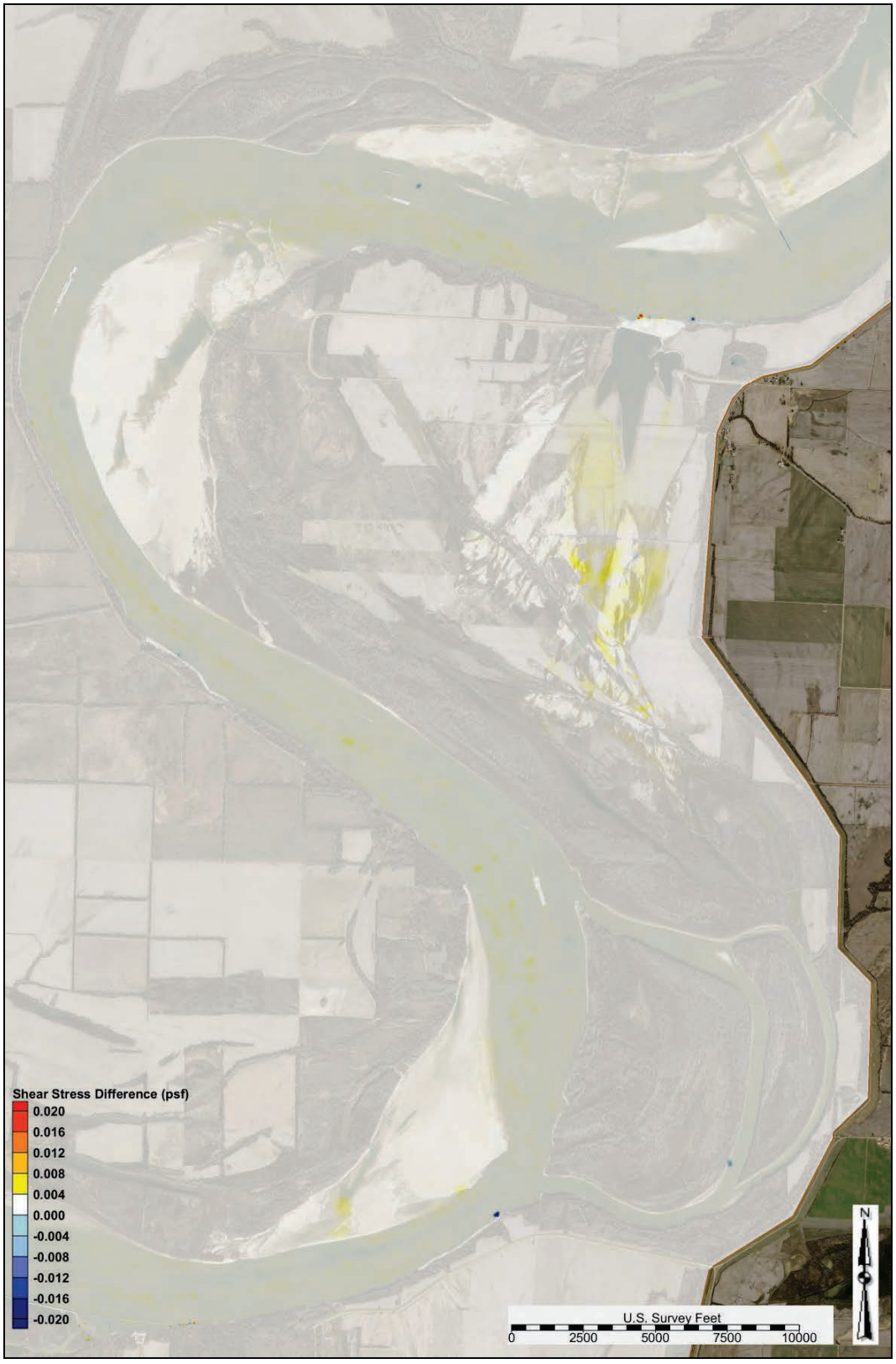


Figure C-231. Local Scour Countermeasure 2 shear stress difference—1,100,000 cfs.

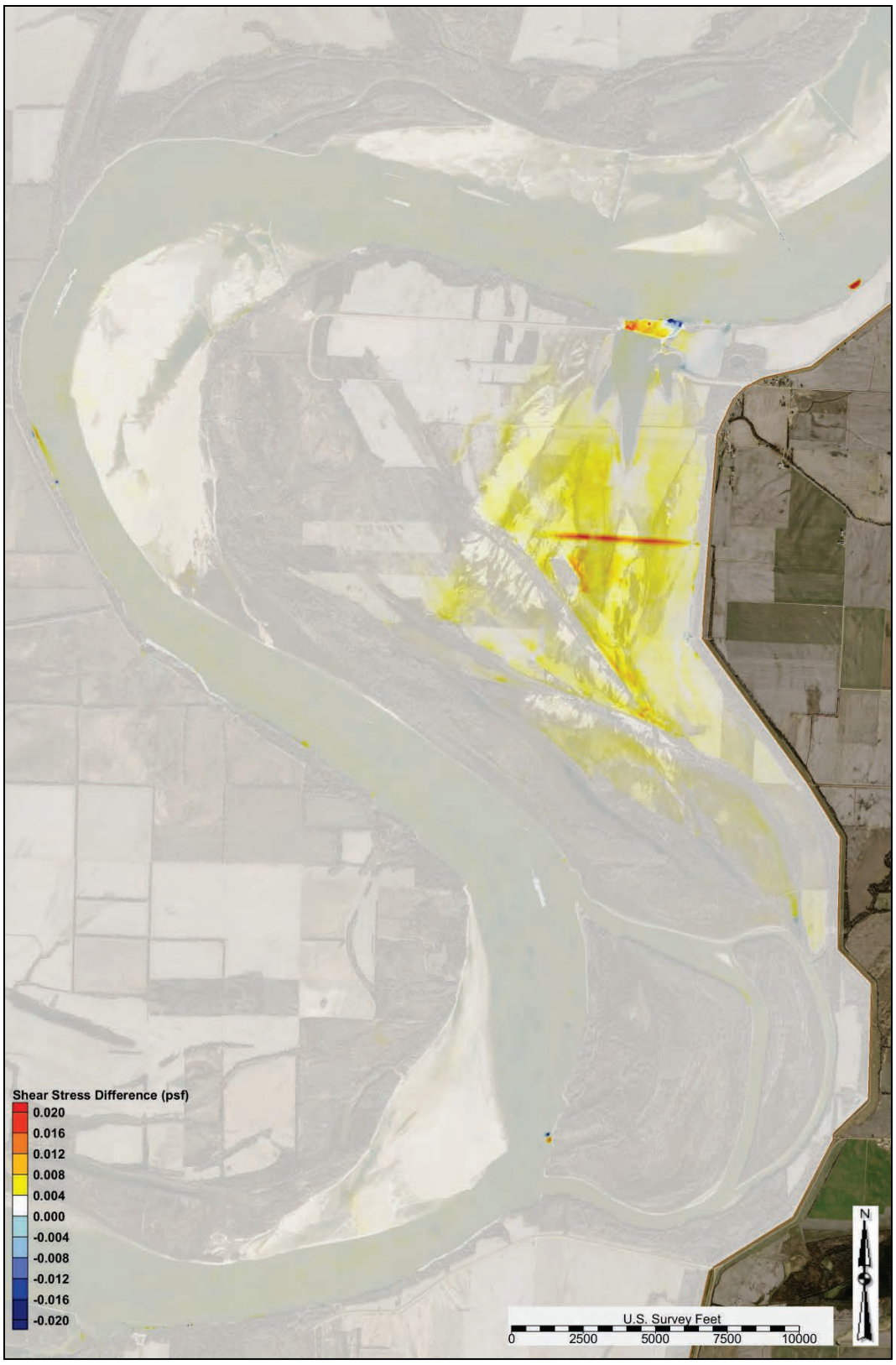


Figure C-232. Local Scour Countermeasure 2 shear stress difference—1,300,000 cfs.

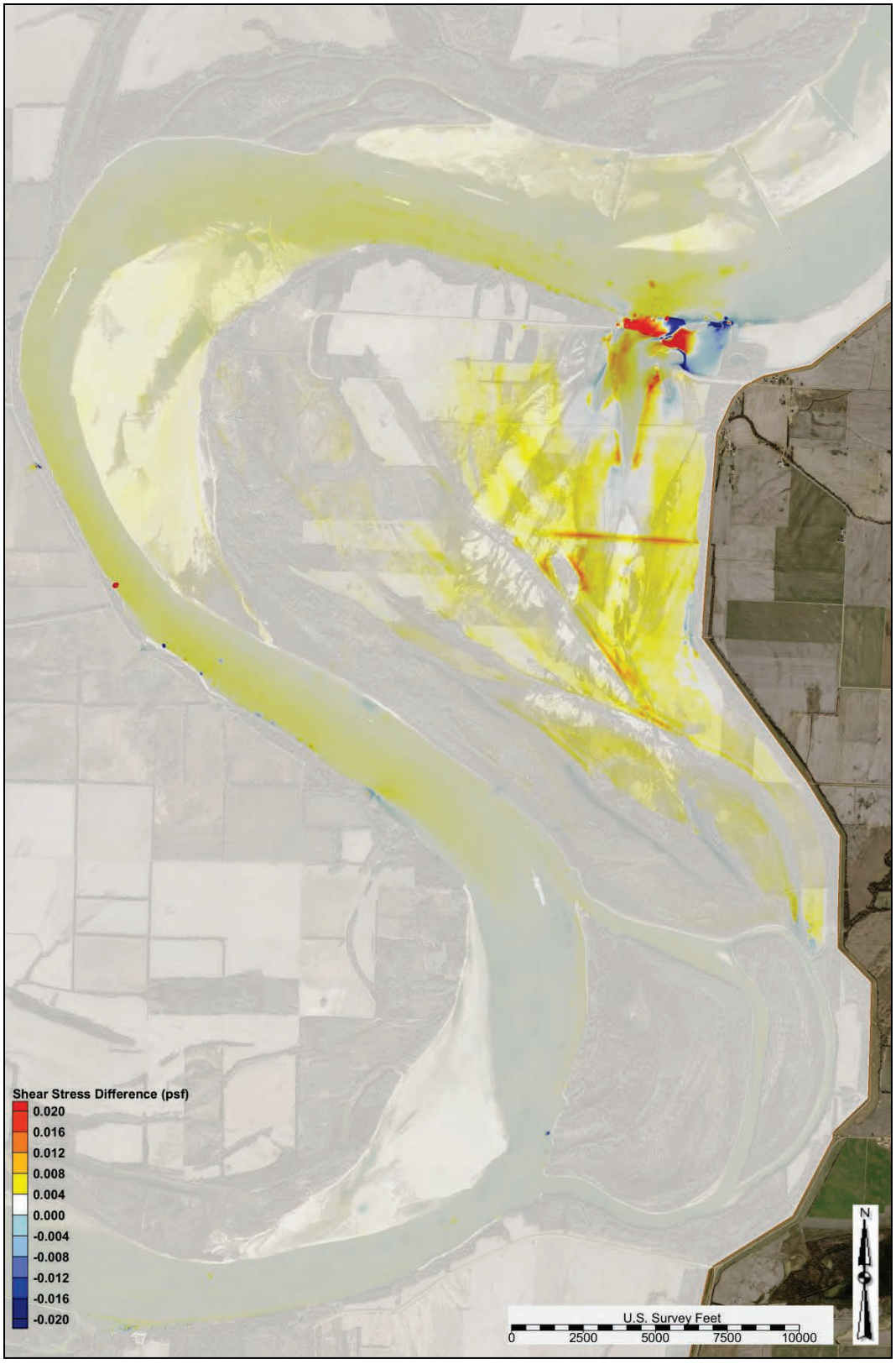


Figure C-233. Local Scour Countermeasure 2 shear stress difference—1,500,000 cfs.

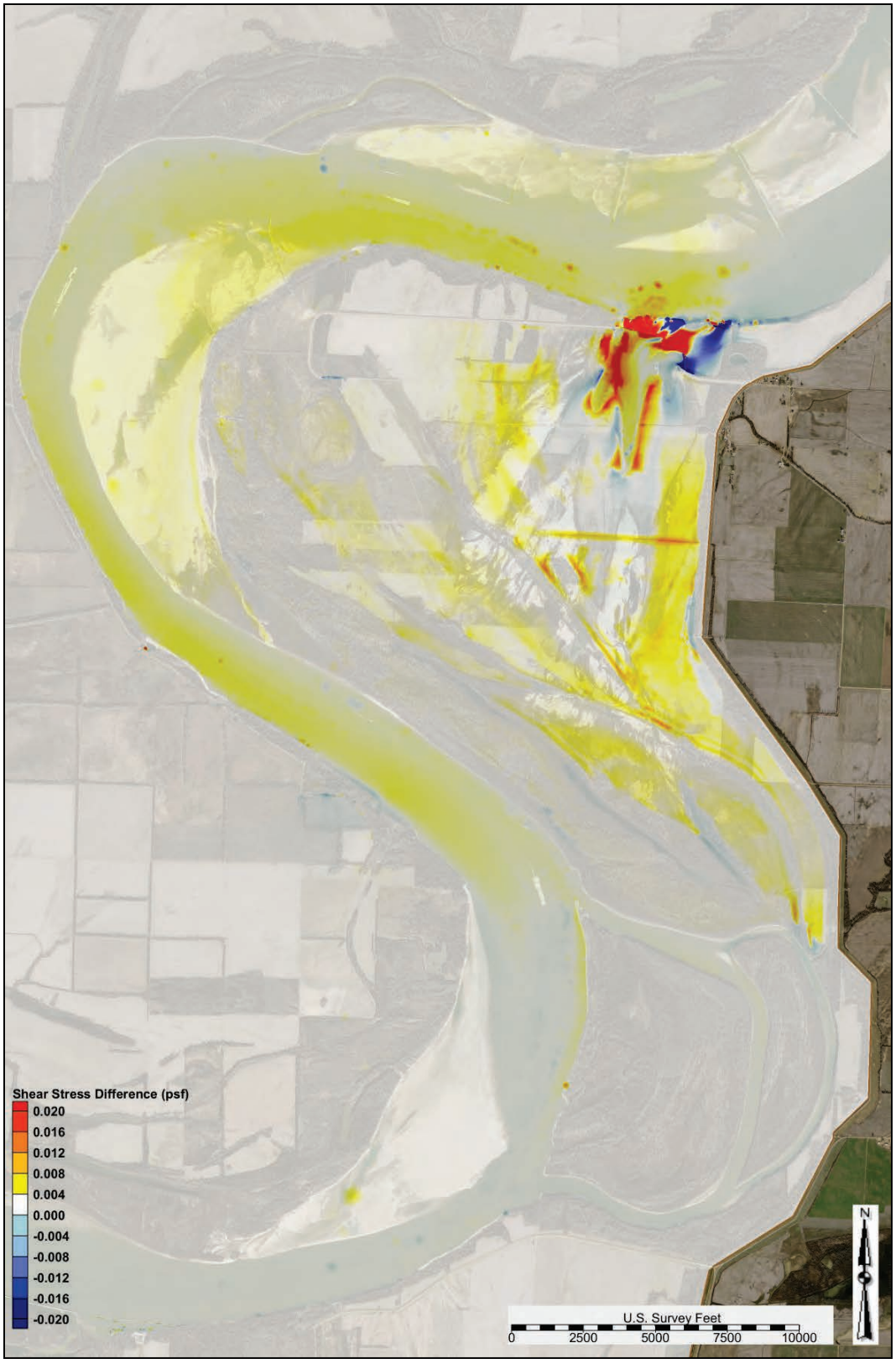


Figure C-234. Local Scour Countermeasure 2 shear stress difference—1,700,000 cfs.

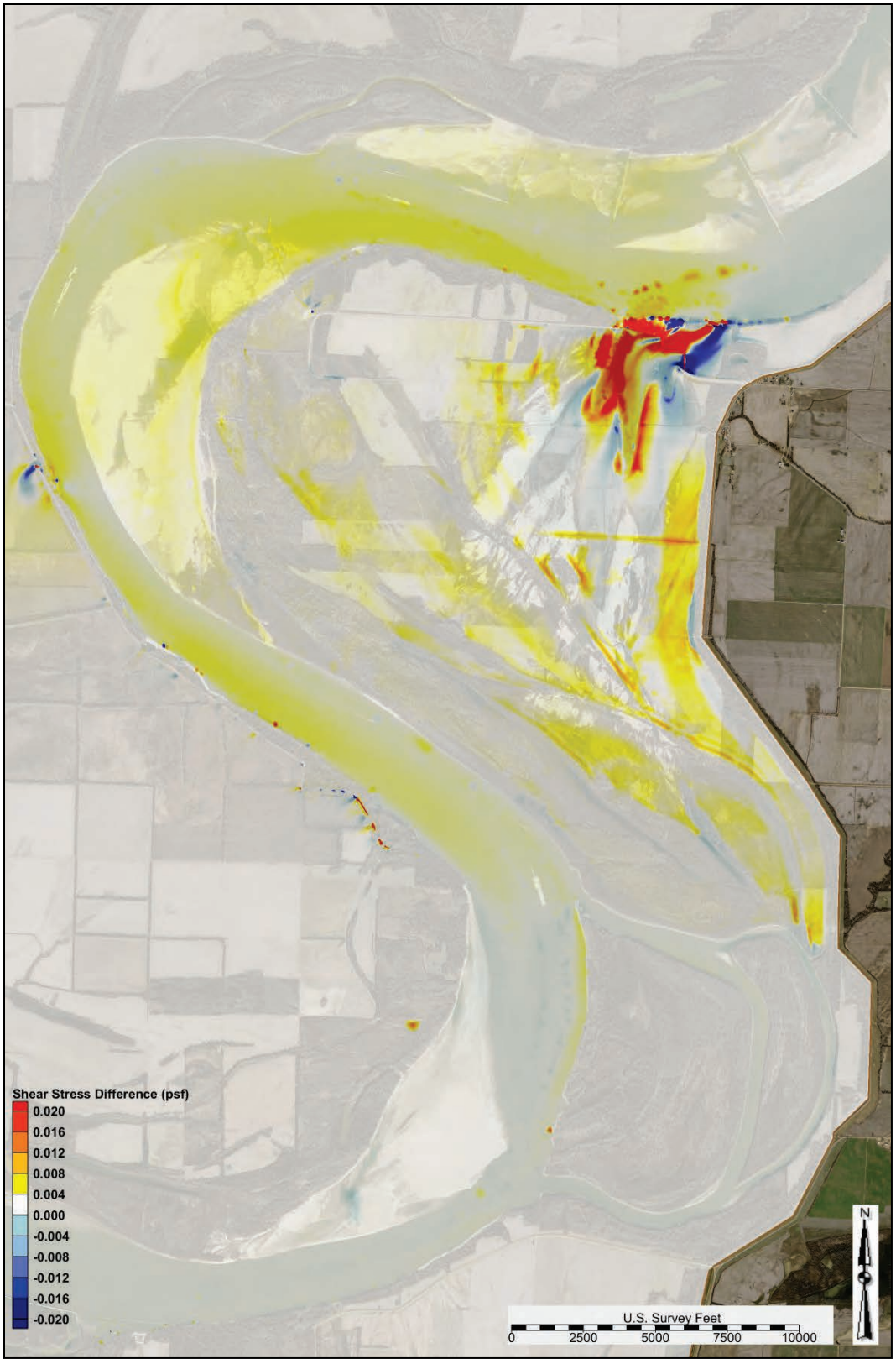


Figure C-235. Local Scour Countermeasure 2 shear stress difference—1,900,000 cfs.

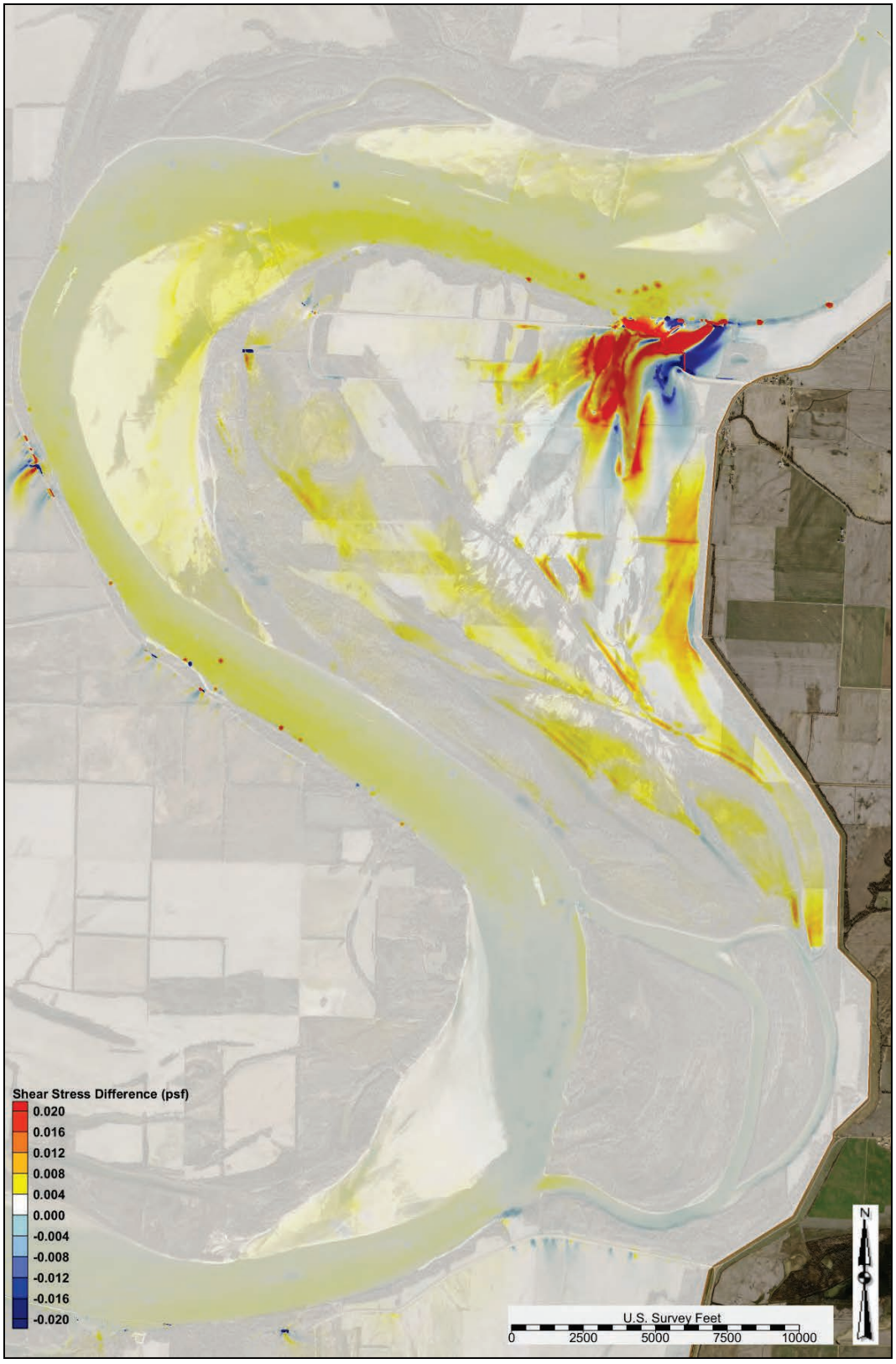
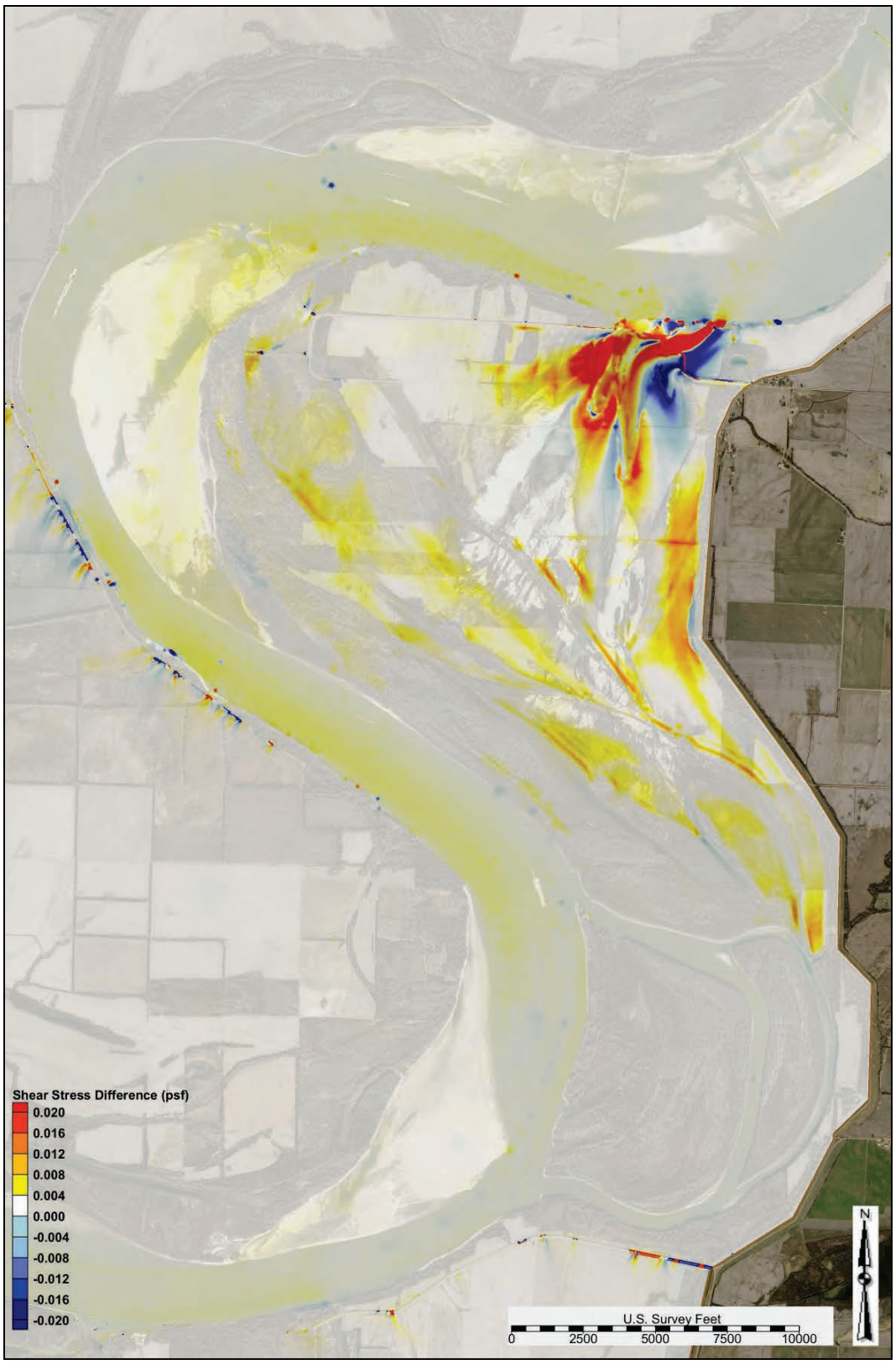


Figure C-236. Local Scour Countermeasure 2 shear stress difference—2,100,000 cfs.



WSEL

Figure C-237 depicts the water surface elevation profiles in the study reach for the following flows: 1,100,000 cfs, 1,500,000 cfs, 1,900,000 cfs, and 2,100,000 cfs.

Sediment diversion grain size distribution

Table C-10 lists the sediment diversion grain size distribution for flows ranging from 870,000 cfs to 2,000,000 cfs.

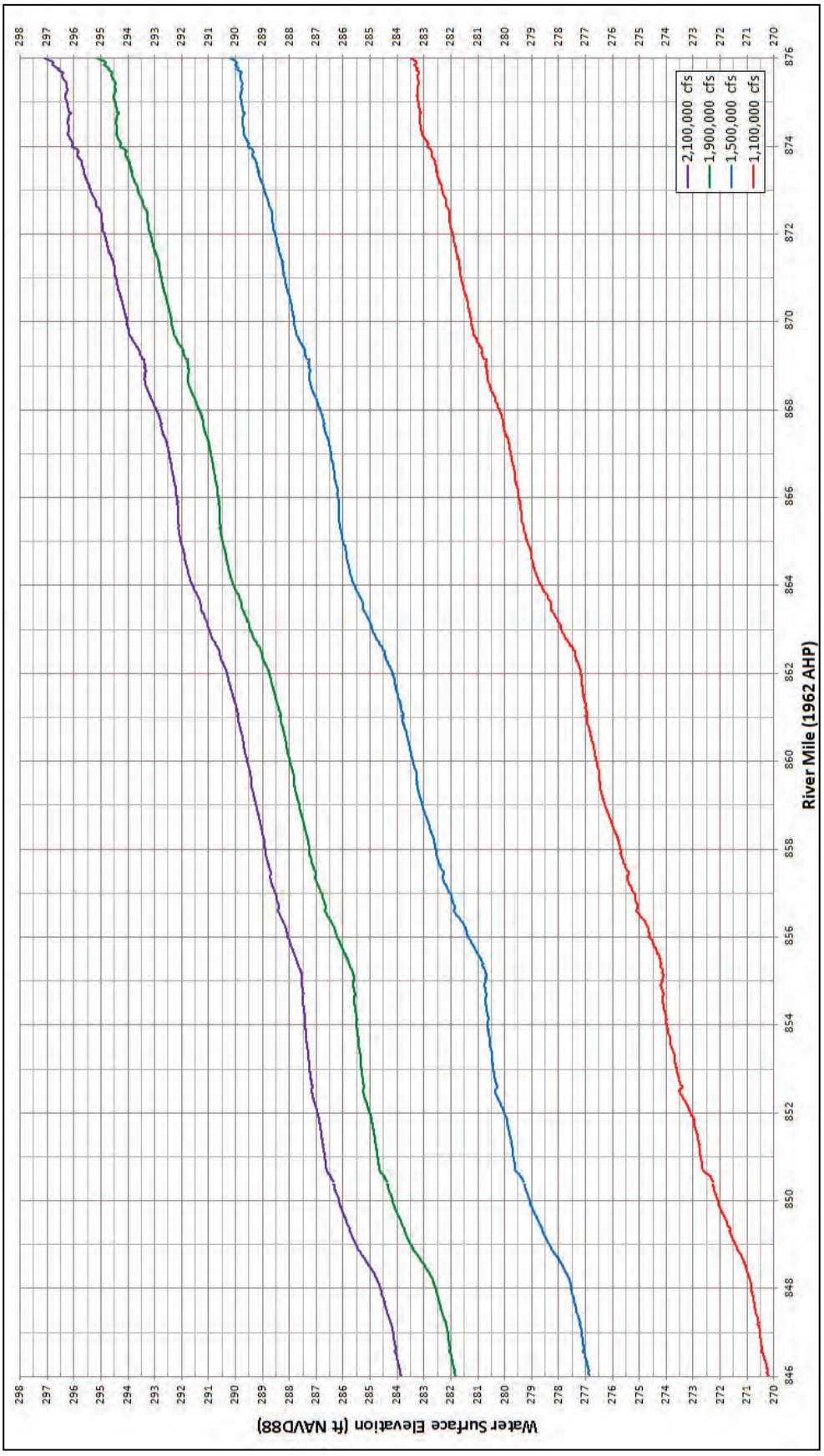


Figure C-237. Local Scour Countermeasure 2 WSEL profile.

Table C-10. Local Scour Countermeasure 2 diversion grain size distribution.

Main Channel Flow US of Crevasse (cfs)	Total Diversion Load Grain Size Fraction Distribution									
	Coarse Silt	Very Fine Sand	Fine Sand	Medium Sand	Coarse Sand	Very Coarse Sand	Very Fine Pebble	Fine Pebble	Medium Pebble	Coarse Pebble
870,000	0.0000	0.9513	0.0482	0.0005	0.0000	0.0000	0.0000	0.0000	0.0000	0.0000
900,000	0.0000	0.8959	0.1024	0.0017	0.0000	0.0000	0.0000	0.0000	0.0000	0.0000
1,000,000	0.0000	0.4112	0.4316	0.1232	0.0279	0.0062	0.0000	0.0000	0.0000	0.0000
1,100,000	0.0000	0.2146	0.4010	0.2533	0.1086	0.0218	0.0005	0.0001	0.0001	0.0000
1,200,000	0.0000	0.1376	0.3350	0.3239	0.1576	0.0381	0.0057	0.0014	0.0006	0.0001
1,300,000	0.0000	0.1044	0.2750	0.3589	0.2052	0.0477	0.0033	0.0038	0.0015	0.0002
1,400,000	0.0000	0.0925	0.2464	0.3667	0.2285	0.0574	0.0033	0.0023	0.0027	0.0003
1,500,000	0.0000	0.0853	0.2365	0.3651	0.2424	0.0591	0.0041	0.0019	0.0050	0.0006
1,600,000	0.0000	0.0777	0.2294	0.3710	0.2456	0.0615	0.0066	0.0024	0.0047	0.0012
1,700,000	0.0000	0.0704	0.2193	0.3795	0.2523	0.0610	0.0088	0.0032	0.0036	0.0017
1,800,000	0.0000	0.0667	0.2140	0.3845	0.2556	0.0616	0.0077	0.0043	0.0035	0.0021
1,900,000	0.0000	0.0639	0.2108	0.3886	0.2572	0.0615	0.0073	0.0043	0.0039	0.0026
2,000,000	0.0000	0.0584	0.1977	0.4364	0.2401	0.0595	0.0032	0.0015	0.0019	0.0013
2,100,000	0.0000	0.0559	0.1965	0.3686	0.2856	0.0668	0.0113	0.0048	0.0061	0.0045

Local scour countermeasures compared to base condition

WSEL

Figures C-238 through C-241 depict the water surface elevation profiles compared to the base condition for the following flows: 1,100,000 cfs, 1,500,000 cfs, 1,900,000 cfs, and 2,100,000 cfs.

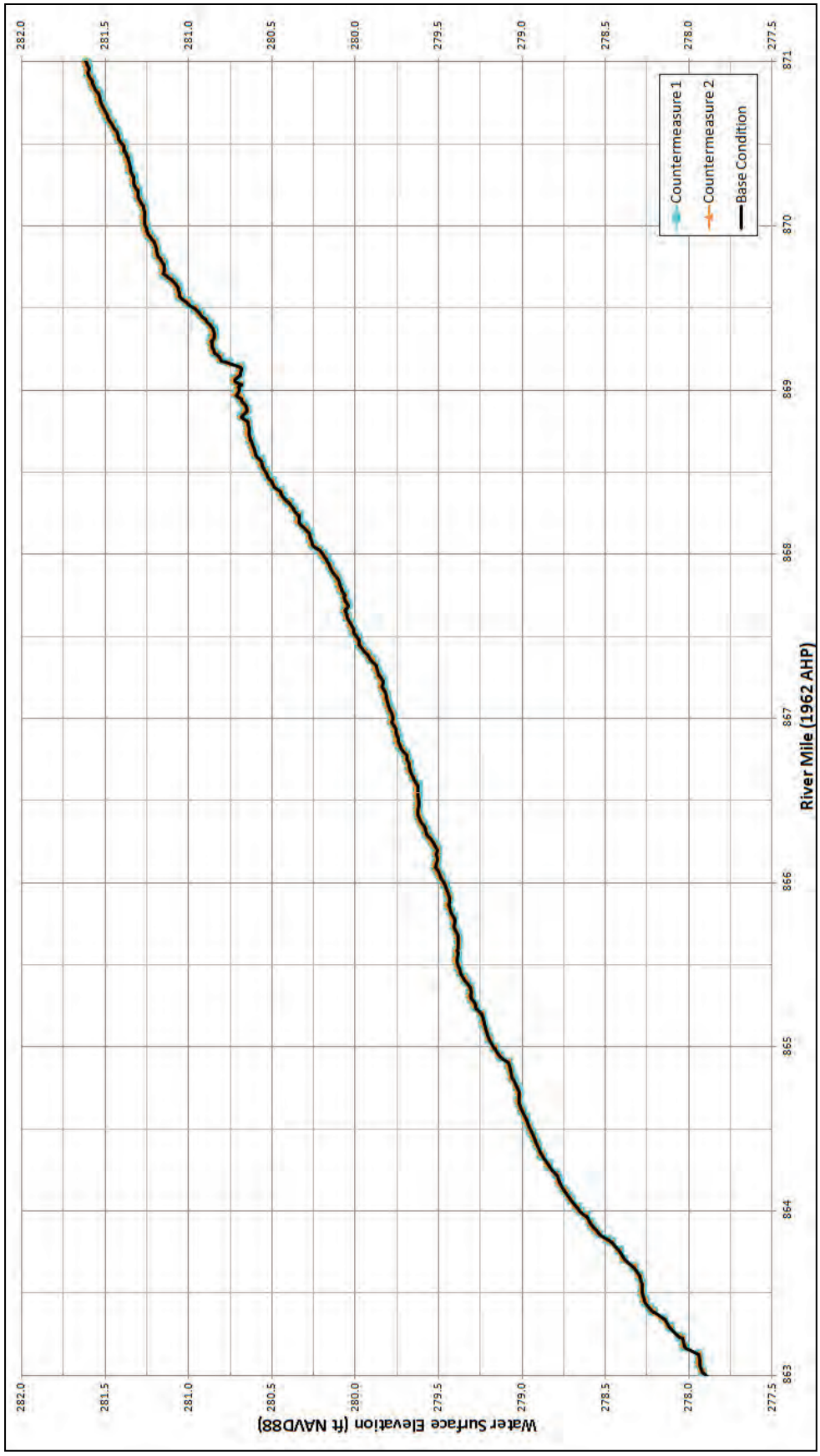


Figure C-238. Local scour countermeasures vs. base condition WSEL profile 1,100,000 cfs.

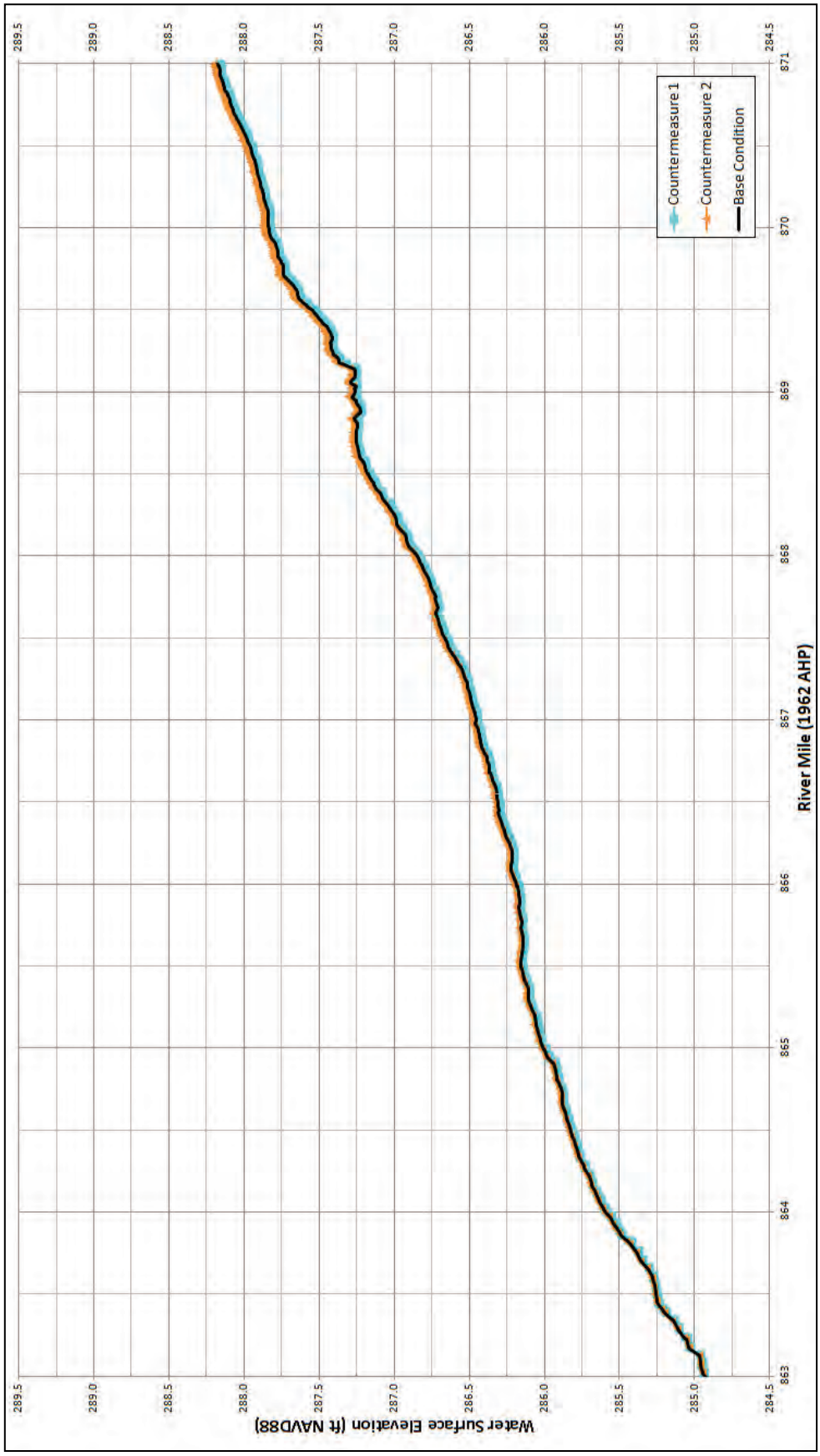


Figure C-239. Local scour countermeasures vs. base condition WSEL profile 1,500,000 cfs.

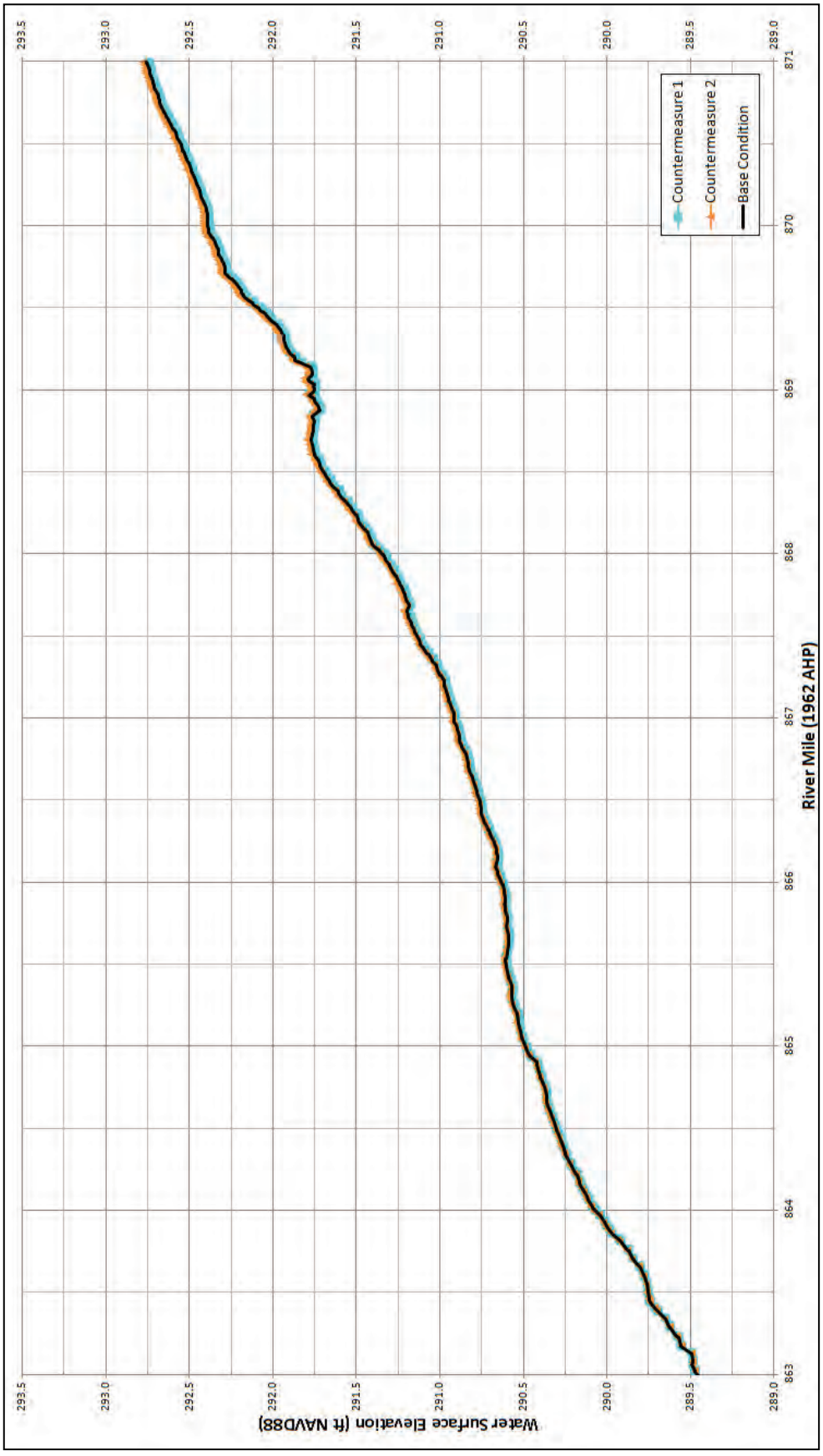


Figure C-240. Local scour countermeasures vs. base condition WSEL profile 1,900,000 cfs.

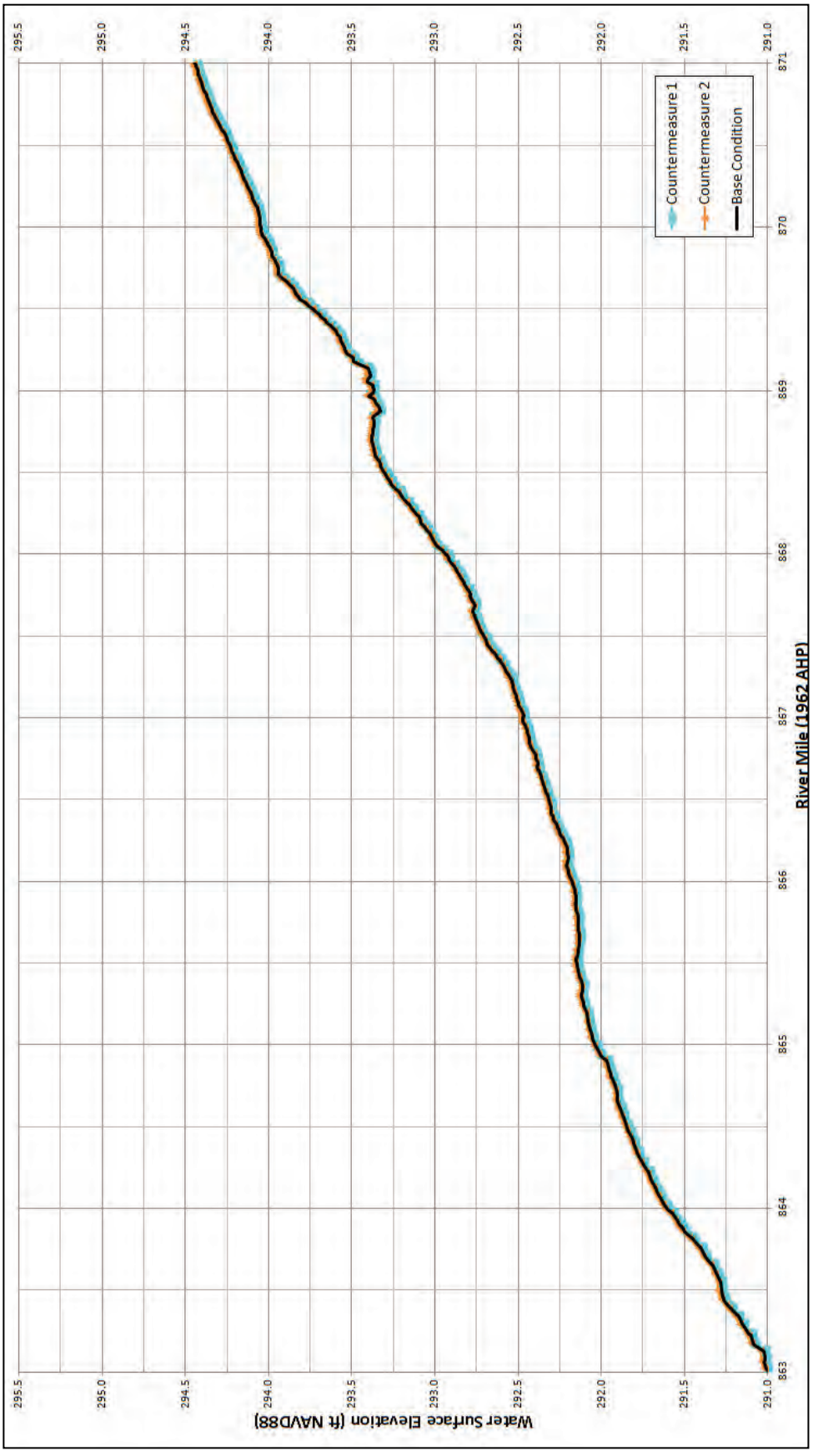


Figure C-241. Local scour countermeasures vs. base condition WSEL profile 2,100,000 cfs.

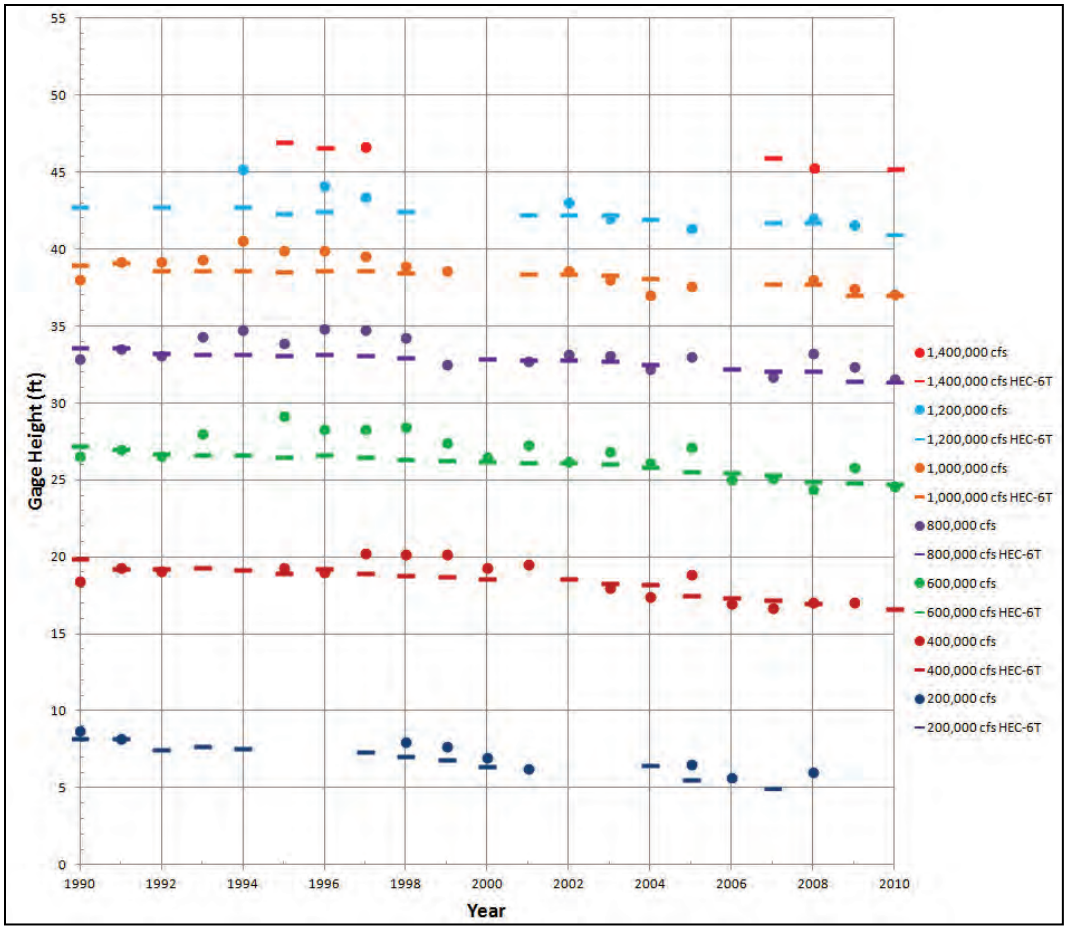
Appendix D: 1D Modeling Analysis

Appendix D contains detailed HEC-6T model output and analysis.

Sediment calibration

Figure D-1 depicts the HEC-6T index flow vs. specific gage plot at Hickman, KY. Figures D-2 through D-13 depict the calibration and validation cross-section analysis at four model locations (RM 846.40, RM 856.99, RM 864.76, and RM 870.2) for 1993, 2004, and 2010.

Figure D-1. HEC-6T index flow and Hickman, KY, specific gage plot.



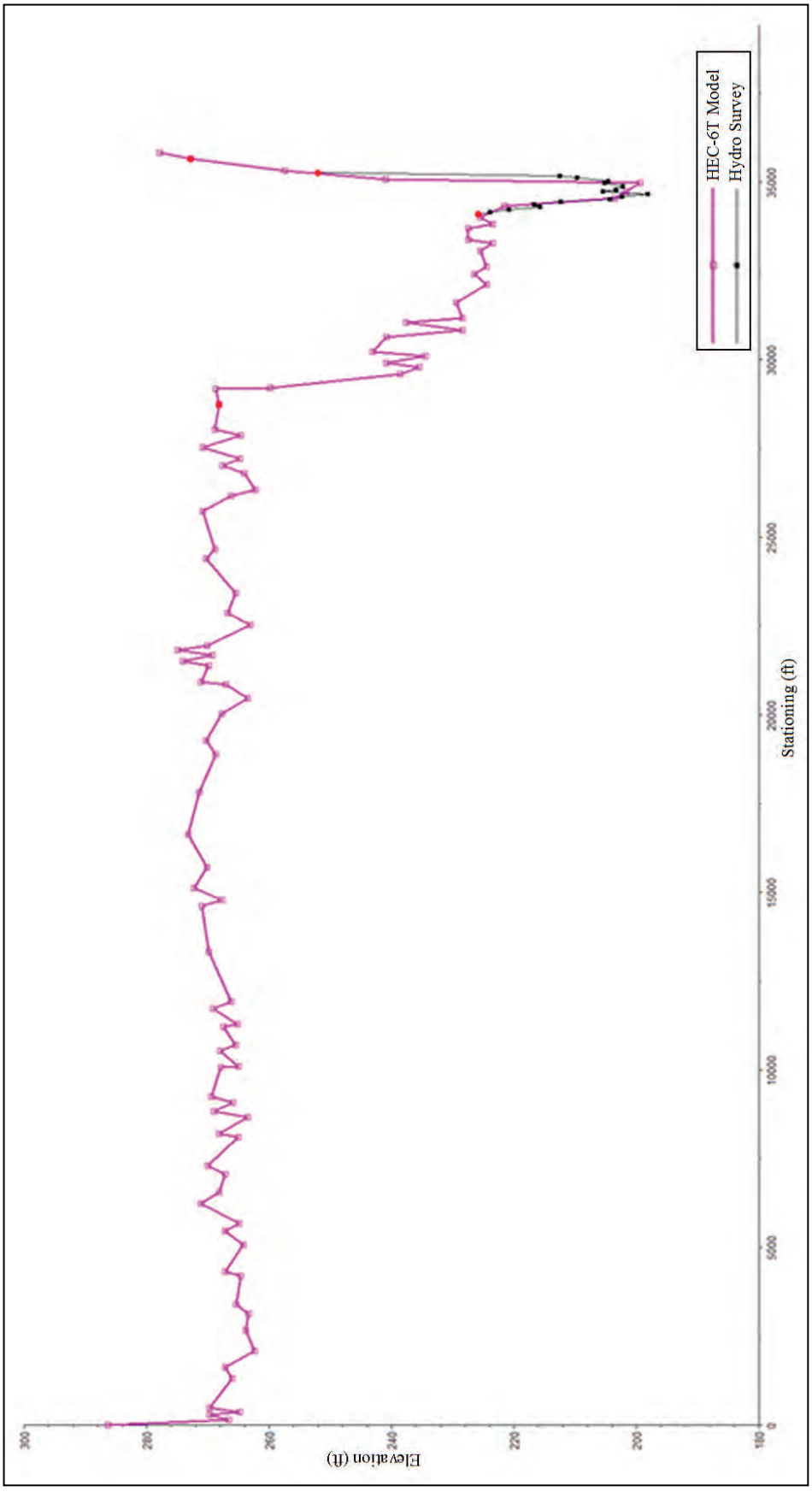


Figure D-2. HEC-6T 1993 sediment calibration at RM 846.40.

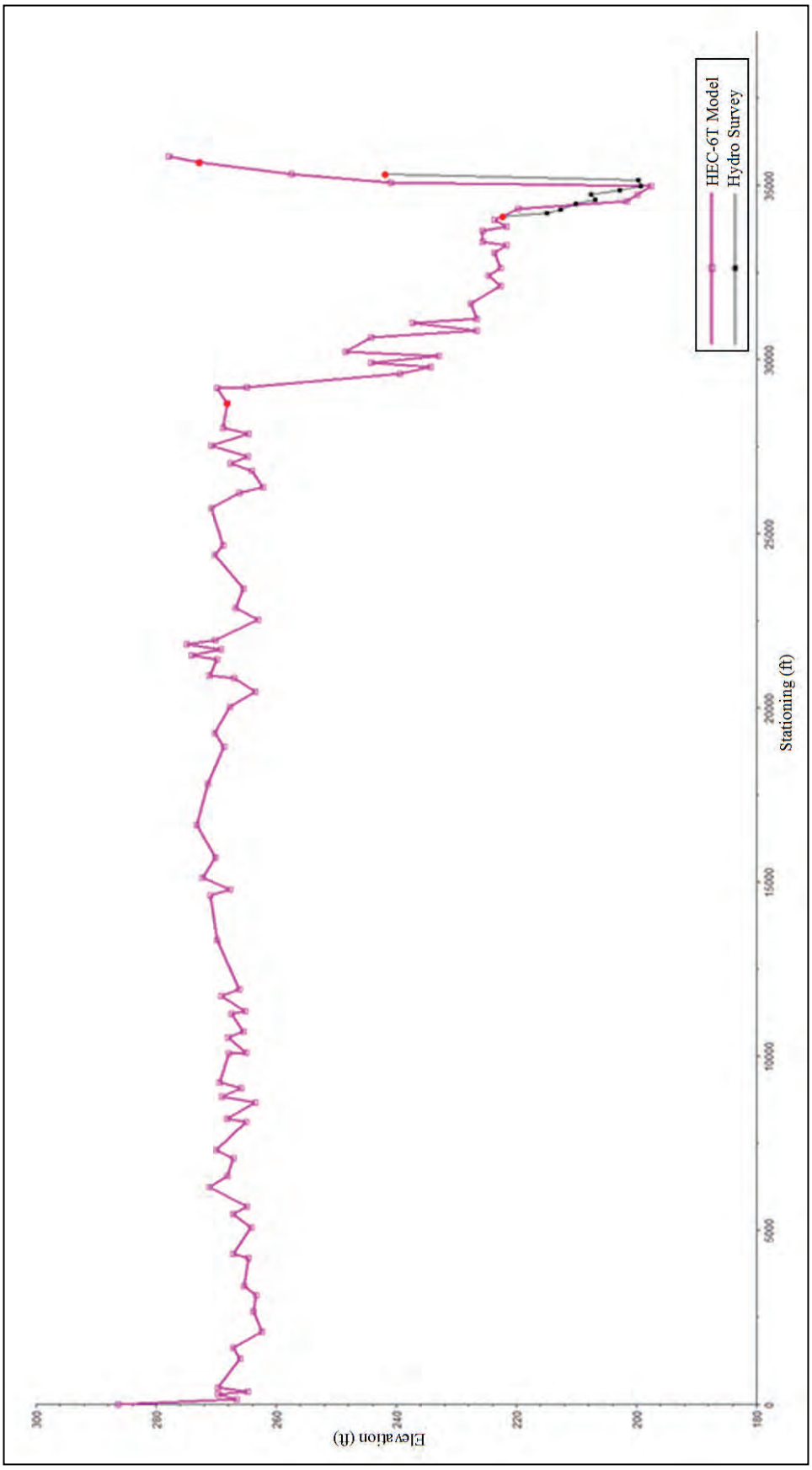


Figure D-3. HEC-6T 2004 sediment calibration at RM 846.40.

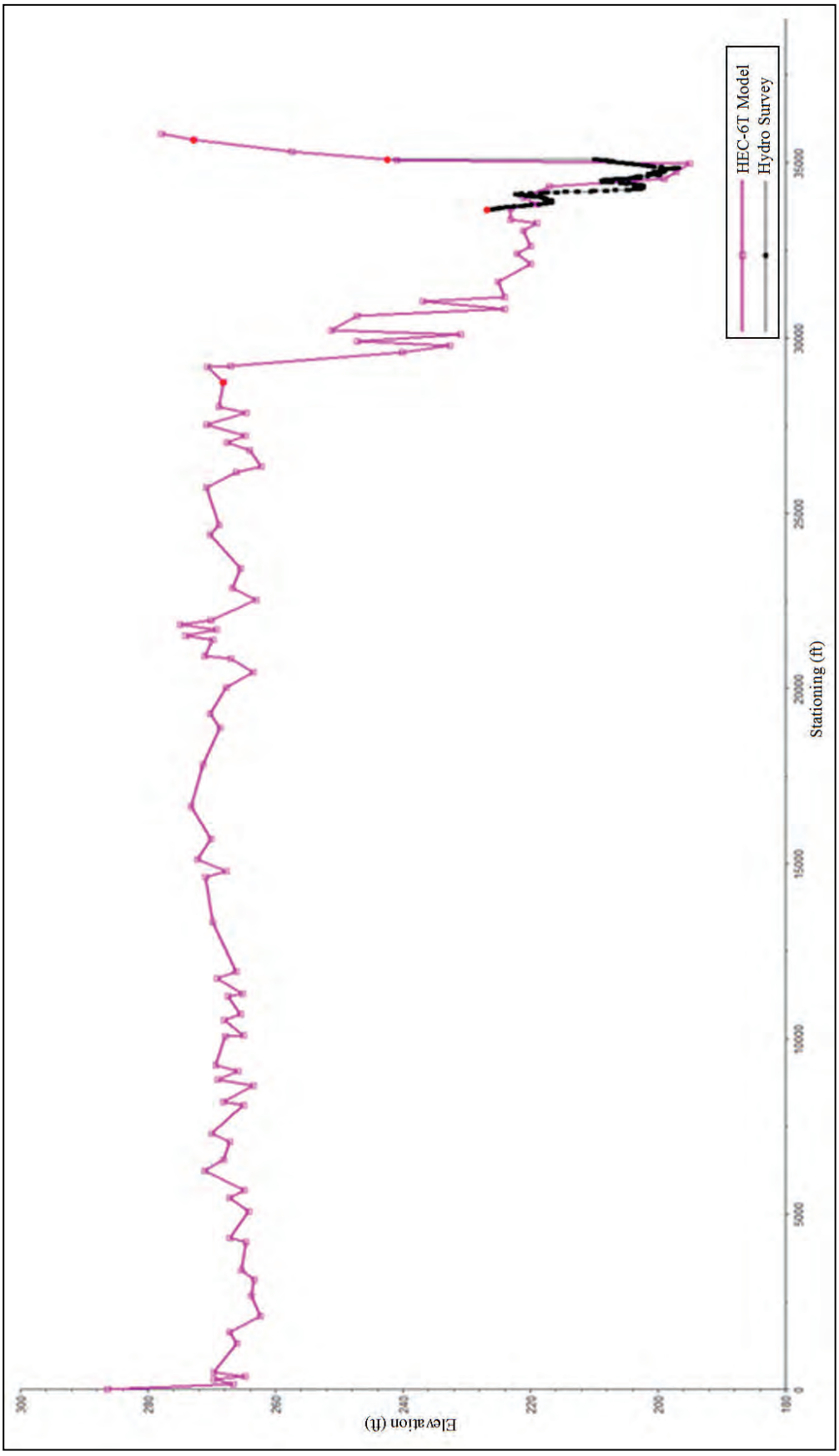


Figure D-4. HEC-6T 2010 sediment validation at RM 846.40.

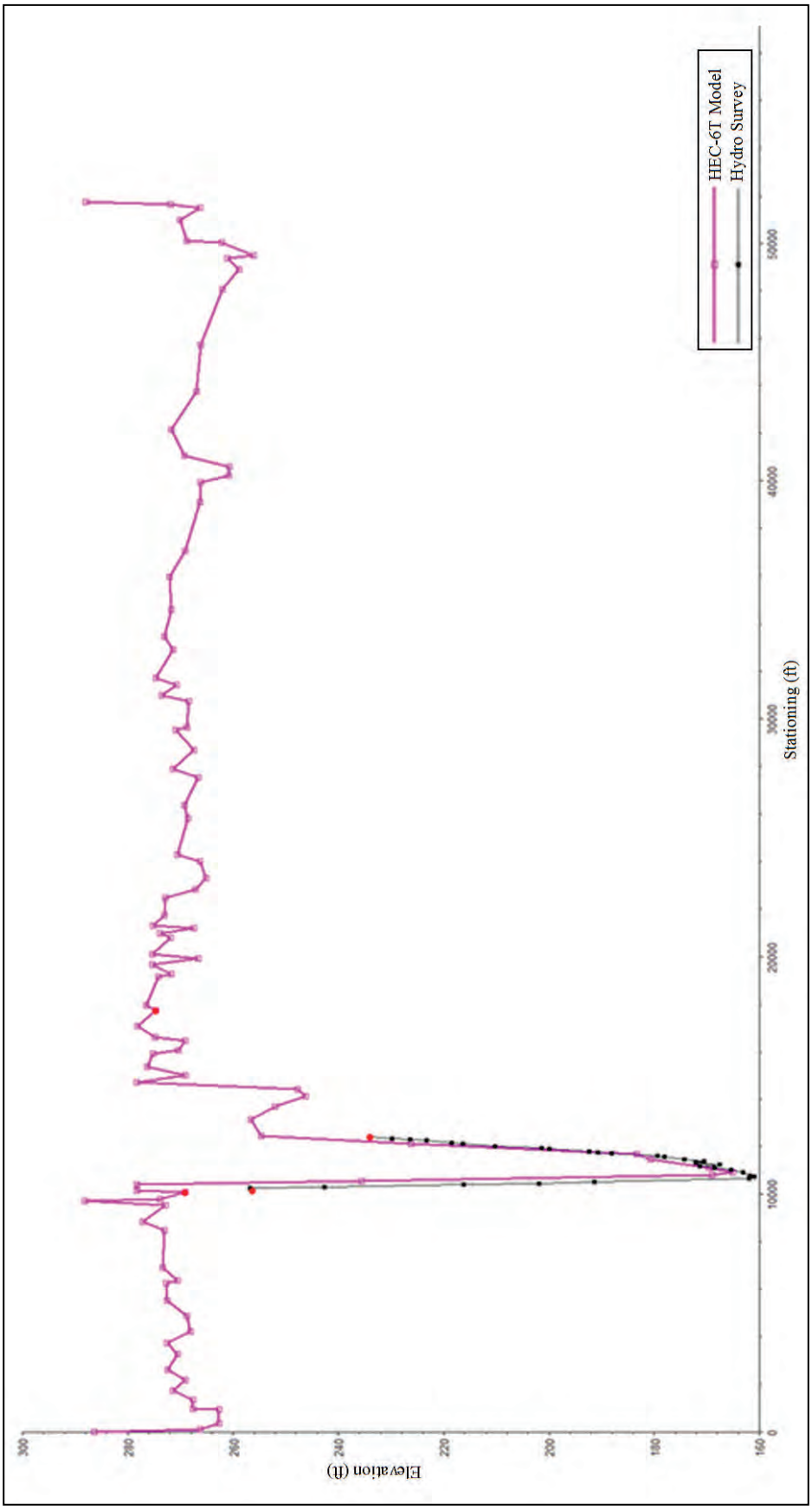


Figure D-5. HEC-6T 1993 sediment calibration at RM 856.99.

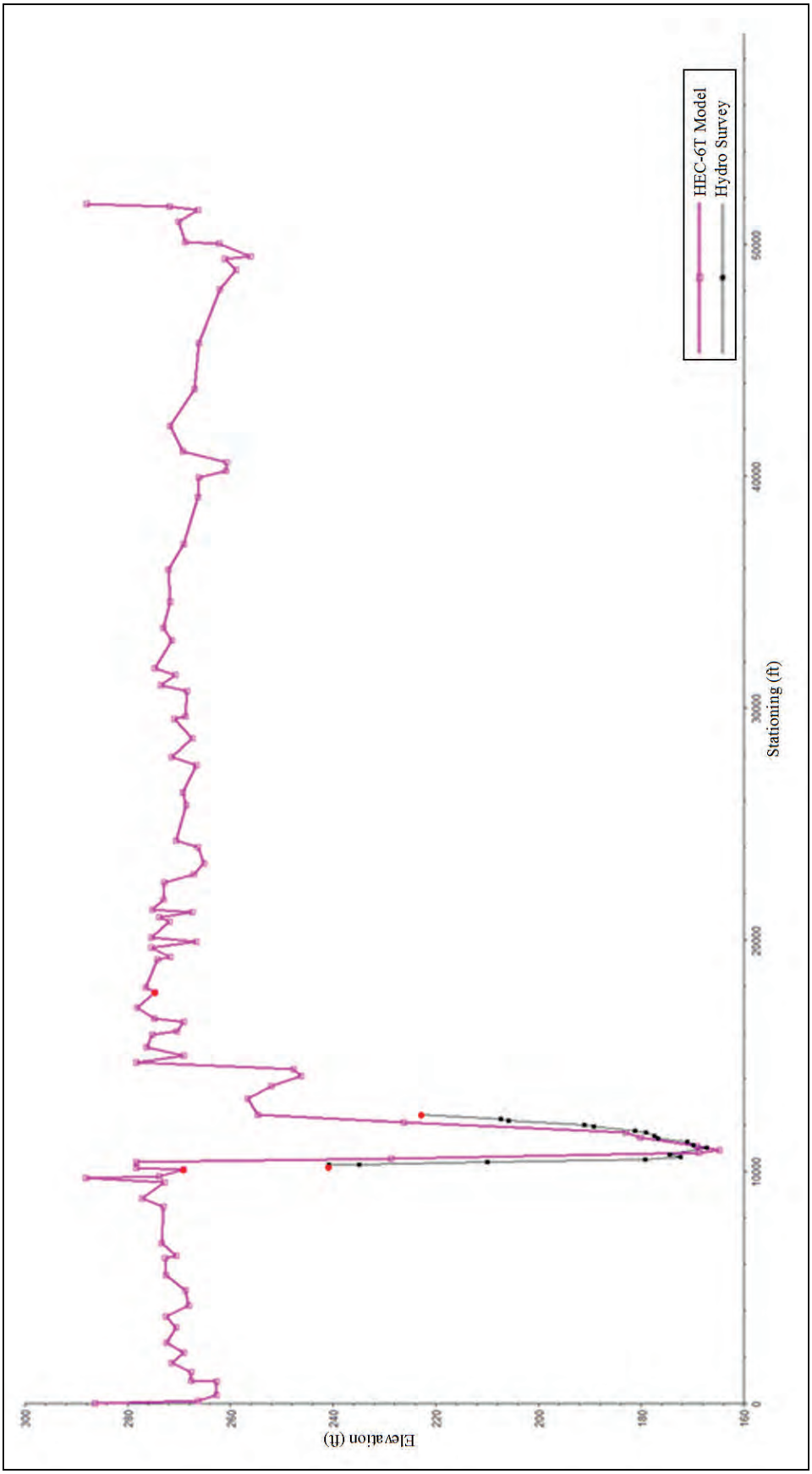


Figure D-6. HEC-6T 2004 sediment calibration at RM 856.99.

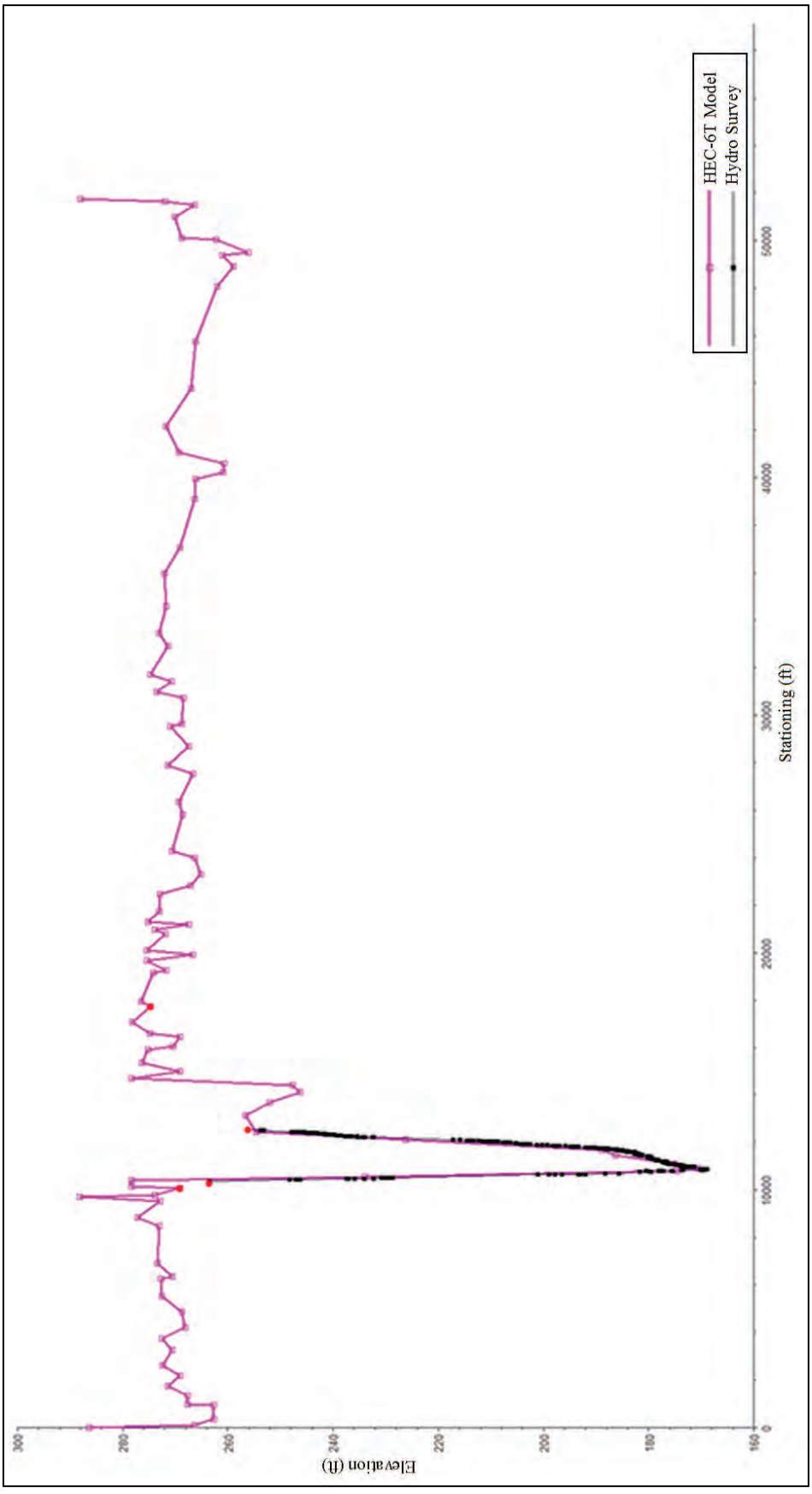


Figure D-7. HEC-6T 2010 sediment validation at RM 856.99.

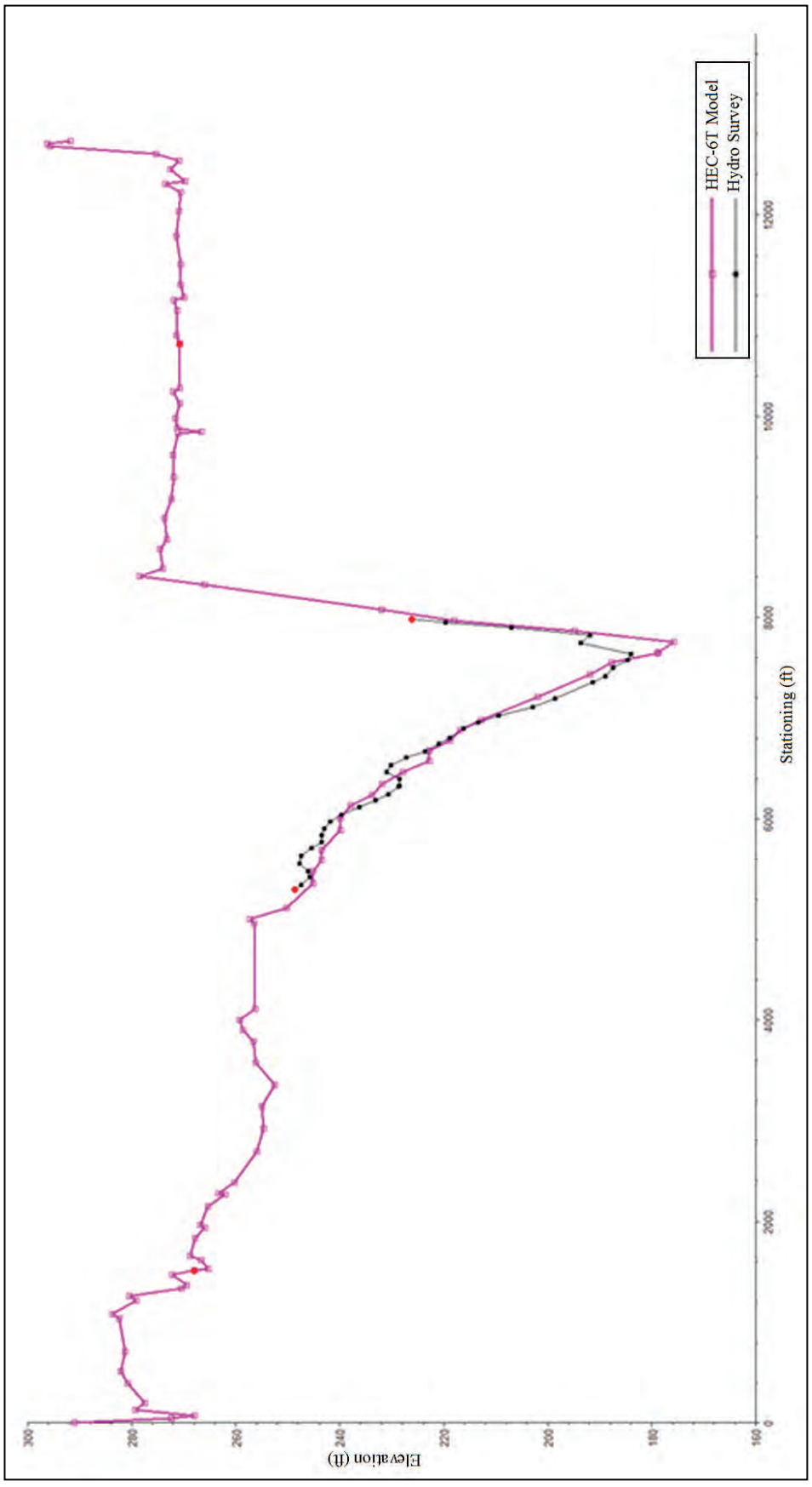


Figure D-8. HEC-6T 1993 sediment calibration at RM 864.76.

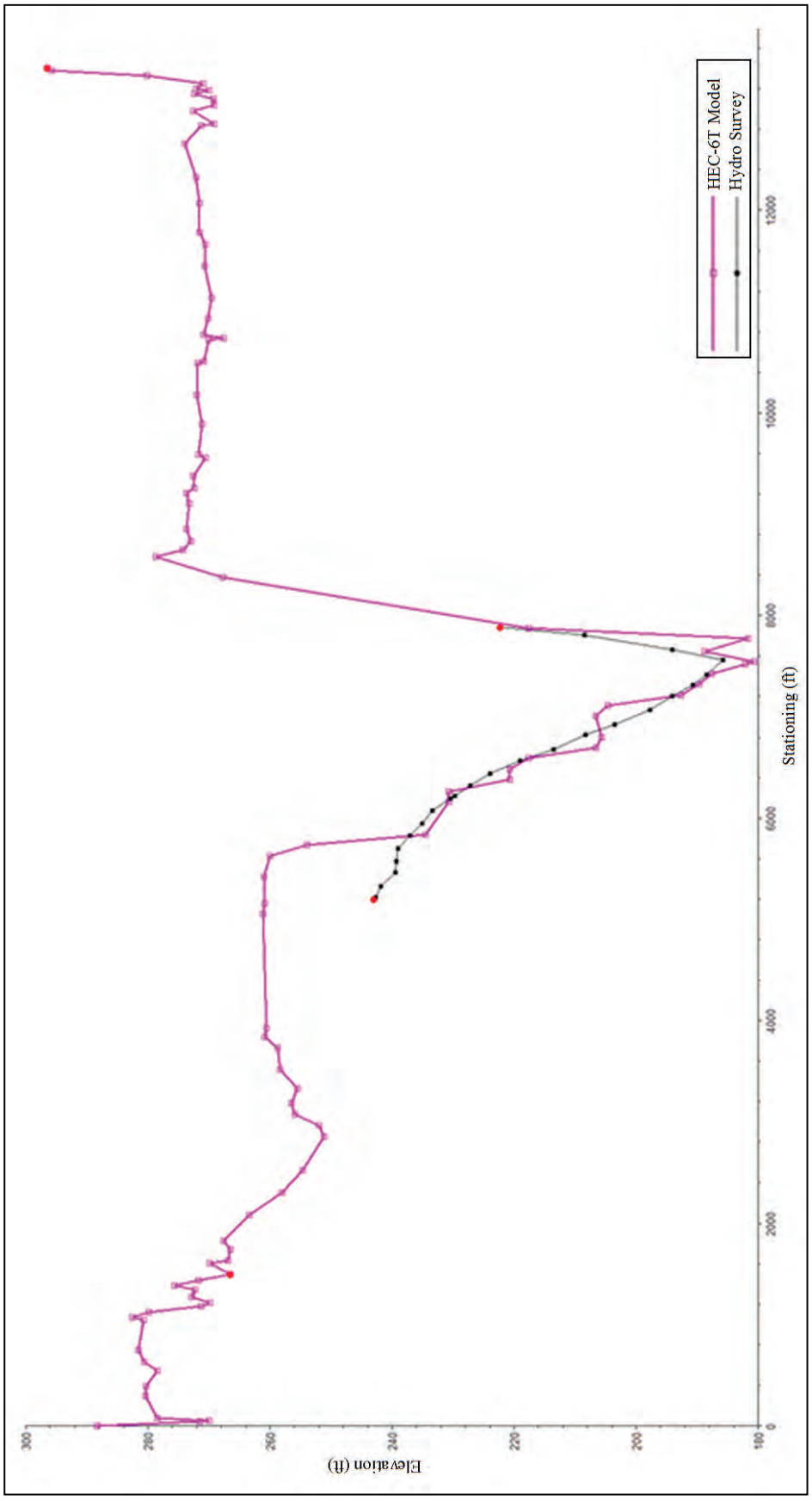


Figure D-9. HEC-6T 2004 sediment calibration at RM 864.76.

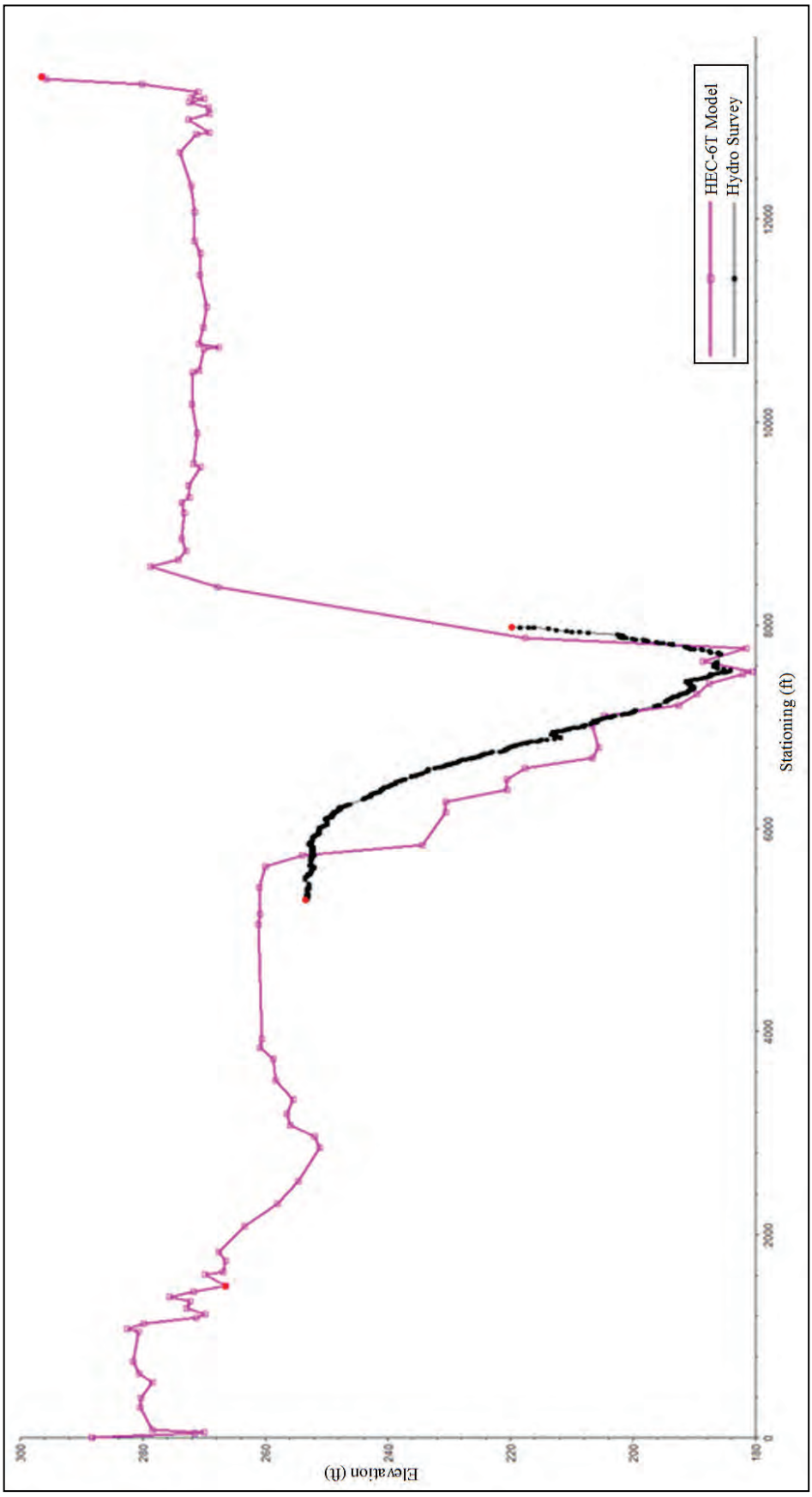


Figure D-10. HEC-6T 2010 sediment validation at RM 864.76.

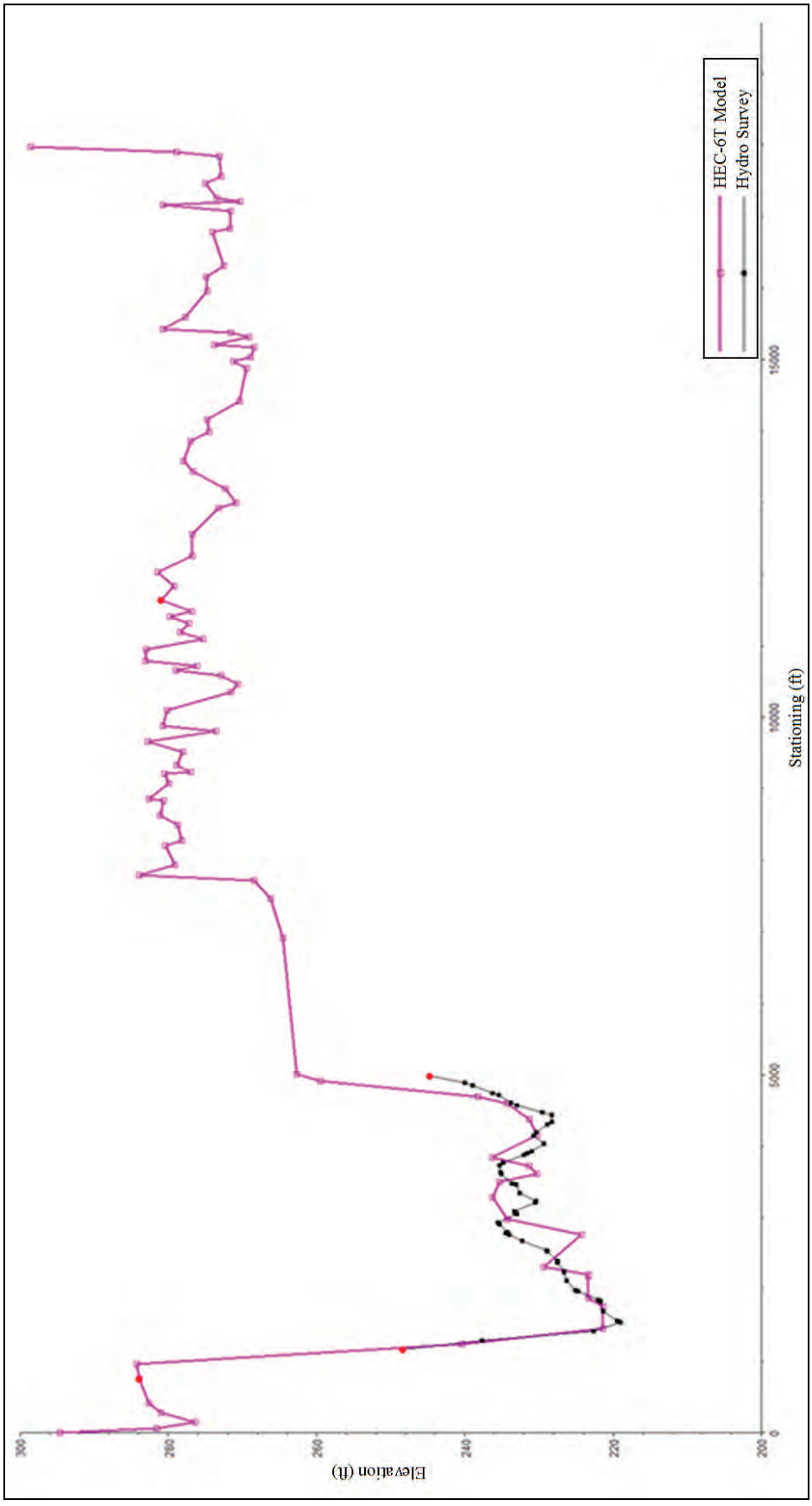


Figure D-11. HEC-6T 1993 sediment calibration at RM 870.20.

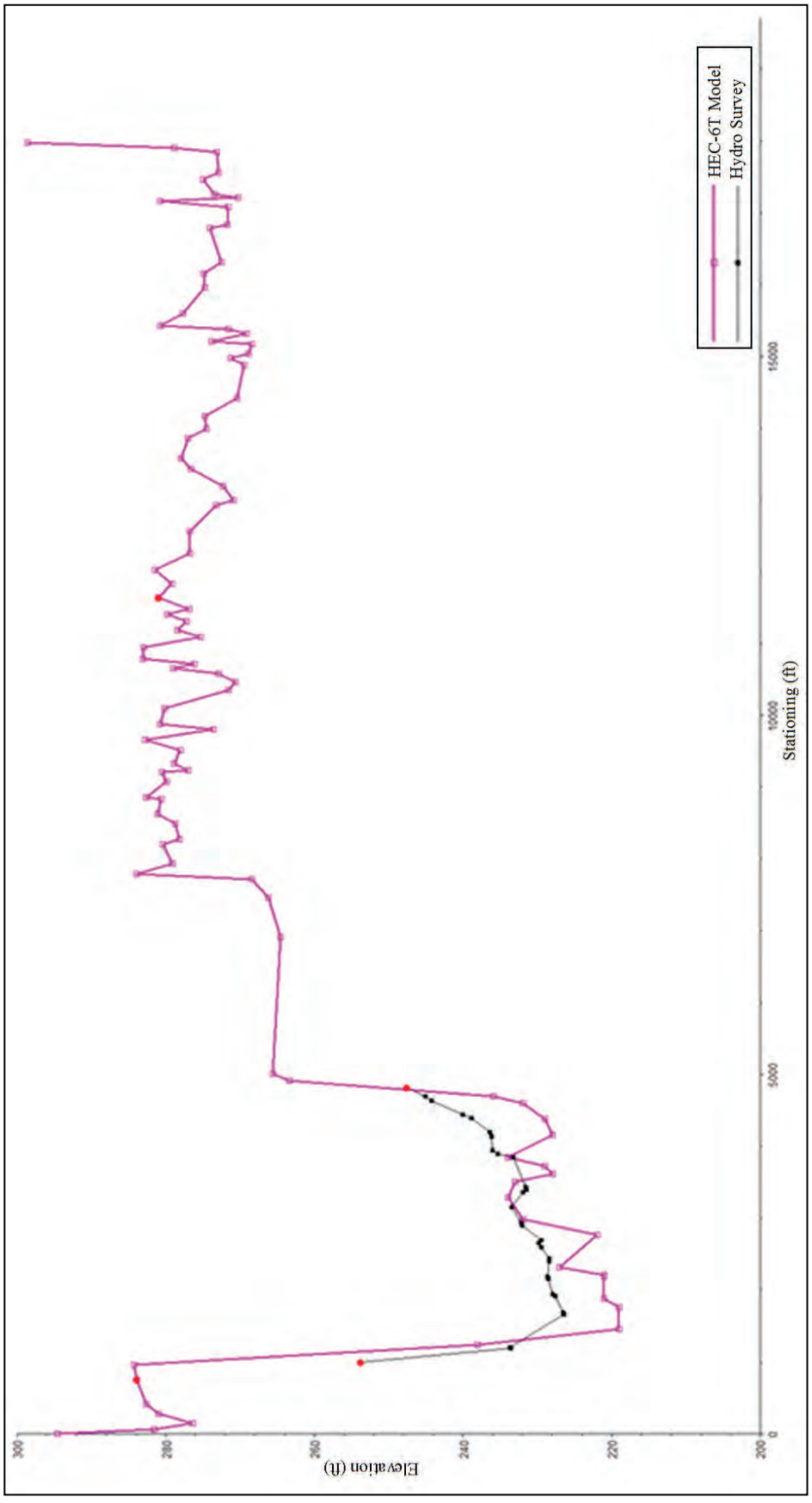


Figure D-12. HEC-6T 2004 sediment calibration at RM 870.20.

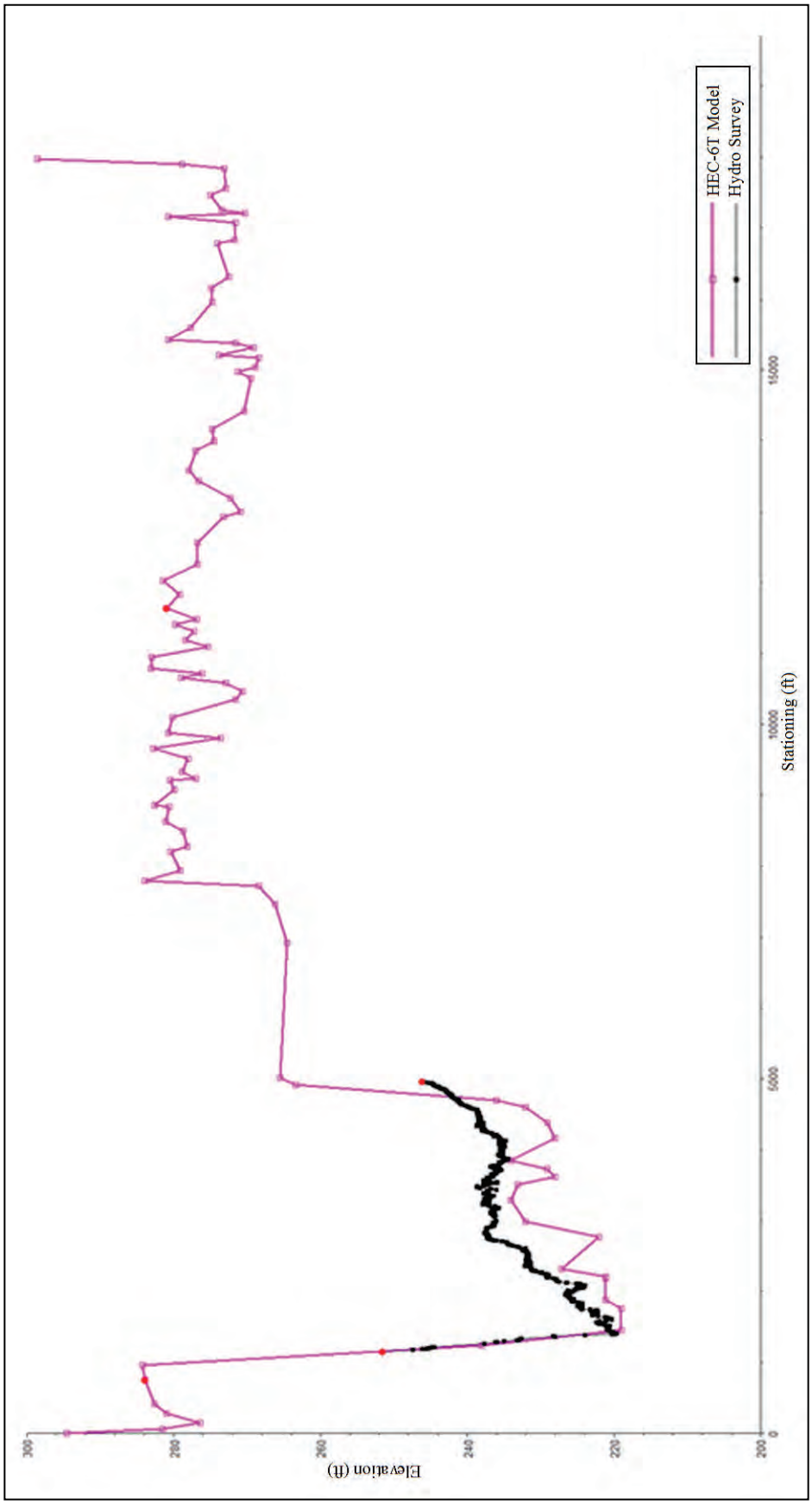


Figure D-13. HEC-6T 2010 sediment validation at RM 870.20.

Plan comparison

Figures D-14 through D-17 depict the index flow line comparison for Alternative 5 for Alternative 5 to the base condition at four model locations (RM 846.40, RM 856.99, RM 864.76, and RM 870.2).

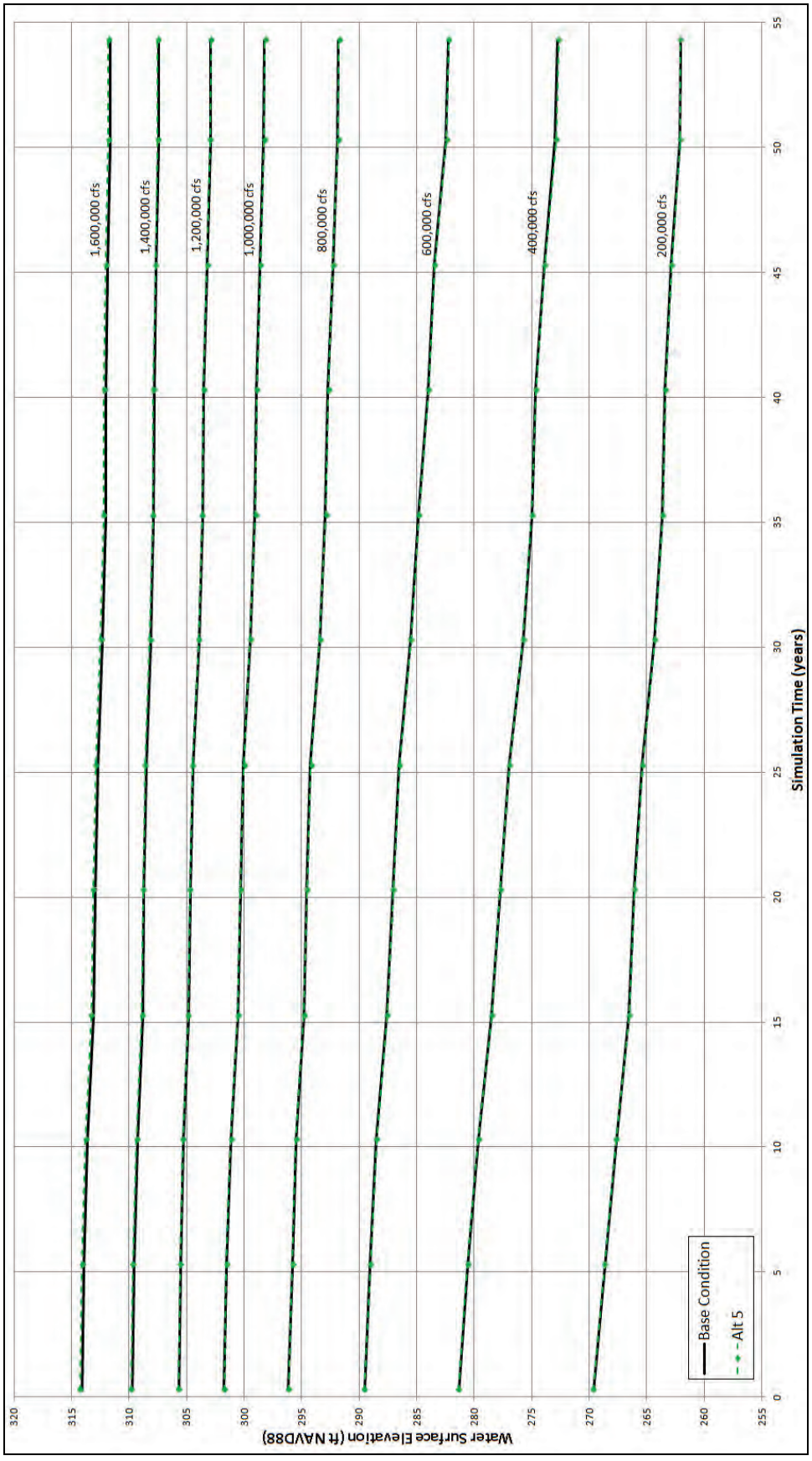


Figure D-14. HEC-6T base condition vs. Alternative 5 index flows at RM 846.20.

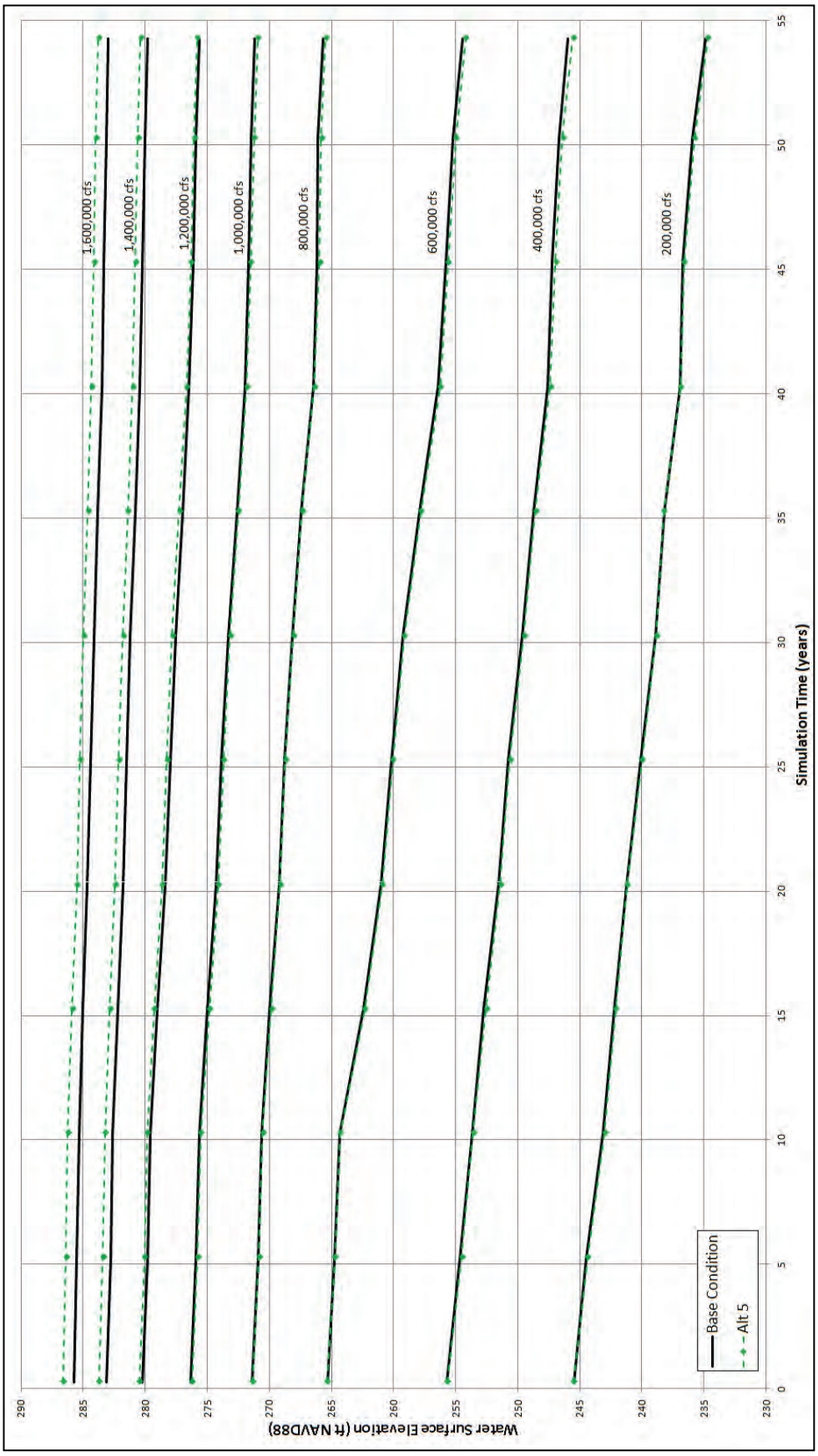


Figure D-15. HEC-6T base condition vs. Alternative 5 index flows at RM 869.08.

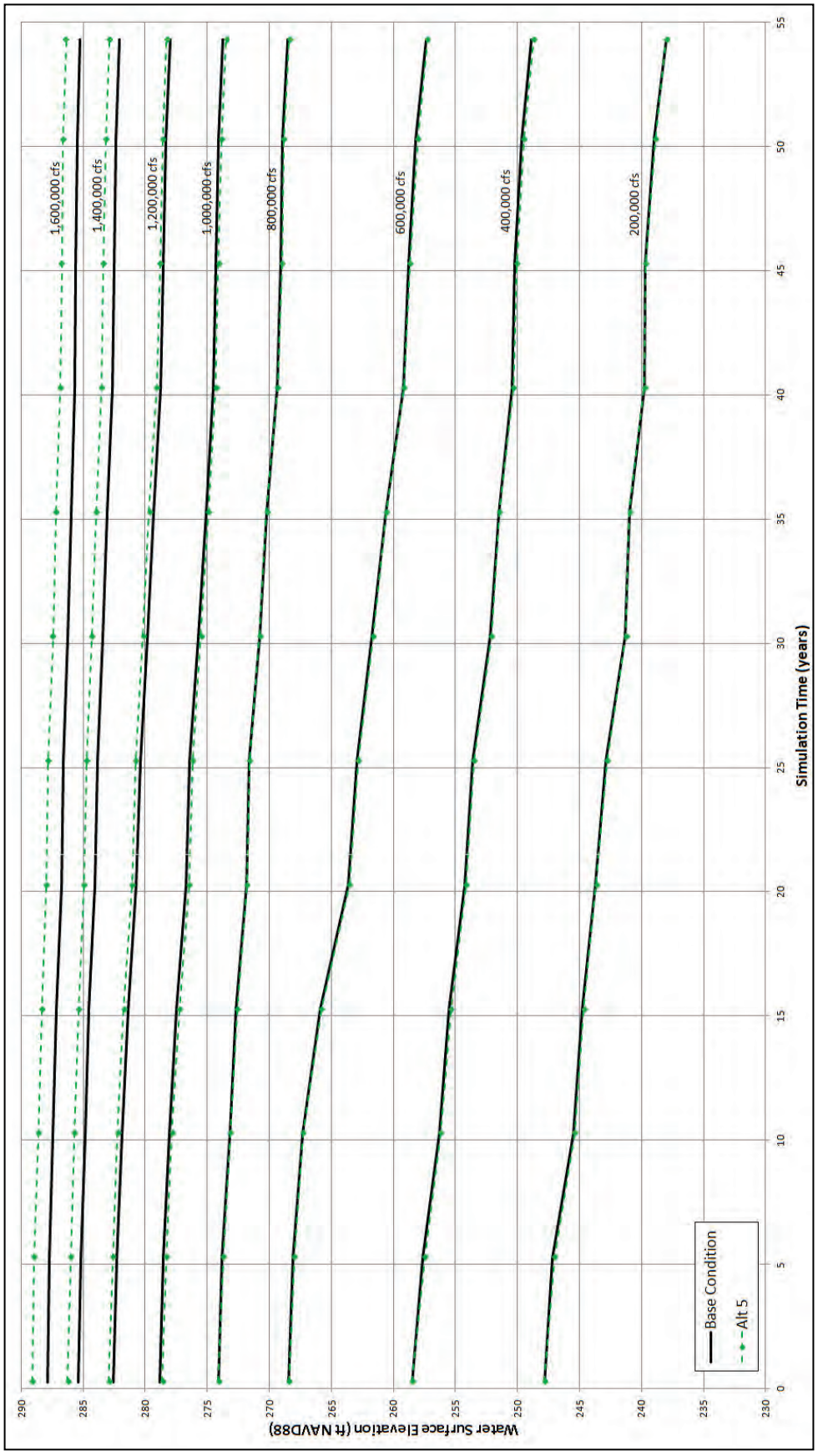


Figure D-16. HEC-6T base condition vs. Alternative 5 index flows at RM 873.04.

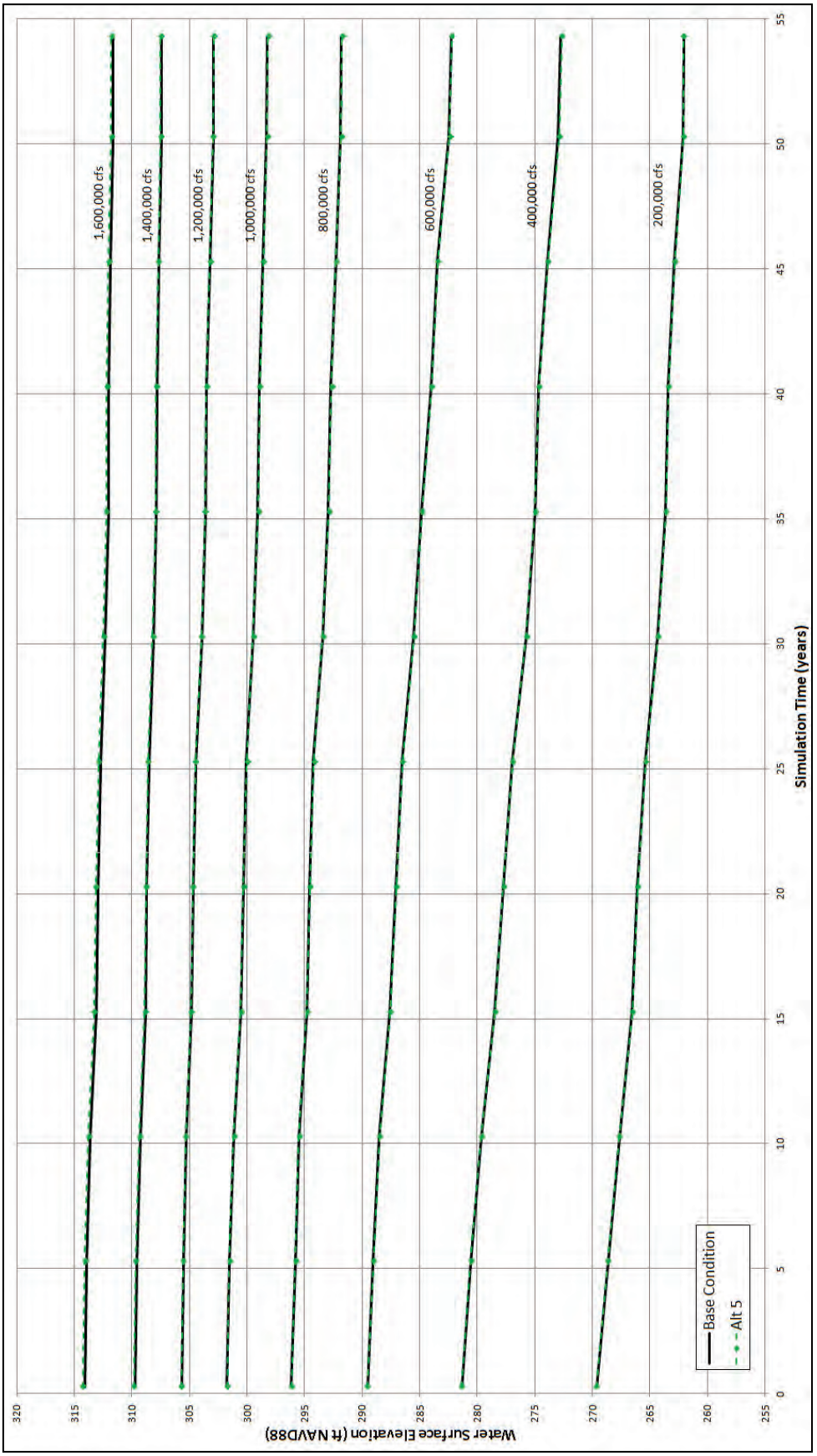


Figure D-17. HEC-6T base condition vs. Alternative 5 index flows at RM 922.00.

REPORT DOCUMENTATION PAGE

Form Approved
OMB No. 0704-0188

The public reporting burden for this collection of information is estimated to average 1 hour per response, including the time for reviewing instructions, searching existing data sources, gathering and maintaining the data needed, and completing and reviewing the collection of information. Send comments regarding this burden estimate or any other aspect of this collection of information, including suggestions for reducing the burden, to Department of Defense, Washington Headquarters Services, Directorate for Information Operations and Reports (0704-0188), 1215 Jefferson Davis Highway, Suite 1204, Arlington, VA 22202-4302. Respondents should be aware that notwithstanding any other provision of law, no person shall be subject to any penalty for failing to comply with a collection of information if it does not display a currently valid OMB control number.
PLEASE DO NOT RETURN YOUR FORM TO THE ABOVE ADDRESS.

1. REPORT DATE	2. REPORT TYPE	3. DATES COVERED *(From - To)*
May 2017	Final	

4. TITLE AND SUBTITLE

Merriwether-Cherokee Potamology Study

5a. CONTRACT NUMBER

5b. GRANT NUMBER

5c. PROGRAM ELEMENT NUMBER

6. AUTHOR(S)

Brian M. Hall, Roger A. Gaines, L. Yu Lin, and Kandi H. Waller

5d. PROJECT NUMBER
127672

5e. TASK NUMBER
A1920

5f. WORK UNIT NUMBER

7. PERFORMING ORGANIZATION NAME(S) AND ADDRESS(ES)

U.S. Army Engineer Memphis District
167 North Main Street
Memphis, TN 38103-1894

8. PERFORMING ORGANIZATION REPORT NUMBER

MRG&P Report No. 9

9. SPONSORING/MONITORING AGENCY NAME(S) AND ADDRESS(ES)

U.S. Army Corps of Engineers, Mississippi Valley Division
Mississippi River Geomorphology and Potamology Program
1400 Walnut Street
Vicksburg, MS 39180

10. SPONSOR/MONITOR'S ACRONYM(S)
CEMVD MRG&P

11. SPONSOR/MONITOR'S REPORT NUMBER(S)

12. DISTRIBUTION/AVAILABILITY STATEMENT

Approved for public release; distribution is unlimited.

13. SUPPLEMENTARY NOTES

14. ABSTRACT

This report documents the analysis performed for the Merriwether-Cherokee Potamology Study. The investigation included the following: infrastructure analysis, Low Water Reference Plane analysis, thalweg and tertiary layer analysis, volumetric analysis, specific gage analysis, duration analysis, multidimensional modeling analysis, one-dimensional modeling analysis, and a navigation assessment. A concern was that without modification of the western spur levee and Island 13 overbank, the Mississippi River will continue to form a 9-mile cutoff. If a cutoff were to form, potential adverse impacts include changes in long-term reach dynamics, navigation outdraft conditions, increased dredging operations, hydrodynamic condition changes in close proximity to a Mississippi River Levee mainline levee (Tiptonville-Obion Levee), endangerment of existing channel improvement features ($60M), endangerment of completed crevasse repairs ($27M), and endangerment of planned crevasse repairs. The analysis conducted on the base condition indicated that there is a moderate risk for cutoff formation. Alternatives were investigated to mitigate the risk for cutoff formation. The analysis conducted on the base condition indicated that there is a severe risk for local scour at the closure structure. Local scour countermeasures were investigated to mitigate the risk of closure structure failure.

15. SUBJECT TERMS

Cutoff formation, Geomorphic assessment, Levee Breech, Mississippi River, Navigation, Navigation assessment, Numerical modeling, Overbank scour, Potamology, Sediment transport

16. SECURITY CLASSIFICATION OF:			17. LIMITATION OF ABSTRACT	18. NUMBER OF PAGES	19a. NAME OF RESPONSIBLE PERSON
a. REPORT	b. ABSTRACT	c. THIS PAGE			Brian M. Hall
Unlimited	Unlimited	Unlimited	SAR	627	19b. TELEPHONE NUMBER *(Include area code)* (303) 963-4560